Sulfur recycling and degassing in subduction zone : Insights from volatile element and sulfur isotope compositions of olivine-hosted melt inclusions from Kyushu Island volcanoes, Japan

Masataka Kawaguchi

UNIVERSITÉ CLERMONT AUVERGNE, FRANCE
Sciences Fondamentales
Laboratoire Magmas et Volcans
&
KUMAMOTO UNIVERSITY, JAPON
Graduate School of Science and Technology

THÈSE DE DOCTORAT EN COTUTELLE

Présentée pour obtenir le grade de

DOCTEUR D'UNIVERSITÉ

Spécialité : *Structure et évolution de la Terre et des autres planètes*

Par

Masataka KAWAGUCHI

Titulaire d'un Master Recherche de l'Université de Kumamoto, Japon

Sulfur recycling and degassing in subduction zone: Insights from volatile element and sulfur isotope compositions of olivine-hosted melt inclusions from Kyushu Island volcanoes, Japan

Soutenue publiquement le 3 août 2021 devant le jury :

Yves Moussallam	Lamont Doherty Earth Observatory, NY, USA	Rapporteur
Tatsuhiko Kawamoto	Shizuoka University, Japon	Rapporteur
Yuki Suzuki	Waseda University, Japon	Examinatrice
Hiroshi Isobe	Kumamoto University, Japon	Président
Yasuo Miyabuchi	Kumamoto University, Japon	Examinateur
Estelle Rose-Koga	LMV, Université Clermont Auvergne, France	Directrice de Thèse
Kenneth Koga	LMV, Université Clermont Auvergne, France	Directeur de Thèse
Akira Yoshiasa	Kumamoto University, Japon	Directeur de Thèse

Acknowledgements

I would first like to thank my advisors Prof. Akira Yoshiasa, Dr. Estelle F. Rose-Koga and Dr. Kenneth T. Koga for all supports through this PhD project. I am grateful to you for giving me a chance to work on this great international project and to all efforts for lead through the conclusion of the co-tutorship agreement. I appreciate all long discussions and patience you invested precious times and passions, giving many important findings on scientific and personal aspects. Estelle also took care of all complicated administrative paperwork in French, and helped to make me possible to focus on scientific works. She always tried to find the best way for me, and clarified the needs to progress in work. Ken has taught me the importance of attitude that deepen the question to explore more fundamental problems. The discussions with him updated my knowledges in many aspects, inspired me and enable to develop myself. I thank to Prof. Akira Yoshiasa for his advises and acceptance of supervision to lead this collaboration. They always encouraged me and gave critical advises at the specific time. I also thank to Prof. Toshiaki Hasenaka who supervised me since my bachelor research project to the first year of PhD, and encouraged and inspired me unwaveringly as mentor all time. All daily discussions and findings in fields and seminars are basics of my idea. He always pushed my back for challenges. During the stay in France, he and his wife, Ms. Kazue, sent heart-warming letters and relief supplies, and encouraged me in tough time.

And I thank to Dr. Atsushi Yasuda and Ms. Natsumi Hokanishi for technical support of EPMA and FTIR analyses at the Earthquake Research Institute, the University of Tokyo, to Dr. Yasushi Mori for XRF analysis at Kitakyushu Museum of Natural History and Human History, and to Prof. Tadao Nishiyama and Prof. Hiroshi Isobe for their support of EPMA analysis at Kumamoto University. Administrative staff of Earth and Environmental Sciences department of Kumamoto University, Ms. Kaori Ban, cooperated for most of paper works from distance. I

am also grateful to her encouragements and critical advises saved me. I acknowledge the financial support from the French Embassy in Tokyo, Japan and from the French government through a “Bourse du Gouvernement Françsais” for this project. This scholarship allowed me to continue the research through this PhD work. Campus France helped me to get settled during stay in France.

The works in France after early 2020 is conducted under the coronavirus global health crisis (COVID-19 pandemic). In this unstable period, this PhD project would not have been possible without any of the support from all people involved. The laboratory director, Dr. Didier Laporte, and all staffs of LMV helped me to work pleasant in many aspects. Dr. Nicolas Cluzel helped with homogenization experiment using microscope heating stage. Ms. Claire Fonquernie and Ms. Chantal Bosq helped with sample preparation. Dr. Jean-Luc Devidal helped with long analytical sessions. I thank all your supports in difficult time schedules under sanitary operation. I deeply thank to Dr. Kenji Shimizu and Dr. Takayuki Ushikubo for helping with SIMS measurements at Kochi on tight schedule. Their contributions for this PhD projects are really significant and unstinting supports for measurements and preparation techniques saved this project. I am grateful to Dr. Yasuhisa Tajima and Dr. Hideto Naruo for their help on the field and on-spot discussions clarified the geological context. I also thank to Prof. Mitsuru Okuno and Mr. Tomohisa Tamura for providing articles and information on the outcrops.

During intermitted long confinement I felt disappearing my personality and it was really hard time to work. The presence of PhD colleagues and co-workers shared the time gave me energies to keep running and inspirations. Especially the officemates, Mr. Guillaume Georgeais, Ms. Roxane Buso, Ms. Sophie Pailot-Bonnetat, Mr. Paul Chauvigné, Mr. Freddy Vasconez, helped me in daily works, shared lunches and taught me French cultures. Guillaume also helped field survey for this project in Japan. I also thank you, Drs. Diego Narvaez, Ines Pereira, Alessandro Tadini, Taya Flaherty, Luca Terray, Pierre Faure, Paul Frossard, Claudine Israel,

Damien Freitas, Mr. Rémy Pierru, Mr. Cyril Aumar, Mr. Quentin Dumont, and many others. All you made my study life filled in bright and pleasant. When it was allowed, Estelle and Ken brought me to the hike and field excursion many times and giving me a chance for refreshing and learning geologies in nature. It helped me a lot to take breath in positive mind. All experiences I could have during this time are my treasure and foundation forever.

Lastly, I thank to my family for heartfelt supports and understanding to continue studies in anytime. I also extend my gratitude to friends, Mr. Naoki Tomita, Mr. Yuya Tamai, Ms. Azusa Okumura and Dr. Yuki Tomimatsu and the dearest friend, Ms. Manaka Kawaguchi, for encouraging and believing me from distance.

Abstract

Sulfur is a volatile element that outgasses from magmas. Its role in volcanology and mantle geochemistry, therefore, needs to be assessed through primitive magmas, to exclude the influence of magma evolution process and degassing. In my thesis, the primary goal is to find these primitive magmas, and characterize their volatile element concentrations and sulfur isotopic compositions. My research covers two important processes of the sulfur cycle in a subduction zone. 1) First, the transport of material from the subducting plate (slab) to the mantle wedge, because the nature of the sulfur dissolved in the fluids escaping from the slab, as well as its speciation and sulfur isotopic composition, remain poorly constrained. 2) Second is the degassing of primitive magma during its ascent, prior to eruption at arc volcanoes, because this process is critical in understanding the observed global discrepancies between total sulfur masses discharged and dissolved sulfur in magmas estimated by petrology, commonly referred to as "excess degassing of sulfur".

Melt inclusions of Aso volcano (Japan) allows to identify the primitive mafic magma responsible for the deep volatile element flux in a mature volcano, providing petrological constraints on (1) the depths of the magma reservoirs, as well as (2) the origin of the observed volcanic gases. In this study, I analyzed melt inclusions and phenocrysts of Holocene basaltic eruptions, and reported their concentrations of major and volatile elements. The samples showed clear evidences of magma mixing, such as reverse mineral zonation, and highly variable mineral and glass compositions. I found that the pre-eruptive storage depths were 2 km and 4 km below the edifice, for the Strombolian eruption and the sub-Plinian eruption, respectively. The most volatile-rich primitive magma, which is one of the magmas participating in the mixing, originates from a deeper level (>10 km). I determined the initial volatile element concentrations of the primitive magma: >4.68 wt% H_2O, 400 - 750 ppm CO_2, 3750 ppm S, 716 ppm Cl and 324 ppm F.

I then studied melt inclusions trapped in olivines from nine volcanoes on Kyushu Island, Japan to understand the systematics of sulfur behavior in the primary magmas along this arc segment. I measured major, trace, and volatile elements as well as sulfur isotopes in olivine melt inclusions from tephra of Oninomi, Yufu, Kuju, and Aso, to southern Kyushu with Kirishima (2 cones), Sumiyoshi-ike, and Kaimon, and one back-arc volcano, Fukue. For each edifice, I identified the least degassed compositions and selected melt inclusions from the primary magma. Sr/Y ratios highlight a compositional dichotomy between volcanoes in northern Kyushu (Sr/Y>20) and southern Kyushu (Sr/Y<20), separated by the Kyushu-Palau ridge. Trace element systematics records a stronger slab melt signature, with residual garnet, in northern Kyushu. Two volcanoes, Fukue and Oninomi, lie outside these two groups and are interpreted as originating from a mantle wedge with weak slab inputs. The $\delta^{34}S$ in melt inclusions range from -0.32±0.79 ‰ to +9.43±0.47 ‰ (2σ) and trace the source of magma from the different volcanoes, rather than degassing or crustal fractionation processes. The $\delta^{34}S$ variation is not controlled by the nature of the fluid (aqueous or silicate liquid) metasomatizing the mantle wedge. Rather, this study highlights the need for a component with a high $\delta^{34}S$, such as seawater sulfates in the agent metasomatizing the mantle wedge.

Résumé

Le soufre est un élément volatile qui dégaze des magmas. Son rôle en volcanologie et en géochimie du manteau doit donc être évalué à partir des magmas primitifs pour exclure l'influence du processus d'évolution du magma et du dégazage. Dans ma thèse, l'objectif principal est de trouver les magmas primitifs, et de caractériser leurs concentrations en éléments volatils et leurs compositions isotopiques en soufre. Mes recherches portent sur deux processus importants du cycle du soufre dans une zone de subduction. 1) Le premier est le transport de matériel de la plaque plongeante vers le coin mantellique, car la nature du soufre dissout dans les fluides s'échappant de cette dernière, ainsi que sa spéciation et sa composition isotopique, restent mal connues. 2) Le second est le dégazage du magma primitif au cours de son ascension, avant l'éruption au niveau des volcans d'arc, car ce processus est essentiel pour comprendre les écarts mondiaux observés entre les masses totales de soufre évacuées et le soufre dissout dans les magmas estimés par la pétrologie, communément appelé "excès de soufre dégazé".

Les inclusions magmatiques du volcan Aso (Japon) permettent d'identifier le magma mafique primitif responsable du flux profond d'éléments volatils dans ce volcan mature, fournissant des contraintes pétrologiques sur (1) les profondeurs des réservoirs magmatiques, ainsi que sur (2) l'origine des gaz volcaniques observés. Dans cette étude, j'ai analysé des inclusions magmatiques et des phénocristaux provenant d'éruptions basaltiques holocènes, et j'ai rapporté leurs concentrations en éléments majeurs et volatils. Les échantillons présentaient des signes évidents de mélange magmatique, comme une zonation minérale inversée, et des compositions minérales et vitreuses très variables. J'ai déterminé des profondeurs de stockage pré-éruptif de 2 km et 4 km sous l'édifice, pour l'éruption strombolienne et l'éruption sub-plinienne, respectivement. Le magma primitif le plus riche en éléments volatils, qui est l'un des magmas participant au mélange, provient d'un niveau plus profond (>10 km). J'ai déterminé

les concentrations initiales en éléments volatils du magma primitif : >4,68 % en poids de H2O, 400 - 750 ppm de CO2, 3750 ppm de S, 716 ppm de Cl et 324 ppm de F.

J'ai ensuite étudié les inclusions magmatiques piégées dans les olivines de neuf volcans de l'île de Kyushu, au Japon, afin de comprendre la systématique du comportement du soufre dans les magmas primaires le long de ce segment d'arc. J'ai mesuré les éléments majeurs, traces et volatils ainsi que les isotopes du soufre dans les inclusions magmatiques d'olivines provenant des téphras d'Oninomi, Yufu, Kuju et Aso, du sud de Kyushu avec Kirishima (2 cônes), Sumiyoshi-ike et Kaimon, et d'un volcan de l'arrière-arc, Fukue. Pour chaque édifice, j'ai identifié les compositions les moins dégazées et sélectionné les inclusions magmatiques du magma primaire. Les rapports Sr/Y mettent en évidence une dichotomie de composition entre les volcans du nord de Kyushu (Sr/Y>20) et du sud de Kyushu (Sr/Y<20), séparés par la crête Kyushu-Palau. La systématique des éléments traces enregistre une signature de fusion de la plaque plongeante plus forte, avec du grenat résiduel, dans le nord de Kyushu. Deux volcans, Fukue et Oninomi, se situent à l'extérieur de ces deux groupes et sont interprétés comme provenant d'un coin mantellique avec de faibles apports de la plaque plongeante. Les $\delta^{34}S$ dans les inclusions de fusion varient de -0,32±0,79 ‰ à +9,43±0,47 ‰ (2σ) et retracent la source du magma des différents volcans, plutôt que des processus de dégazage ou de fractionnement crustal. La variation du $\delta^{34}S$ n'est pas contrôlée par la nature du fluide (aqueux ou liquide silicaté) métasomatisant le coin mantellique. Cette étude met plutôt en évidence la nécessité d'un composant avec un $\delta^{34}S$ élevé, comme les sulfates d'eau de mer, dans l'agent métasomatisant le coin mantellique.

Table of contents

Chapter 1 General introduction 1

1.1. Volatile recycling and outgassing in subduction zone 1

1.2. Sulfur cycle and isotopic fractionation on the Earth surface 3

1.2.1. Why sulfur isotope study is needed in arc volcanoes? 3

1.2.2. Basic principles 5

1.2.2.1. Terminology of sulfur isotopes 5

1.2.2.2. Isotopic fractionation factors 6

1.2.2.3. Equilibrium fractionation factor 6

1.2.3. Sulfur isotope variations in the Earth's surface reservoirs 11

1.2.4. Remaining problems for sulfur transport in subduction zone 19

1.3. Scientific problems and approach 22

1.4. Dissertation organization 24

Chapter 2 Sample and methods 26

2.1. Melt inclusion 26

2.1.1. Use of melt inclusion 26

2.1.2. Post-entrapment processes 27

2.1.2.1. Post-entrapment crystallization and diffusive Fe-Mg exchange 27

2.1.2.2. Diffusive hydrogen loss 28

2.1.2.3. Vapor-bubble formation 30

2.2. Sampling strategy 32

2.3. Sample preparation 33

2.3.1. Selection and polishing of melt inclusion 33

2.3.2. Re-homogenization of crystallized melt inclusion using heating stage 33

2.4. Analytical methods 35

2.4.1. Secondary ion mass spectrometry (SIMS) 35

2.4.2. Electron probe micro-analyzer (EPMA) 36
2.4.3. Laser ablation inductively coupled plasma mass spectrometer (LA-ICP-MS)....37
Chapter 3 Persistent gas emission originating from a deep basaltic magma reservoir of an active volcano: the case of Aso volcano, Japan..... 39
3.1. Introduction 39
3.2. Samples and methods 41
3.2.1. Geological setting of Aso volcano and its cones....41
3.2.2. Tephra and scoria descriptions....42
3.2.3. Melt inclusion preparation 45
3.2.4. Analytical methods....45
3.2.4.1. Bulk rock major and trace elements....45
3.2.4.2. Major and volatile elements in melt inclusion, mineral and glass....46
3.2.4.3. Sulfur speciation analysis 48
3.2.5. Data processing: Post-entrapment crystallization correction....49
3.3. Results 50
3.3.1. Petrography 55
3.3.2. Host mineral compositions....55
3.3.3. Major and volatile elements in melt inclusions....57
3.4. Discussion....59
3.4.1. Evidence for magma mixing 59
3.4.2. Characterization of mixing endmembers 60
3.4.3. Volatile concentrations of primitive basaltic melt 63
3.4.4. Storage depth of the magma mixture 68
3.4.5. Persistent degassing from a deeper magma reservoir (>10km) 72
3.4.5.1. Excess degassing of SO_2 and CO_2 from Nakadake 2014 eruption 72
3.4.5.2. Modelling degassing of the deep magma reservoir 74

3.4.6. Implications for understanding current Aso volcanic activity 79
3.5. Summary and conclusion.....82
3.6. Bridge between Chapter 3 and Chapter 4 83
Chapter 4 Sulfur isotopes systematics in arc: seeing through the degassing via a melt inclusion study of Kyushu Island volcanoes, Japan 84
4.1. Introduction 84
4.2. Geological setting 85
4.2.1. Tectonic setting 85
4.2.2. Volcanism.....86
4.3. Samples and Methods 89
4.3.1. Sample description 89
4.3.2. Melt inclusion preparation 92
4.3.3. Analytical methods.....92
4.4. Correction for post-entrapment modification 95
4.4.1. Post-entrapment crystallization 95
4.4.2. Vapor-bubble formation 96
4.5. Results 98
4.5.1. Major element compositions 98
4.5.2. Trace element compositions.....99
4.5.3. Volatile element and sulfur isotope compositions 99
4.6. Discussions 103
4.6.1. Major and trace element composition of the primitive melt of each volcano....104
4.6.2. Volatile concentrations in primitive magma 108
4.6.3. S isotope composition of primitive magma and influence of degassing on the S isotope compositions 117

4.6.4. The three magma groups of Kyushu 120
4.6.5. Geodynamic significance of source region 124
4.6.6. Assessment of individual volcanoes 129
4.6.7. Implications for sulfur isotope in subduction zone 131
4.7. Conclusions 137
Chapter 5 General conclusions and perspectives 138
5.1. General conclusions 138
5.2. Perspectives 139
References 142
Appendices 179
Appendix A Supplementary materials for Chapter 3 180
Table A1. Uncorrected not-normalized to 100% and corrected compositions of all melt inclusions and host minerals 181
Table A2. All groundmass glass analyses 202
Table A3. All core and rim compositions of phenocrysts 208
A4. Supplementary discussion 252
Magma mixing model 252
Calculation of the total mass of emitted gas and exsolved volatile from erupted magma 256
Comparison of degassing models 257
Comparison of H_2O-CO_2 solubility models 259
Microscopic photo of typical melt inclusions 261
Supplementary references 262

Appendix B Supplementary materials for Chapter 4 265
Table B1. Physical descriptions of olivine-hosted melt inclusions 266
Table B2. Melt inclusion compositions corrected for post-entrapment crystallization and bubble 269
Table B3. Uncorrected major element and sulfur speciation analyses of melt inclusions 277
Table B4. Volatile and P_2O_5 concentrations uncorrected for post-entrapment modification and S isotope compositions of olivine-hosted melt inclusions 282
Table B5. Measured trace element concentrations (uncorrected) in olivine hosted melt inclusions 287
Table B6. Calculated CO_2 concentration in bubble and parameters used to calculation 293
Table B7. Host olivine compositions 296
Table B8. Model parameters and estimated slab melt/fluid composition 298
B9. Supplementary discussion 299
Heating experiment 299
Correction of post-entrapment diffusive Fe-loss 300
Identification of the primitive melt composition 302
Sulfur isotope fractionation 308
Calculation of trace element composition in slab-component 311
Supplementary references 315
B10. Microscopic photos of melt inclusions 321

List of figures

1.1. Equilibrium isotopic fractionation factors of sulfur compounds with respect to H_2S 10

1.2. Sulfur isotope variations in natural rocks, sulfide and sulfate minerals.....15

1.3. Schematic summary of $\delta^{34}S$ compositions in Earth's surface reservoirs 16

1.4. Schematic evolution of sulfur isotope composition and sulfide-sulfur concentration during serpentinization and hydrothermal alteration of oceanic peridotite 18

2.1. Vernadsky-type microscope heating stage designed by Sobolev et al. (1980) 34

3.1. Locations of volcanic cones and sampling sites of the study.....44

3.2. Microscope photographs (a-d) and backscatter electron images (e, f) of representative phenocrysts and textures from Holocene basaltic tephra products in Aso central cones 56

3.3. Major element and volatile concentrations in melt inclusions from Holocene basaltic tephra products in Aso central cones 58

3.4. Ratios of volatiles/K_2O vs. K_2O in melt inclusions and groundmass glasses 64

3.5. (a) Variations in S and total FeO concentrations of melt inclusions and groundmass glasses 66

3.5. (b) Measured S concentration in olivine-hosted melt inclusions as a function of sulfur concentration at sulfide saturation (SCSS) 66

3.6. Variations in Cl and F concentrations of melt inclusions (KSS and NKD14) 68

3.7. Pre-eruptive temperatures and water concentrations calculated from the compositions of plagioclase rim and groundmass glass 71

3.8. Evolution of H_2O/S, CO_2/S, and Cl/S molar ratios of magmatic gases in equilibrium with the primitive basaltic melt plotted against pressure.....77

3.9. Observed volcanic gas compositions emitted from Aso volcano compared with modelled variation in CO_2/SO_2 and H_2O/CO_2 molar ratios.....79
3.10. Schematic summary of the magma and gas evolution in the Aso plumbing system 81
4.1. Map of the Japanese Islands arc and Kyushu sample locations 88
4.2. Total alkali ($Na_2O + K_2O$) vs. SiO_2 diagram for olivine-hosted melt inclusions..101
4.3. Primitive mantle-normalized trace element compositions of melt inclusions.....102
4.4. H_2O and CO_2 concentrations in melt inclusions.....103
4.5. Variations of incompatible element concentrations in melt inclusions.....108
4.6. K_2O normalized volatile element abundances in the melt inclusion.....115
4.7. Comparison of measured sulfur concentrations in primitive melt inclusions with the sulfur content at sulfide saturation (SCSS).....117
4.8. Sulfur isotope composition is plotted against sulfur abundance 120
4.9. Slab-derived material contribution into the magma source.....123
4.10. Sr/Y ratio and Y concentration of melt inclusions 124
4.11. Mixing and melting trajectories of subduction zone endmembers.....128
4.12. Results of mixing calculations for the primitive end members.....129
4.13. Isotopic composition of sulfur plotted against trace element ratios 136
4.14. Isotopic composition of sulfur plotted against trace element ratios.....136

List of tables

1.1. Absolute sulfur isotope abundance ratios of reference materials 6

1.2. Coefficients of the polynomial equation for equilibrium isotopic fractionation factors of sulfur compounds with respect to H_2S 9

1.3. Summary of reported $\delta^{34}S$ values for surface sulfur reservoirs 13

3.1. Tephra samples used in this study. 45

3.2. Major and trace element compositions of bulk tephra samples 51

3.3. PEC corrected and normalized to 100%, major element and volatile concentrations in representative melt inclusions 52

3.4. Major element and volatile contents in groundmass glasses 54

3.5. Results of thermo-barometric calculation for mixed magma 70

3.6. Comparison of the measured volatile emission with petrological estimation for Nakadake 2014 eruption 75

4.1. Sample list 91

4.2. Major, trace and volatile element concentrations and S isotope composition of melt inclusions selected as primitive represents 110

4.3. Comparison of H_2O/K_2O ratio between melt inclusion measurements and plagioclase-hygrometer results, and estimated minimum H_2O concentration in primitive magma 112

Chapter 1

General introduction

1.1. Volatile recycling and outgassing in subduction zone

Volatile elements (H_2O, CO_2, S, Cl and F) have a role in subduction zone magmatism. Magmas produced in subduction zone are generally richer in fluid-mobile element, such as volatile and large-ion lithophile elements (LILE) (HFSE; Gill, 1981; Pearce, 1982; Arculus and Powell, 1986; Elliott et al., 1997), compared to those of the mid-ocean ridge basalt (MORB), which were generated by the adiabatic decompression of the upper mantle. This difference is generally explained by an addition of volatile-rich material into the sub-arc mantle from subducting slab (e.g. Elliott, 2003; Pearce et al., 2005). An oceanic plate subducting beneath arc mantle is typically composed of lithospheric mantle, gabbro, altered- and unaltered-volcanic rocks and marine sediments, carrying H_2O and other volatile elements into sub-arc depth (e.g., Schmidt and Poli, 1998; Nakamura and Iwamori, 2009). Such a subducting slab is progressively dehydrated, releasing the H_2O into overlying mantle, due to the increase of pressure and temperature, as demonstrated by metamorphic rocks and geophysical studies (e.g., Bebout et al., 1999; Iwamori and Zhao, 2000). The current consensus is that such H_2O-rich fluid addition causes a decrease of the solidus temperature of mantle peridotite and melts mantle, although the details of the melt generation process in the mantle wedge are complex and there remain competing hypotheses.

The variation of geochemical characteristic of primitive magma, such as volatile and trace element abundances, indicates the diversity of magma generation processes in subduction zones and within the same volcanic group. Global compilation of subducting sediment data and geochemical systematics of arc magma shows good agreement between bulk composition

and those of regional sediment in terms of geochemical tracers (e.g., Pb isotope, Th/La), indicating significant input of sediment component for magma genesis (Plank and Langmuir, 1998; Plank, 2005, 2014). In addition, high-pressure experiments of sediment and basalt demonstrated the generation of different fluid phases called aqueous fluid, silicate melt and supercritical fluid depending on the temperature, accompanied with various degree of fractionation of elements between fluid and solid (Kessel et al., 2005; Mibe et al 2011). These high-pressure fluid and melt are considered as main carrier of volatile elements (e.g., Spandler and Pirard, 2013). While the aqueous fluid generated by the dehydration of slab are enriched in fluid-mobile elements (volatile elements and LILE), silicate melt generated from the slab melting are enriched in both fluid-mobile elements and fluid-immobile elements (HFSE, light rare earth element). The supercritical fluid is stable at the high-temperature and -pressure condition exceeded critical endpoint, in which the intermediate fluid composition exists (Mibe et al., 2011). Such supercritical fluid potentially separates into aqueous fluid and silicate melt during its ascent within the mantle wedge, producing primitive basalt and andesite at the simultameously (Kawamoto et al., 2012). Recent experimental study identified partitioning coefficients of fluid-mobile elements (Pb, Rb, Sr) between supercritical fluid and silicate melt increase with an increase of pressure and salinity (Cl-bearing solution) (Kawamoto et al., 2014). These geochemical constraints indicate the characteristics of slab-derived fluid is governed by factors such as chemical composition, phase equilibrium of subducting slab and thermal structure of mantle wedge. The interaction of generated slab-derived fluid and sub-arc mantle produces a wide range of geochemical features in primitive magmas.

Volatile elements supplied from the slab are released into the atmosphere via volcanic degassing from magma. Volatile element behavior in magmas is typically governed by its solubility, which strongly depends on pressure, temperature and the chemical composition of magma (e.g., Dixon et al., 1995). Volatiles are dissolved in the magma at greater depths, but

the saturation of volatile elements at a shallow depth leads to exsolution and nucleates bubbles. This gas exsolution causes rapid magma ascent, eruption and fragmentation (Roggensack et al., 1997; Piolo et al., 2009; Edmonds and Wallace, 2017).

Gas emission is commonly monitored volcanic activities, and it occurs during eruptions and in quiescent periods (e.g., Miyakejima, Shinohara et al., 2003; Stromboli, Burton et al., 2007). Persistent degassing of active volcanoes reflects the degassing of magma beneath volcanoes. From such data, several studies have pointed out that the greater total masses of measured emitted gas than the budget of dissolved gas in magma from petrological estimations (e.g., Wallace et al., 2005; Shinohara, 2008). This is commonly referred to as "excess degassing", observed in subduction zone volcanism (e.g., Métrich and Wallace, 2008; Roberge et al., 2009; Wallace and Edmonds, 2011; de Moor et al., 2017). The reconciliation of this imbalance is an outstanding volcanology challenge today.

Geochemical characteristics of volatile elements in arc magma are closely linked to the nature of subducting oceanic slab. Nearly all of discharged volcanic carbon (80 – 95%) from arc volcanoes is originated from the subducting sediment based on the systematics of C isotope and C-S-He composition of volcanic gases (Plank and Manning, 2019). A global compilation of high-temperature volcanic gases identifies CO_2/S^{Total} ratio of volcanic gases correlate with that of subducted sediments (Aiuppa et al., 2017). These observations strongly indicate that the subducting sediment makes significant contributions of the volatile element to arc magma source.

1.2. Sulfur cycle and isotopic fractionation on the Earth surface

1.2.1. Why sulfur isotope study is needed in arc volcanoes?

The subduction zone magmatism is a system of sulfur cycle providing its flux to the Earth atmosphere. Sulfur is the third most abundant volatile element found in volcanic gasses after hydrogen (as a form of water) and carbon (as a form of carbon dioxide), and its degassing

has a significant impact on the atmospheric environment of the Earth. Gaseous volcanic sulfur compounds in high-temperature fumarole gases, in which high-temperature means magmatic origin with minimal crustal contributions, is predominantly released as sulfur dioxide, SO_2, followed by hydrogen sulfide, H_2S, in general (e.g., Symonds et al., 1994; Shinohara, 2008). Global volcanic SO_2 emission rate is ~23±2 Tg/yr for 2005–2015 using the Ozone Monitoring Instrument on NASA's Aura satellite (Carn et al., 2017). Approximately 80% of this total SO_2 flux was emitted from 30 volcanoes, which are mostly subduction-related arc volcanoes (Carn et al., 2017).

The transport mechanisms of sulfur in subduction zone are still controversial despite the significance of sulfur in magmatic activity. Sulfur behaves in the most complex manner among magmatic volatile elements, with its multiple oxidation states in natural conditions varying from -2 to +6. The addition of variably oxidized or reduced subducted sulfur to the mantle potentially affect the oxidation condition of the mantle. In addition, high sulfide-silicate melt partition coefficients for chalcophile element allows metal transport and accumulation at sub-arc condition, in combination with its redox sensitive sulfide breakdown (e.g., Canil and Fellows, 2017). Therefore, the slab-fluid characteristics, such as sulfur and trace element abundance and proportion of sulfur species (so that redox condition), is a critical information to understand slab-mantle material transport and redox evolution of the upper mantle.

The stable isotopes of sulfur are useful indicator to assess the source of sulfur and chemical exchange among sulfur species. Researchers have pointed out that sulfur in arc magma is probably originated from the seawater sulfate as the sulfur isotopic composition, $\delta^{34}S$, of volcanic rocks and high-temperature volcanic gases from the subduction zone is significantly higher than those of oceanic volcanoes ($\delta^{34}S$ values are ~+21‰, +5±3‰ and 0±2‰ for modern seawater sulfate, arc and oceanic volcanoes, respectively; Ono et al., 2012; Labidi et al., 2012, 2014; Ohmoto, 2020 and references therein). However, the transformation

mechanisms of seawater sulfate to magmatic sulfur in subduction zone are poorly constrained and the research community has not reached to consensus. One of the reasons for this problem is due to the complexity of magma generation and slab-dehydration processes as mentioned in previous section. In addition, the sulfur isotope composition of magma is expected to fractionate during sulfur degassing as inferred by theoretical and experimental studies (Marinit et al., 2011; Fiege et al., 2014, 2015). Since available sulfur isotope data are obtained from bulk rock samples, which are the remnants after sulfur degassing due to low-solubility of sulfur under atmospheric pressure, the reported $\delta^{34}S$ values of arc rocks are fractionated from the initial values by extensive degassing (e.g., Mandeville et al., 1998). Non-degassed, volatile-rich, primitive samples are needed to know the sulfur istopic composition of the source.

1.2.2. Basic principles

1.2.2.1. Terminology of sulfur isotopes

Sulfur has four stable isotopes, which are ^{32}S, ^{33}S, ^{34}S, and ^{36}S. The abundances of stable isotopes are ^{32}S = 94.99%, ^{33}S = 0.75%, ^{34}S = 4.25%, and ^{36}S = 0.01% (De Laeter et al., 2003). The isotope composition of sulfur is expressed as the deviation relative to the same ratio in a reference standard in per-mil (‰) using delta notation, which is defined by following equation:

$$\delta^{j}S\ (‰) = \left[\left({}^{j}S/{}^{i}S\right)_{sample} / \left({}^{j}S/{}^{i}S\right)_{standard} - 1\right] \times 10^{3}$$

where i =32 and j = 33, 34, and 36. In earlier studies, troilite (FeS) of the Canyon Diablo iron meteorite (CDT) has been used as an international reference (Macnamara and Thode, 1950; Thode et al., 1961). However, as it has been proven the original CDT is not homogeneous in sulfur isotopic composition (e.g. Beaudoin et al., 1994), a Vienna-CDT (V-CDT) scale has been introduced by an advisory committee of IAEA in 1993, recommending an artificially prepared reference material Ag_2S (IAEA-S-1) with $\delta^{34}S_{VCDT}$ of -0.3‰ (Gonfiantini et al., 1993; Robinson, 1993). Absolute $^{32}S/^{33}S$ and $^{32}S/^{34}S$ ratios of reference materials were determined

by Ding et al. (2001) and are reported in Table 1.1. Consequently, all δ-values are reported as V-CDT scale in this paper.

Table 1.1. Absolute sulfur isotope abundance ratios of reference materials (Ding et al. 2001)

Sample	$^{32}S/^{33}S$	$^{32}S/^{34}S$
IAEA-S-1	126.942 (±0.047)	22.6504 (±0.0020)
IAEA-S-2	125.473 (±0.055)	22.1424 (±0.0020)
IAEA-S-3	129.072 (±0.032)	23.3933 (±0.0017)
V-CDT	126.948 (±0.047)	22.6436 (±0.0020)

1.2.2.2. Isotopic fractionation factors

The isotopic relation between two coexisting, not necessarily in equilibrium, phases A and B has been termed the "isotopic fractionation factor" or "isotopic enrichment factor" and is expressed by $\Delta_{A\text{-}B}$, $\varepsilon_{A\text{-}B}$, or $\alpha_{A\text{-}B}$, which are defined as

$$\Delta_{A-B} = \varepsilon_{A-B} = \delta_A - \delta_B$$

and

$$\alpha_{A-B} = R_A/R_B = (\delta_A + 1000)/(\delta_B + 1000)$$

where R_A and R_B are the $^{34}S/^{32}S$ ratios of compound A and B, respectively (Ohmoto and Goldhaber, 1997). Since the α values are typically very close to 1 in sulfur isotope systems, the relationship is explained as

$$1000 \ln \alpha_{A-B} \approx (\alpha_{A-B} - 1) \times 1000 \approx \Delta_{A-B}.$$

1.2.2.3. Equilibrium fractionation factor

When the isotopic equilibrium is attained between two sulfur compounds, an equilibrium reaction can be written as follows:

$$H_2{}^{34}S + {}^{32}SO_4{}^{2-} = H_2{}^{32}S + {}^{34}SO_4{}^{2-}.$$

The equilibrium constant of the isotope exchange reaction between H_2S and SO_4^{2-}, K, is expressed as follows and is also same with the equilibrium isotopic fractionation factor:

$$K = \frac{[{H_2}^{32}S][{^{34}SO_4}^{2-}]}{[{H_2}^{34}S][{^{32}SO_4}^{2-}]} = \frac{({}^{34}S/{}^{32}S)_{SO_4^{2-}}}{({}^{34}S/{}^{32}S)_{H_2S}} = \alpha_{SO_4^{2-}-H_2S}.$$

In the case of reaction of simple molecules, containing one atom of the isotope-exchanging element, α is equal to K, but when the number of atoms of the element of interest, n, is different from 1, $\alpha = K^{1/n}$ (Richet et al., 1977; Marini et al., 2011).

Physically, the fractionation factor between a given molecule and the element in monoatomic state, so called β factor, is expressed as:

$${}^{34}\beta_{SO_4^{2-}} = \frac{[{^{34}SO_4}^{2-}]/[{^{32}SO_4}^{2-}]}{[{}^{34}S]/[{}^{32}S]} \text{ and } {}^{34}\beta_{H_2S} = \frac{[{H_2}^{34}S]/[{H_2}^{32}S]}{[{}^{34}S]/[{}^{32}S]}.$$

Assuming that the compounds are in isotopic exchange equilibrium, the fractionation factor α should be equal to the ratio of β factors:

$$\alpha_{SO_4^{2-}-H_2S} = {}^{34}\beta_{SO_4^{2-}}/{}^{34}\beta_{H_2S}.$$

Theoretically, the β factor is calculated using the Bigeleisen-Mayer equation (Bigeleisen and Mayer, 1947; Urey, 1947) with the Born-Oppenheimer and harmonic oscillator approximation:

$${}^{34}\beta = \prod_{j=1}^{f} \frac{{}^{34}U_j}{{}^{32}U_j} \frac{e^{-{}^{34}U_j/2}/(1-e^{-{}^{34}U_j})}{e^{-{}^{32}U_j/2}/(1-e^{-{}^{32}U_j})}$$

where $U_j = hv_j/kT$ is the dimensionless normal frequency, f is the number of degrees of freedom for the vibrational mode ($f = 3N - 5$ for linear molecules and $f = 3N - 6$ for other molecules, where N is number of atoms), h is the Plank's constant, k is the Boltzmann's constant, T is temperature in Kelvin, and v_j is the harmonic vibrational frequency of the vibration mode j in s^{-1}:

$$v_j = \omega_j c$$

where ω_j is the harmonic frequency in cm^{-1} and c is the speed of light. It is well known that the β factor depends on the temperature (Richet et al., 1977; Otake et al., 2008), hence, the α value is primarily controlled by temperature.

The temperature dependence of equilibrium isotopic fractionation factors is often expressed as polynomial functions of $1/T^2$ (e.g., Ohmoto and Rye, 1979):

$$1000 \ln \alpha = \frac{A \times 10^6}{T^2} + \frac{B \times 10^3}{T} + C \ (T \text{ in kelvins}).$$

where A, B and C represent constant coefficients (Table 1.2). The equilibrium isotope fractionation factors of sulfur compounds with respect to H_2S determined from the experiment are summarized in Table 1.2 and Figure 1.1. As shown in Figure 1.1, 1) the magnitude of fractionation factor depends primarily on temperature, becoming smaller with temperature increase, 2) sulfur species of higher valence tend to be more enriched in the heavier isotope at the equilibrium; $\delta^{34}S_{SO_4} > \delta^{34}S_{SO_2} > \delta^{34}S_{S_2} > \delta^{34}S_{H_2S}$ (Ohmoto and Goldhaber, 1997).

In the case of the degassing of magmas, the α value between gas and silicate melt phases is theoretically explained as

$$\begin{aligned} 1000 \ln \alpha_{\text{gas-melt}} &= \delta^{34}S_{\text{gas}} - \delta^{34}S_{\text{melt}} \\ &= \left[X\delta^{34}S_{SO_2} + (1-X)\delta^{34}S_{H_2S}\right] - \left[Y\delta^{34}S_{S^{2-}} + (1-Y)\delta^{34}S_{SO_4^{2-}}\right] \\ &= X1000 \ln \alpha_{SO_2-H_2S} + Y1000 \ln \alpha_{SO_4^{2-}-S^{2-}} + 1000 \ln \alpha_{H_2S-SO_4^{2-}} \end{aligned}$$

where X is the mole fraction of SO_2 in gaseous sulfur (SO_2 + H_2S) and Y is the mole fraction of sulfide sulfur in the total sulfur in the melt (Sakai et al., 1982; Marini et al., 2011). Fractionation factors of each reactions are constrained by previous studies (Table 1.2). Recent experiment of fluid-melt isotope fractionation by Fiege et al. (2015) shows the clear discrepancy between results of the study and Miyoshi et al. (1984) at reduced conditions, indicating the temperature dependence determined by Miyoshi (1984) for $\alpha_{SO_4^{2-}-S^{2-}}$ is less likely applicable to the silicate system as the previous experiment conducted for molten salt.

Table 1.2. Coefficients of the polynomial equation for equilibrium isotopic fractionation factors of sulfur compounds with respect to H_2S (from the compilation of Ohmoto and Goldhaber, 1997)

$1000 \ln\alpha_{i\text{-}H_2S} = A \times 10^6/T^2 + B \times 10^3/T + C$ (T in kelvins)				
Compound (i)	A	B	C	T range (˚C)
Dissolved sulfates and sulfate minerals	6.463	0.56		200 – 400
Sulfites	4.12	5.82	-5.0	>25
SO_2	4.70		-0.5	>350
SCO	0.67	0.43	-1.15	>25
CaS, SrS, BaS	0.6			
MgS	0.5			
MoS_2	0.45			
FeS_2	0.40			200 – 700
CoS_2, NiS_2, MnS_2	0.40			
ZnS	0.10			50 – 705
FeS	0.10			200 – 600
MnS, CoS, NiS	0.10			
$CuFe_2S_3$	0.05			
$CuFeS_2$	-0.05			200 – 600
S (= S_8)	-0.16			200 – 400
HS^-	-0.06		-0.6	50 – 350
Cu_5FeS_4	-0.25			
CdS, CuS	-0.4			
SnS	-0.45			
PbS	-0.63			50 – 700
HgS	-0.7			
Cu_2S, Sb_2S_3	-0.75			
Ag_2S	-0.8			
S^{2-}	-0.21	-1.23	-1.23	>25

As mentioned by Fiege et al. (2015), it is expected that the bonding energy of S^{2-} in a molten salt is probably different significantly from that in a Fe-bearing silicate melt. Since the relationship between atomic mass and bonding energy affects the equilibrium isotope

fractionation (e.g., O'Neil, 1986), the differences are most likely related to the significant differences in melt composition and structure. Updated temperature dependence of α value for H_2S-S^{2-} is proposed as

$$1000 \ln \alpha_{H_2S-S^{2-}} = 10.84 \times (10^3/T)^2 - 2.50$$

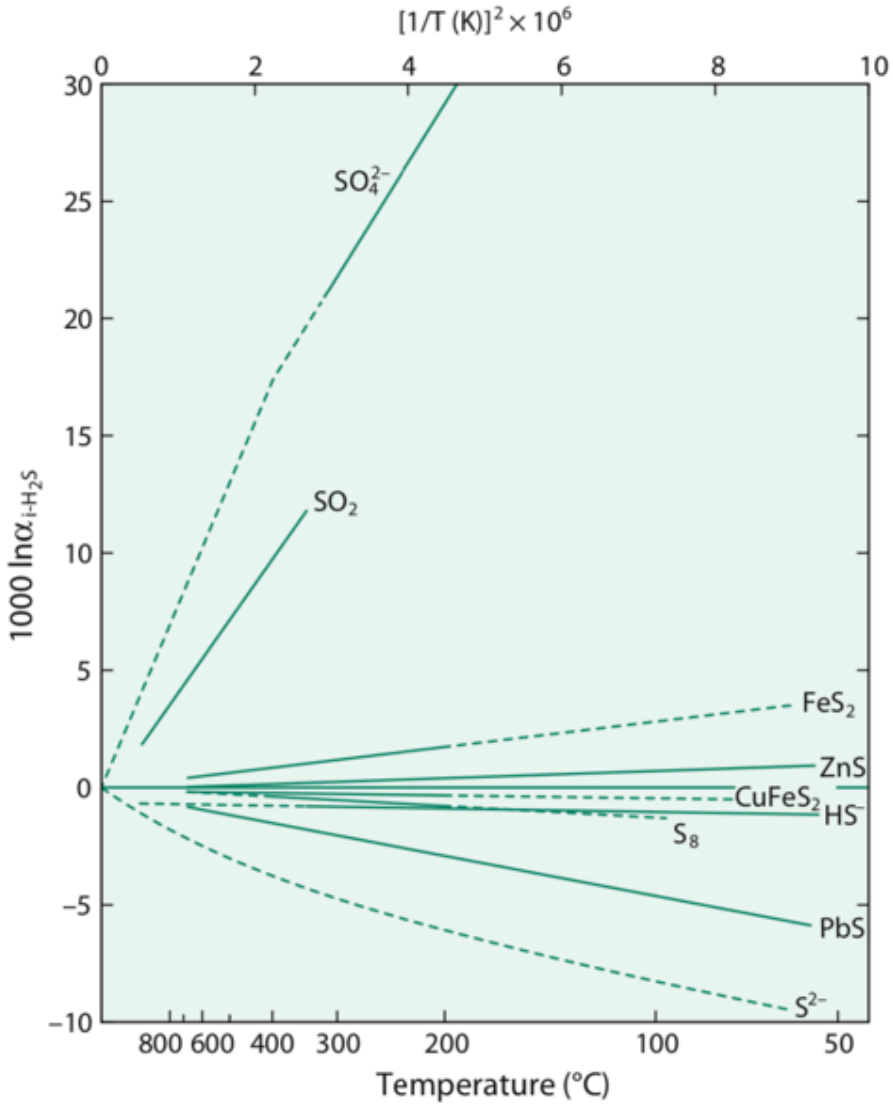

Figure 1.1. Equilibrium isotopic fractionation factors of sulfur compounds with respect to H_2S. Solid lines and dashed lines represent experimentally determined values and extrapolated or theoretically calculated values, respectively. Figure is taken from Hoefs (2018).

with one sigma of ~0.0010 (Fiege et al., 2015). Consequently, the α value for SO_4^{2-}-S^{2-} is theoretically constrained as

$$1000 \ln \alpha_{SO_4^{2-}-S^{2-}} = 1000 \ln \alpha_{SO_4^{2-}-H_2S} + 1000 \ln \alpha_{H_2S-S^{2-}} .$$

Their fractionation model shows closed-system degassing of basaltic melts induce the $\alpha_{\text{gas-melt}}$ of positive value in reduced condition (~QFM) and of negative value in oxidized condition (~QFM+4) at 1040 – 1200 ˚C (Fiege et al., 2015). The variations of $\delta^{34}S_{melt}$ value caused by closed- and open-system isothermal degassing are described as:

$$\delta^{34}S_{melt}^{final} = \delta^{34}S_{melt}^{initial} - (1 - F) \times 1000 \ln \alpha_{gas-melt}$$

$$\delta^{34}S_{melt}^{final} = \delta^{34}S_{melt}^{initial} + 1000 \times (F^{\alpha_{gas-melt}-1} - 1)$$

respectively, where $F = C_S^{final}/C_S^{initial}$ is the fraction of sulfur remaining in the melt (Holloway and Blank, 1994; Marini et al., 1994). Such degassing model indicates that the $\delta^{34}S_{melt}$ value changes drastically, especially if open-system degassing occurs (Marini et al., 2011).

The α value between immiscible sulfide and dissolved sulfur in silicate melt at the magmatic condition has never been determined experimentally, however, it is petrologically constrained from the natural sample studies (e.g. Chaussidon et al., 1989). Recent study of MORB and the Garrett intra-transform lava samples reported the lack of significant evolution of $\delta^{34}S$ values with melting degree of source mantle and sulfide fractionation proxies at the α value of 1.0000 ± 0.0003 (Labidi et al. 2014; Labidi and Cartigny, 2016). These estimates indicate that no preferential enrichment of heavier S isotopes in fractionated sulfides, at least, under the conditions of MORB petrogenesis (i.e. at ~1200 ˚C and with pressure less than 30 kbars; Labidi and Cartigny, 2016).

1.2.3. Sulfur isotope variations in the Earth's surface reservoirs

Isotopic composition of sulfur shows a wide range of values reflecting its reaction histories. Seawater is a largest reservoir of sulfur on the Earth surface, and sulfur exists as

dissolved sulfate. In the lithosphere, sulfur is dominantly present as sulfur-bearing minerals such as sulfides and anhydrite in the rocks. Previously reported $\delta^{34}S$ values are summarized in Table 1.3 and Figure 1.2 and 1.3. The $\delta^{34}S$ value of modern seawater is ~+21 ‰ (Peters et al., 2010; Ono et al., 2012). Precipitated marine sulfate and ancient evaporite have similar $\delta^{34}S$ values to the seawater. The variation of ancient evaporites is attributed to reflect the evolution of $\delta^{34}S$ value in source seawater through geologic times. Fresh MORB, derived from un-metasomatized depleted mantle, shows narrow range of $\delta^{34}S$ values with -0.91 ±0.50 ‰ (Labidi et al., 2012, 2014). The $\delta^{34}S$ value is not expected to be largely fractionated during mantle processes such as mantle melting, because of minimal isotope fractionation at high temperature (e.g., Ohmoto and Goldhaber, 1997; Marini et al., 2011) and the lack of significant evolution of MORB $\delta^{34}S$ values with the melting degree of source mantle (Labidi et al. 2014; Labidi and Cartigny, 2016). Therefore, these MORB $\delta^{34}S$ values reflect isotopic composition of depleted upper mantle, and estimated $\delta^{34}S$ value of depleted mantle is -1.40±0.50‰ (Labidi et al., 2014). It should be noted that $\delta^{34}S$ value of MORB in early measurement is reported as a very narrow range of values clustering around zero (Sakai et al., 1982, 1984). However, recent new high-precision measurements showed that these published MORB data are affected by incomplete sulfur recovery during analytical extraction (Labidi et al., 2012). Negative $\delta^{34}S$ values of the upper mantle probably reflect the recycle of ancient low-$\delta^{34}S$ altered oceanic crust (Cabral et al., 2013) or isotopic fractionation during core-mantle segregation (Labidi et al., 2013).

Dissolved seawater sulfate is incorporated into sea floor sediment and oceanic crust during the hydrothermal alteration processes, as sulfide and sulfate minerals with various $\delta^{34}S$ values. Although fractionation processes are complicated and depends on the physical environments such as temperature (e.g., Ohmoto and Goldhaber, 1997), hydrothermal sulfide and sulfate inherit $\delta^{34}S$ values of their source fluids in general. In a hydrothermal system, reduced H_2S-rich hydrothermal fluid and oxidized sulfate-rich seawater are mixing, and its

Table 1.3. Summary of reported $\delta^{34}S$ values for surface sulfur reservoirs

Reservoir	Material	$\delta^{34}S_{VCDT}$ (‰)	References*
Modern sea water	Seawater sulfate	20.4 to 21.5	[1], [2], [3], [4]
Subducting slab			
Sea floor sediments	Marine evaporite (Quaternary to late-Proterozoic)		[5] and references therein
	Precipitated marine sulfate (modern)	17.5 to 22.0	[2], [6]
	Hydrothermal sulfate	10.5 to 24.9	[6], [7], [8], [9], [10]
	Diagenetic sulfate	21.3 to 77.4	[6], [11], [12], [13]
	Hydrothermal sulfide	-5.3 to 8.9	[2], [7], [9], [14], [15], [16], [17]
	Sedimentary sulfide (abiogenic and biogenic)	-25.1 to 6.5	[2]
Alteared oceanic crust	Altered sea floor basalt, gabbro, websteritic cumulate (WR)	-25.8 to 16.1	[2], [4], [18], [19], [20], [21], [22], [23]
	Sulfide from vein in oceanic crust	-41.4 to 0.1	[23], [24]
Lithospheric mantle	Low-temperature lizardite serpentinite (WR)	-44.2 to 20.2	[4], [25] and references therein
	High-temperature lizardite serpentinite (WR)	-4.0 to 19.7	[25] and references therein, [26], [27]
Metamorphosed slab			
Metasediment	Micaschist (WR)	-12.0 to -8.0	[28]
	Metamorphic sulfide in calc-schist and spessartine-quartzite	-32.4 to -11.0	[29]
Metacrust	Eclogite and blueschist (WR)	-7.2 to 3.6	[27], [28], [30]
	Metamorphic sulfide in eclogite and blueschist	-4.3 to 13.5	[29]
Lithospheric mantle	Antigorite serpentinite (WR)	-3.5 to 14.3	[27], [28], [31]
	Chlorite harzburgite (WR)	-6.6 to 4.6	[31]
Volcanic gas	High-temperature volcanic gas	-8.6 to 12.0	[32] and references therein
Basaltic magma			
MORB	WR, GL	-1.9 to 1.9	[2], [3], [4], [33], [34], [35], [36]
	WR, GL (new protocol only)	-1.91 to 0.35	[3], [36]
OIB	WR, GL	-9.6 to 3.6	[37], [34], [38], [39]
	MI	-5.9 to 8.8	[39], [40]
	Magmatic sulfide	-17.3 to -7.5	[41]
Arc Basalt	WR, GL	-5.3 to 21.0	[42], [43], [44], [45], [46], [47], [48], [49], [50], [51]
	MI	-9.0 to 12.3	[51], [52]
Intra plate volcanoes	WR	-2.7 to 8.9	[53], [54]
Back arc basin	WR	-1.0 to 2.2	[7], [46]
Crustal rock			
Granite and metamorphic rock	Granitoid, gabbroid, granulite (WR)	-10.6 to 9.4	[55], [56], [57], [58]
	Scapolite in granulite	-0.5 to 4.0	[59]
Mafic cumulate	Pyroxenite (WR)	-0.1 to 4.5	[30]
Sedimentary rock	Sandstone, siltstone, claystone, shale and hornfels (WR)	-41.6 to 2.4	[55], [60]
Mantle			
Depleted upper mantle	Estimation from MORB	-1.40 ±0.50	[3], [36]
Subcontinental mantle	Peridotite and pyroxenite xenolith (WR)	-4.5 to 9.0	[60], [61], [62]
	Sulfide in peridotite and pyroxenite xenolith	-5.9 to 4.8	[62], [63]

WR = whole rock; GL = glass; MI = melt inclusion.

*See next page for references.

drastic change of temperature and oxidation states promotes the formation of hydrothermal sulfide and sulfate. In response to the reactions, hydrothermal sulfate and sulfide shows similar $\delta^{34}S$ values with seawater sulfate and MORB, respectively. And in more mixed cases, $\delta^{34}S$ values shift toward intermediate values between those (Fig. 1.2). In addition, previous sulfur isotope studies show the evidences and role of microbial seawater sulfate reduction within the submarine rocks and vent fluid at low-temperature condition (<110 ˚C, Jørgensen et al., 1992), resulting more fractionated $\delta^{34}S$ values in reactant (e.g., Rouxel et al., 2008). This microbial sulfate reduction modifies the seawater $\delta^{34}S$ composition and generates hydrogen sulfide, H_2S, with lighter $\delta^{34}S$ composition (Alt and Shanks, 1998). In case of the open-system reduction with respect to seawater sulfate, microbial sulfate reduction leads low-$\delta^{34}S$ values in reacted sulfide, for example up to -25.8 ‰ in biogenic sedimentary sulfide (Canfield, 2001; Peter et al., 2010). At the same time, microbial sulfate reduction leads to an enrichment of ^{34}S in the

---

*Reference for Table 1.3: [1] Rees et al. (1978); [2] Peters et al. (2010); [3] Labidi et al. (2012); [4] Ono et al. (2012); [5] Veizer et al. (1980); [6] Paytan et al. (2002); [7] Kusakabe et al. (1990); [8] Urabe and Kusakabe (1990); [9] Lüders et al. (2001); [10] de Ronde et al. (2003); [11] Greinert et al. (2002); [12] Klügel et al. (2011); [13] Eickmann et al. (2014); [14] Zierenberg et al. (1984); [15] Herzig et al. (1998); [16] Shanks (2001); [17] Ono et al. (2007); [18] Alt and Anderson (1991); [19] Alt (1994); [20] Alt et al. (1995); [21] Rouxel et al. (2008); [22] Alford et al. (2011); [23] Alt and Shanks (2011); [24] Alt and Burdett (1992); [25] Alt et al. (2013); [26] Alt and Shanks (2003); [27] Alt et al. (2012b); [28] Li et al. (2020a); [29] Walters et al. (2019); [30] Lee et al. (2018); [31] Alt et al. (2012a); [32] Kagoshima et al. (2015); [33] Kanehira et al. (1973); [34] Sakai et al. (1984); [35] Chaussidon et al. (1991); [36] Labidi et al. (2014); [37] Sakai (1982); [38] Labidi et al. (2015); [39] Beaudry et al. (2018); [40] Gurenko et al. (2001); [41] Cabral et al. (2013); [42] Hubberten et al. (1975); [43] Ueda and Sakai (1984); [44] Woodhead et al. (1987); [45] Imai et al. (1993); [46] Alt et al. (1993); [47] Bernard et al. (1996); [48] Mandeville et al. (1998); [49] Marini et al. (1998); [50] de Hoog et al. (2001); [51] Gurenko et al. (2018); [52] Bouvier et al. (2008); [53] Schneider (1970); [54] Harmon et al. (1987); [55] Sasaki and Ishihara (1979); [56] Hoefs et al. (1981); [57] Ishihara and Sasaki (1989); [58] Iyer et al. (1992); [59] Hammerli et al. (2017); [60] Cruse and Lyons (2004); [61] Ionov et al. (1992); [62] Wilson et al. (1996); [63] Giuliani et al. (2016); [64] Chaussidon and Lorand (1990).

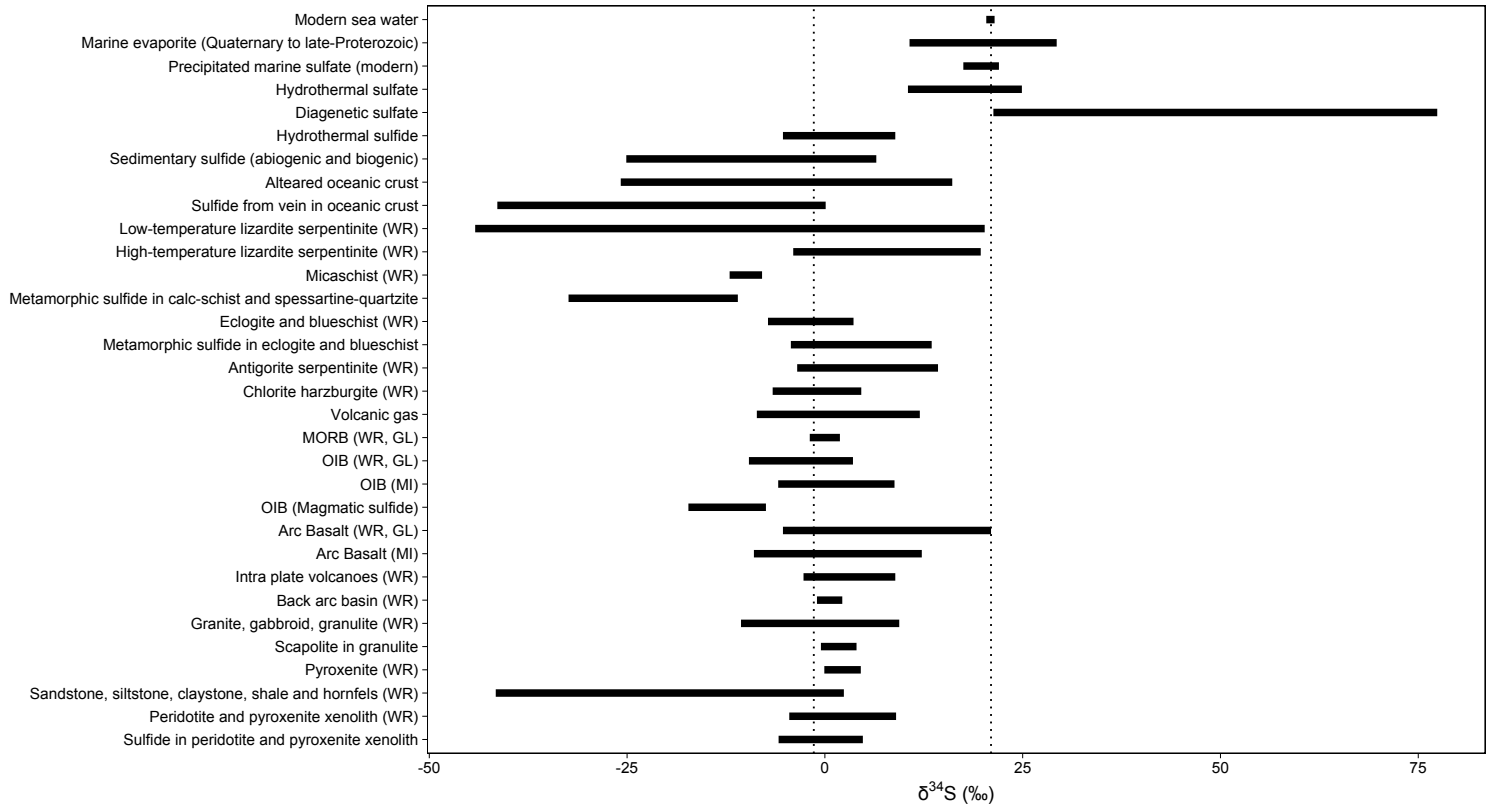

Figure 1.2. Sulfur isotope variations in natural rocks, sulfide and sulfate minerals. The $\delta^{34}S$ value is relative to VCDT. Data source is same with Table 1.2. Two dotted lines represent $\delta^{34}S$ values of -1.40 ‰ and +21 ‰ for depleted upper mantle and modern seawater, respectively (Ono et al., 2012; Labidi et al., 2014). WR = whole rock; GL = glass; MI = melt inclusion.

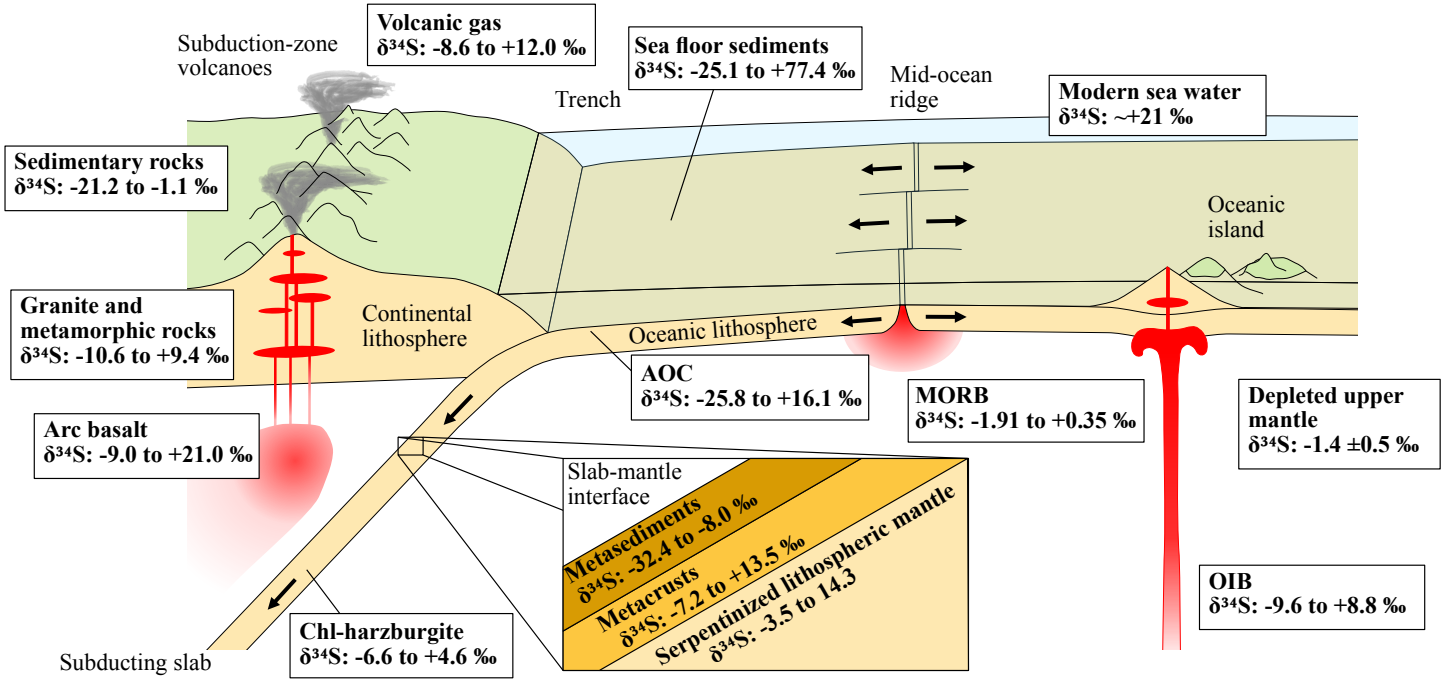

Figure 1.3. Schematic summary of $\delta^{34}S$ compositions in Earth's surface reservoirs. Only bulk rock and melt inclusion data is shown to represent bulk sulfur isotope values. Data source is same with Table 1.2. Value of depleted upper mantle is estimated value from unaltered MORB (Labidi et al., 2014). Only recent data is shown for MORB due to incomplete sulfur recovery during analytical extraction (Labidi et al., 2012).

residual sulfate in fluid, resulting high $\delta^{34}S$ value of precipitated sulfate (diagenetic sulfate) such as barite found in active chimneys (e.g., Eickmann et al., 2014). In case of the closed-system (Rayleigh fractionation) sulfate reduction, progressive microbial sulfur addition leads elevated $\delta^{34}S$ value of sulfide sulfur. Depending on the fractionation factor and openness of the system, $\delta^{34}S$ value of altered oceanic crust varies from -25.8 to +16.1 ‰.

Similar to altered oceanic crust, the studies of abyssal peridotite and ophiolite showed that the oceanic mantle has experienced serpentinization over a wide range of fluid-rock ratio, temperature and redox conditions with various sulfur isotope composition. Such mantle peridotites are often exposed and hydrated at the seafloor on spreading region (Deschamps et al., 2013). In addition, oceanic mantle is hydrated due to infiltration of seawater along fractures of the bending slab at the outer rise before subduction (e.g., Kerrick, 2002; Ranero et al., 2003). Oceanic serpentinites contain up to 10 – 15 wt. % H_2O and 1.1 wt.% S (Alt and Shanks, 1998, 2003; Delacour et al., 2008) and stable to at high temperature and pressure conditions (620 – 720 ˚C, 2 – 5 GPa; Ulmer and Trommsdorff, 1995). In the case of low-pressure serpentinite (lizardite-serpentinite), the range of reported $\delta^{34}S$ value are different between high-temperature serpentinites (higher than ~200 ˚C) and low-temperature serpentinites (lower than ~200 ˚C; Alt et al., 2007, 2013). As shown in Figure 1.2, the $\delta^{34}S$ values of high-temperature serpentinite varied from -4.0 to +19.7 ‰ while the values of low-temperature serpentinites extended to low-$\delta^{34}S$ values up to -44.2 ‰. This contrast reflects the effect of microbial sulfate reduction, leading low-$\delta^{34}S$ value by open-system reduction (Figure 1.4). For high-temperature serpentinites, the range of $\delta^{34}S$ values between mantle to seawater sulfate reflect the addition of sulfur stemmed from hydrothermal alteration (Fig. 1.4, Alt et al., 2007).

The bulk rock $\delta^{34}S$ values of arc basalts range from -5.3 to +21.0 ‰. As mentioned in previous section, this variation reflects the source mantle variability and complex magmatic processes such as magma mixing and degassing. Only two published articles are available for

$\delta^{34}S$ data of un-degassed primitive olivine-hosted melt inclusions (Bouvier et al., 2008; Gurenko et al., 2018). Volatile-rich melt inclusions show similar range of $\delta^{34}S$ value to those of reported bulk rock data, indicating a range of the slab-material addition into source mantle (Figure 1.2). The $\delta^{34}S$ composition of volcanic gases and granitic rocks are also similar to those of arc basalts, varying from -8.6 to +12.0 ‰ and from -10.6 to +9.4 ‰, respectively. The $\delta^{34}S$ value of basalts from oceanic island, intra plate volcanoes, shows moderate variation than arc basalts but significantly variable than MORB (Figure 1.2). The $\delta^{34}S$ value of sub-continental peridotites also show similar variations. with those of ocean island basalts, indicating the presence of metasomatic agent (e.g. Giuliani et al., 2016).

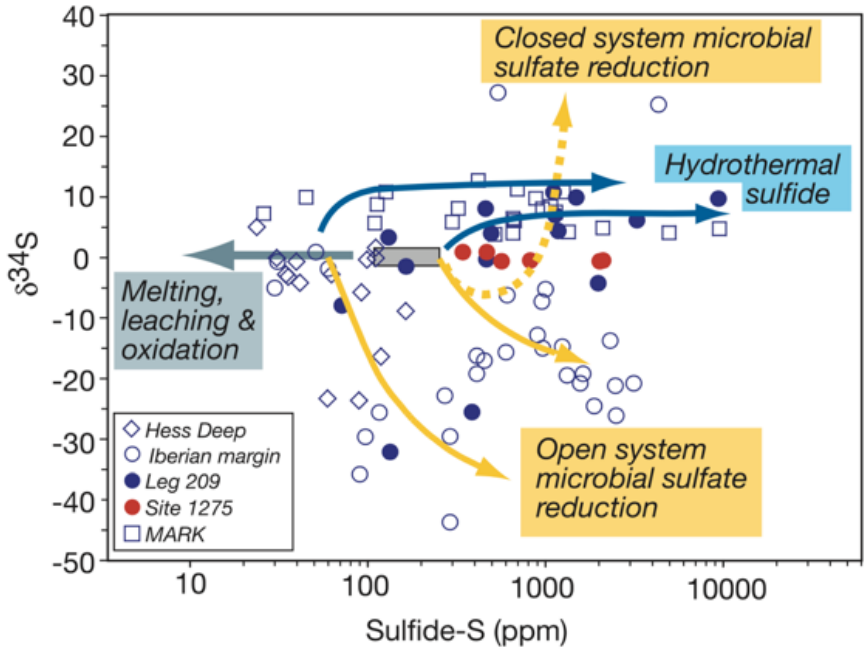

Figure 1.4. Schematic evolution of sulfur isotope composition and sulfide-sulfur concentration during serpentinization and hydrothermal alteration of oceanic peridotite. Data points are composition of recovered oceanic peridotite and gabbro (Alt and Shanks, 1998, 2003; Alt et al., 2007). Grey rectangular indicates unmodified mantle value. Figure is taken from Alt et al. (2007).

1.2.4. Remaining problems for sulfur transport in subduction zone

Controversial questions regarding the sulfur transport in subduction zones are: what is the composition of slab-derived fluid? is there slab-derived melt, what are the sulfur speciation and isotope composition in them? Characteristics of sulfur-bearing slab-fluids are estimated based on the geochemical data of natural metamorphic rocks, which is the remnant of the material released the fluid. These assessments outline three hypotheses: A) Slab-fluid is sulfate dominant and has positive $\delta^{34}S$ value (e.g., Alt et al., 2013), B) Slab-derived sulfur is released as reduced sulfur species and slab-fluid has negative $\delta^{34}S$ value (e.g., Jégo and Dasgupta, 2013, 2014; Li et al., 2020b), C) Slab fluid is oxidized and has various sulfur isotope compositions from negative to positive $\delta^{34}S$ values (e.g., Walters et al., 2019).

A subducting slab, which is composed of sediment, altered oceanic crust and lithospheric mantle, is progressively metamorphosed and dehydrated along subduction. Most of sulfate in marine sediments and altered oceanic crust is retained in the form of pore-water or labile sulfate (e.g., Alt and Burdett, 1992). It is expected that such pore-water is expelled from the slab during the early stage of slab dehydration and compaction (e.g., Peacock, 1990; Hacker, 2008). Since sulfate mineral is highly soluble in NaCl-bearing fluid (e.g., Newton and Manning, 2005), labile water-soluble sulfate would also be removed with dehydrated fluid. Thermodynamic simulation of Tomkins and Evans (2015) showed that the breakdown of anhydrite occurred at the low-temperature (~450 – 650 ˚C) across the transition from blueschist to eclogite facies whereas sulfide mineral such as pyrite is more stable at high temperature. This result indicated the subducting sulfur is mainly transported as sulfide minerals, but not as sulfate minerals, into sub-arc depth (Lee et al., 2018). Overall, it is expected that slab-fluid composition at sub-arc depth is may largely contributed by the breakdown of incorporated sulfide having various $\delta^{34}S$ values and partitioning of sulfur between slab and fluid (or melt).

Alternatively, noble gas and halogen compositions of pore-fluid in exhumed mantle wedge peridotite require the subduction of marine pore-fluid to at least 100 km depth (Sumino et al., 2010). In this case, it is expected that dissolved sulfur in seawater probably be subducting as sulfate, not as sulfide minerals. It should be note that the presence of biogenic sulfide in oceanic crust and peridotite (e.g., Ono et al., 2012) indicates some pore-water sulfates are retained in the slab as sulfide mineral transformed by microbial sulfate reduction, and may transported to sub-arc depth.

Alt et al. (2012, 2013) argued that slab-derived fluid has a positive $\delta^{34}S$ value and subducted sulfur is discharged as sulfate phase (hypothesis A), based on the mass-balance of sulfur along slab-dehydration processes from the high-pressure serpentinites and chlorite-harzburgite representing early stage of subduction-zone metamorphism. Their argument is that the dehydration of subducted serpentinite has a main contribution to the fluid composition and mantle oxidization through the release of sulfate-bearing fluid at sub-arc depth because the dehydration of sediment and altered oceanic crust occurred at shallower depth and low-temperature condition of less than ~500 ˚C. In summary, sulfur loss during dehydration of antigorite-serpentinite to chlorite-harzburgite is estimated at 260 ppm S as sulfate sulfur, having $\delta^{34}S$ = ~+14.5‰.

In contrast to the hypothesis A, Li et al. (2020b) concluded subducted sulfur is predominantly released at 70 – 100 km depth as sulfide-phases with negative $\delta^{34}S$ value of -2.5±3‰ (hypothesis B), based on the textural analysis of metamorphic rocks and mass-balance of sulfur using Deep Earth Water model, which predicts equilibrium constants involving many aqueous species using the equation of state method at high pressure condition (Sverjensky et al., 2014; Huang and Sverjensky, 2019). Moreover, they argued that sulfate sulfur is not the slab-derived oxidizing agent of sub-arc mantle because sulfate species are negligible in estimated fluid. Instead, they suggest that the high fO_2 of sub-arc mantle may result from

addition of slab H_2O and CO_2, and negative-to-positive shift in the $\delta^{34}S$ composition of arc magma must happen as part of the partial melting processes. Their conclusion depends on the $\delta^{34}S$ value of altered oceanic crust-derived fluid because of its major fluid flux and relatively high initial sulfur concentration (0.74 wt. % S in their model). High-pressure experiment of fluid-saturated altered oceanic crust melting shows, at any fO_2 condition, main sulfur species in fluid is sulfide with high-S concentration up to 15 wt.% (Jégo and Dasgupta, 2013, 2014), in agreement with hypothesis B.

Similar to Li et al. (2020b)'s approach, Walters et al. (2019) concluded that the sulfur isotope composition of the slab-derived fluid is a range of $\delta^{34}S$ values from negative to positive (-11‰ to +8‰) from the $\delta^{34}S$ composition of sulfides in metamorphic rocks (hypothesis C). The assumption is that metamorphic sulfides, which represent closed-system crystallization associated with prograde metamorphism and peak in texture, reflect the isotopic composition of protolith whereas metasomatic sulfides records slab-fluid composition. To account for the variation of fluid $\delta^{34}S$ values, they suggest a reactive-transport model that phase separation of fractionation during fluids migration along the slab-mantle interface cause isotopic heterogeneity.

As I explained above, both negative and positive values, and both sulfate-dominant and sulfide-dominant fluids have been estimated from the analysis of metamorphic rocks and these hypotheses are mutually exclusive. The one reason of this disparity is the complexity of the fluid generation and transport processes and the diversity of the source rocks. In addition to the case of slab dehydration, silicate-melt is also produced at many subduction zones by the partial melting of slab (e.g., Ecuador; Narvaez et al., 2018; Cascade, Walowski et al., 2016). Since silicate-melt contains sulfate-sulfur depends on the fO_2 condition even if slab-fluid is sulfide-dominant (Jugo et al., 2010; Jégo and Dasgupta, 2014), sulfate-sulfur in silicate-melt is effective oxidizing agent of sub-arc mantle (for example, one mole of sulfate reduction cause

6 moles of Fe^{2+} oxidation, Tomkins and Evans, 2015) although the flux of sulfur from silicate-melt is probably less than those from aqueous-fluid (Jégo and Dasgupta, 2013). These currently proposed models regard aqueous-fluid as main carrier of sulfur from the slab, however, fluid-melt interaction and the presence of supercritical fluid should also be considered. Therefore, those hypotheses must be evaluated with a novel approach to determine isotopic composition of slab-derived component and magma source material from the magmatic products. Concretely, search of volatile-rich primitive magma (e.g., olivine-hosted melt inclusion) qualifies as such the approach because the primitive $\delta^{34}S$ composition of magma is not modified by sulfur degassing and magma mixing.

1.3. Scientific problems and approach

I focused on two processes in sulfur cycle in subduction zone in this dissertation: 1) slab-material transport into the source mantle region, 2) degassing of primitive magma during its ascent. As summarized in previous section, a remaining problem of process 1 is the isotopic composition and speciation of sulfur transported by slab-fluid. In case of process 2, globally observed "excess degassing" phenomena is a critical problem. The key information tied to these problems is sulfur concentration and isotopic composition in primitive magma.

Measurement of dissolved volatile element concentrations in the primitive magma involves at least two problems. First, magmatic volatiles are degassed after the eruption because of their strong pressure-dependence of solubility in silicate melt (e.g., Dixon et al. 1995). Second, possible crustal magma process, such as fractional crystallization, magma mixing, and crustal assimilation, obscure the primitive magma composition (e.g. Sakuyama, 1979; Hildreth and Moorbath, 1988).

Here, I utilize the melt inclusion hosted in phenocryst minerals to avoid the preceding modifications. Melt inclusion is a tiny droplet of magma trapped inside of phenocrysts at the

time of crystal growth (e.g., Anderson 1973; Wallace 2005). Because the crystalline host acts as vessel to prevent the degassing of melt inclusion and isolate from interaction with surrounding magma, it is possible to directly measure the dissolved volatile concentrations using microscopic analyses such as secondary ion mass spectrometry (SIMS). I chose to study the olivine-hosted melt inclusion to assess the primitive magma composition and volatile concentrations, as olivine crystallizes at the early stage of magma differentiation.

The Kyushu Island, Japan, is a suitable study area to investigate the volcanic processes discussed above. The modern volcanic activities of Kyushu Island are related to the subduction of the Philippine Sea plate composed of two segments with different age divided by remnant island arc (Nakada and Kamata, 1991; Miyoshi et al., 2008; Shibata et al., 2014). Detailed geological and petrological studies provide a comprehensive framework for spatial- and temporal-evolution of geochemical characteristics and volcanism in this region (Kamata and Kodama, 1999; Mahony et al., 2011). On top of it, geophysical and geochemical observations of these highly active volcanoes enable an assessment of the dynamics of the volatile transport in magma, in combination with petrological observation. For example, degassing activity of Aso volcano, one of active volcanoes located in the central Kyushu, is constantly monitored since the 1970s (Mori et al., 2013). Tephrostratigraphic studies (e.g., Okuno, 2002; Miyabuchi, 2009) allow me to collect the best samples, tephra, for melt inclusion approach (e.g., ejected source identification, stratigraphic relationship). I report a comprehensive description of the volatile element variations dissolved in primitive basaltic magmas from the Kyushu Island. Integration of geochemical observations, geophysical observations and thermodynamic principles using comprehensive datasets provides an insight to understand a role of volatile transport in complex subduction zone magmatism, such as magma generation, ascent, and degassing processes.

1.4. Dissertation organization

This dissertation is composed of two stand-alone chapters (Chapter 3 and Chapter 4) presented as individual manuscripts for publication. Both chapters are linked with volatile recycling and transport from mantle to surface in a context of subduction-zone magmatism. Chapter 3 focuses on shallow crustal-level magmatic processes (e.g. magma mixing and degassing), while Chapter 4 investigates deep magmatic processes, such as mantle melting and subducted slab recycling.

In Chapter 2, I briefly describe the preparation and analytical methods of melt inclusion samples.

In Chapter 3, "Persistent gas emission originating from a deep basaltic magma reservoir of an active volcano: the case of Aso volcano, Japan", I illustrate the method to constrain the volatile concentration and storage depth of the pre-eruptive and primitive magma by combined observations of gas measurement and petrological study of Aso volcano, central Kyushu, Japan as a test case of constantly-monitored, persistently-degassing volcano. The results show that a hidden deep magma reservoir is the main degassing body corresponding to the gas observed before and during 2014 – 2015 eruption. This approach identifies the role of a volatile-rich deep magma reservoir on the persistent degassing in a mature active volcano with complex magmatic processes, which provides the critical insight to understand the "excess degassing" phenomena observed world-wide.

In Chapter 4, "Sulfur isotopes systematics in arc: seeing through the degassing via a melt inclusion study of Kyushu Island volcanoes, Japan", I extend the dataset of olivine-hosted melt inclusion to entire Kyushu. This dataset is used to infer the volatile concentrations in primary, mantle-derived magmas in this region related to the Philippine Sea plate subduction. I also provide sulfur isotope data of those primitive melt inclusions, leading to an interpretation for sulfur transport and the nature of slab-derived fluid (aqueous fluid or silicate melt).

In Chapter 5, findings and implications provided in this dissertation are summarized.

Chapter 2

Sample and methods

2.1. Melt inclusion

2.1.1. Use of melt inclusion

Melt inclusion is an un-degassed tiny droplet of magma trapped inside of a crystal formed before eruption (e.g., Anderson, 1973). Since entrapped melts are physically isolated from interactions with the external environment, melt inclusions potentially retain the snapshots of magmatic evolutions. Melt inclusions are powerful tool and are used to investigate a wide range of topics such as the pre-eruptive volatile budget (e.g., Wallace and Gerlach, 1994), the evolution of magma plumbing system (e.g., Druitt et al., 2016), magma source and mantle melting processes (e.g., Portnyagin et al., 2007; Rose-Koga et al., 2012), the oxidation state of magmas (e.g., Kelley and Cottrell, 2009) and timescale of magmatic processes (e.g., Albert et al., 2019). However, modification processes of melt inclusion composition have been recognized and reported in many studies. For example, sufficient temperature decreases of magma induce the crystallization of host mineral or other mineral phases, commonly called as "daughter minerals", inside of melt inclusions (e.g., Danyushevsky et al., 2002a). On top of it, typical high magmatic temperatures allow elements (e.g., H^+, Portnyagin et al., 2008) to diffused out through host minerals, leading the equilibration of trapped melt with host minerals and surrounding magmas. Modifications of olivine-hosted melt inclusion are well studied and correction methods are established. There is no universally accepted correction procedure for melt inclusions hosted by minerals other than olivine, although attempts have been reported (Yasuda et al., 2001; Neave et al., 2017; Hartley et al., 2018). In the following section, I discuss

the post-entrapment processes and correction methods only for olivine-hosted melt inclusion that mainly used material in this paper.

2.1.2. Post-entrapment processes

2.1.2.1. Post-entrapment crystallization and diffusive Fe-Mg exchange

Crystallization of host-olivine or other daughter minerals could occur along the crystal-melt interface or inside of inclusion as the cooling rate of magma is effectively slow. During the crystallization process, composition of newly formed olivine on the inclusion wall progressively evolves toward fayalite (Fe-rich olivine) in consequence to the depletion of olivine component in the residual melt. This variation can be often observed as compositional gradient within inclusion wall (e.g., Danyushevsky et al., 2002b). The simple overgrowth of the host olivine can be corrected by the incremental addition of equilibrium olivine to the trapped melt, if olivine is the only crystallizing phase. The composition of equilibrium olivine is thermodynamically expressed using the Fe-Mg exchange coefficient of Fe and Mg between olivine and melt:

$$K_D{}^{\mathrm{Mg-Fe}}_{\mathrm{Ol-Liq}} = \frac{X^{\mathrm{Mg}}_{\mathrm{Liq}}/X^{\mathrm{Mg}}_{\mathrm{Ol}}}{X^{\mathrm{Fe^{2+}}}_{\mathrm{Liq}}/X^{\mathrm{Fe^{2+}}}_{\mathrm{Ol}}} \approx 0.3$$

where $X^{\mathrm{Mg}}_{\mathrm{Liq}}$ and $X^{\mathrm{Fe^{2+}}}_{\mathrm{Liq}}$ are the mole fraction of Mg and Fe^{2+} in the residual melt and $X^{\mathrm{Mg}}_{\mathrm{Ol}}$ and $X^{\mathrm{Fe^{2+}}}_{\mathrm{Ol}}$ are the mole fraction of Mg and Fe^{2+} in the host olivine (Roeder and Emslie, 1970; Toplis, 2005). The Fe^{2+}/Fe^{Total} ratio in the melt inclusion can be determined by the X-ray absorption near edge structure spectroscopy (XANES) (e.g., Moussallam et al., 2014) or by the thermodynamic equation at given oxygen fugacity (fO_2) and temperature condition (e.g., Kilinc et al., 1983). The fO_2 condition can be determined by the ratio of sulfur speciation in the melt, where based on the S$K\alpha$ peak shifts measured by EPMA (e.g., Wallace and Carmichael, 1994).

In addition to the overgrowth of the host olivine, if the host olivine is kept at high temperature, the re-equilibration of melt inclusion with host olivine would occur. During re-equilibration process, compositional gradient within inclusion wall is homogenized due to the internal diffusion of Fe and Mg. As a consequent, melt inclusion re-equilibrates with the host, leading Fe-depletion in the melt. This process is called "Fe-loss". In this case, the correction by olivine addition leads to a minimum degree of post-entrapment crystallization, and results in less Fe and Mg concentrations than initial values (Danyushevsky et al., 2000). The melt inclusions experienced Fe-loss have high K_D value and tend to show the disparity between Fe concentrations in melt inclusion and in bulk rock with similar SiO_2 abundances. To correct the Fe-loss, commonly used method is to adopt a well-known initial FeO value, if possible, or a estimated FeO value from the bulk rock trend.

Corrections of these post-entrapment processes require assumptions employed to the calculation, for example the initial FeO concentration. The result is a model composition. However, the ratios of incompatible element in melt inclusion are unaffected by post-entrapment crystallization and Fe-loss. Therefore, the use of trace-element ratios eliminates the uncertainty related with these corrections. Similarly, one effective way to compare the major element compositions is to use the pseudo-ternary projection schemes (O'Hara, 1968; Walker et al., 1979). Projection of melt compositions from the olivine apex to a ternary plane eliminates the effect of the olivine controlled post-entrapment crystallization and diffusive Fe-Mg exchange involving olivine component (e.g., Le Voyer et al., 2010).

2.1.2.2. Diffusive hydrogen loss

The H_2O concentration of melt inclusion can be modified by the diffusion of H^+ through host olivine. The exchange of protons between a melt inclusion and the host olivine occurs via the diffusion of metal vacancy on octahedral lattice sites of host olivine (Kohlstedt and

Mackwell, 1998; Gaetani et al., 2012). This H^+ transport is accompanied by O exchange via the reduction or oxidation of Fe on octahedral sites, thus, leading the equilibration of fO_2 of melt inclusion with that of external magma (Gaetani et al., 2012). The experimental studies showed this H^+ transport is a rapid process and a half of initial water concentration in melt inclusion is lost within a few hours of heating at 1200 ˚C (Portnyagin et al., 2008; Chen et al., 2011). Such rapid H^+ diffusion achieves a complete re-equilibration of an originally high H_2O concentration within a few days (e.g., Portnyagin et al., 2008), which is significantly fast compared with the timescale of typical basaltic magma transport from the magma source (e.g., Albert et al., 2016). Recent compilation of global H_2O data of melt inclusion shows nearly all melt inclusions have 2 – 6 wt. % H_2O with a global average of 3.9 ± 0.4 wt.%, corresponding to the solubility at crustal depths (Plank et al., 2013). As a conclusion, the observed H_2O concentration of melt inclusions represents a condition of the last-equilibrium depth.

Diffusive H-loss can occur during post-eruptive cooling or during the final stage of ascent. Clear petrological evidence of diffusive H-loss is identified among different sized fragments (ash, lapilli and bomb) of an eruption event, by Lloyd et al. (2013). Their study showed melt inclusions of bombs experienced large H_2O loss, up to 30% lower than those of ash and lapilli. Therefore, it is highly recommended to use at least lapilli-sized sample to minimize the effect of post-eruptive H-loss.

Unfortunately, a current consensus is that it would not be possible to directly measure the primitive H_2O content from geological materials. The one method to estimate the minimum H_2O content in the primitive magma is to adopt the maximum H_2O and trace element ratio such as H_2O /K_2O. As these elements are incompatible to silicate minerals in basalt, the ratio does not vary with crystallization. Therefore, the highest ratio should indicate the minimum H_2O loss, if a suite of magma shares the same parental magma. In the case of mixed magmas, H_2O/K_2O of the mafic endmember likely defines the least degassed ratio. However, because of

high diffusivity of H_2O, this estimated H_2O concentrations should be treated as minimum H_2O content in the primitive magma, and the primary magma could have an even higher H_2O content.

2.1.2.3. Vapor-bubble formation

Vapor bubble is commonly observed in melt inclusion. It is typically attributed as exsolved volatiles from the melt resulting from the cooling of a magma. In general, more than 40 – 90% of the initial CO_2 that was dissolved in the melt at the time of entrapment is lost to the shrinkage bubbles due to low-solubility of CO_2 (e.g. Wallace et al., 2015). Thus, measured CO_2 concentrations in the melt are fractionated values and do not represent the bulk CO_2 concentration of the melt inclusion. In this case, CO_2 in vapor bubble needs to be added back into that of melt for the reconstruction of the pre-exsolution melt composition.

In the mass balance and numerical model, the total CO_2 concentration in a melt inclusion was calculated as (dissolved + exsolved),

$$CO_2^{Total} = CO_2^{Melt} + \phi \frac{\rho_v}{\rho_m} \times 10^6$$

where CO_2^{Melt} is the dissolved CO_2 concentration in the melt, ϕ is volume fraction of the bubble in the melt inclusion, ρ_v is the volumetric CO_2 vapor density at room temperature, and ρ_m is the melt density (Tucker et al., 2019). The ρ_m could be determined by thermodynamic method (e.g., Ochs and Lange, 1999) using hydrous melt composition measured by EPMA and SIMS. The volume of melt inclusion and inside bubble is possible to obtain by numerical calculation from the optically measured diameters (e.g., Tucker et al., 2019) or by a micro X-ray computed tomography (MXCT) technique (e.g., Hanyu et al., 2020). The ρ_v value is possible to obtain by thermodynamic calculation, such as the ideal gas law method (e.g., Shaw et al., 2008) and the equation of state method (Duan and Zhang, 2006), or by measurement using Raman spectrometry (e.g., Aster et al., 2016).

The reconstructed CO_2 budget have uncertainties inherited from three issues 1) an uncertainty of the melt-vapor volume measurement, 2) a possibility of the non-equilibrium bubble expansion during quench, and 3) a possible entrapment of pre-existed vapor bubble. The uncertainty of volume measurements is large when the melt inclusion volume is determined by two-dimensional section (problem 1). Commonly used assumption is that the third axis of the ellipsoid c equals (i) the smaller of the two visible axes (c = b), (ii) the arithmetic mean of the two visible axes (c = (a + b)/2), and (iii) the geometric mean of the two visible axes (c = $\sqrt{ab}$). A recent numerical simulation reported that the assumption taking an arithmetic mean most closely approximate the true volume, however, yielding a large relative error (1σ) of 37% to 48% (Tucker et al., 2019). This uncertainty of volume estimation is possible to minimize to use MXCT with the high resolution of volumetric analysis (Hanyu et al., 2020).

The non-equilibrium expansion of bubble (problem 2) is stemmed from the competition between the closure temperature of C diffusion and the glass transition temperature of melt. This problem is not a matter if the ρ_v value is directly determined by Raman, but it becomes a problem when the value is estimated by thermodynamic calculation. The thermodynamic method calculates ρ_v under the assumption that bubble and melt were in equilibrium until the bubble ceases to expand. Since the C diffusion is temperature dependent, if the diffusive closure temperature was effectively higher than the glass transition temperature, bubble would expand without C exsolution, resulting in an overestimation of ρ_v and, therefore, of the total CO_2 concentration (e.g. Pichavant et al., 2013; Bali et al., 2018). If this non-equilibrium expansion has occurred, the estimated total CO_2 concentration represents a maximum.

In case of problem 3, if pre-existed bubble were entrapped at melt inclusion, the calculated total CO_2 concentration must be overestimated. This is because the calculation of total CO_2 depended strongly on a fraction of the vapor bubble volume. Therefore, if the pre-

entrapment bubble was present, the observed bubble volume in a quench melt inclusion should be larger than the expected volume of the bubble formed by the cooling. The volume of bubble formed by the cooling, called "shrinkage bubble", can be estimated from the thermal contraction of host-mineral and melt based on the extent of post-entrapment cooling (e.g., Moore et al., 2015). This calculation provides an upper limit of the bubble size that could have formed by post-entrapment cooling and test whether a melt inclusion contained a pre-entrapped bubble or not.

Finally, I should have note that, even after the correction of vapor bubble formation, total CO_2 concentration represent minimum estimation of primitive magma because of possible pre-entrapment CO_2 degassing due to its low-solubility in basaltic melt.

2.2. Sampling strategy

I specifically focused on lapilli-sized tephra samples with olivine phenocryst for the study, to avoid the diffusive volatile-loss and daughter mineral crystallization within melt inclusions (Danyushevsky *et al.* 2002; Lloyd *et al.* 2013). For Chapter 3, I selected five representative tephra samples correspond to recent (3.7 ka to present) eruptions of four cones in Aso volcano: Kishimadake scoria (KSS), Ojodake scoria (OJSU and OJSL), Kamikomezuka scoria (KKO), and Nakadake scoria (NKD14). KSS, OJSU, and OJSL were collected from a tephra deposit site (A9418 section reported by Watanabe 1991; Miyabuchi and Watanabe, 1997). KKO was collected from Kamikomezuka cone, because the tephra deposit away from the edifice has not been identified. NKD14 was collected from the crater rim of Nakadake cone's first crater, immediately after the eruption of Nov 27, 2014. The sample set was used to obtain the information about crustal magma evolution and the volatile characteristics of magmas. For Chapter 4, nine olivine-bearing rocks were selected from 39 samples that I have collected, covering major active volcanoes of the Kyushu Island, Japan. As an exception, I

collected one lava block from a pyroclastic flow deposit for Yufu volcano since no olivine-bearing tephra were found. All melt inclusions of Yufu and Oninomi volcanoes were completely crystallized due to the slow cooling rates of host-rocks (except one melt inclusion of Oninomi). Therefore, I conducted heating experiment to homogenize these crystallized melt inclusions using microscope heating stage. This sample set was used to obtain the information about magma generation processes beneath Kyushu Island.

2.3. Sample preparation

2.3.1. Selection and polishing of melt inclusion

Selected rocks were crushed and sieved from 0.25 to 1 mm. The picked crystals were mounted in resin. And then, the dimensions of inclusion and vapor bubble were measured under microscope according to the recommended practice of Rose-Koga et al. (2021). Fully enclosed inclusions were exposed using silicon carbide mat for coarse polishing, and corundum mats (3 μm and 1 μm mats) were used to complete the polishing. Diamond-based paste was not used to prevent possible carbon contamination. As an exception, melt inclusions used for Chapter 3 were polished by diamond-based paste for the final polishing. Therefore, CO_2 data of those melt inclusions were not used in discussions. Selected polished olivine crystals were subsequently mounted in indium for SIMS analyses, and a final polish with a ¼ μm alumina paste was performed to remove scratches on the exposed surface.

2.3.2. Re-homogenization of crystallized melt inclusion using heating stage

Crystallized olivine-hosted melt inclusions (Yufu and Oninomi) were homogenized using Vernadsky-type microscope heating stage (Fig 2.1) following the procedure described by Le Voyer et al. (2010). Olivine surfaces were roughly polished (without exposing the melt inclusion) to observe the inside of melt inclusions before homogenization. During the

experiments, the oxygen fugacity was kept at a reduced condition less than 10^{-19} atm with a purified He gas of which oxygen is removed by Zr at 650 ˚C. This setting avoids sample oxidization and to ensure an efficient quench. The temperature inside the furnace was measured using a Pt-Pt_{90}-Rh_{10} thermocouple welded to the sample holder and calibrated using Au as temperature standard (melting temperature at 1064 ˚C). Temperature increase was set at ~90 ˚C/min until ~920 ˚C, then slow downed to ~30 ˚C/min until the last crystal disappear. Total duration of one heating experiment was less than 30 minutes. Given a 50 μm radius melt inclusion and 250 – 500 μm radius olivine, the expected water loss is negligible at typical final temperature from 1200 to 1400 ˚C. Even with the smaller temperature ramp rate of 5 ˚C/min (Chen et al., 2011), the water loss is negligible, because heating duration was much less than 10 mins above 1200 ˚C in this study. Homogenized inclusions were carefully exposed after optical observations (see section 2.3.1.1).

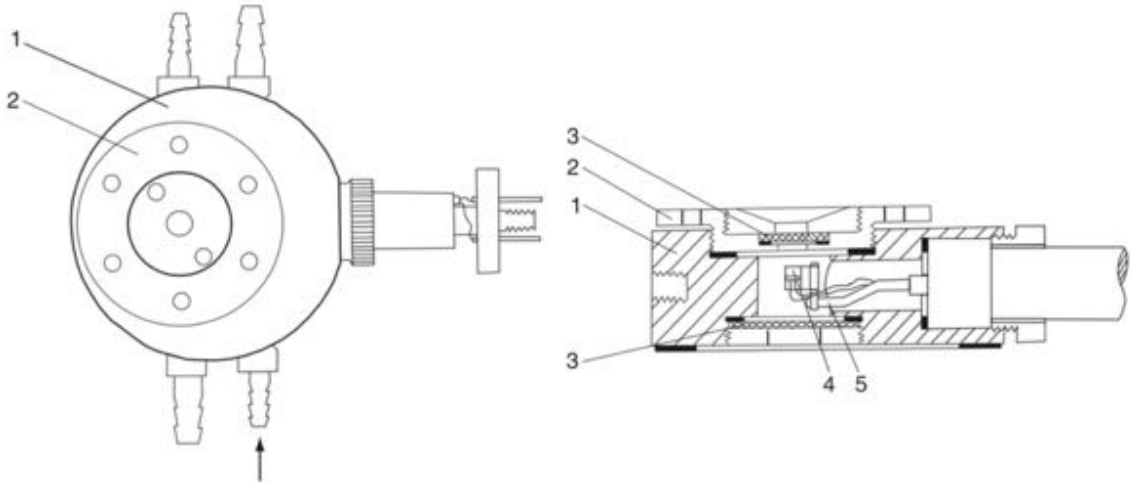

Figure 2.1. Vernadsky-type microscope heating stage designed by Sobolev et al. (1980). (1) Gas-tight sealed body cooled by water; (2) screwed lid; (3) optical quartz glass windows; (4) $Pt_{90}Rh_{10}$ heating element and ring-shaped metallic sample holder with welded Pt–$Pt_{90}Rh_{10}$ thermocouple; (5) electrode. An olivine crystal is placed on a few hundred μm thick sapphire plate in sample holder. Figure is taken from Schiano (2003).

2.4. Analytical methods

2.4.1. Secondary ion mass spectrometry (SIMS)

Volatile element concentrations (H_2O, CO_2, S, Cl, and F) in the inclusions were measured by SIMS (Cameca IMS-1280HR of Kochi Institute of Core Sample Research, JAMSTEC, Japan) following the procedure described by Shimizu *et al.* (2017). In brief, I used a 20 keV Cs+ primary ion beam of 300 – 500 pA defocused to be 10 – 15 μm in diameter. Secondary ions were accelerated at 10 kV. A -10 keV electron beam with a diameter of ~100 μm was applied for electrostatic charge compensation over the area of the Cs beam spot. The field aperture was set to the size corresponding to 5 x 5 μm on the sample surface. Mass resolving power was set at ~6000 to separate mass interferences (for example, to separate $^{34}S^{1}H$ interference on ^{35}Cl requires 5120 MRP; Burdo and Morrison 1971). Negative secondary ions of ^{12}C, ^{16}OH, ^{19}F, ^{30}Si, ^{31}P, ^{32}S, and ^{35}Cl and the mass position of 11.9 amu were measured by an axial electron multiplier using the peak switching method. An analysis consisted of 10 cycles, and the total measurement time for each analysis was ~6 min. Typical relative standard deviations (1σ) obtained from repeated analysis of a secondary basaltic glass standard from the East Pacific Rise, EPR-G3 (Shimizu et al., 2017), were 1.4, 3.2, 0.9, 2.5 and 1.5% for H_2O, CO_2, S, Cl and F, respectively.

Sulfur isotopes in the inclusions were also measured by SIMS at 1) Kochi Institute of Core Sample Research, JAMSTEC, Japan (Cameca IMS-1280HR) and 2) Centre de Recherches Pétrographiques et Géochimiques (CRPG)-CNRS-Nancy, France (Cameca IMS-1270). At Kochi, analyses were conducted following the procedure described by Shimizu et al. (2019c). To summarize, I used a 20 keV Cs+ ion beam of ~0.5 nA defocused to be ~10 μm in diameter. A 10 keV electron beam of ~100 μm diameter was flooded on the sample surface for electrostatic charge compensation. Secondary ions were accelerated to 10 kV. The field aperture was set at the size corresponding to 15 × 15 μm^2 on the sample surface. Negative

secondary ions of ^{32}S and ^{34}S were measured in multi-detection mode with an FC and axial EM, respectively. Mass resolving power was set at ~5000 to separate mass interferences of $^{31}P^{1}H$ on ^{32}S and of $^{33}S^{1}H$ on ^{34}S. Each measurement consisted of 20 s pre-sputtering, 120 s auto-centering of ^{32}S to the field and contrast apertures, and 5s × 50 cycles for measurements. The total measurement time for each analysis was ~7 minutes.

At CRPG, the setting was similar except I used a stronger primary beam of 3 nA defocused to be ~15 μm in diameter. Mass resolving power was set to 4500. Negative secondary ions of ^{32}S and ^{34}S were measured in multi-detection mode with an FC and axial EM, respectively. Each measurement consisted of 60 s pre-sputtering and 5 s × 40 cycles for measurements, giving a total analysis time of ~5 minutes for each spot. Before each measurement, I adjusted the center for ^{32}S. In both cases, the standard basaltic glass, EPR-G3, was systematically measured during the analytical session to define the instrumental mass fractionation factor (IMF) for ^{34}S: $IMF = (^{34}S/^{32}S)_{measured} / (^{34}S/^{32}S)_{reference}$. Sulfur isotopes in the samples are expressed in $\delta^{34}S$ relative to the Vienna Canyon Diablo Troilite (VCDT, $^{34}S/^{32}S = 1/22.6436$; Ding et al., 2001; $\delta^{34}S = [(^{34}S/^{32}S)_{unknown} / IMF / (^{34}S/^{32}S)_{VCDT} - 1] \times 1000$, in per mil). The analytical error (2σ) obtained from repeated measurement of EPR-G3 standard during the analytical session was less than 1.2‰ for both SIMS laboratories.

2.4.2. Electron probe micro-analyzer (EPMA)

Major element compositions of melt inclusion, groundmass glass and host-mineral phenocryst were determined using 1) a JXA8800R electron probe micro-analyzer at the Earthquake Research Institute (ERI), University of Tokyo (Chapter 3), and 2) a CAMECA SX100 electron microprobe at the Laboratoire Magmas et Volcans (LMV), Clermont-Ferrand, France (Chapter 4). At ERI, the analytical settings were 15kV acceleration voltage, 12 nA beam current, with counting times for Na, Al, K, Fe, Mg, Si, Ti, V, Mn, and Ca at 20 s, and 30 s for

Ni, Cr in mafic minerals and for S and Cl in hydrous melt. Beam diameter was set at 10 µm for glass and plagioclase, and focused (1 µm) for other minerals. During melt inclusion and groundmass glass analysis, Na and K were always measured in the first analytical cycle to minimize alkali loss (Devine *et al.* 1995). All analyses applied oxide ZAF correction. Analytical uncertainties are <0.7% relative for Si, <1% relative for Al, Fe, Mg, and Ca, <5% relative for Ti and Na, <10% relative for K, and <20% relative for Mn, V, Ni, Cr, S, and Cl. At LMV, the analytical settings for silicate glass were 15 kV acceleration voltage, 4 nA beam current, with counting times at 30 s for Ti, at 20 s for Si, Al, Fe, Mg, and K, and at 10 s for Mn, Ca, and P. For olivine, I used 15 nA beam current with counting time at 30 s for Ca, at 20 s for Si and Al, at 15 s for Ti and Cr, and at 10 s for Fe, Mn, Mg, and Ni. Beam diameter was set at 5 or 10 µm depending on the size of the inclusion, and focused for olivine measurements. Relative analytical uncertainties (1σ) obtained from repeated measurements of the basaltic glass standard (VG-2, Juan de Fuca ridge basalt, Jarosewich et al., 1980; Dixon et al., 1991) were less than 0.6% for SiO_2, 1% for Al_2O_3, FeO and CaO, 3.5% for TiO_2 and Na_2O, 10% for MnO, 1.5% for MgO, 4.5% for K_2O, 17% for P_2O_5. In addition, S, Cl and F concentration of 12 melt inclusions were also determined, using a 40 nA beam current with counting times of 50 s for S and Cl, and 200 s for F. For each analysis, an average of 5 measurements were taken. The standard deviations (1σ) for S, Cl, and F were less than 143 ppm, 95 ppm, and 397 ppm, respectively.

2.4.3. Laser ablation inductively coupled plasma mass spectrometer (LA-ICP-MS)

Trace element concentrations in melt inclusions were determined using a laser ablation system (193 nm Excimer Resonetics M-50E laser ablation system) coupled with an inductively coupled plasma mass spectrometer, Agilent 7500 cs (LA-ICP-MS) at LMV following the classical procedure described by Rose-Koga et al. (2012, 2017). Analyses were conducted with

a laser pulse frequency of 1–3 Hz, a spot diameter between 15 and 33 μm depending on the melt inclusion size, and a fluence of 2.8 mJ/cm^2. Twenty-six masses were collected: ^{7}Li, ^{45}Sc, ^{51}V, ^{65}Cu, ^{85}Rb, ^{88}Sr, ^{89}Y, ^{90}Zr, ^{93}Nb, ^{137}Ba, ^{139}La, ^{140}Ce, ^{141}Pr, ^{146}Nd, ^{147}Sm, ^{153}Eu, ^{157}Gd, ^{163}Dy, ^{166}Er, ^{172}Yb, ^{175}Lu, ^{178}Hf, ^{181}Ta, ^{208}Pb, ^{232}Th, ^{238}U. The internal reference mass was ^{44}Ca, where the CaO concentrations were measured by electron microprobe. A typical signal acquisition started by collecting a background for 30s, which was followed by the laser firing for 70 s or less depending on the thickness of the MI. Data reduction was performed by the GLITTER software (GEMOC, Macquarie University, Australia). BCR-2G, NIST 610 and NIST 612 glasses (Gao et al., 2002; Gagnon et al.2008) were also analyzed to monitor the reproducibility and accuracy of the analyses. Typical relative standard errors on samples (1σ error of mean; $\sigma/\sqrt{n}$, where n is the number of cycles) were < 5% for V, Rb, Sr, Y, Zr, Ba, La, and Ce, < 8% for Sc, Nb, Pr, and Nd, < 15% for Cu, Sm, Eu, Gd, Dy, Er, Hf, Pb, Th, and U, < 25% for Li, Yb, Lu, and Ta.

Chapter 3

Persistent gas emission originating from a deep basaltic magma reservoir of an active volcano: the case of Aso volcano, Japan

3.1. Introduction

Arc volcanoes are known for their explosive eruptions driven by abundant dissolved volatile elements in their magma. It has been recognized that gas exsolution is the key player triggering rapid magma ascent and eruption (Roggensack *et al.* 1997; Pioli *et al.* 2009; Edmonds and Wallace 2017). Therefore, volcanic gas emission is considered to reflect the degassing of magma beneath volcanoes, and is one of the commonly observed and monitored activities, even in the quiescent period. Such persistent degassing of active volcanoes has been seen in arc volcanoes of the world (e.g. Miyakejima, Shinohara *et al.* 2003; Stromboli, Burton *et al.* 2007). Typically, volatile element behavior in magmas is governed by their solubility, and the amounts of volatile elements issued from magma are closely related to their pre-eruptive abundance. Thus, it is critical to determine the depths at which magmas were present, and their initial compositions through the studies of volcanic products. To investigate pre-eruptive volatile concentration and possibly primitive concentration, the study of melt inclusions is a powerful tool since the melt is trapped in a host crystal at depth, and isolated from interaction with surrounding magma (e.g. Anderson 1973; Sisson and Layne 1993; Wallace 2005). In fact, melt inclusions are not perfectly isolated from surrounding magmas since H^+ can diffuse through the host olivine (e.g. Gaetani *et al.* 2012) and CO_2 can be redistributed in shrinkage bubbles (e.g. Tucker *et al.* 2019). Therefore, H_2O and CO_2 measurements in melt inclusions are regarded as minimum values indicating the condition of last equilibration. However, several studies have pointed out discrepancies between total

masses of emitted gas measurements and melt inclusion-estimation of dissolved gas in glasses (e.g. Wallace 2005; Shinohara 2008). This is commonly referred to as “excess degassing”, and is observed in subduction zone volcanism (e.g. Métrich and Wallace 2008; Roberge et al. 2009; Wallace and Edmonds 2011; de Moor et al. 2017). It appears necessary to reconcile the melt inclusion-based volatile budget with the surface observation and this is the task I want to tackle in this study.

Aso volcano (Japan) is the ideal study site to compare gas emissions and petrological samples, including melt inclusions. It is a constantly monitored persistent degassing volcano since the 1970s, emitting more than 100 - 200 tons of SO_2 a day, even during the quiescent period (e.g. Mori *et al.* 2013; Shinohara *et al.* 2018; Japan Meteorological Agency (JMA) 2020). In addition, Holocene eruptions from Aso produced olivine-bearing tephra samples, ideal for finding quenched melt inclusions. For example, a recent melt inclusion study of historical Aso eruption products reported a shallow storage depth of erupted magma and a large excess of SO_2 degassing from Aso volcano (Saito *et al.* 2018). However, this previous study did not report volatile element concentrations of a primitive magma. Moreover, geophysical studies revealed multiple magma reservoirs with depths down to 24 km (below sea level: bsl) (Sudo and Kong 2001; Sudo *et al.* 2006; Abe *et al.* 2010; Hata *et al.* 2016).

In this study, I analyzed the bulk tephra of less evolved erupted products, matrix glasses, melt inclusions (glass and host minerals) to obtain information on the pre-eruptive magma process, storage depth and characteristics of primitive magma of Aso volcano. This paper reports the first petrological description of the deep magma reservoirs of Aso volcano using melt inclusion data and corroborating gas composition model. Our petrological constraints on a magma plumbing system give us the primitive H_2O, CO_2, F, Cl, and S concentrations of Aso, a persistently-degassing active volcano.

3.2. Samples and methods

3.2.1. Geological setting of Aso volcano and its cones

Aso volcano, located in central Kyushu Island of the Southwest Japan Arc, is one of the most active volcanoes of the volcanic front related to the Philippine sea plate subduction (Nakada and Kamata 1991; Kamata 1998; Miyoshi *et al.* 2008a, b). It has been active for at least 0.8 million years (e.g. Watanabe *et al.* 1989). Its activity is characterized by two different types of volcanisms: caldera-forming gigantic pyroclastic-flow eruptions (from 270 ka to 89 ka), and post-caldera extrusive activities (<89 ka) (Ono and Watanabe 1985). In the post-caldera stage, various types of magma (basalt to rhyolite) were erupted from, at least, 17 observable vents in the caldera (Watanabe 2001; Miyoshi *et al.* 2005).

Holocene activities are well described in tephrostratigraphic studies (Miyabuchi and Watanabe 1997; Miyabuchi 2009, 2010, 2017). The tephra is mostly basaltic and limited to the ejections from central cones. The last silicic eruption deposited Aso central cone pumice 1 (ACP1; Takada 1989) at 4.0 ka (Miyabuchi and Watanabe 1997; Hirata *et al.* 2020). ACP1 is the only silicic product in Holocene, which is dacitic banded pumice related to the effusion of Akamizu andesite lava flow (Miyabuchi 2017). Subsequently, volcanic activity of Kishimadake (3.7 ka), Ojodake (3.5 ka), Komezuka and Kamikomezuka cones (3.0 ka) was derived from basaltic to basaltic andesite magmas (Fig. 3.1; Miyabuchi and Watanabe 1997; Miyabuchi 2010; Hirata *et al.* 2020). Nakadake cone is formed in three stages: old volcanic (22 – 7.3 ka), young volcanic (7.3 – 3.7 ka) and youngest pyroclastic stages (<3.7 ka; Ono and Watanabe 1985; Miyabuchi 2009). Today, Nakadake is the only active central cone since the last eruption of Kamikomezuka (*ca.* 3.0 ka). All basaltic rocks in the post-caldera stage of Aso volcano evolved to low-Mg high-alumina basalt (MgO < 6.1 wt.%; Kuno 1960; Sisson and Grove 1993).

The magma chambers beneath Aso caldera have been described by geophysical surveys. Abe *et al.* (2010) reported a large low-velocity layer (LVL) from a depth of 11 to 25 km (for consistency hereafter, all the depths in the paper are referred as depths from the vent of the edifice, adding 1 km to the depth below sea level), by receiver function tomography. Hata *et al.* (2016) identified the magma pathway from 21 km deep beneath the caldera by electromagnetic survey, and reported two anomaly centers (C1 and C2) separated by 3 km in horizontal distance. C1 is located 5 km beneath Kishimadake cone, which corresponds to the main magma chamber feeding present-day Nakadake eruptions. This is in good agreement with earlier studies that reported the C1 chamber between 4 and 10 km depth, by deformation analysis of the volcano (Sudo *et al.* 2006) and seismic low-velocity anomaly (Sudo and Kong 2001). C2 is located 3 km beneath Nakadake cone. However, this C2 anomaly is geographically offset from the crater of Nakadake, and instead, a crack-like conduit extending from 0.3 to 2.8 km. A continuing passage was identified beneath this cracked-conduit, based on a region of lack of seismic reflectors at a depth from 2.5 to 4.5 km beneath the crater based on a 3-D seismic reflection analysis (Tsutsui and Sudo 2004). In this paper, I call this shallow magma passage as C2.

3.2.2. Tephra and scoria descriptions

I collected tephra deposits of eruptions from Kishimadake (*ca.* 3.7 ka), Ojodake (*ca.* 3.5 ka), Kamikomezuka (*ca.* 3.0 ka) and Nakadake (the youngest pyroclastic cone; <3.7 ka). Tephra samples were specifically collected to avoid the diffusive volatile-loss and daughter mineral crystallization within melt inclusions (Danyushevsky *et al.* 2002; Lloyd *et al.* 2013). Furthermore, I focused on recent (3.7 ka to present) eruption activities of basalt to basaltic andesite composition involving olivine phenocrysts. The sample set was therefore used to obtain information about crustal magma evolution and the volatile characteristics of magmas.

All tephra samples contain phenocrysts of plagioclase, olivine, clinopyroxene, orthopyroxene, and opaque minerals. Detailed descriptions of these tephras are found in Miyabuchi (2009, 2010).

Five tephra samples used in this study correspond to the eruptions of four cones: Kishimadake scoria (KSS), Ojodake scoria (OJSU and OJSL), Kamikomezuka scoria (KKO), and Nakadake scoria (NKD14) (Table 3.1). Specifically, KSS, OJSU, and OJSL were collected from a tephra deposit site (A9418 section reported by Watanabe 1991; Miyabuchi and Watanabe 1997; Fig. 3.1). KSS was collected from the lowest unit of sub-Plinian scoria-fall deposits in the N6 stage. It is a vesicular basaltic black scoria with a maximum size of 4.8 cm (Miyabuchi and Watanabe 1997). OJSU and OJSL were collected from the uppermost and lowest unit of sub-Plinian scoria-fall deposits in the N4 stage, respectively. OJSU and OJSL are reddish-brown, weakly altered basaltic scoria, with a maximum size of 4.6 cm (Miyabuchi and Watanabe 1997). These deposits represent sub-Plinian eruption events, which are the biggest eruption events in Holocene (each with approximately 0.06 km^3, VEI 3, Miyabuchi 2009). KKO was collected from Kamikomezuka cone, because the tephra deposit away from the edifice has not been identified presently. I sampled the black scoria from the outer part of the edifice from a road-cut outcrop, avoiding oxidized reddish scoria. KKO is poorly sorted, non-welded, vesicular scoria, ranging from cm-size to cow-dung bomb (tens of cm). NKD14 was collected from the crater rim of Nakadake cone's first crater, immediately after the eruption of Nov. 27, 2014. The samples were cm-size, well-vesiculated, black scoria. The eruption of Nakadake cone in the period 2014 - 2015 is the first magmatic eruption in 24 years (Ikebe *et al.* 2008; JMA 2016). In the most violent phase, Strombolian eruptions occurred with ejections of scoria lapilli and bombs at Nakadake cone's first crater (Yokoo and Miyabuchi 2015).

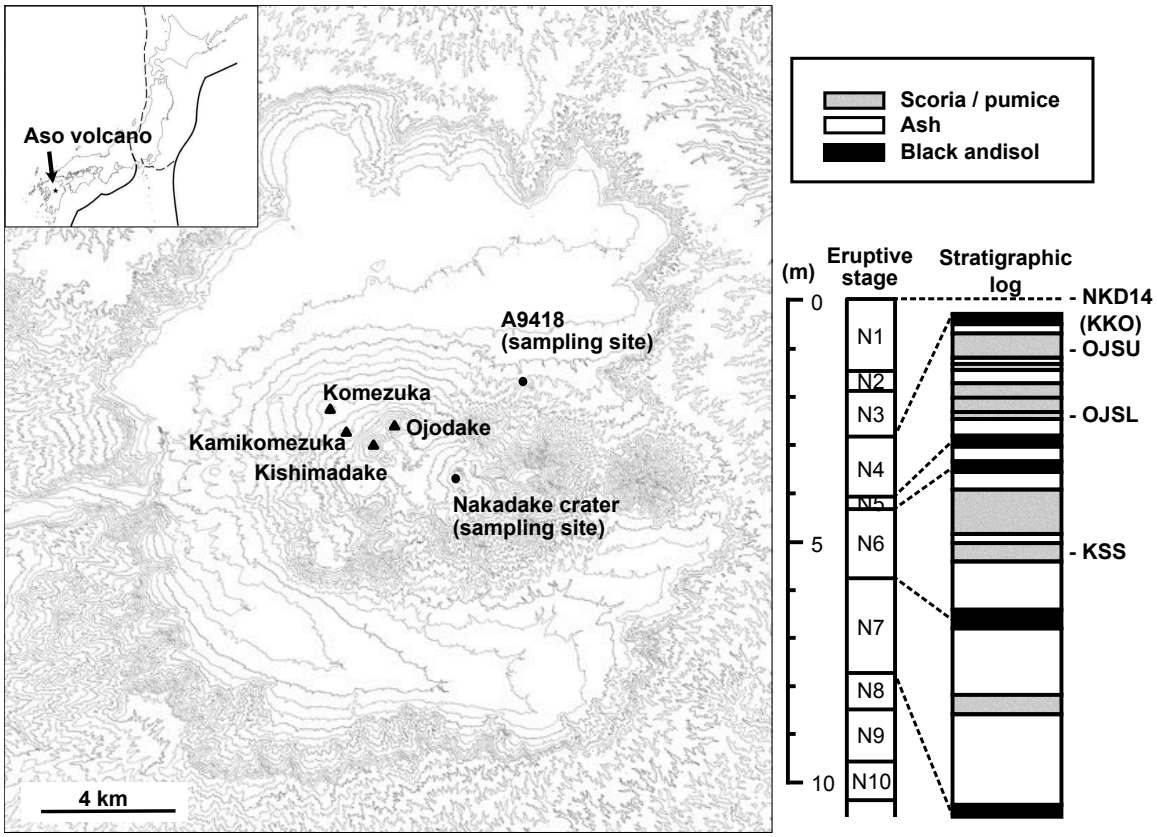

Figure 3.1. Locations of volcanic cones and sampling sites of the study. Main map shows topography of Aso volcano with a 50 m contour interval. Volcanic cones are indicated by solid triangles. Sampling sites are indicated by solid circles. Location of Aso volcano is indicated in an inset in the top left corner, showing Japanese islands with plate boundaries: solid line, active subduction plate boundary, and dashed line, diffused plate boundary. Stratigraphic log shows corresponding eruption stages and nature of volcanic deposits in A9418 site (Miyabuchi and Watanabe 1997). Kishimadake scoria (KSS) and Ojodake scoria (OJSL and OJSU) were collected at the indicated units. Kamikomezuka scoria (KKO) and Nakadake scoria (NKD14) were collected at the location indicated by field symbols. KKO in parenthesis indicates the relative eruption age (top of N4 stage).

Table 3.1. Tephra samples used in this study.

Sample ID	Cone	Age	Eruption style	Sampling site
NKD14	Nakadake	Nov. 27, 2014	Strombolian	1st crater rim
KKO	Kamikomezuka	3.0 ka	Strombolian	Edifice
OJSU	Ojodake	3.5 ka	Sub-Plinian	A9418
OJSL			Sub-Plinian	A9418
KSS	Kishimadake	3.7 ka	Sub-Plinian	A9418

3.2.3. Melt inclusion preparation

These 5 tephra samples were used for petrological observation and chemical analysis (*i.e.* bulk rock, phenocrysts and melt inclusions). Samples were washed in an ultrasonic bath, and only lapilli-size scorias (up to 6 cm) were chosen. Five grams of each sample were powdered using a ball milling machine with an alumina cup and a ball, for bulk rock X-ray fluorescence analysis (XRF). Olivine, pyroxene, and plagioclase crystals were handpicked under an optical microscope from scoria crushed by hand and sieved (from 0.25 to 1 mm). The picked crystals were mounted in resin and polished until the melt inclusion was exposed. They were then measured using an electron probe micro-analyzer (EPMA) and a reflectance Fourier transform infrared spectroscope (FTIR). Selected olivine crystals hosting melt inclusions of KSS and NKD14 were removed from the resin after EPMA and FTIR analyses, then mounted together in indium for secondary ion mass spectrometry (SIMS).

3.2.4. Analytical methods

3.2.4.1. Bulk rock major and trace elements

Bulk rock major and trace elements were determined by XRF on flux-fused disks using a Philips PANalytical MagiX PRO spectrometer at the Kitakyushu Museum of Natural History and Human History. The detailed analytical procedures are described by Mori and Mashima

(Mori and Mashima 2005). Accuracy was reported as ±0.1 % relative for SiO_2 and for trace elements, and varied from 5 to 25 ppm (Table 3.2).

3.2.4.2. Major and volatile elements in melt inclusion, mineral and glass

Major elements, S, and Cl concentrations were determined in melt inclusions, host minerals and groundmass glasses using a JXA8800R electron probe microanalyzer at the Earthquake Research Institute (ERI), University of Tokyo. The analytical settings were 15kV acceleration voltage, 12 nA beam current, with counting times for Na, Al, K, Fe, Mg, Si, Ti, V, Mn, and Ca at 20 s, and 30 s for Ni, Cr in mafic minerals and for S and Cl in hydrous melt. Beam diameter was set at 10 μm for glass and plagioclase, and focused (1 μm) for other minerals. During melt inclusion and groundmass glass analysis, Na and K were always measured in the first analytical cycle to minimize alkali loss (Devine *et al.* 1995). All analyses applied oxide ZAF correction. Analytical uncertainties are <0.7% relative for Si, <1% relative for Al, Fe, Mg, and Ca, <5% relative for Ti and Na, <10% relative for K, and <20% relative for Mn, V, Ni, Cr, S, and Cl.

In addition to the EPMA analysis, the core and rim compositions of phenocrysts were analyzed by energy-dispersive X-ray spectroscopy (EDS, AZtec system; Oxford Instruments) connected to a JEOL JSM-7001F field-emission electron microscope (FE-SEM) at Kumamoto University, using 15 kV acceleration voltage and 1 nA beam current. The beam diameter settings were the same as the EPMA setting at the University of Tokyo for all the host minerals. Analytical uncertainties are typically 0.5% relative for SiO_2, 1% relative for Al_2O_3, 1.5% relative for FeO, 0.5% relative for MgO, 2% relative for TiO_2 and Na_2O, 1.5% relative for K_2O, 1% relative for CaO. Other minor elements such as MnO and P_2O_5 can be as high as 20% relative.

Water concentrations in melt inclusions were determined by FTIR micro-reflectance spectroscopy using a JASCO FT-IR-660 plus, equipped with an IRT-30VC analytical microscope at the ERI, following the procedures described by Yasuda (2014). The IR spectra were obtained using 15 × 15 to 60 × 60 μm^2 rectangular apertures, and by accumulating 220 to 1500 scans, over a range of 400 to 7800 cm^{-1}. A gold mirror was used as a reflectance reference. Water concentrations were quantified using an empirical linear relationship for basalt to rhyolite compositions for total H_2O concentrations, measured in the 3650 cm^{-1} wavelength region. The analytical uncertainty (2σ) of the FTIR reflectance spectroscopy was < 0.3 wt. %. While the detection limit of the method strongly depended on the sample, I estimated the detection limits as 0.14 wt. % (Yasuda 2014).

H_2O, CO_2, F, S, and Cl concentrations in selected melt inclusions were determined by a SIMS (Cameca IMS-1280HR of Kochi Institute, JAMSTEC, Japan) following the procedure described by Shimizu *et al.* (2017). This analytical method favors a weaker primary current (up to 0.5 nA) than in previous studies (1-1.5 nA primary current; Le Voyer *et al.* 2010; Helo *et al.* 2011; Rose-Koga *et al.* 2012, 2014; 20 nA primary current in Hauri *et al.* 2002) and uses in-house standards covering the concentration range found in the natural samples in this study. In short, a 20 keV (10 keV at the ion source and 10 keV at the sample surface) Cs^+ ion beam of 300–500 pA was defocused to be 10-15 μm in diameter. Secondary ions were accelerated at 10 kV. A -10 keV electron beam with a diameter of ~100 μm was applied for electrostatic charge compensation of the analysis area. The field aperture was set at the size corresponding to 5 x 5 μm on the sample surface. Mass resolving power was set at ~6000 to separate mass interferences (for example, to separate $^{34}S^1H$ interference on ^{35}Cl requires 5120 MRP; Burdo and Morrison 1971). Negative secondary ions of ^{12}C, ^{16}OH, ^{19}F, ^{30}Si, ^{31}P, ^{32}S, and ^{35}Cl and the mass position of 11.9 amu were measured by an axial electron multiplier using the peak switching method. An analysis consisted of 10 cycles, and the total measurement time for each

analysis was ~6 min. Repeated analysis of a secondary basaltic glass standard from East Pacific Rise, EPR-G3 (Shimizu *et al.* 2017), yielded a relative standard deviation (1σ) for H_2O, CO_2, F, Cl, and S of 1.4, 3.2, 1.5, 2.5, and 0.9%, respectively. This SIMS analysis was conducted after EPMA analysis. Therefore, although I was careful to polish the sample with alumina powder again before SIMS analysis, measured CO_2 concentrations were reported in the supplementary material but not used due to possible carbon contamination. The measured values for S and Cl agreed within 25% between EPMA and SIMS analysis. So when volatile elements were measured by two methods, I adopted SIMS values rather than EPMA because analytical uncertainty of these elements by SIMS are generally lower (e.g. Rose-Koga *et al.* 2020). In this study, I did not find satisfactory agreement between H_2O determined by FTIR and by SIMS (uncertainty of FTIR measurements is close to 40%) so in the following, I only consider H_2O concentrations measured by SIMS, based on the better detection limit and precision of the method.

3.2.4.3. Sulfur speciation analysis

Selected inclusions were analyzed for S*Kα* peak positions to constrain the fO_2 conditions of the glasses. The wavelength of S*Kα* radiation [λ(S*Kα*)] for melt inclusions was measured using the EPMA following the procedures described by Yasuda *et al.* (2001), based on the method of Wallace and Carmichael (1994) and Carroll and Rutherford (1988). Sulfur speciation as the proportion of S^{6+} over a total S content was determined by measuring a relative shift from the peak position of an anhydrite mineral (Carroll and Rutherford 1988), with an assumption that S^{2-} and S^{6+} are the only two relevant species in silicate melt (Jugo *et al.* 2010). To avoid sulfur oxidation due to prolonged beam exposure (*i.e.* Rowe *et al.* 2007), I conducted a measurement with multiple spots for each melt inclusion. Therefore, I added up the wavelength scan data of individual spots to determine the precise peak position. A Gaussian

curve fitting was used for sulfur peak deconvolution. Analytical uncertainty ranges from 5 to 10% relative (Table A1).

3.2.5. Data processing: Post-entrapment crystallization correction

Major and volatile element data for all melt inclusions hosted in olivine were corrected for the effects of post-entrapment crystallization (PEC; e.g. Danyushevsky et al. 2000) by incremental calculation of equilibrium olivine (0.1 wt. % step) adding into the residual melt, until the melt reaching equilibrium with host olivine (Toplis 2005), following the procedures described in Danyushevsky *et al.* (2000). The melt Fe^{2+}/Fe^{Total} ratios were calculated from the empirical equation of Kilinc *et al.* (1983), assuming a constant fO_2 (ΔFMQ +1.0) based on measured S*Kα* peak shifts of all eruptions (Jugo *et al.* 2010). Temperatures of olivine-melt equilibrium were calculated using the olivine-saturated melt thermometer of Sugawara (2000), corrected for the effect of water on olivine liquidus temperature according to Médard and Grove (2008). I assumed an average H_2O concentration of NKD14 and KSS analyzed by SIMS for melt inclusions that were not analyzed individually for H_2O. Note, K_D and temperature were recalculated at each increment of olivine addition. The melt inclusions were not corrected for post-entrapment diffusive Fe-loss (Danyushevsky et al. 2000), as total FeO concentrations in melt inclusions are either the same or higher than those in bulk rocks. Corrected volatile concentrations were adjusted assuming volatiles are perfectly incompatible to host minerals and corrected values are used in the figures and reported in Table 3.3 (raw uncorrected data in supplementary material A1).

Plagioclase-, clinopyroxene-, and orthopyroxene-hosted melt inclusions were not corrected for PEC because there is no universally accepted procedure, although some attempts have been reported (Yasuda *et al.* 2001; Neave *et al.* 2017; Hartley *et al.* 2018). Among these samples, only the melt inclusions in equilibrium with host minerals were used for the magmatic

temperature calculation, in which the exchange coefficients were within expected range of basaltic composition: ($K_D(Fe\text{-}Mg)_{cpx\text{-}liq}$ = 0.28 ± 0.08, $K_D(Fe\text{-}Mg)_{opx\text{-}liq}$ = 0.29 ± 0.06, and $K_D(An\text{-}Ab)_{pl\text{-}liq}$ = 0.27 ± 0.01 or 0.1 ± 0.05 (depending on the calculated temperature; Putirka 2008).

3.3. Results

The analysis of five scoria from Aso edifices produced data of major elements for bulk rocks along with 204 melt inclusion data (major and volatile element concentrations) and host mineral compositions. More than 890 point-analyses were made to determine major element compositions of groundmass glasses and phenocrysts (core and rim; Tables 3.2 – 3.4 and A1 – A3).

Table 3.2. Major and trace element compositions of bulk tephra samples

Volcanic cone	Nakadake	Kamikomezuka	Kishimadake	RSTD (%)[b]	Detection limit
Sample	NKD14	KKO	KSS		
Major elements (wt.%)[a]					
SiO_2	54.26	51.49	53.22	0.1	–
TiO_2	0.94	0.94	1.00	0.3	–
Al_2O_3	17.84	18.52	18.48	0.1	–
FeO[c]	8.78	10.07	9.62	0.1	–
MnO	0.16	0.18	0.17	0.3	–
MgO	3.91	5.56	4.45	0.1	–
CaO	8.77	9.38	8.71	0.1	–
Na_2O	3.05	2.49	2.61	0.2	–
K_2O	2.00	1.16	1.51	0.3	–
P_2O_5	0.28	0.21	0.22	0.4	–
Total[d]	99.75	99.93	99.50	–	–
Trace elements (ppm)					
Sc	26	31	30	2.4	4.6
V	260	320	283	0.5	5.4
Cr	n.d.	11	12	8.9	3.7
Ni	n.d.	21	18	6.2	5.1
Cu	209	202	131	0.7	5.3
Zn	81	88	81	0.7	2.9
Rb	58	31	45	0.7	1.4
Sr	566	588	598	0.2	2.7
Y	26	21	23	2.3	2.5
Zr	139	88	121	0.6	2.4
Nb	7	5	7	6.3	1.5
Ba	369	277	328	0.7	9.8
La	18	13	15	11.2	6.1
Ce	82	33	33	4.2	5.4
Nd	25	16	18	7.3	5.5
Pb	13	7	18	3.8	2.4

[a] All oxides were normalized to 100 wt.%.

[b] Relative standard deviation (RSTD) of major elements were from Mori and Mashima (2005). RSTD of trace elements were calculated for KSS using the relationship between RSTD and concentration reported in Mori and Mashima (2005).

[c] Total iron as FeO calculated by following equation: $FeO = 0.8998*Fe_2O_3$.

[d] Total of the raw data.

Table 3.3. PEC corrected and normalized to 100%, major element and volatile concentrations in representative melt inclusions

Sample	NKD14						KKO						OJSU				
Host mineral[a]	OL	OL	OL	PL	CPX	OPX	OL	OL	PL	PL	CPX	OPX	OL	OL	PL	PL	CPX
Melt ID	1-m1	2-m1	4-m4	a3-m1	c5-m1	4-m6	2-m1	3-m3	a2-m1	Cb3-m1	d2-m1	1-m2	1-m5	1-m13	1-m1	1-m4	1-m2
SiO_2 (wt.%)[b]	59.21	56.44	57.22	57.71	60.22	59.88	48.53	49.29	57.65	52.53	61.65	59.09	59.68	54.30	59.11	55.74	57.45
TiO_2	1.33	1.01	1.35	1.48	1.45	1.25	0.86	1.07	1.15	1.25	1.39	1.36	0.97	1.15	1.10	1.33	1.60
Al_2O_3	14.43	14.82	14.33	14.61	14.23	14.37	18.08	19.52	17.10	13.35	13.69	14.90	14.42	16.77	16.91	15.34	15.47
FeO^{Total}	10.08	11.63	10.63	11.16	10.06	9.45	11.85	10.50	8.34	13.85	9.31	9.24	9.45	9.88	7.39	10.14	10.04
MnO	0.23	0.22	0.21	0.23	0.18	0.24	0.13	0.19	0.15	0.28	0.21	0.19	0.19	0.17	0.14	0.21	0.19
MgO	3.10	3.59	3.23	2.68	2.05	2.33	6.88	5.60	2.48	5.90	1.86	2.76	2.98	3.87	2.50	3.84	2.17
CaO	5.13	6.50	6.38	5.83	4.90	5.24	10.37	10.60	6.86	8.85	4.71	5.87	5.72	8.50	5.92	7.51	5.27
Na_2O	2.86	3.49	3.03	2.55	2.97	3.63	2.61	2.48	2.44	1.81	3.16	3.40	3.02	3.10	3.49	3.11	3.09
K_2O	3.16	1.94	3.09	3.23	3.36	3.35	0.53	0.58	3.62	1.98	3.78	2.78	3.14	1.95	2.97	2.46	4.07
P_2O_5	0.48	0.37	0.53	0.52	0.57	0.26	0.16	0.17	0.21	0.20	0.23	0.40	0.44	0.31	0.46	0.31	0.64
S (EPMA)	0.010	0.044	0.022	0.009	0.013	0.019	0.378	0.251	0.004	0.097	0.022	0.014	0.019	0.143	0.011	0.041	0.021
Cl (EPMA)	0.087	0.122	0.085	0.099	0.131	0.096	0.054	0.098	0.053	0.070	0.104	0.074	0.090	0.072	0.094	0.073	0.217
H_2O (SIMS)	-	-	0.48	-	-	-	-	-	-	-	-	-	-	-	-	-	-
S ppm (SIMS)	-	-	199	-	-	-	-	-	-	-	-	-	-	-	-	-	-
Cl ppm (SIMS)	-	-	835	-	-	-	-	-	-	-	-	-	-	-	-	-	-
F ppm (SIMS)	-	-	727	-	-	-	-	-	-	-	-	-	-	-	-	-	-
P_2O_5 (SIMS)	-	-	0.49	-	-	-	-	-	-	-	-	-	-	-	-	-	-
H_2O/K_2O	-	-	0.154	-	-	-	-	-	-	-	-	-	-	-	-	-	-
S/K_2O	0.003	0.022	0.006	0.003	0.004	0.006	0.711	0.434	0.001	0.049	0.006	0.005	0.006	0.073	0.004	0.017	0.005
Cl/K_2O	0.028	0.063	0.027	0.031	0.039	0.029	0.101	0.170	0.015	0.035	0.028	0.027	0.028	0.037	0.032	0.029	0.053
F/K_2O	-	-	0.024	-	-	-	-	-	-	-	-	-	-	-	-	-	-
PEC%[c]	1.3	1.6	1.4	-	-	-	5.6	0.1	-	-	-	-	0.7	0.1	-	-	-
Host Mg#/An[d]	66.2	66.0	65.6	66.8	69.6	69.2	80.7	79.0	66.7	89.6	69.2	68.9	67.7	74.5	65.7	80.8	69.6

Table 3.3. (continued)

Sample	OJSL								KSS							
Host mineral[a]	OPX	OL	OL	PL	PL	CPX	CPX	OPX	OL	OL	OL	PL	PL	CPX	CPX	OPX
Melt ID	1-m2	1-m2	1-m3	1-m1	1-m6	1-m6	O1-m7	1-m8	2-m1	3-m4	4-m6	c1-m1	d2-m1	a2-m1	b5-m1	3-m2
SiO_2 (wt.%)[b]	61.75	52.24	61.21	56.12	59.57	58.65	60.87	62.08	48.18	56.92	60.40	59.81	67.77	55.90	59.58	58.78
TiO_2	0.76	1.08	0.79	1.48	1.19	1.24	1.27	1.21	0.99	0.56	1.25	0.98	1.01	1.37	1.41	1.36
Al_2O_3	14.16	16.91	13.34	16.56	16.37	15.31	15.22	14.53	17.89	13.04	12.71	16.61	15.89	16.09	14.99	14.51
FeO^{Total}	8.68	11.50	9.60	9.41	8.01	9.66	7.55	7.67	11.72	10.28	10.56	7.31	4.20	10.25	9.44	10.48
MnO	0.16	0.16	0.20	0.20	0.13	0.18	0.16	0.16	0.18	0.17	0.27	0.20	0.10	0.23	0.24	0.17
MgO	2.45	4.63	2.74	2.82	2.13	2.44	2.18	2.11	6.58	3.13	3.16	3.19	0.83	3.55	1.99	1.92
CaO	5.45	9.35	5.49	7.01	5.78	5.50	4.59	4.68	10.99	6.14	5.97	6.94	2.99	7.28	5.09	5.27
Na_2O	3.91	2.77	2.89	2.78	3.36	2.96	3.58	3.40	2.50	2.81	3.15	2.24	2.04	3.16	2.79	3.08
K_2O	2.55	1.08	3.25	2.76	3.11	3.50	4.12	3.74	0.73	1.84	2.10	2.42	4.77	1.84	3.87	3.83
P_2O_5	0.12	0.29	0.49	0.86	0.36	0.56	0.45	0.41	0.23	0.35	0.43	0.30	0.41	0.34	0.60	0.60
S (EPMA)	0.033	0.203	0.006	0.026	0.007	0.021	0.008	0.013	0.180	0.068	0.017	0.008	0.006	0.081	0.042	0.038
Cl (EPMA)	0.045	0.058	0.101	0.078	0.071	0.103	0.143	0.096	0.071	0.153	0.085	0.067	0.143	0.109	0.123	0.118
H_2O (SIMS)	-	-	-	-	-	-	-	-	2.62	2.52	2.58	-	-	-	-	-
S ppm (SIMS)	-	-	-	-	-	-	-	-	2962	1075	164	-	-	-	-	-
Cl ppm (SIMS)	-	-	-	-	-	-	-	-	731	1311	801	-	-	-	-	-
F ppm (SIMS)	-	-	-	-	-	-	-	-	331	853	578	-	-	-	-	-
P_2O_5 (SIMS)	-	-	-	-	-	-	-	-	0.22	0.40	0.50	-	-	-	-	-
H_2O/K_2O	-	-	-	-	-	-	-	-	3.591	1.375	1.232	-	-	-	-	-
S/K_2O	0.013	0.188	0.002	0.009	0.002	0.006	0.002	0.003	0.406	0.059	0.008	0.003	0.001	0.044	0.011	0.010
Cl/K_2O	0.018	0.054	0.031	0.028	0.023	0.030	0.035	0.026	0.100	0.071	0.038	0.028	0.030	0.059	0.032	0.031
F/K_2O	-	-	-	-	-	-	-	-	0.045	0.047	0.028	-	-	-	-	-
PEC%[c]	-	2.3	0.1	-	-	-	-	-	8.7	1.3	0.3	-	-	-	-	-
Host Mg#/An[d]	70.4	74.9	64.5	81.8	66.4	71.1	69.2	66.7	81.0	66.1	66.0	76.7	56.8	76.4	69.4	66.2

[a] OL: olivine, PL: plagioclase, CPX: clinopyroxene, OPX: orthopyroxene. b All major oxides were normalized to 100 wt.% as volatile-free. c Degree of post-entrapment crystallization (wt.%) based on the addition of equilibrium olivine. Oxide concentrations presented in this table were corrected values. d Mg# = Mg/(Fe+Mg), An = Ca/(Ca+Na), in mole%.

Table 3.4. Major element and volatile contents in groundmass glasses

Volcanic cone	Nakadake		Kamikomezuka		Ojodake				Kishimadake	
Sample	NKD14		KKO		OJSU		OJSL		KSS	
	Avr.	Std.	Avr.	Std.	Avr.	Std.	Avr.	Std.	Avr.	Std.
N = [a]	17		8		14		13		18	
SiO_2 (wt.%)[b]	58.94	0.30	57.58	0.46	56.19	0.95	55.03	0.33	57.15	0.63
TiO_2	1.39	0.05	1.56	0.06	1.32	0.06	1.30	0.05	1.24	0.05
Al_2O_3	14.66	0.35	14.14	0.23	15.01	0.43	15.40	0.55	15.77	0.32
FeO^{Total}	9.60	0.26	12.11	0.43	10.36	0.35	10.87	0.42	9.40	0.36
MnO	0.21	0.02	0.23	0.02	0.21	0.02	0.22	0.02	0.21	0.02
MgO	2.70	0.15	3.28	0.15	3.80	0.19	3.96	0.22	3.55	0.17
CaO	6.05	0.23	6.67	1.12	7.29	0.34	7.84	0.28	7.29	0.36
Na_2O	2.87	0.23	2.15	0.66	3.33	0.18	3.28	0.31	2.73	0.22
K_2O	3.09	0.09	2.01	0.45	2.22	0.10	1.86	0.29	2.30	0.15
P_2O_5	0.48	0.04	0.28	0.05	0.26	0.04	0.23	0.03	0.36	0.05
S	0.008	0.011	0.003	0.005	0.012	0.018	0.006	0.008	0.006	0.006
Cl	0.088	0.013	0.062	0.016	0.065	0.014	0.048	0.008	0.072	0.012

[a] Number of analyses.

[b] All major oxides were normalized to 100 wt.% excluding S and Cl.

3.3.1. Petrography

All samples were porphyritic with approximately 40 vol.% crystals. Plagioclase, clinopyroxene, olivine plus minor orthopyroxene, and opaque minerals were present. In all samples, plagioclase phenocrysts commonly showed dusty zone and honeycomb texture (Fig. 3.2a), and all orthopyroxene phenocrysts had reaction rims of olivine and clinopyroxene (Fig. 3.2b). Aggregates of phenocrysts (i.e. plagioclase, clinopyroxene, olivine, and opaque minerals) were frequently found in all samples (Fig. 3.2c). The groundmass consisted of microlites of plagioclase, clinopyroxene, olivine, and magnetite. The groundmass of KSS occasionally showed the heterogeneous mingling texture where crystals are relatively abundant (Fig. 3.2d).

3.3.2. Host mineral compositions

The olivine phenocrysts were grouped into two types based on the core Fo contents [Mg / (Fe + Mg) × 100 in mole], as low-Fo (62 to 72) and high-Fo (72 to 82) (Fig. 3.3a). High-Fo olivine was observed only in KKO, OJSU, OJSL, and KSS. Low-Fo olivine was found in all samples. As Fo content of the phenocryst rims ranged from 68 to 78 in KKO, OJSU, OJSL, and KSS, and from 64 to 67 in NKD14 (Table A3), generally low-Fo olivine phenocrysts were reversely zoned, whereas olivine phenocrysts in NKD14 were homogeneous. All high-Fo olivine phenocrysts were normally zoned. Clinopyroxene and orthopyroxene phenocryst cores in all samples were in the range of 65-76 and 61-71, respectively (Mg# = [Mg / (Fe + Mg) × 100 in mole]). The majority of clinopyroxene phenocrysts in KKO, OJSU, OJSL, and KSS were reversely zoned. Mg# of NKD14 varied little, at ~70. The compositions in the rims of olivine and clinopyroxene phenocrysts were the same as the minerals found in reaction rims of orthopyroxene phenocrysts. The plagioclase phenocrysts were also divided into two types

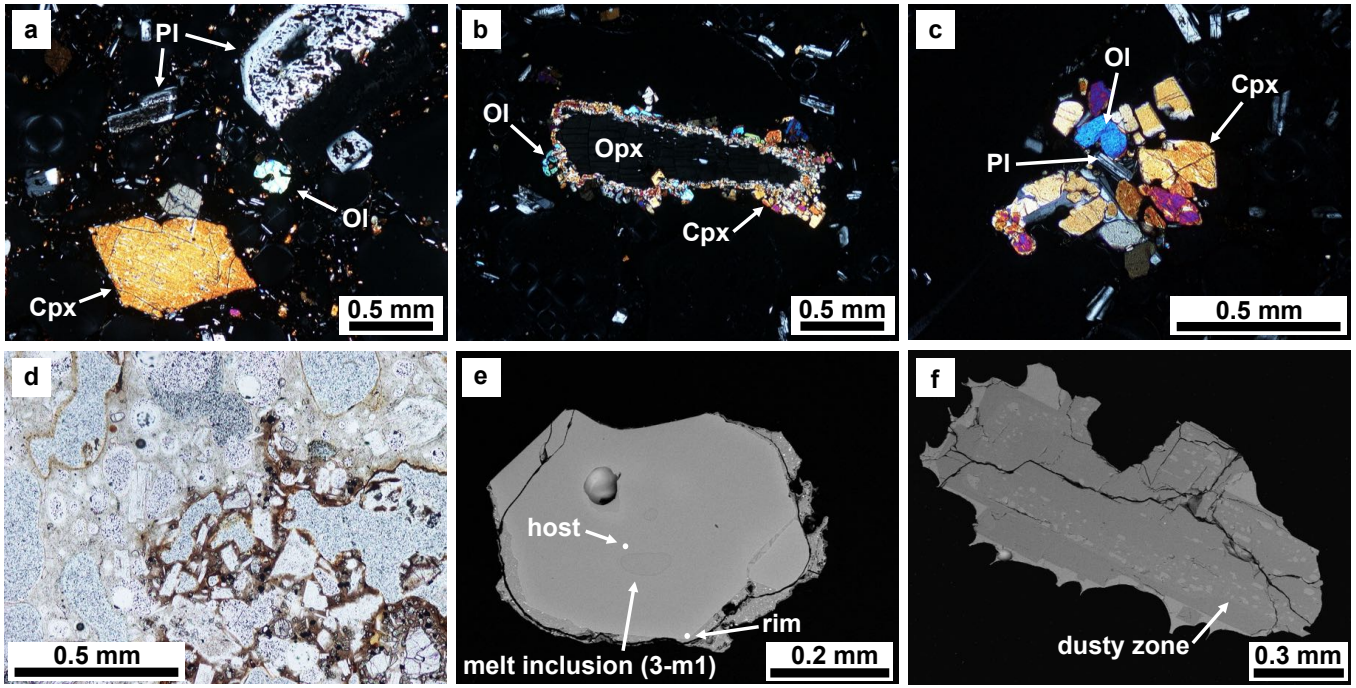

Figure 3.2. Microscope photographs (a-d) and backscatter electron images (e, f) of representative phenocrysts and textures from Holocene basaltic tephra products in Aso central cones. (a) Plagioclase (Pl) phenocrysts with honeycomb texture in KKO, under cross-polarized light. Clinopyroxene (Cpx) and olivine (Ol) phenocrysts also present. (b) An orthopyroxene (Opx) phenocryst with reaction rim consisted of clinopyroxene and olivine in KSS, under cross-polarized light. (c) An aggregate of phenocryst consisted of plagioclase, clinopyroxene and olivine in KSS, under cross-polarized light. (d) A microlite-rich part of groundmass in KSS with abundant crystals, under plain-polarized light. (e) High-Fo olivine phenocryst and its melt inclusions observed in KSS. (f) A texture of plagioclase phenocryst with (optically) dusty zone, in the middle part of the crystal, observed in NKD14.

based on the normal and reverse zoning patterns. The An content [Ca / (Ca + Na) × 100 in mole] of the plagioclase phenocryst cores was within the 55-93 range.

3.3.3. Major and volatile elements in melt inclusions

The tephra samples of this study were basaltic to basaltic andesite with SiO_2 ranging from 51.5 to 54.3 wt. % (large circles in Fig. 3.3c). Melt composition in inclusions varied significantly more than that of the bulk tephra composition: SiO_2 ranging from 46.0 to 65.8 wt. %. This range mostly overlapped with the compositional variation of post-caldera volcanic products (grey circles in Fig. 3.3c). The melt inclusion compositions of NKD14 were generally similar to evolved matrix glass and varied little, and were distinguished from the melt inclusions of KKO, OJSU, OJSL, and KSS.

In our sample set, the core composition of host olivines were clearly divided into two groups with Fo72 representing the divide (Fig. 3.3a). I interpreted that olivines have grown from two distinctively different lavas, which I called mafic and felsic. Based on the anti-correlation of SiO_2 concentration in olivine-hosted melt inclusions with host Fo content, I concluded that magma composition can be divided into two groups above and below 55 wt.% SiO_2. The high SiO_2 corresponded to low-Fo olivine and low SiO_2 corresponded to high-Fo olivine. Thus, in the following I grouped all the melt inclusions lower than 55 wt.% SiO_2 in a mafic group, and others in a felsic group. S concentration in melt inclusions correlates well with host Fo content and is anti-correlated with SiO_2 (Fig. 3.3a) and K_2O, indicating a mafic volatile-rich (with S up to 3750 ppm and Cl up to 1311 ppm) magma, and a felsic volatile-poor magma (Fig. 3.3b). NKD14 inclusions were notably different, with less than 434 ppm S, indicating extensive degassing. Melt inclusion Cl concentrations varied from 530 ppm to 1311 ppm (Table 3.3 and Table A1; SIMS value is preferred to EMP value when both are reported). F concentrations were determined only on a subset of olivine-hosted melt inclusions and

therefore there are fewer data. F concentrations varied between 258 and 853 ppm (Table 3.3 and Table A1). F and Cl correlates with SiO_2 and K_2O and anti-correlate with host Fo content. H_2O concentrations measured in melt inclusions vary between 0.47 to 2.89 wt.% (NKD14-Olivine-4-m4 and KSS-Olivine-4-m11, respectively; Table 3.3 and Table A1).

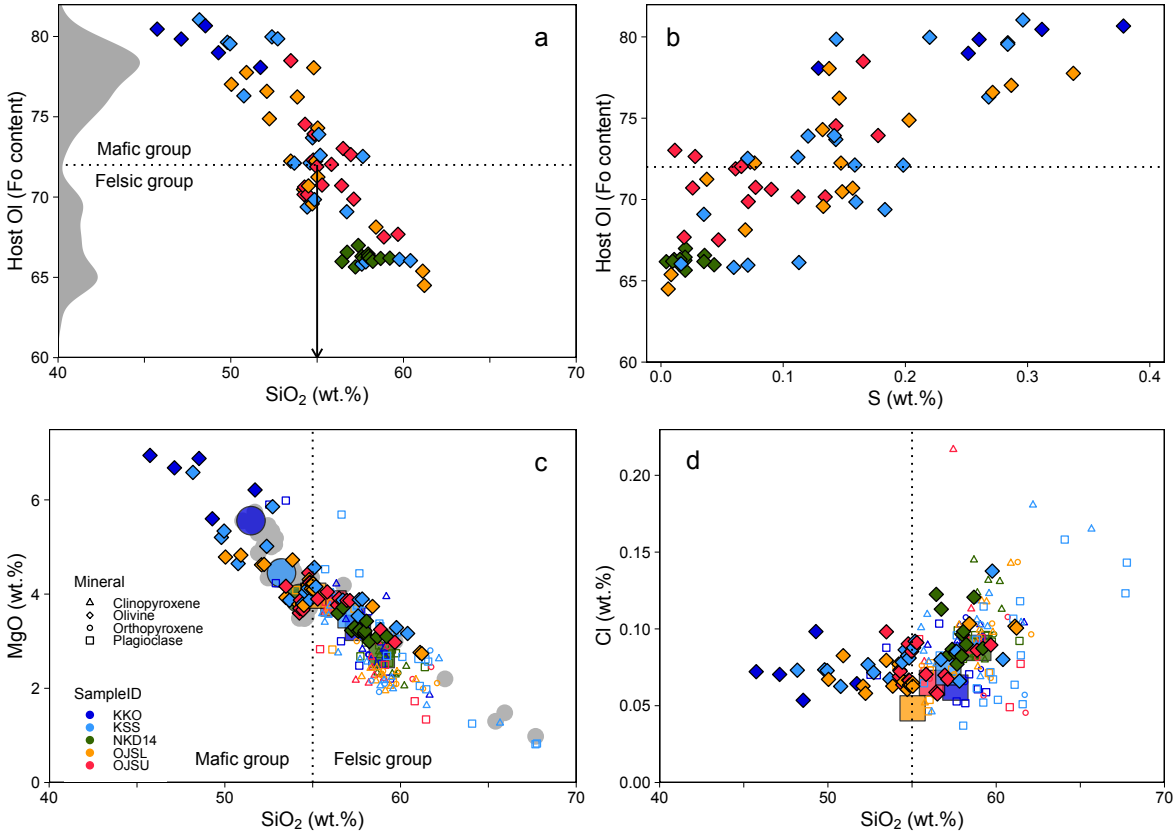

Figure 3.3. Major element and volatile concentrations in melt inclusions from Holocene basaltic tephra products in Aso central cones. Melt inclusion data from minerals other than olivine are shown as open symbols. The melt inclusion data are compared to bulk tephra and average groundmass glass compositions, solid circles, and solid squares, respectively. The distribution of Fo content in all olivine cores is shown as a relative density function on the left side of (a). The dashed line in Figure 3a and 3b indicates the value Fo72. Bulk lava compositions of late-Holocene volcanic products, reported previously, are also shown as solid grey circles in (c) (Miyoshi *et al.* 2005; Miyabuchi 2010, 2017; Saito *et al.* 2018). All oxide concentrations were normalized to 100 wt. %, excluding volatile element abundance.

3.4. Discussion

3.4.1. Evidence for magma mixing

Zoning in magmatic minerals characterizes their crystallization in a magma chamber and can trace the history of magma cooling (e.g. Costa *et al.* 2008), and magma mixing (e.g. Sakuyama 1979). Among the tephra samples in this study, phenocrysts in every sample indicate textural evidence of magma mixing that could have been produced by the introduction of hotter magma: for example, the reverse zoning and disequilibrium texture, such as the honey-comb texture of plagioclase and reaction rim of orthopyroxene (Fig. 3.2a and 3.2b; Tsuchiyama 1985). The coexistence of normally zoned plagioclase and olivine phenocrysts with these disequilibrium phenocrysts suggests that magma mixing of at least two distinct components has occurred (e.g. Sakuyama 1979). This interpretation is supported by the compositional variation of the melt inclusions; felsic melt inclusions are hosted in reversely zoned phenocrysts such as plagioclase, clinopyroxene, orthopyroxene, and low-Fo olivine. Mafic melt inclusions are hosted in high-Fo olivine and some of plagioclase (Fig. 3.3).

The presence of orthopyroxenes surrounded by reaction rims and An-rich zones in the middle part of plagioclases in NKD14 (Fig. 3.2f) indicates that the 2014 magma is also the result of mixing. Such petrological features are found in magmatic products of every Nakadake eruption (Miyoshi *et al.* 2005). Thus, I consider that all the Nakadake eruption products are the result of magma mixing, rather than the derivatives from a single parental magma. In addition, Miyoshi *et al.* (2005) also show that the compositional variation in the trace elements in the post-caldera basaltic rocks of Aso volcano is consistent with a magma mixing model and not with a fractional crystallization process. Therefore, at least two types of magmas are present beneath the Nakadake cone, and feed its eruption.

3.4.2. Characterization of mixing endmembers

I conducted a two-component mixing model calculation of two distinct magmas, one silicic endmember and one mafic endmember, based on the major element variation of melt inclusions (see Supplementary document A4). The model used the most primitive basaltic melt (Melt ID: 2-m1 hosted in an olivine) and the most SiO_2-rich dacitic melt (Melt ID: d2-m1 hosted in a plagioclase) of KSS as the mafic and silicic endmember, respectively. The major element variation was well reproduced with the mixing model for melt inclusions of all host minerals (Fig. A4-5). While the major variance of concentration variations was explained by a simple mixing process, in close inspection of trends, it is likely that crystal fractionation contributed to the dispersion from the mixing model. It should also be noted that the mixing model required the presence of independent mixing endmembers, it does not constrain their origin.

It is important to note that there is a surface expression of this silicic endmember in the Aso eruption products, while the mixing endmember is set by a melt inclusion. Major element compositions of ACP1 dacitic pumice (Takada 1989), the only Holocene felsic product erupted three hundred years before that of KSS, are similar to the endmember, and this indicates the presence of the silicic magma. Furthermore, the presence of a banded pumice was reported in ACP1 prior to KSS (Miyabuchi 2017). This banded texture is evidence of magma mingling and therefore the mixing trend is unlikely a result of assimilation and crystal fractionation of single parental magma. The cores of reversely zoned phenocrysts of KSS scoria samples were formed at equilibrium conditions with the silicic endmember. Therefore, the temperature of silicic endmember magma was determined with a two-pyroxene thermometer by pairing core compositions (Putirka 2008). The estimated temperatures of the silicic endmember are 1010-1025ºC for KKO, OJSU, OJSL, and KSS (± 13˚C, 1σ for samples, while standard error of the thermometer is ±38 ˚C). I adopted this estimated range as the temperature of the silicic

endmember magma. These estimated temperatures are higher than those of typical dacitic magma with 4 - 5 wt. % H_2O (e.g. 770 – 915 ˚C for Mount St. Helens, Gardner *et al.* 1995) and lower than that estimated for a completely anhydrous dacitic magmas, for example Puna Geothermal Venture Wellfield, Hawaii have the highest temperature estimates 1050ºC (Teplow *et al.* 2009). This silicic endmember magma (T between 1010-1025ºC) will mix with the mafic endmember (most likely hotter) magma at temperature presumably higher than 1010-1025ºC.

Basaltic lava corresponding to the pure mafic endmember is absent among the eruption products of the entire post caldera stage (Miyoshi *et al.* 2005), while it is found in olivine-hosted melt inclusion. Many tephras of this study also contain normally zoned phenocrysts with high-Fo and high-An cores. As for the case of the silicic endmember, it is possible to assume the equilibrium of these cores with the mafic endmember melt. I therefore calculated the magmatic temperature of the pure mafic endmember, using Sakuyama's method (Sakuyama *et al.* 2014), which involves the combined application of a plagioclase-melt hygrometer (Lange *et al.* 2009) and an olivine-saturated melt geothermometer (Sugawara 2000; Médard and Grove 2008). This method accounts for the H_2O-dependency of the olivine thermometer by simultaneously solving for H_2O and temperature using an additional constraint from the plagioclase hygrometer. The resulting temperature of mafic endmember magma varies between 1051 – 1063 ˚C, depending on the assumed pressure condition of the magma chamber (0.1 - 0.5 GPa, respectively). In addition, the entrapment temperature of the endmember inclusion (KSS-2-m1) is 1092 ˚C based on the olivine-liquidus thermometer (Table A1, Sugawara 2000; Médard and Grove 2008). Considering the uncertainties of the thermometry methods, these temperature estimates are likely representing the range for the mafic magma. By taking the high temperature result (~1090 ˚C), the temperature difference between mafic and felsic (1010-1025 ˚C) endmembers is at least 65 ˚C.

The mixing trend among volatile elements is present and generally consistent with the trend of major elements. However, in detail, there are systematic disparities from the mixing curve (Supplementary document A4). Notably, abundances of H_2O, S, and Cl for NKD14 sample, are depleted compared to the mixing trend traced by KSS melt inclusions (Fig. A4-4). This is best explained by significant degassing occurring during/after magma mixing. Furthermore, there is no single melt inclusion uniquely representing suitable mafic endmember volatile concentrations. The sample KSS-2-m1 is selected as the major element endmember, but its H_2O contents are not the highest values. From the inspection of the trend, I inferred that the mafic endmember must have higher volatile content thus most likely lost water after its entrapment. If melt inclusions formed at a deeper depth, and were stored in a shallower magma chamber, it is expected that H^+ diffusion through the olivine would equilibrate the melt inclusion with the surrounding magma (Portnyagin *et al.* 2008; Chen *et al.* 2011; Gaetani *et al.* 2012; Bucholz *et al.* 2013; Ferriss *et al.* 2018). Complete re-equilibrated melt inclusion would have erased the mixing trend. It is not the case here, I have found suitable endmember volatile element concentrations that satisfy the general trend. Because the mafic endmember magma is expected to be volatile-rich, its H_2O concentration has to be higher than the H_2O of the mixed-magma (e.g. that of the melt inclusions). The maximum estimated H_2O concentration (4.68 wt. %) based on the hygrometer discussed above is therefore taken as the concentration for the volatile-rich mafic endmember. This value of 4.68 wt.% H_2O is higher, by about 2 wt. %, than the highest H_2O concentration measured in the melt inclusion. Sakuyama's method implicitly ignores the CO_2 activity in magma, and predicts lower H_2O content when considering CO_2-bearing system (by 0.9 wt. % less H_2O, assessed from an experimental result of Melekhova *et al.* 2017). Furthermore, this volatile content is the value at the condition of olivine - plagioclase crystallization, most likely of the cooling magma in the crust. At this point, I have no other

constraint on the H_2O concentration of the mafic endmember and the primary magma could have an even higher H_2O content.

3.4.3. Volatile concentrations of primitive basaltic melt

The melt inclusions similar to the mafic endmember of the mixing model showed element concentrations with primitive character, such as low incompatible element concentrations (low K_2O, Cl, and F), and higher volatile element such as S. However, H_2O concentration is likely equilibrated to a lower pressure conditions, and CO_2 concentration in melt inclusion appears to be low. While these melt inclusions are hosted in high Fo olivine, the H_2O and CO_2 abundances are not of primitive character. On the contrary, as F, S, and Cl are not expected to diffuse through the host olivine, and at the time of entrapment, they retain the value closest to the primitive magma. In an attempt to constrain the mafic endmember composition, compositional trends are examined with ratios of S, Cl, and F over K_2O. These ratios are less affected by crystallization within melt inclusions and before entrapment, assuming the strong incompatibility of K_2O in magmatic minerals near basaltic liquidus (Fig. 3.4). Because the composition of the mafic endmember points towards that of the primitive magma, the maximum values are taken from Fig. 3.4a, b, and c, as the primitive volatile ratios: $S/K_2O = 0.711$, $Cl/K_2O = 0.170$, and $F/K_2O = 0.047$.

Dissolved S concentrations, up to 3750 ppm in the mafic group melt inclusions, are higher than many melt inclusions from subduction-like hydrous basalt (Fig. 3.5a; S mostly between 900 and 2500 ppm; e.g. Wallace 2005), while high S content appears to occur in oxidized magmas (Roggensack 2001; Webster *et al.* 2010). Our primitive magma S estimate is therefore 3750 ppm, the highest measured concentration in a melt inclusion of the mafic group. I also noted that S concentration of half of the melt inclusions are supersaturated in sulfide, plotting above the sulfur concentration at sulfide saturation (SCSS, Fig. 3.5b), while

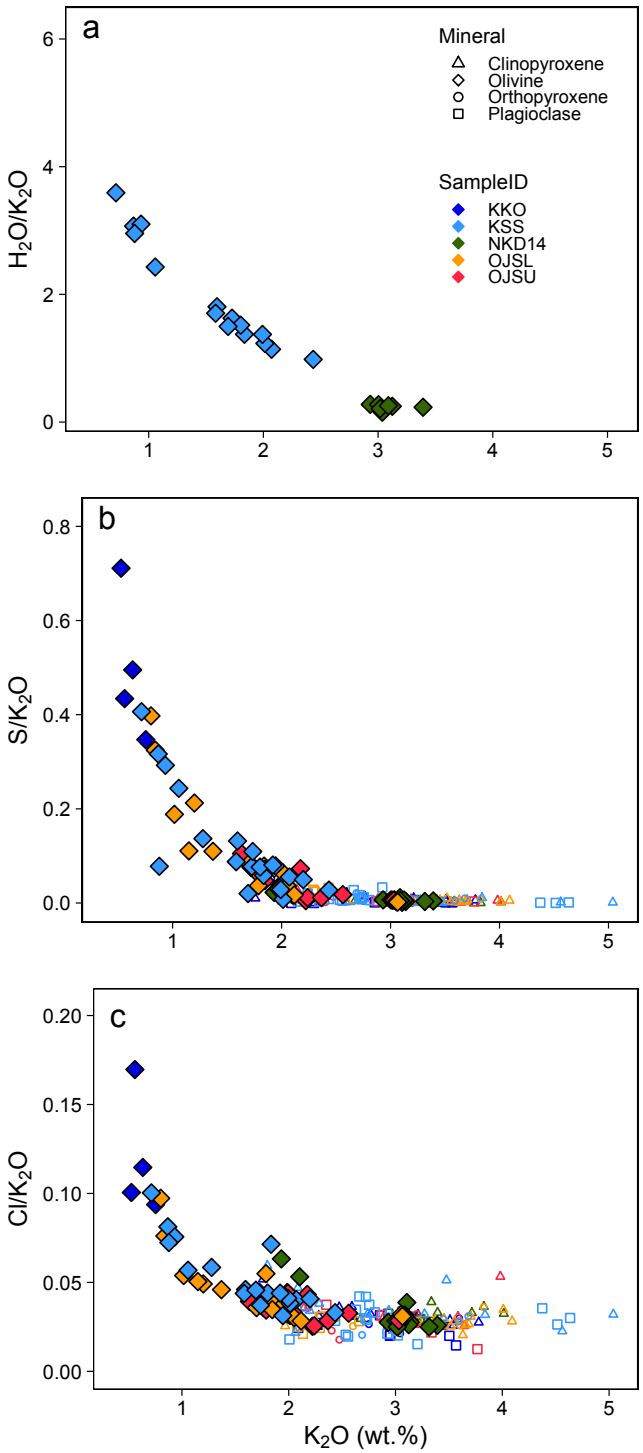

Figure 3.4. Ratios of volatiles/K_2O vs. K_2O in melt inclusions and groundmass glasses (the same symbols as Fig. 3). All volatile elements showed a systematic decrease (a, H_2O/K_2O; b, S/K_2O; c, Cl/K_2O) with respect to increasing K_2O. High volatile/K_2O corresponds to high volatile concentration as well as low K_2O.

no sulfide is found in the melt inclusions or in the groundmass. These sulfide supersaturated melt inclusions must be at high fO_2 condition, so that the concentration of sulfide-precipitating S^{2-} in magma is lower than SCSS. In fact, it has been shown that arc basalt magmas have higher oxygen fugacities than MORB magmas (e.g. Wallace 2005; Kelley and Cottrell 2009). In addition to this, the redox state of the melt inclusions was determined and ranges from FMQ + 0.68 to FMQ + 1.41 (Average = 1.05, 1σ = 0.17, corresponding to S^{6+}/S_{total} = 0.14 - 0.85, Table A1). Such oxidizing conditions allow for (i) higher S solubility in the mafic magma (Carroll and Rutherford 1985; Jugo *et al.* 2010) and (ii) the presence of both S^{2-} and S^{6+} in the melt. Fig. 3.5b also shows a dashed line expected for the SCSS corrected for abundance of S^{2-} species (S^{6+}/S_{total} = 0.85). Such first order correction puts all of our melt inclusion to be below sulfur saturation, consistent with our observation. Also, S concentrations of all the melt inclusions are under-saturated with respect to anhydrite saturation (SCAS was from 5300 to 6000 ppm, Li and Ripley 2009; Baker and Moretti 2011). The elevated S concentrations in the undersaturated oxidized melt are therefore considered to represent, less-degassed, non-sulfide-fractionated, S concentrations, at least at the condition of the shallow storage depth.

Similarly, I also consider that the mafic endmember Cl and F concentrations are representative of primary concentrations, as the exsolution pressure of Cl and F is at shallower depths (~100 MPa for Cl and ~10 MPa for F; Spilliaert *et al.* 2006) than for other volatile species. Cl concentration in the Aso primitive magma was 716 ppm (took the value of the mafic end member melt inclusion: KSS-2-m1) which is higher than that of MORB (Fig. 3.6; max 500 ppm Cl, Le Voyer *et al.* 2015), as it is interpreted as the addition of Cl to the subarc mantle from the subducting slab (e.g. Straub and Layne 2003). On the contrary, F concentration in the primitive magma was 324 ppm, which is the same order of magnitude as that of MORB (max

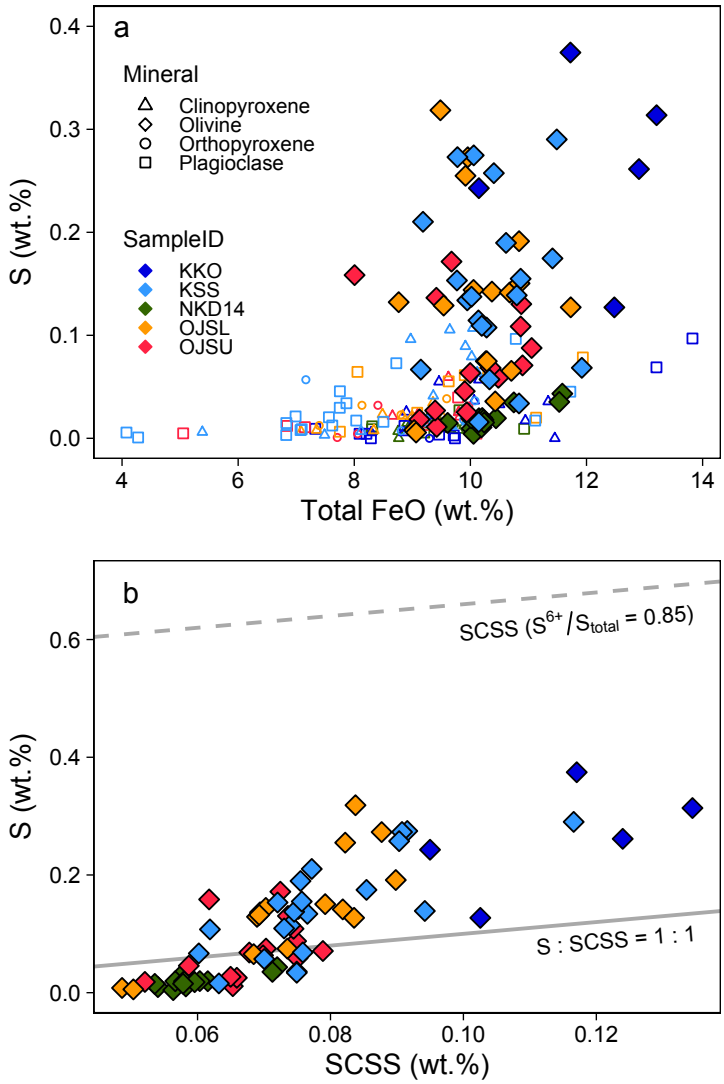

Figure 3.5. (a) Variations in S and total FeO concentrations of melt inclusions and groundmass glasses. Symbols are the same as Fig. 3. Melt inclusions hosted in olivine show abrupt decrease in S content, and the change lacks correlation with FeO. **Figure 3.5.** (b) Measured S concentration in olivine-hosted melt inclusions as a function of sulfur concentration at sulfide saturation (SCSS). In this figure, the samples at the saturation can be seen on the solid grey line (1:1 line). The dashed line shows the SCSS corrected for abundance of S^{2-}, which was 0.85, the maximum value. All data plots below the corrected SCSS. SCSS is calculated according to Fortin *et al.* (2015) using the trapping temperature (T_{trap}) of the melt inclusion (Table A1) at 0.05 GPa (for NKD14) and 0.1 GPa (for KKO, OJSU, OJSL, and KSS) based on estimated volatile saturation pressure of the pre-eruptive magma reservoir. For melt inclusions without measured H_2O concentration, I attributed average H_2O concentrations (by SIMS) of NKD14 and KSS.

500 ppm, Le Voyer *et al.* 2015). This suggests that F addition to the subarc mantle was insignificant.

The Cl/F ratios of melt inclusions globally reflect the composition of the slab-agent added to the mantle source as F fractionate from Cl depending on the physical character of the flux leaving the slab (Le Voyer *et al.* 2010; Van den Bleeken and Koga 2015; Narvaez *et al.* 2018). Observed Cl/F ratio of melt inclusions from Aso volcano are relatively high (from 1 to 2.5, Fig. 3.6) compared with that of MORB (Saal *et al.* 2002; Wanless and Shaw 2012; Wanless *et al.* 2014, 2015; Le Voyer *et al.* 2017; Shimizu *et al.* 2019b). Because Cl/F values in arc magma are characterized by several parameters such as the composition of slab, nature of the fluid and fractionating minerals in residual slab, and the degree of melting of arc magma, the physical character of slab derived flux is determined with a set of assumptions. In any case, the primitive magmas with MORB-like F concentration and a high Cl/F value (2.2) are found among the melt inclusions of calc-alkaline arc magmas in a typically “cold” subduction setting (Straub and Layne 2003; Rose-Koga *et al.* 2014). The halogen characteristics of our Aso melt inclusions were in the range of typical arc magma, and the value of the primitive magma was close to the melt inclusions of Iwate volcano, a prototypical example of the arc magma derived from aqueous fluid driven from a cold oceanic crust (Rose-Koga *et al.* 2014). This indication is consistent with studies based on high bulk B/Nb ratios indicating aqueous fluid additions from the subducting Philippine sea plate in the source of the Aso basalt-basaltic andesite rocks (Miyoshi *et al.* 2008a, b). Other studies based on Sr, Nd, and Pb isotope variations of Quaternary lavas in the northern Kyushu area also support the model of slab-derived aqueous fluid addition from the subducted Philippine sea plate beneath Aso volcano (Shibata *et al.* 2014).

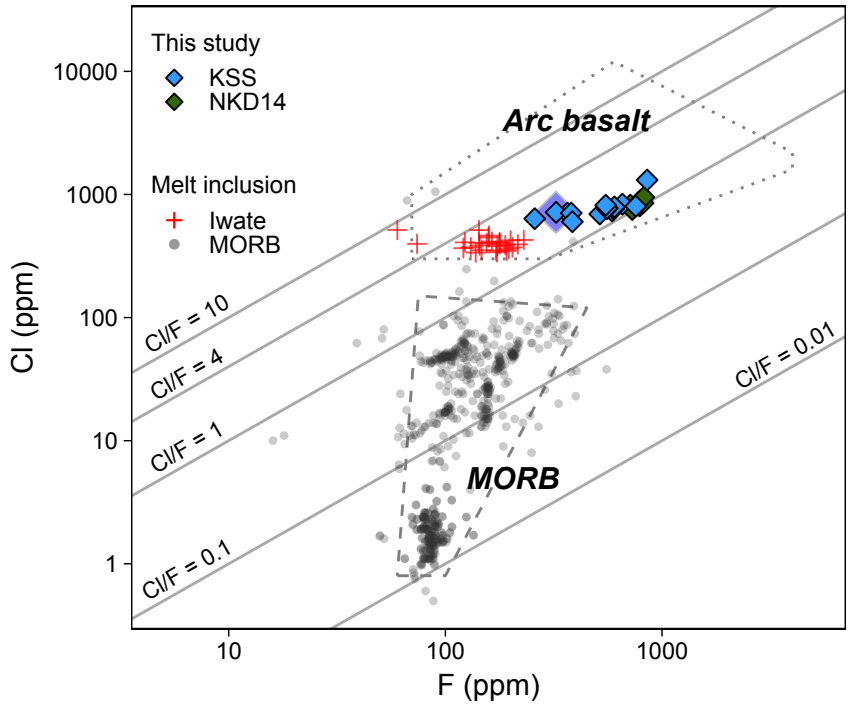

Figure 3.6. Variations in Cl and F concentrations of melt inclusions (KSS and NKD14) plotted in decadic log scale. The KSS and NKD14 data are compared with the volatile rich mafic primitive magma, represented by a large blue diamond. The two areas are indicated to show the Cl and F concentrations in primitive arc basalt and MORB, which were measured in olivine-hosted melt inclusions (taken from Van den Bleeken and Koga 2015). MORB melt inclusions were plotted as solid light-grey circles (Saal *et al.* 2002; Wanless and Shaw 2012; Wanless *et al.* 2014, 2015; Le Voyer *et al.* 2017; Shimizu *et al.* 2019b) including Cl-rich data of assimilated MORB samples by seawater derived component. Melt inclusions from Iwate volcanoes, one of low F concentration arc lava from Japan arc, is shown as an example of a cold subduction zone (red plus sign, Rose-Koga *et al.* 2014). The lines show the constant Cl/F values, and the values are indicated above the line.

3.4.4. Storage depth of the magma mixture

Solubility of volatiles in magma strongly depends on pressure and temperature conditions, and the chemical composition of the magma (e.g. Dixon *et al.* 1995). In this section, I discuss the storage depth of the mixed-magma based on H_2O concentration. For example, measured volatile concentrations of melt inclusions are considered to be re-equilibrated to a

condition of a magma storage. Alternatively, it is also possible to determine H_2O concentrations estimated from plagioclase rim and groundmass glass pairs (geo-hygrometer, Lange *et al.* 2009), likely corresponding to the value of the mixed magma during the plagioclase rim growth. The H_2O concentrations of such mixed magmas are, ~2 wt.% for NKD14 and KKO, and ~3 wt.% for OJSU, OJSL and KSS (Table 3.5). Here, the hygrometer calibrated for the total fluid pressure is equal to $P(H_2O)$, neglecting the role of CO_2. Yet, these values are comparable to those measured in the melt inclusions, and indicate a magma chamber pressures of 0.5 kbar for NKD14 and KKO, and 1.0 kbar for OJSU, OJSL, and KSS (*i.e.* 2.1 and 4 km deep, respectively, Fig. 3.7, note the depth is calculated using a density of 2200 kg/m^3 for the first 1 km and 2700 kg/m^3 for the crust at greater depths (Komazawa 1995), by solving for the depth, h [m], P = g {2200 (1000) + 2700 (h-1000)}). Because CO_2 concentrations in the felsic group melt inclusions are notably low (0 - 77 ppm, Table A1), it makes negligible changes to the calculated equilibrium pressure (~20 MPa, using RhyoliteMELTS/MagmaSat, Ghiorso and Gualda 2015). These pressures correspond to the depths of magma storage after mixing, since (1) the last growth rim of plagioclase must have occurred after mixing, as both normal and reverse zoning plagioclase have the same rim composition. (2) It is less likely that plagioclase rim significantly grew during sub-Plinian and Strombolian eruption. Melt inclusion H_2O concentrations range from 0.47 to 2.89 wt. %, indicating the minimum equilibrium pressure in agreement with the plagioclase-rim method. Two magma chambers, C2 and C1, detected by geophysical studies are also located at similar depths, 1 - 4 and 3 - 10 km, respectively (Tsutsui and Sudo 2004; Sudo *et al.* 2006; Hata *et al.* 2016; Fig. 3.7). At the depths, because the solubility of CO_2 is so low, the conclusion presented here would remain the same even if the hygrometer calculation does not account for CO_2.

Table 3.5. Results of thermo-barometric calculation for mixed magma

Volcanic cone	Nakadake	Kamikomezuka	Ojodake		Kishimadake
Sample	NKD14	KKO	OJSU	OJSL	KSS
An content (Pl-rim)[a]	63	70	77	79	78
Temperature (˚C)[b]	1039–1047	1062–1070	1036–1046	1033–1044	1027–1037
H_2O in melt (wt.%)[b]	1.97–2.26	1.54–1.83	2.83–3.10	3.01–3.30	2.91–3.20

[a] Mode of plagioclase-rim composition.

[b] Temperature and H_2O content are estimated based on groundmass glasses and plagioclase compositions after Sakuyama et al. (2014). Ranges of estimated values correspond with the range of assuming crustal condition (0.1–0.5 GPa).

The magma of the mafic endmember is expected to have more than 4.68 wt. % H_2O, and it is therefore derived from a greater depth than these C1 and C2 storage depths. The corresponding equilibrium pressure is approximately 2.7 kbar (SolEx, Witham *et al.* 2012; note MagmaSat give 2.3 kbar, Ghiorso and Gualda 2015; with CO_2 of 340 ppm reported in a melt inclusion from Nakadake by Saito *et al.* 2018) that is about 10 km deep below the edifice. As gas bubbles were seen in melt inclusions, large amounts of CO_2 incorporated in such shrinkage bubbles significantly increases the entrapment pressure estimation (e.g. Moore *et al.* 2015). Therefore, our pressure estimations are minimum and true entrapment pressures of the basaltic magma certainly occurred at a depth greater than 10 km. Recent melt inclusion studies reported more than 40-90 % of the initial CO_2 that was dissolved in the melt at the time of entrapment was lost to shrinkage bubbles, with an average loss of 75-80 % (Hartley *et al.* 2014; Moore *et al.* 2015; Wallace *et al.* 2015). If 90 % of initial CO_2 is present in the shrinkage bubble and a maximum CO_2 value of 340 ppm is assumed in the melt (from Saito *et al.* 2018), then the expected initial value of the melt would reach 3400 ppm. This value is in the same order of magnitude as the initial CO_2 concentration in a typical primary arc magma (Aster *et al.* 2016), and in this case the saturation pressure would exceed 5 kbar (~19 km depth equivalent).

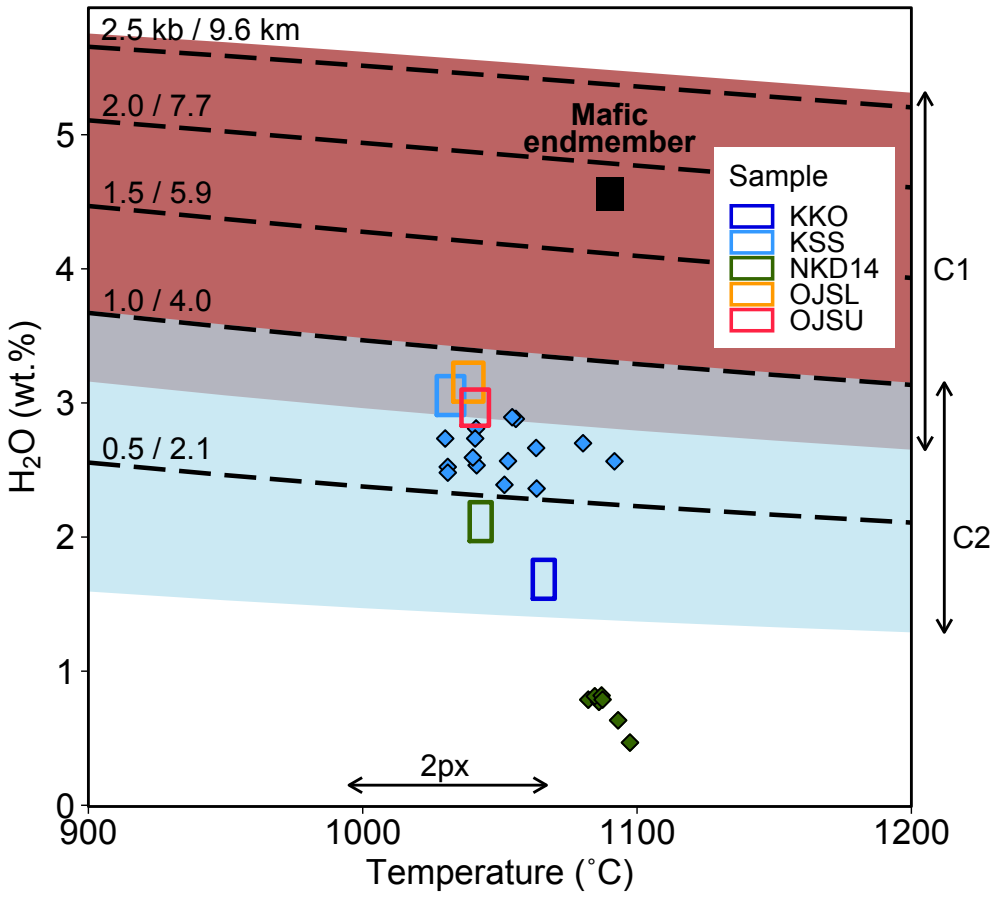

Figure 3.7. Pre-eruptive temperatures and water concentrations calculated from the compositions of plagioclase rim and groundmass glass. The squares represent the estimated range of temperature and H_2O concentration. The calculation was based on a combination of a plagioclase-olivine-liquid hygrometer (Lange *et al.* 2009) and olivine-saturated liquid geothermometer (Sugawara 2000; Médard and Grove 2008) according to Sakuyama et al. (2014), assuming the crustal conditions (0.1 – 0.5 GPa). Standard deviations (1σ) of the difference in temperature and H2O concentration between estimation and expectations using this method were 23 ˚C and 0.6 wt. %, respectively. The dashed lines represent water saturation isobars for groundmass glass composition of KSS calculated according to Moore *et al.* (1998); the corresponding pressures (kbar) and the depths (km) are indicated to the left of the line. The depth in the crust was calculated assuming a density of 2200 kg/m^3 for less than 1 km depth and a density of 2700 kg/m^3 for depth greater than 1 km (Komazawa 1995). The red and blue colors show the range of the magma storage depths: red, C1 from 3 to 10 km depth, and blue, C2 from 1 to 4 km depth beneath Nakadake's first crater (Sudo and Kong 2001; Sudo *et al.* 2006; Hata *et al.* 2016).

However, at the time of this study, bubble sizes were not documented with impossibility to go back to measuring them *a posteriori* since most are now polished away. In this case, I chose not to use the CO_2 data of the melt inclusions. Hata *et al.* (2016) also reported a magma pathway from depths deeper than 11 km, feeding the deeper C1 reservoir. Also, the presence of a seismic low-velocity layer at 11 - 25 km depth was reported and attributed to a magma ponding location beneath the Aso caldera (Abe *et al.* 2010). These observations are in good agreement with our petrological implication for the presence of volatile-rich basaltic magma beneath C1 magma reservoir at a depth greater than 10 km.

3.4.5. Persistent degassing from a deeper magma reservoir (>10km)

3.4.5.1. Excess degassing of SO_2 and CO_2 from Nakadake 2014 eruption

Decomposition of magma mixing endmembers and the subsequent identification of the primitive magma composition provide critical information for investigating volcanic emission of gas and its mass balance. For the 2014 eruption of Aso volcano, the mass of erupted magma is insufficient to account for the mass of the observed SO_2 gas emissions (Saito *et al.* 2018), which is commonly reported in many active volcanoes and is called “excess degassing”. For Aso, approximately 90 – 140 times more magma than the erupted tephra mass is needed to account for the observed total SO_2 emission of 1.4 – 2.2 $\times 10^5$ tons for the period of 70 days from Nov. 2014 to Feb. 2015 (Table 3.6 and; also Saito *et al.* 2018). As demonstrated in the sections above, NKD magma is a mixed magma, so the gas phase must have come from the degassing of mafic and felsic endmember magmas. For this reason, I have used the highest volatile element concentrations determined for Nakadake samples (*i.e.* mixed magmas) for the sulfur budget calculation (Supplementary material A4). This calculation simply demonstrates that the mixed magmas are inadequate sources of the observed volcanic gas flux. The most commonly proposed explanation for this excess is the existence of a gas/fluid phase in the

magma, possibly containing C-O-H-S and co-existing with the magma prior to the eruption (e.g. Anderson 1973; Wallace 2001; Scaillet and Pichavant 2003; Shinohara 2008). The magmatic volatile component must originate from the volatile-rich magma corresponding to the basaltic/mafic endmember. This magma must degas at a deeper depth than that indicated by the equilibrium solubility depth of NKD samples (~2 km at the depth of C2). Therefore, the degree of S excess should be re-assessed with a deeper, volatile-rich, basaltic magma. It should be noted that the observation of S-excess is common (*e.g.* Wallace and Edmonds 2011) and I simply point out here that the eruption of Nakadake edifice of Aso also shows such excess.

There are geophysical observations indicating that degassing is fed by volcanic activities corresponding to depths deeper than ~2 km. The SO_2 gas emission of Aso volcano is continuously monitored during the eruptive and the quiescent periods. The amount of SO_2 emission during the quiescent period (alternatively, "persistent degassing"; Shinohara 2008) is more than 100 – 200 tons/day from 1975 to 2006 (Mori *et al.* 2013). Ground deformation measurements since 1937 revealed deformation (deflation) of the deeper C1 magma reservoir synchronous to gas emission from Nakadake cone during the quiescent period (Sudo *et al.* 2006). This C1 deformation, located approximately 3 km West of Nakadake, causes no significant deformation on the surface around the crater. This degassing is therefore interpreted as open-system degassing of the C1 magma reservoir through stable conduit passages to Nakadake crater (Yamamoto *et al.* 1999; Sudo *et al.* 2006). Furthermore, deflation of the C1 reservoir was seen to slow down from 2008 to early 2014, before acceleration of inflation of the C1 reservoir from July 2014, shortly before the eruption in November (Ohkura *et al.* 2015; JMA 2016). These changes were accompanied by a sudden increase in persistent SO_2 gas emission in September 2013, considered as a precursor to the 2014 - 2015 eruptive period (JMA 2016). These temporal and spatial relationships of geophysical observation and degassing activities strongly indicate the role of the deeper C1 reservoir during degassing.

However, to sustain replenishment of the Cl reservoir, the magma must be supplied from an even deeper depth (greater than 10 km; Sudo *et al.* 2006; Hata *et al.* 2016). For example, the slowing down of deflation in 2008 and subsequent inflation in 2014 can be interpreted as events relating to magma replenishment of the Cl reservoir (Ohkura *et al.* 2015, 2017).

I also found excess degassing of CO_2 for this eruption period. Using the maximum pre-eruptive CO_2 concentration of 340 ppm measured in a melt inclusion of Nakadake eruption products (Saito *et al.* 2018), and assuming there is no pre-eruptive vapor phase approximately 1700 – 2700 times more dissolved CO_2 is required to account for the observed 0.77 – 1.2 $\times 10^6$ tons of CO_2 emission (Table 3.6). In the case of Aso, the gas phase must be derived from a depth greater than that of the C1 reservoir.

3.4.5.2. Modelling degassing of the deep magma reservoir

In the sections above, the equilibrium depths of volatile concentration in magma were used to indicate magma storage depth, where stagnated-magma and gas remain at equilibrium. Equilibrium gas composition at that depth should be the source of the gas composition observed at the surface, only if the gas segregated and travelled to the surface without precipitating solids or re-dissolving gas in between. In detail, the speciation of mixed gas is a function of pressure, temperature, and oxygen fugacity, but the gas system composition can be considered closed. With this hypothesis, it is possible to determine the depth at which the observed gas composition is in equilibrium with a magma (e.g. Burton *et al.* 2007; Allard 2010).

Fig. 3.8 is a result of such a calculation using SolEx (Witham *et al.* 2012), showing the variations in H_2O/S, CO_2/S, and Cl/S molar ratios of gas in equilibrium with a magma as a function of pressure. The observed H_2O/S gas composition of the 2014 eruption (shown as horizontal dotted red lines) intersects with the equilibrium gas composition (plain lines Fig. 3.8) between 2.6 to 3.3 kbars. These pressures correspond to 10 - 13 km depth below the edifice. The family of curved lines represent the results of the model with varying initial CO_2

Table 3.6. Comparison of the measured volatile emission with petrological estimation for Nakadake 2014 eruption

		H_2O	CO_2	SO_2	HCl
Total emitted mass (ton)[a]	min	1.2×10^6	7.7×10^5	1.4×10^5	5.6×10^3
	max	1.8×10^6	1.2×10^6	2.2×10^5	8.7×10^3
Pre-eruptive concentration in melt (wt.%)[b]		1.08	0.034	0.069[d]	0.196[d]
Exsolved volatile from magma (ton)[c]		14000	440	1600	1400

[a] Total mass of each volatile species were computed from observed gas composition of $CO_2/SO_2 = 8$, $H_2O/SO_2 = 30$ and $HCl/SO_2 = 0.07$ in mole (Shinohara 2013, 2018) assuming observed average SO_2 emission rate of 2000 - 3100 ton/day from November 18, 2014 to January 9, 2015 (JMA 2016, 2020) for 70 days.

[b] Pre-eruptive volatile concentrations were estimated for an average K2O concentration of groundmass glass times the maximum volatiles/K_2O ratios of NKD14 melt inclusions. For pre-eruptive CO_2 concentration, I chose the highest reported value (340 ppm) of Nakadake eruption products (Saito et al. 2018).

[c] Total masses of exsolved volatiles from erupted magma were calculated using the total mass of erupted products of 2.0×10^6 ton during the eruption of 2014 - 2015 (Yokoo and Miyabuchi 2015) assuming all S degassed as SO_2.

[d]Values with asterisk are shown as S and Cl.

concentration (400, 750, and 1000 ppm), as the initial CO_2 concentration was unknown (but for sure higher than 340 ppm). For the range of degassing trajectory, the observed Cl/S values (horizontal dotted blue line) intersect with the model calculations between 2.6 and 3.8 kbars. H_2O/S and CO_2/S are less sensitive to the variation of the initial CO_2 concentration. It should be noted that the closed system degassing path here is used to find a unique pressure condition at which the observed high temperature gas composition is at the equilibrium with a mafic magma. The systematics shows that only CO_2 concentrations between 400 and 750 ppm can produce the observed gas composition at pressures between 2.6 to 3.3 kbars, satisfying the observed ranges of H_2O/S, CO_2/S, and Cl/S all at once.

Therefore, the observed gas composition must have been derived from the depth of about 10 to 13 km (~2.6 to 3.3 kb) at which it was in equilibrium with a magma with the initial magmatic CO_2 concentration between 400 to 750 ppm (Fig. 3.8). The determination of initial CO_2 is strongly tied to the Cl and S partitioning into H_2O-CO_2 fluid, and I think that these values may need to be revised once we have a better understanding of Cl and S element partitioning. Lastly, this conclusion is highly model dependent. Here, I chose to use SolEx for its agreement with the variation of S in the melt inclusions. However, one must be cautious with the use of SolEx, because it is shown to fail to reproduce degassing trajectories of other volcanoes (e.g., Werner et al. 2020).

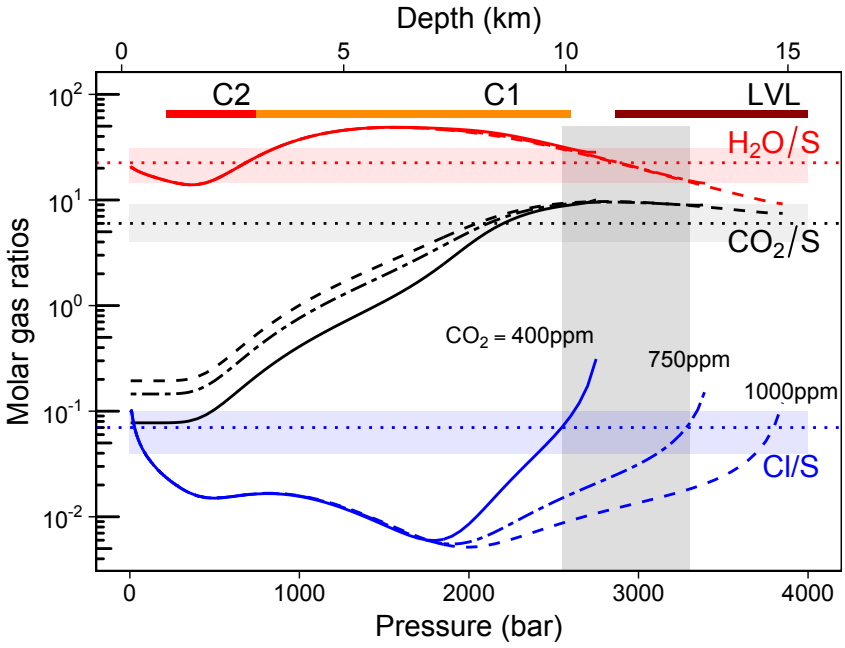

Figure 3.8. Evolution of H_2O/S, CO_2/S, and Cl/S molar ratios of magmatic gases in equilibrium with the primitive basaltic melt plotted against pressure. Horizontal dotted lines indicate measured gas compositions of $H_2O/S = 22.5$, $CO_2/S = 6$, and $Cl/S = 0.07$ (S as total sulfur) with the variation observed with propagated measurement uncertainties shown by shaded regions. The values correspond to high-pressure gas component A reported in previous studies (Shinohara 2013; Shinohara *et al.* 2018). SO_2 and H_2S components were added to calculate the total S. Horizontal colored bars at the top of the panel show pressure ranges corresponding to the C1, C2, and LVL. To evaluate the evolution of the gas composition of the basaltic magma from a great depth, I modelled the equilibrium compositions of gas and magma for a closed system magma ascent using SolEx (Witham *et al.* 2012). Grey field indicates the pressure range of 2.3 – 2.9 kbars, at which conditions the modeled gas compositions (solid and dashed curves) intersect with measured gas ratios. Thus, the observed gas composition potentially originated at these depths. I chose the primitive magma composition (discussed in the text) with values of FMQ+1.4 and 1090 ˚C based on the individual melt analyses. I tested initial CO_2 contents of 400, 750 and 1000 ppm for the calculation, as the CO_2 concentration was unknown to us. In combination with H_2O/S and Cl/S, the initial CO_2 concentration from 400 to 750 ppm produced the gas composition evolution curves that agree at a similar depth.

Fig. 3.9 shows the observed gas composition emitted from Aso volcano in the quiescent period and eruptive period. The gas data shown in Fig. 3.8 correspond to the eruptive period data (orange). While Fig. 3.8 demonstrated the occurrence of deep gas segregation, it does not explain the range of gas composition observed before and, even, during the eruption of the Nakadake cone. I modelled the variation in gas composition using (1) a degassing trend (solid line), the same model as that used in Fig. 3.8, and it fits the data with some scatter and (2) a mixing line (dotted line) between a deep reservoir, for example at the storage depth around 10 km, and a shallow reservoir (C2 or top of C1). Both explain the data (Fig. 3.9). Thus, on the one hand, it is possible to consider the variation in gas composition as the variation in gas segregation depth. On the other hand, the observed gas composition variation potentially represents the different degrees of mixing between discharged gas from NKD14 magma at shallow depth and segregated gas from a deep reservoir (*i.e.* gas segregation depth at 10 km; Fig. 3.8 and 3.10). Case 1 is less likely to apply here. Because of the closed-system degassing model (solid line), the ascending primitive magma would have been expected to be in equilibrium with gas all the time until it reaches near the surface. Therefore, the gas composition representing the low pressure must have been in equilibrium with the mafic magmas at the shallowest depth. However, no volcanic product of primitive composition was found during the eruption of Nakadake cone. Instead, observed volcanic products were all the result of mixing. As case 1 is unlikely, I conclude that the mixing of gases (case 2) is the process explaining the observed compositional variation. The gas mixing could have been possible, for example, by bubble accumulation at the roof of a magma chamber (Jaupart and Vergniolle 1988, 1989).

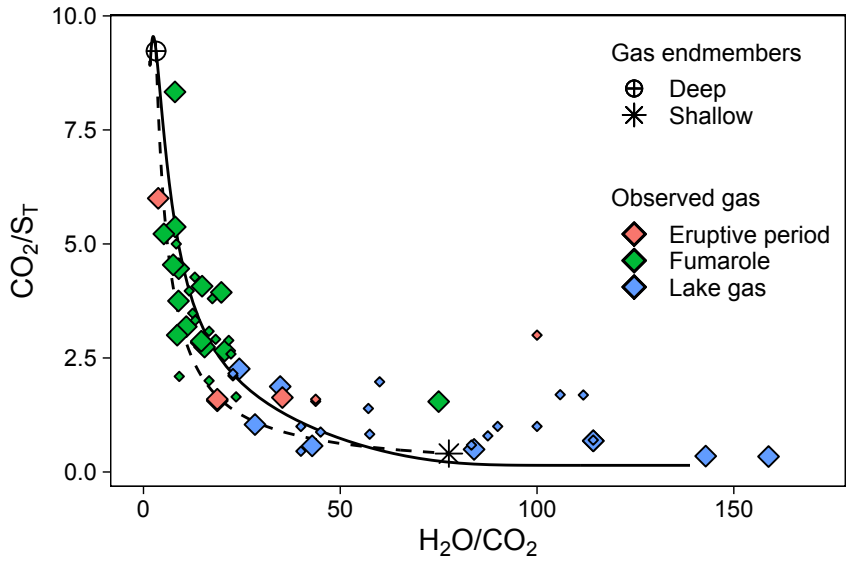

Figure 3.9. Observed volcanic gas compositions emitted from Aso volcano compared with modelled variation in CO_2/SO_2 and H_2O/CO_2 molar ratios. Observed gas compositions are those during quiescent periods (fumarole and lake gases) and during eruptive periods (Shinohara *et al.* 2018). Some data points were reported as poor-quality observations due to atmospheric H_2O, and they are plotted as smaller symbols. Note that apparent equilibrium temperatures (AET; Matsuo, 1960; Ohba et al., 1994) of all observed gas data presented here are higher than 480 ˚C and 81% of sufficient-quality data including lake gas has higher AETs than 600 ˚C. Solid curve is a modeled gas composition of closed-system ascent of primitive magma with 750 ppm initial CO_2 concentration, which is the same as that used in Fig. 8. The gas compositions on the curve indicate the different depths of gas segregation, and thus, the variation among observations can be attributed to a variation in segregation depths. Dashed curve shows a mixing curve between a CO_2-rich gas in equilibrium with the deep primitive magma at 2.6 kbar (crossed circle) and a gas discharged from NKD14 magma at shallow depth (asterisk) representing the gas stored at the shallow reservoir. The

3.4.6. Implications for understanding current Aso volcanic activity

This study identified the role of a volatile-rich, primitive magma during volcanic degassing (Fig. 3.10). During ascent, the volatile-rich primitive magma started to degas at a depth between 11 and 13 km (2.8 to 3.5 kbars, SolEx) based on the initial volatile concentration. The gas and magma reached 10 km depth maintaining equilibrium. At that depth, the gas segregated from the magma and moved to the surface without any significant modification.

The separation of gas from magma was potentially caused by stopping of magma ascent, which contributed to overpressuring of C1 observed by the deformation of the edifice. The magma then moved upwards and mixed with silicic magma in the C1 magma reservoir. While the exact depth of mixing was undetermined, the mixed magma was eventually stored at depths of C1 and C2 (for example 2 km (C2) for NKD14 and KKO samples, and 4 km (C1) for OJSU, OJSL, and KSS samples).

The segregated deep gas mixed with the shallow gases upon its ascent at shallower levels. I was unable to constrain the exact mechanism of the deep gas transport to the shallow depth without significant interaction. One possibility is the presence of porosity providing connected gas passages. However, this mechanism implies the rigid structure at a temperature lower than magmatic conditions, and this contradicts with the observation of the high temperature gas indicating magmatic degassing. Alternatively, a convection within C1 and C2 potentially serves a "gas pump". In this scenario, a shallow mixed magma (devoid of volatile elements) descends by convection to the bottom of C1 where gas segregation is occurring. Upon the return of such magma to shallow depth, it drags the gas component with it. Such parcel of magma may further pull gas bubbles from the shallow depth and result in a bulk system of mixed gas. If the magma degases completely, the resulting gas composition will be identical to the result of the gas mixing. This scenario would fail if some batch of magma do not degas and remain in some depth; it requires complete degassing. Shinohara (2018) proposed a model which suggested that the observed chemical variation in gases during eruption was caused by mixing of gases derived from magmas at different depths. This model is consistent with our gas mixing model. Our model furthered understanding of Aso activity, by (1) quantifying the volatile concentration of primitive mafic magma, and (2) by determining its degassing, segregation, and storage depths.

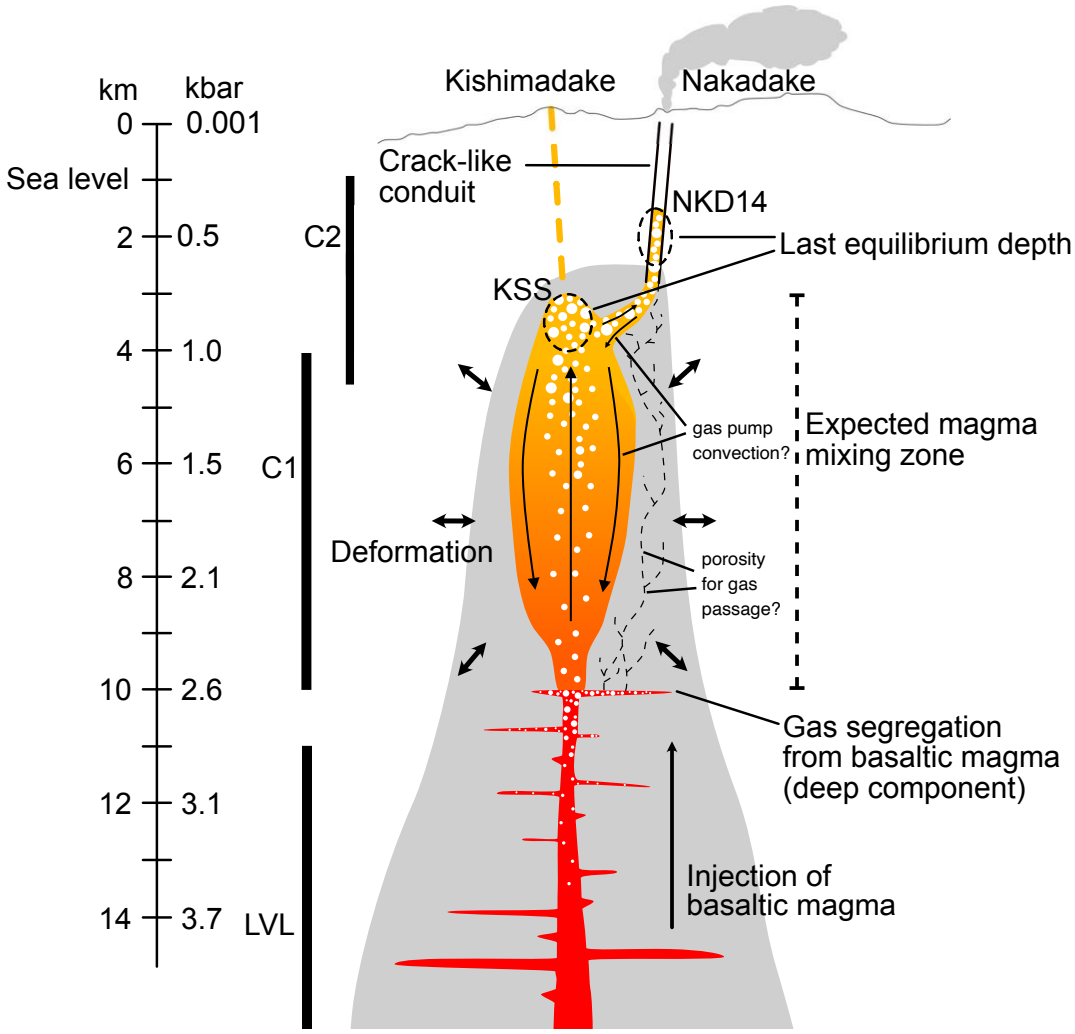

Figure 3.10. Schematic summary of the magma and gas evolution in the Aso plumbing system. Magma passage is indicated by the color ranging red-orange-yellow. The gas is white, and the grey zone corresponds to the conductivity anomaly (Hata *et al.* 2016). C1, C2, and LVL (black thick bars) are the zones of magma stagnations determined by geophysical methods (Yamamoto *et al.* 1999; Sudo and Kong 2001; Tsutsui and Sudo 2004; Sudo *et al.* 2006; Abe *et al.* 2010; Hata *et al.* 2016).

3.5. Summary and conclusion

Petrological analyses of melt inclusions in basaltic tephras from the late Holocene eruption of Aso volcano provided us with insights into the process of the persistent degassing in a magma plumbing system.

(1) The compositions of melt inclusions in phenocrysts from recent eruption products (Nov. 2014) of Nakadake cone were homogeneous, evolved and degassed (S < 434 ppm), while compositions of melt inclusions in phenocrysts from Kishimadake and other related cones (ca. 3.0 – 3.7 ka) showed variable compositions with two extreme endmembers. One was mafic (SiO_2 < 55wt.%) and volatile-rich, and the other was felsic (SiO_2 > 55wt.%) and relatively degassed. Mafic melt inclusions were hosted in high-Fo olivine and some plagioclase, whereas felsic melt inclusions were hosted in plagioclase, clinopyroxene, orthopyroxene and low-Fo olivine.

(2) Reverse mineral zoning, and highly variable mineral and glass compositions indicated a mixing process during which volatile-rich basaltic magma was injected in a degassed shallower magma.

(3) The estimated depths of pre-eruptive magma were approximately 2 km (C2 magma reservoir) for Strombolian eruption of Nakadake cone (Nov. 27, 2014) and Kamikomezuka cone (3.0 ka) and approximately 4 km (top of C1 magma reservoir) for sub-Plinian eruption of Ojodake and Kishimadake cones in 3.5 – 3.7 ka. These depths corresponded to the partially melted zones characterized by geophysical investigations (e.g. Hata *et al.* 2016). Furthermore, volatile-rich primitive magma originated from a deeper level (greater than 10 km) than these two magma reservoirs.

(4) Even with the highest S concentration of NKD14, it was impossible to account for the excess S gas emission. This suggests an addition of gas derived from the deep magma reservoir (greater than 10 km depth).

(5) Initial volatile concentrations of the volatile-rich primitive magma were determined from the systematics of melt inclusion, plagioclase compositions, and degassing model: >4.68 wt.% H_2O, 3750 ppm S, 716 ppm Cl and 324 ppm F.

(6) Emitted gas compositions constrained the initial CO_2 concentration ranges in the magma, between 400 and 750 ppm.

(7) The variation observed in volcanic gas composition was best explained by the mixing of the gas segregated at 10 km depth with those from the shallow reservoirs.

3.6. Bridge between Chapter 3 and Chapter 4

In the preceding chapter, the systematics of melt inclusion and host mineral compositions constraint on the storage depths and initial volatile concentrations of primitive magma beneath Aso volcano by combination with available gas measurement data. The next chapter uses the volatile concentrations, major and trace elements, and S isotope compositions of olivine-hosted melt inclusions from Aso and eight additional volcanoes in Kyushu subduction zone to investigate magma generation processes and mantle condition beneath Kyushu Island.

Chapter 4

Sulfur isotopes systematics in arc: seeing through the degassing via a melt inclusion study of Kyushu Island volcanoes, Japan

4.1. Introduction

Behavior of sulfur (and of its isotopes) in magma is complex because of its multiple valency and its partitioning into gas phase as well as solid. Because sulfur can be saturated in the magmatic system and crystallize sulfide, its geochemical behavior is expected to differ significantly from lithophile trace elements, such as lanthanide series rare earth elements (REE), or high field strength elements (Nb, Ta, Hf: HFSE). Yet, assessments of sulfur budget and its evolution in magma are the first order interest of volcanology and mantle geochemistry, especially since SO_2 in volcanic gas is considered as an indicator of magmatic flux beneath a volcano (e.g. Symonds et al. 1994; Métrich and Mandeville, 2010). Furthermore, sulfur isotope composition of arc magma sources is so far not determined precisely, partly because significant sulfur isotope fractionation is overprinted in erupted products (e.g. Mandeville et al., 2009). It appears nearly impossible to determine the source sulfur isotope composition through subaerial eruption products. This justifies systematic study of sulfur isotope composition in olivine-hosted magmatic inclusions, as the olivine-host can prevent diffusive sulfur-loss through the host crystal (e.g. Bucholz et al., 2013). However, olivine inclusions do not assure successful sampling of undegassed magmas; the melt inclusion studies of Lesser Antilles and Kamchatka have found indications of degassing (Bouvier et al., 2008; Gurenko et al., 2018), while $\delta^{34}S$ values were -9.0 to +7.0 ‰ and -1.6 to +12.3 ‰, respectively. These studies did not provide further assessments about the S isotopic compositions of the magma source. Clearly,

continuing efforts to understand sulfur systematics in different arc systems can help advance our understanding of the sulfur cycle in subduction zones.

Kyushu Island is one of the four main islands of Japan and known for its high concentration of active volcanoes; 12 volcanoes are considered active along the 240 km segment of Kyushu. This provides an ideal locality to sample Holocene eruption samples along an arc section. Despite this ideal setting, there are no systematic studies reporting melt inclusion compositions along this arc and characterizing the variations of the mantle below these arc volcanoes. Furthermore, sulfur fluxes out of the volcanoes are well-monitored, and for example, Aso volcano is known for its persistent sulfur emission (approximately 600 tons per day; Carn et al. 2017; Japan Meteorological Agency, 2020). It is therefore an ideal arc to investigate sulfur systematically along the arc segment. This study reports the sulfur isotope variation recorded in this volcanic segment, and its relation to the geodynamic setting of this arc.

4.2. Geological setting

4.2.1. Tectonic setting

The modern volcanic activities of Kyushu Island are related to the subduction of the Philippine Sea plate (Nakada and Kamata, 1991; Miyoshi et al., 2008ab, 2010; Shibata et al., 2014) composed of two segments of different ages divided by Kyushu-Palau ridge (Fig. 4.1a): young and hot northern segment (Shikoku Basin, 15 – 26 Ma; Okino et al., 1994), old and cold southern segment (West Philippine Basin, 30 – 54 Ma; Shibata et al., 1977; Deschamps and Lallemand, 2002; Ishizuka et al., 2018). Kyushu-Palau ridge is a remnant of Eocene–Oligocene arc that split away from the Izu-Bonin-Mariana arc, due to the spreading in the Shikoku Basin (e.g., Seno and Maruyama, 1984). Recent seismic and geomagnetic studies report the presence of the subducting Kyushu-Palau ridge beneath central Kyushu, precisely beneath the non-volcanic region between Aso and Kirishima volcanoes (e.g. Park et al., 2009; Fig. 4.1b). The

slab has been subducting aseismically, down to 430 km depth beneath Kyushu Island (Zhao et al., 2012; Fig. 4.1b).

P- and S-wave seismic tomography images identify a low-velocity zone along the subducting slab down to 300 – 400 km depth (Zhao et al., 2012; Liu and Zhao, 2016). The receiver function tomography instead shows dehydration at much shallower depths, which the hydrated oceanic crust is present to a depth of 70 km beneath Southern Kyushu, while it reaches 50 km beneath Northern Kyushu (Abe et al., 2013). This suggests the extensive dehydration beneath the fore-arc region in the north. Lastly, numerical simulations report the location of the low-velocity zone beneath the volcanic front to fore-arc region in Northern Kyushu and beneath the volcanic front to the back-arc side in the case of central to Southern Kyushu. This north-south dichotomy is due to the contrasting thermal state of the slab because of its age variation (Iwamori, 2007).

Low-velocity and high-Poisson's ratio anomalies are identified in the upper mantle beneath the back-arc region (Huang et al., 2013; Asamori and Zhao, 2015). This anomalous region extends from the Tsushima Strait in the north (between Korean peninsula and Kyushu Island) to the southern edge of the Kyushu Island. This anomaly extends beneath the back-arc to a depth of more than 200 km, reaching below the slab. It potentially indicates the existence of mantle upwelling, induced by a slab window. This mantle upwelling, originating beneath the Philippine Sea plate, is possibly caused by a deep dehydration reaction of the Pacific slab located below, suggesting a presence of a convective circulation of the "big" mantle wedge delimited by the larger (and deeper) Pacific slab (Zhao et al., 2009; Zhao and Tian, 2013).

4.2.2. Volcanism

The modern volcanism in Kyushu Island is grouped into three main volcanic provinces based on the distribution and geochemical signature: the Northern Kyushu, the Southern

Kyushu, and the back-arc region. The volcanic activity in the frontal-arc of the Northern Kyushu is characterized by hot-subduction zone magmatism, such as the eruption of adakitic-magmas from Yufu-Tsurumi volcano (YF in Fig. 4.1b; Sugimoto et al., 2006; Shibata et al., 2014) and the calc-alkaline high-magnesium andesites (6 – 3 Ma; Nakada and Kamata, 1991; Kakubuchi et al., 1995). Also in the north, High-alumina island-arc basalts are found in Kuju (KJ) and Aso (AS) volcanoes in 2 – 0 Ma (Nakada and Kamata, 1991; Mahony et al., 2011). The temporal evolution of the source mantle by progressive increase of the slab component potentially explains the variations of major and trace element signatures of the area (Nakada and Kamata, 1991). Oninomi (ON) basalt is an exception with an adakite and OIB-like affinity (i.e. high Sr/Y no HFSE depletion), and an eruption age of 16 ka (Ohta et al., 1992; Shitaoka et al., 2014).

In the Southern Kyushu, the modern activity is characterized by calc-alkaline magma for both the back-arc (7.6 – 0.4 Ma; Nagao et al., 1999) and the volcanic front, where Kirishima (KR) Sumiyoshi-ike (SM), Sakurajima (SK) and Kaimondake (KM) volcanoes are located (Mahony et al., 2011). Small amount of alkali basalts erupted at ~1 Ma (in the back-arc side, Uto and Uchiumi, 1997; Kita et al., 2012) and at 0.08 Ma (Aojiki cone adjacent to Sumiyoshi-ike volcano, Kita et al., 2012). In the back-arc region, alkali to tholeiitic basalts episodically erupted since ~15 Ma (Mahony et al., 2011). Onidake volcano on Fukue Island (FK, Fig. 4.1b; referred to as Fukue hereafter) is a typical active back-arc volcano in this region. Both alkali basalts and calc-alkaline andesites erupted at similar ages, in a zone between the frontal-arc and back-arc regions, such as Unzen volcano (UZ, Fig. 4.1b) and adjacent area, (Sugimoto et al., 2005; Kita et al., 2001).

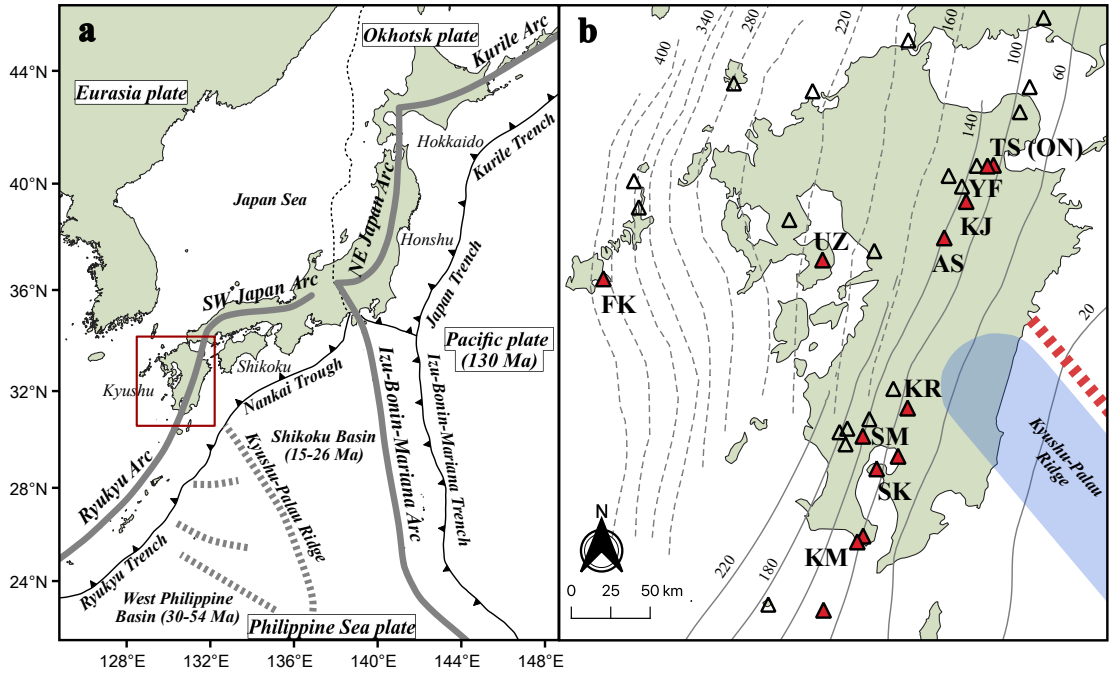

Figure 4.1. Map of the Japanese Islands arc and Kyushu sample locations. a) Map shows the major tectonic setting of Japanese Islands (after Miyoshi et al., 2008 and Mahony et al., 2011). Gray solid lines represent the volcanic front. Major ridge and plateau of the Philippine Sea plate are indicated by gray dashed lines. The formation ages of Philippine Sea plate are from Okino et al. (1994, 1998) and Deschamps and Lallemand (2002), and that of the Pacific plate is from Müller et al. (2008). Location of the study area is indicated by a red square. b) Map of the Kyushu Island showing target volcanoes. Open and solid triangles indicate the locations of Quaternary volcanoes. Active volcanoes are shown as solid. Gray solid lines and dotted lines denote the iso-depth contours to the upper boundary of the seismic (Nakamura and Kaneshiro, 2000; Baba et al., 2002; Nakajima and Hasegawa, 2007; Hirose et al., 2008; Saito, 2017) and aseismic parts of the subducting plate (Zhao et al., 2012), respectively. Blue field and red dotted line mark the inferred subducting Kyushu-Palau ridge and slab fracture, respectively (Park et al., 2009). FK: Fukue, UZ: Unzen, TS: Tsurumi, ON: Oninomi, YF: Yufu, KJ: Kuju, AS: Aso, KR: Kirishima, SM: Sumiyoshi-ike, SK: Sakurajima, KM: Kaimondake.

Magmatic H_2O concentrations are estimated to be 3.6 – 6.0 wt. % for Northern Kyushu volcanoes, calculated from the observed high-An plagioclase and whole rock compositions (Zellmer et al., 2012). This indicates basaltic primary magma were potentially water-rich, although source lithology and slab-derived fluid/melt characteristics are poorly constrained. Miyoshi et al. (2008ab; 2010) determined boron concentration in basaltic rock and identified B/Nb ratio increase from Yufu toward Kirishima, interpreted as an increase of slab-derived fluid contribution. Similarly, the partial melting of the subducted young Philippine Sea plate was suggested from the systematics of adakitic signature and Sr-Nd-Pb isotope ratios of rocks in Northern Kyushu (Sugimoto et al., 2006; Shibata et al., 2014).

4.3. Samples and Methods

4.3.1. Sample description

Nine olivine-bearing rocks were selected from 49 samples that I have collected, covering major active volcanoes of the Kyushu Island (Fig. 4.1ab and Table 4.1). I focused on the lapilli-sized samples to have higher chances of finding quenched volcanic products (no daughter mineral crystallization) and to minimize the effect of the diffusive volatile-loss (Danyushevsky et al., 2002; Lloyd et al., 2013). As an exception, I collected one lava block from a pyroclastic flow deposit from Yufu volcano (YF1L) since no olivine-bearing tephra were found. In this study, I examined only olivine-hosted melt inclusions from the collected samples. The inclusions of Kuju (KJ5S), Aso (KSS), Kirishima-Ohachidake (KROHTH), Kirishima-Shinmoedake (KRSM11), Sumiyoshi-ike (SM1S), Kaimondake (KM1S12a) and Fukue (FKONON) were glassy while those of YF1L were completely crystallized except for one sample. In the case of Oninomi (ON2S), the inclusions hosted in the core of olivines were mostly rounded and crystallized, while glass found at the rim of skeletal olivines tend to be clear, tubular and often connected with outside. Although olivines of FKONON were also

skeletal, the melt inclusions were fully enclosed. Complete descriptions about the appearance and size of the samples are given in Supplementary material Table B1 and document B10, following the recommended practices for melt inclusions study (Rose-Koga et al., 2021).

Whole rock sample descriptions are from the literature: YF1L is a mafic enclave found in Nonokusa pyroclastic-flow deposit (Ohta et al., 1990; Okuno et al., 1999), which is interpreted as an equivalent to the mafic endmember of Yufu-Tsurumi volcanic group (Ohta and Aoki, 1991); ON2S is a black coarse scoria forming the edifice of Oninomi scoria cone. It contains abundant granitic xenolith (Ohta et al., 1992); KJ5S is the Hiijidake scoria, a brown scoria fall deposit, erupted from the Hiijidake cone of Kuju volcano (Kamata, 1997; Nagaoka and Okuno, 2014; Kawanabe et al., 2015); KSS is the Kishimadake scoria, a black coarse scoria fall deposit, erupted from Kishimadake cone of Aso volcano (Miyabuchi and Watanabe, 1997), which is the same sample as in Kawaguchi et al. (2021); KROHTH is the Takaharu scoria, a black vesiculated scoria fall deposit, erupted from Ohachidake cone, from the Kirishima volcanic group, which corresponds to the fall unit ThT of Tsutsui et al. (2007); KRSM11 is a mixed andesitic pumice erupted in 2011 from Shinmoedake cone, from the Kirishima volcanic group, and corresponds to the Unit 2 of Miyabuchi et al. (2013); SM1S is a black fine to coarse scoria produced by a phreatomagmatic eruption of Sumiyoshi-ike volcano (Moriwaki et al., 1986); KM1S12a is a lithic-rich dense to vesiculated scoria, and corresponds to the fall unit Km12a of Fujino and Kobayashi (1997), erupted from Kaimondake volcano (Kawanabe and Sakaguchi, 2005); FKONON is a vesiculated coarse scoria, and corresponds to the Onidake scoria fall unit of Nagaoka and Furuyama (2004), erupted from the Onidake cone, from Fukue volcanic group.

Table 4.1. Sample list

Sample ID	Volcano	Cone	Latitude (N)	Longitude (E)	Sample type	Unit name	Eruption age
ON2S	Oninomi	Oninomi	33°19'00.65"	131°24'35.44"	Scoria	Oninomi	15.8 ± 2.5 ka[1]
YF1L	Yufu	Yufudake	33°15'58.52"	131°23'44.16"	Lava block	Nonokusa	2.1 - 2.5 ka[2]*
KJ5S	Kuju	Hiijidake	33°08'02.41"	131°16'57.50"	Scoria	Hiijidake	11.6 - 12.8 ka[3, 4, 5]*
KSS	Aso	Kishimadake	32°54'56.04"	131°06'25.95"	Scoria	Kishimadake	3.7 ka[6, 7]
KROHTH	Kirishima	Ohachidake	31°52'03.60"	130°56'33.29"	Scoria	Takaharu	AD 1235[8, 9]
KRSM11	Kirishima	Shinmoedake	31°53'33.38"	130°54'07.72"	Pumice	Unit 2 (Layer 2 - 4)	AD 2011[10, 11, 12]
SM1S	Sumiyoshiike	Sumiyoshiike	31°46'10.80"	130°35'21.28"	Scoria	Sumiyoshiike	8.2 ka[13, 14]
KM1S12a	Kaimondake	Kaimondake	31°10'18.57"	130°34'18.37"	Scoria	Km12a	AD 874[15]
FKONON	Fukue	Onidake	32°39'23.37"	128°51'20.29"	Scoria	Onidake	21.7 - 22.3 ka[16]*

*Reported ^{14}C ages were converted using Calib Rev 8.1.0 program (Stuiver and Reimer 1993; Stuiver et al. 2020) and the IntCal20 calibration curve (Reimer et al. 2020) to calendar age.

Reference: 1. Shitaoka et al. (2014), 2. Okuno et al. (1999), 3. Kamata and Kobayashi (1997), 4. Nagaoka and Okuno (2014), 5. Kawanabe et al. (2015), 6. Miyabuchi and Watanabe (1997), 7. Hirata et al. (2020), 8. Okuno et al. (1998), 9. Tsutsui et al. (2007), 10. Miyabuchi et al. (2013), 11. Nakada et al. (2013), 12. Iriyama and Toramaru (2015), 13. Moriwaki et al. (2002), 14. Okuno (2002), 15. Fujino and Kobayashi (1997), 16. Nagaoka and Furuyama (2004)

4.3.2. Melt inclusion preparation

Olivine-hosted melt inclusions of these nine samples were prepared for chemical analysis. Loose olivine crystals (250 to 630 μm) were hand-picked from crushed and sieved samples. The dimensions of inclusion and vapor bubble were measured under a microscope (Table B1). Crystallized inclusions of YF1L and ON2S were homogenized using a Vernadsky-type microscope heating stage following the method described by Le Voyer et al. (2010). A detailed description of the heating procedure was given in Supplementary material document B9. Fully enclosed inclusions were exposed using a silicon carbide mat for coarse polishing, and corundum mats (3 μm and 1 μm mats) were used to complete the polishing. To avoid possible carbon contamination, diamond-based paste was avoided. Polished olivine crystals were subsequently mounted in indium for analyses, and a final polish with a ¼ μm alumina paste was performed to remove scratches on the exposed surface.

4.3.3. Analytical methods

Volatile element concentrations (H_2O, CO_2, S, Cl, and F) in the inclusions were measured by SIMS (Cameca IMS-1280HR of Kochi Institute of Core Sample Research, JAMSTEC, Japan) following the procedure described by Shimizu *et al.* (2017), comparable to that of Rose-Koga et al. (2020) for F, S and Cl. In brief, I used a 20 keV Cs+ primary ion beam of 300 – 500 pA defocused to be 10 – 15 μm in diameter. Secondary ions were accelerated at 10 kV. A -10 keV electron beam with a diameter of ~100 μm was applied for electrostatic charge compensation over the area of the Cs beam spot. The field aperture was set to the size corresponding to 5 x 5 μm on the sample surface. Mass resolving power was set at ~6000 to separate mass interferences (for example, to separate $^{34}S^{1}H$ interference on ^{35}Cl requires 5120 MRP; Burdo and Morrison 1971). Negative secondary ions of ^{12}C, ^{16}OH, ^{19}F, ^{30}Si, ^{31}P, ^{32}S, and ^{35}Cl and the mass position of 11.9 amu were measured by an axial electron multiplier using the

peak switching method. An analysis consisted of 10 cycles, and the total measurement time for each analysis was ~6 min. Typical relative standard deviations (1σ) obtained from repeated analysis of a secondary basaltic glass standard from the East Pacific Rise, EPR-G3 (Shimizu et al., 2017), were 1.4, 3.2, 0.9, 2.5 and 1.5% for H_2O, CO_2, S, Cl and F, respectively.

Sulfur isotopes in the inclusions were measured by SIMS at 1) Kochi Institute of Core Sample Research, JAMSTEC, Japan (Cameca IMS-1280HR) and 2) Centre de Recherches Pétrographiques et Géochimiques (CRPG)-CNRS-Nancy, France (Cameca IMS-1270). At Kochi, analyses were conducted following the procedure described by Shimizu et al. (2019c). To summarize, I used a 20 keV Cs+ ion beam of ~0.5 nA defocused to be ~10 μm in diameter. A 10 keV electron beam of ~100 μm diameter was flooded on the sample surface for electrostatic charge compensation. Secondary ions were accelerated to 10 kV. The field aperture was set at the size corresponding to 15 × 15 μm^2 on the sample surface. Negative secondary ions of ^{32}S and ^{34}S were measured in multi-detection mode with an FC and axial EM, respectively. Mass resolving power was set at ~2200 and ~5000 for FC and EM detectors, respectively, to separate mass interferences of $^{31}P^1H$ on ^{32}S and of $^{33}S^1H$ on ^{34}S. Each measurement consisted of 20 s pre-sputtering, 120 s auto-centering of ^{32}S to the field and contrast apertures, and 5 s × 50 cycles for measurements. The total measurement time for each analysis was ~7 minutes. At CRPG, the setting was similar except I used a stronger primary beam of 3 nA defocused to be ~15 μm in diameter. Mass resolving power was set to 4500. Negative secondary ions of ^{32}S and ^{34}S were measured in the multi-detection mode with an FC and axial EM, respectively. Each measurement consisted of 60 s pre-sputtering and 5 s × 40 cycles for measurements, giving a total analysis time of ~5 minutes for each spot. Before each measurement, I adjusted the center for ^{32}S. In both cases, the standard basaltic glass, EPR-G3, was systematically measured during the analytical session to monitor EM drift and to define the instrumental mass fractionation factor (IMF) for ^{34}S: $IMF = (^{34}S/^{32}S)_{measured}/(^{34}S/^{32}S)_{reference}$.

Sulfur isotopes in the samples are expressed in $\delta^{34}S$ relative to the Vienna Canyon Diablo Troilite (VCDT, $^{34}S/^{32}S = 1/22.6436$; Ding et al., 2001; $\delta^{34}S = [(^{34}S/^{32}S)_{unknown}/IMF/(^{34}S/^{32}S)_{VCDT} - 1] \times 1000$, in per mil). The analytical error (2σ) obtained from repeated measurement of EPR-G3 standard during the analytical session was less than 1.2‰ for both SIMS laboratories.

Major element compositions of melt inclusion and host-olivine phenocryst were determined using a CAMECA SX100 electron microprobe at the Laboratoire Magmas et Volcans, Clermont-Ferrand, France (LMV). The analytical settings for silicate glass were 15 kV acceleration voltage, 4 nA beam current, with counting times at 30 s for Ti, at 20 s for Si, Al, Fe, Mg, and K, and at 10 s for Mn, Ca, and P. For olivine, I used 15 nA beam current with counting time at 30 s for Ca, at 20 s for Si and Al, at 15 s for Ti and Cr, and at 10 s for Fe, Mn, Mg, and Ni. Beam diameter was set at 5 or 10 μm depending on the size of the inclusion, and focused for olivine measurements. Relative analytical uncertainties (1σ) obtained from repeated measurements of the basaltic glass standard (VG-2, Juan de Fuca ridge basalt, Jarosewich et al., 1980; Dixon et al., 1991) were less than 0.6% for SiO_2, 1% for Al_2O_3, FeO and CaO, 3.5% for TiO_2 and Na_2O, 10% for MnO, 1.5% for MgO, 4.5% for K_2O, 17% for P_2O_5.

In addition, S, Cl and F concentration of 12 melt inclusions were also determined, using a 40 nA beam current with counting times of 50 s for S and Cl, and 200 s for F. For each analysis, an average of 5 measurements were taken. The standard deviations (1σ) for S, Cl, and F were less than 143 ppm, 95 ppm, and 397 ppm, respectively.

Sulfur speciation of selected inclusions was determined by measuring a relative sulfur *Kα* peak position in a melt inclusion sample compared to the standard anhydrite mineral using the EPMA (Carroll and Rutherford, 1988), with an assumption that S^{2-} and S^{6+} are the only two relevant species in silicate melt (e.g. Jugo et al., 2010). I took an average of 3 spots per melt

inclusion, and the standard error (1σ) is approximately ±10% S^{6+}/S^{Total} for samples with S concentration > 1000 ppm.

Trace element concentrations in melt inclusions were determined using a laser ablation system (193 nm Excimer Resonetics M-50E laser ablation system) coupled with an inductively coupled plasma mass spectrometer, Agilent 7500 cs (LA-ICP-MS) at LMV following the classical procedure described by Rose-Koga et al. (2012, 2017). Analyses were conducted with a laser pulse frequency of 1–3 Hz, a spot diameter between 15 and 33 µm depending on the MI size, and a fluence of 2.8 mJ/cm^2. Twenty-six masses were collected: ^{7}Li, ^{45}Sc, ^{51}V, ^{65}Cu, ^{85}Rb, ^{88}Sr, ^{89}Y, ^{90}Zr, ^{93}Nb, ^{137}Ba, ^{139}La, ^{140}Ce, ^{141}Pr, ^{146}Nd, ^{147}Sm, ^{153}Eu, ^{157}Gd, ^{163}Dy, ^{166}Er, ^{172}Yb, ^{175}Lu, ^{178}Hf, ^{181}Ta, ^{208}Pb, ^{232}Th, ^{238}U. The internal reference mass was ^{44}Ca, where the CaO concentrations were measured by electron microprobe. A typical signal acquisition started by collecting a background for 30s, which was followed by the laser firing for 70 s or less depending on the thickness of the inclusion. Data reduction was performed by the GLITTER software (GEMOC, Macquarie University, Australia). BCR-2G, NIST 610 and NIST 612 glasses (Gao et al., 2002; Gagnon et al. 2008) were also analyzed to monitor the reproducibility and accuracy of the analyses. Typical relative standard errors on samples (1σ error of mean; $\sigma/\sqrt{n}$, where n is the number of cycles) were < 5% for V, Rb, Sr, Y, Zr, Ba, La, and Ce, < 8% for Sc, Nb, Pr, and Nd, < 15% for Cu, Sm, Eu, Gd, Dy, Er, Hf, Pb, Th, and U, < 25% for Li, Yb, Lu, and Ta.

4.4. Correction for post-entrapment modification

4.4.1. Post-entrapment crystallization

Major, volatile and trace element concentrations of melt inclusions were corrected for the post-entrapment crystallization (PEC; e.g., Danyushevsky et al., 2000) by incremental addition of equilibrium olivine (0.1 wt. % step) into the melt, until it reaches equilibrium with

host olivine (Toplis, 2005). I adopted a constant Fe^{2+}/Fe^{Total} ratio calculated from the empirical equation of Kilinc et al. (1983) from the averages of measured S*K*α peak shifts. A single fO_2 value is assumed to represent a rock sample (Jugo et al., 2010). Olivine-melt equilibrium temperatures were calculated using the olivine-saturated melt thermometer of Sugawara (2000), corrected for the effect of H_2O on the olivine liquidus temperature (Médard and Grove, 2008). The correction for post-entrapment Fe-Mg exchange (also called "diffusive Fe-loss"; Danyushevsky et al., 2000) was not necessary (see Supplementary material document B9), because the FeO concentration in melt inclusion plot along the compositional trend defined by the whole rock data. Concentration of volatile and trace elements was adjusted by assuming their perfect incompatibility in the host olivine (Table B2). The corrected concentrations were used throughout the paper (Table B8). Raw data are reported in supplementary, Tables B3, B4 and B5).

4.4.2. Vapor-bubble formation

In general, more than 40 – 90% of the initial CO_2 that was dissolved in the melt at the time of entrapment is lost to the shrinkage bubbles, when a vapor bubble growth occurs within an inclusion (e.g. Wallace et al., 2015). Therefore, the total CO_2 concentration in a melt inclusion was determined as (dissolved + exsolved),

$$CO_2^{Total} = CO_2^{Melt} + \phi \frac{\rho_v}{\rho_m} \times 10^6$$

where CO_2^{Melt} is the dissolved CO_2 concentration in the melt, ϕ is volume fraction of the bubble in the melt inclusion, ρ_v is the volumetric CO_2 vapor density, and ρ_m is the melt density, calculated from the glass composition. The ϕ is determined based on measurements of the two visible axes, a and b, under the microscope (Table B1) assuming the length of the third axis as c = (a + b) / 2 (e.g. Tucker et al., 2019). The ρ_v value was estimated using RhyoliteMELTS ver. 1.2.0 (Ghiorso and Sack, 1995; Gualda et al., 2012; Ghiorso and Gualda, 2015), based on a

CO_2-H_2O solubility at the glass transition temperature, T_{glass}, and an equation of state (EOS) for the fluid (Duan and Zhang, 2006). The T_{glass} value was calculated from the temperature dependence of the viscosity with the given hydrous glass composition and a constant viscosity of 10^{12} Pa·s (Giordano et al., 2005, 2008). The total CO_2 concentrations were first calculated using measured glass composition and the equation above, and then, they were corrected for PEC similarly to other volatile elements. This EOS method calculates ρ_v under the assumption that bubble and melt were in equilibrium until the bubble ceases to expand. Since carbon (C) diffusion is temperature dependent, if the diffusive closure temperature was effectively higher than T_{glass}, bubble would expand without C exsolution, resulting in an overestimation of ρ_v and of the total CO_2 concentration (e.g. Pichavant et al., 2013; Bali et al., 2018). If this non-equilibrium expansion has occurred, the estimated total CO_2 concentration represents a maximum value.

As an additional test, I calculated the expected vapor bubble volume in a melt inclusion based on the method of Moore et al. (2015), which uses the extent of post-entrapment cooling and thermal contraction of the melt and host olivine. This calculation provides an upper limit of the bubble size that could have formed by post-entrapment cooling and tests whether a melt inclusion contained a pre-entrapped bubble or not. The "CO_2 bubble correction" was not applied for the inclusions that had a bubble volume fraction exceeding the expected value. This was because the calculation of total CO_2 depended strongly on the bubble volume fraction. Therefore, if the pre-entrapment bubble was present, the observed bubble volume would have been larger than the expected shrinkage bubble. This would result in an overestimation of the total CO_2.

The major source of error of the total CO_2 in the inclusions was the uncertainty of the melt inclusion volume, as the volume is estimated assuming an ellipsoid with measurements of only two axes. A recent numerical simulation reported that the assumption taking an

arithmetic mean for the third ellipsoid axis yields a relative error (1σ) of 37% to 48% (Tucker et al., 2019). I conservatively assigned a 50 % (1σ) relative uncertainty to inclusion volumes. The uncertainties (1σ) on the total CO_2 concentration range from 10 to 50% after accounting for the volume error (Table B6).

4.5. Results

4.5.1. Major element compositions

Melt inclusion of this study varied from compositions of basalt to andesite with SiO_2 ranging from 40.3 to 60.7 wt. % (Table B2, Fig. 4.2). Fo content [Mg / (Fe + Mg) × 100 in mole] of host olivine varied from 65.2 to 83.1 (Table B7). The composition of melt inclusions forms tight clusters for each tephra sample, except Aso and Oninomi. The melt inclusions of Fukue, Yufu and Sumiyoshi-ike were classified as alkali-basalt to picrobasalt and basanite. Those of Kuju, Kirishima-Ohachidake, Kirishima-Shinmoedake and Kaimondake were sub-alkaline basaltic andesite. Melt inclusions of Aso exhibited a wide range of SiO_2 and were classified as transitional basalt and sub-alkaline basaltic andesite to andesite (Kawaguchi et al., 2021). The melt inclusions of Oninomi varied from basanite to basalt, except for one andesite inclusion. Basanite magma are rare around Kyushu Island especially from the volcanic front (Iwamori, 1991, 1992). Similar basanite rocks were found in the northern part of the Izu-Bonin volcanic arc (Oshika et al., 2014) and in primitive rocks from the central Chugoku district, SW Japan (Iwamori, 1991, 1992). The subalkaline melt inclusions from the Northern Kyushu were higher in total alkali ($Na_2O + K_2O$) compared to those from the Southern Kyushu for the same SiO_2 concentration.

4.5.2. *Trace element compositions*

The melt inclusions in this study were enriched in large-ion lithophile elements (LILE) over high field strength elements (HFSE) resulting high LILE/HFSE values (Fig. 4.3), characteristic of island arc basalts (IAB; e.g., Elliott, 2003). Positive K, Pb and Sr anomalies were present. Positive Sr anomaly in samples from the Northern Kyushu (Yufu, Kuju, Aso) was stronger than that from the Southern Kyushu (Kirishima, Sumiyoshi-ike, Kaimondake). The patterns of Fukue and Oninomi displayed no Nb-Ta negative anomaly and high Nb concentration (Nb ≥ 23 ppm) as it was described with the whole rock data (e.g., Ohta et al., 1992; Miyoshi et al., 2008). Light rare earth element concentrations (LREE) in the melt inclusions of Oninomi were higher and HREE lower compared to those of Fukue (Fig. 4.3). Two melt inclusions of Oninomi were extremely rich in Ba, La, Pr and Nd.

4.5.3. *Volatile element and sulfur isotope compositions*

H_2O and CO_2 concentrations in melt inclusions were corrected for PEC and post-entrapment vapor bubble growth, and the corrected values were used throughout the paper. H_2O concentration varied between 0.01 and 6.06 wt. % (Table B2), and there was no systematic difference between northern and Southern Kyushu. H_2O concentrations within the same tephra sample varied less than approximately 1 to 2 wt. % (Fig. 4.4). CO_2 concentrations ranged from a few ppm to 1.2 wt.% (Fig. 4.4). S, Cl and F concentrations varied from 142 to 3793 ppm, from 89 to 1437 ppm, and from 55 to 1166 ppm, respectively (Table B2). The high volatile contents indicated the successful sampling of less-degassed, near-primitive volatile in magmas.

Chlorine concentrations in the melt inclusions varied from 89 to 1437 ppm but with less than 7% of the melt inclusions with Cl <500ppm (8 out of 117; Table B2). These Cl concentrations were higher than those of MORB (max ~500 ppm Cl; e.g. Le Voyer et al., 2015), indicating the addition of Cl to the sub-arc mantle from the subducting slab (e.g., Straub and

Layne, 2003). Similarly, F concentrations in melt inclusions (55 to 1166 ppm) were higher than that of MORB (71 to 576 ppm; e.g. Le Voyer et al., 2015), indicating the variable degree of F addition from the subducted slab. Those elevated Cl and F values were characteristics of typical arc basalts (e.g., Rose-Koga et al., 2014; Van den Bleeken and Koga, 2015).

Measured $\delta^{34}S$ values ranged from -0.3 ± 0.8 ‰ to +9.4 ± 0.5 ‰ (Table B4), and were significantly higher than those of typical MORB (-0.91±0.50‰, Kanehira et al., 1973; Sakai et al., 1984; Peters et al., 2010; Labidi et al., 2012, 2014), and within a range of reported bulk S data of Japanese arc volcanic rocks (from -0.2 to +18.3‰, Ueda and Sakai, 1984). Fukue and Oninomi showed relatively lower $\delta^{34}S$ values, a maximum of +3.6 ± 1.2‰ compared with those of other samples, which majority were higher than +3.4‰ (Table B4).

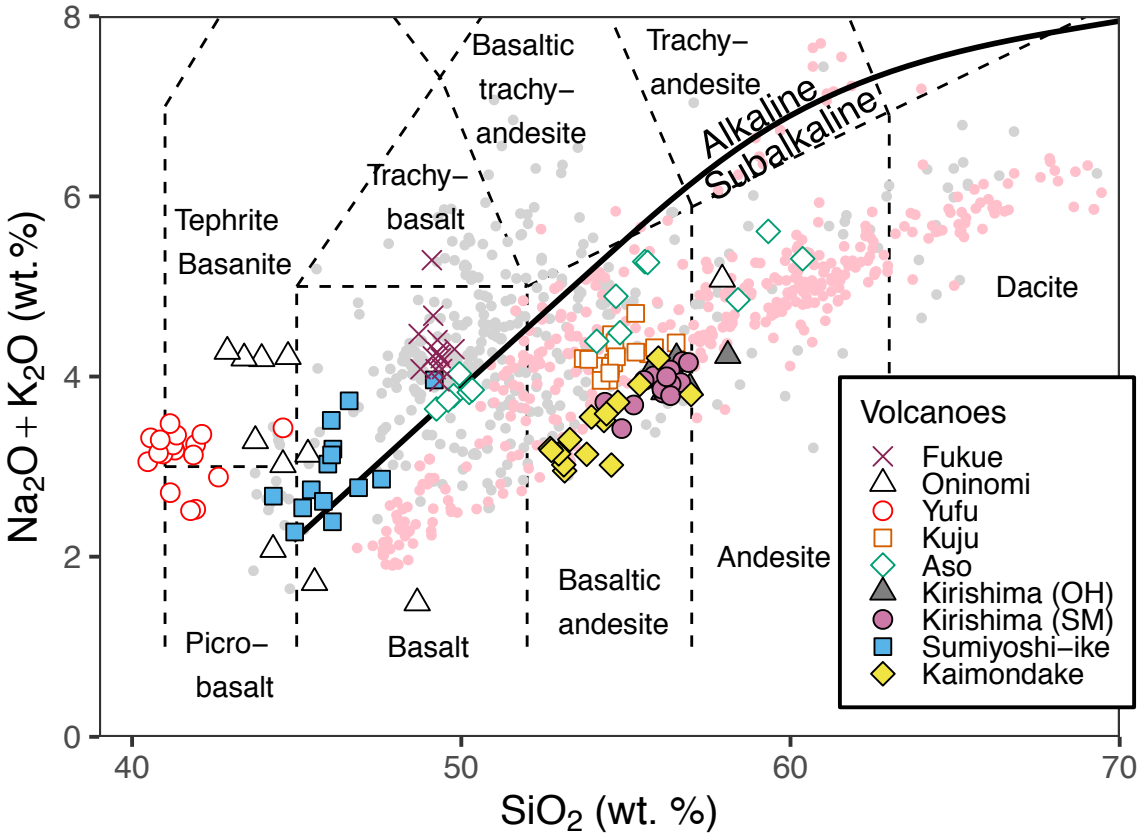

Figure 4.2. Total alkali ($Na_2O + K_2O$) vs. SiO_2 diagram for olivine-hosted melt inclusions. Dashed lines represent boundaries of classification of volcanic rocks (Le Maitre et al., 2002). Black solid line indicates the boundary between alkalic and sub-alkalic volcanic rocks (Miyashiro, 1978). All oxide concentrations were corrected for post-entrapment crystallization and normalized to 100 wt. % as volatile-free. Reported whole rock compositions of Kyushu Island volcanic rocks are shown as small solid circles for comparison: pink, volcanic rocks along the volcanic front; grey, other volcanic rocks of Kyushu. WR data: Sawamura and Matsui, 1957; Shinno, 1966; Nakamura, 1971; Nakada, 1986; Nakada and Kamata, 1988; Kakubuchi and Matsumoto, 1990; Ohta et al., 1990, 1992, Ohta and Aoki, 1991; Iwamori et al., 1991, 1992; Nagao et al., 1992; Kakubuchi et al., 1995; Imura and Kobayashi, 2001; Kita et al., 2001, 2012; Uto et al., 2004; Kawanabe and Sakaguchi, 2005; Sugimoto et al., 2005, 2006; Miyoshi et al., 2005, 2008a, b, 2010, 2011; Sakuyama et al., 2009, 2014; Hoang et al., 2013; Tajima et al., 2013, 2014; Shibata et al., 2013, 2014; Kawanabe et al., 2015; Yamasaki et al., 2016; Kuritani et al., 2017; Brown et al., 2020; Nche et al., 2021.

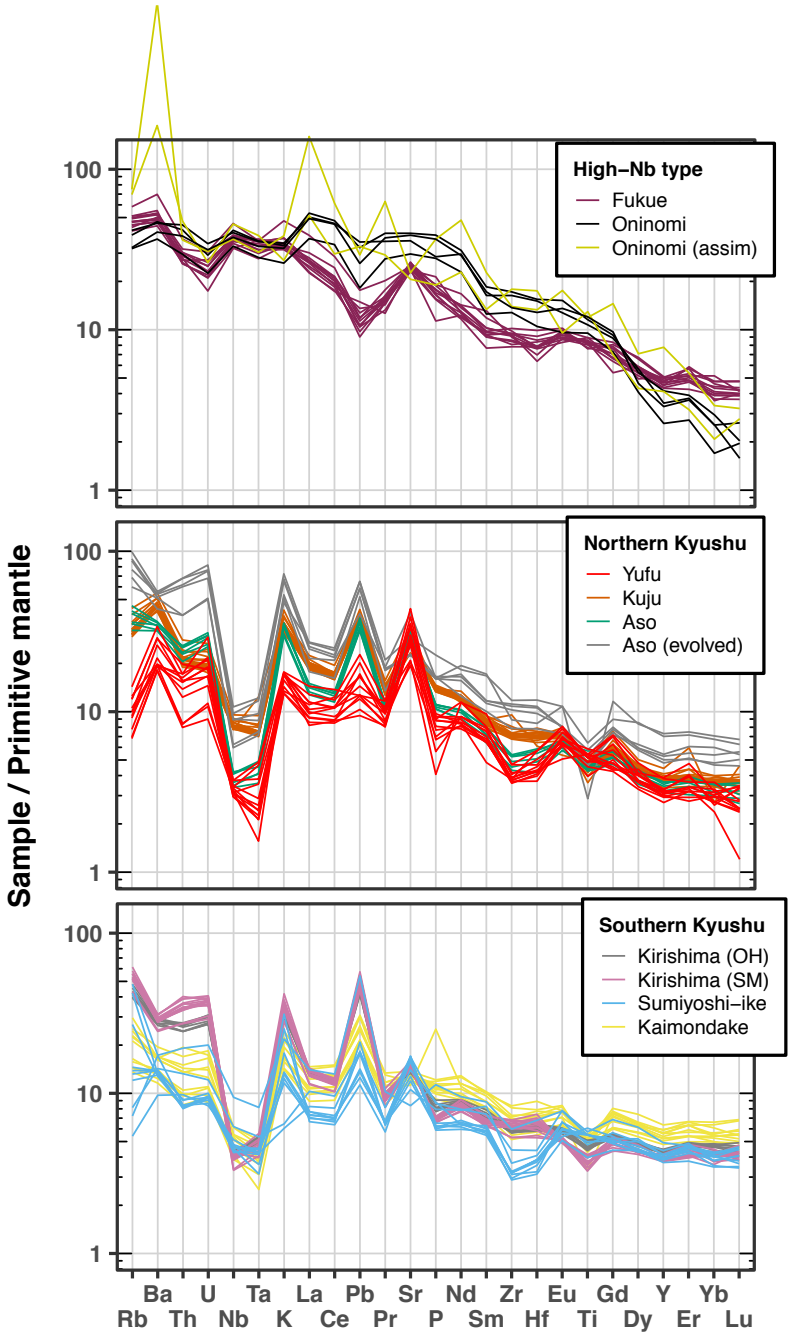

Figure 4.3. Primitive mantle-normalized trace element compositions of melt inclusions. The evolved melt inclusions of KSS (higher than 52 wt.% SiO_2 on hydrous basis) and assimilated inclusions of ON2S were indicated by different colors, as they may be influenced by secondary processes. Composition of the primitive mantle was taken from Sun and McDonough (1989). The order of elements after Pearce et al. (2005).

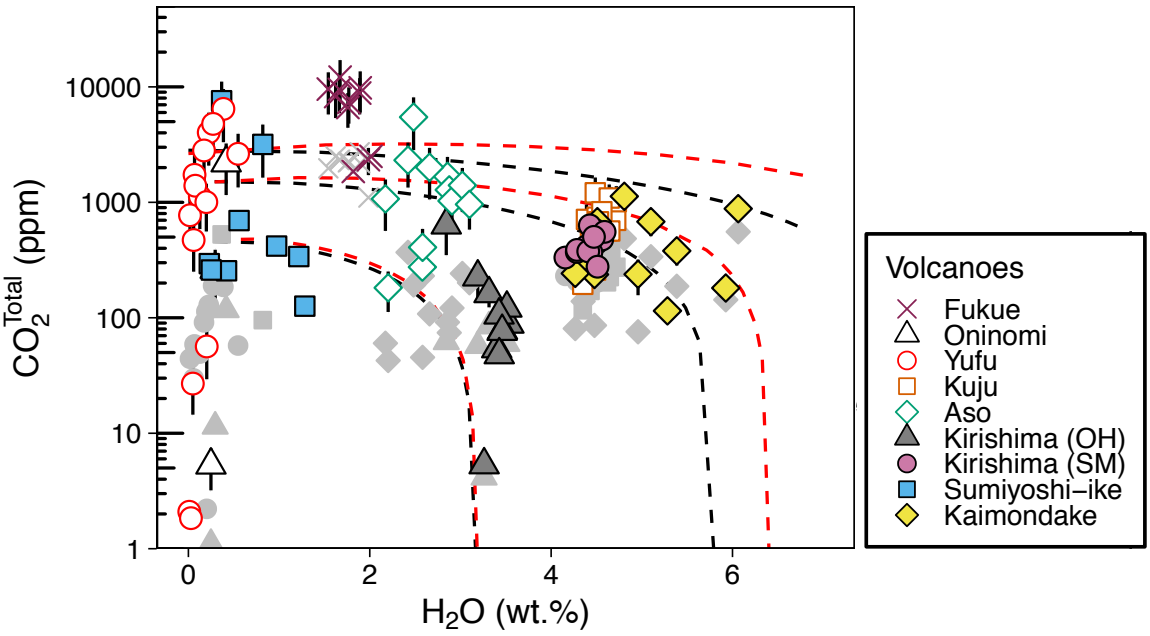

Figure 4.4. H_2O and CO_2 concentrations in melt inclusions. The concentration was corrected for PEC and for gas bubbles. Gas bubble-uncorrected CO_2 concentrations measured in melt inclusion were also shown as light grey symbols. Dashed contour lines represent solubility at 1, 3 and 5 kbar (from inside to outside) with 1100 ˚C, calculated for typical basaltic melt of 49 wt.% SiO_2 and 1100 ˚C using VolatileCalc (black lines, Newman and Lowenstern, 2002) and for our K-rich melt inclusion (FKONON-O-I) using MagmaSat (red lines, Ghiorso and Gualda, 2015). Error bar is standard error (1σ).

4.6. Discussions

I first seek to identify the primitive magma of each volcano, seeing through potential crustal modifications, then discuss melting processes and characteristics of slab-derived components added to the source mantle. While an olivine-hosted melt inclusion is considered as a droplet of magma trapped early in the growing crystal, and it is little modified by crystal fractionation in the crust. However, the observed geochemical variations in melt inclusions

may not be completely free from pre-entrapment modifications. Therefore, it is necessary to exclude the effect of any pre-entrapment crustal processes such as crystal fractionation, magma mixing, wall-rock assimilation, and pre-entrapment volatile element degassing, before interpreting the chemical variations of melt inclusion compositions. Once such analysis is done, the remaining variation represents the melting and metasomatic processes in the source region.

4.6.1. Major and trace element composition of the primitive melt of each volcano

The combinations of incompatible and compatible elements and their ratios are useful indicators to discriminate the effects of fractional crystallization, magma mixing and partial melting of source (e.g. Fourcade and Allegre, 1981; Schiano et al., 2010). Following the method of Schiano et al. (2010), I decipher for each volcano, if the variation in melt inclusion composition is due to mixing, partial melting or crystal fractionation (Supplementary material document B9). In detail, in some cases, the inclusions showed insignificant compositional variation within a sample (Fig. 4.5a), and those compositions were placed at the mafic end of whole rock variation (Fig. B9-4). In other cases, the inclusions showed variations of Ba/Nb ratio, which is a trace element ratio of two highly incompatible elements considered to be unmodifiable during mantle partial melting and crystal fractionation in magma (Fig. 4.5b). Overall, each sample appears to form a distinct cluster (e.g. Kirishima, Kuju), or on the contrary, a trend (e.g. Kaimondake, Yufu), when plotted on different sets of major and trace elements (Fig. 4.5a). From this general inspection, I concluded that a distinct primitive magma (or magmas) exists for each sample, and I could therefore propose a primitive melt composition for each volcano.

All inclusion samples, except for those of Fukue, show significant variations of trace element ratios, such as Rb/Nd and Th/Nd, indicating that magma mixing and/or partial melting is the dominant process rather than fractional crystallization (Fig. B9-3). Those incompatible

element ratios do not fractionate with early crystallization of phases such as olivine, plagioclase, and pyroxene (see inset, Fig. B9-3). Then, I investigated the geochemical variations by individual volcano (Fig. B9-4). In brief, I found that the magmas of Yufu, Aso, Sumiyoshi-ike and Kaimondake showed geochemical systematics indicating magma mixing and/or crustal assimilation. Then, element fractionation during partial melting was identified for the magmas of Kuju, Kirishima-OH and Kirishima-SM. And the variations of the final group, Fukue and Oninomi, were best explained by crystal fractionation (Fig. B9-3). Because the major and trace element data of Fukue formed a tight cluster, I chose the least evolved melt based on trace elements (i.e. lowest concentrations), as representative of the primitive melt of Fukue (A-I, Fig. B9-3).

Compositions of primitive magmas of the studied volcanoes are summarized in Table 4.2. These primitive melt compositions have the lowest SiO_2 contents among the magma series of each volcano, with high MgO, and low incompatible element concentration. Trace element ratios are expected to reflect the composition of mantle derived magma, before modification in the crust. The Fo contents of the host-olivines were more evolved (from 73 to 83) than the expected mantle value of 89. This suggests that our "primitive magmas" potentially have suffered from influence of pre-entrapment crystal fractionation and/or pre-entrapment magma mixing. Alternatively, low Fo content can be acquired through Fe-Mg exchange with evolved magma while maintaining the trace element abundance at the time of entrapment (e.g. Cottrell et al., 2002; Rose-Koga et al., 2021). In this case, primitive trace element and isotope compositions are conserved in the inclusion.

Melt inclusions of Oninomi show a wide range of SiO_2 concentration from 42.7 to 58.6 wt.% and the variation is larger than that reported for the bulk rocks (51.0 – 54.5 wt. % SiO_2, Ohta et al., 1992). While 10 out of 11 inclusions are less than 48.5 wt. % SiO_2, one melt inclusion has an andesitic composition (U-I, 58.6 wt. % SiO_2, Table B2). This andesitic

inclusion is tubular and glassy, trapped in the rim of an olivine, indicating a late-stage entrapment during the crystallization of a cooler magma (Table B1 and Supplementary document B10). I exclude this inclusion in the rest of the discussion, because of its texture, and the reported evidence of crustal assimilation in Oninomi basaltic lava, such as presences of granitic xenoliths and disequilibrium quartz phenocrysts (Ohta et al., 1992), and a high $^{87}Sr/^{86}Sr$ ratio (0.704821±0.000011, Kita et al., 2001; Shibata et al. 2014). Similarly, the anomalous enrichment of Ba, and LREE found in the two melt inclusions (L-I and DZ-I) is again attributed as indication of crustal assimilation (Fig. 4.3). The remaining inclusions show nearly identical trace element pattern (Fig. 4.3), suggesting a similarity in their origin. I chose the least evolved melt in this group as the primitive melt composition, representing Oninomi volcano (Z-I).

The melt inclusions from Aso volcanoes (KSS), especially the ones from the eruptions of the last 3700 years, were previously described and showed compositional variations and phenocryst textures consistent with magma mixing (Kawaguchi et al., 2021). Typically, evolved melt inclusions were trapped in reversely zoned olivine, with lower Fo content in the core (< 72) than the rim (68-78), while primitive melts were trapped in normally zoned olivine. The data in this study corroborates such a conclusion. As shown in Fig. B9-4, the melt inclusions and reported bulk rock data of Aso volcano indicates the systematic of magma mixing (Schiano et al., 2010). For Aso (KSS), the least evolved melt of the mafic endmember is taken as the closest to the primitive composition (K-II).

There is no previous trace element data reported for Kaimondake volcano, and this limited our “test” to find definitive conclusions on the systematics of its magma composition. Kaimondake illustrates a weak concave-down curve on Rb versus Rb/V and Rb versus Rb/Sr indicating magma mixing between a mafic magma and a more evolved magma (Fig. B9-4). From this systematics, the composition of a melt inclusions from the mafic endmember was chosen as the primitive magma composition (J-I).

Melt inclusions of Sumiyoshi-ike (SM1S) show a variation requiring three component mixing (Supplementary material document B9). First, significant variations in K_2O (or K_2O/TiO_2), Rb and Ba/Nb are seen for a given SiO_2 (Fig. 4.5, and Fig. B9-5), indicating that the presence of at least two distinct parental magmas since such incompatible element variations are not possible to generate by fractional crystallization or partial melting of a single source. Furthermore, the plot of Ba/Nb against K_2O/TiO_2 (or Rb/Sr) shows that a third component is required to explain the compositional variation of the inclusions (Fig. B9-5ab). One component appears to be a granite added via crust assimilation previously described by Pb isotope systematics (Brown et al., 2020). The other two endmembers are the low K_2O/TiO_2 with lowest Ba/Nb endmember (S-II), and the low K_2O/TiO_2 with the highest Ba/Nb (AA-I), and they are considered as the two endmembers of primitive magmas.

For Yufu volcano (YF1L), a negative linear correlation between SiO_2 and incompatible element concentrations, such as K_2O and Rb, indicates the mixing of two magmas. This correlation is independent from the mixing reported from the bulk rock chemical variations between a basaltic and a dacitic magma (Fig. 4.5 and Fig. B9-4, Ohta et al., 1990; Ohta and Aoki, 1991). Furthermore, this negative correlation cannot be generated by crustal assimilation, since the partial melt of a crust is SiO_2-rich melt (e.g. granite) with high incompatible element concentrations (e.g., DePaolo, 1981). Melt inclusions of Yufu show significant variation in Ba/Nb, which anti-correlate with SiO_2 concentration. The lack of correlation with K_2O/TiO_2 or CaO/Al_2O_3 ratios (not shown) indicates the Ba/Nb variations are not due to the assimilation of plagioclase or of crustal rocks. Therefore, the geochemical systematics of Yufu melt inclusions indicate a mixing, and the two endmembers have two distinct primitive melt compositions: high and low Ba/Nb (I selected BQ-III and BD-I, respectively).

Magmas of Kirishima (KROHTH, KRSM11) and Kuju (KJ5S) show geochemical systematics consistent with a variation of degrees of partial melting from a single source (Fig.

B9-4). For Kirishima volcano, this interpretation is consistent with whole rock studies showing the existence of two parental magmas generated by different degrees of partial melting of a similar source (Inoue, 1985; Miyamoto, 1997). The SiO_2 variations are so restricted that I decided to rely on trace elements for the choice of the most primitive compositions. I chose the melt inclusions with consistently the lowest trace element concentrations (i.e. highest degree of partial melting) representing the primitive magma compositions for Kuju (AD-V) and Kirishima (Ohachidake, G-I and Shinmoedake, E-II).

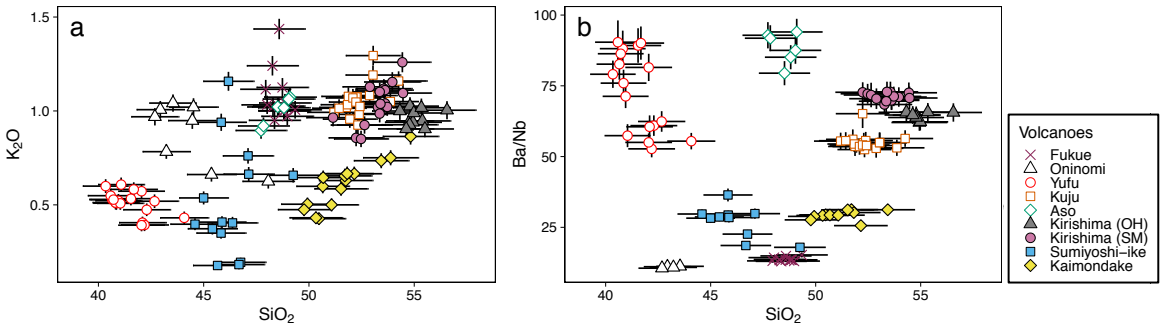

Figure 4.5. Variations of incompatible element concentrations in melt inclusions. (a) K_2O vs. SiO_2 shows absence of global correlation of Kyushu magmas. For individual volcanoes, Kaimondake and Kirishinma-Shinmoedake (SM) magmas show a positive correlation and Yufu shows weak negative correlation. (b) Ba/Nb vs. SiO_2 shows presence or absence of mixing, either of the source, magma, or crust. Yufu and Sumiyoshi-ike magmas show negative slope. Note, evolved melt inclusions of Aso are excluded for clarity (higher than 52 wt.% SiO_2 on hydrous basis).

4.6.2. Volatile concentrations in primitive magma

Volatile concentrations, especially concentration of H_2O and CO_2, in primitive arc magmas are critical geochemical parameters that can constrain models of magma genesis. While it has been studied extensively, a current consensus is that it would not be possible to

directly measure the primitive H_2O and CO_2 content from geological materials. In fact, because of the high-diffusivity of H_2O in host-olivines, measured H_2O concentrations of melt inclusions are likely equilibrated at crustal magma chamber depths (Portnyagin et al., 2008; Chen et al. 2011; Gaetani et al., 2012; Ferriss et al., 2018). Nevertheless, the H_2O concentrations trapped in melt inclusions are higher than those of erupted lava and therefore, it is considered to provide a minimum estimate. On the contrary to H_2O, the other volatile elements such as CO_2, S, Cl and F do not diffuse out through the host-olivine within the lifetime of a magma (e.g. Bucholz et al., 2013) and, they retain the values at the time of entrapment. It should be noted if CO_2 degassing starts before entrapment of the melt in the host olivine, the primitive CO_2 composition cannot be trapped in a melt inclusion.

In this study, several methods were combined to estimate the minimum H_2O content in the primitive magmas of each edifice and the values are reported in Table 4.2. First, the melt inclusions from Kuju, Kirishima, and Kaimondake displayed H_2O values from 2.8 to 6.1 wt. % (Table B2). These would commonly qualify as "high-H_2O" values for the arc magma (e.g. see compilation Cooper et al., 2012). Alternatively, H_2O content in magma can be estimated using plagioclase-hygrometer (Lange et al., 2009; Waters and Lange, 2015). It should be cautioned that the hygrometer records the water content in the magma at the time of plagioclase crystallization, which may happen after melt entrapment in olivine. Again, this is a minimum H_2O estimate for the primitive magma. For example, for the case of Aso, plagioclase hygrometer gives H_2O concentration of 4.7 wt. %, while measured H_2O concentration in melt

Table 4.2. Major, trace and volatile element concentrations and S isotope composition of melt inclusions selected as primitive represents

Sample ID	ON2S	YF1L		KJ5S	KSS	KROHTH	KRSM11	SM1S		KM1S12a	FKONON
Melt ID	Z-I	BD-I	BQ-III	AD-V	K-II	G-I	E-II	AA-I	S-II	J-I	A-I
SiO_2 (wt. %)	42.68	42.19	40.58	51.94	47.72	54.98	52.47	45.82	46.68	49.93	48.36
TiO_2	2.61	1.18	1.17	0.93	0.95	0.95	0.87	1.08	1.19	1.11	1.94
Al_2O_3	16.15	17.99	16.79	16.49	19.53	16.13	17.30	18.35	18.17	17.70	18.59
FeO^{Total}	13.25	13.12	16.74	10.58	9.33	9.85	8.37	12.37	14.98	9.38	8.64
MnO	0.28	0.13	0.14	0.22	0.09	0.16	0.20	0.20	0.11	0.27	0.17
MgO	9.05	11.07	10.12	4.25	4.74	4.22	3.76	5.88	6.19	4.72	5.61
CaO	10.43	11.65	10.52	7.26	10.73	7.52	8.34	13.26	8.97	8.50	10.56
Na_2O	3.29	2.87	2.59	2.87	2.63	2.82	2.65	2.02	3.55	2.53	2.92
K_2O	0.97	0.39	0.55	0.96	0.90	0.99	0.85	0.35	0.18	0.50	0.95
P_2O_5	0.80	0.03	0.26	0.18	0.29	0.19	0.18	0.10	0.14	0.11	0.28
P_2O_5 (SIMS)	0.80	0.15	0.20	0.29	0.23	0.17	0.14	0.13	0.17	0.24	0.34
H_2O[a]	2.31	2.36	3.29	4.39	5.75	4.55	4.59	0.97	1.28	6.06	2.01
CO_2^{Total} (ppm)[b]	2195	6450	6450	1210	5472	636	631	7583	7583	1127	12148
1 s.e. (rel. %)	47	49	49	36	48	45	28	47	47	29	40
S (ppm)	2078	2934	3487	2752	2952	800	1957	2694	3439	2326	1278
Cl (ppm)	783	1272	1212	1006	736	754	715	704	639	938	581
F (ppm)	1160	446	594	500	364	338	336	245	333	557	495
$\delta^{34}S_{V\text{-}CDT}$ (‰)	1.45	5.18	4.73	8.01	6.34	7.33	9.43	6.42	3.65	7.07	2.31
2 s.e.	0.79	1.13	0.79	0.47	0.55	0.67	0.47	1.02	0.55	0.57	0.49
Li (ppm)	6.90	–	–	9.35	7.98	15.52	12.89	–	1.38	5.60	–
Sc	19.8	66.1	53.1	23.3	27.7	34.4	32.3	47.3	52.3	34.2	27.2
V	229.3	374.3	344.9	237.9	364.0	358.1	313.6	442.5	470.0	263.9	251.9
Cu	24.5	45.5	37.4	7.1	137.4	108.6	49.7	35.2	64.6	5.8	21.8
Rb	20.63	4.42	8.16	18.57	20.40	24.95	26.72	4.59	3.43	10.44	29.71
Sr	818.6	587.0	819.6	544.9	664.0	289.4	319.5	269.3	222.5	274.6	511.8
Y	15.1	14.9	15.8	16.9	14.2	19.2	17.1	17.7	20.0	23.0	21.4
Zr	153.5	43.7	50.5	76.1	48.3	65.6	59.4	35.6	41.0	67.5	94.6
Nb	26.84	2.38	2.44	5.58	2.40	3.06	2.36	3.30	3.66	3.24	25.97
Ba	283.6	125.5	220.6	301.5	223.0	190.7	170.2	120.1	68.0	93.5	337.4
La	33.83	6.28	9.51	13.06	8.76	9.12	7.81	5.06	5.68	7.01	17.09
Ce	80.73	15.59	19.58	29.29	20.36	21.11	18.19	12.39	14.35	18.57	34.46
Pr	10.31	2.26	3.40	3.71	2.71	2.58	2.26	1.83	1.80	2.62	4.05
Nd	39.29	11.14	13.07	16.03	12.24	12.11	10.57	9.17	10.63	12.70	17.24
Sm	7.64	2.85	3.60	3.79	3.08	3.35	2.78	2.66	3.68	3.48	4.00
Eu	2.28	0.85	1.18	1.19	0.97	0.97	0.86	1.02	1.10	1.05	1.40
Gd	5.77	2.63	2.42	3.58	2.86	3.30	2.61	3.02	2.95	3.63	3.96
Dy	3.41	2.98	2.32	3.12	2.60	3.50	3.06	3.33	3.69	4.17	4.19
Er	1.75	1.89	1.80	1.93	1.46	2.34	1.90	2.17	2.34	2.58	2.31
Yb	1.26	1.35	1.85	1.80	1.47	2.18	2.08	2.02	1.87	2.59	2.18
Lu	0.12	0.18	0.22	0.27	0.20	0.31	0.31	0.27	0.30	0.37	0.32
Hf	3.96	1.34	1.04	2.05	1.29	1.97	1.63	1.19	1.26	1.93	2.35
Ta	1.36	0.10	–	0.29	0.15	0.20	0.17	0.17	0.17	0.15	1.29
Pb	4.79	1.75	3.05	7.20	5.93	7.70	8.13	2.62	3.25	3.99	1.67
Th	3.26	0.71	1.41	1.68	1.74	2.28	2.33	0.72	0.83	0.89	2.50
U	0.66	0.24	0.38	0.39	0.53	0.65	0.64	0.19	0.18	0.23	0.49
PEC%[c]	0	0	0	2.0	1.5	2.8	2.2	5.4	5.9	0	1.8
Olivine Fo%[d]	83.1	81.3	80.9	73.6	78.9	73.1	74.4	78.9	75.4	72.7	82.8

[a] Estimated minimum H_2O concentration (Table 4.3). See discussion for details.

[b] CO_2 concentration represent the highest value from each cone after corrections of post-entrapment crystallization and vapor bubble growth.

[c] Degree of post-entrapment crystallization in wt. % based on the equilibrium olivine addition.

[d] Fo content of host-olivine: Fo = Mg/(Fe+Mg)×100 in mole%.

inclusions is approximately 3.0 wt. % (Table B2, and Kawaguchi et al., 2021). In this case, 4.7 wt. % is reported as the minimum primitive H_2O content.

Another method for estimating H_2O content in magma is to adopt the maximum H_2O/K_2O ratio of the melt inclusions (Fig. 4.6a). As these elements are incompatible to silicate minerals in basalt, the ratio does not vary with crystallization. The highest ratio should indicate the minimum H_2O loss, if a magmatic suite shares the same parental magma. In the case of mixed magmas, H_2O/K_2O of the mafic endmember likely defines the least degassed ratio. This K_2O normalization also eliminates the effect of post-entrapment crystallization. Specifically, I looked for the highest H_2O/K_2O values of the melt inclusions and previous studies, in which H_2O content from the plagioclase hygrometer is combined with K_2O concentration of the whole rock sample (Table 4.3; Zellmer et al., 2012; 2014; Kawaguchi et al., 2021). The H_2O concentration is then calculated by multiplying the highest H_2O/K_2O ratio by K_2O concentration in the selected primitive melt (Table 4.2). This approach is especially effective for the samples from Oninomi, Yufu, Aso, and Kirishima samples, as H_2O in the inclusions was re-equilibrated to low values. It should be noted that the highest H_2O/K_2O ratios among the melt inclusions of each edifice, correspond to that of the selected primitive ones discussed in the previous section (Table B2), confirming the least degassed characteristic of our chosen primitive magma compositions. The exceptions were for Kuju, Yufu, and Sumiyoshi-ike, for which the highest H_2O/K_2O is not that of the selected inclusions representing primitive magma compositions. For Kuju, the difference of H_2O/K_2O between the highest melt inclusion and the selected primitive endmember were within the measurement uncertainty, so I chose to present the value of melt inclusion AD-V, which has the primitive character. Yufu and Sumiyoshi-ike melt inclusions both have two parental magmas (see previous sections) possibly indicating two sources with different H_2O concentrations; H_2O/K_2O of the magma cannot be assumed to be constant throughout mixing. On top of this, judging from the low H_2O

Table 4.3. Comparison of H_2O/K_2O ratio between melt inclusion measurements and plagioclase-hygrometer results, and estimated minimum H_2O concentration in primitive magma

Volcano	Oninomi	Yufu			Kuju		Aso	Kirishima			Sumiyoshiike		Kaimondake	Fukue
Cone	Oninomi	Yufudake			Hiijidake		Kishimadake	Ohachidake		Shinmoedake	Sumiyoshiike		Kaimondake	Onidake
1. Measurement of melt inclusion (this study)														
ID	Z-I	AH-I	BD-I	BQ-III	AK-I	AD-V	K-II	L-II	G-I	E-II	AA-I	S-II	J-I	A-I
H2O	0.42	0.55	0.22	0.02	4.66	4.39	3.02	3.43	3.43	4.59	0.97	1.28	6.06	2.01
K2O	0.97	0.43	0.39	0.55	0.92	0.96	0.9	0.9	0.99	0.85	0.35	0.18	0.5	0.95
H2O/K2O	0.43	1.27	0.57	0.03	5.04	4.59	3.37	3.79	3.46	5.39	2.78	7.06	12.04	2.12
2. Plagioclase-hygrometer														
H2O	3.6	6.0			5.0		4.68	~4.0		No available data				
K2O	1.51	1.00			2.10		0.73	0.87						
H2O/K2O	2.38	6.00			2.38		6.42	4.6						
Reference	1	1			1		2	3						
3. Representative estimated H2O concentration in primitive magma														
Highest H2O/K2O	2.38	6			5.04		6.42	4.6		5.39	7.06		12.04	2.12
ID	Z-I	BD-I	BQ-III		AD-V		K-II	G-I		E-II	AA-I	S-II	J-I	A-I
K2O in primitive magma	0.97	0.39	0.55		0.96		0.9	0.99		0.85	0.35	0.18	0.5	0.95
Representative primitive H2O	2.31	2.36	3.29		4.82		5.75	4.55		4.59	2.47	1.28	6.06	2.01

Reference: 1. Zellmer et al. (2012), Kawaguchi et al. (2021), Zellmer et al. (2014)

concentrations, these melt inclusions significantly lost their initial water. While I kept the same approach to present the highest H_2O concentrations, those of Yufu and Sumiyoshi-ike remain truly minimum estimates.

I used the maximum CO_2 concentration of each sample as the minimum estimate for the primitive value, using a similar reasoning as for H_2O. I considered the bubbles present in melt inclusions as an exsolved fluid phase, and "added the CO_2 back" in the melt using the equation of state method (e.g., Tucker et al., 2019). The CO_2 content in melt inclusion reported in Table B2, is therefore much higher than the measured value, up to 1.2 wt.%. The highest CO_2 content is found in the alkali basalt of Fukue. Taking these corrected values, nearly all melt inclusions were formed at depths exceeding 10 km, and 20 km for Fukue, Sumiyoshi-ike, Yufu, Aso, Oninomi, and Kuju.

Cl and F concentrations in primitive magmas are likely representative of primary concentrations, since the exsolution pressure of those elements are at shallow depths (~100 MPa for Cl and ~10 MPa for F; Spilliaert et al., 2006). In addition, the expected minimum entrapment depth inferred from H_2O and CO_2 concentrations in magma is mostly greater than 100 MPa, so that Cl and F could not have exsolved before entrapment. Therefore, the Cl and F concentrations of the selected melt inclusions (Table 4.2) are considered as those of the primitive melt compositions.

In basalts, sulfur solubility depends on redox conditions and therefore on the relative proportions of sulfide and sulfate ions in the melt (e.g. Carrol and Webster, 1994; Jugo et al., 2005). Observed high dissolved S concentrations are characteristics of oxidized- and hydrous-basalts found in subduction zones (Roggensack, 2001; Wallace, 2005; Webster et al., 2010, Narvaez et al., 2018). Melt inclusions of our samples (except Kirishima-Ohachidake, Fukue and Oninomi) plot above the S concentration at sulfide saturation (SCSS) curve (Fig. 4.7) and appear supersaturated in sulfide. The SCSS is calculated based on the saturation of FeS in

which S^{2-} is the dominant S species. However, no sulfide was found in these samples, suggesting that a fraction of S is in the form of S^{6+}, preventing the formation of FeS. The remaining fraction of S is in the form of S^{2-}. Therefore, samples are in fact undersaturated, because the concentration of S^{2-} is lower than SCSS. A few inclusions (Y-I and BC-I of Sumiyoshi-ike) are the exceptions as sulfide globules were present, suggesting that SCSS is reached for some compositions. Lastly, S concentrations of all our melt inclusions are under-saturated with respect to anhydrite saturation (SCAS), indicating sulfate fractionation had not occurred (Li and Repley, 2009; calculated SCAS between 5270 to 8560 ppm for our samples).

Fukue and Oninomi are at sulfide saturation (Fig. 4.7). This is consistent with the observations of sulfide globules commonly found in the whole rock samples. For these samples, clearly it is not possible to determine the primitive S concentrations. If the redox state of the sub-arc mantle is reduced, sulfide saturated at the surface is also saturated at the depth of melting, as solubility decreases with pressure (e.g. Mavrogenes and O'Neill, 1999; Hart and Gaetani, 2006). Alternatively, because the sub-arc mantle is oxidized (e.g. Parkinson and Arculus, 1999; Kelley and Cottrell, 2009), then the magma remains undersaturated and the melt inclusions potentially record the primitive S compositions. In the latter case, the magmas of Fukue and Oninomi became reduced late, prior to eruption, to explain the presence of sulfides. Kirishima-Ohachidake plots on the SCSS, but no sulfides were observed in melt inclusions (Fig. 4.7). The sample has an elevated proportion of S^{6+} (0.5-0.9, Table B2), explaining the absence of sulfide (based on visual inspection of hand samples). Therefore, I report the sulfur concentration of the previously selected G-I melt inclusions (800 ppm) as the primitive value.

Sulfur may leave the magma through partitioning into the fluid during degassing (i.e. degassing of H_2O and CO_2). This S-loss via degassing results in a positive correlation between H_2O and S as reported in natural and experimental samples (e.g. Spilliaert et al. 2006; Lesne et

al. 2011). Such correlations were found among the inclusions from Kirishima SM, Kaimondake, Kuju, but not for Sumiyoshi-ike, and Yufu. The correlation of H_2O and S can be alternatively derived from mixing, which is confirmed by correlations between non-degassing elements F and S (Fig. 4.6b). It is possible to conclude that S variation is in fact due to processes other than degassing, and the S concentration of the mafic endmember can therefore represent primitive composition (e.g. Kaimondake).

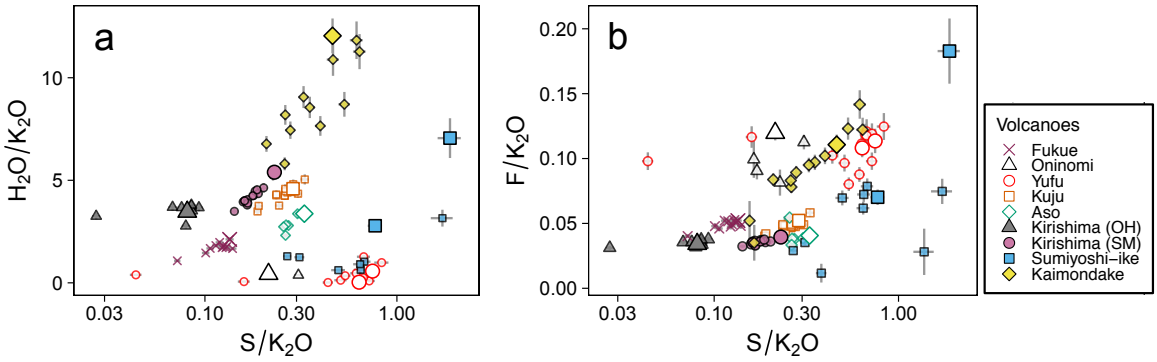

Figure 4.6. K_2O normalized volatile element abundances in the melt inclusion. (a) H_2O and S show a positive correlation (except for Oninomi, Sumiyoshi-ike, and Yufu). Such correlation is often interpreted as a result of magmatic degassing. However (b) F vs. S also shows a strong correlation (i.e. Kaimon) indicating that the correlation is not caused by H_2O-loss through degassing because F is only weakly soluble to magmatic fluid. Note, the horizontal axis is on log-scale to illustrate the wide range of S/K_2O values.

The compositional variations of Kuju and Kirishima were considered to represent a melting process. In such a case, the highest degree melt represents the least fractionation from the source. Therefore, the source magma S concentration was derived from the melt inclusions with the lowest trace element concentration (Table 4.2).

For Yufu, there is a paradox about S concentrations. The Yufu samples plot above SCSS (Fig. 4.7; for example, up to 3793) suggesting a high proportion of S^{6+} in the magmas. However, the measured S speciation gives negligible S^{6+} abundances in the melt inclusions, implying reduced fO_2 conditions (Table B3). Furthermore, if the melt inclusion is really reduced, sulfide should precipitate and S concentration should be at SCSS, but no sulfides were found in Yufu melt inclusions. This paradox is simply the consequence of the heating procedure. As Yufu melt inclusions were partially crystallized, they were re-homogenized in a heating stage (e.g. Le Voyer et al., 2010). During this process, a purified He flux is flushed in the stage and the oxygen fugacity was kept between 10^{-10} and 10^{-9} atm, to avoid oxidation of the host mineral and to ensure an efficient quench. These extremely reduced conditions have affected the S speciation of the melt inclusion, even if the sample were originally oxidized. In fact, reported amphibole compositions of basaltic mafic enclaves found in Yufu indicate oxidized condition (ΔNNO+1 ± 0.4; Ohta et al., 1990; Ridolfi et al., 2010). Thus, I concluded that the Yufu magma was originally oxidized and the high-S concentrations of its melt inclusions reflect the value at the time of entrapment.

Mineral phases such as carbonates, sulfides, sulfates and native sulfur were reported inside the bubbles upon cooling (Kamenetsky et al., 2002, Moore et al., 2015; Robidoux et al., 2018). If such S-bearing phases were present on the wall of the vapor bubble, primary S concentrations would significantly be underestimated. Although it is impossible to examine the exposed vapor bubble *a posteriori* after polishing, the bubbles in the melt inclusions of this study did not contain visible solid precipitates (inspection under an optical microscope). Without this quantification, I assumed our oxidized melt inclusions are undersaturated and did not crystallize neither anhydrite nor sulfide.

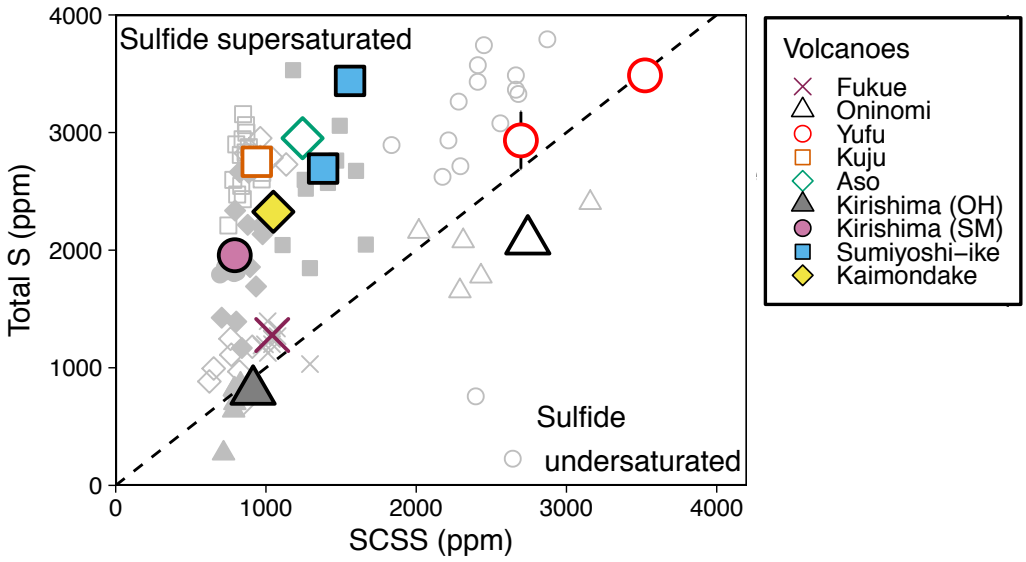

Figure 4.7. Comparison of measured sulfur concentrations in primitive melt inclusions with the sulfur content at sulfide saturation (SCSS). Concentrations for all the other melt inclusions are shown as grey symbols. Symbols are the same as in Figure 2. Dashed black line indicates the 1:1 line. SCSS was calculated according to Fortin et al. (2015) using measured H_2O concentration and the trapping temperature (T_{trap} of Table B7) of melt inclusions at 0.1 GPa. For primitive melt inclusion, I used minimum H_2O concentrations estimated from the highest H_2O/K_2O ratio (Table 3). I took the average measured H_2O concentration of the melt inclusions from each edifice and assigned this value to the melt inclusions of the same edifice that did not have H_2O data. Decrease of SCSS caused by pressure increment does not change our conclusions, since it does not significantly decrease the S concentration. For example a decrease in pressure from 0.1 GPa to 0.5 GPa decreases the S concentration in the primitive melt inclusions by a maximum of 300 ppm.

4.6.3. S isotope composition of primitive magma and influence of degassing on the S isotope compositions

Identifying the source of magmatic volatiles through S-isotope characterization requires careful evaluation of potential modifications of the initial isotopic signature. In general, the modification and variation of sulfur isotope compositions is caused by two processes: mixing

of sulfur coming from isotopically distinct sources, and isotopic fractionation due to changes of sulfur speciation. For the latter case, a significant equilibrium sulfur isotope fractionation factor ($\alpha_{gas\text{-}melt}$) was calculated for a degassing of a magma ($\alpha_{gas\text{-}melt}$ = 0.996 to 0.998 at degassing conditions of the Mazama magma, e.g. Mandeville et al., 2009), leading to $\delta^{34}S_{melt}$ heavier than equilibrium $\delta^{34}S_{gas}$ at oxidized condition (typically higher than ~ΔFMQ+1; Marini, 2011; Fiege et al., 2015). The implication was that open-system degassing potentially reaches an even higher $\delta^{34}S_{melt}$ (Marini et al., 1994; example of Krakatau 1883 eruption, Mandeville et al., 1998). For the modification of S-isotope composition due to mixing, earlier studies interpreted variations of S isotope composition of arc lavas as the addition of slab-derived seawater sulfur component into the sub-arc mantle (Sasaki and Ishihara, 1979; Alt et al., 1993, 2012; Evans et al., 2014). However, these studies pointed out that the fractionation of S isotopes during the transformation mechanisms of seawater SO_4^{2-} to dissolved S in primitive arc magma is poorly constrained. The variation of the present sulfur isotope data (Fig. 4.8) is caused by mixing and unlikely influenced by degassing, because the melt inclusions of this study trapped magmas before degassing as inferred from high CO_2 contents (note, the bubble corrected values).

Sulfur fractionation model showed the variation of $\delta^{34}S$ is maximum during open-system degassing (Marini et al., 2011; Supplementary document B9). In detail, that model predicts that even if there was an extensive degassing and all the melt inclusions were affected by an open-system degassing of up to 50% of the initial S, the $\delta^{34}S$ of the melt inclusions would be changed by a maximum 2 ‰, which is the 2σ error of our $\delta^{34}S$ measurements. The $\delta^{34}S$ measurement is insensitive to less than 50% degassing due to its uncertainty in this study. In the case of extremely degassed whole rock, a study has reported $\delta^{34}S$ of +18.0 ‰ for S content down to 9 ppm (Aso Nakadake; Ueda and Saki, 1984). Therefore, a systematic degassing by 50% is unlikely among the inclusion data here, since S concentrations of Kyushu melt

inclusions are in the range of those reported for other primitive arc basalts in the world (e.g., as high as ~3000 ppm in Cascades, Wallace, 2005). The $\delta^{34}S$ values of our primitive melt inclusions therefore reflect the values of the metasomatized mantle below the volcanoes (Table 4.2).

One can expect a correlation between $\delta^{34}S$ and S concentrations, if the magma degassing is significant. There is no such correlation among melt inclusions from each individual Kyushu volcano (Fig. 4.8a). The inclusion data of Yufu is the only sample showing a weak negative correlation (Fig. 4.8a) and the values of other volcanoes are clustered around a single value. Sulfur depletion through degassing can be illustrated by normalizing the concentration with a non-degassing, incompatible element such as K_2O, (Fig. 4.8b). The negative correlations with $\delta^{34}S$ are slightly more apparent for Yufu, Sumiyoshi-ike, and Kaimondake. Given that trace element concentrations of these samples were controlled by mixing rather than degassing, I instead argue that the negative trend is due to mixing. Therefore, the $\delta^{34}S$ values of the mixing endmembers represent the primitive magma values. For Oninomi and Fukue, $\delta^{34}S$ values are systematically lower than other oxidized magmas. In fact, S concentration of these samples was controlled by sulfide saturation, so the low $\delta^{34}S$ values are potentially explained by a fractionation during sulfide precipitation, which leaves the remaining melt slightly lighter than the oxidized magmas (e.g. Marini et al., 2011).

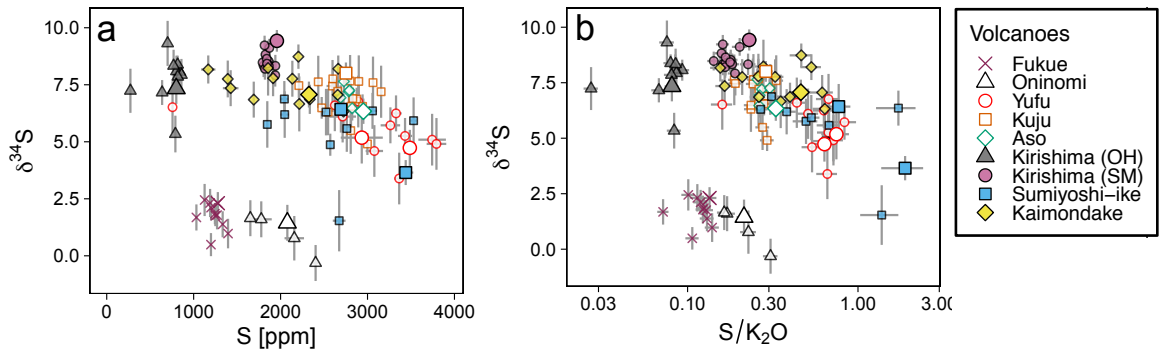

Figure 4.8. Sulfur isotope composition is plotted against sulfur abundance. (a) $\delta^{34}S$ vs. S plot is expected to illustrate the strong fractionation of isotope due to degassing. Here, there is no obvious trend, except perhaps for Yufu. (b) $\delta^{34}S$ vs. S/K_2O plot may illustrate the degassing process better by compensating concentration increase by magma differentiation. Even in this space, Yufu, Kaimondake and Sumiyoshi-ike show a weak negative trend. Error bars represent 2 standard errors, approximately corresponding to 95 % confidence interval.

4.6.4. The three magma groups of Kyushu

Magma sources are identified using trace element ratios of highly incompatible elements. The contribution of slab-derived material to the magma source increases Ba/Zr (Fig. 4.9a; e.g. Leeman et al. 2005). The plot of Ba/Zr against Nb/Zr illustrates the contrast between the mantle array with a well-defined slope of Ba/Nb ~ 7, derived from MORB samples, (also model mantle compositions are indicated). In comparison, arc magmas show elevated Ba compared to Nb. It shows that Fukue and Oninomi magmas plot close to the mantle array, while other Kyushu magmas plot above it and reflect the addition of slab-derived material, rich in Ba. Northern Kyushu magmas (open symbols in Fig. 4.9a) appear to show, in general, higher Ba/Zr (and Ba/Nb), than Southern Kyushu. In brief, there appears to be three distinct groups in these Kyushu magmas.

The distinction of three groups is also clear with Fig. 4.9b (Sr/Y against Th/Nb). The MORB melt inclusion compositions (small light blue triangles) cluster near the values of the model depleted MORB mantle with Sr/Y = 2.3 and Th/Nb = 0.053 (Workman and Hart, 2005). For peridotite partial melting, Sr/Y in MORB melt inclusions show limited variation whereas among the Kyushu melt inclusions the variation covers more than factor of 5 with those of the north (open symbols) plotting at higher Sr/Y values (>30) than those of the south (<30) and MORB. There is also a variation of Th/Nb, a ratio of highly incompatible elements (Fig. 4.9b). This variation is caused by the input of a mobile agent from the slab to the arc magma source (i.e. metasomatism), and the resulting variation is a characteristic of arc magmatism (see light pink solid circle representing arc olivine-hosted melt inclusions). The Th/Nb of the slab agent is potentially characterized both by its physical nature (aqueous flux, silicate melt, or supercritical fluid) and by the source composition (sediment, altered oceanic crust). For example, rutile in the slab fractionate Nb as Nb is strongly partitioned in it, $D_{Nb}^{rutile/melt}$ ranging 14 to 550 (Foley et al. 2000; Klemme et al., 2005), and Th abundance can be controlled by allanite and apatite (Hermann, 2002). As these minerals are commonly found in the sedimentary and magmatic part of the slab, the slab-issued flux can be characterized by these phases (Klimm et al, 2008). Furthermore, The value of Th/Nb in the altered oceanic crust is expected to be similar to that of MORB, and variation of mantle fertility can only vary Th/Nb from 0.05 to 0.14 (Fig. 4.9b). On the contrary, subducting sediments can vary significantly from 0.10 to 1.5 with an average of 0.77 (Plank and Langmuir, 1998). As HFSE elements are poorly soluble into aqueous fluid, it is generally interpreted that only silicate melt, especially the silicate melt from the subducting sediment is the most effective slab agent that can change Th/Nb ratio.

The high Sr/Y values are often interpreted as adakite signatures, as they are the result of the partial melting of the slab having residual garnet (e.g. Defant and Drummond, 1990; Martin et al. 2005). In this scenario, melting, instead of dehydration, is the necessary process to fractionate Sr and Y. High Sr/Y values in Northern Kyushu are comparable to those from other

arc systems, for example, Southern Cascade, (1 to ~10% slab melt addition into source mantle, Walowski et al., 2016). Alternatively, the high Sr/Y is potentially derived from magma interacting with garnet and/or amphibole of the lower arc crust during magma ascent (e.g. Davidson et al., 2007). Because the melt inclusions of this study have experienced negligible crystal fractionation and the primitive chemical components were carefully selected, Sr/Y of our inclusions are unlikely reflecting the lower crust interaction processes.

Among the Kyushu magmas, Oninomi and Fukue both are the closest to the mantle array (Fig. 4.9a) with the most discrete Ba/Zr enrichment of about 1.5 and 1.8, respectively. This slight slab contribution, particularly for Fukue, is explained by its back arc location, where the distance to the slab surface is over 400 km (Fig. 4.1). The restricted Ba/Th enrichment is also seen in Akashima volcano from the same Fukue volcanic group (Kuritani et al., 2017). While Ba/Th and Ba/Nb are close to the mantle values, and Sr/Y is significantly different from the depleted mantle value, both for Fukue and Oninomi. Because the DMM can yield a maximum Sr/Y of ~10 (determined by $[Sr]_{DMM}/[Y]_{DMM} * D_Y^{mantle/melt}/D_{Sr}^{mantle/melt}$) during mantle partial melting (Workman and Hart, 2005), and the Sr/Y values of Fukue and Oninomi are >20, they must reflect the source composition.

The melt inclusions from the other edifices plot above the mantle array (Fig. 4.9a). For example, fluid derived from the slab increased Ba/Zr of melt inclusions (Fig. 4.9a) by a factor of 2.8 (Kaimon) to 9 (Aso). Th/Nb varies up to a factor of 10 (1.0 for Kirishima Shinmoedake) compared to that of the MORB-cluster (~ 0.1). For the two Kirishima samples, Aso and Yufu, the slab contribution is the most significant (Fig. 4.9a) and identified as mainly due to silicate melt addition causing high Th/Nb and Sr/Y (Fig. 4.9ab). On the contrary, for Sumiyoshi-ike and Kaimondake the contribution is weaker and likely due to aqueous fluids.

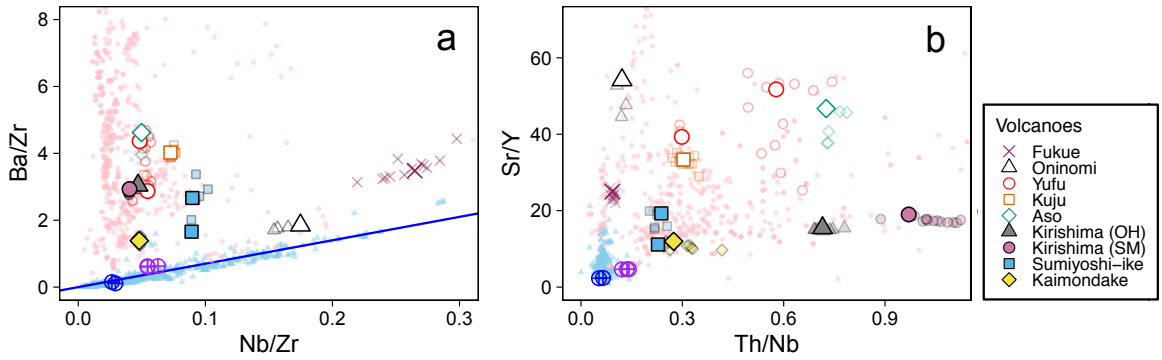

Figure 4.9. Slab-derived material contribution into the magma source. a) Ba/Zr vs. Nb/Zr plot. Small blue triangles are melt inclusion and glass MORB data (Shaw et al. 2010; Wanless et al., 2012; 2014; Le Voyer et al. 2015; 2017; 2019; Shimizu et al. 2019a, b), they define a trend with a slope of Ba/Nb of 7, blue line). The small pink circles are arc melt inclusions (Straub and Layne, 2003; Churikova et al., 2007; Elburg et al., 2007; Portnyagin et al., 2007; Sadofsky et al., 2008; Vigouroux et al., 2008; Wysoczanski et al., 2006; Bouvier et al., 2008, 2010a,b; Sorbadere et al., 2011, 2013; Rose-Koga et al., 2014; Walowski et al., 2016; Narvaez et al., 2018; Barker et al., 2020). Blue circles with a cross indicate the models of the depleted mantle (Workman and Hart 2005; Salters and Stracke 2004). Purple circles with a cross indicate the model bulk silicate Earth (McDonough and Sun 1995; Palme and O'Neill, 2003; Lyubetskaya and Korenaga, 2007). All the melt inclusions from Kyushu volcanoes plot above the blue line, in the arc magma field. b) Sr/Y vs. Th/Nb plot. Melt inclusions from volcanoes of Northern Kyushu (open symbols) have Sr/Y values higher than those from Southern Kyushu volcanoes (filled symbols), with a Sr/Y=20 the value separating the two groups (see text for significance).

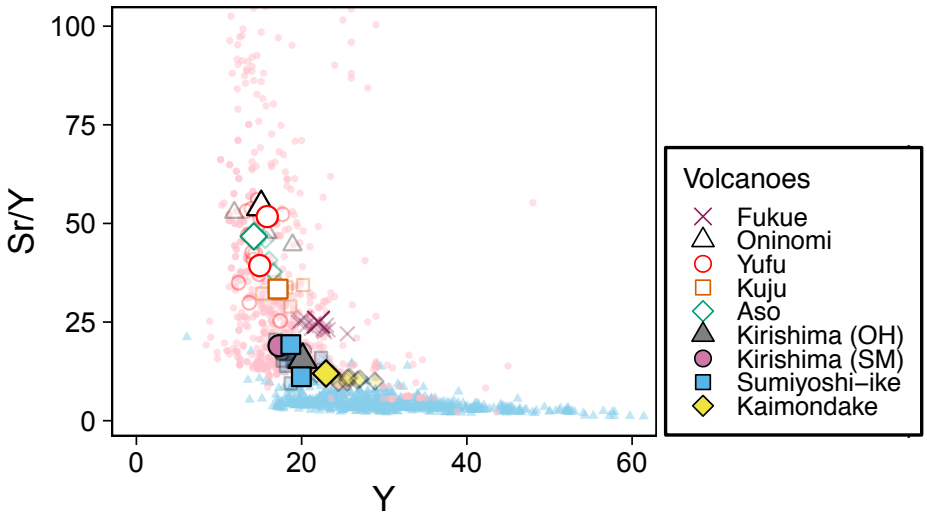

Figure 4.10. Sr/Y ratio and Y concentration of melt inclusions. As in Fig. 9, pink and blue filled symbols indicate olivine hosted melt inclusion compositions for arc magma, and MORB, respectively. Symbols filled in white are samples from Northern Kyushu, and filled with color indicates samples from Southern Kyushu. Sr/Y clearly separates the north from the south. Note the vertical axis is in log scale.

4.6.5. Geodynamic significance of source region

Presence of these three groups of magmas indicates that there exist at least three distinct mechanisms of magma genesis below the Kyushu Island. Variation of arc primitive magmas, excluding the magma evolution in the crust, is derived from variations of mantle composition, quantity and composition of a flux added from the slab, and degrees of melting (e.g. Stolper and Newman, 1994; Tatsumi and Eggins, 1995). Such variation is observed across the scale of arc (1000s of km) to within a single volcano (e.g. Le Voyer et al., 2010). The studied volcanic area spreads across 250 km, and the subducting plate underneath has a discontinuity of the plate age separating young north and older south. A variation of magmas in the area is perhaps expected.

First, I examine the potential heterogeneity of the mantle below Kyushu volcanoes before metasomatism by slab. This is particularly important for the Northern Kyushu volcanoes, for which basalts were previously described as "OIB-like" for their enriched trace element characteristics (e.g., Nakada and Kamata, 1991). In fact, Fukue and Oninomi magmas plot in the region of alkali basalts from oceanic islands, with slightly elevated Th/Nb values (Fig. 4.9b), and Th/Nb is closer to the value of the bulk silicate earth, which is the enriched mantle (McDonough and Sun, 1995; Palme and O'Neill, 2003; Lyubetskaya and Korenaga, 2007). Similar systematics can be recognized with Ba/Zr - Nb/Zr plot (Fig. 4.9a). These diagrams also show that arc magmas in general have significant addition of Ba and Th compared to Nb. The addition of a component rich in Ba and Th to a typical upper mantle (i.e. depleted mantle) potentially creates similar characteristics to an "enriched" mantle and deciphering the difference between the two is not obvious from these diagrams. In detail, the ranges of Th/Nb and Ba/Nb of enriched and depleted mantle are much smaller than the variation of these ratios observed in arcs; I conclude that the initial mantle heterogeneity does not significantly impact the trace element characteristics of arc magmas, so it does not matter if I consider the mantle initially enriched or depleted before the slab agent addition. For the discussion hereafter, I consider depleted mantle (Workman and Hart, 2005; Salters and Stracke, 2004) as the reference mantle composition below the arc volcanoes before the metasomatism.

The dichotomy of Sr/Y values separating north and south Kyushu is then explained by an addition from the slab (Fig. 4.9b and Fig. 4.10). Fractionation of Sr/Y is due to the presence of garnet as a residual phase, and the residual garnet is potentially present in the mantle, metasomatized mantle, and slab (i.e. sediment and AOC). Following the consensus about the thermal structure of the arc mantle (e.g., Syracuse et al. 2010), the hottest part of the mantle below a volcano is located somewhat midway between the bottom of the Moho and the top of the slab, which is approximately 65-75 km (Fig. 4.1). This is not the depth to form melt in garnet peridotite (e.g. Walter, 1998). Considering that there is no strong upward movement of the solid mantle below a volcano, the maximum melting is attained at the level of this hottest

area of the mantle, and that is likely the condition of equilibration between mantle and melt. The garnet signature cannot be produced in the mantle beneath the volcanic front. The residual garnet signature must come from the slab (Defant and Drummond, 1990; Martin et al. 2005), or the metasomatized mantle near the slab-mantle interface (e.g. Lara and Dasgupta, 2020). Furthermore, Sr/Y is more strongly fractionated by the garnet-melt pair, than by garnet-aqueous fluid (Martin et al., 2005). From these bases, the high Sr/Y magmas in Northern Kyushu indicate the presence of silicate melt near the slab - mantle interface with the presence of residual garnet.

There remains a question, does the difference between north and south simply represents the presence/absence of silicate melt or does it represent variable contributions from different lithologies of the slab (i.e. AOC and sediments)? The answer to this question is non-unique, as the exact compositions of the subducting material are undeterminable, as well as the exact pressure-temperature conditions at dehydration/melting reactions. Nevertheless, there exists a wealth of databases allowing educated guesses about the compositions of slab material (e.g. Plank and Langmuir, 1998; Plank, 2014), and geodynamic models of pressure-temperature path along the subduction zones (Syracuse et al., 2010). Here, I used a forward model package, the arc basalt simulator 5 (ABS 5, Kimura 2017), to test the role of the fluxes from sediments and AOC, as well as the presence/absence of silicate melt (Supplementary document B9 for detail). ABS 5 conveniently includes sediments and AOC compositions around Japan. Furthermore, it includes the models of pressure - temperature trajectory, pseudosection diagrams for related lithologies, composite slab with six lithologies, and chromatographic fluid/melt modification adjustments. In Fig. 4.11ab, the endmember fluids/melts derived from a sediment (Nankai sediment, ABS 5) and AOC (Shikoku basin, ABS 5) are plotted together with the depleted mantle. As expected, the Th/Nb ratio of the fluxes derived from AOC is close to the value of the depleted mantle, and that derived from the sediments have significantly higher Th/Nb. Because the composition of the slab derived agent controls the ratios of highly incompatible elements, both fluid/melt phases from sediment and AOC must modify the source mantle to

cover the range of variation observed (see mixing curve in Fig. 4.11b). However, because of the contrast of the proportion of water in the fluid (~90%) and melt (~10%), it requires less amount of aqueous fluid flux to attain the equivalent extent of wet mantle melting. Another way of saying it is, to reach the same amount of melted mantle, the proportion of slab melt needed will be greater than that of fluid. This is why slab derived melt modifies the mantle more than fluid.

The compositions of the mantle fluxing agent illustrate the first-order influence to the trace element characteristics of arc magma, as it has been known and discussed for many years (e.g., Tatsumi, 1989; Kessel et al., 2005). As shown in Fig. 4.11, one approach is to use a detailed forward model to predict the flux from the slab. Alternatively, ABS 5 also includes a function of the inverse fit, by iteratively searching for the best fit solution by changing conditions of fluid release along the slab. On the one hand, our test with the inverse model easily yielded results showing a contrast of slab surface temperatures between north and south Kyushu, by adjusting some of many parameters. I concluded that the fit-results of the inverse calculation of ABS 5 do not strengthen the conclusion already shown with Fig. 4.11. I did not further discuss this. Instead, I have tested a mixing model among three components the depleted mantle, sediment flux, and AOC flux (Table B8), and calculate the proportion of a mixture satisfying the observe incompatible ratios (Th/Nb, Rb/Ba, Ba/Nb, Sr/Y, Sr/Nd, Nb/Zr). The results of the calculation also confirm the conclusion drawn from Fig. 4.9, 4.10, and 4.11. Based on the proportion of the mixing model (Fig. 4.12), Northern Kyushu volcanoes show stronger slab input than the Southern volcanoes, suggesting a higher amount of flux formed due to higher temperature. Sediment - AOC contributions are also variable but do not correlate with the geographical distribution of volcanoes.

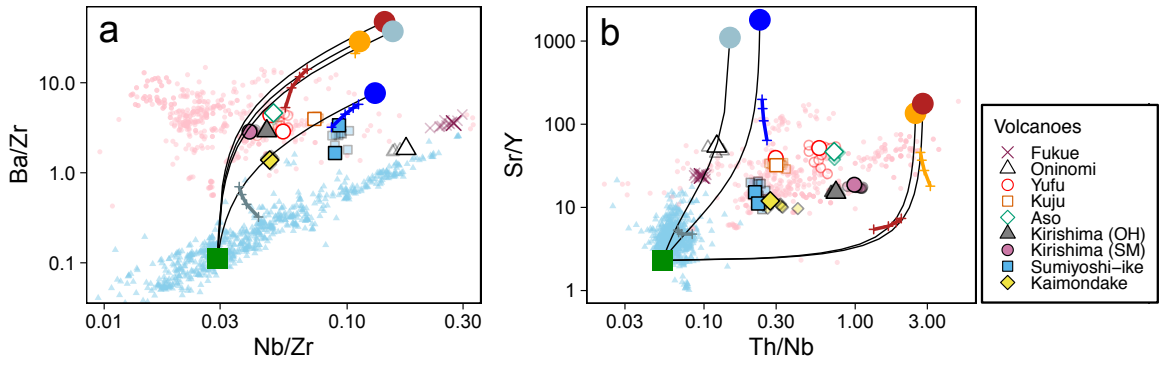

Figure 4.11. Mixing and melting trajectories of subduction zone endmembers are overlaid on Fig. 9ab. Blue cloud is MORB melt inclusion data, and pink cloud is arc basaltic melt inclusion data. Green square indicates the depleted mantle (Workman and Hart, 2005), and filled circles are slab derived fluxes: blue, silicate melt from AOC; light blue, aqueous fluid from AOC; orange, sediment melt; brick, sediment fluid (exact compositions of these fluids are in Table B8). Black lines are mixing curves between a flux and the mantle. Metasomatized mantle plots along this curve. In the case of three component mixing between the mantle and other fluxes, the metasomatized mantle plots in the region between two mixing curves. Thick colored lines indicate the trajectory of a melting model (modified after the flux model of Van den Bleeken and Koga 2015). Each tick mark is a 5% interval of the degree of melting ranging from 5 to 20 %. The larger degree of melting approaches the mixing curve. It should be noted that the variation caused by melting does not deviate significantly from the mixing lines. (a) the figure illustrates a clear mantle array, and the input form the slab is the main cause to deviate from the array. The melt flux is more efficient than the fluid flux, in raising Ba/Zr. (b) the figure indicates the elevation of Sr/Y, signature of residual garnet. Again, the melt flux is more efficient in producing high Sr/Y magmas than the fluid flux.

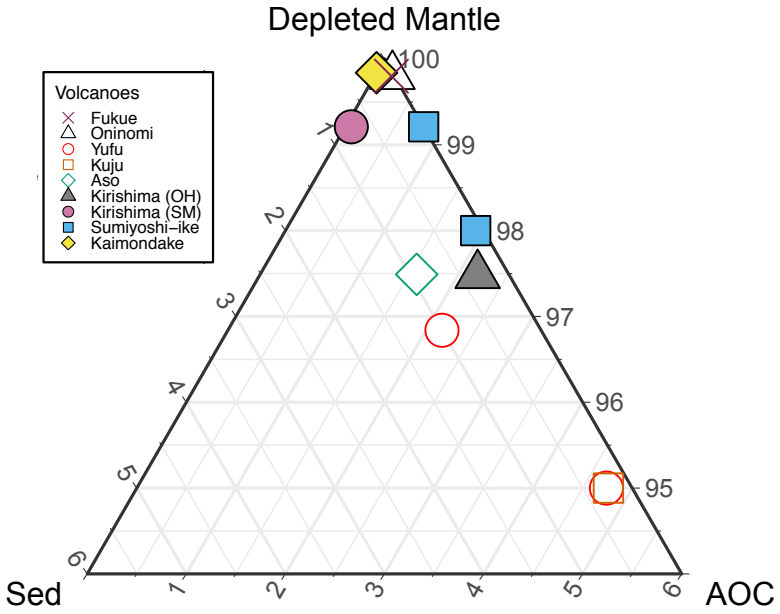

Figure 4.12. Results of mixing calculations for the primitive end members. Note that trace element characteristics are dominantly controlled by the depleted mantle. Small additions of fluxes from the slab are sufficient to satisfy the model. Northern Kyushu samples are more strongly influenced by slab signature, i.e. a slightly smaller fraction of the deleted mantle.

4.6.6. Assessment of individual volcanoes

The Northern Kyushu group, Yufu, Kuju, and Aso associate with silicate melt input from the slab, and south Kyushu group, Kirishima, Sumiyoshi-ike, Kaimondake associate with aqueous fluid (Fig. 4.11b). However, the amount of flux from sediment compared to the amount of flux from AOC shows different sub-groups. Aso, Kirishima and one endmember of

Yufu (BQ-III) have higher Th/Nb values than Kuju, Kaimondake, Sumiyoshi-ike, and the other endmember of Yufu (BD-I). This difference is explained by a higher proportion of sediment flux than that of AOC (Fig. 4.11ab). Aso, Kirishima, and Yufu (BQ-III) plot closer to the mixing curves of sediment-depleted mantle (Fig. 4.11ab). Curiously, this variation of sediment-AOC contributions does not correlate with the geographical north-south separation, neither with the depth to the slab surface, nor the dip of subduction. It should be noted that Yufu volcano melt inclusion magmas are a mixture of both melts, the one fluxed with more sediment and the one fluxed with less sediment. This variability on a single volcano indicates that primitive magmas arriving at the base of the crust can be heterogeneous with different origins. I also note that the degrees of dehydration of the slab in the forearc region along Kyushu are heterogeneous with patchy regions of high and low water contents in the forearc mantle wedge, described by a seismic tomography study (Abe et al. 2013). This indicates that availability of "water" in the slab below the arc volcanic front may vary with respect to spatial and perhaps temporal distributions, causing non-systematic contributions of sediment and AOC fluxes.

Magmas from Fukue and Oninomi are significantly different from those of the main volcanic front. They appear to record significantly different mantle processes. Fukue magma is slightly higher in Ba/Th and Th/Nb than the depleted mantle alignment (Fig. 4.9a). Fukue volcano is located in the back-arc region, where slab surface depth is approximately 400 km. At such a depth, the slab is mostly dehydrated and unlikely to contribute significant aqueous flux, leading to melting. Magma genesis of Fukue instead is caused by mantle upwelling potentially responding to the extension of the back-arc region, because Fukue is located broadly at the northern extension of Okinawa trough. If the degree of partial melting is small, it explains the LREE enriched pattern of the spidergram (Fig. 4.3). Alternatively, the magma genesis is related to a deep fluid released from the older Pacific plate stagnated at the mantle transition zone, extending over a much broader area than the young Philippine sea plate (Kuritani et al., 2017). This model is constrained by isotopic composition of Fukue magmas, being similar to deeply recycled sediment (EM2), and provides the mechanism for broader magmatic activities

extending to China. A recent seismic tomography study appears to indicate that Philippine sea plate is present beneath Fukue (Zhao et al., 2012; Liu and Zhao, 2016), and if the contribution of Pacific plate is critical, such mantle upwelling must flow around the upper Philippine sea plate.

Lastly, Oninomi volcano is unique in its character, standing out from the near-by volcanoes (e.g. Yufu, Kuju, and Tsurumi-dake, not studied). The spidergram of Oninomi magma shows no arc-magma-like character (Fig. 4.3), and it is somewhat similar to that of Fukue. The Ba/Nb and Th/Nb values are close to the depleted mantle, suggesting it records little input form the slab. It appears a small degree of partial melting of a slightly metasomatized mantle is sufficient to explain the magma composition. As the volcano is located in the middle of a 40 km wide graben active for 6 Ma (Kamata and Kodama, 1994), if the extension is accompanied by a lithosphere thinning, corresponding upward decompressing in the mantle below can cause an adiabatic melting (McKenzie and Bickle, 1988). It should be noted that a mantle melting in response to a small change in crustal load has been observed and demonstrated in Iceland, where deglaciation has caused magmatism (Slater et al., 1998). I consider this upward decompression melting in response to the extension the most plausible mechanism explaining the magma genesis of Oninomi.

4.6.7. Implications for sulfur isotope in subduction zone

Sulfur isotope compositions of melt inclusions from Kyushu volcanoes in this study reflect the compositional variation of magma source rather than degassing process. Then, what would be the main contributor of sulfur isotope variation in the subduction zone magmas? In our data set, $\delta^{34}S$ weakly correlates with Th/Nb, which is sensitive to slab input (Fig. 4.13a). As Th/Nb indicates the composition of the metasomatized magma source, and the depleted mantle is at -0.91 ‰ for $\delta^{34}S$, and 0.06 for Th/Nb, the variation is reflecting the input from the slab. Compared to other melt inclusion measurements from Antilles and Kamchatka (Bouvier

et al., 2008; Gurenko et al., 2018; 2021), our data plot in a similar range, showing global systematics. Fig. 4.13b illustrates a lack of systematics of $\delta^{34}S$ and Cl/F, which is strongly influenced by the presence of fluid and hydroxyl minerals (amphibole and mica). It is interpreted as aqueous fluid flux from lithologies with residual hydroxyl minerals yields higher Cl/F than slab melt flux (e.g. Van den Bleeken and Koga, 2015). For example, Cl/F of a cold subduction volcano is 3.0±2.0 (e.g. melt inclusions from Iwate volcano; Rose-Koga et al., 2014), and melt inclusions from typical fresh MORB is expected to have value around 0.4±0.4 (Le Voyer et al., 2015, 2019; Wanless et al., 2014). Now, Kyushu magmas cluster around Cl/F = 2.1±0.8. I conclude from this systematics, that the nature of the fluid (aqueous or melt) is not the first order factor controlling the sulfur isotope variations. I have also examined other trace element indicators that are considered sensitive to fractionation processes rather than source composition. For example, V (either concentration or ratios normalized to other trace elements) does not correlate with $\delta^{34}S$. This suggests that variation of sulfur isotope may not be due to changes in oxidation state of the fluid that carries the sulfur. Similarly, $\delta^{34}S$ does not correlate with Sr/Y (residual garnet), F/Nd (residual hydroxyl minerals or breakdown), or La/Sm (degree of melting). The variation of $\delta^{34}S$ in Kyushu magma must be related to the compositional variation of the slab component, which is transported into the mantle wedge by flux of mobile agents that is likely a solute rich melt.

Positive correlations between $\delta^{34}S$ and trace elements ratios are also found, for example with Rb/Ba, and Pb/Ce, in addition to Th/Nb (Fig. 4.14). Such recurring correlation underlines that the variation of $\delta^{34}S$ of these Kyushu magmas is again somewhat related to the slab flux. Careful inspections of these correlations identify two distinct contributions in addition to the depleted mantle. In Fig. 4.14a, the positive trend for the samples from the main volcanic front (excluding Fukue and Oninomi) can be explained by a mixing between a first endmember with a low $\delta^{34}S$ and a Rb/Ba lower than that of depleted mantle (approximately $\delta^{34}S < +3$ ‰ , Rb/Ba

< 0.03), and a second endmember with a high $\delta^{34}S$ and high Rb/Ba. Along this positive trend the Rb/Ba variations of the slab flux can come from the different source composition, combined with Rb/Ba fractionations due to presence of specific minerals, for example (i) the presence of residual phyllosilicates, which have an affinity for Rb and Ba, can fractionate them from the slab flux, (ii) Ba is preferentially incorporated into feldspar relative to a silica rich melt. As for the sources from the slab, first, the AOC is expected to inherit the Rb/Ba ratio of MORB, because of only slight addition of Rb is expected during MORB alteration (0.09; Staudigel, 2003), and this value is similar to that of the depleted mantle (0.089; Workman and Hart, 2005 and 0.073; Salters and Stracke, 2004). During the subduction of this AOC there is any significant amount of phyllosilicates in the metamorphosed basalt and gabbro, therefore the neither endmembers can be derived from the AOC. I note that altered basalts sampled at the ocean floor often report high Rb/Ba (e.g. Shu et al., 2017; Hickey-Vargas et al., 2018) but such basalts are volumetrically insignificant compared to total mafic material subducted. Second, the sediment flux component used in Fig. 4.11 gives Rb/Ba as 0.007 and 0.009 for fluid and melt respectively. Even considering oceanic manganese nodules and carbonates, they all have Rb/Ba <0.01 (e.g. Li and Schoomaker, 2005). So based on the Rb/Ba, the sediments would be the best candidate for the endmember with low Rb/Ba and low $\delta^{34}S$. Subduction zone sediments are reported to have a range of negative $\delta^{34}S$ values.

For the high Rb/Ba endmember, I considered other specific slab components, such as shales. For example, Rb/Ba ratio of shale is high and reported as 0.24 and seawater has a Rb/Ba = 8 (Li and Schoomaker, 2005). Corresponding $\delta^{34}S$ value ranges -16 to -38 ‰ (Sasaki and Ishihara, 1979; Cruse and Lyons, 2004) for shale, and is +21 ‰ for seawater (Rees et al., 1978). Seawater sulfur is sulfate, and thus seawater derived material rich in sulfate tends to give strong positive sulfur isotope values. The systematics of $\delta^{34}S$ and Rb/Ba suggest a slab component as seawater itself (or rocks impregnated by seawater sulfate). Forearc serpentinites also show

variable but high Rb/Ba, because of varying interactions with seawater (Savov et al. 2005; Deschamps et al., 2010; Albers et al. 2020). Similarly, feldspar-bearing sandstone as well as granite of south-west Japan, are also reported to have high Rb/Ba (Shinjoe 1997; Kiminami et al. 2009). These rocks are magnetite-bearing (and often sulfide-bearing) and salfate is not expected to be stable. Only brown clasts of serpentinites are reported to have oxidized state due to extensive interaction with seawater expected to be formed near seafloor (Albers et al. 2020). Alternatively, serpentinites in subducting slab can potentially carry sulfide with positive $\delta^{34}S$, due to seawater interaction. Such serpentinites are expected to release sulfate bearing fluid with $\delta^{34}S$ = 14 ‰, at the time of serpentinite dehydration to chlorite harzburgite (Alt et al. 2013). It is not clear if these ultramafic rocks are the definitive carrier satisfying both the high $\delta^{34}S$ and high Rb/Ba, but it appears that they are certainly the possible carriers of seawater sulfur isotope signature.

Considering the discussion above and what is known today, I conclude that seawater is a plausible vector responsible for giving the high $\delta^{34}S$ and high Rb/Ba geochemical signature. Direct injection of seawater into the source region of arc magma is a possible scenario as there are reports indicating direct injection of seawater into subduction zone to eclogite facies (seawater fluid inclusions; e.g. Sumino et al., 2010; Kawamoto et al., 2013). This conclusion contradicts with observation of mantle-like sulfur isotope in deep arc cumulates, where the $\delta^{34}S$ in the cumulates correlate with an index of magma evolution indicating that high $\delta^{34}S$ is a result of the crustal assimilation and crystal fractionation process. This in consequence suggests an efficient release of sulfate from the slab before the arc magmatic front, leaving the reduced sulfide with lighter $\delta^{34}S$ as the dominant sulfur species transported to the deep mantle (Lee et al., 2018). I think this disparity illustrates the complexity of sulfur behavior in magma. It should be noted that sulfur in the Kyushu inclusions are dominantly sulfate, while these cumulates

suggest crystallization at reduced condition dominated by sulfide. Such a contrast may suggest a range of redox states of arc magmas controlling the sulfur isotopic signature.

The ratio of Pb/Ce correlates with $\delta^{34}S$. This correlation is consistent with the interpretation based on the systematics of Fig. 4.14a ($\delta^{34}S$ vs. Rb/Ba). The flux from the slab gives Pb/Ce value ranging between 0.13 ~ 0.45 for an AOC-derived flux (ABS 5 model in our study), for a sediment-derived flux, the value ranges from 1.1 to 4.0 and Pb/Ce of seawater is 1.7 (Li and Schoomaker 2005). Furthermore, for Kyushu magmas, no negative $\delta^{34}S$ component is needed to describe the systematics, while strongly negative sulfur isotope component is subducted. For example, sulfide in sediments and oceanic crust is as low as - 40 ‰ (Peters et al., 2010; Alt and Shanks, 2011). The lack of a negative component suggests that the dominant sulfur mobility from the slab is done by sulfate rather than sulfide, and negative $\delta^{34}S$ of sulfide is perhaps not incorporated into the slab flux. While our finding may apply only to local sulfur cycle in Kyushu volcanoes, it shows potential isotopic filters operating at the subduction zone primarily controlled by initial sulfur speciation. Lastly, some negative $\delta^{34}S$ values are reported in melt inclusions and embayments from Lesser Antilles known to have large sediment inputs into the mantle wedge (Bouvier et al., 2008) and a decreasing $\delta^{34}S$ with decreasing S concentrations for melt inclusions from Kamchatka (Gurenko, 2021); they are interpreted as results of sulfur fractionation in the crust (i.e. sulfide precipitation and/or degassing). Presence or absence of negative $\delta^{34}S$ slab flux is critical in understanding S cycle systematics in the subduction zone system.

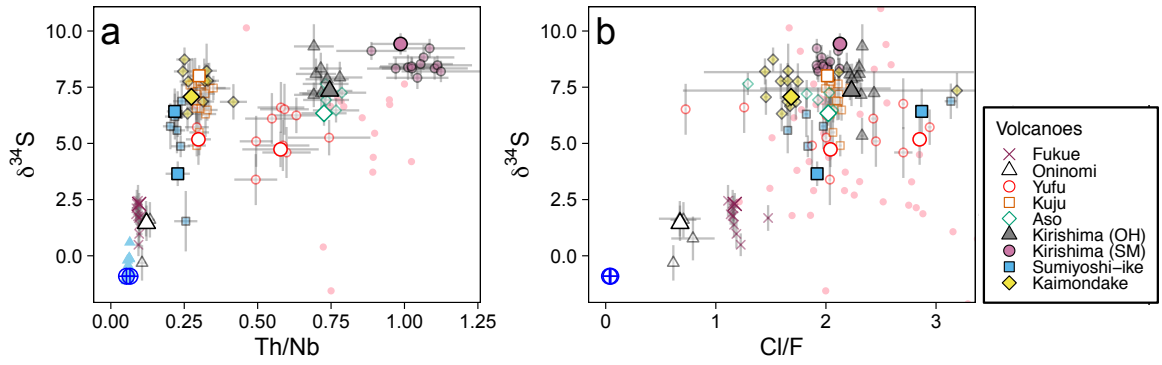

Figure 4.13. Isotopic composition of sulfur plotted against trace element ratios. (a) Against the ratio of Th/Nb, the plot distinguishes AOC and sediment fluxes as illustrated by Fig. 11a. (b) Against Cl/F, the plot potentially separates fluid from melt. However, there is no systematic separation. Blue circles with a cross indicate the depleted mantle. Filled sky blue triangles are the MORB values (Labidi et al., 2012; 2014). Filled pink circles are the arc melt inclusion data (Bouvier et al. 2012; Gurenko et al., 2018; 2021), shown as a comparison.

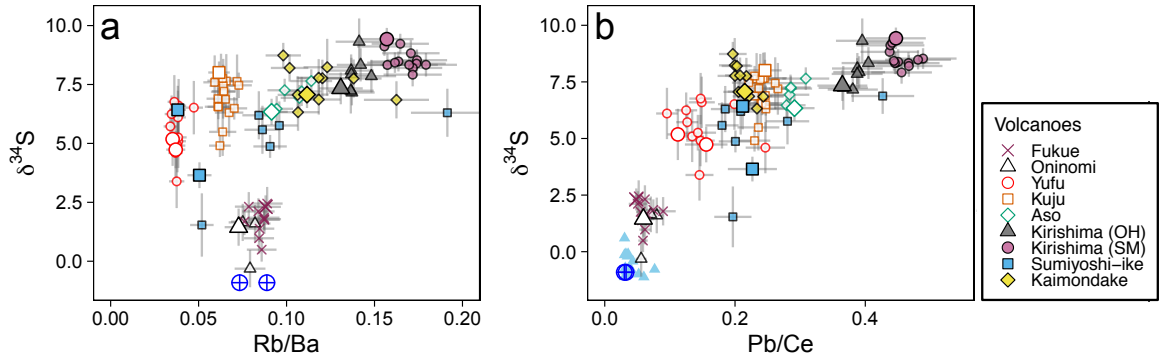

Figure 4.14. Isotopic composition of sulfur plotted against trace element ratios. (a) Against the ratio of Rb/Ba, the plot shows the data distribution that requires three component mixing. (b) Against Pb/Ce, the plot shows Pb input from the slab, correlating with $\delta^{34}S$. Blue circles with cross indicate the depleted mantle. Filled sky blue triangles are the MORB values (Labidi et al., 2012; 2014). The arc melt inclusion data are not shown as Rb and Pb data are not available. Note, the samples with little slab input Fukue and Oninomi) plots close to the depleted mantle and MORB.

4.7. Conclusions

- Olivine-hosted magmatic melt inclusions along the Kyushu arc studied here are from mafic tephra deposits. I identified the melt inclusion the closest to the primitive composition of the magma of each volcano.
- The highest water content found was 6.1 wt % in agreement with the high values of other arcs, while the CO_2 in the inclusions was lost. The highest entrapment pressure determined by a volatile content of an inclusion is at 12 kb (Fukue), and 7.4 kb (Aso) for the inclusion from volcanic front.
- I found three primitive magma groups: north and south Kyushu, and a group with little slab inputs (composed of Oninomi and Fukue). The northern group systematically shows higher Sr/Y values than the southern group. This can be explained by the slab agent being hotter and recording stronger slab melt signature with residual garnet.
- Oninomi volcano magma is likely produced by a small degree of mantle melt with nearly no input from the slab. The crustal extension in the area may have triggered such a small degree of melting.
- Fukue is located in the back-arc and its magma with small slab input is consistent with its geodynamic setting.
- Magma source sulfur isotope composition was determined by carefully examining the trace element systematics and assuring that the melt inclusions were not influenced by a degassing process. Careful analysis of such results reveals that sulfur isotopes of Kyushu arc magmas are characterized by mixture of the depleted mantle, slab sediment, and a third component, which can potentially be seawater.

Chapter 5

General conclusions and perspectives

Source of magmatic sulfur and characteristics of sulfur-bearing slab-fluids are highly controversial questions: whether slab-fluid is sulfate-dominant or sulfide-dominant, with positive $\delta^{34}S$ value or negative $\delta^{34}S$ value (e.g., Alt et al., 2013; Jégo and Dasgupta, 2013, 2014; Walters et al., 2019; Li et al., 2020b). In addition, globally observed "excess degassing" of sulfur is a critical problem for the estimation of volatile-budget and -flux on the Earth's surface. Missing link is volatile content and S-isotope composition of primitive magma. In this dissertation, I used olivine-hosted melt inclusions to obtain the information of least-degassed magma. The determination of major, trace and volatile element concentrations and S isotopic composition in primitive magma synthesizes research on two important processes in subduction zone sulfur cycle: 1) slab-material transport into the sub-arc mantle, 2) degassing of primitive magma during its ascent.

5.1. General conclusions

The melt inclusion study of Aso volcano (Chapter 3) illustrated the method to identify the primitive mafic magma responsible for deep volatile flux in a mature volcano with complex magmatic processes. This study provides petrological constrains (1) on the depths of the magma reservoirs, as well as (2) on the origin of volcanic gases observed today. I analyzed the melt inclusions and phenocryst minerals of Holocene basaltic eruption products, and reported their major and volatile element concentrations. Two pre-eruptive storage depths were confirmed from volatile concentrations: 2 km and 4 km depth for Strombolian eruption and sub-Plinian eruption, respectively. The volatile-rich primitive magma originated from a deeper level (>10 km) than these magma reservoirs. During ascent, the primitive magma started to

degas at a depth between 11 and 13 km, and maintained in equilibrium with gas until 10 km depth. The observed variation of volcanic gas composition was best explained by the mixing of the gas segregated from at least a depth of 10 km, with that from the shallow reservoirs.

The dataset of olivine-hosted melt inclusion is extended to entire Kyushu in order to investigate sulfur systematics in primary magma along the arc segment (Chapter 4). This dataset was used to infer the nature of slab agent metasomatizing the sub-arc mantle wedge. Sr/Y ratios underline a clear compositional dichotomy between volcanoes from north (Sr/Y>20) and south Kyushu (Sr/Y<20), separated by the Kyushu-Palau ridge. Trace element systematics indicated the presence of slab agent being hotter and recording stronger slab-melt signature with residual garnet beneath northern Kyushu.

S isotopes ($\delta^{34}S$) of those primitive melt inclusions were not affected by degassing processes and showed positive values. Positive correlation between $\delta^{34}S$ and indicators of slab flux (e.g., Th/Nb, Pb/Ce) indicated that the source mantle and the slab-fluids are oxidized (sulfate-dominant) and have positive $\delta^{34}S$ values. The nature of the fluid (aqueous or melt) is not the first order factor controlling the sulfur isotope variations. Moreover, $\delta^{34}S$ does not correlate with V concentration or ratio normalized to other trace element (oxidation state), Sr/Y (residual garnet), F/Nd (residual hydroxyl minerals or breakdown), or La/Sm (degree of melting). Therefore, the variation of $\delta^{34}S$ in Kyushu magma must be related to the compositional variation of the slab component. The systematics of $\delta^{34}S$ and Rb/Ba indicated three components as the sulfur source of arc magma: depleted mantle, subducted sediment and high-Rb/Ba material, potentially be seawater.

5.2. Perspectives

To further constraints on sulfur sources and degassing processes, following approaches would be useful:

1. Pursuit of arc sulfur sources using melt inclusions by combination with other slab-input tracers. Coupling of sulfur isotope and trace elements data with other stable-isotopes, especially boron and oxygen, provide more information to clarify seawater component and allow to inspect the contribution of seawater quantitatively. It is well known that O-isotopes ($^{18}O/^{16}O$) of pore-fluids in oceanic sediments are depleted in ^{18}O relative to those of seawater, whereas sediments, AOC, fresh serpentinites and mantle peridotite are enriched in ^{18}O (Eiler, 2001; Bouvier et al., 2019). Similarly, as B-isotopes ($^{11}B/^{10}B$) of seawater is extremely rich in ^{11}B compared with those of other reservoirs, it is useful tracer of seawater addition (e.g., Rose et al., 2001; Bouvier et al., 2008). If pore-fluids are directly subducting at sub-arc depth as suggested by a systematics of noble gas and halogen (Sumino et al., 2010) and metasomatizing source mantle, the seawater-like signature would be found in arc melt inclusions (e.g., Bouvier et al., 2008). Whether S-isotopes and Rb/Ba ratios correlate with B- and O-isotopes is interesting.
2. Comparison with other arcs. Published sulfur isotope data of primitive melt inclusion are from only 2 arcs today (Lesser Antilles, Bouvier et al., 2008; Kurile-Kamchatka, Gurenko et al., 2018, Gurenko, 2021). This study (Kyushu, Japan) is currently the only available melt inclusion S-isotope study with multiple trace-element data including Rb and Ba. Further melt inclusion studies of other arcs are required to assess if our findings are universally accepted or not.
3. Assessment of crustal contamination for olivine-hosted melt inclusions. While S concentration is expected to be low in crustal rocks (<621 ppm in typical continental crust; Rudnick and Gao, 2003), contamination potentially modifies $\delta^{34}S$ of magma. Sr-isotope and Nd-isotope measurement would be useful to quantify the crustal contribution and strengthen the conclusion (e.g., Reinhard et al., 2018).

4. Measurement of S-isotopes in volcanic gases to understand the degassing process from multiple magma reservoirs. In this study, I identified deep and shallow magma reservoirs of an active volcano (Aso volcano, Japan) corresponding to the source of emitted gases. However, actual transportation mechanisms were not constrained. S-isotope composition of volcanic gas should reflect the reaction during gas transport or convective degassing of shallow magma reservoir. For example, in case of convective degassing in conduit and effective gas release, vast S degassing induce large fractionation in $\delta^{34}S$ of magma and gas phase depending on physical condition (e.g., fO_2 and temperature; Marini et al., 2011; de Moor et al., 2013). Combinations of melt inclusion and gas data and theoretical expressions may allow quantitative assessment for the processes such as evolution of $\delta^{34}S$ in degassing magma at shallow reservoir and contribution of shallow magma reservoir and hydrothermal fluid during gas transport from deep magma reservoir.

References

Abe, Y., Ohkura, T., Hirahara, K. & Shibutani, T. (2013). Along-arc variation in water distribution in the uppermost mantle beneath Kyushu, Japan, as derived from receiver function analyses. *Journal of Geophysical Research: Solid Earth* **118**, 3540–3556.

Abe, Y., Ohkura, T., Shibutani, T., Hirahara, K. & Kato, M. (2010). Crustal structure beneath Aso Caldera, Southwest Japan, as derived from receiver function analysis. *Journal of Volcanology and Geothermal Research* **195**, 1–12.

Aiuppa, A., Fischer, T. P., Plank, T., Robidoux, P. & Di Napoli, R. (2017). Along-arc, inter-arc and arc-to-arc variations in volcanic gas CO_2/S_T ratios reveal dual source of carbon in arc volcanism. *Earth-Science Reviews* **168**, 24–47.

Albers, E., Kahl, W.-A., Beyer, L. & Bach, W. (2020). Variant across-forearc compositions of slab-fluids recorded by serpentinites: implications on the mobilization of FMEs from an active subduction zone (Mariana forearc). *Lithos* **364–365**, 105525.

Albert, H., Costa, F., Di Muro, A., Herrin, J., Métrich, N. & Deloule, E. (2019). Magma interactions, crystal mush formation, timescales, and unrest during caldera collapse and lateral eruption at ocean island basaltic volcanoes (Piton de la Fournaise, La Réunion). *Earth and Planetary Science Letters* **515**, 187–199.

Albert, H., Costa, F. & Martí, J. (2016). Years to weeks of seismic unrest and magmatic intrusions precede monogenetic eruptions. *Geology* **44**, 211–214.

Alford, S. E., Alt, J. C. & Shanks, W. C. III. (2011). Sulfur geochemistry and microbial sulfate reduction during low-temperature alteration of uplifted lower oceanic crust: insights from ODP hole 735B. *Chemical Geology* **286**, 185–195.

Allard, P. (2010). A CO_2-rich gas trigger of explosive paroxysms at Stromboli basaltic volcano, Italy. *Journal of Volcanology and Geothermal Research* **189**, 363–374.

Alt, J. C. (1994). A sulfur isotopic profile through the Troodos ophiolite, Cyprus: primary composition and the effects of seawater hydrothermal alteration. *Geochimica et Cosmochimica Acta* **58**, 1825–1840.

Alt, J. C. & Anderson, T. F. (1991). 5. Mineralogy and isotopic composition of sulfur in layer 3 gabbros from the Indian ocean, hole 735B. *Proceedings of the Ocean Drilling Program, Scientific Results* **118**, 113–125.

Alt, J. C. & Burdett, J. W. (1992). Sulfur in Pacific deep-sea sediments (leg 129) and implications for cycling of sediment in subduction zones. *Proceedings of the Ocean Drilling Program, Scientific Results* **129**, 283–294.

Alt, J. C., Garrido, C. J., Shanks, W. C. III., Turchyn, A., Padrón-Navarta, J. A., Sánchez-Vizcaíno, V. L., Pugnaire, M. T. G. & Marchesi, C. (2012a). Recycling of water, carbon, and sulfur during subduction of serpentinites: a stable isotope study of Cerro del Almirez, Spain. *Earth and Planetary Science Letters* **327**–**328**, 50–60.

Alt, J. C., Schwarzenbach, E. M., Früh-Green, G. L., Shanks, W. C. III., Bernasconi, S. M., Garrido, C. J., Crispini, L., Gaggero, L., Padrón-Navarta, J. A. & Marchesi, C. (2013). The role of serpentinites in cycling of carbon and sulfur: seafloor serpentinization and subduction metamorphism. *Lithos* **178**, 40–54.

Alt, J. C. & Shanks, W. C. III. (1998). Sulfur in serpentinized oceanic peridotites: serpentinization processes and microbial sulfate reduction. *Journal of Geophysical Research: Solid Earth* **103**, 9917–9929.

Alt, J. C. & Shanks, W. C. III. (2003). Serpentinization of abyssal peridotites from the MARK area, Mid-Atlantic Ridge: sulfur geochemistry and reaction modeling. *Geochimica et Cosmochimica Acta* **67**, 641–653.

Alt, J. C. & Shanks, W. C. (2011). Microbial sulfate reduction and the sulfur budget for a complete section of altered oceanic basalts, IODP Hole 1256D (eastern Pacific). *Earth and Planetary Science Letters* **310**, 73–83.

Alt, J. C., Shanks, W. C. III., Bach, W., Paulick, H., Garrido, C. J. & Beaudoin, G. (2007). Hydrothermal alteration and microbial sulfate reduction in peridotite and gabbro exposed by detachment faulting at the Mid-Atlantic Ridge, 15°20'N (ODP leg 209): a sulfur and oxygen isotope study. *Geochemistry Geophysics Geosystems* **8**, Q08002.

Alt, J. C., Shanks, W. C. III., Crispini, L., Gaggero, L., Schwarzenbach, E. M., Früh-Green, G. L. & Bernasconi, S. M. (2012b). Uptake of carbon and sulfur during seafloor serpentinization and the effects of subduction metamorphism in Ligurian peridotites. *Chemical Geology* **322**–**323**, 268–277.

Alt, J. C., Shanks, W. C. III. & Jackson, M. C. (1993). Cycling of sulfur in subduction zones: the geochemistry of sulfur in the Mariana Island Arc and back-arc trough. *Earth and Planetary Science Letters* **119**, 477–494.

Alt, J. C., Zuleger, E. & Erzinger, J. (1995). 14. Mineralogy and stable isotopic compositions of the hydrothermally altered lower sheeted dike complex, hole 504B, leg 140. *Proceedings of the Ocean Drilling Program, Scientific Results* **137**/**140**, 155–166.

Anderson, A. T. (1973). The before-eruption water content of some high-alumina magmas. *Bulletin Volcanologique* **37**, 530–552.

Arculus, R. J. & Powell, R. (1986). Source component mixing in the regions of arc magma generation. *Journal of Geophysical Research: Solid Earth* **91**, 5913–5926.

Asamori, K. & Zhao, D. (2015). Teleseismic shear wave tomography of the Japan subduction zone. *Geophysical Journal International* **203**, 1752–1772.

Aster, E. M., Wallace, P. J., Moore, L. R., Watkins, J., Gazel, E. & Bodnar, R. J. (2016). Reconstructing CO_2 concentrations in basaltic melt inclusions using Raman analysis of vapor bubbles. *Journal of Volcanology and Geothermal Research* **323**, 148–162.

Baba, T., Tanioka, Y., Cummins, P. R. & Uhira, K. (2002). The slip distribution of the 1946 Nankai earthquake estimated from tsunami inversion using a new plate model. *Physics of the Earth and Planetary Interiors* **132**, 59–73.

Baker, D. R. & Moretti, R. (2011). Modeling the solubility of sulfur in magmas: a 50-year old geochemical challenge. *Reviews in Mineralogy and Geochemistry* **73**, 167–213.

Bali, E., Hartley, M. E., Halldórsson, S. A., Gudfinnsson, G. H. & Jakobsson, S. (2018). Melt inclusion constraints on volatile systematics and degassing history of the 2014–2015 Holuhraun eruption, Iceland. *Contributions to Mineralogy and Petrology*. Springer Berlin Heidelberg **173**, 9.

Barker, S. J., Rowe, M. C., Wilson, C. J. N., Gamble, J. A., Rooyakkers, S. M., Wysoczanski, R. J., Illsley-Kemp, F. & Kenworthy, C. C. (2020). What lies beneath? Reconstructing the primitive magmas fueling voluminous silicic volcanism using olivine-hosted melt inclusions. *Geology* **48**, 504–508.

Beaudoin, G., Taylor, B. E., Rumble, D. III. & Thiemens, M. (1994). Variations in the sulfur isotope composition of troilite from the Cañon Diablo iron meteorite. *Geochimica et Cosmochimica Acta* **58**, 4253–4255.

Beaudry, P., Longpré, M.-A., Economos, R., Wing, B. A., Bui, T. H. & Stix, J. (2018). Degassing-induced fractionation of multiple sulphur isotopes unveils post-Archaean recycled oceanic crust signal in hotspot lava. *Nature Communications* **9**, 5093.

Bebout, G. E., Ryan, J. G., Leeman, W. P. & Bebout, A. E. (1999). Fractionation of trace elements by subduction-zone metamorphism – effect of convergent-margin thermal evolution. *Earth and Planetary Science Letters* **171**, 63–81.

Bernard, A., Knittel, U., Weber, B., Weis, D., Albrecht, A., Hattori, K., Klein, J. & Oles, D. (1996). Petrology and geochemistry of the 1991 eruption products of Mount Pinatubo. *Fire and mud: eruptions and lahars of Mount Pinatubo, Philippines,* 767–797.

Bigeleisen, J. & Mayer, M. G. (1947). Calculation of equilibrium constants for isotopic exchange reactions. *The Journal of Chemical Physics* **15**, 261–267.

Bouvier, A.-S., Deloule, E. & Métrich, N. (2010a). Fluid inputs to magma sources of St.Vincent and Grenada (Lesser Antilles): new insights from trace elements in olivine-

hosted melt inclusions. *Journal of Petrology* **51**, 1597–1615.

Bouvier, A.-S., Manzini, M., Rose-Koga, E. F., Nichols, A. R. L. & Baumgartner, L. P. (2019). Tracing of Cl input into the sub-arc mantle through the combined analysis of B, O and Cl isotopes in melt inclusions. *Earth and Planetary Science Letters* **507**, 30–39.

Bouvier, A.-S., Métrich, N. & Deloule, E. (2008). Slab-derived fluids in the magma sources of St. Vincent (Lesser Antilles arc): volatile and light element imprints. *Journal of Petrology* **49**, 1427–1448.

Bouvier, A.-S., Métrich, N. & Deloule, E. (2010b). Light elements, volatiles, and stable isotopes in basaltic melt inclusions from Grenada, Lesser Antilles: inferences for magma genesis. *Geochemistry, Geophysics, Geosystems* **11**, Q09004.

Brown, J. R., Taylor, R. N. & Iguchi, M. (2020). Using high-resolution Pb isotopes to unravel the petrogenesis of Sakurajima volcano, Japan. *Bulletin of Volcanology* **82**, 36.

Bucholz, C. E., Gaetani, G. A., Behn, M. D. & Shimizu, N. (2013). Post-entrapment modification of volatiles and oxygen fugacity in olivine-hosted melt inclusions. *Earth and Planetary Science Letters* **374**, 145–155.

Burdo, R. A. & Morrison, H. G. (1971). *Table of atomic and molecular lines for spark source mass spectrometry of complex sample-graphite mixes*. *Report 1670*. Ithaca, New York: Materials Science Center, Cornell University.

Burton, M. R., Allard, P., Muré, F. & La Spina, A. (2007). Magmatic gas composition reveals the source depth of slug-driven Strombolian explosive activity. *Science* **317**, 227–230.

Cabral, R. A., Jackson, M. G., Rose-Koga, E. F., Koga, K. T., Whitehouse, M. J., Antonelli, M. A., Farquhar, J., Day, J. M. D. & Hauri, E. H. (2013). Anomalous sulphur isotopes in plume lavas reveal deep mantle storage of Archaean crust. *Nature* **496**, 490–493.

Canfield, D. E. (2001). Biogeochemistry of sulfur isotopes. *Reviews in Mineralogy and Geochemistry* **43**, 607–636.

Canil, D. & Fellows, S. A. (2017). Sulphide-sulphate stability and melting in subducted sediment and its role in arc mantle redox and chalcophile cycling in space and time. *Earth and Planetary Science Letters* **470**, 73–86.

Carn, S. A., Fioletov, V. E., Mclinden, C. A., Li, C. & Krotkov, N. A. (2017). A decade of global volcanic SO_2 emissions measured from space. *Scientific Reports* **7**, 44095.

Carroll, M. R. & Rutherford, M. J. (1988). Sulfur speciation in hydrous experimental glasses of varying oxidation state: results from measured wavelength shifts of sulfur X-rays. *American Journal of Science* **73**, 845–849.

Carroll, M. R. & Webster, J. D. (1994). Solubilities of sulfur, noble gases, nitrogen, chlorine and fluorine in magmas. *Reviews in Mineralogy and Geochemistry* **30**, 231–280.

Chaussidon, M., Albarède, F. & Sheppard, S. M. F. (1989). Sulphur isotope variations in the mantle from ion microprobe analyses of micro-sulphide inclusions. *Earth and Planetary Science Letters* **92**, 144–156.

Chaussidon, M. & Lorand, J.-P. (1990). Sulphur isotope composition of orogenic spinel lherzolite massifs from Ariege (North-Eastern Pyrenees, France): an ion microprobe study. *Geochimica et Cosmochimica Acta* **54**, 2835–2846.

Chaussidon, M., Sheppard, S. M. F. & Michard, A. (1991). Hydrogen, sulphur and neodymium isotope variations in the mantle beneath the EPR at 12˚50'N. *Stable isotope geochemistry: A tribute to Samuel Epstein*, 325–337.

Chen, Y., Provost, A., Schiano, P. & Cluzel, N. (2011). The rate of water loss from olivine-hosted melt inclusions. *Contributions to Mineralogy and Petrology* **162**, 625–636.

Churikova, T., Wörner, G., Mironov, N. & Kronz, A. (2007). Volatile (S, Cl and F) and fluid mobile trace element compositions in melt inclusions: implications for variable fluid sources across the Kamchatka arc. *Contributions to Mineralogy and Petrology* **154**, 217–239.

Cooper, L. B., Ruscitto, D. M., Plank, T., Wallace, P. J., Syracuse, E. M. & Manning, C. E. (2012). Global variations in H_2O/Ce: 1. Slab surface temperatures beneath volcanic arcs. *Geochemistry, Geophysics, Geosystems* **13**, Q03024.

Costa, F., Dohmen, R. & Chakraborty, S. (2008). Time scales of magmatic processes from modeling the zoning patterns of crystals. *Reviews in Mineralogy and Geochemistry* **69**, 545–594.

Cottrell, E., Spiegelman, M. & Langmuir, C. H. (2002). Consequences of diffusive reequilibration for the interpretation of melt inclusions. *Geochemistry, Geophysics, Geosystems* **3**, 1–26.

Cruse, A. M. & Lyons, T. W. (2004). Trace metal records of regional paleoenvironmental variability in Pennsylvanian (Upper Carboniferous) black shales. *Chemical Geology* **206**, 319–345.

Danyushevsky, L. V., Della-Pasqua, F. N. & Sokolov, S. (2000). Re-equilibration of melt inclusions trapped by magnesian olivine phenocrysts from subduction-related magmas: petrological implications. *Contributions to Mineralogy and Petrology* **138**, 68–83.

Danyushevsky, L. V., McNeill, A. W. & Sobolev, A. V. (2002a). Experimental and petrological studies of melt inclusions in phenocrysts from mantle-derived magmas: an

overview of techniques, advantages and complications. *Chemical Geology* **183**, 5–24.

Danyushevsky, L. V., Sokolov, S. & Falloon, T. J. (2002b). Melt inclusions in olivine phenocrysts: using diffusive re-equilibration to determine the cooling history of a crystal, with implications for the origin of olivine-phyric volcanic rocks. *Journal of Petrology* **43**, 1651–1671.

Davidson, J., Turner, S., Handley, H., Macpherson, C. & Dosseto, A. (2007). Amphibole "sponge" in arc crust? *Geology* **35**, 787–790.

de Hoog, J. C. M., Taylor, B. E. & van Bergen, M. J. (2001). Sulfur isotope systematics of basaltic lavas from Indonesia: implications for the sulfur cycle in subduction zones. *Earth and Planetary Science Letters* **189**, 237–252.

De Laeter, J. R., Böhlke, J. K., De Bièvre, P., Hidaka, H., Peiser, H. S., Rosman, K. J. R. & Taylor, P. D. P. (2003). Atomic weights of the elements: review 2000 (IUPAC technical report). *Pure and Applied chemistry* **75**, 683–800.

de Moor, J. M., Fischer, T. P., Sharp, Z. D., King, P. L., Wilke, M., Botcharnikov, R. E., Cottrell, E., Zelenski, M., Marty, B., Klimm, K., Rivard, C., Ayalew, D., Ramirez, C. & Kelley, K. A. (2013). Sulfur degassing at Erta Ale (Ethiopia) and Masaya (Nicaragua) volcanoes: implications for degassing processes and oxygen fugacities of basaltic systems. *Geochemistry, Geophysics, Geosystems* **14**, 4076–4108.

de Moor, J. M., Kern, C., Avard, G., Muller, C., Aiuppa, A., Saballos, A., Ibarra, M., LaFemina, P., Protti, M. & Fischer, T. P. (2017). A new sulfur and carbon degassing inventory for the Southern Central American Volcanic Arc: the importance of accurate time-series data sets and possible tectonic processes responsible for temporal variations in arc-scale volatile emissions. *Geochemistry, Geophysics, Geosystems* **18**, 4437–4468.

de Ronde, C. E. J., Faure, K., Bray, C. J., Chappell, D. A. & Wright, I. C. (2003). Hydrothermal fluids associated with seafloor mineralization at two southern Kermadec arc volcanoes, offshore New Zealand. *Mineralium Deposita* **38**, 217–233.

Defant, M. J. & Drummond, M. S. (1990). Derivation of some modern arc magmas by melting of young subducted lithosphere. *Nature* **347**, 662–665.

Delacour, A., Früh-Green, G. L., Bernasconi, S. M. & Kelley, D. S. (2008). Sulfur in peridotites and gabbros at Lost City (30˚N, MAR): implications for hydrothermal alteration and microbial activity during serpentinization. *Geochimica et Cosmochimica Acta* **72**, 5090–5110.

DePaolo, D. J. (1981). Trace element and isotopic effects of combined wallrock assimilation and fractional crystallization. *Earth and Planetary Science Letters* **53**, 189–202.

Deschamps, A. & Lallemand, S. (2002). The West Philippine Basin: an Eocene to early Oligocene back arc basin opened between two opposed subduction zones. *Journal of Geophysical Research: Solid Earth* **107**, 2322.

Deschamps, F., Godard, M., Guillot, S. & Hattori, K. (2013). Geochemistry of subduction zone serpentinites: a review. *Lithos* **178**, 96–127.

Deschamps, F., Guillot, S., Godard, M., Chauvel, C., Andreani, M. & Hattori, K. (2010). In situ characterization of serpentinites from forearc mantle wedges: timing of serpentinization and behavior of fluid-mobile elements in subduction zones. *Chemical Geology* **269**, 262–277.

Devine, J. D., Gardner, J. E., Brack, H. P., Layne, G. D. & Rutherford, M. J. (1995). Comparison of microanalytical methods for estimating H_2O contents of silicic volcanic glasses. *American Mineralogist* **80**, 319–328.

Ding, T., Valkiers, S., Kipphardt, H., De Bièvre, P., Taylor, P. D. P., Gonfiantini, R. & Krouse, R. (2001). Calibrated sulfur isotope abundance ratios three IAEA sulfur isotope reference materials and V-CDT with a reassessment of the atomic weight of sulfur. *Geochimica et Cosmochimica Acta* **65**, 2433–2437.

Dixon, J. E., Clague, D. A. & Stolper, E. M. (1991). Degassing history of water, sulfur, and carbon in submarine lavas from Kilauea volcano, Hawaii. *Journal of Geology* **99**, 371–394.

Dixon, J. E., Stolper, E. M. & Holloway, J. R. (1995). An experimental study of water and carbon dioxide solubilities in mid-ocean ridge basaltic liquids. Part I: calibration and solubility models. *Journal of Petrology* **36**, 1607–1631.

Druitt, T. H., Mercier, M., Florentin, L., Deloule, E., Cluzel, N., Flaherty, T., Médard, E. & Cadoux, A. (2016). Magma storage and extraction associated with plinian and interplinian activity at Santorini caldera (Greece). *Journal of Petrology* **57**, 461–494.

Duan, Z. & Zhang, Z. (2006). Equation of state of the H_2O, CO_2, and H_2O–CO_2 systems up to 10 GPa and 2573.15 K: molecular dynamics simulations with ab initio potential surface. *Geochimica et Cosmochimica Acta* **70**, 2311–2324.

Edmonds, M. & Wallace, P. J. (2017). Volatiles and exsolved vapor in volcanic systems. *Elements* **13**, 29–34.

Eickmann, B., Thorseth, I. H., Peters, M., Strauss, H., Bröcker, M. & Pedersen, R. B. (2014). Barite in hydrothermal environments as a recorder of subseafloor processes: a multiple-isotope study from the Loki's Castle vent field. *Geobiology* **12**, 308–321.

Eiler, J. M. (2001). Oxygen isotope variations of basaltic lavas and upper mantle rocks.

Reviews in Mineralogy and Geochemistry **43**, 319–364.

Elburg, M. A., Kamenetsky, V. S., Foden, J. D. & Sobolev, A. (2007). The origin of medium-K ankaramitic arc magmas from Lombok (Sunda arc, Indonesia): mineral and melt inclusion evidence. *Chemical Geology* **240**, 260–279.

Elliott, T. (2003). Tracers of the slab. In: Eiler, J. M. (ed.) *Inside the Subduction Factory*. American Geophysical Union, 23–45.

Elliott, T., Plank, T., Zindler, A., White, W. & Bourdon, B. (1997). Element transport from slab to volcanic front at the Mariana arc. *Journal of Geophysical Research: Solid Earth* **102**, 14991–15018.

Evans, K. A., Tomkins, A. G., Cliff, J. & Fiorentini, M. L. (2014). Insights into subduction zone sulfur recycling from isotopic analysis of eclogite-hosted sulfides. *Chemical Geology* **365**, 1–19.

Ferriss, E., Plank, T., Newcombe, M., Walker, D. & Hauri, E. (2018). Rates of dehydration of olivines from San Carlos and Kilauea Iki. *Geochimica et Cosmochimica Acta* **242**, 165–190.

Fiege, A., Holtz, F., Behrens, H., Mandeville, C. W., Shimizu, N., Crede, L. S. & Göttlicher, J. (2015). Experimental investigation of the S and S-isotope distribution between H_2O–S ± Cl fluids and basaltic melts during decompression. *Chemical Geology* **393**–**394**, 36–54.

Fiege, A., Holtz, F., Shimizu, N., Mandeville, C. W., Behrens, H. & Knipping, J. L. (2014). Sulfur isotope fractionation between fluid and andesitic melt: an experimental study. *Geochimica et Cosmochimica Acta* **142**, 501–521.

Foley, S. F., Barth, M. G. & Jenner, G. A. (2000). Rutile/melt partition coefficients for trace elements and an assessment of the influence of rutile on the trace element characteristics of subduction zone magmas. *Geochimica et Cosmochimica Acta* **64**, 933–938.

Fortin, M.-A., Riddle, J., Desjardins-Langlais, Y. & Baker, D. R. (2015). The effect of water on the sulfur concentration at sulfide saturation (SCSS) in natural melts. *Geochimica et Cosmochimica Acta* **160**, 100–116.

Fourcade, S. & Allegre, C. J. (1981). Trace element behavior in granite genesis: a case study The calc-alkaline plutonic association from the Querigut Complex (Pyrénées, France). *Contributions to Mineralogy and Petrology* **76**, 177–195.

Fujino, N. & Kobayashi, T. (1997). Eruption history of Kaimondake volcano, southern Kyushu, Japan. *Bulletin of the volcanological society of Japan* **42**, 195-211 (in Japanese with English abstract).

Gaetani, G. A., O'Leary, J. A., Shimizu, N., Bucholz, C. E. & Newville, M. (2012). Rapid

reequilibration of H_2O and oxygen fugacity in olivine-hosted melt inclusions. *Geology* **40**, 915–918.

Gagnon, J. E., Fryer, B. J., Samson, I. M. & Williams-Jones, A. E. (2008). Quantitative analysis of silicate certified reference materials by LA-ICPMS with and without an internal standard. *Journal of Analytical Atomic Spectrometry* **23**, 1529–1537.

Gao, S., Liu, X., Yuan, H., Hattendorf, B., Günther, D., Chen, L. & Hu, S. (2002). Determination of Forty Two Major and Trace Elements in USGS and NIST SRM Glasses by Laser Ablation-Inductively Coupled Plasma-Mass Spectrometry. *Geostandards and Geoanalytical Research* **26**, 181–196.

Gardner, J. E., Rutherford, M., Carey, S. & Sigurdsson, H. (1995). Experimental constraints on pre-eruptive water contents and changing magma storage prior to explosive eruptions of Mount St Helens volcano. *Bulletin of Volcanology* **57**, 1–17.

Ghiorso, M. S. & Gualda, G. A. R. (2015). An H_2O–CO_2 mixed fluid saturation model compatible with rhyolite-MELTS. *Contributions to Mineralogy and Petrology* **169**, 1–30.

Ghiorso, M. S. & Sack, R. O. (1995). Chemical mass transfer in magmatic processes IV. A revised and internally consistent thermodynamic model for the interpolation and extrapolation of liquid-solid equilibria in magmatic systems at elevated temperatures and pressures. *Contributions to Mineralogy and Petrology* **119**, 197–212.

Gill, J. B. (1981). *Orogenic andesites and plate tectonics*. Springer, Berlin, Heiledberg.

Giordano, D., Nichols, A. R. L. & Dingwell, D. B. (2005). Glass transition temperatures of natural hydrous melts: A relationship with shear viscosity and implications for the welding process. *Journal of Volcanology and Geothermal Research* **142**, 105–118.

Giordano, D., Russell, J. K. & Dingwell, D. B. (2008). Viscosity of magmatic liquids: a model. *Earth and Planetary Science Letters* **271**, 123–134.

Giuliani, A., Fiorentini, M. L., Martin, L. A. J., Farquhar, J., Phillips, D., Griffin, W. L. & LaFlamme, C. (2016). Sulfur isotope composition of metasomatised mantle xenoliths from the Bultfontein kimberlite (Kimberley, South Africa): contribution from subducted sediments and the effect of sulfide alteration on S isotope systematics. *Earth and Planetary Science Letters* **445**, 114–124.

Gonfiantini, R., Stichler, W. & Rozanski, K. (1993). Standards and intercomparison materials distributed by the international atomic energy agency for stable isotope measurements. *Proceedings of a consultants meeting held in Vienna, 1-3 December 1993*, 13–30.

Greinert, J., Bollwerk, S. M., Derkachev, A., Bohrmann, G. & Suess, E. (2002). Massive barite deposits and carbonate mineralization in the Derugin Basin, Sea of Okhotsk: precipitation

processes at cold seep sites. *Earth and Planetary Science Letters* **203**, 165–180.

Gualda, G. A. R., Ghiorso, M. S., Lemons, R. V. & Carley, T. L. (2012). Rhyolite-MELTS: a modified calibration of MELTS optimized for silica-rich, fluid-bearing magmatic systems. *Journal of Petrology* **53**, 875–890.

Gurenko, A. A. (2021). Origin of sulphur in relation to silicate-sulphide immiscibility in Tolbachik primitive arc magma (Kamchatka, Russia): insights from sulphur and boron isotopes. *Chemical Geology* **576**, 120244.

Gurenko, A. A., Belousov, A. B., Kamenetsky, V. S. & Zelenski, M. E. (2018). Origin of volatiles emitted by Plinian mafic eruptions of the Chikurachki volcano, Kurile arc, Russia: trace element, boron and sulphur isotope constraints. *Chemical Geology* **478**, 131–147.

Gurenko, A. A., Chaussidon, M. & Schmincke, H.-U. (2001). Magma ascent and contamination beneath one intraplate volcano: evidence from S and O isotopes in glass inclusions and their host clinopyroxenes from Miocene basaltic hyaloclastites southwest of Gran Canaria (Canary island). *Geochimica et Cosmochimica Acta* **65**, 4359–4374.

Hacker, B. R. (2008). H_2O subduction beyond arcs. *Geochemistry, Geophysics, Geosystems* **9**, Q03001.

Hammerli, J., Kemp, A. I. S., Barrett, N., Wing, B. A., Roberts, M., Arculus, R. J., Boivin, P., Nude, P. M. & Rankenburg, K. (2017). Sulfur isotope signatures in the lower crust: a SIMS study on S-rich scapolite of granulites. *Chemical Geology* **454**, 54–66.

Hanyu, T., Yamamoto, J., Kimoto, K., Shimizu, K. & Ushikubo, T. (2020). Determination of total CO_2 in melt inclusions with shrinkage bubbles. *Chemical Geology* **557**, 119855.

Harmon, R. S., Hoefs, J. & Wedepohl, K. H. (1987). Stable isotope (O, H, S) relationships in Tertiary basalts and their mantle xenoliths from the Northern Hessian Depression, W.-Germany. *Contributions to Mineralogy and Petrology* **95**, 350–369.

Hart, S. R. & Gaetani, G. A. (2006). Mantle Pb paradoxes: the sulfide solution. *Contributions to Mineralogy and Petrology* **152**, 295–308.

Hartley, M. E., Bali, E., Maclennan, J., Neave, D. A. & Halldórsson, S. A. (2018). Melt inclusion constraints on petrogenesis of the 2014–2015 Holuhraun eruption, Iceland. *Contributions to Mineralogy and Petrology* **173**, 10.

Hata, M., Takakura, S., Matsushima, N., Hashimoto, T. & Utsugi, M. (2016). Crustal magma pathway beneath Aso caldera inferred from three-dimensional electrical resistivity structure. *Geophysical Research Letters* **43**, 10720–10727.

Hauri, E., Wang, J., Dixon, J. E., King, P. L., Mandeville, C. & Newman, S. (2002). SIMS

analysis of volatiles in silicate glasses 1. Calibration, matrix effects and comparisons with FTIR. *Chemical Geology* **183**, 99–114.

Helo, C., Longpré, M.-A., Shimizu, N., Clague, D. A. & Stix, J. (2011). Explosive eruptions at mid-ocean ridges driven by CO_2-rich magmas. *Nature Geoscience*. Nature Publishing Group **4**, 260–263.

Hermann, J. (2002). Allanite: thorium and light rare earth element carrier in subducted crust. *Chemical Geology* **192**, 289–306.

Herzig, P. M., Petersen, S. & Hannington, M. D. (1998). Geochemistry and sulfur-isotopic composition of the TAG hydrothermal mound, Mid-Atlantic Ridge, 26°N. *Proceedings of the Ocean Drilling Program: Scientific Results* **158**, 47–70.

Hickey-Vargas, R., Yogodzinski, G. M., Ishizuka, O., McCarthy, A., Bizimis, M., Kusano, Y., Savov, I. P. & Arculus, R. (2018). Origin of depleted basalts during subduction initiation and early development of the Izu-Bonin-Mariana island arc: evidence from IODP expedition 351 site U1438, Amami-Sankaku basin. *Geochimica et Cosmochimica Acta* **229**, 85–111.

Hildreth, W. & Moorbath, S. (1988). Crustal contributions to arc magmatism in the Andes of Central Chile. *Contributions to Mineralogy and Petrology* **98**, 455–489.

Hirata, Y., Ueta, K., Miyawaki, R., Iemura, K., Yokoyoma, T. & Miyawaki, A. (2020). Tephra stratigraphy and an about 4000-year-old slope failure on Janoo volcano, NW Aso caldera. *Transactions, Japanese Geomorphological Union* **41**, 27-47 (in Japanese with English abstract).

Hirose, F., Nakajima, J. & Hasegawa, A. (2008). Three-dimensional seismic velocity structure and configuration of the Philippine Sea slab in southwestern Japan estimated by double-difference tomography. *Journal of Geophysical Research: Solid Earth* **113**, B09315.

Hoefs, J. (2018). *Stable isotope geochemistry*. Springer Nature Switzerland AG.

Hoefs, J., Coolen, J. J. M. & Touret, J. (1981). The sulfur and carbon isotope composition of scapolite-rich granulites from southern Tanzania. *Contributions to Mineralogy and Petrology* **78**, 332–336.

Holloway, J. R. & Blank, J. G. (1994). Application of experimental results to C-O-H species in natural melts. *Reviews in Mineralogy and Geochemistry* **30**, 187–230.

Huang, F. & Sverjensky, D. A. (2019). Extended Deep Earth Water model for predicting major element mantle metasomatism. *Geochimica et Cosmochimica Acta* **254**, 192–230.

Huang, Z., Zhao, D., Hasegawa, A., Umino, N., Park, J.-H. & Kang, I.-B. (2013). Aseismic deep subduction of the Philippine Sea plate and slab window. *Journal of Asian Earth*

Sciences **75**, 82–94.

Hubberten, H. W., Nielsen, H. & Puchelt, H. (1975). The enrichment of ^{34}S in the solfataras of the Nea Kameni volcano, Santorini Archipelago, Greece. *Chemical Geology* **16**, 197–205.

Ikebe, S., Watanabe, K. & Miyabuchi, Y. (2008). The sequence and style of the 1988-1955 eruption of Nakadake Aso volcano, Kyushu, Japan. *Bulletin of the volcanological society of Japan* **53**, 15-33 (in Japanese with English abstract).

Imai, A., Listanco, E. L. & Fujii, T. (1993). Petrologic and sulfur isotopic significance of highly oxidized and sulfur-rich magma of Mt. Pinatubo, Philippines. *Geology* **21**, 699.

Imura, R. & Kobayashi, T. (2001). *Geological map of Kirishima volcano, 1:50,000*. *Geological map of volcanoes 11*.

Inoue, K. (1985). Lateral variations of K_2O, Rb in Kirishima volcano. *Programme and abstracts of the Volcanological Society of Japan 2017 fall meeting* 313 (in Japanese).

Ionov, D. A., Hoefs, J., Wedepohl, K. H. & Wiechert, U. (1992). Content and isotopic composition of sulphur in ultramafic xenoliths from central Asia. *Earth and Planetary Science Letters* **111**, 269–286.

Iriyama, Y. & Toramaru, A. (2015). Stratigraphic variations in grain-size characteristics of pyroclastic fall deposits during the 2011 subplinian eruption of Shinmoedake, Kirishima volcano, Japan. *Bulletin of the volcanological society of Japan* **60**, 399-410 (in Japanese with English abstract).

Ishihara, S. & Chappell, B. W. (2010). Chemical compositions of the Miocene granitoids of the Okueyama, Hoei mine and Takakumayama plutons, Outer Zone of SW Japan. *Bulletin of the Geological Survey of Japan* **61**, 17–38.

Ishihara, S. & Sasaki, A. (1989). Sulfur isotopic ratios of the magnetite-series and ilmenite-series granitoids of the Sierra Nevada batholith—A reconnaissance study. *Geology* **17**, 788–791.

Ishizuka, O., Hickey-Vargas, R., Arculus, R. J., Yogodzinski, G. M., Savov, I. P., Kusano, Y., McCarthy, A., Brandl, P. A. & Sudo, M. (2018). Age of Izu–Bonin–Mariana arc basement. *Earth and Planetary Science Letters* **481**, 80–90.

Iwamori, H. (1991). Zonal structure of Cenozoic basalts related to mantle upwelling in southwest Japan. *Journal of Geophysical Research* **96**, 6157–6170.

Iwamori, H. (1992). Degree of melting and source composition of Cenozoic basalts in southwest Japan: evidence for mantle upwelling by flux melting. *Journal of Geophysical Research: Solid Earth* **97**, 10983–10995.

Iwamori, H. (2007). Transportation of H_2O beneath the Japan arcs and its implications for global water circulation. *Chemical Geology* **239**, 182–198.

Iwamori, H. & Zhao, D. (2000). Melting and seismic structure beneath the northeast Japan Arc. *Geophysical Research Letters* **27**, 425–428.

Iyer, S. S., de Oliveira, M. A. F., Hoefs, J. & Krouse, H. R. (1992). Sulfur and carbon isotopes in scapolite-bearing granulites of the São José do Rio Pardo area, Brazil. *Journal of South American Earth Sciences* **6**, 59–66.

Japan Meteorological Agency (2016). Volcanic activity of Asosan volcano —October 2014–February 2015—. *Report of Coordinating Comittee for Prediction of Volcanic Eruption* **120**, 166-186 (in Japanese).

Japan Meteorological Agency (2020). *Results of volcanic gas observation at Aso volcano*. http://www.data.jma.go.jp/svd/vois/data/fukuoka/rovdm/Asosan_rovdm/Asosan_rovdm.html (accessed April 20, 2020).

Jarosewich, E., Nelen, J. A. & Norberg, J. A. (1980). Reference samples for electron microprobe analysis. *Geostandards Newsletter* **4**, 43–47.

Jégo, S. & Dasgupta, R. (2013). Fluid-present melting of sulfide-bearing ocean-crust: experimental constraints on the transport of sulfur from subducting slab to mantle wedge. *Geochimica et Cosmochimica Acta* **110**, 106–134.

Jégo, S. & Dasgupta, R. (2014). The fate of sulfur during fluid-present melting of subducting basaltic crust at variable oxygen fugacity. *Journal of Petrology* **55**, 1019–1050.

Jørgensen, B. B., Isaksen, M. F. & Jannasch, H. W. (1992). Bacterial sulfate reduction above 100˚C in deep-sea hydrothermal vent sediments. *Science* **258**, 1756–1757.

Jugo, P. J., Luth, R. W. & Richards, J. P. (2005). An experimental study of the sulfur content in basaltic melts saturated with immiscible sulfide or sulfate liquids at 1300 ˚C and 1.0 GPa. *Journal of Petrology* **46**, 783–798.

Jugo, P. J., Wilke, M. & Botcharnikov, R. E. (2010). Sulfur K-edge XANES analysis of natural and synthetic basaltic glasses: implications for S speciation and S content as function of oxygen fugacity. *Geochimica et Cosmochimica Acta* **74**, 5926–5938.

Kagoshima, T., Sano, Y., Takahata, N., Maruoka, T., Fischer, T. P. & Hattori, K. (2015). Sulphur geodynamic cycle. *Scientific Reports* **5**, 8330.

Kakubuchi, S., Kido, M. & Hikosan Collaborative Research Group (1995). High-magnesian andesites from the northwestern margin of the Pliocene Kuju-Beppu Tectonic Basin, northern Kyushu, Japan. *Memoir of the Geological Society of Japan* **44**, 125-138 (in Japanese with English abstract).

Kakubuchi, S. & Matsumoto, Y. (1990). Primitive tholeiitic basalt from the Yabakei district, Oita Prefecture, southwest Japan. *Journal of Mineralogy, Petrology and Economic Geology* **85**, 559–568.

Kamata, H. (1998). Quaternary volcanic front at the junction of the South-west Japan Arc and the Ryukyu Arc. *Journal of Asian Earth Sciences* **16**, 67–75.

Kamata, H. & Kobayashi, T. (1997). The eruptive rate and history of Kuju volcano in Japan during the past 15,000 years. *Journal of Volcanology and Geothermal Research* **76**, 163–171.

Kamata, H. & Kodama, K. (1994). Tectonics of an arc-arc junction: an example from Kyushu Island at the junction of the southwest Japan arc and the Ryukyu arc. *Tectonophysics* **233**, 69–81.

Kamata, H. & Kodama, K. (1999). Volcanic history and tectonics of the southwest Japan arc. *The Island Arc* **8**, 393–403.

Kamenetsky, V. S., Sobolev, A. V., Eggins, S. M., Crawford, A. J. & Arculus, R. J. (2002). Olivine-enriched melt inclusions in chromites from low-Ca boninites, Cape Vogel, Papua New Guinea: evidence for ultramafic primary magma, refractory mantle source and enriched components. *Chemical Geology* **183**, 287–303.

Kanehira, K., Yui, S., Sakai, H. & Sasaki, A. (1973). Sulphide globules and sulphur isotope ratios in the abyssal tholeiite from the Mid-Atlantic Ridge near 30˚N latitude. *Geochemical Journal* **7**, 89–96.

Kawaguchi, M., Hasenaka, T., Koga, K. T., Rose, E. F., Yasuda, A., Hokanishi, N., Mori, Y., Shimizu, K. & Ushikubo, T. (2021). Persistent gas emission originating from a deep basaltic magma reservoir of an active volcano: the case of Aso volcano, Japan. *Contributions to Mineralogy and Petrology* **176**, 6.

Kawamoto, T., Kanzaki, M., Mibe, K., Matsukage, K. N. & Ono, S. (2012). Separation of supercritical slab-fluids to form aqueous fluid and melt components in subduction zone magmatism. *Proceedings of the National Academy of Sciences* **109**, 18695–18700.

Kawamoto, T., Mibe, K., Bureau, H., Reguer, S., Mocuta, C., Kubsky, S., Thiaudière, D., Ono, S. & Kogiso, T. (2014). Large-ion lithophile elements delivered by saline fluids to the sub-arc mantle. *Earth, Planets and Space* **66**, 61.

Kawamoto, T., Yoshikawa, M., Kumagai, Y., Mirabueno, M. H. T., Okuno, M. & Kobayashi, T. (2013). Mantle wedge infiltrated with saline fluids from dehydration and decarbonation of subducting slab. *Proceedings of the National Academy of Sciences* **110**, 9663–9668.

Kawanabe, Y., Hoshizumi, H., Itoh, J. & Yamasaki, S. (2015). *Geological map of Kuju volcano*.

Geological map of volcanoes 19.

Kawanabe, Y. & Sakaguchi, K. (2005). *Geology of the Kaimon Dake district*. *Quadrangle Series, 1:50,000*. Geological Survey of Japan, AIST.

Kelley, K. A. & Cottrell, E. (2009). Water and the oxidation state of subduction zone magmas. *Science* **325**, 605–607.

Kerrick, D. (2002). Serpentinite seduction. *Science* **298**, 1344–1345.

Kessel, R., Schmidt, M. W., Ulmer, P. & Pettke, T. (2005). Trace element signature of subduction-zone fluids, melts and supercritical liquids at 120-180 km depth. *Nature* **437**, 724–727.

Kilinc, A., Carmichael, I. S. E., Rivers, M. L. & Sack, R. O. (1983). The ferric-ferrous ratio of natural silicate liquids equilibrated in air. *Contributions to Mineralogy and Petrology* **83**, 136–140.

Kiminami, K., Kishita, S. & Imaoka, T. (2009). Marked change in sandstone composition during the Middle Jurassic in Jurassic accretionary complexes of SW Japan, and geologic significance. *The Journal of the Geological Society of Japan* **115**, 578-596 (in Japanese with English abstract).

Kimura, J.-I. (2017). Modeling chemical geodynamics of subduction zones using the Arc Basalt Simulator version 5. *Geosphere* **13**, 992–1025.

Kita, I., Asakawa, Y., Yuri, T., Yasui, M., Shimoike, Y., Yamamoto, M., Hasegawa, H., Taguchi, S. & Sumino, H. (2012). Rifting of Kyushu, Japan, based on the fault-controlled concurrent eruption of oceanic island basalt-type and island arc-type lavas. *Bulletin of Volcanology* **74**, 1121–1139.

Kita, I., Yamamoto, M., Asakawa, Y., Nakagawa, M., Taguchi, S. & Hasegawa, H. (2001). Contemporaneous ascent of within-plate type and island-arc type magmas in the Beppu-Shimabara graben system, Kyushu island, Japan. *Journal of Volcanology and Geothermal Research* **111**, 99–109.

Klemme, S., Prowatke, S., Hametner, K. & Günther, D. (2005). Partitioning of trace elements between rutile and silicate melts: implications for subduction zones. *Geochimica et Cosmochimica Acta* **69**, 2361–2371.

Klimm, K., Blundy, J. D. & Green, T. H. (2008). Trace element partitioning and accessory phase saturation during H_2O-saturated melting of basalt with implications for subduction zone chemical fluxes. *Journal of Petrology* **49**, 523–553.

Klügel, A., Hansteen, T. H., van den Bogaard, P., Strauss, H. & Hauff, F. (2011). Holocene fluid venting at an extinct Cretaceous seamount, Canary archipelago. *Geology* **39**, 855–

858.

Kohlstedt, D. L. & Mackwell, S. J. (1998). Diffusion of hydrogen and intrinsic point defects in olivine. *Zeitschrift für Physikalische Chemie* **207**, 147–162.

Komazawa, M. (1995). Gravimetric analysis of Aso volcano and its interpretation. *Journal of the Geodetic Society of Japan* **41**, 17–45.

Kuno, H. (1960). High-alumina basalt. *Journal of Petrology* **1**, 121–145.

Kuritani, T., Sakuyama, T., Kamada, N., Yokoyama, T. & Nakagawa, M. (2017). Fluid-fluxed melting of mantle versus decompression melting of hydrous mantle plume as the cause of intraplate magmatism over a stagnant slab: implications from Fukue Volcano Group, SW Japan. *Lithos* **282**–**283**, 98–110.

Kusakabe, M., Mayeda, S. & Nakamura, E. (1990). S, O and Sr isotope systematics of active vent materials from the Mariana backarc basin spreading axis at 18°N. *Earth and Planetary Science Letters* **100**, 275–282.

Labidi, J. & Cartigny, P. (2016). Negligible sulfur isotope fractionation during partial melting: evidence from Garrett transform fault basalts, implications for the late-veneer and the hadean matte. *Earth and Planetary Science Letters*. Elsevier B.V. **451**, 196–207.

Labidi, J., Cartigny, P., Birck, J. L., Assayag, N. & Bourrand, J. J. (2012). Determination of multiple sulfur isotopes in glasses: a reappraisal of the MORB $\delta^{34}S$. *Chemical Geology* **334**, 189–198.

Labidi, J., Cartigny, P., Hamelin, C., Moreira, M. & Dosso, L. (2014). Sulfur isotope budget (^{32}S, ^{33}S, ^{34}S and ^{36}S) in Pacific-Antarctic ridge basalts: a record of mantle source heterogeneity and hydrothermal sulfide assimilation. *Geochimica et Cosmochimica Acta* **133**, 47–67.

Labidi, J., Cartigny, P. & Jackson, M. G. (2015). Multiple sulfur isotope composition of oxidized Samoan melts and the implications of a sulfur isotope 'mantle array' in chemical geodynamics. *Earth and Planetary Science Letters* **417**, 28–39.

Labidi, J., Cartigny, P. & Moreira, M. (2013). Non-chondritic sulphur isotope composition of the terrestrial mantle. *Nature* **501**, 208–211.

Lange, R. A., Frey, H. M. & Hector, J. (2009). A thermodynamic model for the plagioclase-liquid hygrometer/thermometer. *American Mineralogist* **94**, 494–506.

Lara, M. & Dasgupta, R. (2020). Partial melting of a depleted peridotite metasomatized by a MORB-derived hydrous silicate melt – Implications for subduction zone magmatism. *Geochimica et Cosmochimica Acta* **290**, 137–161.

Le Maitre, R. W., Streckeisen, A., Zanettin, B., Le Bas, M. J., Bonin, B. & Bateman, P. (2002). *Igneous rocks: A classification and glossary of terms: recommendations of the International Union of Geological Sciences subcommission on the systematics of igneous Rocks (2nd ed.)*. Cambridge: Cambridge University Press.

Le Voyer, M., Cottrell, E., Kelley, K. A., Brounce, M. & Hauri, E. H. (2015). The effect of primary versus secondary processes on the volatile content of MORB glasses: an example from the equatorial Mid-Atlantic Ridge (5°N–3°S). *Journal of Geophysical Research: Solid Earth* **120**, 125–144.

Le Voyer, M., Hauri, E. H., Cottrell, E., Kelley, K. A., Salters, V. J. M., Langmuir, C. H., Hilton, D. R., Barry, P. H. & Füri, E. (2019). Carbon fluxes and primary magma CO_2 contents along the global mid-ocean ridge system. *Geochemistry, Geophysics, Geosystems* **20**, 1387–1424.

Le Voyer, M., Kelley, K. A., Cottrell, E. & Hauri, E. H. (2017). Heterogeneity in mantle carbon content from CO_2-undersaturated basalts. *Nature Communications*. Nature Publishing Group **8**, 14062.

Le Voyer, M., Rose-Koga, E. F., Shimizu, N., Grove, T. L. & Schiano, P. (2010). Two contrasting H_2O-rich components in primary melt inclusions from Mount Shasta. *Journal of Petrology* **51**, 1571–1595.

Lee, C.-T. A., Erdman, M., Yang, W., Ingram, L., Chin, E. J. & DePaolo, D. J. (2018). Sulfur isotopic compositions of deep arc cumulates. *Earth and Planetary Science Letters* **500**, 76–85.

Leeman, W. P., Lewis, J. F., Evarts, R. C., Conrey, R. M. & Streck, M. J. (2005). Petrologic constraints on the thermal structure of the Cascades arc. *Journal of Volcanology and Geothermal Research* **140**, 67–105.

Lesne, P., Kohn, S. C., Blundy, J., Witham, F., Botcharnikov, R. E. & Behrens, H. (2011). Experimental simulation of closed-system degassing in the system basalt–H_2O–CO_2–S–Cl. *Journal of Petrology* **52**, 1737–1762.

Li, C. & Ripley, E. M. (2009). Sulfur contents at sulfide-liquid or anhydrite saturation in silicate melts: empirical equations and example applications. *Economic Geology* **104**, 405–412.

Li, J.-L., Klemd, R., Huang, G.-F., Ague, J. J. & Gao, J. (2020a). Unravelling slab δ34S compositions from in-situ sulphide δ34S studies of high-pressure metamorphic rocks. *International Geology Review* **63**, 109–129.

Li, J.-L., Schwarzenbach, E. M., John, T., Ague, J. J., Huang, F., Gao, J., Klemd, R., Whitehouse, M. J. & Wang, X.-S. (2020b). Uncovering and quantifying the subduction

zone sulfur cycle from the slab perspective. *Nature Communications* **11**, 514.

Li, Y.-H. & Schoonmaker, J. E. (2003). Chemical composition and mineralogy of marine sediments. *Treatise on Geochemistry* **7**, 1–35.

Liu, X. & Zhao, D. (2016). P and S wave tomography of Japan subduction zone from joint inversions of local and teleseismic travel times and surface-wave data. *Physics of the Earth and Planetary Interiors* **252**, 1–22.

Lloyd, A. S., Plank, T., Ruprecht, P., Hauri, E. H. & Rose, W. (2013). Volatile loss from melt inclusions in pyroclasts of differing sizes. *Contributions to Mineralogy and Petrology* **165**, 129–153.

Lüders, V., Pracejus, B. & Halbach, P. (2001). Fluid inclusion and sulfur isotope studies in probable modern analogue Kuroko-type ores from the JADE hydrothermal field (Central Okinawa Trough, Japan). *Chemical Geology* **173**, 45–58.

Lyubetskaya, T. & Korenaga, J. (2007). Chemical composition of Earth's primitive mantle and its variance: 1. method and results. *Journal of Geophysical Research: Solid Earth* **112**, B03211.

Macnamara, J. & Thode, H. G. (1950). Comparison of the isotopic constitution of terrestrial and meteoritic sulfur. *Physical Review* **78**, 307–308.

Mahony, S. H., Wallace, L. M., Miyoshi, M., Villamor, P., Sparks, R. S. J. & Hasenaka, T. (2011). Volcano-tectonic interactions during rapid plate-boundary evolution in the Kyushu region, SW Japan. *Bulletin of the Geological Society of America* **123**, 2201–2223.

Mandeville, C. W., Sasaki, A., Saito, G., Faure, K., King, R. & Hauri, E. (1998). Open-system degassing of sulfur from Krakatau 1883 magma. *Earth and Planetary Science Letters* **160**, 709–722.

Mandeville, C. W., Webster, J. D., Tappen, C., Taylor, B. E., Timbal, A., Sasaki, A., Hauri, E. & Bacon, C. R. (2009). Stable isotope and petrologic evidence for open-system degassing during the climactic and pre-climactic eruptions of Mt . Mazama , Crater Lake, Oregon. *Geochimica et Cosmochimica Acta* **73**, 2978–3012.

Marini, L., Chiappini, V., Cioni, R., Cortecci, G., Dinelli, E., Principe, C. & Ferrara, G. (1998). Effect of degassing on sulfur contents and $\delta^{34}S$ values in Somma-Vesuvius magmas. *Bulletin of Volcanology* **60**, 187–194.

Marini, L., Moretti, R. & Accornero, M. (2011). Sulfur isotopes in magmatic-hydrothermal systems, melts, and magmas. *Reviews in Mineralogy and Geochemistry* **73**, 423–492.

Marini, L., Paiotti, A., Principe, C., Ferrara, G. & Cioni, R. (1994). Isotopic ratio and concentration of sulfur in the undersaturated alkaline magmas of Vulture volcano (Italy).

Bulletin of Volcanology **56**, 487–492.

Martin, H., Smithies, R. H., Rapp, R., Moyen, J. F. & Champion, D. (2005). An overview of adakite, tonalite–trondhjemite–granodiorite (TTG), and sanukitoid: relationships and some implications for crustal evolution. *Lithos* **79**, 1–24.

Matsuo, S. (1960). On the origin of volcanic gases. *The Journal of Earth Sciences, Nagoya University* **8**, 222–245.

Mavrogenes, J. A. & O'Neill, H. S. C. (1999). The relative effects of pressure, temperature and oxygen fugacity on the solubility of sulfide in mafic magmas. *Geochimica et Cosmochimica Acta* **63**, 1173–1180.

McDonough, W. F. & Sun, S. -s. (1995). The composition of the Earth. *Chemical Geology* **120**, 223–253.

Mckenzie, D. & Bickle, M. J. (1988). The volume and composition of melt generated by extension of the lithosphere. *Journal of Petrology* **29**, 625–679.

Médard, E. & Grove, T. L. (2008). The effect of H_2O on the olivine liquidus of basaltic melts: experiments and thermodynamic models. *Contributions to Mineralogy and Petrology* **155**, 417–432.

Melekhova, E., Blundy, J., Martin, R., Arculus, R. & Pichavant, M. (2017). Petrological and experimental evidence for differentiation of water-rich magmas beneath St. Kitts, Lesser Antilles. *Contributions to Mineralogy and Petrology*. Springer Berlin Heidelberg **172**, 98.

Métrich, N. & Mandeville, C. W. (2010). Sulfur in Magmas. *Elements* **6**, 81–86.

Métrich, N. & Wallace, P. J. (2008). Volatile abundances in basaltic magmas and their degassing paths tracked by melt inclusions. *Reviews in Mineralogy and Geochemistry* **69**, 363–402.

Mibe, K., Kawamoto, T., Matsukage, K. N., Fei, Y. & Ono, S. (2011). Slab melting versus slab dehydration in subduction-zone magmatism. *Proceedings of the National Academy of Sciences of the United States of America* **108**, 8177–8182.

Miyabuchi, Y. (2009). A 90,000-year tephrostratigraphic framework of Aso volcano, Japan. *Sedimentary Geology* **220**, 169–189.

Miyabuchi, Y. (2010). Eruption age of Komezuka at Aso volcano, Japan. *Bulletin of the volcanological society of Japan* **55**, 219-225 (in Japanese with English abstract).

Miyabuchi, Y. (2017). Eruption history of Janoo volcano in the Northwestern part of Aso caldera, Japan. *Bulletin of the volcanological society of Japan* **62**, 1-12 (in Japanese with English abstract).

Miyabuchi, Y., Hanada, D., Niimi, H. & Kobayashi, T. (2013). Stratigraphy, grain-size and component characteristics of the 2011 Shinmoedake eruption deposits, Kirishima Volcano, Japan. *Journal of Volcanology and Geothermal Research* **258**, 31–46.

Miyabuchi, Y. & Watanabe, K. (1997). Eruption ages of Holocene tephras from Aso volcano, southwestern Japan, inferred from ^{14}C ages of buried andisols. *Bulletin of the Volcanological Society of Japan* **42**, 403-408 (in Japanese with English abstract).

Miyamoto, T. (1997). The evolution of magmas in Kirishima volcanoes. *Bulletin of the Earthquake Research Institute, University of Tokyo* (in Japanese).

Miyashiro, A. (1978). Nature of alkalic volcanic rock series. *Contributions to Mineralogy and Petrology* **66**, 91–104.

Miyoshi, M., Fukuoka, T., Sano, T. & Hasenaka, T. (2008a). Subduction influence of Philippine Sea plate on the mantle beneath northern Kyushu, SW Japan: an examination of boron contents in basaltic rocks. *Journal of Volcanology and Geothermal Research* **171**, 73–87.

Miyoshi, M., Hasenaka, T. & Sano, T. (2005). Genetic relationship of the compositionally diverse magmas from Aso post-caldera volcanism. *Bulletin of the volcanological society of Japan* **50**, 269-283 (in Japanese with English abstract).

Miyoshi, M., Shibata, T., Yoshikawa, M., Sano, T., Shinmura, T. & Hasenaka, T. (2011). Genetic relationship between post-caldera and caldera-forming magmas from Aso volcano, SW Japan: constraints from Sr isotope and trace element compositions. *Journal of Mineralogical and Petrological Sciences* **106**, 114–119.

Miyoshi, M., Shimono, M., Hasenaka, T., Sano, T. & Fukuoka, T. (2008b). Determination of boron and other elements in volcanic rocks by prompt gamma-ray analysis: an application to magma genesis in Kyushu island, SW-Japan. *Journal of Radioanalytical and Nuclear Chemistry* **278**, 343–347.

Miyoshi, M., Shimono, M., Hasenaka, T., Sano, T., Mori, Y. & Fukuoka, T. (2010). Boron systematics of Hisatsu and Kirishima basaltic rocks from southern Kyushu, Japan. *Geochemical Journal* **44**, 359–369.

Miyoshi, T., Sakai, H. & Chiba, H. (1984). Experimental study of sulfur isotope fractionation factors between sulfate and sulfide in high temperature melts. *Geochemical Journal* **18**, 75–84.

Moore, G., Vennemann, T. & Carmichael, I. S. E. (1998). An empirical model for the solubility of H_2O in magmas to 3 kilobars. *American Mineralogist* **83**, 36–42.

Moore, L. R., Gazel, E., Tuohy, R., Lloyd, A. S., Esposito, R., Steele-MacInnis, M., Hauri, E.

H., Wallace, P. J., Plank, T. & Bodnar, R. J. (2015). Bubbles matter: an assessment of the contribution of vapor bubbles to melt inclusion volatile budgets. *American Mineralogist* **100**, 806–823.

Mori, T., Shinohara, H., Kazahaya, K., Hirabayashi, J., Matsushima, T., Mori, T., Ohwada, M., Odai, M., Iino, H. & Miyashita, M. (2013). Time-averaged SO_2 fluxes of subduction-zone volcanoes: example of a 32-year exhaustive survey for Japanese volcanoes. *Journal of Geophysical Research Atmospheres* **118**, 8662–8674.

Mori, Y. & Mashima, H. (2005). X-ray fluorescence analysis of major and trace elements in silicate rocks using 1:5 dilution glass beads. *Bulletin of Kitakyushu Museum of Natural History and Human History, Series A* **3**, 1–12.

Moriwaki, H., Machida, H., Hatsumi, Y. & Matsushima, Y. (1986). Phreatomagmatic eruptions affected by postglacial transgression in the northern coastal area of Kagoshima bay, southern Kyushu, Japan. *Journal of Geography* **95**, 24-43 (in Japanese with English abstract).

Moriwaki, H., Matsushima, Y., Iwai, M., Arai, F. & Fujiwara, O. (2002). Holocene geomorphic evolution around the Aira caldera, south Japan. *The Quaternary Research* **41**, 253-268 (in Japanese with English abstract).

Moussallam, Y., Oppenheimer, C., Scaillet, B., Gaillard, F., Kyle, P., Peters, N., Hartley, M., Berlo, K. & Donovan, A. (2014). Tracking the changing oxidation state of Erebus magmas, from mantle to surface, driven by magma ascent and degassing. *Earth and Planetary Science Letters* **393**, 200–209.

Müller, R. D., Sdrolias, M., Gaina, C. & Roest, W. R. (2008). Age, spreading rates, and spreading asymmetry of the world's ocean crust. *Geochemistry, Geophysics, Geosystems* **9**, 1–19.

Nagao, T., Hase, Y., Nagamine, S., Kakubuchi, S. & Sakaguchi, K. (1999). Late Miocene to middle Pleistocene Hisatsu volcanic rocks generated from heterogeneous magma sources: evidence form temporal-spatial variation of distribution and chemistry of rocks. *Journal of Mineralogy, Petrology and Economic Geology* **94**, 461-481 (in Japanese with English abstract).

Nagao, T., Sawai, O., Itaya, T. & Kakubuchi, S. (1992). K-Ar ages and petrological characteristics of the tholeiitic basalts and high-magnesian andesite from Amakusa-Shimoshima, Kumamoto Prefecture, SW Japan. *Journal of Mineralogy, Petrology and Economic Geology* **87**, 283-290 (in Japanese with English abstract).

Nagaoka, S. & Furuyama, K. (2004). Eruptive history of the Onidake volcano group on Fukue island, western Japan. *Journal of Geography (Chigaku Zasshi)* **113**, 349-382 (in Japanese with English abstract).

Nagaoka, S. & Okuno, M. (2014). Tephra-stratigraphy of Kuju volcano in southwestern Japan. *Chikyu monthly* **36**, 281-296 (in Japanese).

Nakada, S. (1986). Comparative study of chemistry of rocks from the Kirishima, and Daisen Volcanic Belts in Kyushu, southwest Japan. *Bulletin of the volcanological society of Japan* **31**, 95-110 (in Japanese with English abstract).

Nakada, S. & Kamata, H. (1988). Petrogenetical relationship of basalts and andesites in southern part of Shimabara Peninsula, Kyushu, Japan. *Bulletin of the Volcanological Society of Japan* **33**, 273–289.

Nakada, S. & Kamata, H. (1991). Temporal change in chemistry of magma source under Central Kyushu, Southwest Japan: progressive contamination of mantle wedge. *Bulletin of Volcanology* **53**, 182–194.

Nakada, S., Nagai, M., Kaneko, T., Suzuki, Y. & Maeno, F. (2013). The outline of the 2011 eruption at Shinmoe-dake (Kirishima), Japan. *Earth, Planets and Space* **65**, 475–488.

Nakajima, J. & Hasegawa, A. (2007). Subduction of the Philippine Sea plate beneath southwestern Japan: slab geometry and its relationship to arc magmatism. *Journal of Geophysical Research: Solid Earth* **112**, B08306.

Nakamura, H. & Iwamori, H. (2009). Contribution of slab-fluid in arc magmas beneath the Japan arcs. *Gondwana Research* **16**, 431–445.

Nakamura, M. (1971). Petrology of Kaimon-dake volcano. *Journal of Geological Society of Japan* **77**, 359-364 (in Japanese with English abstract).

Nakamura, M. & Kaneshiro, S. (2000). Determination of subducted Philippine Sea Plate in the Nansei islands deduced from hypocenter data. *Bulletin of the College of Science, University of the Ryukyu* **70**, 73-82 (in Japanese with English abstract).

Narvaez, D. F., Rose-Koga, E. F., Samaniego, P., Koga, K. T. & Hidalgo, S. (2018). Constraining magma sources using primitive olivine-hosted melt inclusions from Puñalica and Sangay volcanoes (Ecuador). *Contributions to Mineralogy and Petrology* **173**, 80.

Neave, D. A., Hartley, M. E., Maclennan, J., Edmonds, M. & Thordarson, T. (2017). Volatile and light lithophile elements in high-anorthite plagioclase-hosted melt inclusions from Iceland. *Geochimica et Cosmochimica Acta*. The Author(s) **205**, 100–118.

Newman, S. & Lowenstern, J. B. (2002). VolatileCalc: a silicate melt–H_2O–CO_2 solution model written in Visual Basic for excel. *Computers and Geosciences* **28**, 597–604.

Newton, R. C. & Manning, C. E. (2005). Solubility of anhydrite, $CaSO_4$, in NaCl–H_2O solutions at high pressures and temperatures: applications to fluid–rock interaction. *Journal of Petrology* **46**, 701–716.

O'Hara, M. J. (1968). The bearing of phase equilibria studies in synthetic and natural systems on the origin and evolution of basic and ultrabasic rocks. *Earth-Science Reviews* **4**, 69–133.

O'Neil, J. R. (1986). Theoretical and experimental aspects of isotopic fractionation. *Reviews in Mineralogy and geochemistry* **16**, 1–40.

Ochs, F. A. III. & Lange, R. A. (1999). The density of hydrous magmatic liquids. *Science* **283**, 1314–1317.

Ohba, T., Hirabayashi, J.-I. & Yoshida, M. (1994). Equilibrium temperature and redox state of volcanic gas at Unzen volcano, Japan. *Journal of Volcanology and Geothermal Research* **60**, 263–272.

Ohkura, T., Utsugi, M., Yokoo, A., Yoshikawa, S., Inoue, H. & Kagiyama, T. (2015). Eruptive activities of Aso volcano, 2014-2015. *Japan Geoscience Union Meeting 2015* SVC45-04.

Ohkura, T., Utsugi, M., Yokoo, A., Yoshikawa, S., Inoue, H., Kagiyama, T., Yamamoto, M. & Oikawa, J. (2017). Eruptive activities of Aso Volcano, 2014-2016. *Programme and abstracts of the Volcanological Society of Japan 2017 fall meeting* A3-20 (in Japanese).

Ohmoto, H. (2020). A seawater-sulfate origin for early Earth's volcanic sulfur. *Nature Geoscience* **13**, 576–583.

Ohmoto, H. & Goldhaber, M. B. (1997). Sulfur and carbon isotopes. *Geochemistry of Hydrothermal Ore Deposits*, 517–611.

Ohmoto, H. & Rye, R. O. (1979). Isotopes of sulfur and carbon. *Geochemistry of hydrothermal ore deposits*, 509–567.

Ohta, T. & Aoki, K. (1991). Origin of andesitic magma in Yufu-Tsurumi volcano group – a binary mixing model –. *Journal of Mineralogy, Petrology and Economic Geology* **86**, 1-15 (in Japanese with English abstract).

Ohta, T., Hasenaka, T., Ban, M. & Sasaki, M. (1992). Characteristic geology and petrology of non-arc type volcanism at Oninomi monogenetic volcano, Yufu-Tsurumi graben. *Bulletin of the volcanological society of Japan* **37**, 119-131 (in Japanese with English abstract).

Ohta, T., Hasenaka, T. & Fujimaki, H. (1990). Geology and petrography of Yufu-Tsurumi volcano group, Oita Prefecture. *Journal of Mineralogy, Petrology and Economic Geology* **85**, 113-129 (in Japanese with English abstract).

Okino, K., Kasuga, S. & Ohara, Y. (1998). A new scenario of the Parece Vela Basin genesis. *Marine Geophysical Research* **20**, 21–40.

Okino, K., Shimakawa, Y. & Nagaoka, S. (1994). Evolution of the Shikoku Basin. *Journal of*

geomagnetism and geoelectricity **46**, 463–479.

Okuno, M. (2002). Chronology of tephra layers in southern Kyushu, SW Japan, for the last 30,000 years. *The Quaternary Researchu* **41**, 225-236 (in Japanese with English abstract).

Okuno, M., Fujisawa, Y., Kusanagi-Tajima, M., Ui, T., Nakamura, T. & Kobayashi, T. (1999). AMS radiocarbon dates of the Ikeshiro and Nonokusa pyroclastic-flow deposits from Yufu-dake volcano, northeastern Kyushu, Japan. *Summaries of Researchers using AMS at Nagoya University* **10**, 199-205 (in Japanese with English abstract).

Okuno, M., Nakamura, T. & Kobayashi, T. (1998). AMS ^{14}C dating of historic eruptions of the Kirishima, Sakurajima and Kaimondake volcanoes, southern Kyushu, Japan. *Radiocarbon* **40**, 825–832.

Ono, K. & Watanabe, K. (1985). *Geological map of Aso volcano, 1:50,000*. *Geological map of volcanoes 4*. Geological Survey of Japan (in Japanese with English abstract).

Ono, S., Keller, N. S., Rouxel, O. & Alt, J. C. (2012). Sulfur-33 constraints on the origin of secondary pyrite in altered oceanic basement. *Geochimica et Cosmochimica Acta* **87**, 323–340.

Ono, S., Shanks, W. C. III., Rouxel, O. J. & Rumble, D. (2007). S-33 constraints on the seawater sulfate contribution in modern seafloor hydrothermal vent sulfides. *Geochimica et Cosmochimica Acta* **71**, 1170–1182.

Otake, T., Lasaga, A. C. & Ohmoto, H. (2008). Ab initio calculations for equilibrium fractionations in multiple sulfur isotope systems. *Chemical Geology* **249**, 357–376.

Palme, H. & O'Neill, H. S. C. (2007). Cosmochemical estimates of mantle composition. *Treatise on Geochemistry* **2**, 1–38.

Park, J.-O., Hori, T. & Kaneda, Y. (2009). Seismotectonic implications of the Kyushu-Palau ridge subducting beneath the westernmost Nankai forearc. *Earth, Planets and Space* **61**, 1013–1018.

Parkinson, I. J. & Arculus, R. J. (1999). The redox state of subduction zones: insights from arc-peridotites. *Chemical Geology* **160**, 409–423.

Paytan, A., Mearon, S., Cobb, K. & Kastner, M. (2002). Origin of marine barite deposits: Sr and S isotope characterization. *Geology* **30**, 747–750.

Peacock, S. A. (1990). Fluid processes in subduction zones. *Science* **248**, 329–337.

Pearce, J. A. (1982). Trace element characteristics of lavas from destructive plate boundaries. *Andesites: Orogenic andesites and related rocks*, 525–548.

Pearce, J. A., Stern, R. J., Bloomer, S. H. & Fryer, P. (2005). Geochemical mapping of the Mariana arc-basin system: implications for the nature and distribution of subduction components. *Geochemistry, Geophysics, Geosystems* **6**, Q07006.

Peters, M., Strauss, H., Farquhar, J., Ockert, C., Eickmann, B. & Jost, C. L. (2010). Sulfur cycling at the mid-Atlantic ridge: a multiple sulfur isotope approach. *Chemical Geology* **269**, 180–196.

Pichavant, M., Di Carlo, I., Rotolo, S. G., Scaillet, B., Burgisser, A., Le Gall, N. & Martel, C. (2013). Generation of CO_2-rich melts during basalt magma ascent and degassing. *Contributions to Mineralogy and Petrology* **166**, 545–561.

Pioli, L., Azzopardi, B. J. & Cashman, K. V. (2009). Controls on the explosivity of scoria cone eruptions: magma segregation at conduit junctions. *Journal of Volcanology and Geothermal Research* **186**, 407–415.

Plank, T. (2005). Constraints from thorium/lanthanum on sediment recycling at subduction zones and the evolution of the continents. *Journal of Petrology* **46**, 921–944.

Plank, T. (2014). The chemical composition of subducting sediments. *Treatise on Geochemistry: Second Edition* **4**, 607–629.

Plank, T., Kelley, K. A., Zimmer, M. M., Hauri, E. H. & Wallace, P. J. (2013). Why do mafic arc magmas contain ~4wt% water on average? *Earth and Planetary Science Letters* **364**, 168–179.

Plank, T. & Langmuir, C. H. (1998). The chemical composition of subducting sediment and its consequences for the crust and mantle. *Chemical Geology* **145**, 325–394.

Plank, T. & Manning, C. E. (2019). Subducting carbon. *Nature* **574**, 343–352.

Portnyagin, M., Almeev, R., Matveev, S. & Holtz, F. (2008). Experimental evidence for rapid water exchange between melt inclusions in olivine and host magma. *Earth and Planetary Science Letters* **272**, 541–552.

Portnyagin, M., Hoernle, K., Plechov, P., Mironov, N. & Khubunaya, S. (2007). Constraints on mantle melting and composition and nature of slab components in volcanic arcs from volatiles (H_2O, S, Cl, F) and trace elements in melt inclusions from the Kamchatka Arc. *Earth and Planetary Science Letters* **255**, 53–69.

Putirka, K. D. (2008). Thermometers and barometers for volcanic systems. *Reviews in Mineralogy and Geochemistry* **69**, 61–120.

Ranero, C. R., Phipps Morgan, J., McIntosh, K. D. & Reichert, C. (2003). Bending-related faulting and mantle serpentinization at the Middle America trench. *Nature* **425**, 367–373.

Rees C. E., Jenkins, W. J. & Monster, J. (1978). The sulphur isotopic composition of ocean water sulphate. *Geochimca et Cosmochimica Acta* **42**, 377–381.

Reimer, P. J., Austin, W. E. N., Bard, E., Bayliss, A., Blackwell, P. G., Bronk Ramsey, C., Butzin, M., Cheng, H., Edwards, R. L., Friedrich, M., Grootes, P. M., Guilderson, T. P., Hajdas, I., Heaton, T. J., Hogg, A. G., Hughen, K. A., Kromer, B., Manning, S. W., Muscheler, R., Palmer, J. G., Pearson, C., van der Plicht, J., Reimer, R. W., Richards, D. A., Scott, E. M., Southon, J. R., Turney, C. S. M., Wacker, L., Adolphi, F., Büntgen, U., Capano, M., Fahrni, S. M., Fogtmann-Schulz, A., Friedrich, R., Köhler, P., Kudsk, S., Miyake, F., Olsen, J., Reinig, F., Sakamoto, M., Sookdeo, A. & Talamo, S. (2020). The IntCal20 nothern hemisphere radiocarbon age calibration curve (0-55 cal kBP). *Radiocarbon* **62**, 725–757.

Reinhard, A. A., Jackson, M. G., Koornneef, J. M., Rose-Koga, E. F., Blusztajn, J., Konter, J. G., Koga, K. T., Wallace, P. J. & Harvey, J. (2018). Sr and Nd isotopic compositions of individual olivine-hosted melt inclusions from Hawai'i and Samoa: implications for the origin of isotopic heterogeneity in melt inclusions from OIB lavas. *Chemical Geology* **495**, 36–49.

Richet, P., Bottinga, Y. & Javoy, M. (1977). A review of hydrogen, carbon, nitrogen, oxygen, sulphur, and chlorine stable isotope fractionation among gaseous molecules. *Annual Review of Earth and Planetary Sciences* **5**, 65–110.

Ridolfi, F., Renzulli, A. & Puerini, M. (2010). Stability and chemical equilibrium of amphibole in calc-alkaline magmas: an overview, new thermobarometric formulations and application to subduction-related volcanoes. *Contributions to Mineralogy and Petrology* **160**, 45–66.

Roberge, J., Delgado-Granados, H. & Wallace, P. J. (2009). Mafic magma recharge supplies high CO_2 and SO_2 gas fluxes from Popocatépetl volcano, Mexico. *Geology* **37**, 107–110.

Robidoux, P., Frezzotti, M. L., Hauri, E. H. & Aiuppa, A. (2018). Shrinkage bubbles: the C-O-H-S magmatic fluid system at San Cristóbal volcano. *Journal of Petrology* **59**, 2093–2122.

Robinson, B. W. (1993). Sulphur isotope standards. *Proceedings of a consultants meeting held in Vienna, 1-3 December 1993*, 39–46.

Roeder, P. L. & Emslie, R. F. (1970). Olivine-liquid equilibrium. *Contributions to Mineralogy and Petrology* **29**, 275–289.

Roggensack, K. (2001). Unraveling the 1974 eruption of Fuego volcano (Guatemala) with small crystals and their young melt inclusions. *Geology* **29**, 911–914.

Roggensack, K., Hervig, R. L., McKnight, S. B. & Williams, S. N. (1997). Explosive basaltic

volcanism from Cerro Negro volcano: influence of volatiles on eruptive style. *Science* **277**, 1639–1642.

Rose-Koga, E. F., Bouvier, A.-S., Gaetani, G. A., Wallace, P. J., Allison, C. M., Andrys, J. A., Angeles de la Torre, C. A., Barth, A., Bodnar, R. J., Bracco Gartner, A. J. J., Butters, D., Castillejo, A., Chilson-Parks, B., Choudhary, B. R., Cluzel, N., Cole, M., Cottrell, E., Daly, A., Danyushevsky, L. V., DeVitre, C. L., Drignon, M. J., France, L., Gaborieau, M., Garcia, M. O., Gatti, E., Genske, F. S., Hartley, M. E., Hughes, E. C., Iveson, A. A., Johnson, E. R., Jones, M., Kagoshima, T., Katzir, Y., Kawaguchi, M., Kawamoto, T., Kelley, K. A., Koornneef, J. M., Kurz, M. D., Laubier, M., Layne, G. D., Lerner, A., Lin, K.-Y., Liu, P.-P., Lorenzo-Merino, A., Luciani, N., Magalhães, N., Marschall, H. R., Michael, P. J., Monteleone, B. D., Moore, L. R., Moussallam, Y., Muth, M., Myers, M. L., Narváez, D. F., Navon, O., Newcombe, M. E., Nichols, A. R. L., Nielsen, R. L., Pamukcu, A., Plank, T., Rasmussen, D. J., Roberge, J., Schiavi, F., Schwartz, D., Shimizu, K., Shimizu, N., Thomas, J. B., Thompson, G. T., Tucker, J. M., Ustunisik, G., Waelkens, C., Zhang, Y. & Zhou, T. (2021). Silicate melt inclusions in the new millennium: a review of recommended practices for preparation, analysis, and data presentation. *Chemical Geology* **570**, 120145.

Rose-Koga, E. F., Koga, K. T., Devidal, J.-L., Shimizu, N., Le Voyer, M., Dalou, C. & Döbeli, M. (2020). In-situ measurements of magmatic volatile elements, F, S, and Cl, by electron microprobe, secondary ion mass spectrometry, and heavy ion elastic recoil detection analysis. *American Mineralogist* **105**, 616–626.

Rose-Koga, E. F., Koga, K. T., Hamada, M., Hélouis, T., Whitehouse, M. J. & Shimizu, N. (2014). Volatile (F and Cl) concentrations in Iwate olivine-hosted melt inclusions indicating low-temperature subduction. *Earth, Planets and Space* **66**, 81.

Rose-Koga, E. F., Koga, K. T., Moreira, M., Vlastelic, I., Jackson, M. G., Whitehouse, M. J., Shimizu, N. & Habib, N. (2017). Geochemical systematics of Pb isotopes, fluorine, and sulfur in melt inclusions from São Miguel, Azores. *Chemical Geology* **458**, 22–37.

Rose-Koga, E. F., Koga, K. T., Schiano, P., Le Voyer, M., Shimizu, N., Whitehouse, M. J. & Clocchiatti, R. (2012). Mantle source heterogeneity for South Tyrrhenian magmas revealed by Pb isotopes and halogen contents of olivine-hosted melt inclusions. *Chemical Geology* **334**, 266–279.

Rose, E. F., Shimizu, N., Layne, G. D. & Grove, T. L. (2001). Melt production beneath Mt. Shasta from boron data in primitive melt inclusions. *Science* **293**, 281–283.

Rouxel, O., Ono, S., Alt, J., Rumble, D. & Ludden, J. (2008). Sulfur isotope evidence for microbial sulfate reduction in altered oceanic basalts at ODP Site 801. *Earth and Planetary Science Letters* **268**, 110–123.

Rowe, M. C., Kent, A. J. R. & Nielsen, R. L. (2007). Determination of sulfur speciation and

oxidation state of olivine hosted melt inclusions. *Chemical Geology* **236**, 303–322.

Rudnick, R. L. & Gao, S. (2003). Composition of the continental crust. *Treatise on Geochemistry* **3**, 1–64.

Saal, A. E., Hauri, E. H., Langmuir, C. H. & Perfit, M. R. (2002). Vapour undersaturation in primitive mid-ocean-ridge basalt and the volatile content of earth's upper mantle. *Nature* **419**, 451–455.

Sadofsky, S. J., Portnyagin, M., Hoernle, K. & van den Bogaard, P. (2008). Subduction cycling of volatiles and trace elements through the Central American volcanic arc: evidence from melt inclusions. *Contributions to Mineralogy and Petrology* **155**, 433–456.

Saito, E. (2017). GIS data of the depth of the oceanic plate surfaces beneath the Japanese archipelago. *GSJ Open-File Report, no. 647, Geological Survey of Japan, AIST* (in Japanese).

Saito, G., Ishizuka, O., Ishizuka, Y., Hoshizumi, H. & Miyagi, I. (2018). Petrological characteristics and volatile content of magma of the 1979, 1989, and 2014 eruptions of Nakadake, Aso volcano, Japan. *Earth, Planets and Space*. Springer Berlin Heidelberg **70**, 197.

Sakai, H., Casadevall, T. J. & Moore, J. G. (1982). Chemistry and isotope ratios of sulfur in basalts and volcanic gases at Kilauea volcano, Hawaii. *Geochimica et Cosmochimica Acta* **46**, 729–738.

Sakai, H., Marais, D. J. D., Ueda, A. & Moore, J. G. (1984). Concentrations and isotope ratios of carbon, nitrogen and sulfur in ocean-floor basalts. *Geochimica et Cosmochimica Acta* **48**, 2433–2441.

Sakuyama, M. (1979). Evidence of magma mixing: petrological study of Shirouma-Oike calc-alkaline andesite volcano, Japan. *Journal of Volcanology and Geothermal Research* **5**, 179–208.

Sakuyama, T., Nakai, S., Yoshikawa, M., Shibata, T. & Ozawa, K. (2014). Progressive interaction between dry and wet mantle during high-temperature diapiric upwelling: constraints from cenozoic Kita-Matsuura intraplate basalt province, Northwestern Kyushu, Japan. *Journal of Petrology* **55**, 1083–1128.

Sakuyama, T., Ozawa, K., Sumino, H. & Nagao, K. (2009). Progressive melt extraction from upwelling mantle constrained by the Kita-Matsuura basalts in NW Kyushu, SW Japan. *Journal of Petrology* **50**, 725–779.

Salters, V. J. M. & Stracke, A. (2004). Composition of the depleted mantle. *Geochemistry, Geophysics, Geosystems* **5**, Q05B07.

Sasaki, A. & Ishihara, S. (1979). Sulfur isotopic composition of the magnetite-series and ilmenite-series granitoids in Japan. *Contributions to Mineralogy and Petrology* **68**, 107–115.

Savov, I. P., Ryan, J. G., D'Antonio, M., Kelley, K. & Mattie, P. (2005). Geochemistry of serpentinized peridotites from the Mariana forearc Conical Seamount, ODP leg 125: implications for the elemental recycling at subduction zones. *Geochemistry, Geophysics, Geosystems* **6**, Q04J15.

Sawamura, K. & Matsui, K. (1957). *Explanatory text of the geological map of Japan, "Kirishimayama", Scale 1:50,000*. *Geological Survey of Japan*.

Scaillet, B. & Pichavant, M. (2003). Experimental constraints on volatile abundances in arc magmas and their implications for degassing processes. *Geological Society, London, Special Publications Special Publication* **213**, 23–52.

Schiano, P. (2003). Primitive mantle magmas recorded as silicate melt inclusions in igneous minerals. *Earth-Science Reviews* **63**, 121–144.

Schiano, P., Monzier, M., Eissen, J.-P., Martin, H. & Koga, K. T. (2010). Simple mixing as the major control of the evolution of volcanic suites in the Ecuadorian Andes. *Contributions to Mineralogy and Petrology* **160**, 297–312.

Schmidt, M. W. & Poli, S. (1998). Experimentally based water budgets for dehydrating slabs and consequences for arc magma generation. *Earth and Planetary Science Letters* **163**, 361–379.

Schneider, A. (1970). The sulfur isotope composition of basaltic rocks. *Contributions to Mineralogy and Petrology* **25**, 95–124.

Seno, T. & Maruyama, S. (1984). Paleogeographic reconstruction and origin of the Philippine Sea. *Tectonophysics* **102**, 53–84.

Shanks, W. C. III. (2001). Stable Isotopes in seafloor hydrothermal systems: vent fluids, hydrothermal deposits, hydrothermal alteration, and microbial processes. *Reviews in Mineralogy and Geochemistry* **43**, 469–525.

Shaw, A. M., Behn, M. D., Humphris, S. E., Sohn, R. A. & Gregg, P. M. (2010). Deep pooling of low degree melts and volatile fluxes at the 85˚E segment of the Gakkel Ridge: evidence from olivine-hosted melt inclusions and glasses. *Earth and Planetary Science Letters* **289**, 311–322.

Shaw, A. M., Hauri, E. H., Fischer, T. P., Hilton, D. R. & Kelley, K. A. (2008). Hydrogen isotopes in Mariana arc melt inclusions: implications for subduction dehydration and the deep-Earth water cycle. *Earth and Planetary Science Letters* **275**, 138–145.

Shibata, K., Mizuno, A., Yuasa, M., Uchiumi, S. & Nakagawa, T. (1977). Further K-Ar dating of tonalite dredged from the Komahashi-daini seamount. *Bulletin of the Geological Survey of Japan* **28**, 1–4.

Shibata, T., Suzuki, J., Yoshikawa, M., Kobayashi, T., Miki, D. & Takemura, K. (2013). Geochemical and Sr-Nd-Pb isotopic constraints on the origin and magmatic evolution of Quaternary lavas of Sakurajima volcano, southern Kyushu Island, Japan. *Bulletin of the volcanological society of Japan* **58**, 43–58.

Shibata, T., Yoshikawa, M., Itoh, J., Ujike, O., Miyoshi, M. & Takemura, K. (2014). Along-arc geochemical variations in Quaternary magmas of northern Kyushu Island, Japan. *Geological Society Special Publication* **385**, 15–29.

Shimizu, K., Ito, M., Chang, Q., Miyazaki, T., Ueki, K., Toyama, C., Senda, R., Vaglarov, B. S., Ishikawa, T. & Kimura, J.-I. (2019a). Identifying volatile mantle trend with the water–fluorine–cerium systematics of basaltic glass. *Chemical Geology* **522**, 283–294.

Shimizu, K., Saal, A. E., Hauri, E. H., Perfit, M. R. & Hékinian, R. (2019b). Evaluating the roles of melt-rock interaction and partial degassing on the CO_2/Ba ratios of MORB: implications for the CO_2 budget in the Earth's depleted upper mantle. *Geochimica et Cosmochimica Acta* **260**, 29–48.

Shimizu, K., Ushikubo, T., Hamada, M., Itoh, S., Higashi, Y., Takahashi, E. & Ito, M. (2017). H_2O, CO_2, F, S, Cl, and P_2O_5 analyses of silicate glasses using SIMS: report of volatile standard glasses. *Geochemical Journal* **51**, 299–313.

Shimizu, K., Ushikubo, T., Murai, T., Matsu'ura, F. & Ueno, Y. (2019c). In situ analyses of hydrogen and sulfur isotope ratios in basaltic glass using SIMS. *Geochemical Journal* **53**, 195–207.

Shinjoe, H. (1997). Origin of the granodiorite in the forearc region of southwest Japan: melting of the Shimanto accretionary prism. *Chemical Geology* **134**, 237–255.

Shinno, I. (1966). Petrology of the Kirishima volcano. *Journal of Mineralogy, Petrology and Economic Geology* **56**, 56-74 (in Japanese with English abstract).

Shinohara, H. (2008). Excess degassing from volcanoes and its role on eruptive and intrusive activity. *Reviews of Geophysics* **46**, RG4005.

Shinohara, H. (2013). Volatile flux from subduction zone volcanoes: insights from a detailed evaluation of the fluxes from volcanoes in Japan. *Journal of Volcanology and Geothermal Research* **268**, 46–63.

Shinohara, H., Kazahaya, K., Saito, G., Fukui, K. & Odai, M. (2003). Variation of CO_2/SO_2 ratio in volcanic plumes of Miyakejima: stable degassing deduced from heliborne

measurements. *Geophysical Research Letters* **30**.

Shinohara, H., Yokoo, A. & Kazahaya, R. (2018). Variation of volcanic gas composition during the eruptive period in 2014–2015 at Nakadake crater, Aso volcano, Japan. *Earth, Planets and Space*. Springer Berlin Heidelberg **70**, 151.

Shitaoka, Y., Miyoshi, M., Yamamoto, J., Shibata, T., Nagatomo, T. & Takemura, K. (2014). Thermoluminescence age of quartz xenocrysts in basaltic lava from Oninomi monogenetic Volcano, Northern Kyushu, Japan. *Geochronometria* **41**, 30–35.

Shu, Y., Nielsen, S. G., Zeng, Z., Shinjo, R., Blusztajn, J., Wang, X. & Chen, S. (2017). Tracing subducted sediment inputs to the Ryukyu arc-Okinawa Trough system: evidence from thallium isotopes. *Geochimica et Cosmochimica Acta* **217**, 462–491.

Sisson, T. W. & Grove, T. L. (1993). Temperatures and H_2O contents of low-MgO high-alumina basalts. *Contributions to Mineralogy and Petrology* **113**, 167–184.

Sisson, T. W. & Layne, G. D. (1993). H_2O in basalt and basaltic andesite glass inclusions from four subduction-related volcanoes. *Earth and Planetary Science Letters* **117**, 619–635.

Slater, L., Jull, M., McKenzie, D. & Gronvöld, K. (1998). Deglaciation effects on mantle melting under Iceland: results from the northern volcanic zone. *Earth and Planetary Science Letters* **164**, 151–164.

Sobolev, A. V, Dmitriev, L. V, Barsukov, V. L., Nevsorov, V. N. & Slutsky, A. B. (1980). The formation conditions of the high-magnesium olivines from the monomineralic fraction of Luna 24 regolith. *Lunar and Planetary Science Conference Proceedings* **11**, 105–116.

Sorbadere, F., Schiano, P. & Métrich, N. (2013). Constraints on the origin of nepheline-normative primitive magmas in Island arcs inferred from olivine-hosted melt inclusion compositions. *Journal of Petrology* **54**, 215–233.

Sorbadere, F., Schiano, P., Métrich, N. & Garaebiti, E. (2011). Insights into the origin of primitive silica-undersaturated arc magmas of Aoba volcano (Vanuatu arc). *Contributions to Mineralogy and Petrology* **162**, 995–1009.

Spandler, C. & Pirard, C. (2013). Element recycling from subducting slabs to arc crust: a review. *Lithos* **170**–**171**, 208–223.

Spilliaert, N., Métrich, N. & Allard, P. (2006). S-Cl-F degassing pattern of water-rich alkali basalt: modelling and relationship with eruption styles on Mount Etna volcano. *Earth and Planetary Science Letters* **248**, 772–786.

Staudigel, H. (2003). Hydrothermal alteration processes in the oceanic crust. *Treatise on Geochemistry* **3**, 511–535.

Stolper, E. & Newman, S. (1994). The role of water in the petrogenesis of Mariana trough magmas. *Earth and Planetary Science Letters* **121**, 293–325.

Straub, S. M. & Layne, G. D. (2003). The systematics of chlorine, fluorine, and water in Izu arc front volcanic rocks: implications for volatile recycling in subduction zones. *Geochimica et Cosmochimica Acta* **67**, 4179–4203.

Stuiver, M. & Reimer, P. J. (1993). Extended ^{14}C data base and revised CALIB 3.0 ^{14}C age calibration program. *Radiocarbon* **35**, 215–230.

Stuiver, M., Reimer, P. J. & W, R. R. (2020). *CALIB 8.2*. http://calib.org (accessed November 26, 2020).

Sudo, Y. & Kong, L. S. L. (2001). Three-dimensional seismic velocity structure beneath Aso volcano, Kyushu, Japan. *Bulletin of Volcanology* **63**, 326–344.

Sudo, Y., Tsutsui, T., Nakaboh, M., Yoshikawa, M., Yoshikawa, S. & Inoue, H. (2006). Ground deformation and magma reservoir at Aso volcano: location of deflation source derived from long-term geodetic surveys. *Bulletin of the volcanological society of Japan* **51**, 291-309 (in Japanese with English abstract).

Sugawara, T. (2000). Empirical relationships between temperature, pressure, and MgO content in olivine and pyroxene saturated liquid. *Journal of Geophysical Research: Solid Earth* **105**, 8457–8472.

Sugimoto, T., Ishibashi, H., Wakamatsu, S. & Yanagi, T. (2005). Petrologic evolution of Pre-Unzen and Unzen magma chambers beneath the Shimabara Peninsula, Kyushu, Japan: Evidence from petrography and bulk rock chemistry. *Geochemical Journal* **39**, 241–256.

Sugimoto, T., Shibata, T., Yoshikawa, M. & Takemura, K. (2006). Sr-Nd-Pb isotopic and major and trace element compositions of the Yufu-Tsurumi volcanic rocks: implications for the magma genesis of the Yufu-Tsurumi volcanoes, northeast Kyushu, Japan. *Journal of Mineralogical and Petrological Sciences* **101**, 270–275.

Sumino, H., Burgess, R., Mizukami, T., Wallis, S. R., Holland, G. & Ballentine, C. J. (2010). Seawater-derived noble gases and halogens preserved in exhumed mantle wedge peridotite. *Earth and Planetary Science Letters* **294**, 163–172.

Sun, S. -s. & McDonough, W. F. (1989). Chemical and isotopic systematics of oceanic basalts: implications for mantle composition and processes. *Geological Society, London, Special Publications* **42**, 313–345.

Sverjensky, D. A., Stagno, V. & Huang, F. (2014). Important role for organic carbon in subduction-zone fluids in the deep carbon cycle. *Nature Geoscience* **7**, 909–913.

Symonds, R. B., Rose, W. I., Bluth, G. J. S. & Gerlach, T. M. (1994). Volcanic-gas studies:

methods, results, and applications. *Volatiles in Magmas*. Reviews in Mineralogy and geochemistry **30**, 1–66.

Syracuse, E. M., van Keken, P. E. & Abers, G. A. (2010). The global range of subduction zone thermal models. *Physics of the Earth and Planetary Interiors* **183**, 73–90.

Tajima, Y., Hayashi, S., Yasuda, A. & Itoh, H. (2013). Tephrostratigraphy and eruptive history of Shinmoedake volcano of the Kirishima volcanoes, Kyushu, Japan. *The Quaternary Research* **52**, 151-171 (in Japanese with English abstract).

Tajima, Y., Matsuo, Y., Shoji, T. & Kobayashi, T. (2014). Eruptive history of Ebinokogen volcanic area of Kirishima volcanoes for the past 15,000 years in Kyushu, Japan. *Bulletin of the volcanological society of Japan* **59**, 55-75 (in Japanese with English abstract).

Takada, H. (1989). Preliminary report on tephra from Aso central cones. *Journal of the Kumamoto Geoscience Association* **90**, 8-11 (in Japanese).

Tatsumi, Y. & Eggins, S. (1995). *Subduction zone magmatism*. Boston, Blackwell Science.

Teplow, W., Marsh, B., Hulen, J., Spielman, P., Kaleikini, M., Fitch, D. & Rickard, W. (2009). Dacite melt at the Puna Geothermal Venture wellfield, Big Island of Hawaii. *Geothermal resources council transactions* **33**, 989–994.

Thode, H. G., Monster, J. & Dunford, H. B. (1961). Sulphur isotope geochemistry. *Geochimica et Cosmochimica Acta* **25**, 159–174.

Tomkins, A. G. & Evans, K. A. (2015). Separate zones of sulfate and sulfide release from subducted mafic oceanic crust. *Earth and Planetary Science Letters* **428**, 73–83.

Toplis, M. J. (2005). The thermodynamics of iron and magnesium partitioning between olivine and liquid: criteria for assessing and predicting equilibrium in natural and experimental systems. *Contributions to Mineralogy and Petrology* **149**, 22–39.

Tsuchiyama, A. (1985). Dissolution kinetics of plagioclase in the melt of the system diopside-albite-anorthite, and origin of dusty plagioclase in andesites. *Contributions to Mineralogy and Petrology* **89**, 1–16.

Tsutsui, M., Okuno, M. & Kobayashi, T. (2007). Eruptive history of Ohachi volcano, Kirishima volcano group, southern Kyushu, Japan. *Bulletin of the Volcanological Society of Japan* **52**, 1-21 (in Japanese with English abstract).

Tsutsui, T. & Sudo, Y. (2004). Seismic reflectors beneath the central cones of Aso Volcano, Kyushu, Japan. *Journal of Volcanology and Geothermal Research* **131**, 33–58.

Tucker, J. M., Hauri, E. H., Pietruszka, A. J., Garcia, M. O., Marske, J. P. & Trusdell, F. A. (2019). A high carbon content of the Hawaiian mantle from olivine-hosted melt inclusions.

Geochimica et Cosmochimica Acta **254**, 156–172.

Ueda, A. & Sakai, H. (1984). Sulfur isotope study of Quaternary volcanic rocks from the Japanese islands arc. *Geochimica et Cosmochimica Acta* **48**, 1837–1848.

Ulmer, P. & Trommsdorff, V. (1995). Serpentine stability to mantle depths and subduction-related magmatism. *Science* **268**, 858–861.

Urabe, T. & Kusakabe, M. (1990). Barite silica chimneys from the Sumisu Rift, Izu-Bonin arc: possible analog to hematitic chert associated with Kuroko deposits. *Earth and Planetary Science Letters* **100**, 283–290.

Urey, H. C. (1947). The thermodynamic properties of isotopic substances. *Journal of the Chemical Society (Resumed),* 562–581.

Uto, K., Hoang, N. & Matsui, K. (2004). Cenozoic lithospheric extension induced magmatism in southwest Japan. *Tectonophysics* **393**, 281–299.

Uto, K. & Uchiumi, S. (1997). K-Ar ages of Maruyama lava domes in Hiwaki town, Kagoshima Prefectures, southwest Japan: a Quaternary volcano constituting a second volcanic row of Ryukyu arc. *Bulletin of the Volcanological Society of Japan* **42**, 299-302 (in Japanese).

Van den Bleeken, G. & Koga, K. T. (2015). Experimentally determined distribution of fluorine and chlorine upon hydrous slab melting, and implications for F-Cl cycling through subduction zones. *Geochimica et Cosmochimica Acta* **171**, 353–373.

Veizer, J., Holser, W. T. & Wilgus, C. K. (1980). Correlation of $^{13}C/^{12}C$ and $^{34}S/^{32}S$ secular variations. *Geochimica et Cosmochimica Acta* **44**, 579–587.

Vigouroux, N., Wallace, P. J. & Kent, A. J. R. (2008). Volatiles in high-K magmas from the western trans-Mexican volcanic belt: evidence for fluid fluxing and extreme enrichment of the mantle wedge by subduction processes. *Journal of Petrology* **49**, 1589–1618.

Walker, D., Shibata, T. & DeLong, S. E. (1979). Abyssal tholeiites from the Oceanographer Fracture Zone. *Contributions to Mineralogy and Petrology* **70**, 111–125.

Wallace, P. J. (2001). Volcanic SO_2 emissions and the abundance and distribution of exsolved gas in magma bodies. *Journal of Volcanology and Geothermal Research* **108**, 85–106.

Wallace, P. J. (2005). Volatiles in subduction zone magmas: concentrations and fluxes based on melt inclusion and volcanic gas data. *Journal of Volcanology and Geothermal Research* **140**, 217–240.

Wallace, P. J. & Carmichael, I. S. E. (1994). S speciation in submarine basaltic glasses as determined by measurements of S*Kα* X-ray wavelength shifts. *American Mineralogist* **79**,

161–167.

Wallace, P. J. & Edmonds, M. (2011). The sulfur budget in magmas: evidence from melt inclusions, submarine glasses, and volcanic gas emissions. *Reviews in Mineralogy and Geochemistry* **73**, 215–246.

Wallace, P. J. & Gerlach, T. M. (1994). Magmatic vapor source for sulfur dioxide released during volcanic eruptions: evidence from Mount Pinatubo. *Science* **265**, 497–499.

Wallace, P. J., Kamenetsky, V. S. & Cervantes, P. (2015). Melt inclusion CO_2 contents, pressures of olivine crystallization, and the problem of shrinkage bubbles. *American Mineralogist* **100**, 787–794.

Walowski, K. J., Wallace, P. J., Clynne, M. A., Rasmussen, D. J. & Weis, D. (2016). Slab melting and magma formation beneath the southern Cascade arc. *Earth and Planetary Science Letters* **446**, 100–112.

Walter, M. J. (1998). Melting of garnet peridotite and the origin of Komatiite and depleted lithosphere. *Journal of Petrology* **39**, 29–60.

Walters, J. B., Cruz-Uribe, A. M. & Marschall, H. R. (2019). Isotopic compositions of sulfides in exhumed high-pressure terranes: implications for sulfur cycling in subduction zones. *Geochemistry, Geophysics, Geosystems* **20**, 3347–3374.

Wanless, V. D., Behn, M. D., Shaw, A. M. & Plank, T. (2014). Variations in melting dynamics and mantle compositions along the eastern volcanic zone of the Gakkel ridge: insights from olivine-hosted melt inclusions. *Contributions to Mineralogy and Petrology* **167**, 1005.

Wanless, V. D. & Shaw, A. M. (2012). Lower crustal crystallization and melt evolution at mid-ocean ridges. *Nature Geoscience* **5**, 651–655.

Wanless, V. D., Shaw, A. M., Behn, M. D., Soule, S. A., Escartín, J. & Hamelin, C. (2015). Magmatic plumbing at Lucky Strike volcano based on olivine-hosted melt inclusion compositions. *Geochemistry Geophysics Geosystems* **16**, 126–147.

Watanabe, K. (1991). Volcanic activity of Nakadake, Aso volcano. *Journal of the Kumamoto Geoscience Association* **98**, 2-13 (in Japanese).

Watanabe, K. (2001). *History and activity of Aso volcano (Japanese title "Aso kazan no oitachi")*. Ichinomiya-cho, Japan (in Japanese).

Watanabe, K., Itaya, T., Ono, K. & takada (1989). K-Ar ages of dike rocks in the Southwestern region of Aso caldera, Kyushu, Japan. *Bulletin of the volcanological society of Japan* **34**, 189-195 (in Japanese with English abstract).

Waters, L. E. & Lange, R. A. (2015). An updated calibration of the plagioclase-liquid hygrometer-thermometer applicable to basalts through rhyolites. *American Mineralogist* **100**, 2172–2184.

Webster, J. D., Mandeville, C. W., Goldoff, B., Coombs, M. L. & Tappen, C. (2010). Augustine Volcano—The influence of volatile components in magmas erupted A.D. 2006 to 2,100 years before present. In: Power, J. A., Coombs, M. L. & Freymueller, J. T. (eds) *The 2006 eruption of Augustine Volcano, Alaska: U.S. Geological Survey Professional Paper 1769*.

Werner, C., Rasmussen, D. J., Plank, T., Kelly, P. J., Kern, C., Lopez, T., Gliss, J., Power, J. A., Roman, D. C., Izbekov, P. & Lyons, J. (2020). Linking subsurface to surface using gas emission and melt inclusion data at Mount Cleveland volcano, Alaska. *Geochemistry, Geophysics, Geosystems* **125**, e2019GC008882.

Wilson, M. R., Kyser, T. K. & Fagan, R. (1996). Sulfur isotope systematics and platinum group element behavior in REE-enriched metasomatic fluids: a study of mantle xenoliths from Dish Hill, California, USA. *Geochimica et Cosmochimica Acta* **60**, 1933–1942.

Witham, F., Blundy, J., Kohn, S. C., Lesne, P., Dixon, J., Churakov, S. V. & Botcharnikov, R. (2012). SolEx: a model for mixed COHSCl-volatile solubilities and exsolved gas compositions in basalt. *Computers and Geosciences* **45**, 87–97.

Woodhead, J. D., Harmon, R. S. & Fraser, D. G. (1987). O, S, Sr, and Pb isotope variations in volcanic rocks from the Northern Mariana Islands: implications for crustal recycling in intra-oceanic arcs. *Earth and Planetary Science Letters* **83**, 39–52.

Workman, R. K. & Hart, S. R. (2005). Major and trace element composition of the depleted MORB mantle (DMM). *Earth and Planetary Science Letters* **231**, 53–72.

Wysoczanski, R. J., Wright, I. C., Gamble, J. A., Hauri, E. H., Luhr, J. F., Eggins, S. M. & Handler, M. R. (2006). Volatile contents of Kermadec arc-Havre trough pillow glasses: fingerprinting slab-derived aqueous fluids in the mantle sources of arc and back-arc lavas. *Journal of Volcanology and Geothermal Research* **152**, 51–73.

Yamamoto, M., Kawakatsu, H., Kaneshima, S., Mori, T., Tsutsui, T., Sudo, Y. & Morita, Y. (1999). Detection of a crack-like conduit beneath the active crater at Aso volcano. *Geophysical Research Letters* **26**, 3677–3680.

Yamasaki, S., Hoshizumi, H. & Matsumoto, A. (2016). Growth history of western to central part of Kuju volcanic group, Kyushu, Japan. *Bulletin of the Volcanological Society of Japan* **61**, 519-531 (in Japanese with English abstract).

Yasuda, A. (2014). A new technique using FT-IR micro-reflectance spectroscopy for measurement of water concentrations in melt inclusions. *Earth, Planets and Space* **66**, 34.

Yasuda, A., Nakada, S. & Fujii, T. (2001). Sulfur abundance and redox state of melt inclusions from Miyake-jima 2000 eruption products. *Bulletin of the volcanological society of Japan* **46**, 165-173 (in Japanese with English abstract).

Yokoo, A. & Miyabuchi, Y. (2015). Eruption at the Nakadake 1st crater of Aso volcano started in November 2014. *Bulletin of the volcanological society of Japan* **60**, 275-278 (in Japanese).

Zellmer, G. F., Iizuka, Y., Miyoshi, M., Tamura, Y. & Tatsumi, Y. (2012). Lower crustal H_2O controls on the formation of adakitic melts. *Geology* **40**, 487–490.

Zellmer, G. F., Sakamoto, N., Iizuka, Y., Miyoshi, M., Tamura, Y., Hsieh, H.-H. & Yurimoto, H. (2014). Crystal uptake into aphyric arc melts: insights from two-pyroxene pseudo-decompression path, plagioclase hygrometry, and measurement of hydrogen in olivines from mafic volcanics of SW Japan. *Geological Society, London, Special Publications* **385**, 161–184.

Zhao, D. & Tian, Y. (2013). Changbai intraplate volcanism and deep earthquakes in East Asia: a possible link? *Geophysical Journal International* **195**, 706–724.

Zhao, D., Tian, Y., Lei, J., Liu, L. & Zheng, S. (2009). Seismic image and origin of the Changbai intraplate volcano in East Asia: role of big mantle wedge above the stagnant Pacific slab. *Physics of the Earth and Planetary Interiors* **173**, 197–206.

Zhao, D., Yanada, T., Hasegawa, A., Umino, N. & Wei, W. (2012). Imaging the subducting slabs and mantle upwelling under the Japan Islands. *Geophysical Journal International* **190**, 816–828.

Zierenberg, R. A., Shanks, W. C. III. & Bischoff, J. L. (1984). Massive sulfide deposits at 21˚N, East Pacific Rise: chemical composition, stable isotopes, and phase equilibria. *Geological Society of America Bulletin* **95**, 922–929.

Appendices

Appendix A
Supplementary materials for Chapter 3

Table A1. Uncorrected not-normalized to 100% and corrected compositions of all melt inclusions and host minerals

Volcanic cone	Nakadake																			
Sample ID	NKD14																			
Host mineral	Clinopyroxene											Olivine								
Melt ID	a1-m1	b1-m1	b1-m2	b3-m1	c3-m1	c4-m1	c5-m1	d3-m1	d4-m1	d5-m1	O4-m4	1-m1	1-m2	2-m1	2-m2	3-m1	4-m1	4-m2	4-m3	4-m4
Uncorrected melt compositions (wt.%)																				
SiO_2	58.03	58.16	58.71	58.51	58.57	58.21	59.82	58.68	58.79	59.90	56.29	59.14	58.80	56.55	56.58	58.34	57.04	57.90	57.07	56.46
TiO_2	1.36	1.37	1.24	1.31	1.49	1.37	1.44	1.26	1.27	1.24	1.25	1.34	1.35	1.02	1.19	1.31	1.37	1.36	1.33	1.35
Al_2O_3	14.37	14.86	14.63	14.12	14.72	14.43	14.14	15.12	14.95	14.45	14.50	14.53	14.41	15.01	14.84	14.94	14.46	14.82	14.48	14.27
FeO^{Total}	9.89	9.47	8.91	9.79	9.66	9.62	10.00	8.93	8.76	9.38	8.77	9.67	9.65	11.18	11.02	9.88	9.33	9.72	9.76	10.07
MnO	0.25	0.17	0.18	0.18	0.20	0.23	0.18	0.25	0.16	0.17	0.18	0.23	0.25	0.22	0.24	0.25	0.20	0.20	0.20	0.21
MgO	2.74	2.27	3.09	2.24	2.52	2.67	2.04	2.59	2.28	2.45	2.23	2.64	2.57	3.04	3.01	2.28	2.58	2.58	2.62	2.70
CaO	5.88	5.10	6.49	5.52	5.87	5.88	4.87	5.72	5.06	5.00	5.25	5.17	5.82	6.58	6.11	6.21	5.71	5.89	5.89	6.35
Na_2O	2.72	3.01	2.57	2.77	3.25	2.96	2.95	2.96	2.87	2.82	3.26	2.88	2.98	3.54	3.23	2.04	2.91	3.10	3.07	3.02
K_2O	3.00	3.72	2.68	3.09	3.17	3.18	3.34	3.19	4.01	3.39	3.83	3.18	3.15	1.96	2.15	3.19	3.43	3.17	3.37	3.08
P_2O_5	0.51	0.64	0.48	0.44	0.43	0.45	0.57	0.55	0.62	0.51	0.38	0.48	0.51	0.37	0.44	0.46	0.47	0.42	0.55	0.52
S (EPMA)	0.012	0.010	0.015	0.008	0.009	0.015	0.013	0.010	0.007	0.014	0.000	0.010	0.004	0.044	0.036	0.036	0.018	0.021	0.011	0.022
Cl (EPMA)	0.080	0.122	0.079	0.089	0.083	0.084	0.130	0.097	0.130	0.112	0.139	0.088	0.122	0.124	0.114	0.101	0.086	0.073	0.084	0.085
Total[a]	98.91	98.92	99.10	98.11	100.02	99.09	99.51	99.39	98.90	99.48	96.03	99.38	99.65	99.73	99.00	99.11	97.65	99.32	98.50	98.23
H_2O (FTIR)	-	-	-	-	-	-	-	-	-	-	-	1.11	1.00	-	-	-	-	-	-	-
H_2O (SIMS)	-	-	-	-	-	-	-	-	-	-	-	-	-	-	-	-	0.80	0.78	-	0.47
CO_2 ppm (SIMS)[a]	-	-	-	-	-	-	-	-	-	-	-	-	-	-	-	-	19	11	-	79
S ppm (SIMS)	-	-	-	-	-	-	-	-	-	-	-	-	-	-	-	-	151	198	-	198
Cl ppm (SIMS)	-	-	-	-	-	-	-	-	-	-	-	-	-	-	-	-	886	832	-	832
F ppm (SIMS)	-	-	-	-	-	-	-	-	-	-	-	-	-	-	-	-	794	795	-	724
P_2O_5 (SIMS)	-	-	-	-	-	-	-	-	-	-	-	-	-	-	-	-	0.54	0.50	-	0.49
S^{6+}/S_{total}	-	-	-	-	-	-	-	-	-	-	-	-	-	0.41	-	-	-	-	-	-
1 s.e.[b]	-	-	-	-	-	-	-	-	-	-	-	-	-	0.04	-	-	-	-	-	-
T_{erupt} (°C)[c]	1054	1034	1069	1031	1042	1041	1019	1054	1037	1042	1036	1065	1066	1084	1085	1067	1075	1074	1078	1087
$K_{D\ uncorrected}$[a]	0.24	0.22	0.31	0.20	0.23	0.23	0.20	0.23	0.26	0.23	0.25	0.55	0.56	0.56	0.55	0.56	0.56	0.55	0.55	0.57
Corrected melt compositions for post-entrapment crystallization (wt.%)																				
SiO_2	-	-	-	-	-	-	-	-	-	-	-	58.86	58.47	56.24	56.19	57.63	56.83	57.56	56.75	56.18
TiO_2	-	-	-	-	-	-	-	-	-	-	-	1.32	1.33	1.00	1.17	1.27	1.35	1.34	1.31	1.33
Al_2O_3	-	-	-	-	-	-	-	-	-	-	-	14.34	14.20	14.77	14.55	14.45	14.31	14.59	14.25	14.07
FeO^{Total}	-	-	-	-	-	-	-	-	-	-	-	10.02	10.05	11.58	11.53	10.75	9.61	10.15	10.19	10.44
MnO	-	-	-	-	-	-	-	-	-	-	-	0.23	0.24	0.22	0.23	0.25	0.20	0.20	0.19	0.21
MgO	-	-	-	-	-	-	-	-	-	-	-	3.08	3.08	3.58	3.68	3.40	2.92	3.13	3.17	3.17
CaO	-	-	-	-	-	-	-	-	-	-	-	5.10	5.74	6.47	5.99	6.01	5.66	5.79	5.80	6.26
Na_2O	-	-	-	-	-	-	-	-	-	-	-	2.84	2.93	3.48	3.16	1.97	2.88	3.05	3.02	2.97
K_2O	-	-	-	-	-	-	-	-	-	-	-	3.14	3.11	1.93	2.10	3.09	3.39	3.12	3.31	3.04
P_2O_5	-	-	-	-	-	-	-	-	-	-	-	0.47	0.50	0.36	0.43	0.44	0.46	0.42	0.54	0.52
S	-	-	-	-	-	-	-	-	-	-	-	0.009	0.004	0.043	0.035	0.035	0.018	0.021	0.011	0.022
Cl	-	-	-	-	-	-	-	-	-	-	-	0.087	0.120	0.122	0.112	0.098	0.085	0.072	0.083	0.084

Table A1. (continued)

Volcanic cone	Nakadake																			
Sample ID	NKD14																			
Host mineral	Clinopyroxene											Olivine								
Melt ID	a1-m1	b1-m1	b1-m2	b3-m1	c3-m1	c4-m1	c5-m1	d3-m1	d4-m1	d5-m1	O4-m4	1-m1	1-m2	2-m1	2-m2	3-m1	4-m1	4-m2	4-m3	4-m4
H_2O (FTIR)	-	-	-	-	-	-	-	-	-	-	-	1.10	0.99	-	-	-	-	-	-	-
H_2O (SIMS)	-	-	-	-	-	-	-	-	-	-	-	-	-	-	-	-	0.79	0.77	-	0.47
CO_2 ppm (SIMS)[d]	-	-	-	-	-	-	-	-	-	-	-	-	-	-	-	-	18	11	-	77
S ppm (SIMS)	-	-	-	-	-	-	-	-	-	-	-	-	-	-	-	-	149	194	-	195
Cl ppm (SIMS)	-	-	-	-	-	-	-	-	-	-	-	-	-	-	-	-	877	819	-	820
F ppm (SIMS)	-	-	-	-	-	-	-	-	-	-	-	-	-	-	-	-	786	783	-	714
P_2O_5 (SIMS)	-	-	-	-	-	-	-	-	-	-	-	-	-	-	-	-	0.54	0.49	-	0.48
T_{trap} (°C)[c]	-	-	-	-	-	-	-	-	-	-	-	1075	1077	1096	1100	1092	1082	1086	1089	1097
PEC%[e]	-	-	-	-	-	-	-	-	-	-	-	1.3	1.5	1.6	2.0	3.3	1.0	1.6	1.6	1.4
Host mineral compositions (wt.%)																				
SiO_2	52.56	52.71	52.79	51.93	52.70	52.55	52.09	52.59	52.18	52.19	49.54	37.13	38.00	37.89	37.51	-	37.51	37.74	37.76	37.00
TiO_2	0.55	0.57	0.61	0.53	0.57	0.57	0.63	0.56	0.66	0.60	0.63	0.04	0.00	0.02	0.00	-	0.01	0.05	0.03	0.00
Al_2O_3	2.38	2.32	2.32	2.31	2.25	2.34	2.07	2.83	2.52	2.69	2.85	0.02	0.04	0.01	0.04	-	0.04	0.02	0.00	0.00
Cr_2O_3	0.00	0.00	0.01	0.00	0.00	0.01	0.01	0.14	0.01	0.01	0.01	-	-	-	-	-	0.00	0.00	0.00	0.03
FeO^{Total}	10.47	11.07	11.04	10.32	11.02	10.36	12.04	9.50	12.03	10.60	11.41	29.89	29.03	30.10	29.12	-	29.95	30.01	30.07	29.81
MnO	0.36	0.33	0.43	0.37	0.39	0.32	0.39	0.28	0.41	0.35	0.31	0.65	0.66	0.63	0.63	-	0.60	0.63	0.54	0.61
MgO	15.27	15.50	15.70	15.24	15.63	15.50	15.50	15.05	15.09	15.38	14.83	32.84	31.86	32.76	32.52	-	32.61	33.06	33.19	31.96
CaO	19.42	18.54	18.01	19.27	18.32	18.90	17.89	19.86	18.41	19.25	18.54	0.23	0.20	0.22	0.22	-	0.23	0.26	0.24	0.23
Na_2O	0.25	0.27	0.24	0.24	0.25	0.22	0.26	0.29	0.27	0.28	0.29	0.00	0.00	0.00	0.00	-	0.00	0.02	0.02	0.00
K_2O	0.01	0.03	0.00	0.00	0.00	0.00	0.00	0.00	0.00	0.00	0.01	0.00	0.01	0.01	0.02	-	0.00	0.01	0.02	0.00
NiO	0.00	0.00	0.00	0.03	0.00	0.03	0.00	0.01	0.00	0.03	0.00	-	-	-	-	-	0.02	0.01	0.01	0.00
V_2O_3	0.13	0.06	0.08	0.07	0.05	0.07	0.06	0.04	0.00	0.11	0.09	0.00	0.02	0.02	0.01	-	0.00	0.00	0.00	0.00
P_2O_5	-	-	-	-	-	-	-	-	-	-	-	-	-	-	-	-	-	-	-	-
Total[a]	101.40	101.39	101.24	100.30	101.19	100.87	100.93	101.15	101.59	101.47	98.51	100.86	99.84	101.68	100.09	-	100.97	101.82	101.87	99.63
Cations																				
Si	7.73	7.75	7.76	7.72	7.76	7.75	7.73	7.72	7.70	7.68	7.56	5.97	6.13	6.04	6.05	6.01	6.02	6.01	6.00	6.03
Ti	0.06	0.06	0.07	0.06	0.06	0.06	0.07	0.06	0.07	0.07	0.07	0.00	0.00	0.00	0.00	0.01	0.00	0.01	0.00	0.00
Al	0.41	0.40	0.40	0.41	0.39	0.41	0.36	0.49	0.44	0.47	0.51	0.00	0.01	0.00	0.01	0.01	0.01	0.00	0.00	0.00
Cr	0.00	0.00	0.00	0.00	0.00	0.00	0.00	0.02	0.00	0.00	0.00	-	-	-	-	-	0.00	0.00	0.00	0.00
Fe2+	1.29	1.36	1.36	1.28	1.36	1.28	1.49	1.17	1.48	1.30	1.46	4.02	3.92	4.01	3.93	3.99	4.02	3.99	4.00	4.06
Mn	0.04	0.04	0.05	0.05	0.05	0.04	0.05	0.04	0.05	0.04	0.04	0.09	0.09	0.08	0.09	0.09	0.08	0.08	0.07	0.08
Mg	3.35	3.40	3.44	3.38	3.43	3.41	3.43	3.29	3.32	3.37	3.37	7.87	7.66	7.78	7.82	7.82	7.80	7.84	7.87	7.76
Ca	3.06	2.92	2.84	3.07	2.89	2.99	2.84	3.13	2.91	3.03	3.03	0.04	0.03	0.04	0.04	0.04	0.04	0.04	0.04	0.04
Na	0.07	0.08	0.07	0.07	0.07	0.06	0.07	0.08	0.08	0.08	0.09	0.00	0.00	0.00	0.00	0.00	0.00	0.01	0.01	0.00
K	0.00	0.01	0.00	0.00	0.00	0.00	0.00	0.00	0.00	0.00	0.00	0.00	0.00	0.00	0.00	0.00	0.00	0.00	0.00	0.00
Ni	0.00	0.00	0.00	0.00	0.00	0.00	0.00	0.00	0.00	0.00	0.00	-	-	-	-	-	0.00	0.00	0.00	0.00
V	0.02	0.01	0.01	0.01	0.01	0.01	0.01	0.00	0.00	0.01	0.01	0.00	0.00	0.00	0.00	0.00	0.00	0.00	0.00	0.00
P	-	-	-	-	-	-	-	-	-	-	-	0.01	0.00	0.00	0.00	0.01	-	-	-	-
Cation total	16.03	16.02	16.00	16.05	16.02	16.01	16.06	16.00	16.05	16.06	16.15	18.01	17.86	17.96	17.94	17.97	17.98	17.99	18.00	17.97
Mg# / An[f]	72.2	71.4	71.7	72.5	71.7	72.7	69.6	73.9	69.1	72.1	69.9	66.2	66.2	66.0	66.6	66.2	66.0	66.3	66.3	65.6

Table A1. (continued)

Volcanic cone																Kamikomezuka					
Sample ID																KKO					
Host mineral					Orthopyroxene	Plagioclase										Clinopyroxene					
Melt ID	O4-m1	O4-m2	O4-m3	O4-m5	4-m6	a1-m1	a2-m1	a2-m2	a3-m1	a3-m2	a4-m1	a4-m2	b1-m1	b3-m1	b4-m1	a1-m1	a1-m2	a6-m1	b5-m1	b5-m2	
Uncorrected melt compositions (wt.%)																					
SiO_2	57.22	56.76	56.64	57.54	58.36	59.94	56.95	58.45	56.50	58.17	58.60	57.10	58.77	57.85	57.73	55.67	56.08	57.63	57.28	57.79	
TiO_2	1.37	1.33	1.30	1.34	1.22	1.29	1.36	1.46	1.45	1.24	1.35	1.58	1.42	1.42	1.34	1.24	1.24	1.46	1.30	1.36	
Al_2O_3	14.43	14.43	14.19	14.46	14.00	14.19	14.35	14.44	14.30	15.96	14.35	14.26	14.20	14.38	14.41	14.54	14.09	14.42	14.83	14.85	
FeO^{Total}	9.66	9.80	9.90	9.81	9.21	8.31	9.81	9.34	10.93	8.31	9.21	10.14	9.40	10.08	9.41	10.07	11.34	10.50	9.46	10.15	
MnO	0.20	0.18	0.21	0.20	0.24	0.21	0.24	0.23	0.23	0.19	0.21	0.20	0.21	0.21	0.18	0.18	0.21	0.22	0.23	0.21	
MgO	2.68	2.73	2.76	2.63	2.27	2.39	2.92	2.77	2.62	2.49	2.69	3.01	2.71	2.86	2.47	3.99	4.20	2.82	3.22	3.32	
CaO	5.97	6.09	5.81	5.72	5.10	5.30	6.23	5.67	5.71	6.40	5.78	6.19	5.94	5.70	5.59	7.28	7.96	6.05	6.57	6.42	
Na_2O	3.34	3.48	3.49	3.35	3.54	2.21	2.41	2.16	2.50	2.95	2.40	2.28	2.50	2.32	2.35	3.57	1.86	2.96	3.33	3.29	
K_2O	2.97	3.05	3.05	3.14	3.27	3.44	2.93	3.22	3.16	2.93	3.07	3.01	3.23	3.03	3.34	2.77	2.27	3.21	2.60	2.47	
P_2O_5	0.30	0.36	0.29	0.30	0.25	0.37	0.95	0.48	0.51	0.39	0.43	0.61	0.54	0.56	0.46	0.25	0.28	0.38	0.24	0.33	
S (EPMA)	0.014	0.015	0.010	0.024	0.019	0.009	0.027	0.020	0.009	0.012	0.006	0.014	0.016	0.018	0.012	0.036	0.036	0.033	0.055	0.057	
Cl (EPMA)	0.083	0.084	0.084	0.087	0.094	0.090	0.079	0.094	0.097	0.095	0.090	0.087	0.095	0.082	0.093	0.089	0.057	0.102	0.080	0.089	
Total[a]	98.28	98.35	97.75	98.65	97.62	97.79	98.29	98.41	98.04	99.19	98.24	98.55	99.07	98.57	97.42	99.83	99.81	99.91	99.42	100.56	
H_2O (FTIR)	-	-	-	-	-	-	-	-	-	-	-	-	-	-	-	n.d.	n.d.	n.d.	-	-	
H_2O (SIMS)	0.82	0.83	0.64	0.80	-	-	-	-	-	-	-	-	-	-	-	-	-	-	-	-	
CO_2 ppm (SIMS)[d]	11	10	10	37	-	-	-	-	-	-	-	-	-	-	-	-	-	-	-	-	
S ppm (SIMS)	197	200	181	156	-	-	-	-	-	-	-	-	-	-	-	-	-	-	-	-	
Cl ppm (SIMS)	819	866	763	966	-	-	-	-	-	-	-	-	-	-	-	-	-	-	-	-	
F ppm (SIMS)	799	830	737	838	-	-	-	-	-	-	-	-	-	-	-	-	-	-	-	-	
P_2O_5 (SIMS)	0.49	0.50	0.48	0.58	-	-	-	-	-	-	-	-	-	-	-	-	-	-	-	-	
S^{0+}/S_{total}	-	-	-	-	-	-	-	-	-	-	-	-	-	-	-	-	-	0.14	-	-	
1 s.e.[b]	-	-	-	-	-	-	-	-	-	-	-	-	-	-	-	-	-	0.05	-	-	
T_{erupt} (°C)[c]	1075	1076	1084	1076	1112	1069	1090	1079	1083	1096	1082	1089	-	1083	1080	-	1098	1037	1048	1057	
$K_{D\ uncorrected}$[d]	0.55	0.54	0.55	0.55	0.25	0.21	0.21	0.23	0.19	0.24	0.20	0.21	0.13	0.20	0.20	0.37	0.34	0.26	0.27	0.29	
Corrected melt compositions for post-entrapment crystallization (wt.%)																					
SiO_2	56.96	56.46	56.40	57.22	-	-	-	-	-	-	-	-	-	-	-	-	-	-	-	-	
TiO_2	1.35	1.31	1.29	1.32	-	-	-	-	-	-	-	-	-	-	-	-	-	-	-	-	
Al_2O_3	14.24	14.22	14.02	14.23	-	-	-	-	-	-	-	-	-	-	-	-	-	-	-	-	
FeO^{Total}	10.01	10.20	10.23	10.24	-	-	-	-	-	-	-	-	-	-	-	-	-	-	-	-	
MnO	0.20	0.18	0.21	0.20	-	-	-	-	-	-	-	-	-	-	-	-	-	-	-	-	
MgO	3.12	3.24	3.16	3.18	-	-	-	-	-	-	-	-	-	-	-	-	-	-	-	-	
CaO	5.89	6.00	5.74	5.63	-	-	-	-	-	-	-	-	-	-	-	-	-	-	-	-	
Na_2O	3.29	3.43	3.45	3.29	-	-	-	-	-	-	-	-	-	-	-	-	-	-	-	-	
K_2O	2.93	3.00	3.02	3.09	-	-	-	-	-	-	-	-	-	-	-	-	-	-	-	-	
P_2O_5	0.29	0.36	0.28	0.30	-	-	-	-	-	-	-	-	-	-	-	-	-	-	-	-	
S	0.013	0.015	0.009	0.024	-	-	-	-	-	-	-	-	-	-	-	-	-	-	-	-	
Cl	0.082	0.083	0.083	0.086	-	-	-	-	-	-	-	-	-	-	-	-	-	-	-	-	

Table A1. (continued)

Volcanic cone																	Kamikomezuka					
Sample ID																	KKO					
Host mineral					Orthopyroxene	Plagioclase											Clinopyroxene					
Melt ID	O4-m1	O4-m2	O4-m3	O4-m5	4-m6	a1-m1	a2-m1	a2-m2	a3-m1	a3-m2	a4-m1	a4-m2	b1-m1	b3-m1	b4-m1	a1-m1	a1-m2	a6-m1	b5-m1	b5-m2		
H_2O (FTIR)	-	-	-	-	-	-	-	-	-	-	-	-	-	-	-	-	-	-	-	-	-	-
H_2O (SIMS)	0.81	0.82	0.63	0.79	-	-	-	-	-	-	-	-	-	-	-	-	-	-	-	-	-	-
CO_2 ppm (SIMS)[d]	11	10	10	36	-	-	-	-	-	-	-	-	-	-	-	-	-	-	-	-	-	-
S ppm (SIMS)	194	197	179	153	-	-	-	-	-	-	-	-	-	-	-	-	-	-	-	-	-	-
Cl ppm (SIMS)	808	853	754	951	-	-	-	-	-	-	-	-	-	-	-	-	-	-	-	-	-	-
F ppm (SIMS)	789	817	729	825	-	-	-	-	-	-	-	-	-	-	-	-	-	-	-	-	-	-
P_2O_5 (SIMS)	0.48	0.49	0.48	0.57	-	-	-	-	-	-	-	-	-	-	-	-	-	-	-	-	-	-
T_{trap} (°C)[c]	1085	1087	1093	1087	-	-	-	-	-	-	-	-	-	-	-	-	-	-	-	-	-	-
PEC%[e]	1.3	1.5	1.2	1.6	-	-	-	-	-	-	-	-	-	-	-	-	-	-	-	-	-	-
Host mineral compositions (wt.%)																						
SiO_2	37.07	37.56	37.14	37.53	53.10	54.19	53.54	54.15	53.34	55.04	53.60	53.19	51.24	52.54	53.49	51.85	52.85	52.10	52.69	52.49		
TiO_2	0.00	0.00	0.04	0.00	0.34	0.03	0.05	0.06	0.05	0.07	0.06	0.06	0.05	0.07	0.02	0.65	0.53	0.55	0.56	0.61		
Al_2O_3	0.03	0.03	0.02	0.03	1.38	29.16	29.50	29.38	29.13	28.70	29.69	29.86	30.94	29.28	29.46	2.79	2.25	2.60	2.45	2.65		
Cr_2O_3	0.00	0.00	0.00	0.02	0.00	-	-	-	-	-	-	-	-	-	-	0.04	0.02	0.01	0.02	0.00		
FeO^{Total}	30.09	29.70	30.36	30.17	18.95	0.86	0.82	0.92	0.88	0.82	0.86	0.79	0.90	0.91	0.82	11.08	10.94	11.49	9.97	10.64		
MnO	0.61	0.63	0.60	0.60	0.53	0.02	0.01	0.00	0.00	0.06	0.00	0.00	0.00	0.00	0.02	0.38	0.30	0.40	0.30	0.31		
MgO	33.43	33.81	33.36	33.33	23.83	0.13	0.13	0.12	0.09	0.13	0.11	0.12	0.12	0.13	0.12	14.89	15.29	14.94	15.72	15.43		
CaO	0.23	0.24	0.25	0.20	2.15	12.46	12.90	12.60	12.96	11.95	12.84	13.28	14.53	12.53	12.67	18.85	18.93	18.15	19.41	18.74		
Na_2O	0.06	0.02	0.01	0.02	0.06	3.93	3.54	3.78	3.57	4.14	3.61	3.45	2.89	3.54	3.58	0.27	0.26	0.28	0.27	0.31		
K_2O	0.03	0.00	0.02	0.00	0.00	0.46	0.39	0.42	0.42	0.47	0.37	0.38	0.29	0.41	0.44	0.05	0.03	0.03	0.03	0.04		
NiO	0.07	0.00	0.00	0.06	0.02	-	-	-	-	-	-	-	-	-	-	0.03	0.03	0.00	0.01	0.00		
V_2O_3	0.00	0.03	0.00	0.01	0.03	0.00	0.00	0.02	0.00	0.00	0.01	0.00	0.00	0.02	0.00	0.05	0.09	0.10	0.06	0.07		
P_2O_5	-	-	-	-	-	0.02	0.00	0.03	0.00	0.02	0.03	0.01	0.00	0.03	0.03	-	-	-	-	-		
Total[a]	101.60	102.01	101.79	101.97	100.40	101.27	100.90	101.48	100.45	101.42	101.19	101.15	100.97	99.46	100.64	100.98	101.54	100.64	101.52	101.30		
Cations																						
Si	5.93	5.96	5.93	5.97	7.80	7.29	7.23	7.27	7.24	7.38	7.22	7.17	6.96	7.20	7.24	7.68	7.76	7.73	7.72	7.72		
Ti	0.00	0.00	0.01	0.00	0.04	0.00	0.01	0.01	0.00	0.01	0.01	0.01	0.01	0.01	0.00	0.07	0.06	0.06	0.06	0.07		
Al	0.01	0.01	0.00	0.01	0.24	4.62	4.69	4.65	4.66	4.53	4.71	4.75	4.95	4.73	4.70	0.49	0.39	0.46	0.42	0.46		
Cr	0.00	0.00	0.00	0.00	0.00	-	-	-	-	-	-	-	-	-	-	0.01	0.00	0.00	0.00	0.00		
Fe2+	4.02	3.94	4.05	4.01	2.33	0.10	0.09	0.10	0.10	0.09	0.10	0.09	0.10	0.10	0.09	1.37	1.34	1.43	1.22	1.31		
Mn	0.08	0.09	0.08	0.08	0.07	0.00	0.00	0.00	0.00	0.01	0.00	0.00	0.00	0.00	0.00	0.05	0.04	0.05	0.04	0.04		
Mg	7.97	8.00	7.94	7.90	5.22	0.03	0.03	0.02	0.02	0.03	0.02	0.02	0.02	0.03	0.02	3.29	3.35	3.30	3.43	3.38		
Ca	0.04	0.04	0.04	0.03	0.34	1.80	1.87	1.81	1.89	1.72	1.85	1.92	2.11	1.84	1.84	2.99	2.98	2.89	3.05	2.95		
Na	0.02	0.00	0.00	0.01	0.02	1.03	0.93	0.98	0.94	1.08	0.94	0.90	0.76	0.94	0.94	0.08	0.07	0.08	0.08	0.09		
K	0.01	0.00	0.00	0.00	0.00	0.08	0.07	0.07	0.07	0.08	0.06	0.07	0.05	0.07	0.08	0.01	0.01	0.01	0.01	0.01		
Ni	0.01	0.00	0.00	0.01	0.00	-	-	-	-	-	-	-	-	-	-	0.00	0.00	0.00	0.00	0.00		
V	0.00	0.00	0.00	0.00	0.00	0.00	0.00	0.00	0.00	0.00	0.00	0.00	0.00	0.00	0.00	0.01	0.01	0.01	0.01	0.01		
P	-	-	-	-	-	0.00	0.00	0.00	0.00	0.00	0.00	0.00	0.00	0.00	0.00	-	-	-	-	-		
Cation total	18.08	18.04	18.07	18.03	16.05	14.94	14.91	14.92	14.93	14.92	14.91	14.93	14.97	14.93	14.91	16.04	16.02	16.01	16.04	16.03		
Mg# / An[f]	66.5	67.0	66.2	66.3	69.2	63.7	66.8	64.8	66.8	61.5	66.3	68.0	73.6	66.2	66.2	70.5	71.3	69.9	73.8	72.1		

Table A1. (continued)

Volcanic cone																					
Sample ID																					
Host mineral							Olivine					Orthopyroxene			Plagioclase						
Melt ID	c6-m1	c6-m2	d2-m1	e3-m1	e3-m2	Pe4-m1	2-m1	2-m2	3-m2	3-m3	4-m1	1-m2	5-m1	5-m2	a2-m1	a6-m1	a7-m1	c2-m1	c5-m1	c5-m2	Cb3-m1
Uncorrected melt compositions (wt.%)																					
SiO_2	58.70	58.05	61.67	58.55	56.96	56.99	48.54	46.77	51.72	47.61	47.85	58.43	57.83	57.92	56.78	52.25	57.42	59.39	58.02	59.62	52.43
TiO_2	1.36	1.34	1.39	1.29	1.41	1.56	0.90	0.94	1.09	1.03	0.94	1.34	1.44	1.39	1.14	1.07	1.43	1.48	1.21	0.96	1.25
Al_2O_3	14.65	14.76	13.70	14.42	14.79	14.68	18.93	20.81	16.27	18.87	19.39	14.73	14.55	14.66	16.85	19.35	15.12	15.42	15.82	17.49	13.32
FeO^{Total}	8.85	8.90	9.31	8.29	11.45	10.95	10.14	10.60	11.03	10.12	11.29	9.14	10.05	9.30	8.21	8.29	9.73	9.46	8.09	7.33	13.83
MnO	0.22	0.15	0.22	0.21	0.20	0.18	0.13	0.16	0.22	0.19	0.21	0.19	0.27	0.19	0.14	0.10	0.23	0.16	0.19	0.10	0.28
MgO	2.66	2.78	1.86	3.91	3.46	3.60	4.95	3.75	4.33	5.37	4.72	2.73	2.71	2.70	2.44	4.18	3.59	2.54	2.56	2.22	5.89
CaO	5.81	5.35	4.72	6.89	7.21	6.72	10.86	12.13	8.94	10.25	11.57	5.81	5.88	6.07	6.76	7.12	6.22	5.86	5.83	6.50	8.83
Na_2O	3.15	3.09	3.16	2.42	2.09	1.98	2.73	3.01	1.98	2.40	2.56	3.36	3.21	3.09	2.40	3.71	2.52	3.17	3.72	2.89	1.80
K_2O	3.54	3.51	3.78	2.59	2.28	1.76	0.56	0.70	1.86	0.56	0.80	2.75	3.04	3.60	3.57	2.30	2.09	2.86	3.50	2.95	1.97
P_2O_5	0.31	0.39	0.23	0.35	0.25	0.36	0.17	0.16	0.28	0.16	0.09	0.40	0.45	0.63	0.21	0.40	0.37	0.45	0.43	0.31	0.20
S (EPMA)	0.006	0.026	0.022	0.006	0.000	0.017	0.396	0.346	0.134	0.243	0.278	0.014	0.000	0.000	0.004	0.000	0.000	0.004	0.004	0.009	0.097
Cl (EPMA)	0.091	0.101	0.104	0.094	0.071	0.091	0.056	0.080	0.067	0.095	0.075	0.073	0.065	0.107	0.052	0.069	0.051	0.090	0.070	0.059	0.070
Total[a]	99.53	98.59	100.29	99.18	100.35	99.08	99.01	100.03	98.15	97.28	100.24	98.99	99.53	99.64	98.67	98.93	98.94	100.97	99.48	100.59	100.22
H_2O (FTIR)	-	-	0.77	-	n.d.	-	-	-	-	-	-	-	-	-	-	-	n.d.	n.d.	-	n.d.	-
H_2O (SIMS)	-	-	-	-	-	-	-	-	-	-	-	-	-	-	-	-	-	-	-	-	-
CO_2 ppm (SIMS)[a]	-	-	-	-	-	-	-	-	-	-	-	-	-	-	-	-	-	-	-	-	-
S ppm (SIMS)	-	-	-	-	-	-	-	-	-	-	-	-	-	-	-	-	-	-	-	-	-
Cl ppm (SIMS)	-	-	-	-	-	-	-	-	-	-	-	-	-	-	-	-	-	-	-	-	-
F ppm (SIMS)	-	-	-	-	-	-	-	-	-	-	-	-	-	-	-	-	-	-	-	-	-
P_2O_5 (SIMS)	-	-	-	-	-	-	-	-	-	-	-	-	-	-	-	-	-	-	-	-	-
S^{6+}/S_{total}	-	-	-	-	-	-	-	-	-	-	-	-	-	-	-	-	-	-	-	-	-
1 s.e.[b]	-	-	-	-	-	-	-	-	-	-	-	-	-	-	-	-	-	-	-	-	-
T_{erupt} (°C)[c]	1032	1040	1019	-	1068	1077	1057	1029	1047	1069	1050	1076	1077	1069	-	1068	-	-	-	-	-
$K_{D\ uncorrected}$[a]	0.26	0.26	0.20	0.43	0.25	0.21	0.26	0.26	0.31	0.29	0.27	0.30	0.29	0.32	0.27	0.22	0.22	0.17	0.16	0.27	0.09
Corrected melt compositions for post-entrapment crystallization (wt.%)																					
SiO_2	-	-	-	-	-	-	48.03	46.03	51.02	47.60	47.33	-	-	-	-	-	-	-	-	-	-
TiO_2	-	-	-	-	-	-	0.85	0.85	1.03	1.03	0.88	-	-	-	-	-	-	-	-	-	-
Al_2O_3	-	-	-	-	-	-	17.90	18.89	15.42	18.85	18.26	-	-	-	-	-	-	-	-	-	-
FeO^{Total}	-	-	-	-	-	-	11.72	13.21	12.48	10.15	12.90	-	-	-	-	-	-	-	-	-	-
MnO	-	-	-	-	-	-	0.12	0.15	0.21	0.19	0.19	-	-	-	-	-	-	-	-	-	-
MgO	-	-	-	-	-	-	6.81	6.99	6.13	5.41	6.71	-	-	-	-	-	-	-	-	-	-
CaO	-	-	-	-	-	-	10.27	11.01	8.47	10.24	10.89	-	-	-	-	-	-	-	-	-	-
Na_2O	-	-	-	-	-	-	2.58	2.73	1.88	2.40	2.41	-	-	-	-	-	-	-	-	-	-
K_2O	-	-	-	-	-	-	0.53	0.63	1.76	0.56	0.75	-	-	-	-	-	-	-	-	-	-
P_2O_5	-	-	-	-	-	-	0.16	0.15	0.26	0.16	0.08	-	-	-	-	-	-	-	-	-	-
S	-	-	-	-	-	-	0.375	0.314	0.127	0.243	0.261	-	-	-	-	-	-	-	-	-	-
Cl	-	-	-	-	-	-	0.053	0.073	0.063	0.095	0.071	-	-	-	-	-	-	-	-	-	-

Table A1. (continued) s

Volcanic cone																							
Sample ID																							
Host mineral							Olivine					Orthopyroxene			Plagioclase								
Melt ID	c6-m1	c6-m2	d2-m1	e3-m1	e3-m2	Pe4-m1	2-m1	2-m2	3-m2	3-m3	4-m1	1-m2	5-m1	5-m2	a2-m1	a6-m1	a7-m1	c2-m1	c5-m1	c5-m2	Cb3-m1		
H_2O (FTIR)	-	-	-	-	-	-	-	-	-	-	-	-	-	-	-	-	-	-	-	-	-		
H_2O (SIMS)	-	-	-	-	-	-	-	-	-	-	-	-	-	-	-	-	-	-	-	-	-		
CO_2 ppm (SIMS)[a]	-	-	-	-	-	-	-	-	-	-	-	-	-	-	-	-	-	-	-	-	-		
S ppm (SIMS)	-	-	-	-	-	-	-	-	-	-	-	-	-	-	-	-	-	-	-	-	-		
Cl ppm (SIMS)	-	-	-	-	-	-	-	-	-	-	-	-	-	-	-	-	-	-	-	-	-		
F ppm (SIMS)	-	-	-	-	-	-	-	-	-	-	-	-	-	-	-	-	-	-	-	-	-		
P_2O_5 (SIMS)	-	-	-	-	-	-	-	-	-	-	-	-	-	-	-	-	-	-	-	-	-		
T_{trap} (°C)[c]	-	-	-	-	-	-	1100	1105	1090	1069	1096	-	-	-	-	-	-	-	-	-	-		
PEC%[c]	-	-	-	-	-	-	5.6	9.7	5.4	0.1	6.0	-	-	-	-	-	-	-	-	-	-		
Host mineral compositions (wt.%)																							
SiO_2	52.62	52.19	52.58	52.51	52.86	51.56	-	40.23	39.04	39.32	39.80	53.24	52.85	52.89	52.71	52.72	52.69	53.62	53.69	54.49	46.51		
TiO_2	0.60	0.59	0.69	0.66	0.56	0.75	-	0.03	0.00	0.03	0.02	0.31	0.36	0.32	0.06	0.06	0.08	0.01	0.07	0.04	0.02		
Al_2O_3	2.68	2.39	1.98	2.70	2.37	4.66	-	0.02	0.03	0.03	0.04	1.45	1.58	1.36	29.73	29.41	29.25	29.43	28.99	28.73	34.35		
Cr_2O_3	0.00	0.00	0.00	0.02	0.01	0.04	-	0.00	0.01	0.00	0.01	0.00	0.01	0.01	-	-	-	-	-	-	-		
FeO^{Total}	10.24	10.22	11.58	11.22	10.23	7.64	-	18.30	20.43	19.65	18.79	19.06	20.28	20.32	0.76	0.81	0.82	0.78	0.74	0.77	0.74		
MnO	0.34	0.38	0.44	0.36	0.36	0.20	-	0.28	0.27	0.29	0.28	0.52	0.61	0.59	0.02	0.00	0.01	0.00	0.00	0.04	0.01		
MgO	15.06	15.34	14.58	15.44	15.61	14.83	-	42.28	40.81	41.45	41.74	23.66	23.43	23.33	0.09	0.12	0.11	0.13	0.12	0.11	0.09		
CaO	19.73	19.07	17.86	18.39	18.91	21.69	-	0.12	0.17	0.15	0.11	2.14	1.98	2.07	13.00	13.34	12.96	12.49	12.26	11.67	17.92		
Na_2O	0.29	0.32	0.31	0.33	0.27	0.29	-	0.00	0.01	0.00	0.00	0.05	0.04	0.04	3.59	3.52	3.72	3.85	3.90	3.98	1.14		
K_2O	0.04	0.06	0.05	0.01	0.02	0.05	-	0.00	0.03	0.01	0.01	0.00	0.00	0.00	0.38	0.41	0.37	0.47	0.48	0.45	0.08		
NiO	0.01	0.00	0.00	0.02	0.00	0.03	-	0.09	0.07	0.01	0.05	0.00	0.00	0.02	-	-	-	-	-	-	-		
V_2O_3	0.03	0.09	0.06	0.09	0.00	0.13	-	0.03	0.00	0.00	0.04	0.00	0.05	0.10	-	-	-	-	-	-	-		
P_2O_5	-	-	-	-	-	-	-	-	-	-	-	-	-	-	0.00	0.00	0.00	0.08	0.03	0.01	0.04		
Total[a]	101.66	100.67	100.14	101.79	101.19	101.87	-	101.37	100.87	100.94	100.89	100.42	101.17	101.05	100.49	100.55	100.17	101.00	100.44	100.42	101.02		
Cations																							
Si	7.71	7.73	7.84	7.70	7.76	7.50	6.03	6.06	5.98	6.00	6.04	7.82	7.75	7.77	7.16	7.17	7.19	7.24	7.28	7.37	6.38		
Ti	0.07	0.07	0.08	0.07	0.06	0.08	0.00	0.00	0.00	0.00	0.00	0.03	0.04	0.04	0.01	0.01	0.01	0.00	0.01	0.00	0.00		
Al	0.46	0.42	0.35	0.47	0.41	0.80	0.00	0.00	0.01	0.01	0.01	0.25	0.27	0.24	4.76	4.72	4.70	4.68	4.64	4.58	5.55		
Cr	0.00	0.00	0.00	0.00	0.00	0.00	0.00	0.00	0.00	0.00	0.00	0.00	0.00	0.00	-	-	-	-	-	-	-		
Fe2+	1.26	1.27	1.44	1.38	1.26	0.93	2.29	2.31	2.62	2.51	2.39	2.34	2.49	2.50	0.09	0.09	0.09	0.09	0.08	0.09	0.08		
Mn	0.04	0.05	0.06	0.04	0.05	0.02	0.04	0.04	0.04	0.04	0.04	0.06	0.08	0.07	0.00	0.00	0.00	0.00	0.00	0.00	0.00		
Mg	3.29	3.38	3.24	3.38	3.42	3.22	9.56	9.49	9.33	9.42	9.45	5.18	5.12	5.11	0.02	0.03	0.02	0.03	0.02	0.02	0.02		
Ca	3.10	3.03	2.85	2.89	2.98	3.38	0.03	0.02	0.03	0.02	0.02	0.34	0.31	0.33	1.89	1.94	1.89	1.81	1.78	1.69	2.63		
Na	0.08	0.09	0.09	0.09	0.08	0.08	0.00	0.00	0.00	0.00	0.00	0.01	0.01	0.01	0.95	0.93	0.98	1.01	1.02	1.04	0.30		
K	0.01	0.01	0.01	0.00	0.00	0.01	0.00	0.00	0.01	0.00	0.00	0.00	0.00	0.00	0.07	0.07	0.06	0.08	0.08	0.08	0.01		
Ni	0.00	0.00	0.00	0.00	0.00	0.00	0.01	0.01	0.01	0.00	0.01	0.00	0.00	0.00	-	-	-	-	-	-	-		
V	0.00	0.01	0.01	0.01	0.00	0.02	0.00	0.00	0.00	0.00	0.01	0.00	0.01	0.01	-	-	-	-	-	-	-		
P	-	-	-	-	-	-	-	-	-	-	-	-	-	-	0.00	0.00	0.00	0.01	0.00	0.00	0.00		
Cation total	16.03	16.05	15.96	16.04	16.01	16.05	17.97	17.93	18.02	18.00	17.95	16.03	16.08	16.07	14.96	14.97	14.98	14.95	14.94	14.89	15.00		
Mg# / An[f]	72.4	72.8	69.2	71.0	73.1	77.6	80.7	80.5	78.1	79.0	79.8	68.9	67.3	67.2	66.7	67.7	65.8	64.2	63.5	61.8	89.6		

Table A1. (continued)

Volcanic cone				Ojodake																	
Sample ID				OJSU																	
Host mineral				Clinopyroxene								Olivine									
Melt ID	Cb3-m2	e5-m1	e5-m2	1-m1	1-m2	1-m3	1-m4	1-m5	1-m6	1-m7	O1-m7	1-m1	1-m10	1-m11	1-m12	1-m13	1-m14	1-m15	1-m2	1-m3	1-m4
Uncorrected melt compositions (wt.%)																					
SiO_2	53.01	56.37	59.21	57.54	56.18	56.57	56.68	56.95	57.28	53.85	56.78	55.37	53.64	53.70	51.20	51.77	57.53	55.28	55.33	53.29	55.02
TiO_2	1.36	1.66	1.42	1.17	1.56	1.36	1.51	1.48	1.26	1.18	1.03	1.28	1.14	1.14	0.92	1.10	0.99	1.24	1.37	1.23	0.84
Al_2O_3	13.04	15.58	15.08	15.45	15.13	15.07	14.86	14.74	14.89	15.48	14.57	15.42	15.57	15.45	18.51	16.00	14.20	15.05	15.05	15.36	15.00
FeO^{Total}	13.21	9.71	8.87	8.66	9.82	9.26	10.11	9.53	9.09	9.62	9.80	9.05	9.96	9.81	7.97	9.39	9.46	9.57	8.70	9.88	9.61
MnO	0.27	0.19	0.19	0.19	0.19	0.17	0.18	0.20	0.17	0.20	0.16	0.18	0.20	0.20	0.14	0.16	0.19	0.18	0.16	0.18	0.22
MgO	5.93	2.99	3.01	2.16	2.12	2.37	2.06	2.22	2.92	3.53	2.59	3.37	3.39	2.95	3.95	3.66	2.61	3.23	2.90	3.32	2.77
CaO	8.11	6.05	6.17	5.37	5.16	5.40	4.88	5.40	5.83	7.36	5.54	6.93	7.40	7.66	7.40	8.11	5.97	7.04	6.46	7.50	6.24
Na_2O	2.01	3.46	3.33	3.07	3.03	2.97	2.90	2.78	2.79	2.94	3.49	3.20	2.99	2.88	3.05	2.96	2.95	3.22	3.16	2.80	2.96
K_2O	1.99	3.07	2.95	3.42	3.98	3.31	3.64	3.59	2.88	2.14	3.19	2.25	2.01	2.07	2.18	1.86	2.60	2.27	2.42	2.01	2.05
P_2O_5	0.22	0.49	0.30	0.41	0.62	0.42	0.60	0.44	0.47	0.32	0.20	0.34	0.23	0.37	0.38	0.30	0.44	0.31	0.46	0.38	0.34
S (EPMA)	0.069	0.003	0.012	0.022	0.021	0.011	0.002	0.012	0.023	0.059	0.025	0.011	0.076	0.074	0.159	0.137	0.046	0.026	0.028	0.060	0.070
Cl (EPMA)	0.087	0.103	0.061	0.089	0.212	0.083	0.093	0.110	0.086	0.076	0.084	0.057	0.089	0.091	0.094	0.069	0.085	0.058	0.069	0.084	0.066
Total[a]	99.51	99.75	100.76	97.60	98.03	96.98	97.56	97.49	97.73	96.92	97.51	97.52	96.83	96.55	96.24	95.74	97.19	97.52	96.19	96.21	95.30
H_2O (FTIR)	-	n.d.	n.d.	0.57	0.92	0.71	0.81	0.72	2.40	2.03	-	-	-	-	-	2.05	-	1.74	-	-	-
H_2O (SIMS)	-	-	-	-	-	-	-	-	-	-	-	-	-	-	-	-	-	-	-	-	-
CO_2 ppm (SIMS)[a]	-	-	-	-	-	-	-	-	-	-	-	-	-	-	-	-	-	-	-	-	-
S ppm (SIMS)	-	-	-	-	-	-	-	-	-	-	-	-	-	-	-	-	-	-	-	-	-
Cl ppm (SIMS)	-	-	-	-	-	-	-	-	-	-	-	-	-	-	-	-	-	-	-	-	-
F ppm (SIMS)	-	-	-	-	-	-	-	-	-	-	-	-	-	-	-	-	-	-	-	-	-
P_2O_5 (SIMS)	-	-	-	-	-	-	-	-	-	-	-	-	-	-	-	-	-	-	-	-	-
S^{6+}/S_{total}	-	-	-	-	-	-	-	-	-	-	-	-	-	-	0.53	0.43	-	-	-	0.43	-
1 s.e.[b]	-	-	-	-	-	-	-	-	-	-	-	-	-	-	0.04	0.04	-	-	-	0.04	-
T_{erupt} (°C)[c]	1048	-	-	1031	1026	1034	1028	1018	931	1052	1024	1032	1032	1022	1048	1055	1017	1056	1024	1031	1022
$K_{D\ uncorrected}$[a]	0.10	0.17	0.17	0.22	0.21	0.24	0.20	0.21	0.22	0.30	0.22	0.40	0.45	0.42	0.30	0.37	0.52	0.45	0.41	0.42	0.47
Corrected melt compositions for post-entrapment crystallization (wt.%)																					
SiO_2	-	-	-	-	-	-	-	-	-	-	-	55.14	53.46	53.07	51.19	51.75	57.20	55.05	54.92	52.95	54.55
TiO_2	-	-	-	-	-	-	-	-	-	-	-	1.26	1.13	1.09	0.92	1.10	0.97	1.22	1.34	1.21	0.81
Al_2O_3	-	-	-	-	-	-	-	-	-	-	-	15.22	15.40	14.84	18.49	15.98	13.97	14.85	14.70	15.03	14.60
FeO^{Total}	-	-	-	-	-	-	-	-	-	-	-	9.42	10.27	10.90	8.01	9.41	9.90	9.94	9.39	10.48	10.35
MnO	-	-	-	-	-	-	-	-	-	-	-	0.18	0.20	0.19	0.14	0.16	0.19	0.17	0.16	0.17	0.21
MgO	-	-	-	-	-	-	-	-	-	-	-	3.82	3.77	4.31	3.99	3.69	3.15	3.68	3.73	4.07	3.69
CaO	-	-	-	-	-	-	-	-	-	-	-	6.84	7.32	7.36	7.39	8.10	5.88	6.95	6.31	7.33	6.07
Na_2O	-	-	-	-	-	-	-	-	-	-	-	3.15	2.95	2.77	3.05	2.95	2.91	3.18	3.09	2.74	2.88
K_2O	-	-	-	-	-	-	-	-	-	-	-	2.22	1.99	1.99	2.17	1.86	2.56	2.24	2.37	1.97	1.99
P_2O_5	-	-	-	-	-	-	-	-	-	-	-	0.33	0.22	0.36	0.38	0.30	0.44	0.30	0.45	0.37	0.33
S	-	-	-	-	-	-	-	-	-	-	-	0.011	0.075	0.071	0.158	0.136	0.046	0.025	0.027	0.059	0.068
Cl	-	-	-	-	-	-	-	-	-	-	-	0.056	0.088	0.087	0.094	0.069	0.084	0.057	0.067	0.082	0.064

Table A1. (continued)

Volcanic cone				Ojodake																		
Sample ID				OJSU																		
Host mineral				Clinopyroxene									Olivine									
Melt ID	Cb3-m2	e5-m1	e5-m2	1-m1	1-m2	1-m3	1-m4	1-m5	1-m6	1-m7	O1-m7	1-m1	1-m10	1-m11	1-m12	1-m13	1-m14	1-m15	1-m2	1-m3	1-m4	
H_2O (FTIR)	-	-	-	-	-	-	-	-	-	-	-	-	-	-	-	2.05	-	1.72	-	-	-	
H_2O (SIMS)	-	-	-	-	-	-	-	-	-	-	-	-	-	-	-	-	-	-	-	-	-	
CO_2 ppm (SIMS)[a]	-	-	-	-	-	-	-	-	-	-	-	-	-	-	-	-	-	-	-	-	-	
S ppm (SIMS)	-	-	-	-	-	-	-	-	-	-	-	-	-	-	-	-	-	-	-	-	-	
Cl ppm (SIMS)	-	-	-	-	-	-	-	-	-	-	-	-	-	-	-	-	-	-	-	-	-	
F ppm (SIMS)	-	-	-	-	-	-	-	-	-	-	-	-	-	-	-	-	-	-	-	-	-	
P_2O_5 (SIMS)	-	-	-	-	-	-	-	-	-	-	-	-	-	-	-	-	-	-	-	-	-	
T_{trap} (°C)[c]	-	-	-	-	-	-	-	-	-	-	-	1042	1041	1054	1048	1055	1030	1066	1043	1048	1044	
PEC%[c]	-	-	-	-	-	-	-	-	-	-	-	1.3	1.1	4.0	0.1	0.1	1.6	1.3	2.4	2.2	2.7	
Host mineral compositions (wt.%)																						
SiO_2	47.33	53.85	53.78	51.18	51.08	51.18	51.43	51.07	50.72	51.05	51.77	38.80	38.06	38.45	39.12	38.52	37.57	38.28	38.15	38.15	38.00	
TiO_2	0.00	0.05	0.06	0.52	0.54	0.52	0.61	0.59	0.56	0.58	0.64	0.00	0.00	0.02	0.00	0.01	0.00	0.00	0.01	0.00	0.00	
Al_2O_3	33.27	29.25	29.05	2.47	2.54	2.52	2.34	2.21	2.68	2.57	2.29	0.06	0.00	0.01	0.02	0.02	0.03	0.04	0.03	0.03	0.01	
Cr_2O_3	-	-	-	0.00	0.02	0.01	0.00	0.03	0.00	0.01	0.01	0.01	0.01	0.00	0.03	0.00	0.01	0.00	0.00	0.00	0.00	
FeO^{Total}	0.61	0.81	0.88	10.43	11.83	11.01	11.52	10.63	8.55	9.69	10.55	24.15	26.12	25.06	20.04	23.15	28.47	26.49	24.20	25.51	26.91	
MnO	0.01	0.02	0.01	0.34	0.36	0.32	0.37	0.33	0.24	0.29	0.32	0.48	0.49	0.46	0.30	0.43	0.58	0.52	0.47	0.48	0.50	
MgO	0.10	0.13	0.13	15.08	15.17	14.86	14.64	15.08	15.51	15.10	15.70	36.67	35.44	36.71	41.03	38.01	33.20	35.87	36.04	36.59	35.01	
CaO	17.53	12.79	12.62	19.74	18.76	19.78	19.43	19.66	22.14	20.99	18.88	0.21	0.26	0.21	0.14	0.22	0.19	0.20	0.24	0.21	0.18	
Na_2O	1.49	3.76	3.88	0.26	0.28	0.23	0.29	0.23	0.23	0.26	0.28	0.00	0.01	0.01	0.01	0.00	0.01	0.00	0.02	0.00	0.00	
K_2O	0.08	0.44	0.49	0.00	0.00	0.00	0.00	0.02	0.02	0.03	0.01	0.00	0.00	0.00	0.00	0.00	0.00	0.01	0.01	0.00	0.00	
NiO	-	-	-	0.00	0.00	0.01	0.00	0.03	0.06	0.00	0.02	0.05	0.00	0.01	0.05	0.01	0.04	0.04	0.03	0.00	0.06	
V_2O_3	-	-	-	0.09	0.07	0.06	0.04	0.03	0.01	0.06	0.04	0.00	0.05	0.04	0.00	0.01	0.00	0.00	0.02	0.03	0.07	
P_2O_5	0.02	0.01	0.02	-	-	-	-	-	-	-	-	-	-	-	-	-	-	-	-	-	-	
Total[a]	100.58	101.25	101.05	100.11	100.64	100.51	100.67	99.90	100.71	100.63	100.50	100.41	100.43	100.96	100.72	100.38	100.08	101.44	99.22	101.00	100.73	
Cations																						
Si	6.51	7.26	7.27	7.65	7.63	7.64	7.67	7.66	7.54	7.60	7.69	6.08	6.03	6.02	5.99	6.01	6.04	6.01	6.06	5.99	6.02	
Ti	0.00	0.00	0.01	0.06	0.06	0.06	0.07	0.07	0.06	0.06	0.07	0.00	0.00	0.00	0.00	0.00	0.00	0.00	0.00	0.00	0.00	
Al	5.39	4.65	4.63	0.44	0.45	0.44	0.41	0.39	0.47	0.45	0.40	0.01	0.00	0.00	0.00	0.00	0.01	0.01	0.01	0.01	0.00	
Cr	-	-	-	0.00	0.00	0.00	0.00	0.00	0.00	0.00	0.00	0.00	0.00	0.00	0.00	0.00	0.00	0.00	0.00	0.00	0.00	
Fe2+	0.07	0.09	0.10	1.30	1.48	1.37	1.44	1.33	1.06	1.21	1.31	3.16	3.46	3.28	2.57	3.02	3.83	3.48	3.21	3.35	3.57	
Mn	0.00	0.00	0.00	0.04	0.05	0.04	0.05	0.04	0.03	0.04	0.04	0.06	0.07	0.06	0.04	0.06	0.08	0.07	0.06	0.06	0.07	
Mg	0.02	0.03	0.03	3.36	3.38	3.31	3.26	3.37	3.44	3.35	3.47	8.56	8.36	8.57	9.37	8.85	7.96	8.39	8.54	8.56	8.27	
Ca	2.58	1.85	1.83	3.16	3.00	3.16	3.11	3.16	3.53	3.35	3.00	0.04	0.04	0.04	0.02	0.04	0.03	0.03	0.04	0.03	0.03	
Na	0.40	0.98	1.02	0.08	0.08	0.07	0.08	0.07	0.07	0.08	0.08	0.00	0.00	0.00	0.00	0.00	0.00	0.00	0.01	0.00	0.00	
K	0.01	0.08	0.08	0.00	0.00	0.00	0.00	0.00	0.00	0.01	0.00	0.00	0.00	0.00	0.00	0.00	0.00	0.00	0.00	0.00	0.00	
Ni	-	-	-	0.00	0.00	0.00	0.00	0.00	0.01	0.00	0.00	0.01	0.00	0.00	0.01	0.00	0.00	0.01	0.00	0.00	0.01	
V	-	-	-	0.01	0.01	0.01	0.01	0.00	0.00	0.01	0.00	0.00	0.01	0.00	0.00	0.00	0.00	0.00	0.00	0.00	0.01	
P	0.00	0.00	0.00	-	-	-	-	-	-	-	-	-	-	-	-	-	-	-	-	-	-	
Cation total	15.00	14.94	14.96	16.10	16.13	16.11	16.09	16.11	16.20	16.15	16.08	17.92	17.97	17.98	18.01	17.98	17.96	17.99	17.94	18.01	17.97	
Mg# / An[f]	86.7	65.3	64.2	72.0	69.6	70.6	69.4	71.7	76.4	73.5	72.6	73.0	70.7	72.3	78.5	74.5	67.5	70.7	72.6	71.9	69.9	

Table A1. (continued)

Volcanic cone																	Ojodake				
Sample ID																	OJSL				
Host mineral						Orthopyroxene						Plagioclase					Clinopyroxene				
Melt ID	1-m5	1-m6	1-m7	1-m8	1-m9	O1-m6	1-m1	1-m2	1-m3	1-m4	1-m5	1-m1	1-m4	1-m5	1-m6	1-m7	1-m1	1-m2	1-m3	1-m4	1-m5
Uncorrected melt compositions (wt.%)																					
SiO_2	57.75	54.08	52.94	52.77	52.63	53.15	57.65	59.83	56.64	53.95	58.00	57.17	53.79	52.26	58.26	58.08	57.88	53.76	58.24	57.52	57.51
TiO_2	0.94	1.24	1.09	0.78	0.91	1.16	0.64	0.74	1.47	1.12	1.11	1.06	1.29	1.35	1.04	0.81	1.29	1.24	1.45	1.39	1.52
Al_2O_3	14.02	15.42	15.75	15.42	15.79	16.26	15.33	13.72	13.43	14.44	14.43	16.36	14.80	15.78	15.88	16.92	15.42	14.92	14.68	15.10	14.85
FeO^{Total}	8.93	9.52	10.69	10.68	10.82	9.30	8.06	8.41	9.97	10.31	7.71	7.15	9.79	9.11	6.84	5.05	8.83	9.90	9.35	9.36	9.00
MnO	0.18	0.20	0.19	0.21	0.20	0.19	0.21	0.16	0.19	0.20	0.20	0.14	0.21	0.22	0.11	0.12	0.14	0.18	0.16	0.17	0.17
MgO	2.63	3.32	3.12	3.31	3.42	3.65	2.81	2.38	3.00	3.73	2.10	2.42	3.70	2.67	1.65	1.27	2.26	3.91	2.24	2.12	1.90
CaO	5.56	6.87	8.00	8.38	8.25	7.30	6.24	5.28	5.82	6.76	4.93	5.73	7.25	6.88	4.84	4.84	5.37	7.46	5.39	5.36	4.71
Na_2O	2.93	3.07	2.99	2.95	2.90	3.49	3.80	3.79	3.17	3.43	3.60	3.38	3.00	2.86	2.93	3.67	2.93	2.63	2.83	3.09	2.88
K_2O	3.05	2.07	1.87	1.80	1.72	1.65	2.40	2.47	2.18	2.08	3.20	2.87	2.37	2.35	3.77	3.34	3.63	1.97	3.69	3.52	4.09
P_2O_5	0.43	0.29	0.30	0.33	0.31	0.17	0.17	0.12	0.34	0.24	0.30	0.45	0.30	0.81	0.48	0.42	0.49	0.46	0.66	0.53	0.62
S (EPMA)	0.018	0.064	0.089	0.109	0.131	0.174	0.004	0.032	0.031	0.074	0.001	0.011	0.040	0.020	0.012	0.005	0.022	0.050	0.011	0.034	0.021
Cl (EPMA)	0.087	0.069	0.072	0.062	0.067	0.065	0.055	0.044	0.078	0.065	0.103	0.091	0.070	0.088	0.047	0.073	0.074	0.050	0.098	0.089	0.115
Total[a]	96.55	96.36	97.27	96.99	97.34	96.87	97.40	97.03	96.38	96.54	95.68	96.85	96.67	94.46	95.94	94.62	98.42	96.64	98.85	98.35	97.43
H_2O (FTIR)	-	-	-	-	-	-	-	-	-	-	-	-	-	-	2.11	4.71	1.31	2.52	-	0.99	-
H_2O (SIMS)	-	-	-	-	-	-	-	-	-	-	-	-	-	-	-	-	-	-	-	-	-
CO_2 ppm (SIMS)[a]	-	-	-	-	-	-	-	-	-	-	-	-	-	-	-	-	-	-	-	-	-
S ppm (SIMS)	-	-	-	-	-	-	-	-	-	-	-	-	-	-	-	-	-	-	-	-	-
Cl ppm (SIMS)	-	-	-	-	-	-	-	-	-	-	-	-	-	-	-	-	-	-	-	-	-
F ppm (SIMS)	-	-	-	-	-	-	-	-	-	-	-	-	-	-	-	-	-	-	-	-	-
P_2O_5 (SIMS)	-	-	-	-	-	-	-	-	-	-	-	-	-	-	-	-	-	-	-	-	-
S^{6+}/S_{total}	-	-	-	-	-	-	-	-	-	-	-	-	-	-	-	-	-	-	-	-	-
1 s.e.[b]	-	-	-	-	-	-	-	-	-	-	-	-	-	-	-	-	-	-	-	-	-
T_{erupt} (°C)[c]	1019	1032	1025	1027	1030	1039	1065	1076	1081	1096	1068	-	-	1060	-	969	1026	-	1006	1019	978
$K_{D\ uncorrected}$[a]	0.52	0.42	0.45	0.46	0.46	0.38	0.32	0.27	0.32	0.34	0.26	0.17	0.10	0.18	0.17	0.13	0.25	0.38	0.23	0.21	0.21
Corrected melt compositions for post-entrapment crystallization (wt.%)																					
SiO_2	57.61	53.81	52.72	52.66	52.60	52.96	-	-	-	-	-	-	-	-	-	-	-	-	-	-	-
TiO_2	0.93	1.22	1.08	0.78	0.90	1.15	-	-	-	-	-	-	-	-	-	-	-	-	-	-	-
Al_2O_3	13.92	15.16	15.53	15.31	15.75	16.05	-	-	-	-	-	-	-	-	-	-	-	-	-	-	-
FeO^{Total}	9.12	10.00	11.06	10.87	10.88	9.68	-	-	-	-	-	-	-	-	-	-	-	-	-	-	-
MnO	0.18	0.19	0.18	0.21	0.20	0.19	-	-	-	-	-	-	-	-	-	-	-	-	-	-	-
MgO	2.87	3.90	3.59	3.55	3.49	4.09	-	-	-	-	-	-	-	-	-	-	-	-	-	-	-
CaO	5.52	6.76	7.89	8.32	8.23	7.20	-	-	-	-	-	-	-	-	-	-	-	-	-	-	-
Na_2O	2.91	3.02	2.95	2.93	2.89	3.44	-	-	-	-	-	-	-	-	-	-	-	-	-	-	-
K_2O	3.03	2.04	1.85	1.79	1.72	1.63	-	-	-	-	-	-	-	-	-	-	-	-	-	-	-
P_2O_5	0.42	0.29	0.30	0.32	0.31	0.17	-	-	-	-	-	-	-	-	-	-	-	-	-	-	-
S	0.018	0.063	0.088	0.109	0.130	0.172	-	-	-	-	-	-	-	-	-	-	-	-	-	-	-
Cl	0.086	0.068	0.071	0.062	0.067	0.064	-	-	-	-	-	-	-	-	-	-	-	-	-	-	-

Table A1. (continued)

Volcanic cone																		Ojodake					
Sample ID																		OJSL					
Host mineral							Orthopyroxene					Plagioclase						Clinopyroxene					
Melt ID	1-m5	1-m6	1-m7	1-m8	1-m9	O1-m6	1-m1	1-m2	1-m3	1-m4	1-m5	1-m1	1-m4	1-m5	1-m6	1-m7		1-m1	1-m2	1-m3	1-m4	1-m5	
H_2O (FTIR)	-	-	-	-	-	-	-	-	-	-	-	-	-	-	-	-		-	-	-	-	-	-
H_2O (SIMS)	-	-	-	-	-	-	-	-	-	-	-	-	-	-	-	-		-	-	-	-	-	-
CO_2 ppm (SIMS)[a]	-	-	-	-	-	-	-	-	-	-	-	-	-	-	-	-		-	-	-	-	-	-
S ppm (SIMS)	-	-	-	-	-	-	-	-	-	-	-	-	-	-	-	-		-	-	-	-	-	-
Cl ppm (SIMS)	-	-	-	-	-	-	-	-	-	-	-	-	-	-	-	-		-	-	-	-	-	-
F ppm (SIMS)	-	-	-	-	-	-	-	-	-	-	-	-	-	-	-	-		-	-	-	-	-	-
P_2O_5 (SIMS)	-	-	-	-	-	-	-	-	-	-	-	-	-	-	-	-		-	-	-	-	-	-
T_{trap} (°C)[c]	1024	1046	1036	1032	1031	1049	-	-	-	-	-	-	-	-	-	-		-	-	-	-	-	-
PEC%[c]	0.7	1.7	1.4	0.7	0.2	1.3	-	-	-	-	-	-	-	-	-	-		-	-	-	-	-	-
Host mineral compositions (wt.%)																							
SiO_2	37.68	38.68	37.56	38.01	38.01	-	53.55	53.81	53.07	53.69	53.16	52.68	48.50	51.11	53.21	52.43		51.26	50.94	51.63	51.30	51.74	
TiO_2	0.00	0.06	0.00	0.01	0.01	-	0.31	0.33	0.32	0.29	0.27	0.02	0.03	0.04	0.02	0.04		0.63	0.61	0.61	0.54	0.57	
Al_2O_3	0.02	0.02	0.04	0.04	0.04	-	1.40	1.33	1.33	1.47	1.31	29.32	32.44	30.59	28.50	29.48		2.67	2.50	2.19	2.26	2.01	
Cr_2O_3	0.00	0.00	0.00	0.00	0.00	-	0.02	0.01	0.02	0.00	0.01	-	-	-	-	-		0.00	0.00	0.00	0.01	0.01	
FeO^{Total}	28.33	25.06	26.48	26.67	26.67	-	18.12	18.38	19.75	18.23	18.38	0.82	0.91	0.90	0.86	0.81		11.24	11.54	11.49	11.18	11.86	
MnO	0.54	0.50	0.45	0.49	0.49	-	0.50	0.49	0.56	0.44	0.52	0.01	0.00	0.00	0.02	0.00		0.35	0.33	0.39	0.33	0.41	
MgO	33.29	36.21	35.71	35.18	35.18	-	25.07	24.56	23.18	24.29	24.34	0.10	0.08	0.11	0.12	0.09		14.79	15.09	15.00	14.97	15.03	
CaO	0.22	0.24	0.21	0.25	0.25	-	2.05	2.07	2.11	2.11	2.03	11.99	15.67	13.32	11.76	12.33		19.35	19.51	19.22	19.50	19.04	
Na_2O	0.00	0.00	0.00	0.01	0.01	-	0.03	0.02	0.03	0.04	0.04	3.47	2.05	2.86	3.71	3.48		0.25	0.25	0.24	0.25	0.23	
K_2O	0.00	0.01	0.01	0.00	0.00	-	0.01	0.00	0.00	0.01	0.00	0.46	0.18	0.36	0.59	0.45		0.00	0.01	0.00	0.00	0.01	
NiO	0.03	0.01	0.04	0.01	0.01	-	0.03	0.00	0.03	0.06	0.05	-	-	-	-	-		0.00	0.01	0.00	0.05	0.01	
V_2O_3	0.01	0.00	0.04	0.02	0.02	-	0.00	0.07	0.05	0.00	0.09	0.01	0.00	0.00	0.01	0.00		0.06	0.11	0.06	0.06	0.08	
P_2O_5	-	-	-	-	-	-	-	-	-	-	-	0.05	0.00	0.00	0.04	0.04		-	-	-	-	-	
Total[a]	100.13	100.79	100.53	100.69	100.69	-	101.08	101.06	100.45	100.64	100.20	98.91	99.88	99.29	98.84	99.16		100.60	100.89	100.83	100.43	100.99	
Cations																							
Si	6.05	6.06	5.96	6.02	6.02	5.98	7.78	7.82	7.82	7.83	7.80	7.24	6.68	7.03	7.32	7.20		7.64	7.60	7.68	7.67	7.70	
Ti	0.00	0.01	0.00	0.00	0.00	0.00	0.03	0.04	0.04	0.03	0.03	0.00	0.00	0.00	0.00	0.00		0.07	0.07	0.07	0.06	0.06	
Al	0.00	0.00	0.01	0.01	0.01	0.00	0.24	0.23	0.23	0.25	0.23	4.75	5.27	4.96	4.62	4.77		0.47	0.44	0.38	0.40	0.35	
Cr	0.00	0.00	0.00	0.00	0.00	0.00	0.00	0.00	0.00	0.00	0.00	-	-	-	-	-		0.00	0.00	0.00	0.00	0.00	
Fe2+	3.81	3.28	3.51	3.53	3.53	3.11	2.20	2.23	2.43	2.22	2.26	0.09	0.10	0.10	0.10	0.09		1.40	1.44	1.43	1.40	1.48	
Mn	0.07	0.07	0.06	0.07	0.07	0.06	0.06	0.06	0.07	0.05	0.06	0.00	0.00	0.00	0.00	0.00		0.04	0.04	0.05	0.04	0.05	
Mg	7.97	8.46	8.45	8.30	8.30	8.81	5.43	5.32	5.09	5.28	5.33	0.02	0.02	0.02	0.02	0.02		3.29	3.35	3.33	3.33	3.33	
Ca	0.04	0.04	0.04	0.04	0.04	0.03	0.32	0.32	0.33	0.33	0.32	1.77	2.31	1.96	1.73	1.81		3.09	3.12	3.06	3.12	3.04	
Na	0.00	0.00	0.00	0.00	0.00	0.01	0.01	0.00	0.01	0.01	0.01	0.92	0.55	0.76	0.99	0.93		0.07	0.07	0.07	0.07	0.07	
K	0.00	0.00	0.00	0.00	0.00	0.00	0.00	0.00	0.00	0.00	0.00	0.08	0.03	0.06	0.10	0.08		0.00	0.00	0.00	0.00	0.00	
Ni	0.00	0.00	0.01	0.00	0.00	0.01	0.00	0.00	0.00	0.01	0.01	-	-	-	-	-		0.00	0.00	0.00	0.01	0.00	
V	0.00	0.00	0.00	0.00	0.00	0.00	0.00	0.01	0.01	0.00	0.01	0.00	0.00	0.00	0.00	0.00		0.01	0.01	0.01	0.01	0.01	
P	-	-	-	-	-	-	-	-	-	-	-	0.01	0.00	0.00	0.00	0.01		-	-	-	-	-	
Cation total	17.95	17.93	18.03	17.98	17.98	18.01	16.07	16.03	16.03	16.02	16.05	14.88	14.97	14.90	14.90	14.91		16.09	16.15	16.09	16.11	16.09	
Mg# / An[f]	67.7	72.0	70.6	70.2	70.2	73.9	71.2	70.4	67.7	70.4	70.3	65.7	80.8	72.0	63.7	66.2		70.1	70.0	69.9	70.5	69.3	

Table A1. (continued)

Volcanic cone																						
Sample ID																						
Host mineral							Olivine															
Melt ID	1-m6	1-m7	O1-m2	O1-m3	O1-m7	O1-m9	1-m1	1-m10	1-m11	1-m12	1-m13	1-m14	1-m15	1-m16	1-m17	1-m2	1-m3	1-m5	1-m6	1-m7	1-m8	
Uncorrected melt compositions (wt.%)																						
SiO_2	57.83	56.41	56.87	58.09	59.26	57.58	51.73	58.82	53.83	53.91	52.67	52.74	48.06	52.85	48.93	49.51	57.80	52.91	53.29	52.65	47.64	
TiO_2	1.22	1.23	1.31	1.18	1.24	1.25	1.09	0.66	1.15	1.18	1.07	1.10	0.65	1.11	0.88	1.04	0.74	1.24	0.85	0.65	0.67	
Al_2O_3	15.10	16.72	14.40	15.90	14.82	15.06	15.85	13.45	16.52	15.59	16.22	16.09	17.92	16.26	16.95	16.31	12.60	15.03	15.86	14.97	17.87	
FeO^{Total}	9.52	8.34	10.14	7.08	7.35	8.49	10.34	9.00	9.16	9.81	10.03	9.69	9.45	8.32	9.89	10.20	9.04	9.96	9.18	11.29	9.93	
MnO	0.18	0.16	0.17	0.13	0.16	0.19	0.17	0.21	0.19	0.20	0.17	0.21	0.17	0.15	0.18	0.16	0.19	0.22	0.23	0.18	0.17	
MgO	2.40	2.20	2.37	2.29	2.13	1.98	3.77	2.62	3.67	3.44	3.64	3.39	4.52	3.62	4.31	3.58	2.55	3.34	1.47	3.44	4.52	
CaO	5.43	5.40	5.24	5.11	4.47	4.86	8.60	5.32	7.20	7.67	8.35	8.26	10.14	8.22	8.45	9.02	5.19	7.15	9.40	8.09	10.94	
Na_2O	2.92	3.17	3.42	3.36	3.48	3.45	2.87	2.61	3.14	3.17	2.83	2.84	2.38	2.97	2.84	2.68	2.73	2.99	2.99	2.69	2.37	
K_2O	3.45	3.55	3.37	3.66	4.01	3.70	1.93	3.06	2.04	2.09	1.84	1.76	0.80	1.87	1.20	1.04	3.07	2.15	1.46	1.17	0.84	
P_2O_5	0.55	0.44	0.30	0.35	0.44	0.34	0.35	0.46	0.34	0.35	0.28	0.29	0.26	0.38	0.27	0.28	0.47	0.38	0.29	0.34	0.23	
S (EPMA)	0.020	0.008	0.009	0.006	0.008	0.023	0.143	0.008	0.131	0.076	0.144	0.147	0.319	0.134	0.255	0.196	0.006	0.036	0.160	0.129	0.273	
Cl (EPMA)	0.102	0.100	0.097	0.095	0.139	0.114	0.077	0.098	0.064	0.063	0.075	0.063	0.078	0.065	0.059	0.056	0.095	0.061	0.067	0.059	0.064	
Total[a]	98.80	97.73	97.69	97.28	97.54	97.10	97.21	96.30	97.65	97.69	97.58	96.84	95.22	96.20	94.62	94.37	94.46	95.55	95.53	95.88	95.94	
H_2O (FTIR)	-	-	-	-	-	-	-	-	-	-	1.61	-	-	-	-	3.22	4.32	-	-	-	-	
H_2O (SIMS)	-	-	-	-	-	-	-	-	-	-	-	-	-	-	-	-	-	-	-	-	-	
CO_2 ppm (SIMS)[a]	-	-	-	-	-	-	-	-	-	-	-	-	-	-	-	-	-	-	-	-	-	
S ppm (SIMS)	-	-	-	-	-	-	-	-	-	-	-	-	-	-	-	-	-	-	-	-	-	
Cl ppm (SIMS)	-	-	-	-	-	-	-	-	-	-	-	-	-	-	-	-	-	-	-	-	-	
F ppm (SIMS)	-	-	-	-	-	-	-	-	-	-	-	-	-	-	-	-	-	-	-	-	-	
P_2O_5 (SIMS)	-	-	-	-	-	-	-	-	-	-	-	-	-	-	-	-	-	-	-	-	-	
S^{6+}/S_{total}	-	-	-	-	-	-	-	-	-	0.37	0.38	-	-	-	-	0.59	-	-	-	0.40	-	
1 s.e.[b]	-	-	-	-	-	-	-	-	-	0.03	0.03	-	-	-	-	0.03	-	-	-	0.03	-	
T_{erupt} (°C)[c]	1010	998	1014	1014	994	998	1037	1018	1039	1032	1035	1030	1051	1035	1053	1021	1018	1033	982	1031	1048	
$K_{D\ uncorrected}$[a]	0.23	0.21	0.20	0.27	0.29	0.20	0.42	0.58	0.38	0.42	0.46	0.34	0.31	0.31	0.33	0.36	0.60	0.44	0.45	0.48	0.32	
Corrected melt compositions for post-entrapment crystallization (wt.%)																						
SiO_2	-	-	-	-	-	-	51.72	58.79	53.63	53.64	52.65	52.24	48.05	52.63	48.92	49.25	57.78	52.65	52.26	52.39	47.63	
TiO_2	-	-	-	-	-	-	1.09	0.65	1.13	1.16	1.07	1.06	0.65	1.10	0.88	1.02	0.74	1.21	0.80	0.64	0.67	
Al_2O_3	-	-	-	-	-	-	15.83	13.43	16.31	15.32	16.21	15.53	17.90	16.02	16.93	15.94	12.59	14.78	14.89	14.72	17.85	
FeO^{Total}	-	-	-	-	-	-	10.37	9.03	9.54	10.28	10.05	10.68	9.48	8.77	9.92	10.84	9.06	10.43	10.85	11.73	9.95	
MnO	-	-	-	-	-	-	0.17	0.21	0.19	0.19	0.17	0.21	0.17	0.14	0.18	0.15	0.19	0.21	0.22	0.18	0.17	
MgO	-	-	-	-	-	-	3.80	2.66	4.11	4.02	3.68	4.58	4.56	4.14	4.34	4.36	2.58	3.92	3.61	4.01	4.56	
CaO	-	-	-	-	-	-	8.59	5.32	7.10	7.54	8.34	7.97	10.13	8.10	8.44	8.82	5.18	7.03	8.82	7.96	10.93	
Na_2O	-	-	-	-	-	-	2.87	2.61	3.10	3.11	2.83	2.75	2.38	2.92	2.84	2.62	2.73	2.94	2.81	2.64	2.37	
K_2O	-	-	-	-	-	-	1.93	3.05	2.01	2.05	1.84	1.70	0.80	1.85	1.20	1.02	3.06	2.12	1.37	1.15	0.84	
P_2O_5	-	-	-	-	-	-	0.34	0.45	0.33	0.35	0.28	0.28	0.26	0.38	0.27	0.27	0.47	0.37	0.27	0.34	0.23	
S	-	-	-	-	-	-	0.142	0.008	0.129	0.075	0.144	0.142	0.318	0.132	0.255	0.191	0.006	0.036	0.150	0.127	0.273	
Cl	-	-	-	-	-	-	0.077	0.098	0.063	0.062	0.075	0.061	0.078	0.064	0.059	0.055	0.095	0.060	0.063	0.058	0.064	

Table A1. (continued)

Volcanic cone																						
Sample ID																						
Host mineral							Olivine															
Melt ID	1-m6	1-m7	O1-m2	O1-m3	O1-m7	O1-m9	1-m1	1-m10	1-m11	1-m12	1-m13	1-m14	1-m15	1-m16	1-m17	1-m2	1-m3	1-m5	1-m6	1-m7	1-m8	
H_2O (FTIR)	-	-	-	-	-	-	-	-	-	-	-	-	-	-	-	3.15	-	-	-	-	-	-
H_2O (SIMS)	-	-	-	-	-	-	-	-	-	-	-	-	-	-	-	-	-	-	-	-	-	-
CO_2 ppm (SIMS)[4]	-	-	-	-	-	-	-	-	-	-	-	-	-	-	-	-	-	-	-	-	-	-
S ppm (SIMS)	-	-	-	-	-	-	-	-	-	-	-	-	-	-	-	-	-	-	-	-	-	-
Cl ppm (SIMS)	-	-	-	-	-	-	-	-	-	-	-	-	-	-	-	-	-	-	-	-	-	-
F ppm (SIMS)	-	-	-	-	-	-	-	-	-	-	-	-	-	-	-	-	-	-	-	-	-	-
P_2O_5 (SIMS)	-	-	-	-	-	-	-	-	-	-	-	-	-	-	-	-	-	-	-	-	-	-
T_{trap} (°C)[c]	-	-	-	-	-	-	1037	1018	1049	1045	1035	1058	1051	1047	1053	1040	1018	1046	1035	1044	1048	
PEC%[c]	-	-	-	-	-	-	0.1	0.1	1.3	1.7	0.1	3.5	0.1	1.5	0.1	2.3	0.1	1.7	6.3	1.7	0.1	
Host mineral compositions (wt.%)																						
SiO_2	51.51	51.36	51.25	51.55	50.88	50.65	37.73	37.29	-	38.30	38.25	38.85	38.89	39.01	38.55	38.00	36.62	37.50	37.79	37.93	39.00	
TiO_2	0.65	0.58	0.48	0.53	0.62	0.65	0.02	0.00	-	0.01	0.02	0.00	0.00	0.00	0.01	0.05	0.00	0.00	0.00	0.00	0.01	
Al_2O_3	2.44	2.92	2.35	2.32	2.22	2.92	0.02	0.05	-	0.05	0.03	0.06	0.03	0.02	0.03	0.01	0.04	0.01	0.01	0.03	0.01	
Cr_2O_3	0.03	0.02	0.01	0.00	0.02	0.02	0.01	0.01	-	0.00	0.00	0.00	0.00	0.00	0.02	0.00	0.01	0.00	0.03	0.00	0.00	
FeO^{Total}	10.98	9.15	10.13	10.12	12.03	9.93	24.91	29.11	-	25.24	26.54	21.46	20.72	20.01	21.62	22.45	31.10	25.47	26.28	26.91	20.85	
MnO	0.36	0.28	0.29	0.32	0.37	0.32	0.48	0.57	-	0.47	0.51	0.38	0.35	0.31	0.35	0.38	0.55	0.48	0.51	0.48	0.37	
MgO	15.17	14.68	14.99	15.04	15.17	14.61	36.37	30.85	-	36.85	35.54	38.62	40.63	39.92	39.67	37.53	31.70	35.40	35.56	34.52	39.20	
CaO	19.23	21.27	19.44	19.39	17.94	20.04	0.26	0.25	-	0.22	0.25	0.16	0.19	0.16	0.15	0.18	0.21	0.16	0.23	0.19	0.20	
Na_2O	0.24	0.22	0.28	0.27	0.31	0.28	0.00	0.00	-	0.02	0.01	0.01	0.00	0.00	0.00	0.03	0.01	0.01	0.00	0.02	0.01	
K_2O	0.01	0.02	0.00	0.01	0.01	0.00	0.00	0.00	-	0.00	0.00	0.01	0.00	0.00	0.02	0.00	0.02	0.00	0.00	0.00	0.00	
NiO	0.00	0.02	0.00	0.00	0.01	0.00	0.05	0.00	-	0.05	0.06	0.05	0.07	0.07	0.05	0.05	0.03	0.07	0.00	0.00	0.14	
V_2O_3	0.09	0.08	0.01	0.01	0.06	0.11	0.00	0.00	-	0.06	0.02	0.00	0.00	0.00	0.03	0.00	0.07	0.01	0.00	0.00	0.00	
P_2O_5	-	-	-	-	-	-	-	-	-	-	-	-	-	-	-	-	-	-	-	-	-	
Total[a]	100.70	100.60	99.23	99.56	99.64	99.53	99.85	98.11	-	101.28	101.22	99.59	100.90	99.49	100.50	98.66	100.36	99.11	100.41	100.08	99.79	
Cations																						
Si	7.66	7.62	7.71	7.72	7.67	7.61	5.98	6.14	5.98	5.99	6.02	6.06	5.97	6.05	5.97	6.02	5.96	6.01	5.99	6.05	6.06	
Ti	0.07	0.06	0.05	0.06	0.07	0.07	0.00	0.00	0.00	0.00	0.00	0.00	0.00	0.00	0.00	0.01	0.00	0.00	0.00	0.00	0.00	
Al	0.43	0.51	0.42	0.41	0.39	0.52	0.00	0.01	0.01	0.01	0.01	0.01	0.01	0.00	0.01	0.00	0.01	0.00	0.00	0.01	0.00	
Cr	0.00	0.00	0.00	0.00	0.00	0.00	0.00	0.00	0.00	0.00	0.00	0.00	0.00	0.00	0.00	0.00	0.00	0.00	0.00	0.00	0.00	
Fe2+	1.37	1.14	1.27	1.27	1.52	1.25	3.30	4.01	3.07	3.30	3.49	2.80	2.66	2.59	2.80	2.98	4.24	3.41	3.49	3.59	2.71	
Mn	0.04	0.03	0.04	0.04	0.05	0.04	0.06	0.08	0.05	0.06	0.07	0.05	0.05	0.04	0.05	0.05	0.08	0.07	0.07	0.06	0.05	
Mg	3.36	3.25	3.36	3.36	3.41	3.27	8.60	7.57	8.88	8.59	8.34	8.98	9.30	9.23	9.16	8.87	7.69	8.46	8.41	8.21	9.07	
Ca	3.06	3.38	3.13	3.11	2.90	3.23	0.04	0.04	0.03	0.04	0.04	0.03	0.03	0.03	0.02	0.03	0.04	0.03	0.04	0.03	0.03	
Na	0.07	0.06	0.08	0.08	0.09	0.08	0.00	0.00	0.00	0.00	0.00	0.00	0.00	0.00	0.00	0.01	0.00	0.00	0.00	0.01	0.00	
K	0.00	0.00	0.00	0.00	0.00	0.00	0.00	0.00	0.00	0.00	0.00	0.00	0.00	0.00	0.00	0.00	0.00	0.00	0.00	0.00	0.00	
Ni	0.00	0.00	0.00	0.00	0.00	0.00	0.01	0.00	0.01	0.01	0.01	0.01	0.01	0.01	0.01	0.01	0.00	0.01	0.00	0.00	0.02	
V	0.01	0.01	0.00	0.00	0.01	0.01	0.00	0.00	0.00	0.01	0.00	0.00	0.00	0.00	0.00	0.00	0.01	0.00	0.00	0.00	0.00	
P	-	-	-	-	-	-	-	-	-	-	-	-	-	-	-	-	-	-	-	-	-	
Cation total	16.08	16.08	16.07	16.05	16.11	16.09	18.01	17.85	18.02	18.01	17.98	17.94	18.03	17.95	18.02	17.97	18.03	17.99	18.00	17.95	17.94	
Mg# / An[f]	71.1	74.1	72.5	72.6	69.2	72.4	72.2	65.4	74.3	72.2	70.5	76.2	77.8	78.1	76.6	74.9	64.5	71.2	70.7	69.6	77.0	

Table A1. (continued)

Volcanic cone																						
Sample ID																		Kishimadake KSS				
Host mineral		Orthopyroxene							Plagioclase									Clinopyroxene				
Melt ID	1-m9	1-m1	1-m10	1-m11	1-m4	1-m5	1-m6	1-m8	1-m1	1-m2	1-m3	1-m4	1-m5	1-m6	1-m7	1-m8	a2-m1	a2-m2	b5-m1	b5-m2	b5-m3	
Uncorrected melt compositions (wt.%)																						
SiO_2	55.59	58.31	54.64	57.87	57.45	54.02	58.92	59.85	54.20	54.66	54.54	54.32	53.18	57.68	54.18	54.84	54.65	53.38	59.06	54.79	58.61	
TiO_2	0.64	1.30	1.42	1.11	1.32	1.09	1.28	1.17	1.43	0.90	1.01	1.46	1.32	1.15	1.36	1.28	1.34	1.24	1.40	1.17	1.32	
Al_2O_3	13.53	14.53	13.44	13.59	14.88	15.21	13.82	14.01	16.00	15.69	15.29	14.14	14.32	15.85	15.09	15.25	15.73	15.77	14.86	16.35	14.66	
FeO^{Total}	10.47	9.00	10.44	9.59	8.81	10.16	8.13	7.40	9.08	8.06	9.63	11.13	11.94	7.75	9.94	9.90	10.02	10.04	9.36	9.65	9.94	
MnO	0.20	0.16	0.21	0.21	0.20	0.20	0.20	0.16	0.20	0.18	0.16	0.23	0.25	0.13	0.18	0.19	0.22	0.24	0.24	0.18	0.21	
MgO	3.24	2.04	2.85	2.84	2.30	3.88	1.92	2.04	2.73	3.52	3.70	3.55	4.02	2.07	3.52	3.52	3.47	3.26	1.97	2.67	2.20	
CaO	5.97	4.98	6.35	5.78	5.23	7.33	4.43	4.51	6.77	6.81	7.20	7.01	7.63	5.60	6.95	6.76	7.11	6.87	5.04	6.33	5.36	
Na_2O	2.94	3.31	3.03	3.23	3.63	3.27	3.24	3.28	2.68	2.89	3.10	2.76	2.95	3.26	2.91	2.88	3.09	2.99	2.76	3.36	2.94	
K_2O	1.80	3.60	2.35	2.60	3.21	1.88	3.83	3.60	2.66	2.29	2.31	2.13	2.43	3.01	2.08	2.29	1.80	1.79	3.84	2.20	2.94	
P_2O_5	0.37	0.35	0.28	0.16	0.34	0.16	0.39	0.40	0.83	0.28	0.37	0.37	0.33	0.35	0.48	0.31	0.33	0.27	0.60	0.37	0.36	
S (EPMA)	0.066	0.008	0.020	0.038	0.023	0.065	0.032	0.012	0.025	0.064	0.055	0.020	0.078	0.006	0.023	0.061	0.079	0.107	0.041	0.105	0.016	
Cl (EPMA)	0.099	0.101	0.067	0.066	0.092	0.074	0.138	0.093	0.075	0.070	0.071	0.045	0.075	0.069	0.052	0.056	0.107	0.082	0.122	0.075	0.100	
Total[a]	95.05	97.73	95.18	97.18	97.55	97.47	96.34	96.53	96.74	95.52	97.55	97.26	98.67	96.93	96.90	97.47	98.12	96.29	99.38	97.45	98.69	
H_2O (FTIR)	2.49	-	-	-	-	-	-	-	1.68	-	1.04	-	-	-	-	-	-	-	0.95	-	-	
H_2O (SIMS)	-	-	-	-	-	-	-	-	-	-	-	-	-	-	-	-	-	-	-	-	-	
CO_2 ppm (SIMS)[a]	-	-	-	-	-	-	-	-	-	-	-	-	-	-	-	-	-	-	-	-	-	
S ppm (SIMS)	-	-	-	-	-	-	-	-	-	-	-	-	-	-	-	-	-	-	-	-	-	
Cl ppm (SIMS)	-	-	-	-	-	-	-	-	-	-	-	-	-	-	-	-	-	-	-	-	-	
F ppm (SIMS)	-	-	-	-	-	-	-	-	-	-	-	-	-	-	-	-	-	-	-	-	-	
P_2O_5 (SIMS)	-	-	-	-	-	-	-	-	-	-	-	-	-	-	-	-	-	-	-	-	-	
S^{6+}/S_{total}	0.32	-	-	-	-	-	-	-	-	-	-	-	-	-	-	-	-	0.67	-	-	-	
1 s.e.[b]	0.04	-	-	-	-	-	-	-	-	-	-	-	-	-	-	-	-	0.05	-	-	-	
T_{erupt} (°C)[c]	1037	1075	1094	1077	1079	-	1059	1046	-	-	-	-	-	-	1051	-	1069	1057	1021	1030	1016	
$K_{D\ uncorrected}$[a]	0.51	0.25	0.27	0.32	0.26	0.36	0.27	0.31	0.11	0.11	0.21	0.04	0.07	0.16	0.22	0.11	0.24	0.24	0.21	0.23	0.22	
Corrected melt compositions for post-entrapment crystallization (wt.%)																						
SiO_2	55.42	-	-	-	-	-	-	-	-	-	-	-	-	-	-	-	-	-	-	-	-	
TiO_2	0.64	-	-	-	-	-	-	-	-	-	-	-	-	-	-	-	-	-	-	-	-	
Al_2O_3	13.40	-	-	-	-	-	-	-	-	-	-	-	-	-	-	-	-	-	-	-	-	
FeO^{Total}	10.71	-	-	-	-	-	-	-	-	-	-	-	-	-	-	-	-	-	-	-	-	
MnO	0.20	-	-	-	-	-	-	-	-	-	-	-	-	-	-	-	-	-	-	-	-	
MgO	3.55	-	-	-	-	-	-	-	-	-	-	-	-	-	-	-	-	-	-	-	-	
CaO	5.92	-	-	-	-	-	-	-	-	-	-	-	-	-	-	-	-	-	-	-	-	
Na_2O	2.91	-	-	-	-	-	-	-	-	-	-	-	-	-	-	-	-	-	-	-	-	
K_2O	1.79	-	-	-	-	-	-	-	-	-	-	-	-	-	-	-	-	-	-	-	-	
P_2O_5	0.36	-	-	-	-	-	-	-	-	-	-	-	-	-	-	-	-	-	-	-	-	
S	0.065	-	-	-	-	-	-	-	-	-	-	-	-	-	-	-	-	-	-	-	-	
Cl	0.098	-	-	-	-	-	-	-	-	-	-	-	-	-	-	-	-	-	-	-	-	

Table A1. (continued)

Volcanic cone																		Kishimadake					
Sample ID																		KSS					
Host mineral		Orthopyroxene							Plagioclase									Clinopyroxene					
Melt ID	1-m9	1-m1	1-m10	1-m11	1-m4	1-m5	1-m6	1-m8	1-m1	1-m2	1-m3	1-m4	1-m5	1-m6	1-m7	1-m8		a2-m1	a2-m2	b5-m1	b5-m2	b5-m3	
H_2O (FTIR)	2.47	-	-	-	-	-	-	-	-	-	-	-	-	-	-	-	-	-	-	-	-	-	-
H_2O (SIMS)	-	-	-	-	-	-	-	-	-	-	-	-	-	-	-	-	-	-	-	-	-	-	-
CO_2 ppm (SIMS)[a]	-	-	-	-	-	-	-	-	-	-	-	-	-	-	-	-	-	-	-	-	-	-	-
S ppm (SIMS)	-	-	-	-	-	-	-	-	-	-	-	-	-	-	-	-	-	-	-	-	-	-	-
Cl ppm (SIMS)	-	-	-	-	-	-	-	-	-	-	-	-	-	-	-	-	-	-	-	-	-	-	-
F ppm (SIMS)	-	-	-	-	-	-	-	-	-	-	-	-	-	-	-	-	-	-	-	-	-	-	-
P_2O_5 (SIMS)	-	-	-	-	-	-	-	-	-	-	-	-	-	-	-	-	-	-	-	-	-	-	-
T_{trap} (°C)[c]	1044	-	-	-	-	-	-	-	-	-	-	-	-	-	-	-	-	-	-	-	-	-	-
PEC%[c]	0.9	-	-	-	-	-	-	-	-	-	-	-	-	-	-	-	-	-	-	-	-	-	-
Host mineral compositions (wt.%)																							
SiO_2	37.32	52.81	51.66	53.04	53.25	53.70	52.73	52.12	48.64	48.73	52.65	45.16	46.96	52.50	52.08	48.78		51.50	50.89	51.71	51.96	51.80	
TiO_2	0.00	0.27	0.33	0.30	0.31	0.34	0.33	0.38	0.00	0.03	0.02	0.00	0.05	0.00	0.03	0.03		0.61	0.74	0.67	0.57	0.66	
Al_2O_3	0.02	1.32	1.46	1.48	1.37	1.38	1.04	1.16	32.76	32.37	29.54	35.30	33.98	29.67	29.76	32.67		3.39	3.66	2.53	2.23	2.64	
Cr_2O_3	0.00	0.02	0.01	0.00	0.01	0.01	0.00	0.00	-	-	-	-	-	-	-	-		0.04	0.03	0.01	0.00	0.02	
FeO^{Total}	27.71	19.70	18.65	19.98	18.61	18.09	20.74	20.50	0.92	0.81	0.80	0.57	0.79	0.88	0.80	0.93		8.25	8.62	11.76	10.29	11.63	
MnO	0.54	0.57	0.49	0.63	0.52	0.51	0.60	0.57	0.00	0.00	0.01	0.01	0.00	0.00	0.01	0.02		0.23	0.26	0.39	0.42	0.39	
MgO	33.24	22.98	23.92	23.24	24.04	24.40	22.54	22.99	0.08	0.08	0.12	0.06	0.08	0.10	0.11	0.12		14.96	14.58	14.96	15.50	15.04	
CaO	0.22	2.01	2.06	2.03	2.09	2.04	1.91	2.07	15.68	15.34	12.44	18.55	16.96	12.20	12.61	15.51		21.28	21.16	18.75	18.95	18.13	
Na_2O	0.00	0.02	0.05	0.04	0.03	0.05	0.04	0.07	1.93	2.08	3.46	0.84	1.47	3.42	3.46	2.14		0.32	0.28	0.28	0.27	0.31	
K_2O	0.01	0.01	0.01	0.01	0.01	0.03	0.00	0.01	0.21	0.22	0.43	0.03	0.08	0.42	0.35	0.16		0.02	0.00	0.00	0.01	0.00	
NiO	0.01	0.00	0.00	0.03	0.00	0.02	0.00	0.00	-	-	-	-	-	-	-	-		0.00	0.00	0.00	0.00	0.00	
V_2O_3	0.00	0.05	0.00	0.05	0.06	0.00	0.01	0.07	0.00	0.01	0.01	0.00	0.02	0.00	0.02	0.03		0.07	0.06	0.08	0.08	0.00	
P_2O_5	-	-	-	-	-	-	-	-	0.03	0.01	0.04	0.05	0.02	0.01	0.00	0.01		-	-	-	-	-	
Total[a]	99.06	99.76	98.65	100.83	100.30	100.55	99.93	99.93	100.27	99.70	99.52	100.57	100.43	99.19	99.26	100.40		100.67	100.26	101.14	100.28	100.62	
Cations																							
Si	6.05	7.83	7.73	7.79	7.81	7.83	7.84	7.76	6.67	6.71	7.20	6.22	6.46	7.20	7.15	6.68		7.60	7.56	7.67	7.72	7.70	
Ti	0.00	0.03	0.04	0.03	0.03	0.04	0.04	0.04	0.00	0.00	0.00	0.00	0.01	0.00	0.00	0.00		0.07	0.08	0.08	0.06	0.07	
Al	0.00	0.23	0.26	0.26	0.24	0.24	0.18	0.20	5.30	5.26	4.76	5.73	5.51	4.80	4.81	5.28		0.59	0.64	0.44	0.39	0.46	
Cr	0.00	0.00	0.00	0.00	0.00	0.00	0.00	0.00	-	-	-	-	-	-	-	-		0.00	0.00	0.00	0.00	0.00	
Fe2+	3.76	2.44	2.33	2.46	2.28	2.21	2.58	2.55	0.11	0.09	0.09	0.07	0.09	0.10	0.09	0.11		1.02	1.07	1.46	1.28	1.45	
Mn	0.07	0.07	0.06	0.08	0.06	0.06	0.08	0.07	0.00	0.00	0.00	0.00	0.00	0.00	0.00	0.00		0.03	0.03	0.05	0.05	0.05	
Mg	8.03	5.08	5.34	5.09	5.26	5.30	5.00	5.11	0.02	0.02	0.02	0.01	0.02	0.02	0.02	0.02		3.29	3.23	3.31	3.43	3.33	
Ca	0.04	0.32	0.33	0.32	0.33	0.32	0.30	0.33	2.30	2.27	1.82	2.74	2.50	1.79	1.85	2.28		3.37	3.37	2.98	3.02	2.89	
Na	0.00	0.01	0.02	0.01	0.01	0.01	0.01	0.02	0.51	0.56	0.92	0.22	0.39	0.91	0.92	0.57		0.09	0.08	0.08	0.08	0.09	
K	0.00	0.00	0.00	0.00	0.00	0.00	0.00	0.00	0.04	0.04	0.08	0.01	0.01	0.07	0.06	0.03		0.00	0.00	0.00	0.00	0.00	
Ni	0.00	0.00	0.00	0.00	0.00	0.00	0.00	0.00	-	-	-	-	-	-	-	-		0.00	0.00	0.00	0.00	0.00	
V	0.00	0.01	0.00	0.01	0.01	0.00	0.00	0.01	0.00	0.00	0.00	0.00	0.00	0.00	0.00	0.00		0.01	0.01	0.01	0.01	0.00	
P	-	-	-	-	-	-	-	-	0.00	0.00	0.00	0.01	0.00	0.00	0.00	0.00		-	-	-	-	-	
Cation total	17.95	16.02	16.11	16.05	16.04	16.02	16.03	16.10	14.95	14.95	14.90	15.01	14.99	14.89	14.92	14.97		16.07	16.07	16.07	16.05	16.04	
Mg# / An[f]	68.1	67.5	69.6	67.5	69.7	70.6	65.9	66.7	81.8	80.3	66.5	92.5	86.5	66.4	66.8	80.1		76.4	75.1	69.4	72.9	69.7	

Table A1. (continued)

Volcanic cone																					
Sample ID																					
Host mineral												Olivine									
Melt ID	c2-m1	c3-m1-1	c3-m2	c4-m1	c4-m2	c4-m3	c4-m4	c5-m1	d1-m1	d3-m1	O3-m5	1-m1	2-m1	3-m1	3-m2	3-m4	3-m5	3-m6	4-m1	4-m10	4-m11
Uncorrected melt compositions (wt.%)																					
SiO_2	60.76	54.93	61.27	56.88	57.23	58.26	56.00	53.99	58.35	54.81	64.07	48.61	47.96	50.39	53.26	57.18	51.83	54.87	52.79	51.56	48.13
TiO_2	1.28	1.28	0.93	1.52	1.48	1.40	1.21	1.25	1.58	1.20	0.70	0.93	1.05	0.96	1.17	0.56	1.19	1.31	1.19	1.19	0.92
Al_2O_3	14.82	15.73	14.04	14.86	14.35	15.03	16.69	15.51	14.59	15.50	14.52	18.57	19.13	17.87	15.79	13.21	14.74	15.17	15.43	16.20	18.61
FeO^{Total}	8.12	9.67	7.49	10.10	9.11	9.69	8.97	9.91	10.47	10.12	5.38	9.32	8.99	8.37	8.49	9.93	9.89	8.01	9.63	9.56	9.04
MnO	0.19	0.23	0.19	0.22	0.21	0.22	0.18	0.21	0.25	0.25	0.13	0.16	0.19	0.15	0.17	0.17	0.19	0.14	0.21	0.24	0.16
MgO	1.62	3.94	2.59	2.51	3.23	2.14	2.54	3.48	2.04	3.67	1.23	4.31	3.49	3.86	2.35	2.69	3.95	2.30	3.48	4.20	4.14
CaO	4.00	6.66	5.34	5.59	6.15	5.36	5.80	7.45	5.37	7.29	3.21	10.74	11.75	8.86	7.46	6.22	7.95	5.87	8.15	8.15	10.77
Na_2O	3.08	2.94	2.53	3.06	2.74	3.16	3.22	3.02	2.68	2.98	3.06	2.59	2.67	2.74	2.85	2.85	2.72	2.83	2.87	2.87	2.69
K_2O	4.56	2.06	3.48	2.74	2.29	2.98	2.13	2.09	3.27	1.80	5.04	0.89	0.78	1.64	2.20	1.86	1.73	2.53	1.83	1.65	0.96
P_2O_5	0.39	0.35	0.66	0.45	0.52	0.43	0.32	0.30	0.56	0.29	0.25	0.19	0.25	0.20	0.27	0.36	0.25	0.26	0.25	0.30	0.24
S (EPMA)	0.007	0.012	0.003	0.016	0.018	0.012	0.096	0.089	0.019	0.064	0.006	0.176	0.192	0.164	0.091	0.068	0.092	0.041	0.145	0.133	0.328
Cl (EPMA)	0.103	0.045	0.178	0.088	0.087	0.068	0.085	0.098	0.105	0.077	0.161	0.082	0.076	0.055	0.088	0.155	0.068	0.077	0.089	0.057	0.078
Total[a]	98.91	97.94	98.68	98.11	97.48	98.79	97.42	97.57	99.33	98.19	97.73	96.86	96.89	95.53	94.37	95.36	94.79	93.51	96.33	96.33	96.60
H_2O (FTIR)	-	-	-	-	-	-	-	-	-	-	-	-	2.19	-	-	-	1.93	-	2.53	2.00	-
H_2O (SIMS)	-	-	-	-	-	-	-	-	-	-	-	2.73	2.80	2.96	2.50	2.56	2.81	2.48	2.77	2.82	2.97
CO_2 ppm (SIMS)[a]	-	-	-	-	-	-	-	-	-	-	-	187	220	45	71	*416*	58	-	52	22	140
S ppm (SIMS)	-	-	-	-	-	-	-	-	-	-	-	2817	3165	2160	1213	1089	1342	694	1394	1449	2799
Cl ppm (SIMS)	-	-	-	-	-	-	-	-	-	-	-	723	781	754	884	1328	767	834	804	724	724
F ppm (SIMS)	-	-	-	-	-	-	-	-	-	-	-	375	354	604	695	865	598	787	611	539	391
P_2O_5 (SIMS)	-	-	-	-	-	-	-	-	-	-	-	0.23	0.23	0.23	0.40	0.40	0.34	0.41	0.35	0.31	0.23
S^{6+}/S_{total}	-	-	-	-	-	-	-	-	-	0.59	-	0.59	0.62	0.53	-	-	0.30	-	-	-	-
1 s.e.[b]	-	-	-	-	-	-	-	-	-	0.05	-	0.03	0.03	0.03	-	-	0.05	-	-	-	-
T_{erupt} (°C)[c]	972	-	-	1034	1059	-	1013	1060	1001	1076	939	1043	1021	1033	1015	1021	1040	1019	1030	1046	1034
$K_{D\ uncorrected}$[a]	0.20	0.40	0.41	0.21	0.30	0.19	0.20	0.30	0.20	0.28	0.26	0.28	0.25	0.27	0.38	0.56	0.38	0.41	0.39	0.27	0.28
Corrected melt compositions for post-entrapment crystallization (wt.%)																					
SiO_2	-	-	-	-	-	-	-	-	-	-	-	48.37	47.21	50.08	52.38	56.92	51.80	54.20	52.58	51.03	47.91
TiO_2	-	-	-	-	-	-	-	-	-	-	-	0.91	0.97	0.93	1.10	0.56	1.18	1.26	1.18	1.14	0.90
Al_2O_3	-	-	-	-	-	-	-	-	-	-	-	18.11	17.53	17.40	14.90	13.04	14.71	14.59	15.22	15.51	18.15
FeO^{Total}	-	-	-	-	-	-	-	-	-	-	-	10.06	11.49	9.18	10.14	10.28	9.95	9.15	10.02	10.80	9.78
MnO	-	-	-	-	-	-	-	-	-	-	-	0.15	0.17	0.15	0.16	0.17	0.19	0.13	0.21	0.23	0.15
MgO	-	-	-	-	-	-	-	-	-	-	-	5.17	6.45	4.79	4.34	3.13	4.02	3.65	3.96	5.67	5.01
CaO	-	-	-	-	-	-	-	-	-	-	-	10.47	10.77	8.62	7.04	6.14	7.93	5.64	8.03	7.80	10.51
Na_2O	-	-	-	-	-	-	-	-	-	-	-	2.53	2.45	2.67	2.69	2.81	2.71	2.72	2.83	2.75	2.63
K_2O	-	-	-	-	-	-	-	-	-	-	-	0.87	0.71	1.60	2.07	1.84	1.73	2.43	1.80	1.58	0.93
P_2O_5	-	-	-	-	-	-	-	-	-	-	-	0.18	0.23	0.19	0.25	0.35	0.25	0.25	0.24	0.28	0.24
S	-	-	-	-	-	-	-	-	-	-	-	0.172	0.176	0.160	0.086	0.068	0.092	0.040	0.143	0.128	0.320
Cl	-	-	-	-	-	-	-	-	-	-	-	0.080	0.070	0.054	0.083	0.153	0.068	0.074	0.088	0.055	0.076

Table A1. (continued)

Volcanic cone																						
Sample ID																						
Host mineral												Olivine										
Melt ID	c2-m1	c3-m1-1	c3-m2	c4-m1	c4-m2	c4-m3	c4-m4	c5-m1	d1-m1	d3-m1	O3-m5	1-m1	2-m1	3-m1	3-m2	3-m4	3-m5	3-m6	4-m1	4-m10	4-m11	
H_2O (FTIR)	-	-	-	-	-	-	-	-	-	-	-	-	2.01	-	-	-	1.93	-	2.49	1.91	-	
H_2O (SIMS)	-	-	-	-	-	-	-	-	-	-	-	2.66	2.56	2.88	2.36	2.52	2.81	2.39	2.74	2.70	2.89	
CO_2 ppm (SIMS)[4]	-	-	-	-	-	-	-	-	-	-	-	182	202	44	67	411	58	-	51	21	137	
S ppm (SIMS)	-	-	-	-	-	-	-	-	-	-	-	2747	2902	2102	1144	1075	1339	667	1375	1388	2730	
Cl ppm (SIMS)	-	-	-	-	-	-	-	-	-	-	-	705	716	734	834	1311	766	802	793	693	706	
F ppm (SIMS)	-	-	-	-	-	-	-	-	-	-	-	366	324	588	656	853	597	757	603	516	381	
P_2O_5 (SIMS)	-	-	-	-	-	-	-	-	-	-	-	0.22	0.21	0.22	0.37	0.40	0.34	0.39	0.34	0.29	0.23	
T_{trap} (°C)[c]	-	-	-	-	-	-	-	-	-	-	-	1063	1092	1056	1063	1031	1041	1052	1041	1080	1054	
PEC%[c]	-	-	-	-	-	-	-	-	-	-	-	2.5	8.7	2.7	5.8	1.3	0.2	3.9	1.4	4.3	2.5	
Host mineral compositions (wt.%)																						
SiO_2	51.93	52.45	51.52	51.25	52.73	52.36	51.24	51.34	52.43	51.77	50.93	38.64	39.99	-	38.37	37.56	38.62	38.27	38.42	39.17	39.23	
TiO_2	0.68	0.63	0.62	0.53	0.63	0.56	0.59	0.64	0.60	0.61	0.63	0.01	0.01	-	0.02	0.01	0.00	0.00	0.00	0.00	0.02	
Al_2O_3	2.12	2.14	2.41	2.43	2.47	2.28	3.02	2.85	2.28	2.50	2.12	0.05	0.02	-	0.00	0.03	0.02	0.00	0.04	0.04	0.03	
Cr_2O_3	0.01	0.00	0.00	0.00	0.01	0.00	0.04	0.00	0.02	0.01	0.01	0.00	0.02	-	0.00	0.00	0.01	0.01	0.00	0.02	0.00	
FeO^{Total}	11.62	11.46	13.08	10.59	10.31	10.68	8.43	10.17	12.02	9.73	12.31	19.27	17.96	-	23.57	29.25	23.74	24.63	24.43	19.24	19.36	
MnO	0.36	0.43	0.48	0.40	0.31	0.39	0.23	0.34	0.43	0.38	0.48	0.29	0.26	-	0.38	0.58	0.43	0.45	0.49	0.34	0.32	
MgO	15.00	14.70	14.11	15.49	15.64	15.92	15.32	15.14	15.07	15.84	13.73	42.04	43.06	-	37.44	32.03	37.76	36.48	38.38	42.79	42.48	
CaO	19.10	18.53	18.09	18.55	18.99	18.77	21.34	19.63	18.12	19.66	19.70	0.19	0.22	-	0.17	0.20	0.24	0.17	0.21	0.17	0.17	
Na_2O	0.30	0.33	0.27	0.34	0.30	0.30	0.23	0.25	0.26	0.31	0.26	0.00	0.00	-	0.00	0.03	0.00	0.01	0.00	0.00	0.00	
K_2O	0.00	0.00	0.00	0.00	0.03	0.01	0.00	0.02	0.00	0.00	0.01	0.00	0.01	-	0.00	0.01	0.00	0.00	0.00	0.00	0.00	
NiO	0.00	0.00	0.00	0.00	0.04	0.00	0.00	0.05	0.00	0.03	0.01	0.11	0.08	-	0.01	0.04	0.03	0.07	0.01	0.08	0.08	
V_2O_3	0.06	0.05	0.06	0.09	0.11	0.11	0.09	0.06	0.00	0.05	0.08	0.00	0.10	-	0.03	0.00	0.00	0.00	0.00	0.01	0.00	
P_2O_5	-	-	-	-	-	-	-	-	-	-	-	-	-	-	-	-	-	-	-	-	-	
Total[a]	101.18	100.72	100.63	99.67	101.56	101.37	100.53	100.49	101.23	100.88	100.27	100.60	101.73	-	100.00	99.74	100.85	100.09	101.98	101.85	101.68	
Cations																						
Si	7.70	7.78	7.71	7.68	7.73	7.70	7.59	7.63	7.75	7.65	7.68	5.92	6.00	6.18	6.02	6.08	6.02	6.04	5.94	5.92	5.94	
Ti	0.08	0.07	0.07	0.06	0.07	0.06	0.07	0.07	0.07	0.07	0.07	0.00	0.00	0.00	0.00	0.00	0.00	0.00	0.00	0.00	0.00	
Al	0.37	0.37	0.42	0.43	0.43	0.40	0.53	0.50	0.40	0.44	0.38	0.01	0.00	0.00	0.00	0.01	0.00	0.00	0.01	0.01	0.01	
Cr	0.00	0.00	0.00	0.00	0.00	0.00	0.00	0.00	0.00	0.00	0.00	0.00	0.00	0.00	0.00	0.00	0.00	0.00	0.00	0.00	0.00	
Fe2+	1.44	1.42	1.64	1.33	1.26	1.31	1.04	1.26	1.49	1.20	1.55	2.47	2.25	2.31	3.09	3.96	3.09	3.25	3.16	2.43	2.45	
Mn	0.05	0.05	0.06	0.05	0.04	0.05	0.03	0.04	0.05	0.05	0.06	0.04	0.03	0.03	0.05	0.08	0.06	0.06	0.06	0.04	0.04	
Mg	3.31	3.25	3.15	3.46	3.42	3.49	3.38	3.35	3.32	3.49	3.09	9.60	9.63	9.24	8.76	7.73	8.77	8.58	8.85	9.64	9.59	
Ca	3.03	2.95	2.90	2.98	2.98	2.96	3.39	3.13	2.87	3.11	3.18	0.03	0.04	0.03	0.03	0.03	0.04	0.03	0.03	0.03	0.03	
Na	0.09	0.09	0.08	0.10	0.08	0.08	0.08	0.07	0.07	0.08	0.09	0.08	0.00	0.00	0.00	0.01	0.00	0.00	0.00	0.00	0.00	
K	0.00	0.00	0.00	0.00	0.01	0.00	0.00	0.00	0.00	0.00	0.00	0.00	0.00	0.00	0.00	0.00	0.00	0.00	0.00	0.00	0.00	
Ni	0.00	0.00	0.00	0.00	0.00	0.00	0.00	0.01	0.00	0.00	0.00	0.01	0.01	0.01	0.00	0.01	0.00	0.01	0.00	0.01	0.01	
V	0.01	0.01	0.01	0.01	0.01	0.01	0.01	0.01	0.00	0.01	0.01	0.00	0.01	0.00	0.00	0.00	0.00	0.00	0.00	0.00	0.00	
P	-	-	-	-	-	-	-	-	-	-	-	-	-	-	-	-	-	-	-	-	-	
Cation total	16.08	16.00	16.04	16.09	16.03	16.07	16.11	16.08	16.02	16.11	16.10	18.08	17.99	17.82	17.97	17.92	17.98	17.96	18.06	18.08	18.06	
Mg# / An[f]	69.7	69.6	65.8	72.3	73.0	72.6	76.4	72.6	69.1	74.4	66.5	79.5	81.0	80.0	73.9	66.1	73.9	72.5	73.7	79.9	79.6	

Table A1. (continued)

Volcanic cone																						
Sample ID																						
Host mineral											Orthopyroxene				Plagioclase							
Melt ID	4-m12	4-m13	4-m2	4-m3	4-m4	4-m5	4-m6	4-m7	4-m8	4-m9	3-m1	3-m2	3-m3	3-m4	a1-m1	a1-m2	a6-m1	a6-m2	b1-m1	b1-m2	b2-m1	
Uncorrected melt compositions (wt.%)																						
SiO_2	51.49	49.02	55.07	52.13	52.71	54.59	58.07	55.30	53.82	56.07	57.97	56.55	56.80	59.45	58.06	56.91	57.54	57.93	59.33	58.92	62.79	
TiO_2	1.11	1.34	1.06	0.69	1.22	1.27	1.20	1.13	1.18	0.31	1.15	1.31	1.49	0.88	1.50	1.44	1.21	1.18	1.10	1.09	1.04	
Al_2O_3	16.30	17.46	13.95	14.33	15.26	15.91	12.24	13.36	15.75	14.26	15.66	13.96	14.25	14.37	15.27	16.08	14.67	15.10	15.27	15.05	15.18	
FeO^{Total}	10.37	9.61	10.36	10.95	9.74	8.85	10.06	10.30	10.03	11.34	8.81	10.08	9.88	7.17	8.03	7.62	9.21	8.72	7.75	7.87	6.83	
MnO	0.21	0.20	0.20	0.24	0.22	0.19	0.26	0.22	0.22	0.28	0.20	0.17	0.17	0.14	0.15	0.18	0.23	0.21	0.19	0.22	0.17	
MgO	3.39	3.50	3.13	3.00	3.69	2.41	2.94	3.36	2.89	2.98	2.06	1.85	2.10	2.70	2.58	2.58	3.30	3.02	2.53	2.53	1.23	
CaO	7.66	10.17	7.47	9.11	7.93	7.54	5.75	6.93	8.32	7.09	5.13	5.07	5.60	5.34	5.97	6.49	6.57	6.47	5.39	5.67	4.00	
Na_2O	2.93	2.86	2.88	2.67	3.00	3.30	3.04	2.88	2.72	2.46	3.13	2.96	2.97	3.40	2.22	1.93	2.07	2.15	2.07	2.18	2.11	
K_2O	1.75	1.09	1.72	1.30	1.95	2.31	2.02	1.99	1.98	0.90	3.45	3.68	3.59	2.69	2.53	2.56	2.63	2.66	2.72	2.75	4.37	
P_2O_5	0.34	0.22	0.43	0.59	0.34	0.38	0.41	0.49	0.31	0.21	0.54	0.57	0.50	0.23	0.29	0.29	0.45	0.32	0.25	0.29	0.29	
S (EPMA)	0.191	0.270	0.050	0.178	0.153	0.115	0.016	0.052	0.160	0.085	0.007	0.036	0.018	0.057	0.017	0.012	0.017	0.073	0.030	0.034	0.003	
Cl (EPMA)	0.065	0.065	0.085	0.076	0.061	0.094	0.082	0.072	0.087	0.062	0.101	0.114	0.101	0.055	0.052	0.050	0.091	0.112	0.114	0.103	0.155	
Total[a]	96.10	96.24	96.47	95.57	96.57	97.17	96.10	96.21	97.72	96.19	98.22	96.40	97.50	96.59	96.78	96.24	98.06	98.09	96.84	96.74	98.13	
H_2O (FTIR)	-	-	2.79	-	4.31	-	2.48	4.43	-	-	-	-	-	-	-	-	-	-	-	-	-	
H_2O (SIMS)	-	2.64	2.58	-	-	-	2.49	2.74	-	2.65	-	-	-	-	-	-	-	-	-	-	-	
CO_2 ppm (SIMS)[a]	-	326	35	-	-	-	31	62	-	*178*	-	-	-	-	-	-	-	-	-	-	-	
S ppm (SIMS)	-	2647	345	-	-	-	158	572	-	700	-	-	-	-	-	-	-	-	-	-	-	
Cl ppm (SIMS)	-	618	786	-	-	-	772	819	-	650	-	-	-	-	-	-	-	-	-	-	-	
F ppm (SIMS)	-	396	570	-	-	-	557	550	-	265	-	-	-	-	-	-	-	-	-	-	-	
P_2O_5 (SIMS)	-	0.24	0.50	-	-	-	0.48	0.47	-	0.21	-	-	-	-	-	-	-	-	-	-	-	
S^{6+}/S_{total}	-	-	-	-	-	-	-	-	-	-	-	-	-	-	-	-	-	0.58	0.62	-	-	
1 s.e.[b]	-	-	-	-	-	-	-	-	-	-	-	-	-	-	-	-	-	0.06	0.08	-	-	
T_{erupt} (°C)[c]	1034	1030	1027	1017	1037	1010	1029	1030	1018	1022	1073	-	-	-	-	1053	1046	1048	-	1037	-	
$K_{D\ uncorrected}$[a]	0.42	0.34	0.49	0.48	0.47	0.41	0.56	0.56	0.42	0.56	0.24	0.21	0.22	0.38	0.13	0.23	0.07	0.08	0.17	0.11	0.19	
Corrected melt compositions for post-entrapment crystallization (wt.%)																						
SiO_2	51.37	48.73	54.75	51.86	52.70	53.79	58.00	55.28	53.32	55.63	-	-	-	-	-	-	-	-	-	-	-	
TiO_2	1.10	1.30	1.04	0.68	1.22	1.21	1.20	1.13	1.15	0.30	-	-	-	-	-	-	-	-	-	-	-	
Al_2O_3	16.15	16.98	13.70	14.08	15.24	15.16	12.20	13.35	15.27	13.93	-	-	-	-	-	-	-	-	-	-	-	
FeO^{Total}	10.61	10.40	10.84	11.41	9.77	10.20	10.14	10.33	10.87	11.92	-	-	-	-	-	-	-	-	-	-	-	
MnO	0.20	0.19	0.20	0.23	0.22	0.18	0.26	0.22	0.21	0.27	-	-	-	-	-	-	-	-	-	-	-	
MgO	3.70	4.46	3.74	3.61	3.73	4.05	3.04	3.39	3.94	3.75	-	-	-	-	-	-	-	-	-	-	-	
CaO	7.59	9.89	7.33	8.94	7.93	7.19	5.73	6.93	8.07	6.92	-	-	-	-	-	-	-	-	-	-	-	
Na_2O	2.91	2.78	2.83	2.62	2.99	3.15	3.03	2.88	2.64	2.40	-	-	-	-	-	-	-	-	-	-	-	
K_2O	1.74	1.06	1.69	1.28	1.95	2.20	2.01	1.99	1.92	0.88	-	-	-	-	-	-	-	-	-	-	-	
P_2O_5	0.33	0.21	0.42	0.58	0.34	0.36	0.41	0.49	0.30	0.21	-	-	-	-	-	-	-	-	-	-	-	
S	0.190	0.263	0.049	0.175	0.153	0.109	0.016	0.052	0.155	0.083	-	-	-	-	-	-	-	-	-	-	-	
Cl	0.064	0.063	0.083	0.075	0.061	0.090	0.082	0.072	0.084	0.061	-	-	-	-	-	-	-	-	-	-	-	

Table A1. (continued)

Volcanic cone																						
Sample ID																						
Host mineral											Orthopyroxene				Plagioclase							
Melt ID	4-m12	4-m13	4-m2	4-m3	4-m4	4-m5	4-m6	4-m7	4-m8	4-m9	3-m1	3-m2	3-m3	3-m4	a1-m1	a1-m2	a6-m1	a6-m2	b1-m1	b1-m2	b2-m1	
H_2O (FTIR)	-	-	2.74	-	-	-	2.47	-	-	-	-	-	-	-	-	-	-	-	-	-	-	-
H_2O (SIMS)	-	2.57	2.54	-	-	-	2.48	2.73	-	2.59	-	-	-	-	-	-	-	-	-	-	-	-
CO_2 ppm (SIMS)[4]	-	317	34	-	-	-	31	62	-	174	-	-	-	-	-	-	-	-	-	-	-	-
S ppm (SIMS)	-	2574	339	-	-	-	158	572	-	684	-	-	-	-	-	-	-	-	-	-	-	-
Cl ppm (SIMS)	-	601	772	-	-	-	769	818	-	636	-	-	-	-	-	-	-	-	-	-	-	-
F ppm (SIMS)	-	386	560	-	-	-	555	550	-	258	-	-	-	-	-	-	-	-	-	-	-	-
P_2O_5 (SIMS)	-	0.23	0.49	-	-	-	0.48	0.47	-	0.20	-	-	-	-	-	-	-	-	-	-	-	-
T_{trap} (°C)[c]	1040	1053	1042	1032	1037	1050	1031	1030	1043	1040	-	-	-	-	-	-	-	-	-	-	-	-
PEC%[c]	0.9	2.8	1.8	1.8	0.1	4.8	0.3	0.1	3.1	2.3	-	-	-	-	-	-	-	-	-	-	-	-
Host mineral compositions (wt.%)																						
SiO_2	37.41	-	37.50	-	-	-	36.60	37.05	38.06	37.07	52.86	52.72	53.23	53.61	50.53	51.64	47.30	48.01	51.84	49.73	54.68	
TiO_2	0.02	-	0.01	-	-	-	0.00	0.00	0.00	0.00	0.31	0.30	0.29	0.31	0.03	0.00	0.00	0.03	0.08	0.06	0.09	
Al_2O_3	0.02	-	0.02	-	-	-	0.01	0.01	0.01	0.02	1.56	1.41	1.51	1.38	31.74	31.25	33.77	33.69	30.65	32.17	28.36	
Cr_2O_3	0.01	-	0.00	-	-	-	0.03	0.01	0.02	0.00	0.01	0.01	0.01	0.01	-	-	-	-	-	-	-	
FeO^{Total}	25.42	-	28.05	-	-	-	30.53	30.68	25.76	30.63	19.39	20.23	19.28	19.23	0.81	1.08	0.74	0.80	0.83	0.84	0.74	
MnO	0.48	-	0.60	-	-	-	0.58	0.63	0.47	0.67	0.50	0.57	0.49	0.48	0.00	0.00	0.00	0.00	0.00	0.03	0.02	
MgO	36.88	-	35.17	-	-	-	33.31	33.15	37.39	33.30	23.40	22.25	23.12	23.85	0.09	0.15	0.06	0.08	0.10	0.10	0.04	
CaO	0.12	-	0.24	-	-	-	0.23	0.20	0.22	0.17	2.22	2.26	2.30	2.30	15.27	14.31	17.80	17.30	14.21	15.68	11.70	
Na_2O	0.00	-	0.01	-	-	-	0.00	0.00	0.01	0.01	0.04	0.04	0.04	0.02	2.40	2.99	1.26	1.50	3.07	2.23	4.12	
K_2O	0.00	-	0.00	-	-	-	0.01	0.01	0.00	0.01	0.00	0.00	0.02	0.00	0.16	0.19	0.09	0.14	0.19	0.15	0.56	
NiO	0.00	-	0.03	-	-	-	0.02	0.04	0.04	0.04	0.00	0.00	0.00	0.02	-	-	-	-	-	-	-	
V_2O_3	0.02	-	0.00	-	-	-	0.00	0.02	0.01	0.00	0.01	0.01	0.00	0.05	0.00	0.00	0.00	0.00	0.01	0.01	0.00	
P_2O_5	-	-	-	-	-	-	-	-	-	-	-	-	-	-	0.04	0.01	0.00	0.00	0.03	0.01	0.04	
Total[a]	100.39	-	101.62	-	-	-	101.32	101.79	102.00	101.92	100.31	99.80	100.30	101.25	101.09	101.65	101.04	101.53	101.03	101.01	100.35	
Cations																						
Si	5.92	5.89	5.93	5.92	5.91	5.95	5.89	5.93	5.93	5.92	7.79	7.84	7.83	7.81	6.85	6.96	6.47	6.53	7.02	6.77	7.40	
Ti	0.00	0.00	0.00	0.00	0.00	0.00	0.00	0.00	0.00	0.00	0.03	0.03	0.03	0.03	0.00	0.00	0.00	0.00	0.01	0.01	0.01	
Al	0.00	0.00	0.00	0.01	0.00	0.00	0.00	0.00	0.00	0.00	0.27	0.25	0.26	0.24	5.07	4.96	5.45	5.40	4.89	5.16	4.53	
Cr	0.00	0.00	0.00	0.00	0.00	0.00	0.00	0.00	0.00	0.00	0.00	0.00	0.00	0.00	-	-	-	-	-	-	-	
Fe2+	3.36	2.87	3.71	3.69	3.64	3.29	4.11	4.11	3.35	4.09	2.39	2.52	2.37	2.34	0.09	0.12	0.08	0.09	0.09	0.10	0.08	
Mn	0.06	0.05	0.08	0.08	0.07	0.06	0.08	0.09	0.06	0.09	0.06	0.07	0.06	0.06	0.00	0.00	0.00	0.00	0.00	0.00	0.00	
Mg	8.70	9.24	8.29	8.36	8.42	8.70	7.99	7.91	8.68	7.93	5.14	4.93	5.07	5.18	0.02	0.03	0.01	0.02	0.02	0.02	0.01	
Ca	0.02	0.03	0.04	0.04	0.04	0.04	0.04	0.03	0.04	0.03	0.35	0.36	0.36	0.36	2.22	2.07	2.61	2.52	2.06	2.29	1.70	
Na	0.00	0.00	0.00	0.00	0.00	0.00	0.00	0.00	0.00	0.00	0.01	0.01	0.01	0.01	0.63	0.78	0.34	0.39	0.81	0.59	1.08	
K	0.00	0.00	0.00	0.00	0.00	0.00	0.00	0.00	0.00	0.00	0.00	0.00	0.00	0.00	0.03	0.03	0.02	0.02	0.03	0.03	0.10	
Ni	0.00	0.01	0.00	0.00	0.01	0.01	0.00	0.00	0.01	0.00	0.00	0.00	0.00	0.00	-	-	-	-	-	-	-	
V	0.00	0.01	0.00	0.00	0.00	0.00	0.00	0.00	0.00	0.00	0.00	0.00	0.00	0.01	0.00	0.00	0.00	0.00	0.00	0.00	0.00	
P	-	-	-	-	-	-	-	-	-	-	-	-	-	-	0.00	0.00	0.00	0.00	0.00	0.00	0.00	
Cation total	18.07	18.11	18.07	18.08	18.09	18.05	18.11	18.07	18.07	18.08	16.05	16.01	16.01	16.04	14.93	14.96	14.98	14.98	14.94	14.96	14.91	
Mg# / An[f]	72.1	76.3	69.1	69.4	69.8	72.6	66.0	65.8	72.1	66.0	68.3	66.2	68.1	68.9	77.8	72.5	88.6	86.5	71.9	79.5	61.1	

Table A1. (continued)

Volcanic cone													
Sample ID													
Host mineral													
Melt ID	c1-m1	c5-m1	c6-m1	d2-m1	d2-m2	d5-m1	d6-m1	d6-m2	e2-m1	e4-m1	e5-m1	e5-m2	e6-m1
Uncorrected melt compositions (wt.%)													
SiO_2	57.90	55.96	55.64	65.81	65.39	59.17	53.45	56.39	56.45	55.46	58.64	58.57	57.29
TiO_2	0.95	1.45	0.98	0.98	0.95	0.96	1.24	1.25	1.19	1.08	1.02	1.06	0.84
Al_2O_3	16.08	12.56	15.55	15.43	15.35	15.74	13.39	15.33	15.67	12.27	16.30	16.20	15.88
FeO^{Total}	7.08	11.12	7.75	4.08	4.28	6.83	10.78	9.08	8.50	11.72	6.99	7.10	7.56
MnO	0.19	0.27	0.13	0.09	0.12	0.15	0.24	0.18	0.18	0.26	0.16	0.15	0.15
MgO	3.09	4.31	3.14	0.80	0.79	2.47	4.35	3.69	3.69	5.57	1.89	1.97	3.02
CaO	6.72	6.17	6.99	2.90	2.85	5.34	6.70	7.40	7.23	6.66	5.42	5.53	6.70
Na_2O	2.17	2.17	1.81	1.99	1.93	1.95	2.62	2.18	2.16	1.96	1.82	1.84	1.89
K_2O	2.35	2.81	2.24	4.64	4.52	3.21	2.92	2.15	2.01	2.72	2.73	3.02	2.43
P_2O_5	0.29	0.25	0.31	0.40	0.46	0.29	0.26	0.36	0.18	0.22	0.44	0.43	0.27
S (EPMA)	0.008	0.017	0.046	0.006	0.001	0.015	0.097	0.007	0.016	0.045	0.021	0.009	0.020
Cl (EPMA)	0.065	0.093	0.058	0.139	0.119	0.049	0.062	0.080	0.036	0.081	0.079	0.061	0.069
Total[a]	96.90	97.25	94.75	97.28	96.74	96.20	96.29	98.12	97.40	98.13	95.54	95.96	96.17
H_2O (FTIR)	3.10	-	-	1.26	-	-	-	-	2.38	-	2.63	-	-
H_2O (SIMS)	-	-	-	-	-	-	-	-	-	-	-	-	-
CO_2 ppm (SIMS)[a]	-	-	-	-	-	-	-	-	-	-	-	-	-
S ppm (SIMS)	-	-	-	-	-	-	-	-	-	-	-	-	-
Cl ppm (SIMS)	-	-	-	-	-	-	-	-	-	-	-	-	-
F ppm (SIMS)	-	-	-	-	-	-	-	-	-	-	-	-	-
P_2O_5 (SIMS)	-	-	-	-	-	-	-	-	-	-	-	-	-
S^{6+}/S_{total}	-	-	-	-	-	-	-	-	-	-	0.85	-	-
1 s.e.[b]	-	-	-	-	-	-	-	-	-	-	0.19	-	-
T_{erupt} (°C)[c]	-	1027	1061	-	-	1033	1035	1060	1071	1027	-	-	1058
$K_{D\ uncorrected}$[d]	0.17	0.08	0.24	0.17	0.17	0.14	0.11	0.17	0.22	0.06	0.29	0.29	0.16
Corrected melt compositions for post-entrapment crystallization (wt.%)													
SiO_2	-	-	-	-	-	-	-	-	-	-	-	-	-
TiO_2	-	-	-	-	-	-	-	-	-	-	-	-	-
Al_2O_3	-	-	-	-	-	-	-	-	-	-	-	-	-
FeO^{Total}	-	-	-	-	-	-	-	-	-	-	-	-	-
MnO	-	-	-	-	-	-	-	-	-	-	-	-	-
MgO	-	-	-	-	-	-	-	-	-	-	-	-	-
CaO	-	-	-	-	-	-	-	-	-	-	-	-	-
Na_2O	-	-	-	-	-	-	-	-	-	-	-	-	-
K_2O	-	-	-	-	-	-	-	-	-	-	-	-	-
P_2O_5	-	-	-	-	-	-	-	-	-	-	-	-	-
S	-	-	-	-	-	-	-	-	-	-	-	-	-
Cl	-	-	-	-	-	-	-	-	-	-	-	-	-

Table A1. (continued)

Volcanic cone														
Sample ID														
Host mineral														
Melt ID	c1-m1	c5-m1	c6-m1	d2-m1	d2-m2	d5-m1	d6-m1	d6-m2	e2-m1	e4-m1	e5-m1	e5-m2	e6-m1	
H_2O (FTIR)	-	-	-	-	-	-	-	-	-	-	-	-	-	-
H_2O (SIMS)	-	-	-	-	-	-	-	-	-	-	-	-	-	-
CO_2 ppm (SIMS)[d]	-	-	-	-	-	-	-	-	-	-	-	-	-	-
S ppm (SIMS)	-	-	-	-	-	-	-	-	-	-	-	-	-	-
Cl ppm (SIMS)	-	-	-	-	-	-	-	-	-	-	-	-	-	-
F ppm (SIMS)	-	-	-	-	-	-	-	-	-	-	-	-	-	-
P_2O_5 (SIMS)	-	-	-	-	-	-	-	-	-	-	-	-	-	-
T_{trap} (°C)[c]	-	-	-	-	-	-	-	-	-	-	-	-	-	-
PEC%[e]	-	-	-	-	-	-	-	-	-	-	-	-	-	-
Host mineral compositions (wt.%)														
SiO_2	50.01	49.82	50.26	55.68	55.92	49.20	50.03	49.77	50.90	46.87	53.78	53.59	49.41	
TiO_2	0.17	0.32	0.06	0.07	0.06	0.05	0.03	0.06	0.22	0.02	0.06	0.05	0.06	
Al_2O_3	29.68	29.73	30.25	28.11	28.00	31.40	31.56	31.66	28.03	34.32	29.13	29.30	31.95	
Cr_2O_3	-	-	-	-	-	-	-	-	-	-	-	-	-	
FeO^{Total}	1.51	3.00	0.88	0.53	0.55	1.04	1.05	0.82	2.34	0.65	0.84	0.74	0.96	
MnO	0.03	0.09	0.00	0.01	0.00	0.01	0.03	0.02	0.02	0.06	0.02	0.01	0.00	
MgO	0.39	0.77	0.14	0.07	0.08	0.15	0.14	0.11	0.80	0.07	0.12	0.12	0.13	
CaO	14.40	15.30	14.63	10.61	10.68	14.15	15.46	15.27	13.32	17.39	12.40	12.53	15.83	
Na_2O	2.42	1.71	2.74	4.46	4.43	2.31	2.25	2.41	2.68	1.22	3.73	3.75	2.20	
K_2O	0.42	0.47	0.21	0.63	0.64	0.24	0.17	0.16	0.44	0.08	0.40	0.45	0.14	
NiO	-	-	-	-	-	-	-	-	-	-	-	-	-	
V_2O_3	0.00	0.04	0.00	0.01	0.00	0.00	0.00	0.00	0.00	0.00	0.00	0.00	0.00	
P_2O_5	0.03	0.02	0.03	0.04	0.02	0.01	0.05	0.00	0.02	0.03	0.00	0.03	0.00	
Total[a]	99.04	101.28	99.21	100.23	100.40	98.56	100.77	100.27	98.76	100.70	100.48	100.58	100.68	
Cations														
Si	6.95	6.84	6.95	7.51	7.53	6.84	6.82	6.81	7.10	6.43	7.28	7.25	6.75	
Ti	0.02	0.03	0.01	0.01	0.01	0.01	0.00	0.01	0.02	0.00	0.01	0.01	0.01	
Al	4.86	4.81	4.93	4.47	4.44	5.14	5.07	5.11	4.61	5.55	4.65	4.68	5.15	
Cr	-	-	-	-	-	-	-	-	-	-	-	-	-	
Fe2+	0.18	0.34	0.10	0.06	0.06	0.12	0.12	0.09	0.27	0.07	0.10	0.08	0.11	
Mn	0.00	0.01	0.00	0.00	0.00	0.00	0.00	0.00	0.00	0.01	0.00	0.00	0.00	
Mg	0.08	0.16	0.03	0.01	0.02	0.03	0.03	0.02	0.17	0.01	0.02	0.02	0.03	
Ca	2.14	2.25	2.17	1.53	1.54	2.11	2.26	2.24	1.99	2.55	1.80	1.82	2.32	
Na	0.65	0.45	0.74	1.17	1.16	0.62	0.60	0.64	0.72	0.32	0.98	0.98	0.58	
K	0.07	0.08	0.04	0.11	0.11	0.04	0.03	0.03	0.08	0.01	0.07	0.08	0.02	
Ni	-	-	-	-	-	-	-	-	-	-	-	-	-	
V	0.00	0.00	0.00	0.00	0.00	0.00	0.00	0.00	0.00	0.00	0.00	0.00	0.00	
P	0.00	0.00	0.00	0.00	0.00	0.00	0.01	0.00	0.00	0.00	0.00	0.00	0.00	
Cation total	14.96	14.99	14.96	14.88	14.87	14.91	14.94	14.96	14.97	14.96	14.91	14.93	14.97	
Mg# / An[f]	76.7	83.2	74.7	56.8	57.1	77.2	79.1	77.8	73.3	88.8	64.7	64.9	79.9	

(Footnote for **Table A1**)

[a] Analyzed total by EPMA.

[b] Estimated standard error based on the accuracy of gaussian curve fit.

[c] Temperatures calculated based on unccorrected and corrected melt compositions after Sugawara (2000) and Médard and Grove (2008) for olivine-hosted melt, assumed average H_2O concentration (by SIMS) of NKD14 and KSS for not analyzed melt inclusion, and Putirka (2008) for plagioclase- and pyroxene-hosted melt.

[d] The distribution coefficient between melt inclusion and host minerals calculated by following equations: $K_D(Fe\text{-}Mg)^{ol,cpx,opx\text{-}liq} = [(X_{Fe}^{ol,cpx,opx}X_{Mg}^{liq})/(X_{Mg}^{ol,cpx,opx}X_{Fe}^{liq})]$, $K_D(An\text{-}Ab)^{pl\text{-}liq} = (X_{Ab}^{pl}X_{Al2O3}^{liq}X_{Ca}^{liq}/X_{An}^{pl}X_{NaO0.5}^{liq}X_{SiO2}^{liq})$. We assumed $FeO/FeO^{Total} = 0.79$ for pyroxene hosted melt inclusions, equivalent to ~FMQ+1.

[e] Degree of post-entrapment crystallization (wt.%) based on adding calculation.

[f] Mg# = Mg/(Fe+Mg), An = Ca/(Ca+Na), in mole%.

* High concentration values are suspect due to the possible carbon contamination from residual carbon coating from EPMA analysis. Suspected outliers are not reported for the PEC values.

n.d.: not detected.

In this study, we did not find satisfactory agreement between H_2O determined by FTIR and by SIMS (uncertainty of FTIR measurements is close to 40%) so in the following, we only consider H_2O concentrations measured by SIMS, based on the better detection limit and precision of the method

Table A2. All groundmass glass analyses

Volcanic cone	Nakadake											
Sample	NKD14											
ID	a1-gm1	a1-gm2	a1-gm3	a1-gm4	d4-gm1	d4-gm2	d4-gm3	d4-gm4	ol1-gm1	ol1-gm2	ol1-gm3	ol1-gm4
SiO_2 (wt.%)	58.63	58.33	58.09	57.90	58.63	58.01	58.68	58.90	58.60	57.85	58.44	58.27
TiO_2	1.36	1.44	1.37	1.47	1.37	1.38	1.44	1.34	1.36	1.30	1.31	1.42
Al_2O_3	14.47	14.15	14.23	14.05	14.68	14.42	14.32	14.68	14.53	14.43	15.44	14.76
FeO^{Total}	9.35	9.65	9.41	9.69	9.29	9.45	9.73	9.55	9.60	9.82	9.03	9.60
MnO	0.21	0.20	0.19	0.22	0.17	0.25	0.21	0.23	0.22	0.23	0.19	0.20
MgO	2.57	2.60	2.84	2.80	2.74	2.83	2.67	2.74	2.81	2.81	2.49	2.51
CaO	6.15	5.95	5.94	5.69	6.03	5.75	5.90	6.07	5.96	6.26	6.49	6.16
Na_2O	2.55	2.43	2.46	2.45	2.95	2.96	2.98	2.92	2.86	2.85	3.22	2.95
K_2O	3.02	3.07	3.07	3.10	3.06	3.00	3.01	3.09	3.08	3.03	2.77	3.04
P_2O_5	0.45	0.47	0.43	0.53	0.55	0.43	0.42	0.47	0.51	0.50	0.46	0.51
S	0.000	0.000	0.000	0.004	0.008	0.004	0.001	0.000	0.016	0.011	0.000	0.016
Cl	0.078	0.076	0.083	0.097	0.087	0.072	0.098	0.075	0.105	0.077	0.082	0.078
Total	98.91	98.42	98.13	98.02	99.60	98.55	99.50	100.11	99.71	99.19	99.95	99.58

Table A2. (continued)

Volcanic cone	Kamikomezuka											
Sample	KKO											
ID	ol2-gm1	ol2-gm2	ol2-gm3	ol2-gm4	ol2-gm5	ol2-gm1	ol2-gm2	ol2-gm3	ol2-gm4	ol2-gm5	ol2-gm6	ol4-gm1
SiO_2 (wt.%)	58.04	58.39	58.10	58.18	58.28	57.06	57.21	56.89	57.01	56.88	57.83	57.94
TiO_2	1.37	1.38	1.39	1.37	1.31	1.51	1.63	1.50	1.50	1.54	1.51	1.65
Al_2O_3	14.40	14.59	14.45	14.03	15.02	14.08	14.15	14.01	14.42	14.30	14.10	13.86
FeO^{Total}	9.18	9.57	9.45	9.08	9.99	11.20	11.89	12.33	12.02	12.23	11.83	12.47
MnO	0.21	0.22	0.23	0.20	0.21	0.26	0.24	0.24	0.21	0.25	0.20	0.22
MgO	2.66	2.76	2.73	2.67	2.30	3.17	3.35	3.30	3.11	3.41	3.51	3.22
CaO	5.78	5.90	6.02	5.55	6.20	6.45	4.00	7.17	6.57	7.41	7.27	7.23
Na_2O	3.00	2.92	2.94	2.99	2.89	2.39	3.65	1.77	2.16	1.89	1.73	1.91
K_2O	3.11	3.12	3.16	3.11	3.23	2.20	2.99	1.65	1.78	1.73	1.61	1.97
P_2O_5	0.51	0.47	0.46	0.41	0.41	0.30	0.24	0.34	0.29	0.36	0.26	0.21
S	0.006	0.002	0.014	0.009	0.044	0.003	0.000	0.014	0.000	0.000	0.002	0.000
Cl	0.113	0.072	0.086	0.083	0.112	0.069	0.064	0.080	0.068	0.073	0.037	0.039
Total	98.38	99.39	99.08	97.73	100.11	98.72	99.48	99.38	99.19	100.16	99.93	100.79

Table A2. (continued)

Volcanic cone		Ojodake										
Sample		OJSU										
ID	ol4-gm2	opx1-gm1	opx1-gm10	opx1-gm11	opx1-gm12	opx1-gm13	opx1-gm14	opx1-gm2	opx1-gm3	opx1-gm4	opx1-gm5	opx1-gm6
SiO_2 (wt.%)	57.85	55.38	55.64	53.59	55.61	53.86	56.28	55.66	55.77	54.04	53.21	54.60
TiO_2	1.58	1.31	1.29	1.27	1.36	1.14	1.32	1.28	1.24	1.26	1.26	1.39
Al_2O_3	13.70	14.56	14.75	14.71	14.48	14.74	15.25	14.94	15.26	14.43	14.29	13.61
FeO^{Total}	12.53	10.07	9.59	10.31	10.26	9.83	9.95	10.14	9.84	10.18	10.71	10.92
MnO	0.25	0.24	0.22	0.19	0.22	0.19	0.19	0.23	0.21	0.23	0.20	0.24
MgO	3.09	3.60	3.61	3.72	3.54	3.69	3.74	3.70	3.62	3.73	3.97	4.29
CaO	7.04	6.99	6.83	6.96	6.43	6.96	7.27	7.27	7.39	7.72	7.22	7.65
Na_2O	1.63	3.24	3.29	3.10	3.41	3.58	3.04	3.44	3.37	3.21	3.13	2.88
K_2O	2.04	2.21	2.29	2.15	2.30	2.23	2.26	2.29	2.12	2.06	2.15	2.13
P_2O_5	0.22	0.25	0.21	0.16	0.28	0.23	0.26	0.25	0.27	0.26	0.27	0.29
S	0.003	0.000	0.000	0.005	0.000	0.023	0.002	0.000	0.000	0.026	0.032	0.063
Cl	0.062	0.070	0.062	0.062	0.096	0.040	0.071	0.069	0.049	0.071	0.070	0.071
Total	100.06	97.96	97.82	96.29	98.07	96.60	99.67	99.34	99.19	97.28	96.61	98.28

Table A2. (continued)

Volcanic cone												
Sample				OJSL								
ID	opx1-gm7	opx1-gm8	opx1-gm9	pl1-gm1	pl1-gm10	pl1-gm11	pl1-gm12	pl1-gm13	pl1-gm2	pl1-gm3	pl1-gm4	pl1-gm5
SiO_2 (wt.%)	55.47	54.99	55.59	54.26	54.75	54.36	54.42	54.53	53.73	54.55	54.21	54.56
TiO_2	1.32	1.33	1.33	1.26	1.39	1.25	1.23	1.23	1.29	1.23	1.32	1.24
Al_2O_3	14.54	15.06	15.05	15.63	14.64	14.95	16.07	15.89	15.47	15.40	14.76	15.99
FeO^{Total}	10.21	9.97	9.94	10.50	11.81	11.07	10.33	10.57	10.57	10.78	11.10	10.51
MnO	0.17	0.20	0.21	0.20	0.28	0.20	0.19	0.25	0.22	0.21	0.20	0.23
MgO	3.67	3.59	3.61	3.98	4.01	4.13	3.78	3.92	4.06	4.14	4.29	3.48
CaO	7.16	6.79	7.26	7.84	7.86	8.24	8.13	8.13	7.42	7.54	7.60	7.57
Na_2O	3.27	3.41	3.31	3.58	2.87	3.11	3.43	2.90	3.74	3.45	2.95	3.67
K_2O	2.20	1.99	2.06	1.67	1.81	1.63	1.54	1.59	1.58	1.72	1.81	1.56
P_2O_5	0.31	0.24	0.25	0.27	0.20	0.25	0.25	0.26	0.17	0.19	0.21	0.21
S	0.001	0.002	0.005	0.000	0.000	0.023	0.014	0.016	0.000	0.001	0.002	0.001
Cl	0.042	0.051	0.064	0.053	0.039	0.056	0.051	0.046	0.038	0.038	0.044	0.039
Total	98.44	97.69	98.73	99.29	99.70	99.35	99.48	99.43	98.37	99.33	98.56	99.11

Table A2. (continued)

Volcanic cone	Kishimadake											
Sample	KSS											
ID	pl1-gm6	pl1-gm7	pl1-gm8	pl1-gm9	a2-gm	a2-gm2	a2-gm3	a6-gm	a6-gm2	a6-gm3	a6-gm4	a6-gm5
SiO_2 (wt.%)	54.23	54.76	54.41	53.69	55.77	56.14	56.15	56.51	56.66	56.78	56.63	55.84
TiO_2	1.33	1.33	1.31	1.30	1.19	1.15	1.16	1.24	1.26	1.21	1.23	1.22
Al_2O_3	14.89	14.64	14.59	14.84	15.42	16.23	15.75	15.75	15.67	15.83	15.73	15.50
FeO^{Total}	10.57	10.80	10.76	10.14	9.67	8.98	9.28	9.37	8.81	9.71	9.33	9.40
MnO	0.21	0.18	0.22	0.23	0.21	0.23	0.22	0.17	0.18	0.20	0.19	0.20
MgO	3.83	3.88	3.76	3.65	3.55	3.28	3.59	3.60	3.52	3.73	3.87	3.66
CaO	7.73	7.39	7.58	7.61	6.70	7.14	7.28	7.43	7.69	7.77	7.64	7.75
Na_2O	3.03	3.23	3.21	2.89	2.88	3.18	3.09	2.64	2.57	2.77	2.59	2.67
K_2O	2.22	2.28	2.29	2.18	2.36	1.97	2.34	2.11	2.10	2.17	2.19	2.03
P_2O_5	0.27	0.24	0.22	0.25	0.39	0.30	0.42	0.38	0.25	0.33	0.28	0.34
S	0.004	0.010	0.000	0.009	0.001	0.000	0.009	0.010	0.009	0.000	0.000	0.003
Cl	0.047	0.060	0.050	0.059	0.062	0.072	0.073	0.080	0.064	0.084	0.070	0.042
Total	98.41	98.85	98.44	96.90	98.28	98.72	99.40	99.34	98.81	100.67	99.82	98.72

Table A2. (continued)

Volcanic cone										
Sample ID	b2-gm	b2-gm2	b2-gm3	c5-gm	c5-gm2	c6-gm	d5-gm	d5-gm2	d5-gm3	d5-gm4
SiO_2 (wt.%)	57.23	56.66	57.51	54.98	56.04	56.11	56.96	57.04	55.59	56.34
TiO_2	1.22	1.18	1.34	1.18	1.24	1.27	1.21	1.25	1.23	1.19
Al_2O_3	15.46	15.53	15.82	15.26	14.88	15.11	15.69	15.65	15.15	15.63
FeO^{Total}	9.05	10.15	9.17	9.44	9.52	9.44	8.99	8.86	8.86	8.85
MnO	0.18	0.24	0.24	0.22	0.21	0.22	0.23	0.19	0.19	0.21
MgO	3.39	3.24	3.44	3.60	3.40	3.61	3.40	3.46	3.18	3.53
CaO	6.83	7.06	7.17	7.33	7.09	7.20	6.91	6.63	6.73	7.11
Na_2O	2.68	2.93	2.68	2.43	2.47	2.33	2.60	2.60	2.69	2.63
K_2O	2.49	2.34	2.42	2.30	2.36	2.18	2.36	2.38	2.40	2.36
P_2O_5	0.43	0.33	0.34	0.31	0.38	0.43	0.39	0.43	0.39	0.36
S	0.001	0.010	0.000	0.002	0.008	0.002	0.016	0.002	0.021	0.006
Cl	0.070	0.055	0.074	0.062	0.078	0.059	0.081	0.087	0.093	0.067
Total	99.07	99.78	100.21	97.14	97.74	98.01	98.90	98.62	96.62	98.32

Table A3. All core and rim compositions of phenocrysts

Volcanic cone	Nakadake								Kamikomezuka	
Sample	NKD14								KKO	
Mineral[a]	OL	OL	OL	OL	OL	OL	OL	OL	OL	OL
Core ID	a3-ol01-c	a3-ol02-c	OL-m2h-core	OL02-core	OL03-core-1	OL03-core-2	O-core	O3-core	a1c	a2c
Major element (wt.%)[b]										
SiO_2	35.91	36.17	35.91	36.15	36.09	36.10	35.82	36.11	38.14	38.35
TiO_2	0.09	0.00	0.10	0.00	0.00	0.00	0.02	0.00	0.00	0.02
Al_2O_3	0.00	0.01	0.00	0.00	0.00	0.03	0.00	0.00	0.00	0.01
Cr_2O_3	-	-	-	-	-	-	-	-	-	-
FeO[c]	30.76	31.30	30.91	30.79	31.08	30.92	31.50	30.92	19.57	17.60
MnO	0.61	0.54	0.71	0.65	0.54	0.50	0.49	0.53	0.37	0.18
MgO	32.24	31.77	32.09	32.12	32.02	32.17	31.73	32.10	41.79	43.65
CaO	0.26	0.18	0.21	0.27	0.19	0.21	0.25	0.31	0.13	0.19
Na_2O	0.04	0.02	0.02	0.00	0.08	0.00	0.07	0.01	0.00	0.00
K_2O	0.03	0.02	0.03	0.00	0.00	0.01	0.03	0.02	0.00	0.01
NiO	-	-	-	-	-	-	-	-	-	-
V_2O_3	-	-	-	-	-	-	-	-	-	-
P_2O_5	0.06	0.00	0.02	0.02	0.00	0.06	0.10	0.01	0.00	0.00
Total[d]	99.75	100.77	101.13	99.75	99.76	99.66	100.46	100.01	100.52	100.63
Cations										
Si	5.88	5.93	5.88	5.92	5.91	5.90	5.88	5.91	5.90	5.87
Ti	0.01	0.00	0.01	0.00	0.00	0.00	0.00	0.00	0.00	0.00
Al	0.00	0.00	0.00	0.00	0.00	0.00	0.00	0.00	0.00	0.00
Cr	-	-	-	-	-	-	-	-	-	-
Fe2+	4.21	4.29	4.23	4.22	4.26	4.23	4.32	4.23	2.53	2.26
Mn	0.08	0.07	0.10	0.09	0.08	0.07	0.07	0.07	0.05	0.02
Mg	7.87	7.76	7.83	7.84	7.82	7.84	7.76	7.83	9.64	9.97
Ca	0.05	0.03	0.04	0.05	0.03	0.04	0.04	0.05	0.02	0.03
Na	0.01	0.01	0.01	0.00	0.03	0.00	0.02	0.00	0.00	0.00
K	0.01	0.00	0.01	0.00	0.00	0.00	0.01	0.01	0.00	0.00
Ni	-	-	-	-	-	-	-	-	-	-
V	-	-	-	-	-	-	-	-	-	-
P	0.01	0.00	0.00	0.00	0.00	0.01	0.01	0.00	0.00	0.00
Cation total	18.13	18.09	18.11	18.12	18.13	18.09	18.11	18.10	18.14	18.15
Mg# / An[e]	65.1	64.4	64.9	65.0	64.7	65.0	64.2	64.9	79.2	81.5
Lab[f]	1	1	1	1	1	1	1	1	1	1
Mineral[a]	OL	OL	OL	OL	OL	OL	OL	OL	OL	OL
Rim ID	a3-ol01-r	a3-ol02-r	OL-r	OL02-r	OL03-r-1	OL03-r-2	O-r	O3-r	a1r	a2r
Major element (wt.%)[b]										
SiO_2	36.07	36.18	36.00	35.99	36.37	36.24	36.27	36.05	37.02	37.52
TiO_2	0.10	0.14	0.05	0.00	0.12	0.03	0.09	0.05	0.09	0.08
Al_2O_3	0.00	0.02	0.12	0.07	0.05	0.07	0.00	0.02	0.00	0.00
Cr_2O_3	-	-	-	-	-	-	-	-	-	-
FeO[c]	30.41	30.08	29.75	30.88	30.34	30.52	30.19	30.41	25.62	24.56
MnO	0.57	0.50	0.65	0.52	0.54	0.56	0.57	0.64	0.50	0.35
MgO	32.26	32.63	33.01	31.98	32.25	32.29	32.44	32.42	36.46	37.21
CaO	0.42	0.19	0.29	0.36	0.30	0.25	0.30	0.28	0.32	0.26
Na_2O	0.00	0.12	0.05	0.07	0.02	0.00	0.00	0.00	0.00	0.00
K_2O	0.01	0.02	0.00	0.04	0.00	0.03	0.06	0.01	0.00	0.00
NiO	-	-	-	-	-	-	-	-	-	-
V_2O_3	-	-	-	-	-	-	-	-	-	-
P_2O_5	0.17	0.12	0.08	0.09	0.00	0.00	0.09	0.12	0.00	0.01
Total[d]	100.40	100.03	102.33	100.11	99.37	98.97	102.41	100.25	100.93	99.59
Cations										
Si	5.89	5.90	5.86	5.89	5.93	5.92	5.91	5.88	5.90	5.94
Ti	0.01	0.02	0.01	0.00	0.01	0.00	0.01	0.01	0.01	0.01
Al	0.00	0.00	0.02	0.01	0.01	0.01	0.00	0.00	0.00	0.00
Cr	-	-	-	-	-	-	-	-	-	-
Fe2+	4.15	4.10	4.05	4.23	4.14	4.17	4.12	4.15	3.42	3.25
Mn	0.08	0.07	0.09	0.07	0.07	0.08	0.08	0.09	0.07	0.05
Mg	7.85	7.93	8.01	7.80	7.84	7.86	7.88	7.89	8.67	8.77
Ca	0.07	0.03	0.05	0.06	0.05	0.04	0.05	0.05	0.05	0.04
Na	0.00	0.04	0.02	0.02	0.01	0.00	0.00	0.00	0.00	0.00
K	0.00	0.00	0.00	0.01	0.00	0.01	0.01	0.00	0.00	0.00
Ni	-	-	-	-	-	-	-	-	-	-
V	-	-	-	-	-	-	-	-	-	-
P	0.02	0.02	0.01	0.01	0.00	0.00	0.01	0.02	0.00	0.00
Cation total	18.07	18.11	18.12	18.10	18.06	18.09	18.07	18.09	18.12	18.06
Mg# / An[e]	65.4	65.9	66.4	64.8	65.4	65.3	65.7	65.5	71.7	73.0
Lab[f]	1	1	1	1	1	1	1	1	1	1

Table A3. (continued)

Volcanic cone										
Sample										
Mineral[a]	OL	OL	OL	OL	OL	OL	OL	OL	OL	OL
Core ID	a3c	a4c	a5c	b1c	b2c	b3c	b4c	b5c	b6c	c1c
Major element (wt.%) [b]										
SiO_2	38.16	37.86	37.85	37.77	37.99	37.98	38.58	37.98	37.70	38.51
TiO_2	0.04	0.00	0.00	0.05	0.00	0.01	0.00	0.00	0.02	0.00
Al_2O_3	0.00	0.00	0.00	0.00	0.00	0.01	0.00	0.00	0.00	0.01
Cr_2O_3	-	-	-	-	-	-	-	-	-	-
FeO[c]	20.31	21.13	20.38	20.77	21.09	20.13	18.83	20.51	21.47	18.40
MnO	0.24	0.23	0.22	0.30	0.35	0.27	0.18	0.25	0.28	0.40
MgO	41.05	40.44	41.32	40.93	40.42	41.47	42.29	41.07	40.27	42.50
CaO	0.18	0.27	0.16	0.16	0.14	0.09	0.09	0.18	0.18	0.18
Na_2O	0.02	0.04	0.00	0.00	0.00	0.01	0.00	0.00	0.00	0.00
K_2O	0.00	0.04	0.00	0.02	0.00	0.00	0.02	0.01	0.08	0.00
NiO	-	-	-	-	-	-	-	-	-	-
V_2O_3	-	-	-	-	-	-	-	-	-	-
P_2O_5	0.00	0.00	0.07	0.00	0.01	0.03	0.00	0.00	0.00	0.00
Total[d]	100.97	100.75	101.15	101.26	100.98	99.81	99.50	99.09	100.56	99.86
Cations										
Si	5.92	5.90	5.87	5.88	5.91	5.88	5.94	5.89	5.88	5.92
Ti	0.00	0.00	0.00	0.01	0.00	0.00	0.00	0.00	0.00	0.00
Al	0.00	0.00	0.00	0.00	0.00	0.00	0.00	0.00	0.00	0.00
Cr	-	-	-	-	-	-	-	-	-	-
Fe2+	2.64	2.75	2.64	2.70	2.75	2.61	2.43	2.66	2.80	2.37
Mn	0.03	0.03	0.03	0.04	0.05	0.04	0.02	0.03	0.04	0.05
Mg	9.49	9.39	9.55	9.50	9.38	9.57	9.71	9.50	9.37	9.74
Ca	0.03	0.04	0.03	0.03	0.02	0.02	0.01	0.03	0.03	0.03
Na	0.01	0.01	0.00	0.00	0.00	0.00	0.00	0.00	0.00	0.00
K	0.00	0.01	0.00	0.00	0.00	0.00	0.00	0.00	0.02	0.00
Ni	-	-	-	-	-	-	-	-	-	-
V	-	-	-	-	-	-	-	-	-	-
P	0.00	0.00	0.01	0.00	0.00	0.00	0.00	0.00	0.00	0.00
Cation total	18.12	18.13	18.13	18.16	18.11	18.12	18.11	18.11	18.14	18.11
Mg# / An[e]	78.2	77.3	78.3	77.9	77.3	78.6	80.0	78.1	77.0	80.4
Lab[f]	1	1	1	1	1	1	1	1	1	1
Mineral[a]	OL	OL	OL	OL	OL	OL	OL	OL	OL	OL
Rim ID	a3r	a4r	a5r	b1r	b2r	b3r	b4r	b5r	b6r	c1r
Major element (wt.%)[b]										
SiO_2	37.13	37.13	37.30	36.84	36.86	37.18	37.58	36.95	37.27	37.22
TiO_2	0.00	0.00	0.04	0.00	0.01	0.09	0.13	0.06	0.02	0.00
Al_2O_3	0.05	0.05	0.00	0.08	0.00	0.00	0.00	0.04	0.06	0.02
Cr_2O_3	-	-	-	-	-	-	-	-	-	-
FeO[c]	24.80	24.72	24.07	25.57	26.16	24.33	23.37	25.92	24.02	24.88
MnO	0.45	0.49	0.42	0.36	0.39	0.51	0.45	0.54	0.48	0.43
MgO	37.23	37.22	37.89	36.88	36.34	37.57	38.25	36.15	37.87	37.17
CaO	0.33	0.25	0.28	0.27	0.20	0.28	0.18	0.24	0.26	0.26
Na_2O	0.00	0.00	0.00	0.00	0.00	0.00	0.04	0.00	0.02	0.00
K_2O	0.00	0.05	0.00	0.01	0.03	0.00	0.00	0.02	0.00	0.00
NiO	-	-	-	-	-	-	-	-	-	-
V_2O_3	-	-	-	-	-	-	-	-	-	-
P_2O_5	0.00	0.08	0.00	0.00	0.00	0.03	0.00	0.08	0.00	0.02
Total[d]	100.31	99.16	99.96	101.03	98.96	99.13	99.76	99.32	99.27	99.60
Cations										
Si	5.90	5.89	5.90	5.87	5.89	5.89	5.92	5.89	5.89	5.91
Ti	0.00	0.00	0.01	0.00	0.00	0.01	0.02	0.01	0.00	0.00
Al	0.01	0.01	0.00	0.01	0.00	0.00	0.00	0.01	0.01	0.00
Cr	-	-	-	-	-	-	-	-	-	-
Fe2+	3.29	3.28	3.18	3.41	3.49	3.22	3.08	3.46	3.18	3.30
Mn	0.06	0.07	0.06	0.05	0.05	0.07	0.06	0.07	0.07	0.06
Mg	8.82	8.80	8.93	8.76	8.65	8.87	8.98	8.59	8.92	8.79
Ca	0.06	0.04	0.05	0.05	0.04	0.05	0.03	0.04	0.04	0.04
Na	0.00	0.00	0.00	0.00	0.00	0.00	0.01	0.00	0.01	0.00
K	0.00	0.01	0.00	0.00	0.01	0.00	0.00	0.00	0.00	0.00
Ni	-	-	-	-	-	-	-	-	-	-
V	-	-	-	-	-	-	-	-	-	-
P	0.00	0.01	0.00	0.00	0.00	0.00	0.00	0.01	0.00	0.00
Cation total	18.14	18.11	18.13	18.15	18.13	18.11	18.10	18.08	18.12	18.10
Mg# / An[e]	72.8	72.8	73.7	72.0	71.3	73.4	74.5	71.3	73.7	72.7
Lab[f]	1	1	1	1	1	1	1	1	1	1

Table A3. (continued)

Volcanic cone										
Sample										
Mineral[a]	OL	OL	OL	OL	OL	OL	OL	OL	OL	OL
Core ID	c2c	c4c	c5c	c6c	d1c	d2c	d3c	d4c	d5c	d6c
Major element (wt.%) [b]										
SiO_2	37.84	37.91	38.01	38.14	37.95	37.90	37.96	38.20	38.36	38.03
TiO_2	0.07	0.11	0.02	0.05	0.01	0.05	0.00	0.00	0.04	0.02
Al_2O_3	0.00	0.00	0.02	0.00	0.00	0.00	0.00	0.00	0.00	0.00
Cr_2O_3	-	-	-	-	-	-	-	-	-	-
FeO[c]	20.05	20.42	20.58	19.65	19.88	20.50	20.14	19.73	20.12	19.50
MnO	0.33	0.36	0.39	0.30	0.34	0.21	0.32	0.17	0.30	0.33
MgO	41.50	41.08	40.82	41.59	41.65	41.14	41.42	41.78	40.98	41.89
CaO	0.15	0.11	0.16	0.22	0.15	0.20	0.13	0.11	0.17	0.19
Na_2O	0.00	0.01	0.00	0.00	0.01	0.00	0.00	0.01	0.02	0.00
K_2O	0.00	0.00	0.00	0.04	0.00	0.00	0.03	0.00	0.00	0.04
NiO	-	-	-	-	-	-	-	-	-	-
V_2O_3	-	-	-	-	-	-	-	-	-	-
P_2O_5	0.06	0.00	0.00	0.00	0.01	0.00	0.00	0.00	0.00	0.00
Total[d]	100.10	99.51	99.75	99.58	99.97	99.77	100.52	99.65	99.63	100.47
Cations										
Si	5.86	5.88	5.90	5.90	5.88	5.89	5.90	5.91	5.94	5.88
Ti	0.01	0.01	0.00	0.01	0.00	0.01	0.00	0.00	0.00	0.00
Al	0.00	0.00	0.00	0.00	0.00	0.00	0.00	0.00	0.00	0.00
Cr	-	-	-	-	-	-	-	-	-	-
Fe2+	2.60	2.65	2.67	2.54	2.57	2.67	2.62	2.55	2.61	2.52
Mn	0.04	0.05	0.05	0.04	0.05	0.03	0.04	0.02	0.04	0.04
Mg	9.59	9.50	9.45	9.59	9.61	9.54	9.59	9.64	9.46	9.65
Ca	0.02	0.02	0.03	0.04	0.03	0.03	0.02	0.02	0.03	0.03
Na	0.00	0.00	0.00	0.00	0.00	0.00	0.00	0.00	0.01	0.00
K	0.00	0.00	0.00	0.01	0.00	0.00	0.01	0.00	0.00	0.01
Ni	-	-	-	-	-	-	-	-	-	-
V	-	-	-	-	-	-	-	-	-	-
P	0.01	0.00	0.00	0.00	0.00	0.00	0.00	0.00	0.00	0.00
Cation total	18.13	18.11	18.10	18.13	18.14	18.17	18.18	18.14	18.09	18.13
Mg# / An[e]	78.7	78.2	78.0	79.1	78.9	78.1	78.5	79.1	78.4	79.3
Lab[f]	1	1	1	1	1	1	1	1	1	1
Mineral[a]	OL	OL	OL	OL	OL	OL	OL	OL	OL	OL
Rim ID	c2r	c4r	c5r	c6r	d1r	d2r	d3r	d4r	d5r	d6r
Major element (wt.%)[b]										
SiO_2	37.34	37.42	36.79	36.85	37.39	36.78	37.09	37.05	37.26	37.83
TiO_2	0.01	0.00	0.11	0.05	0.02	0.04	0.00	0.00	0.00	0.00
Al_2O_3	0.00	0.00	0.03	0.06	0.00	0.02	0.00	0.00	0.00	0.05
Cr_2O_3	-	-	-	-	-	-	-	-	-	-
FeO[c]	23.71	25.13	25.99	27.09	24.37	27.85	25.35	25.30	23.89	22.41
MnO	0.39	0.47	0.49	0.31	0.43	0.41	0.44	0.33	0.41	0.46
MgO	38.28	36.64	36.27	35.40	37.44	34.60	36.82	37.12	38.16	39.05
CaO	0.24	0.31	0.28	0.23	0.25	0.30	0.25	0.19	0.26	0.20
Na_2O	0.00	0.00	0.04	0.00	0.05	0.00	0.00	0.02	0.00	0.00
K_2O	0.03	0.02	0.00	0.00	0.05	0.00	0.00	0.00	0.02	0.00
NiO	-	-	-	-	-	-	-	-	-	-
V_2O_3	-	-	-	-	-	-	-	-	-	-
P_2O_5	0.00	0.00	0.00	0.00	0.00	0.01	0.05	0.00	0.00	0.00
Total[d]	99.15	99.67	99.36	99.37	99.73	100.39	99.46	99.90	100.67	100.13
Cations										
Si	5.89	5.95	5.88	5.91	5.92	5.92	5.90	5.89	5.89	5.93
Ti	0.00	0.00	0.01	0.01	0.00	0.00	0.00	0.00	0.00	0.00
Al	0.00	0.00	0.01	0.01	0.00	0.00	0.00	0.00	0.00	0.01
Cr	-	-	-	-	-	-	-	-	-	-
Fe2+	3.13	3.34	3.47	3.63	3.23	3.75	3.37	3.37	3.16	2.94
Mn	0.05	0.06	0.07	0.04	0.06	0.06	0.06	0.04	0.05	0.06
Mg	9.00	8.68	8.64	8.46	8.84	8.30	8.73	8.80	8.99	9.12
Ca	0.04	0.05	0.05	0.04	0.04	0.05	0.04	0.03	0.04	0.03
Na	0.00	0.00	0.01	0.00	0.02	0.00	0.00	0.00	0.00	0.00
K	0.01	0.00	0.00	0.00	0.01	0.00	0.00	0.00	0.00	0.00
Ni	-	-	-	-	-	-	-	-	-	-
V	-	-	-	-	-	-	-	-	-	-
P	0.00	0.00	0.00	0.00	0.00	0.00	0.01	0.00	0.00	0.00
Cation total	18.12	18.08	18.14	18.10	18.12	18.08	18.11	18.13	18.13	18.09
Mg# / An[e]	74.2	72.2	71.3	70.0	73.2	68.9	72.1	72.3	74.0	75.6
Lab[f]	1	1	1	1	1	1	1	1	1	1

Table A3. (continued)

Volcanic cone						Ojodake				
Sample						OJSU				
Mineral[a]	OL	OL	OL	OL	OL	OL	OL	OL	OL	OL
Core ID	e1c	e2c	e3c	e4c	e5c	e6c	a1c	a2c	a3c	a4c
Major element (wt.%) [b]										
SiO_2	38.36	37.91	37.97	37.95	38.12	37.91	37.58	36.67	37.32	38.46
TiO_2	0.00	0.04	0.00	0.12	0.00	0.00	0.00	0.00	0.02	0.00
Al_2O_3	0.00	0.01	0.00	0.00	0.00	0.00	0.02	0.09	0.00	0.00
Cr_2O_3	-	-	-	-	-	-	-	-	-	-
FeO[c]	20.35	20.83	21.14	20.15	20.07	20.95	23.02	26.64	24.55	18.58
MnO	0.35	0.32	0.36	0.24	0.34	0.40	0.37	0.45	0.47	0.27
MgO	40.64	40.67	40.33	41.32	41.30	40.55	38.82	35.83	37.43	42.40
CaO	0.15	0.17	0.16	0.15	0.13	0.14	0.17	0.27	0.17	0.17
Na_2O	0.00	0.02	0.00	0.02	0.00	0.04	0.01	0.00	0.01	0.00
K_2O	0.09	0.00	0.01	0.02	0.03	0.01	0.01	0.00	0.02	0.04
NiO	-	-	-	-	-	-	-	-	-	-
V_2O_3	-	-	-	-	-	-	-	-	-	-
P_2O_5	0.06	0.03	0.04	0.03	0.00	0.00	0.00	0.05	0.00	0.08
Total[d]	101.03	100.28	101.10	99.91	99.48	99.81	99.75	100.60	99.38	99.49
Cations										
Si	5.95	5.89	5.91	5.88	5.92	5.90	5.91	5.87	5.91	5.91
Ti	0.00	0.00	0.00	0.01	0.00	0.00	0.00	0.00	0.00	0.00
Al	0.00	0.00	0.00	0.00	0.00	0.00	0.00	0.02	0.00	0.00
Cr	-	-	-	-	-	-	-	-	-	-
Fe2+	2.64	2.71	2.75	2.61	2.61	2.73	3.03	3.57	3.25	2.39
Mn	0.05	0.04	0.05	0.03	0.04	0.05	0.05	0.06	0.06	0.04
Mg	9.40	9.42	9.36	9.55	9.56	9.41	9.10	8.55	8.83	9.72
Ca	0.03	0.03	0.03	0.02	0.02	0.02	0.03	0.05	0.03	0.03
Na	0.00	0.01	0.00	0.01	0.00	0.01	0.00	0.00	0.00	0.00
K	0.02	0.00	0.00	0.00	0.01	0.00	0.00	0.00	0.00	0.01
Ni	-	-	-	-	-	-	-	-	-	-
V	-	-	-	-	-	-	-	-	-	-
P	0.01	0.00	0.01	0.00	0.00	0.00	0.00	0.01	0.00	0.01
Cation total	18.10	18.10	18.11	18.11	18.16	18.12	18.12	18.13	18.08	18.11
Mg# / An[e]	78.1	77.7	77.3	78.5	78.6	77.5	75.0	70.5	73.1	80.3
Lab[f]	1	1	1	1	1	1	1	1	1	1
Mineral[a]	OL	OL	OL	OL	OL	OL	OL	OL	OL	OL
Rim ID	e1r	e2r	e3r	e4r	e5r	e6r	a1r	a2r	a3r	a4r
Major element (wt.%)[b]										
SiO_2	36.71	37.34	36.62	37.18	37.75	37.20	37.07	-	37.00	-
TiO_2	0.04	0.04	0.09	0.06	0.00	0.04	0.00	-	0.00	-
Al_2O_3	0.03	0.00	0.00	0.03	0.01	0.00	0.00	-	0.00	-
Cr_2O_3	-	-	-	-	-	-	-	-	-	-
FeO[c]	26.92	24.40	27.11	24.64	23.44	24.07	25.88	-	26.60	-
MnO	0.47	0.41	0.61	0.57	0.29	0.49	0.42	-	0.44	-
MgO	35.62	37.47	35.25	37.22	38.22	37.79	36.37	-	35.62	-
CaO	0.21	0.31	0.31	0.23	0.22	0.29	0.21	-	0.32	-
Na_2O	0.00	0.00	0.00	0.00	0.00	0.01	0.00	-	0.00	-
K_2O	0.00	0.00	0.00	0.06	0.03	0.01	0.01	-	0.01	-
NiO	-	-	-	-	-	-	-	-	-	-
V_2O_3	-	-	-	-	-	-	-	-	-	-
P_2O_5	0.00	0.04	0.01	0.00	0.03	0.09	0.05	-	0.00	-
Total[d]	99.57	101.12	99.97	99.51	99.15	99.12	97.26	-	101.61	-
Cations								-		-
Si	5.88	5.92	5.88	5.90	5.94	5.88	5.92	-	5.93	-
Ti	0.00	0.00	0.01	0.01	0.00	0.00	0.00	-	0.00	-
Al	0.01	0.00	0.00	0.00	0.00	0.00	0.00	-	0.00	-
Cr	-	-	-	-	-	-	-	-	-	-
Fe2+	3.61	3.23	3.64	3.27	3.08	3.18	3.45	-	3.57	-
Mn	0.06	0.05	0.08	0.08	0.04	0.07	0.06	-	0.06	-
Mg	8.51	8.85	8.44	8.81	8.96	8.90	8.65	-	8.51	-
Ca	0.04	0.05	0.05	0.04	0.04	0.05	0.03	-	0.06	-
Na	0.00	0.00	0.00	0.00	0.00	0.00	0.00	-	0.00	-
K	0.00	0.00	0.00	0.01	0.01	0.00	0.00	-	0.00	-
Ni	-	-	-	-	-	-	-	-	-	-
V	-	-	-	-	-	-	-	-	-	-
P	0.00	0.01	0.00	0.00	0.00	0.01	0.01	-	0.00	-
Cation total	18.11	18.11	18.10	18.12	18.07	18.09	18.12	-	18.13	-
Mg# / An[e]	70.2	73.3	69.9	72.9	74.4	73.7	71.5	-	70.4	-
Lab[f]	1	1	1	1	1	1	1	-	1	-

Table A3. (continued)

Volcanic cone										
Sample										
Mineral[a]	OL	OL	OL	OL	OL	OL	OL	OL	OL	OL
Core ID	a5c	a6c	b1c	b2c	b3c	b4c	b5c	b6c	c1c	c2c
Major element (wt.%) [b]										
SiO_2	36.50	37.67	36.57	36.43	36.04	36.27	37.95	37.53	37.82	36.13
TiO_2	0.04	0.02	0.03	0.00	0.12	0.06	0.03	0.11	0.00	0.09
Al_2O_3	0.00	0.02	0.02	0.00	0.00	0.00	0.06	0.02	0.00	0.00
Cr_2O_3	-	-	-	-	-	-	-	-	-	-
FeO[c]	27.37	22.40	27.73	29.14	30.44	28.95	21.94	22.32	21.26	29.68
MnO	0.59	0.38	0.61	0.63	0.48	0.55	0.33	0.36	0.42	0.61
MgO	35.16	39.35	34.77	33.57	32.58	33.83	39.57	39.43	40.34	33.18
CaO	0.32	0.15	0.24	0.22	0.23	0.23	0.11	0.18	0.16	0.26
Na_2O	0.00	0.00	0.02	0.00	0.00	0.09	0.00	0.00	0.00	0.00
K_2O	0.02	0.00	0.00	0.00	0.00	0.03	0.00	0.04	0.00	0.00
NiO	-	-	-	-	-	-	-	-	-	-
V_2O_3	-	-	-	-	-	-	-	-	-	-
P_2O_5	0.00	0.00	0.00	0.00	0.10	0.00	0.00	0.00	0.00	0.05
Total[d]	99.52	99.31	99.28	99.37	99.21	98.98	98.91	99.19	98.70	99.13
Cations										
Si	5.88	5.90	5.89	5.92	5.88	5.88	5.93	5.88	5.90	5.88
Ti	0.01	0.00	0.00	0.00	0.02	0.01	0.00	0.01	0.00	0.01
Al	0.00	0.00	0.00	0.00	0.00	0.00	0.01	0.00	0.00	0.00
Cr	-	-	-	-	-	-	-	-	-	-
Fe2+	3.69	2.94	3.74	3.96	4.15	3.93	2.86	2.93	2.77	4.04
Mn	0.08	0.05	0.08	0.09	0.07	0.08	0.04	0.05	0.06	0.08
Mg	8.44	9.19	8.35	8.13	7.93	8.17	9.21	9.21	9.37	8.04
Ca	0.06	0.03	0.04	0.04	0.04	0.04	0.02	0.03	0.03	0.04
Na	0.00	0.00	0.01	0.00	0.00	0.03	0.00	0.00	0.00	0.00
K	0.00	0.00	0.00	0.00	0.00	0.01	0.00	0.01	0.00	0.00
Ni	-	-	-	-	-	-	-	-	-	-
V	-	-	-	-	-	-	-	-	-	-
P	0.00	0.00	0.00	0.00	0.01	0.00	0.00	0.00	0.00	0.01
Cation total	18.16	18.11	18.11	18.14	18.10	18.15	18.07	18.12	18.13	18.10
Mg# / An[e]	69.6	75.8	69.1	67.2	65.6	67.5	76.3	75.9	77.2	66.6
Lab[f]	1	1	1	1	1	1	1	1	1	1
Mineral[a]	OL	OL	OL	OL	OL	OL	OL	OL	OL	OL
Rim ID	a5r	a6r	b1r	b2r	b3r	b4r	b5r	b6r	c1r	c2r
Major element (wt.%)[b]										
SiO_2	37.02	37.29	-	37.33	36.72	36.77	36.79	37.23	36.88	37.31
TiO_2	0.01	0.05	-	0.00	0.00	0.05	0.03	0.07	0.00	0.00
Al_2O_3	0.01	0.02	-	0.01	0.00	0.00	0.07	0.06	0.03	0.00
Cr_2O_3	-	-	-	-	-	-	-	-	-	-
FeO[c]	26.14	25.29	-	25.04	25.88	27.42	26.93	25.05	27.16	24.39
MnO	0.56	0.62	-	0.56	0.34	0.56	0.48	0.49	0.52	0.33
MgO	35.99	36.43	-	36.81	36.64	34.88	35.44	36.86	35.12	37.73
CaO	0.25	0.26	-	0.25	0.28	0.24	0.21	0.24	0.27	0.25
Na_2O	0.00	0.00	-	0.00	0.00	0.07	0.00	0.00	0.00	0.00
K_2O	0.02	0.04	-	0.00	0.00	0.01	0.01	0.00	0.01	0.00
NiO	-	-	-	-	-	-	-	-	-	-
V_2O_3	-	-	-	-	-	-	-	-	-	-
P_2O_5	0.00	0.00	-	0.00	0.13	0.00	0.05	0.00	0.01	0.00
Total[d]	97.77	99.81	-	102.31	98.99	98.96	100.09	98.58	96.22	96.85
Cations			-							
Si	5.91	5.94	-	5.93	5.86	5.92	5.89	5.91	5.92	5.91
Ti	0.00	0.01	-	0.00	0.00	0.01	0.00	0.01	0.00	0.00
Al	0.00	0.00	-	0.00	0.00	0.00	0.01	0.01	0.01	0.00
Cr	-	-	-	-	-	-	-	-	-	-
Fe2+	3.49	3.37	-	3.33	3.45	3.69	3.61	3.33	3.65	3.23
Mn	0.08	0.08	-	0.08	0.05	0.08	0.07	0.06	0.07	0.04
Mg	8.57	8.65	-	8.72	8.71	8.36	8.46	8.72	8.40	8.90
Ca	0.04	0.04	-	0.04	0.05	0.04	0.04	0.04	0.05	0.04
Na	0.00	0.00	-	0.00	0.00	0.02	0.00	0.00	0.00	0.00
K	0.00	0.01	-	0.00	0.00	0.00	0.00	0.00	0.00	0.00
Ni	-	-	-	-	-	-	-	-	-	-
V	-	-	-	-	-	-	-	-	-	-
P	0.00	0.00	-	0.00	0.02	0.00	0.01	0.00	0.00	0.00
Cation total	18.09	18.10	-	18.10	18.14	18.12	18.09	18.08	18.10	18.12
Mg# / An[e]	71.1	72.0	-	72.4	71.6	69.4	70.1	72.4	69.7	73.4
Lab[f]	1	1	-	1	1	1	1	1	1	1

Table A3. (continued)

Volcanic cone										
Sample										
Mineral[a]	OL	OL	OL	OL	OL	OL	OL	OL	OL	OL
Core ID	c3c	c4c	c5c	c6c	d1c	d2c	d3c	d5c	d6c	e1c
Major element (wt.%) [b]										
SiO_2	38.24	38.15	38.62	36.38	38.02	38.23	38.00	35.86	38.03	36.23
TiO_2	0.03	0.03	0.05	0.00	0.02	0.06	0.07	0.00	0.00	0.04
Al_2O_3	0.00	0.00	0.03	0.00	0.01	0.00	0.00	0.00	0.00	0.00
Cr_2O_3	-	-	-	-	-	-	-	-	-	-
FeO[c]	19.65	18.98	18.72	29.21	21.30	19.14	21.59	31.59	20.97	30.35
MnO	0.26	0.20	0.32	0.50	0.29	0.33	0.36	0.55	0.34	0.60
MgO	41.64	42.41	42.10	33.68	40.02	42.04	39.85	31.75	40.59	32.52
CaO	0.17	0.19	0.12	0.19	0.20	0.19	0.11	0.25	0.07	0.26
Na_2O	0.00	0.00	0.00	0.04	0.09	0.00	0.00	0.00	0.00	0.00
K_2O	0.00	0.00	0.04	0.00	0.02	0.00	0.01	0.00	0.00	0.00
NiO	-	-	-	-	-	-	-	-	-	-
V_2O_3	-	-	-	-	-	-	-	-	-	-
P_2O_5	0.00	0.04	0.00	0.00	0.02	0.00	0.00	0.00	0.00	0.00
Total[d]	99.06	99.12	99.31	98.74	99.23	99.14	98.97	99.35	98.85	98.81
Cations										
Si	5.92	5.88	5.94	5.91	5.92	5.90	5.93	5.90	5.92	5.91
Ti	0.00	0.00	0.01	0.00	0.00	0.01	0.01	0.00	0.00	0.01
Al	0.00	0.00	0.01	0.00	0.00	0.00	0.00	0.00	0.00	0.00
Cr	-	-	-	-	-	-	-	-	-	-
Fe2+	2.54	2.45	2.41	3.97	2.77	2.47	2.82	4.34	2.73	4.14
Mn	0.03	0.03	0.04	0.07	0.04	0.04	0.05	0.08	0.04	0.08
Mg	9.60	9.74	9.65	8.15	9.29	9.67	9.28	7.78	9.42	7.90
Ca	0.03	0.03	0.02	0.03	0.03	0.03	0.02	0.04	0.01	0.05
Na	0.00	0.00	0.00	0.01	0.03	0.00	0.00	0.00	0.00	0.00
K	0.00	0.00	0.01	0.00	0.00	0.00	0.00	0.00	0.00	0.00
Ni	-	-	-	-	-	-	-	-	-	-
V	-	-	-	-	-	-	-	-	-	-
P	0.00	0.01	0.00	0.00	0.00	0.00	0.00	0.00	0.00	0.00
Cation total	18.12	18.14	18.09	18.14	18.08	18.12	18.11	18.14	18.12	18.09
Mg# / An[e]	79.1	79.9	80.0	67.2	77.0	79.7	76.7	64.2	77.5	65.6
Lab[f]	1	1	1	1	1	1	1	1	1	1
Mineral[a]	OL	OL	OL	OL	OL	OL	OL	OL	OL	OL
Rim ID	c3r	c4r	c5r	c6r	d1r	d2r	d3r	d5r	d6r	e1r
Major element (wt.%)[b]										
SiO_2	36.86	36.89	37.00	37.15	37.24	37.10	36.93	36.79	37.66	-
TiO_2	0.09	0.09	0.15	0.17	0.05	0.07	0.07	0.03	0.00	-
Al_2O_3	0.03	0.00	0.00	0.00	0.03	0.00	0.11	0.03	0.03	-
Cr_2O_3	-	-	-	-	-	-	-	-	-	-
FeO[c]	25.73	25.68	25.71	25.34	25.19	25.33	25.10	26.11	23.33	-
MnO	0.58	0.49	0.44	0.41	0.45	0.45	0.61	0.49	0.41	-
MgO	36.38	36.49	36.30	36.63	36.80	36.84	36.89	36.27	38.35	-
CaO	0.31	0.31	0.25	0.29	0.25	0.22	0.22	0.27	0.22	-
Na_2O	0.00	0.00	0.02	0.01	0.00	0.00	0.06	0.00	0.00	-
K_2O	0.01	0.05	0.03	0.00	0.00	0.00	0.02	0.01	0.00	-
NiO	-	-	-	-	-	-	-	-	-	-
V_2O_3	-	-	-	-	-	-	-	-	-	-
P_2O_5	0.00	0.00	0.10	0.00	0.00	0.00	0.00	0.00	0.00	-
Total[d]	98.55	99.60	99.38	100.48	100.85	102.15	99.09	98.55	102.50	-
Cations										-
Si	5.89	5.89	5.89	5.91	5.92	5.90	5.88	5.88	5.93	-
Ti	0.01	0.01	0.02	0.02	0.01	0.01	0.01	0.00	0.00	-
Al	0.01	0.00	0.00	0.00	0.00	0.00	0.02	0.01	0.00	-
Cr	-	-	-	-	-	-	-	-	-	-
Fe2+	3.43	3.43	3.42	3.37	3.35	3.37	3.34	3.49	3.07	-
Mn	0.08	0.07	0.06	0.06	0.06	0.06	0.08	0.07	0.05	-
Mg	8.66	8.69	8.62	8.69	8.72	8.73	8.75	8.64	9.00	-
Ca	0.05	0.05	0.04	0.05	0.04	0.04	0.04	0.05	0.04	-
Na	0.00	0.00	0.01	0.00	0.00	0.00	0.02	0.00	0.00	-
K	0.00	0.01	0.01	0.00	0.00	0.00	0.00	0.00	0.00	-
Ni	-	-	-	-	-	-	-	-	-	-
V	-	-	-	-	-	-	-	-	-	-
P	0.00	0.00	0.01	0.00	0.00	0.00	0.00	0.00	0.00	-
Cation total	18.13	18.15	18.08	18.10	18.10	18.11	18.14	18.14	18.09	-
Mg# / An[e]	71.6	71.7	71.6	72.1	72.2	72.1	72.4	71.2	74.6	-
Lab[f]	1	1	1	1	1	1	1	1	1	-

Table A3. (continued)

Volcanic cone										
Sample						OJSL				
Mineral[a]	OL	OL	OL	OL	OL	OL	OL	OL	OL	OL
Core ID	e2c	e3c	e4c	e5c	e6c	a1c	a2c	a3c	a4c	a5c
Major element (wt.%) [b]										
SiO_2	36.13	38.00	37.95	37.41	37.59	38.32	36.70	36.19	37.54	37.57
TiO_2	0.01	0.01	0.00	0.00	0.00	0.08	0.00	0.01	0.01	0.00
Al_2O_3	0.00	0.06	0.02	0.01	0.00	0.00	0.03	0.01	0.00	0.00
Cr_2O_3	-	-	-	-	-	-	-	-	-	-
FeO[c]	30.81	21.93	20.72	22.92	22.23	19.26	27.39	28.83	23.69	23.29
MnO	0.52	0.24	0.32	0.35	0.36	0.49	0.45	0.56	0.45	0.35
MgO	32.30	39.65	40.72	38.98	39.64	41.63	35.23	34.13	38.11	38.61
CaO	0.17	0.11	0.21	0.23	0.11	0.22	0.15	0.25	0.14	0.14
Na_2O	0.00	0.00	0.00	0.00	0.00	0.00	0.05	0.00	0.07	0.00
K_2O	0.00	0.00	0.06	0.03	0.05	0.00	0.01	0.01	0.00	0.03
NiO	-	-	-	-	-	-	-	-	-	-
V_2O_3	-	-	-	-	-	-	-	-	-	-
P_2O_5	0.05	0.00	0.00	0.07	0.02	0.00	0.00	0.00	0.00	0.00
Total[d]	99.06	98.87	98.71	99.41	98.89	100.02	98.73	99.19	98.49	98.83
Cations										
Si	5.90	5.94	5.91	5.88	5.89	5.92	5.90	5.87	5.93	5.92
Ti	0.00	0.00	0.00	0.00	0.00	0.01	0.00	0.00	0.00	0.00
Al	0.00	0.01	0.00	0.00	0.00	0.00	0.00	0.00	0.00	0.00
Cr	-	-	-	-	-	-	-	-	-	-
Fe2+	4.21	2.86	2.70	3.01	2.91	2.49	3.68	3.91	3.13	3.07
Mn	0.07	0.03	0.04	0.05	0.05	0.06	0.06	0.08	0.06	0.05
Mg	7.87	9.23	9.45	9.14	9.25	9.58	8.44	8.24	8.98	9.06
Ca	0.03	0.02	0.04	0.04	0.02	0.04	0.03	0.04	0.02	0.02
Na	0.00	0.00	0.00	0.00	0.00	0.00	0.02	0.00	0.02	0.00
K	0.00	0.00	0.01	0.01	0.01	0.00	0.00	0.00	0.00	0.01
Ni	-	-	-	-	-	-	-	-	-	-
V	-	-	-	-	-	-	-	-	-	-
P	0.01	0.00	0.00	0.01	0.00	0.00	0.00	0.00	0.00	0.00
Cation total	18.09	18.09	18.15	18.14	18.13	18.10	18.13	18.14	18.14	18.13
Mg# / An[e]	65.1	76.3	77.8	75.2	76.1	79.4	69.6	67.8	74.2	74.7
Lab[f]	1	1	1	1	1	1	1	1	1	1
Mineral[a]	OL	OL	OL	OL	OL	OL	OL	OL	OL	OL
Rim ID	e2r	e3r	e4r	e5r	e6r	a1r	a2r	a3r	a4r	a5r
Major element (wt.%)[b]										
SiO_2	36.77	37.55	36.46	36.70	37.53	37.14	37.00	37.05	37.18	36.67
TiO_2	0.02	0.11	0.00	0.00	0.05	0.05	0.00	0.00	0.05	0.17
Al_2O_3	0.00	0.00	0.07	0.03	0.00	0.00	0.00	0.00	0.00	0.00
Cr_2O_3	-	-	-	-	-	-	-	-	-	-
FeO[c]	27.13	24.05	28.16	26.87	23.74	24.30	24.96	25.08	25.00	26.78
MnO	0.40	0.40	0.55	0.49	0.49	0.47	0.58	0.38	0.57	0.61
MgO	35.32	37.66	34.34	35.71	37.88	37.77	37.17	37.18	36.92	35.31
CaO	0.27	0.23	0.25	0.20	0.31	0.23	0.24	0.25	0.24	0.28
Na_2O	0.08	0.00	0.10	0.00	0.00	0.04	0.00	0.00	0.00	0.01
K_2O	0.01	0.00	0.00	0.00	0.00	0.00	0.02	0.06	0.00	0.01
NiO	-	-	-	-	-	-	-	-	-	-
V_2O_3	-	-	-	-	-	-	-	-	-	-
P_2O_5	0.00	0.00	0.07	0.00	0.00	0.00	0.03	0.00	0.04	0.16
Total[d]	98.19	96.98	96.81	99.42	100.45	100.64	96.54	99.12	101.18	101.90
Cations										
Si	5.90	5.93	5.88	5.89	5.93	5.88	5.88	5.90	5.91	5.88
Ti	0.00	0.01	0.00	0.00	0.01	0.01	0.00	0.00	0.01	0.02
Al	0.00	0.00	0.01	0.01	0.00	0.00	0.00	0.00	0.00	0.00
Cr	-	-	-	-	-	-	-	-	-	-
Fe2+	3.64	3.17	3.80	3.60	3.14	3.22	3.32	3.34	3.32	3.59
Mn	0.05	0.05	0.08	0.07	0.06	0.06	0.08	0.05	0.08	0.08
Mg	8.45	8.86	8.26	8.54	8.92	8.91	8.80	8.82	8.75	8.43
Ca	0.05	0.04	0.04	0.03	0.05	0.04	0.04	0.04	0.04	0.05
Na	0.03	0.00	0.03	0.00	0.00	0.01	0.00	0.00	0.00	0.00
K	0.00	0.00	0.00	0.00	0.00	0.00	0.00	0.01	0.00	0.00
Ni	-	-	-	-	-	-	-	-	-	-
V	-	-	-	-	-	-	-	-	-	-
P	0.00	0.00	0.01	0.00	0.00	0.00	0.00	0.00	0.00	0.02
Cation total	18.12	18.06	18.11	18.14	18.11	18.13	18.12	18.16	18.11	18.07
Mg# / An[e]	69.9	73.6	68.5	70.3	74.0	73.5	72.6	72.5	72.5	70.1
Lab[f]	1	1	1	1	1	1	1	1	1	1

Table A3. (continued)

Volcanic cone										
Sample										
Mineral[a]	OL	OL	OL	OL	OL	OL	OL	OL	OL	OL
Core ID	a6c	b1c	b2c	b3c	b4c	b5c	b6c	c1c	c2c	c3c
Major element (wt.%) [b]										
SiO_2	35.59	37.56	36.75	36.56	36.16	38.06	38.32	36.08	36.65	36.30
TiO_2	0.00	0.09	0.00	0.07	0.05	0.02	0.06	0.00	0.00	0.00
Al_2O_3	0.02	0.00	0.00	0.05	0.00	0.06	0.00	0.00	0.02	0.00
Cr_2O_3	-	-	-	-	-	-	-	-	-	-
FeO[c]	32.92	22.58	26.66	27.26	28.21	20.00	19.38	30.05	27.33	28.91
MnO	0.68	0.32	0.39	0.54	0.65	0.21	0.33	0.72	0.52	0.51
MgO	30.56	39.25	35.74	35.22	34.73	41.46	41.74	32.85	35.23	34.05
CaO	0.20	0.19	0.28	0.27	0.16	0.08	0.14	0.25	0.22	0.23
Na_2O	0.00	0.00	0.05	0.00	0.00	0.00	0.01	0.04	0.00	0.00
K_2O	0.03	0.01	0.04	0.00	0.04	0.00	0.00	0.01	0.00	0.00
NiO	-	-	-	-	-	-	-	-	-	-
V_2O_3	-	-	-	-	-	-	-	-	-	-
P_2O_5	0.00	0.00	0.08	0.03	0.00	0.10	0.00	0.00	0.02	0.00
Total[d]	98.54	98.91	99.04	98.33	98.91	98.79	98.53	99.11	99.11	97.97
Cations										
Si	5.90	5.89	5.88	5.88	5.85	5.89	5.92	5.89	5.89	5.88
Ti	0.00	0.01	0.00	0.01	0.01	0.00	0.01	0.00	0.00	0.00
Al	0.00	0.00	0.00	0.01	0.00	0.01	0.00	0.00	0.00	0.00
Cr	-	-	-	-	-	-	-	-	-	-
Fe2+	4.56	2.96	3.57	3.66	3.82	2.59	2.50	4.10	3.68	3.92
Mn	0.10	0.04	0.05	0.07	0.09	0.03	0.04	0.10	0.07	0.07
Mg	7.55	9.17	8.53	8.44	8.38	9.56	9.61	7.99	8.45	8.23
Ca	0.04	0.03	0.05	0.05	0.03	0.01	0.02	0.04	0.04	0.04
Na	0.00	0.00	0.02	0.00	0.00	0.00	0.00	0.01	0.00	0.00
K	0.01	0.00	0.01	0.00	0.01	0.00	0.00	0.00	0.00	0.00
Ni	-	-	-	-	-	-	-	-	-	-
V	-	-	-	-	-	-	-	-	-	-
P	0.00	0.00	0.01	0.00	0.00	0.01	0.00	0.00	0.00	0.00
Cation total	18.16	18.10	18.12	18.12	18.19	18.10	18.10	18.13	18.13	18.14
Mg# / An[e]	62.3	75.6	70.5	69.8	68.7	78.7	79.4	66.1	69.7	67.7
Lab[f]	1	1	1	1	1	1	1	1	1	1
Mineral[a]	OL	OL	OL	OL	OL	OL	OL	OL	OL	OL
Rim ID	a6r	b1r	b2r	b3r	b4r	b5r	b6r	c1r	c2r	c3r
Major element (wt.%)[b]										
SiO_2	37.48	36.58	37.27	37.22	37.43	-	38.01	36.37	37.52	37.07
TiO_2	0.05	0.00	0.03	0.00	0.06	-	0.00	0.00	0.09	0.04
Al_2O_3	0.01	0.01	0.00	0.00	0.01	-	0.05	0.00	0.00	0.00
Cr_2O_3	-	-	-	-	-	-	-	-	-	-
FeO[c]	24.07	27.64	25.21	24.85	24.28	-	21.66	28.49	23.92	24.72
MnO	0.45	0.72	0.40	0.37	0.44	-	0.32	0.53	0.50	0.51
MgO	37.70	34.82	36.83	37.22	37.43	-	39.71	34.22	37.70	37.38
CaO	0.23	0.19	0.18	0.29	0.28	-	0.17	0.31	0.27	0.24
Na_2O	0.00	0.00	0.04	0.00	0.00	-	0.00	0.00	0.00	0.01
K_2O	0.00	0.00	0.04	0.04	0.07	-	0.05	0.00	0.00	0.03
NiO	-	-	-	-	-	-	-	-	-	-
V_2O_3	-	-	-	-	-	-	-	-	-	-
P_2O_5	0.00	0.04	0.00	0.01	0.00	-	0.03	0.09	0.00	0.00
Total[d]	99.04	98.74	98.24	102.31	102.59	-	100.78	102.46	103.49	102.39
Cations						-				
Si	5.92	5.89	5.92	5.91	5.92	-	5.93	5.89	5.93	5.89
Ti	0.01	0.00	0.00	0.00	0.01	-	0.00	0.00	0.01	0.00
Al	0.00	0.00	0.00	0.00	0.00	-	0.01	0.00	0.00	0.00
Cr	-	-	-	-	-	-	-	-	-	-
Fe2+	3.18	3.72	3.35	3.30	3.21	-	2.83	3.86	3.16	3.28
Mn	0.06	0.10	0.05	0.05	0.06	-	0.04	0.07	0.07	0.07
Mg	8.88	8.36	8.72	8.80	8.83	-	9.24	8.26	8.88	8.85
Ca	0.04	0.03	0.03	0.05	0.05	-	0.03	0.05	0.05	0.04
Na	0.00	0.00	0.01	0.00	0.00	-	0.00	0.00	0.00	0.00
K	0.00	0.00	0.01	0.01	0.01	-	0.01	0.00	0.00	0.01
Ni	-	-	-	-	-	-	-	-	-	-
V	-	-	-	-	-	-	-	-	-	-
P	0.00	0.01	0.00	0.00	0.00	-	0.00	0.01	0.00	0.00
Cation total	18.09	18.11	18.09	18.12	18.09	-	18.09	18.14	18.10	18.14
Mg# / An[e]	73.6	69.2	72.2	72.7	73.3	-	76.6	68.2	73.8	73.0
Lab[f]	1	1	1	1	1	-	1	1	1	1

Table A3. (continued)

Volcanic cone										
Sample										
Mineral[a]	OL	OL	OL	OL	OL	OL	OL	OL	OL	OL
Core ID	c4c	c5c	c6c	d1c	d2c	d3c	d4c	d5c	d6c	e1c
Major element (wt.%) [b]										
SiO_2	36.94	35.73	37.94	36.68	36.23	36.48	36.69	37.67	36.29	37.67
TiO_2	0.00	0.00	0.06	0.02	0.10	0.00	0.15	0.00	0.16	0.00
Al_2O_3	0.00	0.10	0.00	0.00	0.11	0.00	0.02	0.02	0.00	0.00
Cr_2O_3	-	-	-	-	-	-	-	-	-	-
FeO[c]	24.18	31.83	20.44	28.04	29.63	27.81	27.15	23.19	28.87	22.31
MnO	0.51	0.57	0.31	0.57	0.65	0.54	0.46	0.42	0.53	0.41
MgO	37.97	31.52	40.99	34.51	33.00	34.92	35.32	38.51	33.85	39.44
CaO	0.24	0.25	0.20	0.18	0.26	0.20	0.21	0.19	0.24	0.16
Na_2O	0.04	0.00	0.00	0.00	0.03	0.02	0.00	0.00	0.00	0.00
K_2O	0.03	0.00	0.00	0.00	0.00	0.00	0.00	0.00	0.00	0.00
NiO	-	-	-	-	-	-	-	-	-	-
V_2O_3	-	-	-	-	-	-	-	-	-	-
P_2O_5	0.09	0.00	0.05	0.00	0.00	0.03	0.00	0.00	0.07	0.00
Total[d]	99.60	99.22	98.12	99.84	100.04	101.00	99.70	99.70	100.22	99.99
Cations										
Si	5.85	5.88	5.89	5.91	5.89	5.88	5.89	5.93	5.88	5.90
Ti	0.00	0.00	0.01	0.00	0.01	0.00	0.02	0.00	0.02	0.00
Al	0.00	0.02	0.00	0.00	0.02	0.00	0.00	0.00	0.00	0.00
Cr	-	-	-	-	-	-	-	-	-	-
Fe2+	3.20	4.38	2.65	3.78	4.03	3.75	3.65	3.05	3.91	2.92
Mn	0.07	0.08	0.04	0.08	0.09	0.07	0.06	0.06	0.07	0.05
Mg	8.96	7.73	9.48	8.29	8.00	8.39	8.45	9.03	8.18	9.21
Ca	0.04	0.04	0.03	0.03	0.05	0.03	0.04	0.03	0.04	0.03
Na	0.01	0.00	0.00	0.00	0.01	0.01	0.00	0.00	0.00	0.00
K	0.01	0.00	0.00	0.00	0.00	0.00	0.00	0.00	0.00	0.00
Ni	-	-	-	-	-	-	-	-	-	-
V	-	-	-	-	-	-	-	-	-	-
P	0.01	0.00	0.01	0.00	0.00	0.00	0.00	0.00	0.01	0.00
Cation total	18.15	18.13	18.11	18.09	18.10	18.13	18.11	18.10	18.11	18.11
Mg# / An[e]	73.7	63.8	78.2	68.7	66.5	69.1	69.8	74.8	67.7	75.9
Lab[f]	1	1	1	1	1	1	1	1	1	1
Mineral[a]	OL	OL	OL	OL	OL	OL	OL	OL	OL	OL
Rim ID	c4r	c5r	c6r	d1r	d2r	d3r	d4r	d5r	d6r	e1r
Major element (wt.%)[b]										
SiO_2	-	-	-	37.28	37.19	37.31	37.37	37.54	37.28	36.96
TiO_2	-	-	-	0.00	0.03	0.12	0.08	0.04	0.01	0.10
Al_2O_3	-	-	-	0.00	0.05	0.00	0.00	0.03	0.01	0.00
Cr_2O_3	-	-	-	-	-	-	-	-	-	-
FeO[c]	-	-	-	24.34	25.54	24.40	25.09	23.06	24.20	26.31
MnO	-	-	-	0.50	0.47	0.48	0.49	0.38	0.46	0.50
MgO	-	-	-	37.57	36.48	37.41	36.76	38.60	37.79	35.84
CaO	-	-	-	0.20	0.22	0.29	0.22	0.33	0.18	0.25
Na_2O	-	-	-	0.00	0.00	0.00	0.00	0.02	0.00	0.04
K_2O	-	-	-	0.02	0.00	0.00	0.00	0.01	0.00	0.00
NiO	-	-	-	-	-	-	-	-	-	-
V_2O_3	-	-	-	-	-	-	-	-	-	-
P_2O_5	-	-	-	0.08	0.02	0.00	0.00	0.00	0.07	0.00
Total[d]	-	-	-	103.37	103.67	103.86	100.84	100.84	103.40	101.92
Cations	-	-	-							
Si	-	-	-	5.90	5.92	5.91	5.93	5.90	5.89	5.91
Ti	-	-	-	0.00	0.00	0.01	0.01	0.00	0.00	0.01
Al	-	-	-	0.00	0.01	0.00	0.00	0.00	0.00	0.00
Cr	-	-	-	-	-	-	-	-	-	-
Fe2+	-	-	-	3.22	3.40	3.23	3.33	3.03	3.20	3.52
Mn	-	-	-	0.07	0.06	0.06	0.07	0.05	0.06	0.07
Mg	-	-	-	8.86	8.65	8.83	8.70	9.04	8.90	8.54
Ca	-	-	-	0.03	0.04	0.05	0.04	0.06	0.03	0.04
Na	-	-	-	0.00	0.00	0.00	0.00	0.01	0.00	0.01
K	-	-	-	0.00	0.00	0.00	0.00	0.00	0.00	0.00
Ni	-	-	-	-	-	-	-	-	-	-
V	-	-	-	-	-	-	-	-	-	-
P	-	-	-	0.01	0.00	0.00	0.00	0.00	0.01	0.00
Cation total	-	-	-	18.09	18.08	18.09	18.08	18.09	18.09	18.10
Mg# / An[e]	-	-	-	73.3	71.8	73.2	72.3	74.9	73.6	70.8
Lab[f]	-	-	-	1	1	1	1	1	1	1

Table A3. (continued)

Volcanic cone						Kishimadake				
Sample						KSS				
Mineral[a]	OL	OL	OL	OL	OL	OL	OL	OL	OL	OL
Core ID	e2c	e3c	e4c	e5c	e6c	OL03-a1c	OL03-a2c	OL03-a3c	OL03-a4c	OL03-b1c
Major element (wt.%) [b]										
SiO_2	37.87	37.76	38.08	37.51	37.97	38.11	38.25	38.30	35.77	38.01
TiO_2	0.00	0.00	0.02	0.00	0.06	0.14	0.06	0.01	0.04	0.01
Al_2O_3	0.03	0.00	0.00	0.01	0.00	0.00	0.00	0.00	0.12	0.00
Cr_2O_3	-	-	-	-	-	-	-	-	-	-
FeO[c]	21.65	22.04	20.21	22.94	22.01	19.73	19.26	18.74	31.26	21.51
MnO	0.21	0.38	0.26	0.38	0.38	0.40	0.26	0.47	0.72	0.35
MgO	40.02	39.56	41.20	38.96	39.39	41.43	41.93	42.31	31.64	39.94
CaO	0.15	0.21	0.20	0.16	0.18	0.18	0.11	0.16	0.25	0.16
Na_2O	0.01	0.00	0.00	0.00	0.00	0.00	0.01	0.00	0.06	0.00
K_2O	0.00	0.05	0.03	0.03	0.00	0.01	0.10	0.01	0.05	0.00
NiO	-	-	-	-	-	-	-	-	-	-
V_2O_3	-	-	-	-	-	-	-	-	-	-
P_2O_5	0.06	0.00	0.00	0.00	0.01	0.00	0.02	0.00	0.10	0.03
Total[d]	100.28	100.20	99.59	99.33	100.47	99.90	99.84	99.25	100.71	100.96
Cations										
Si	5.90	5.91	5.90	5.90	5.94	5.90	5.90	5.90	5.87	5.92
Ti	0.00	0.00	0.00	0.00	0.01	0.02	0.01	0.00	0.00	0.00
Al	0.01	0.00	0.00	0.00	0.00	0.00	0.00	0.00	0.02	0.00
Cr	-	-	-	-	-	-	-	-	-	-
Fe2+	2.82	2.89	2.62	3.02	2.88	2.55	2.49	2.42	4.29	2.80
Mn	0.03	0.05	0.03	0.05	0.05	0.05	0.03	0.06	0.10	0.05
Mg	9.30	9.24	9.52	9.13	9.18	9.56	9.64	9.72	7.74	9.28
Ca	0.03	0.03	0.03	0.03	0.03	0.03	0.02	0.03	0.04	0.03
Na	0.00	0.00	0.00	0.00	0.00	0.00	0.00	0.00	0.02	0.00
K	0.00	0.01	0.01	0.01	0.00	0.00	0.02	0.00	0.01	0.00
Ni	-	-	-	-	-	-	-	-	-	-
V	-	-	-	-	-	-	-	-	-	-
P	0.01	0.00	0.00	0.00	0.00	0.00	0.00	0.00	0.01	0.00
Cation total	18.10	18.13	18.11	18.14	18.09	18.11	18.11	18.13	18.10	18.08
Mg# / An[e]	76.7	76.2	78.4	75.1	76.1	78.9	79.5	80.1	64.3	76.8
Lab[f]	1	1	1	1	1	1	1	1	1	1
Mineral[a]	OL	OL	OL	OL	OL	OL	OL	OL	OL	OL
Rim ID	e2r	e3r	e4r	e5r	e6r	OL03-a1r	OL03-a2r	OL03-a3r	OL03-a4r	OL03-b1r
Major element (wt.%)[b]										
SiO_2	-	37.50	37.65	-	37.37	37.69	37.82	37.69	37.02	37.30
TiO_2	-	0.01	0.04	-	0.04	0.02	0.05	0.02	0.00	0.00
Al_2O_3	-	0.05	0.00	-	0.06	0.01	0.04	0.00	0.02	0.00
Cr_2O_3	-	-	-	-	-	-	-	-	-	-
FeO[c]	-	23.39	22.68	-	23.57	22.80	22.88	23.56	24.99	24.50
MnO	-	0.44	0.43	-	0.53	0.55	0.40	0.43	0.50	0.45
MgO	-	38.28	39.06	-	38.11	38.64	38.46	38.01	37.16	37.54
CaO	-	0.33	0.13	-	0.19	0.25	0.26	0.28	0.28	0.15
Na_2O	-	0.00	0.00	-	0.05	0.00	0.05	0.00	0.00	0.00
K_2O	-	0.00	0.01	-	0.05	0.00	0.02	0.01	0.00	0.01
NiO	-	-	-	-	-	-	-	-	-	-
V_2O_3	-	-	-	-	-	-	-	-	-	-
P_2O_5	-	0.00	0.00	-	0.02	0.04	0.02	0.00	0.03	0.05
Total[d]	-	102.81	98.36	-	98.37	99.39	101.82	100.54	101.71	102.07
Cations	-			-						
Si	-	5.91	5.91	-	5.89	5.92	5.93	5.95	5.88	5.91
Ti	-	0.00	0.00	-	0.00	0.00	0.01	0.00	0.00	0.00
Al	-	0.01	0.00	-	0.01	0.00	0.01	0.00	0.00	0.00
Cr	-	-	-	-	-	-	-	-	-	-
Fe2+	-	3.09	2.98	-	3.11	2.99	3.00	3.11	3.32	3.24
Mn	-	0.06	0.06	-	0.07	0.07	0.05	0.06	0.07	0.06
Mg	-	9.00	9.13	-	8.96	9.04	8.99	8.94	8.80	8.86
Ca	-	0.06	0.02	-	0.03	0.04	0.04	0.05	0.05	0.02
Na	-	0.00	0.00	-	0.02	0.00	0.02	0.00	0.00	0.00
K	-	0.00	0.00	-	0.01	0.00	0.00	0.00	0.00	0.00
Ni	-	-	-	-	-	-	-	-	-	-
V	-	-	-	-	-	-	-	-	-	-
P	-	0.00	0.00	-	0.00	0.01	0.00	0.00	0.00	0.01
Cation total	-	18.13	18.10	-	18.10	18.07	18.05	18.11	18.12	18.10
Mg# / An[e]	-	74.4	75.4	-	74.2	75.1	75.0	74.2	72.6	73.2
Lab[f]	-	1	1	-	1	1	1	1	1	1

Table A3. (continued)

Volcanic cone										
Sample										
Mineral[a]	OL	OL	OL	OL	OL	OL	OL	OL	OL	OL
Core ID	OL03-b3c	OL03-b4c	OL03-c1c	OL03-c2c	OL03-c3c	OL03-c4c	OL03-d1c	OL03-d2c	OL03-d3c	OL03-d4c
Major element (wt.%) [b]										
SiO_2	36.18	37.73	37.97	35.83	36.03	37.67	37.36	37.24	37.43	37.70
TiO_2	0.08	0.11	0.00	0.05	0.00	0.00	0.00	0.00	0.00	0.03
Al_2O_3	0.00	0.00	0.00	0.01	0.00	0.00	0.00	0.03	0.01	0.04
Cr_2O_3	-	-	-	-	-	-	-	-	-	-
FeO[c]	29.92	22.13	20.05	30.61	30.95	22.50	23.45	24.88	23.70	21.34
MnO	0.50	0.46	0.28	0.51	0.66	0.58	0.49	0.47	0.29	0.35
MgO	32.92	39.29	41.44	32.67	32.02	39.00	38.44	37.06	38.38	40.33
CaO	0.28	0.16	0.24	0.27	0.32	0.25	0.24	0.29	0.10	0.20
Na_2O	0.02	0.05	0.01	0.02	0.00	0.00	0.03	0.00	0.03	0.00
K_2O	0.03	0.06	0.02	0.00	0.00	0.00	0.00	0.00	0.00	0.01
NiO	-	-	-	-	-	-	-	-	-	-
V_2O_3	-	-	-	-	-	-	-	-	-	-
P_2O_5	0.06	0.01	0.00	0.04	0.03	0.00	0.00	0.04	0.06	0.00
Total[d]	100.32	100.61	100.97	100.95	99.98	100.27	100.53	100.54	100.54	100.61
Cations										
Si	5.90	5.91	5.89	5.86	5.90	5.92	5.90	5.91	5.90	5.88
Ti	0.01	0.01	0.00	0.01	0.00	0.00	0.00	0.00	0.00	0.00
Al	0.00	0.00	0.00	0.00	0.00	0.00	0.00	0.01	0.00	0.01
Cr	-	-	-	-	-	-	-	-	-	-
Fe2+	4.08	2.90	2.60	4.18	4.24	2.96	3.10	3.30	3.12	2.78
Mn	0.07	0.06	0.04	0.07	0.09	0.08	0.06	0.06	0.04	0.05
Mg	8.00	9.17	9.58	7.96	7.82	9.14	9.05	8.76	9.01	9.37
Ca	0.05	0.03	0.04	0.05	0.06	0.04	0.04	0.05	0.02	0.03
Na	0.01	0.01	0.00	0.01	0.00	0.00	0.01	0.00	0.01	0.00
K	0.01	0.01	0.00	0.00	0.00	0.00	0.00	0.00	0.00	0.00
Ni	-	-	-	-	-	-	-	-	-	-
V	-	-	-	-	-	-	-	-	-	-
P	0.01	0.00	0.00	0.00	0.00	0.00	0.00	0.01	0.01	0.00
Cation total	18.14	18.10	18.15	18.14	18.11	18.14	18.16	18.10	18.11	18.12
Mg# / An[e]	66.2	76.0	78.7	65.6	64.8	75.5	74.5	72.6	74.3	77.1
Lab[f]	1	1	1	1	1	1	1	1	1	1
Mineral[a]	OL	OL	OL	OL	OL	OL	OL	OL	OL	OL
Rim ID	OL03-b3r	OL03-b4r	OL03-c1r	OL03-c2r	OL03-c3r	OL03-c4r	OL03-d1r	OL03-d2r	OL03-d3r	OL03-d4r
Major element (wt.%)[b]										
SiO_2	37.08	36.93	37.15	37.26	37.60	37.13	37.15	37.47	37.30	36.98
TiO_2	0.05	0.03	0.13	0.04	0.07	0.04	0.07	0.03	0.02	0.01
Al_2O_3	0.00	0.00	0.01	0.00	0.00	0.00	0.06	0.00	0.05	0.00
Cr_2O_3	-	-	-	-	-	-	-	-	-	-
FeO[c]	24.58	25.54	24.52	25.71	24.02	25.27	25.60	24.36	25.04	26.38
MnO	0.46	0.41	0.38	0.37	0.43	0.60	0.50	0.45	0.43	0.48
MgO	37.48	36.83	37.53	36.40	37.61	36.64	36.29	37.41	36.94	35.73
CaO	0.34	0.19	0.24	0.22	0.26	0.27	0.24	0.26	0.21	0.22
Na_2O	0.00	0.00	0.01	0.00	0.00	0.05	0.06	0.00	0.00	0.05
K_2O	0.01	0.01	0.02	0.00	0.01	0.01	0.03	0.02	0.00	0.06
NiO	-	-	-	-	-	-	-	-	-	-
V_2O_3	-	-	-	-	-	-	-	-	-	-
P_2O_5	0.00	0.06	0.00	0.00	0.00	0.00	0.00	0.00	0.00	0.08
Total[d]	102.40	99.46	96.74	101.44	100.32	101.78	99.07	96.83	98.03	98.34
Cations										
Si	5.89	5.88	5.89	5.93	5.94	5.91	5.92	5.94	5.93	5.91
Ti	0.01	0.00	0.02	0.00	0.01	0.00	0.01	0.00	0.00	0.00
Al	0.00	0.00	0.00	0.00	0.00	0.00	0.01	0.00	0.01	0.00
Cr	-	-	-	-	-	-	-	-	-	-
Fe2+	3.26	3.40	3.25	3.42	3.17	3.36	3.41	3.23	3.33	3.52
Mn	0.06	0.05	0.05	0.05	0.06	0.08	0.07	0.06	0.06	0.07
Mg	8.87	8.74	8.88	8.64	8.85	8.69	8.62	8.83	8.75	8.51
Ca	0.06	0.03	0.04	0.04	0.04	0.04	0.04	0.04	0.04	0.04
Na	0.00	0.00	0.00	0.00	0.00	0.02	0.02	0.00	0.00	0.02
K	0.00	0.00	0.00	0.00	0.00	0.00	0.01	0.00	0.00	0.01
Ni	-	-	-	-	-	-	-	-	-	-
V	-	-	-	-	-	-	-	-	-	-
P	0.00	0.01	0.00	0.00	0.00	0.00	0.00	0.00	0.00	0.01
Cation total	18.15	18.11	18.13	18.08	18.07	18.10	18.11	18.10	18.12	18.09
Mg# / An[e]	73.1	72.0	73.2	71.6	73.6	72.1	71.7	73.2	72.4	70.7
Lab[f]	1	1	1	1	1	1	1	1	1	1

Table A3. (continued)

Volcanic cone	Nakadake									
Sample	NKD14									
Mineral[a]	PL	PL	PL	PL	PL	PL	PL	PL	PL	PL
Core ID	O-pl-c	1-m1,2h-core	a2-c	a3-m1h,core	a4-c	a5-c	a6-c	b1-c	b2-c	b3-c
Major element (wt.%) [b]										
SiO_2	52.13	52.21	50.21	51.39	50.55	51.00	48.53	46.80	51.40	49.31
TiO_2	0.07	0.04	0.00	0.05	0.00	0.08	0.10	0.14	0.00	0.07
Al_2O_3	28.74	28.96	30.84	29.60	30.51	29.95	31.81	33.00	29.98	31.35
Cr_2O_3	-	-	-	-	-	-	-	-	-	-
FeO[c]	1.33	1.03	0.69	1.04	0.93	0.84	0.96	1.01	0.69	0.74
MnO	0.12	0.03	0.02	0.00	0.00	0.00	0.00	0.00	0.02	0.06
MgO	0.16	0.08	0.11	0.17	0.03	0.11	0.04	0.09	0.09	0.10
CaO	12.66	12.95	14.53	13.40	14.15	14.00	15.73	16.95	13.66	15.10
Na_2O	4.33	4.25	3.30	3.84	3.56	3.63	2.66	1.86	3.71	2.98
K_2O	0.46	0.43	0.29	0.49	0.26	0.38	0.18	0.16	0.45	0.28
NiO	-	-	-	-	-	-	-	-	-	-
V_2O_3	-	-	-	-	-	-	-	-	-	-
P_2O_5	0.00	0.02	0.00	0.03	0.01	0.00	0.00	0.00	0.00	0.00
Total[d]	100.54	99.11	99.31	99.44	98.82	99.15	99.26	99.07	98.54	98.56
Cations										
Si	7.18	7.16	6.90	7.06	6.95	7.01	6.71	6.50	7.06	6.79
Ti	0.01	0.00	0.00	0.01	0.00	0.01	0.01	0.02	0.00	0.01
Al	4.66	4.68	5.00	4.79	4.94	4.85	5.18	5.40	4.85	5.09
Cr	-	-	-	-	-	-	-	-	-	-
Fe2+	0.15	0.12	0.08	0.12	0.11	0.10	0.11	0.12	0.08	0.08
Mn	0.01	0.00	0.00	0.00	0.00	0.00	0.00	0.00	0.00	0.01
Mg	0.03	0.02	0.02	0.03	0.01	0.02	0.01	0.02	0.02	0.02
Ca	1.87	1.90	2.14	1.97	2.08	2.06	2.33	2.52	2.01	2.23
Na	1.15	1.13	0.88	1.02	0.95	0.97	0.71	0.50	0.99	0.80
K	0.08	0.08	0.05	0.09	0.05	0.07	0.03	0.03	0.08	0.05
Ni	-	-	-	-	-	-	-	-	-	-
V	-	-	-	-	-	-	-	-	-	-
P	0.00	0.00	0.00	0.00	0.00	0.00	0.00	0.00	0.00	0.00
Cation total	15.14	15.09	15.07	15.09	15.09	15.09	15.09	15.11	15.09	15.08
Mg# / An[e]	61.9	62.7	70.9	65.9	68.6	68.0	76.6	83.4	67.0	73.6
Lab[f]	1	1	1	1	1	1	1	1	1	1
Mineral[a]	PL	PL	PL	PL	PL	PL	PL	PL	PL	PL
Rim ID	O-pl-r	a1-r	a2-r	a3-r	a4-r	a5-r	a6-r	b1-r	b2-r	b3-r
Major element (wt.%)[b]										
SiO_2	52.63	52.21	52.21	52.53	52.61	52.23	52.43	52.20	52.85	51.91
TiO_2	0.12	0.11	0.05	0.05	0.06	0.13	0.07	0.00	0.08	0.03
Al_2O_3	28.89	29.15	28.98	28.79	28.84	29.13	28.81	29.39	28.74	29.18
Cr_2O_3	-	-	-	-	-	-	-	-	-	-
FeO[c]	1.17	1.01	0.98	1.01	1.10	1.02	1.13	0.90	0.86	0.89
MnO	0.01	0.00	0.13	0.08	0.00	0.00	0.08	0.02	0.11	0.00
MgO	0.10	0.20	0.14	0.11	0.15	0.08	0.17	0.08	0.08	0.20
CaO	12.13	12.64	12.83	12.82	12.48	12.82	12.63	12.98	12.51	13.28
Na_2O	4.36	4.26	4.20	4.16	4.30	4.21	4.23	4.07	4.28	4.07
K_2O	0.54	0.43	0.46	0.45	0.47	0.39	0.45	0.37	0.46	0.40
NiO	-	-	-	-	-	-	-	-	-	-
V_2O_3	-	-	-	-	-	-	-	-	-	-
P_2O_5	0.05	0.00	0.00	0.00	0.00	0.00	0.00	0.00	0.01	0.04
Total[d]	100.79	101.06	98.02	98.08	100.27	100.46	98.93	99.03	99.01	99.05
Cations										
Si	7.21	7.16	7.17	7.21	7.21	7.16	7.19	7.15	7.23	7.12
Ti	0.01	0.01	0.01	0.00	0.01	0.01	0.01	0.00	0.01	0.00
Al	4.66	4.71	4.69	4.66	4.66	4.71	4.66	4.74	4.63	4.72
Cr	-	-	-	-	-	-	-	-	-	-
Fe2+	0.13	0.12	0.11	0.12	0.13	0.12	0.13	0.10	0.10	0.10
Mn	0.00	0.00	0.02	0.01	0.00	0.00	0.01	0.00	0.01	0.00
Mg	0.02	0.04	0.03	0.02	0.03	0.02	0.04	0.02	0.02	0.04
Ca	1.78	1.86	1.89	1.89	1.83	1.88	1.86	1.90	1.83	1.95
Na	1.16	1.13	1.12	1.11	1.14	1.12	1.12	1.08	1.14	1.08
K	0.09	0.08	0.08	0.08	0.08	0.07	0.08	0.07	0.08	0.07
Ni	-	-	-	-	-	-	-	-	-	-
V	-	-	-	-	-	-	-	-	-	-
P	0.01	0.00	0.00	0.00	0.00	0.00	0.00	0.00	0.00	0.00
Cation total	15.07	15.11	15.12	15.10	15.09	15.09	15.10	15.06	15.05	15.08
Mg# / An[e]	60.5	62.2	62.8	63.0	61.6	62.7	62.4	63.8	61.6	64.4
Lab[f]	1	1	1	1	1	1	1	1	1	1

Table A3. (continued)

Volcanic cone										
Sample										
Mineral[a]	PL	PL	PL	PL	PL	PL	PL	PL	PL	PL
Core ID	b4-c	b5-c	b6-c	c1a-c	c1b-c	c2-c	c3-c	c4-c1	c5-c	c6-c
Major element (wt.%) [b]										
SiO_2	51.76	50.95	51.44	52.41	51.58	52.35	49.72	51.86	52.43	53.05
TiO_2	0.00	0.15	0.09	0.08	0.00	0.19	0.10	0.00	0.07	0.13
Al_2O_3	29.55	29.94	29.65	29.05	29.61	28.97	31.00	29.52	29.19	28.70
Cr_2O_3	-	-	-	-	-	-	-	-	-	-
FeO[c]	0.86	0.89	0.83	0.69	0.90	0.75	0.85	0.78	0.87	0.89
MnO	0.00	0.08	0.00	0.03	0.05	0.08	0.04	0.08	0.00	0.00
MgO	0.07	0.10	0.09	0.12	0.13	0.15	0.10	0.11	0.10	0.06
CaO	13.39	13.68	13.60	12.77	13.19	12.99	14.75	13.18	12.70	12.31
Na_2O	3.90	3.78	3.92	4.28	4.03	4.13	3.16	4.02	4.20	4.34
K_2O	0.47	0.37	0.37	0.53	0.47	0.38	0.27	0.45	0.44	0.53
NiO	-	-	-	-	-	-	-	-	-	-
V_2O_3	-	-	-	-	-	-	-	-	-	-
P_2O_5	0.00	0.06	0.00	0.05	0.03	0.00	0.00	0.00	0.00	0.00
Total[d]	98.71	98.71	98.50	98.88	98.60	99.02	98.92	98.50	98.62	98.72
Cations										
Si	7.11	7.00	7.06	7.17	7.08	7.17	6.85	7.12	7.18	7.26
Ti	0.00	0.02	0.01	0.01	0.00	0.02	0.01	0.00	0.01	0.01
Al	4.78	4.85	4.80	4.69	4.79	4.68	5.04	4.78	4.71	4.63
Cr	-	-	-	-	-	-	-	-	-	-
Fe2+	0.10	0.10	0.10	0.08	0.10	0.09	0.10	0.09	0.10	0.10
Mn	0.00	0.01	0.00	0.00	0.01	0.01	0.00	0.01	0.00	0.00
Mg	0.02	0.02	0.02	0.02	0.03	0.03	0.02	0.02	0.02	0.01
Ca	1.97	2.01	2.00	1.87	1.94	1.90	2.18	1.94	1.86	1.80
Na	1.04	1.01	1.04	1.13	1.07	1.10	0.85	1.07	1.11	1.15
K	0.08	0.07	0.06	0.09	0.08	0.07	0.05	0.08	0.08	0.09
Ni	-	-	-	-	-	-	-	-	-	-
V	-	-	-	-	-	-	-	-	-	-
P	0.00	0.01	0.00	0.01	0.00	0.00	0.00	0.00	0.00	0.00
Cation total	15.10	15.10	15.09	15.07	15.10	15.07	15.10	15.11	15.07	15.05
Mg# / An[e]	65.4	66.6	65.8	62.3	64.5	63.3	71.9	64.5	62.6	61.0
Lab[f]	1	1	1	1	1	1	1	1	1	1
Mineral[a]	PL	PL	PL	PL	PL	PL	PL	PL	PL	PL
Rim ID	b4-r	b5-r	b6-r	c1a-r	c1b-r	c2-r1	c3-r	c4-r	c5-r	c6-r
Major element (wt.%)[b]										
SiO_2	52.80	52.10	52.11	51.80	52.80	51.25	52.07	52.23	51.83	51.84
TiO_2	0.13	0.10	0.12	0.08	0.00	0.00	0.06	0.04	0.00	0.00
Al_2O_3	28.64	29.12	29.37	29.35	28.60	29.65	29.19	28.99	29.28	29.47
Cr_2O_3	-	-	-	-	-	-	-	-	-	-
FeO[c]	1.10	1.03	0.84	1.04	0.94	1.09	0.82	0.98	1.07	0.99
MnO	0.04	0.00	0.00	0.00	0.12	0.04	0.12	0.10	0.08	0.00
MgO	0.19	0.14	0.12	0.11	0.12	0.19	0.09	0.16	0.17	0.13
CaO	12.31	12.81	12.92	13.10	12.63	13.58	13.00	12.99	13.12	13.22
Na_2O	4.33	4.21	4.09	4.04	4.31	3.76	4.16	4.06	4.02	3.96
K_2O	0.44	0.49	0.43	0.46	0.48	0.45	0.49	0.43	0.42	0.33
NiO	-	-	-	-	-	-	-	-	-	-
V_2O_3	-	-	-	-	-	-	-	-	-	-
P_2O_5	0.01	0.00	0.00	0.02	0.00	0.00	0.00	0.01	0.00	0.06
Total[d]	99.57	98.86	98.13	99.08	99.23	98.53	98.96	98.23	97.93	98.40
Cations										
Si	7.23	7.15	7.14	7.11	7.23	7.05	7.14	7.16	7.11	7.11
Ti	0.01	0.01	0.01	0.01	0.00	0.00	0.01	0.00	0.00	0.00
Al	4.62	4.71	4.74	4.75	4.62	4.81	4.72	4.68	4.74	4.76
Cr	-	-	-	-	-	-	-	-	-	-
Fe2+	0.13	0.12	0.10	0.12	0.11	0.12	0.09	0.11	0.12	0.11
Mn	0.01	0.00	0.00	0.00	0.01	0.01	0.01	0.01	0.01	0.00
Mg	0.04	0.03	0.03	0.02	0.03	0.04	0.02	0.03	0.03	0.03
Ca	1.81	1.88	1.90	1.93	1.85	2.00	1.91	1.91	1.93	1.94
Na	1.15	1.12	1.09	1.07	1.14	1.00	1.11	1.08	1.07	1.05
K	0.08	0.08	0.07	0.08	0.09	0.08	0.09	0.08	0.07	0.06
Ni	-	-	-	-	-	-	-	-	-	-
V	-	-	-	-	-	-	-	-	-	-
P	0.00	0.00	0.00	0.00	0.00	0.00	0.00	0.00	0.00	0.01
Cation total	15.08	15.10	15.08	15.09	15.08	15.11	15.10	15.06	15.08	15.07
Mg# / An[e]	61.1	62.7	63.5	64.3	61.9	66.7	63.2	63.9	64.3	64.9
Lab[f]	1	1	1	1	1	1	1	1	1	1

Table A3. (continued)

Volcanic cone										
Sample										
Mineral[a]	PL	PL	PL	PL	PL	PL	PL	PL	PL	PL
Core ID	d1-c	d2-c	d3-c	d4-c	d5-c	d6a-c	d6b-c	e1-c	e2-c	e5-c
Major element (wt.%) [b]										
SiO_2	51.90	49.96	48.43	52.07	50.73	51.71	48.05	52.60	51.63	49.55
TiO_2	0.00	0.01	0.00	0.15	0.00	0.13	0.05	0.05	0.04	0.01
Al_2O_3	29.44	30.92	31.75	29.48	30.64	29.55	31.63	28.80	29.76	31.13
Cr_2O_3	-	-	-	-	-	-	-	-	-	-
FeO[c]	0.83	0.87	0.85	0.73	0.76	0.87	1.36	0.91	0.87	0.99
MnO	0.03	0.02	0.03	0.00	0.00	0.07	0.00	0.02	0.00	0.00
MgO	0.15	0.16	0.10	0.12	0.00	0.07	0.18	0.10	0.11	0.07
CaO	13.13	14.57	15.96	12.92	14.20	13.27	15.99	12.62	13.25	15.05
Na_2O	3.96	3.23	2.69	4.02	3.39	3.91	2.43	4.41	3.99	2.93
K_2O	0.47	0.25	0.19	0.51	0.29	0.42	0.31	0.49	0.35	0.27
NiO	-	-	-	-	-	-	-	-	-	-
V_2O_3	-	-	-	-	-	-	-	-	-	-
P_2O_5	0.08	0.00	0.00	0.00	0.00	0.00	0.00	0.00	0.00	0.00
Total[d]	99.13	98.49	98.02	98.63	97.98	98.72	98.33	98.84	98.67	98.34
Cations										
Si	7.11	6.87	6.70	7.13	6.97	7.09	6.67	7.21	7.08	6.83
Ti	0.00	0.00	0.00	0.02	0.00	0.01	0.01	0.01	0.00	0.00
Al	4.75	5.01	5.17	4.76	4.96	4.78	5.17	4.66	4.81	5.06
Cr	-	-	-	-	-	-	-	-	-	-
Fe2+	0.10	0.10	0.10	0.08	0.09	0.10	0.16	0.10	0.10	0.11
Mn	0.00	0.00	0.00	0.00	0.00	0.01	0.00	0.00	0.00	0.00
Mg	0.03	0.03	0.02	0.02	0.00	0.01	0.04	0.02	0.02	0.02
Ca	1.93	2.15	2.36	1.90	2.09	1.95	2.38	1.85	1.95	2.22
Na	1.05	0.86	0.72	1.07	0.90	1.04	0.66	1.17	1.06	0.78
K	0.08	0.05	0.03	0.09	0.05	0.07	0.05	0.08	0.06	0.05
Ni	-	-	-	-	-	-	-	-	-	-
V	-	-	-	-	-	-	-	-	-	-
P	0.01	0.00	0.00	0.00	0.00	0.00	0.00	0.00	0.00	0.00
Cation total	15.06	15.07	15.10	15.07	15.06	15.06	15.14	15.10	15.08	15.07
Mg# / An[e]	64.8	71.4	76.6	64.0	69.9	65.2	78.3	61.3	64.8	74.0
Lab[f]	1	1	1	1	1	1	1	1	1	1
Mineral[a]	PL	PL	PL	PL	PL	PL	PL	PL	PL	PL
Rim ID	d1-r	d2-r	d3-r	d4-r	d5-r	d6a-r	d6b-r	e1-r	e2-r	e5-r
Major element (wt.%)[b]										
SiO_2	52.75	51.45	51.61	52.26	52.42	51.23	53.17	52.26	52.09	52.11
TiO_2	0.03	0.07	0.07	0.08	0.01	0.01	0.11	0.05	0.05	0.02
Al_2O_3	28.78	29.56	29.31	29.18	28.86	29.78	28.47	28.94	29.04	29.12
Cr_2O_3	-	-	-	-	-	-	-	-	-	-
FeO[c]	1.14	0.96	1.09	1.07	1.05	1.12	0.96	1.11	1.13	1.16
MnO	0.02	0.13	0.03	0.00	0.02	0.02	0.07	0.00	0.06	0.00
MgO	0.09	0.09	0.11	0.07	0.14	0.12	0.15	0.17	0.13	0.17
CaO	12.28	13.35	13.31	12.91	12.79	13.71	12.02	12.73	12.90	13.00
Na_2O	4.42	3.97	3.98	4.01	4.20	3.68	4.47	4.30	4.11	4.05
K_2O	0.46	0.40	0.50	0.41	0.51	0.33	0.57	0.44	0.47	0.38
NiO	-	-	-	-	-	-	-	-	-	-
V_2O_3	-	-	-	-	-	-	-	-	-	-
P_2O_5	0.03	0.00	0.00	0.01	0.00	0.00	0.01	0.00	0.02	0.00
Total[d]	98.75	98.87	98.60	98.76	98.12	99.34	99.01	100.15	98.31	99.33
Cations										
Si	7.22	7.07	7.10	7.16	7.19	7.04	7.27	7.17	7.15	7.15
Ti	0.00	0.01	0.01	0.01	0.00	0.00	0.01	0.00	0.01	0.00
Al	4.64	4.79	4.75	4.71	4.67	4.82	4.59	4.68	4.70	4.71
Cr	-	-	-	-	-	-	-	-	-	-
Fe2+	0.13	0.11	0.12	0.12	0.12	0.13	0.11	0.13	0.13	0.13
Mn	0.00	0.02	0.00	0.00	0.00	0.00	0.01	0.00	0.01	0.00
Mg	0.02	0.02	0.02	0.01	0.03	0.03	0.03	0.04	0.03	0.04
Ca	1.80	1.97	1.96	1.89	1.88	2.02	1.76	1.87	1.90	1.91
Na	1.17	1.06	1.06	1.07	1.12	0.98	1.19	1.15	1.09	1.08
K	0.08	0.07	0.09	0.07	0.09	0.06	0.10	0.08	0.08	0.07
Ni	-	-	-	-	-	-	-	-	-	-
V	-	-	-	-	-	-	-	-	-	-
P	0.00	0.00	0.00	0.00	0.00	0.00	0.00	0.00	0.00	0.00
Cation total	15.06	15.12	15.11	15.04	15.10	15.08	15.07	15.12	15.10	15.09
Mg# / An[e]	60.6	65.0	64.9	63.9	62.7	67.3	59.7	61.9	63.5	63.9
Lab[f]	1	1	1	1	1	1	1	1	1	1

Table A3. (continued)

Volcanic cone		Kamikomezuka								
Sample		KKO								
Mineral[a]	PL	PL	PL	PL	PL	PL	PL	PL	PL	PL
Core ID	e6-c	PL03-a1-c1	PL03-a2c1	PL03-a4c1	PL03-a6c	PL03-a7c	PL03-b2c2	PL03-b3c	PL03-b4c	PL03-b5c2
Major element (wt.%) [b]										
SiO_2	51.90	49.71	52.29	45.69	52.15	52.16	46.87	52.02	46.86	53.92
TiO_2	0.09	0.15	0.00	0.02	0.00	0.09	0.05	0.02	0.03	0.03
Al_2O_3	29.46	30.96	29.22	34.04	29.71	29.22	33.09	29.52	33.10	28.21
Cr_2O_3	-	-	-	-	-	-	-	-	-	-
FeO[c]	0.93	1.00	0.80	0.62	0.78	0.99	0.71	0.83	0.58	0.87
MnO	0.10	0.00	0.13	0.04	0.01	0.00	0.08	0.12	0.00	0.03
MgO	0.11	0.10	0.12	0.10	0.07	0.10	0.10	0.15	0.10	0.10
CaO	12.84	14.87	12.92	17.99	13.08	13.09	17.23	13.22	17.41	11.99
Na_2O	4.15	2.89	4.09	1.48	3.82	3.96	1.84	3.68	1.81	4.40
K_2O	0.42	0.22	0.43	0.02	0.38	0.40	0.02	0.42	0.04	0.44
NiO	-	-	-	-	-	-	-	-	-	-
V_2O_3	-	-	-	-	-	-	-	-	-	-
P_2O_5	0.00	0.09	0.00	0.00	0.00	0.00	0.00	0.00	0.07	0.00
Total[d]	99.16	97.65	97.91	97.31	98.45	97.46	96.55	97.34	97.62	97.99
Cations										
Si	7.12	6.84	7.17	6.35	7.14	7.16	6.49	7.13	6.48	7.35
Ti	0.01	0.02	0.00	0.00	0.00	0.01	0.01	0.00	0.00	0.00
Al	4.76	5.02	4.72	5.58	4.79	4.73	5.40	4.77	5.40	4.53
Cr	-	-	-	-	-	-	-	-	-	-
Fe2+	0.11	0.12	0.09	0.07	0.09	0.11	0.08	0.10	0.07	0.10
Mn	0.01	0.00	0.02	0.00	0.00	0.00	0.01	0.01	0.00	0.00
Mg	0.02	0.02	0.02	0.02	0.01	0.02	0.02	0.03	0.02	0.02
Ca	1.89	2.19	1.90	2.68	1.92	1.93	2.56	1.94	2.58	1.75
Na	1.10	0.77	1.09	0.40	1.01	1.05	0.50	0.98	0.49	1.16
K	0.07	0.04	0.08	0.00	0.07	0.07	0.00	0.07	0.01	0.08
Ni	-	-	-	-	-	-	-	-	-	-
V	-	-	-	-	-	-	-	-	-	-
P	0.00	0.01	0.00	0.00	0.00	0.00	0.00	0.00	0.01	0.00
Cation total	15.09	15.03	15.08	15.11	15.03	15.07	15.07	15.03	15.05	15.01
Mg# / An[e]	63.2	74.0	63.6	87.0	65.4	64.7	83.8	66.5	84.2	60.1
Lab[f]	1	1	1	1	1	1	1	1	1	1
Mineral[a]	PL	PL	PL	PL	PL	PL	PL	PL	PL	PL
Rim ID	e6-r	PL03-a1r1	PL03-a2r1	PL03-a4r1	PL03-a6r	PL03-a7r	PL03-b2r	PL03-b3r	PL03-b4r	PL03-b5r1
Major element (wt.%)[b]										
SiO_2	52.28	51.06	50.75	48.19	50.97	50.89	45.66	48.96	50.28	-
TiO_2	0.15	0.09	0.03	0.00	0.09	0.03	0.00	0.00	0.15	-
Al_2O_3	29.03	29.75	29.95	31.93	29.96	30.02	33.95	31.37	30.36	-
Cr_2O_3	-	-	-	-	-	-	-	-	-	-
FeO[c]	1.12	1.24	1.22	0.99	1.06	1.15	0.66	0.98	1.07	-
MnO	0.09	0.00	0.04	0.07	0.00	0.00	0.00	0.05	0.00	-
MgO	0.18	0.12	0.20	0.17	0.12	0.07	0.08	0.15	0.17	-
CaO	12.67	14.09	14.17	16.06	13.98	13.99	18.49	15.64	14.64	-
Na_2O	4.06	3.48	3.48	2.51	3.57	3.70	1.12	2.76	3.19	-
K_2O	0.41	0.18	0.15	0.09	0.23	0.16	0.05	0.09	0.13	-
NiO	-	-	-	-	-	-	-	-	-	-
V_2O_3	-	-	-	-	-	-	-	-	-	-
P_2O_5	0.00	0.00	0.00	0.00	0.02	0.00	0.00	0.00	0.00	-
Total[d]	99.66	97.75	97.33	98.87	96.17	99.89	97.79	98.06	98.34	-
Cations										-
Si	7.17	7.03	6.98	6.66	7.00	7.01	6.35	6.77	6.92	-
Ti	0.02	0.01	0.00	0.00	0.01	0.00	0.00	0.00	0.02	-
Al	4.69	4.83	4.86	5.20	4.85	4.87	5.56	5.11	4.93	-
Cr	-	-	-	-	-	-	-	-	-	-
Fe2+	0.13	0.14	0.14	0.11	0.12	0.13	0.08	0.11	0.12	-
Mn	0.01	0.00	0.00	0.01	0.00	0.00	0.00	0.01	0.00	-
Mg	0.04	0.02	0.04	0.03	0.02	0.01	0.02	0.03	0.03	-
Ca	1.86	2.08	2.09	2.38	2.06	2.07	2.75	2.32	2.16	-
Na	1.08	0.93	0.93	0.67	0.95	0.99	0.30	0.74	0.85	-
K	0.07	0.03	0.03	0.02	0.04	0.03	0.01	0.02	0.02	-
Ni	-	-	-	-	-	-	-	-	-	-
V	-	-	-	-	-	-	-	-	-	-
P	0.00	0.00	0.00	0.00	0.00	0.00	0.00	0.00	0.00	-
Cation total	15.07	15.07	15.07	15.09	15.06	15.11	15.06	15.10	15.06	-
Mg# / An[e]	63.3	69.1	69.3	78.0	68.4	67.7	90.1	75.8	71.7	-
Lab[f]	1	1	1	1	1	1	1	1	1	-

Table A3. (continued)

Volcanic cone										
Sample										
Mineral[a]	PL	PL	PL	PL	PL	PL	PL	PL	PL	PL
Core ID	PL03-b6c	PL03-b7c	PL03-c1c	PL03-c2c	PL03-c4c	PL03-c5c	PL03-c6c	PL03-c7c	PL03-d1c	PL03-d2c
Major element (wt.%) [b]										
SiO_2	53.64	51.01	53.64	52.86	48.12	52.89	53.41	52.11	52.89	45.41
TiO_2	0.09	0.10	0.00	0.00	0.12	0.10	0.00	0.05	0.00	0.00
Al_2O_3	28.59	29.96	28.41	29.02	32.06	28.92	28.56	29.26	28.96	34.16
Cr_2O_3	-	-	-	-	-	-	-	-	-	-
FeO[c]	0.82	0.87	0.66	0.77	1.03	0.65	0.76	0.75	1.01	0.78
MnO	0.00	0.01	0.00	0.05	0.00	0.03	0.00	0.12	0.00	0.08
MgO	0.02	0.08	0.08	0.03	0.00	0.19	0.05	0.08	0.15	0.07
CaO	11.94	14.02	12.02	12.78	16.08	12.50	12.54	13.23	12.48	18.36
Na_2O	4.41	3.55	4.64	3.98	2.42	4.23	4.16	3.97	3.99	1.15
K_2O	0.51	0.39	0.49	0.47	0.16	0.49	0.52	0.43	0.52	0.00
NiO	-	-	-	-	-	-	-	-	-	-
V_2O_3	-	-	-	-	-	-	-	-	-	-
P_2O_5	0.00	0.00	0.05	0.02	0.00	0.00	0.00	0.00	0.00	0.00
Total[d]	97.61	97.93	99.03	96.49	97.36	97.73	96.65	97.84	97.29	98.85
Cations										
Si	7.32	7.01	7.32	7.22	6.66	7.23	7.30	7.14	7.23	6.31
Ti	0.01	0.01	0.00	0.00	0.01	0.01	0.00	0.01	0.00	0.00
Al	4.60	4.86	4.57	4.67	5.23	4.66	4.60	4.73	4.66	5.59
Cr	-	-	-	-	-	-	-	-	-	-
Fe2+	0.09	0.10	0.08	0.09	0.12	0.07	0.09	0.09	0.11	0.09
Mn	0.00	0.00	0.00	0.01	0.00	0.00	0.00	0.01	0.00	0.01
Mg	0.00	0.02	0.02	0.01	0.00	0.04	0.01	0.02	0.03	0.01
Ca	1.75	2.06	1.76	1.87	2.38	1.83	1.84	1.94	1.83	2.73
Na	1.17	0.95	1.23	1.06	0.65	1.12	1.10	1.05	1.06	0.31
K	0.09	0.07	0.08	0.08	0.03	0.09	0.09	0.08	0.09	0.00
Ni	-	-	-	-	-	-	-	-	-	-
V	-	-	-	-	-	-	-	-	-	-
P	0.00	0.00	0.01	0.00	0.00	0.00	0.00	0.00	0.00	0.00
Cation total	15.02	15.08	15.05	15.01	15.08	15.06	15.03	15.07	15.02	15.06
Mg# / An[e]	60.0	68.6	58.9	63.9	78.6	62.0	62.5	64.8	63.4	89.9
Lab[f]	1	1	1	1	1	1	1	1	1	1
Mineral[a]	PL	PL	PL	PL	PL	PL	PL	PL	PL	PL
Rim ID	PL03-b6r	PL03-b7r	PL03-c1r	PL03-c2r-ou	PL03-c4r	PL03-c5r	PL03-c6r	PL03-c7r	PL03-d1r	PL03-d2r
Major element (wt.%)[b]										
SiO_2	48.14	47.23	50.90	51.10	47.53	50.39	50.57	50.60	49.70	45.40
TiO_2	0.00	0.05	0.03	0.10	0.02	0.14	0.02	0.12	0.00	0.12
Al_2O_3	32.04	32.67	29.94	29.75	32.29	30.27	30.06	30.11	30.88	34.18
Cr_2O_3	-	-	-	-	-	-	-	-	-	-
FeO[c]	0.99	0.98	1.27	1.13	1.04	1.12	1.17	1.31	0.99	0.58
MnO	0.00	0.00	0.05	0.09	0.00	0.03	0.03	0.00	0.00	0.05
MgO	0.10	0.07	0.17	0.10	0.14	0.17	0.19	0.07	0.19	0.05
CaO	16.35	16.82	14.10	13.97	17.04	14.48	14.36	14.09	15.07	18.50
Na_2O	2.27	2.06	3.43	3.55	1.92	3.27	3.43	3.58	3.07	1.12
K_2O	0.11	0.11	0.10	0.21	0.02	0.14	0.17	0.13	0.11	0.00
NiO	-	-	-	-	-	-	-	-	-	-
V_2O_3	-	-	-	-	-	-	-	-	-	-
P_2O_5	0.00	0.00	0.00	0.00	0.00	0.00	0.00	0.00	0.00	0.00
Total[d]	97.25	97.39	97.13	97.18	96.67	97.39	97.51	98.34	98.45	97.36
Cations										
Si	6.65	6.55	7.00	7.03	6.58	6.93	6.97	6.97	6.86	6.31
Ti	0.00	0.01	0.00	0.01	0.00	0.01	0.00	0.01	0.00	0.01
Al	5.22	5.34	4.85	4.82	5.26	4.91	4.88	4.89	5.02	5.60
Cr	-	-	-	-	-	-	-	-	-	-
Fe2+	0.11	0.11	0.15	0.13	0.12	0.13	0.14	0.15	0.11	0.07
Mn	0.00	0.00	0.01	0.01	0.00	0.00	0.00	0.00	0.00	0.01
Mg	0.02	0.01	0.03	0.02	0.03	0.03	0.04	0.01	0.04	0.01
Ca	2.42	2.50	2.08	2.06	2.53	2.14	2.12	2.08	2.23	2.75
Na	0.61	0.55	0.91	0.95	0.52	0.87	0.92	0.95	0.82	0.30
K	0.02	0.02	0.02	0.04	0.00	0.02	0.03	0.02	0.02	0.00
Ni	-	-	-	-	-	-	-	-	-	-
V	-	-	-	-	-	-	-	-	-	-
P	0.00	0.00	0.00	0.00	0.00	0.00	0.00	0.00	0.00	0.00
Cation total	15.06	15.09	15.04	15.07	15.04	15.06	15.09	15.09	15.10	15.06
Mg# / An[e]	79.9	81.8	69.5	68.5	83.0	71.0	69.8	68.5	73.1	90.1
Lab[f]	1	1	1	1	1	1	1	1	1	1

Table A3. (continued)

Volcanic cone										
Sample										
Mineral[a]	PL	PL	PL	PL	PL	PL	PL	PL	PL	PL
Core ID	PL03-d3c	PL03-d4c	PL03-d5c	PL03-d6c	PL03-d7c	PL03-e1c	PL03-e2c	PL03-e3c	PL03-e5c	PL03-e6c
Major element (wt.%) [b]										
SiO_2	52.61	45.56	52.98	45.53	52.08	54.73	45.40	51.97	53.28	51.72
TiO_2	0.12	0.19	0.00	0.12	0.00	0.12	0.03	0.19	0.12	0.03
Al_2O_3	29.19	34.11	28.81	34.14	29.28	27.77	34.01	29.52	28.71	29.63
Cr_2O_3	-	-	-	-	-	-	-	-	-	-
FeO[c]	0.82	0.72	0.90	0.56	0.89	0.58	0.65	0.86	0.91	0.86
MnO	0.01	0.00	0.00	0.13	0.04	0.00	0.13	0.03	0.00	0.00
MgO	0.10	0.00	0.07	0.03	0.07	0.10	0.00	0.07	0.12	0.05
CaO	12.55	18.13	12.68	18.23	13.28	11.13	18.70	13.09	12.36	13.59
Na_2O	4.11	1.19	4.02	1.18	3.92	4.96	1.07	3.90	4.03	3.79
K_2O	0.43	0.00	0.54	0.09	0.44	0.58	0.01	0.37	0.47	0.33
NiO	-	-	-	-	-	-	-	-	-	-
V_2O_3	-	-	-	-	-	-	-	-	-	-
P_2O_5	0.05	0.09	0.00	0.00	0.00	0.02	0.00	0.00	0.00	0.00
Total[d]	97.63	98.15	98.52	98.58	97.90	96.82	97.07	97.04	97.45	97.50
Cations										
Si	7.19	6.32	7.25	6.33	7.15	7.45	6.32	7.12	7.28	7.09
Ti	0.01	0.02	0.00	0.01	0.00	0.01	0.00	0.02	0.01	0.00
Al	4.70	5.58	4.65	5.59	4.73	4.45	5.58	4.76	4.62	4.79
Cr	-	-	-	-	-	-	-	-	-	-
Fe2+	0.09	0.08	0.10	0.07	0.10	0.07	0.08	0.10	0.10	0.10
Mn	0.00	0.00	0.00	0.02	0.00	0.00	0.02	0.00	0.00	0.00
Mg	0.02	0.00	0.01	0.01	0.01	0.02	0.00	0.01	0.02	0.01
Ca	1.84	2.70	1.86	2.71	1.95	1.62	2.79	1.92	1.81	2.00
Na	1.09	0.32	1.07	0.32	1.04	1.31	0.29	1.04	1.07	1.01
K	0.08	0.00	0.09	0.02	0.08	0.10	0.00	0.07	0.08	0.06
Ni	-	-	-	-	-	-	-	-	-	-
V	-	-	-	-	-	-	-	-	-	-
P	0.01	0.01	0.00	0.00	0.00	0.00	0.00	0.00	0.00	0.00
Cation total	15.03	15.03	15.03	15.06	15.07	15.03	15.07	15.04	14.99	15.06
Mg# / An[e]	62.8	89.3	63.5	89.5	65.2	55.4	90.6	65.0	62.9	66.5
Lab[f]	1	1	1	1	1	1	1	1	1	1
Mineral[a]	PL	PL	PL	PL	PL	PL	PL	PL	PL	PL
Rim ID	PL03-d3r	PL03-d4r	PL03-d5r	PL03-d6r	PL03-d7r	PL03-e1r	PL03-e2r	PL03-e3r	PL03-e5r	PL03-e6r
Major element (wt.%)[b]										
SiO_2	50.04	50.80	51.12	51.17	51.02	51.52	49.47	51.24	50.29	50.26
TiO_2	0.00	0.00	0.10	0.07	0.00	0.12	0.00	0.03	0.05	0.13
Al_2O_3	30.49	29.98	30.02	29.62	30.01	29.43	31.21	29.74	30.23	30.26
Cr_2O_3	-	-	-	-	-	-	-	-	-	-
FeO[c]	1.09	1.20	0.95	1.35	1.04	1.22	0.90	1.04	1.16	1.09
MnO	0.03	0.00	0.12	0.00	0.00	0.08	0.00	0.00	0.07	0.00
MgO	0.12	0.12	0.12	0.14	0.15	0.16	0.15	0.14	0.17	0.18
CaO	14.94	14.32	13.80	13.80	14.18	13.39	15.42	14.10	14.60	14.50
Na_2O	3.15	3.41	3.58	3.70	3.46	3.78	2.71	3.48	3.29	3.36
K_2O	0.12	0.17	0.19	0.16	0.11	0.30	0.14	0.23	0.15	0.12
NiO	-	-	-	-	-	-	-	-	-	-
V_2O_3	-	-	-	-	-	-	-	-	-	-
P_2O_5	0.02	0.00	0.00	0.00	0.02	0.00	0.00	0.00	0.00	0.09
Total[d]	97.61	97.62	100.14	97.54	97.29	101.24	97.52	97.58	98.44	99.36
Cations										
Si	6.89	7.00	7.02	7.04	7.00	7.08	6.82	7.04	6.93	6.92
Ti	0.00	0.00	0.01	0.01	0.00	0.01	0.00	0.00	0.01	0.01
Al	4.95	4.87	4.85	4.80	4.86	4.77	5.07	4.82	4.91	4.91
Cr	-	-	-	-	-	-	-	-	-	-
Fe2+	0.13	0.14	0.11	0.15	0.12	0.14	0.10	0.12	0.13	0.13
Mn	0.00	0.00	0.01	0.00	0.00	0.01	0.00	0.00	0.01	0.00
Mg	0.02	0.02	0.02	0.03	0.03	0.03	0.03	0.03	0.03	0.04
Ca	2.20	2.11	2.03	2.03	2.09	1.97	2.28	2.07	2.16	2.14
Na	0.84	0.91	0.95	0.99	0.92	1.01	0.72	0.93	0.88	0.90
K	0.02	0.03	0.03	0.03	0.02	0.05	0.02	0.04	0.03	0.02
Ni	-	-	-	-	-	-	-	-	-	-
V	-	-	-	-	-	-	-	-	-	-
P	0.00	0.00	0.00	0.00	0.00	0.00	0.00	0.00	0.00	0.01
Cation total	15.06	15.08	15.04	15.09	15.04	15.07	15.06	15.05	15.09	15.07
Mg# / An[e]	72.4	69.9	68.1	67.3	69.3	66.2	75.9	69.1	71.1	70.4
Lab[f]	1	1	1	1	1	1	1	1	1	1

Table A3. (continued)

Volcanic cone							Ojodake			
Sample							OJSU			
Mineral[a]	PL	PL	PL	PL	PL	PL	PL	PL	PL	PL
Core ID	PL03-e7c	PL03-f1c	PL03-f3-1c	PL03-f3-2c	PL03-f6c	PL03-f7c	PL01-a1c	PL01-a2c	PL01-a3c	PL01-a4c
Major element (wt.%) [b]										
SiO_2	53.75	50.35	47.34	48.53	52.17	44.95	52.63	50.01	51.03	48.01
TiO_2	0.07	0.15	0.12	0.07	0.00	0.03	0.04	0.08	0.15	0.05
Al_2O_3	28.12	30.34	32.53	32.17	29.43	34.52	28.77	30.50	29.77	32.34
Cr_2O_3	-	-	-	-	-	-	-	-	-	-
FeO[c]	0.86	0.78	0.90	0.80	0.79	0.72	0.88	0.97	1.04	0.75
MnO	0.01	0.07	0.17	0.00	0.00	0.03	0.11	0.07	0.08	0.00
MgO	0.14	0.10	0.14	0.02	0.14	0.05	0.12	0.05	0.14	0.12
CaO	11.93	14.56	16.75	15.90	13.35	18.76	12.54	14.45	13.53	16.06
Na_2O	4.52	3.21	2.03	2.42	3.78	0.94	4.36	3.59	3.89	2.56
K_2O	0.60	0.34	0.02	0.10	0.35	0.00	0.52	0.28	0.36	0.10
NiO	-	-	-	-	-	-	-	-	-	-
V_2O_3	-	-	-	-	-	-	-	-	-	-
P_2O_5	0.00	0.09	0.00	0.00	0.00	0.00	0.02	0.00	0.00	0.00
Total[d]	97.71	96.96	97.74	96.81	97.60	97.77	98.15	98.71	99.54	98.47
Cations										
Si	7.34	6.92	6.56	6.70	7.15	6.25	7.21	6.90	7.02	6.64
Ti	0.01	0.02	0.01	0.01	0.00	0.00	0.00	0.01	0.02	0.01
Al	4.53	4.92	5.32	5.23	4.75	5.66	4.64	4.96	4.82	5.27
Cr	-	-	-	-	-	-	-	-	-	-
Fe2+	0.10	0.09	0.10	0.09	0.09	0.08	0.10	0.11	0.12	0.09
Mn	0.00	0.01	0.02	0.00	0.00	0.00	0.01	0.01	0.01	0.00
Mg	0.03	0.02	0.03	0.00	0.03	0.01	0.02	0.01	0.03	0.03
Ca	1.75	2.15	2.49	2.35	1.96	2.80	1.84	2.14	1.99	2.38
Na	1.20	0.86	0.55	0.65	1.01	0.25	1.16	0.96	1.04	0.69
K	0.11	0.06	0.00	0.02	0.06	0.00	0.09	0.05	0.06	0.02
Ni	-	-	-	-	-	-	-	-	-	-
V	-	-	-	-	-	-	-	-	-	-
P	0.00	0.01	0.00	0.00	0.00	0.00	0.00	0.00	0.00	0.00
Cation total	15.05	15.05	15.08	15.05	15.04	15.07	15.07	15.15	15.11	15.13
Mg# / An[e]	59.3	71.5	82.0	78.4	66.1	91.7	61.3	69.0	65.7	77.5
Lab[f]	1	1	1	1	1	1	1	1	1	1
Mineral[a]	PL	PL	PL	PL	PL	PL	PL	PL	PL	PL
Rim ID	PL03-e7r	PL03-f1r	PL03-f3-1r	PL03-f3-2r	PL03-f6r	PL03-f7r	PL01-a1r	PL01-a2r	PL01-a3r	PL01-a4r
Major element (wt.%)[b]										
SiO_2	51.10	50.83	50.30	51.36	50.93	50.81	52.13	50.80	51.44	48.68
TiO_2	0.02	0.03	0.03	0.03	0.07	0.05	0.01	0.09	0.11	0.07
Al_2O_3	29.96	29.92	30.28	29.44	30.11	29.95	29.43	29.89	29.66	31.46
Cr_2O_3	-	-	-	-	-	-	-	-	-	-
FeO[c]	1.00	1.20	1.12	1.17	1.00	1.09	0.84	1.27	0.90	1.03
MnO	0.00	0.06	0.05	0.08	0.03	0.07	0.04	0.00	0.09	0.04
MgO	0.07	0.13	0.20	0.07	0.17	0.20	0.11	0.20	0.18	0.15
CaO	14.30	14.12	14.47	13.92	14.14	14.25	12.80	13.57	13.17	15.70
Na_2O	3.47	3.50	3.38	3.65	3.36	3.46	4.26	3.93	4.09	2.68
K_2O	0.09	0.14	0.16	0.28	0.20	0.12	0.37	0.21	0.32	0.20
NiO	-	-	-	-	-	-	-	-	-	-
V_2O_3	-	-	-	-	-	-	-	-	-	-
P_2O_5	0.00	0.05	0.00	0.00	0.00	0.00	0.00	0.05	0.04	0.00
Total[d]	97.56	99.70	97.83	97.81	98.26	99.04	100.12	101.35	100.88	96.29
Cations										
Si	7.03	6.99	6.93	7.07	6.99	6.99	7.14	6.99	7.06	6.73
Ti	0.00	0.00	0.00	0.00	0.01	0.01	0.00	0.01	0.01	0.01
Al	4.86	4.85	4.92	4.78	4.87	4.86	4.75	4.85	4.80	5.13
Cr	-	-	-	-	-	-	-	-	-	-
Fe2+	0.12	0.14	0.13	0.13	0.11	0.13	0.10	0.15	0.10	0.12
Mn	0.00	0.01	0.01	0.01	0.00	0.01	0.00	0.00	0.01	0.01
Mg	0.01	0.03	0.04	0.01	0.03	0.04	0.02	0.04	0.04	0.03
Ca	2.11	2.08	2.14	2.05	2.08	2.10	1.88	2.00	1.94	2.33
Na	0.93	0.93	0.90	0.97	0.90	0.92	1.13	1.05	1.09	0.72
K	0.02	0.03	0.03	0.05	0.03	0.02	0.06	0.04	0.05	0.03
Ni	-	-	-	-	-	-	-	-	-	-
V	-	-	-	-	-	-	-	-	-	-
P	0.00	0.01	0.00	0.00	0.00	0.00	0.00	0.01	0.00	0.00
Cation total	15.07	15.06	15.10	15.09	15.04	15.08	15.08	15.14	15.10	15.11
Mg# / An[e]	69.5	69.0	70.3	67.8	69.9	69.5	62.5	65.6	64.0	76.4
Lab[f]	1	1	1	1	1	1	1	1	1	1

Table A3. (continued)

Volcanic cone										
Sample										
Mineral[a]	PL	PL	PL	PL	PL	PL	PL	PL	PL	PL
Core ID	PL01-a5c	PL01-a6c	PL01-a7c	PL01-b2c	PL01-b3c	PL01-b4c	PL01-b5c	PL01-b6c	PL01-c1c	PL01-c2c
Major element (wt.%) [b]										
SiO_2	53.40	48.93	45.59	52.73	48.65	52.69	49.31	45.33	53.15	46.97
TiO_2	0.07	0.00	0.00	0.04	0.00	0.01	0.05	0.02	0.06	0.06
Al_2O_3	28.32	31.45	33.91	28.86	31.82	29.05	31.11	34.26	28.77	32.80
Cr_2O_3	-	-	-	-	-	-	-	-	-	-
FeO[c]	0.93	1.03	0.80	0.90	0.87	0.82	1.00	0.66	0.78	1.02
MnO	0.00	0.06	0.00	0.00	0.00	0.06	0.00	0.06	0.02	0.14
MgO	0.08	0.08	0.00	0.12	0.06	0.06	0.02	0.07	0.03	0.11
CaO	12.04	15.28	18.34	12.43	15.65	12.41	15.07	18.16	12.21	16.98
Na_2O	4.66	2.99	1.31	4.33	2.79	4.37	3.23	1.39	4.40	1.87
K_2O	0.49	0.18	0.05	0.57	0.16	0.53	0.19	0.04	0.57	0.04
NiO	-	-	-	-	-	-	-	-	-	-
V_2O_3	-	-	-	-	-	-	-	-	-	-
P_2O_5	0.00	0.00	0.00	0.01	0.00	0.00	0.01	0.00	0.00	0.00
Total[d]	97.23	98.00	98.33	98.44	97.85	97.90	98.06	98.56	98.35	97.98
Cations										
Si	7.30	6.76	6.34	7.22	6.73	7.21	6.80	6.30	7.26	6.52
Ti	0.01	0.00	0.00	0.00	0.00	0.00	0.01	0.00	0.01	0.01
Al	4.56	5.12	5.56	4.65	5.19	4.68	5.06	5.61	4.63	5.36
Cr	-	-	-	-	-	-	-	-	-	-
Fe2+	0.11	0.12	0.09	0.10	0.10	0.09	0.11	0.08	0.09	0.12
Mn	0.00	0.01	0.00	0.00	0.00	0.01	0.00	0.01	0.00	0.02
Mg	0.02	0.02	0.00	0.02	0.01	0.01	0.00	0.01	0.01	0.02
Ca	1.76	2.26	2.73	1.82	2.32	1.82	2.23	2.70	1.79	2.52
Na	1.23	0.80	0.35	1.15	0.75	1.16	0.86	0.38	1.17	0.50
K	0.09	0.03	0.01	0.10	0.03	0.09	0.03	0.01	0.10	0.01
Ni	-	-	-	-	-	-	-	-	-	-
V	-	-	-	-	-	-	-	-	-	-
P	0.00	0.00	0.00	0.00	0.00	0.00	0.00	0.00	0.00	0.00
Cation total	15.08	15.12	15.08	15.06	15.13	15.07	15.10	15.10	15.06	15.08
Mg# / An[e]	58.9	73.9	88.6	61.3	75.6	61.1	72.2	87.7	60.5	83.4
Lab[f]	1	1	1	1	1	1	1	1	1	1
Mineral[a]	PL	PL	PL	PL	PL	PL	PL	PL	PL	PL
Rim ID	PL01-a5r	PL01-a6r	PL01-a7r	PL01-b2r	PL01-b3r	PL01-b4r	PL01-b5r	PL01-b6r	PL01-c1r	PL01-c2r
Major element (wt.%)[b]										
SiO_2	47.30	-	49.01	47.41	47.08	45.50	-	46.90	48.43	46.51
TiO_2	0.00	-	0.02	0.02	0.03	0.00	-	0.13	0.03	0.03
Al_2O_3	32.83	-	31.18	32.34	33.03	33.99	-	32.75	31.65	33.28
Cr_2O_3	-	-	-	-	-	-	-	-	-	-
FeO[c]	0.89	-	1.06	0.87	0.81	0.74	-	0.97	1.08	0.87
MnO	0.09	-	0.08	0.12	0.09	0.16	-	0.07	0.04	0.00
MgO	0.03	-	0.06	0.09	0.05	0.09	-	0.13	0.20	0.05
CaO	16.56	-	15.32	16.65	16.94	18.00	-	16.89	15.82	17.31
Na_2O	2.23	-	2.96	2.37	1.95	1.45	-	2.03	2.53	1.79
K_2O	0.08	-	0.24	0.11	0.02	0.07	-	0.12	0.20	0.17
NiO	-	-	-	-	-	-	-	-	-	-
V_2O_3	-	-	-	-	-	-	-	-	-	-
P_2O_5	0.00	-	0.07	0.00	0.00	0.00	-	0.00	0.01	0.00
Total[d]	102.01	-	97.77	96.14	99.96	99.02	-	96.98	98.90	98.87
Cations		-					-			
Si	6.55	-	6.77	6.58	6.52	6.33	-	6.51	6.69	6.46
Ti	0.00	-	0.00	0.00	0.00	0.00	-	0.01	0.00	0.00
Al	5.36	-	5.07	5.29	5.39	5.58	-	5.35	5.16	5.45
Cr	-	-	-	-	-	-	-	-	-	-
Fe2+	0.10	-	0.12	0.10	0.09	0.09	-	0.11	0.13	0.10
Mn	0.01	-	0.01	0.01	0.01	0.02	-	0.01	0.00	0.00
Mg	0.01	-	0.01	0.02	0.01	0.02	-	0.03	0.04	0.01
Ca	2.46	-	2.27	2.47	2.51	2.68	-	2.51	2.34	2.58
Na	0.60	-	0.79	0.64	0.52	0.39	-	0.55	0.68	0.48
K	0.01	-	0.04	0.02	0.00	0.01	-	0.02	0.03	0.03
Ni	-	-	-	-	-	-	-	-	-	-
V	-	-	-	-	-	-	-	-	-	-
P	0.00	-	0.01	0.00	0.00	0.00	-	0.00	0.00	0.00
Cation total	15.10	-	15.09	15.13	15.05	15.12	-	15.10	15.07	15.11
Mg# / An[e]	80.4	-	74.2	79.4	82.8	87.3	-	82.0	77.5	84.3
Lab[f]	1	-	1	1	1	1	-	1	1	1

Table A3. (continued)

Volcanic cone										
Sample										
Mineral[a]	PL	PL	PL	PL	PL	PL	PL	PL	PL	PL
Core ID	PL01-c4c	PL01-c5c	PL01-c6c?	PL01-d1c	PL01-d2c	PL01-d3c	PL01-d4c	PL01-d5c	PL01-e1c	PL01-e2c
Major element (wt.%) [b]										
SiO_2	48.51	52.29	48.72	45.85	45.82	48.54	48.99	52.70	48.33	52.82
TiO_2	0.00	0.00	0.00	0.00	0.09	0.01	0.03	0.06	0.03	0.04
Al_2O_3	31.78	29.31	31.86	33.91	33.52	31.79	31.35	28.82	32.21	28.93
Cr_2O_3	-	-	-	-	-	-	-	-	-	-
FeO[c]	0.80	0.76	0.76	0.72	0.86	0.82	0.84	0.78	0.54	0.73
MnO	0.03	0.07	0.01	0.06	0.12	0.12	0.08	0.02	0.04	0.00
MgO	0.09	0.08	0.13	0.03	0.05	0.07	0.04	0.09	0.04	0.00
CaO	15.96	12.85	15.66	17.83	17.83	15.84	15.47	12.51	15.99	12.48
Na_2O	2.69	4.17	2.70	1.55	1.62	2.68	2.96	4.51	2.70	4.38
K_2O	0.11	0.43	0.15	0.04	0.09	0.12	0.23	0.51	0.11	0.62
NiO	-	-	-	-	-	-	-	-	-	-
V_2O_3	-	-	-	-	-	-	-	-	-	-
P_2O_5	0.02	0.03	0.00	0.00	0.00	0.00	0.00	0.00	0.00	0.00
Total[d]	97.97	98.12	97.67	97.81	98.16	97.67	97.99	97.84	98.07	97.42
Cations										
Si	6.70	7.16	6.73	6.38	6.37	6.71	6.77	7.21	6.67	7.23
Ti	0.00	0.00	0.00	0.00	0.01	0.00	0.00	0.01	0.00	0.00
Al	5.17	4.73	5.19	5.56	5.49	5.18	5.10	4.65	5.24	4.67
Cr	-	-	-	-	-	-	-	-	-	-
Fe2+	0.09	0.09	0.09	0.08	0.10	0.10	0.10	0.09	0.06	0.08
Mn	0.00	0.01	0.00	0.01	0.01	0.01	0.01	0.00	0.00	0.00
Mg	0.02	0.02	0.03	0.01	0.01	0.01	0.01	0.02	0.01	0.00
Ca	2.36	1.88	2.32	2.66	2.66	2.35	2.29	1.83	2.36	1.83
Na	0.72	1.11	0.72	0.42	0.44	0.72	0.79	1.20	0.72	1.16
K	0.02	0.08	0.03	0.01	0.02	0.02	0.04	0.09	0.02	0.11
Ni	-	-	-	-	-	-	-	-	-	-
V	-	-	-	-	-	-	-	-	-	-
P	0.00	0.00	0.00	0.00	0.00	0.00	0.00	0.00	0.00	0.00
Cation total	15.08	15.08	15.11	15.13	15.11	15.10	15.11	15.10	15.08	15.08
Mg# / An[e]	76.6	62.9	76.3	86.4	85.8	76.5	74.4	60.4	76.6	61.2
Lab[f]	1	1	1	1	1	1	1	1	1	1
Mineral[a]	PL	PL	PL	PL	PL	PL	PL	PL	PL	PL
Rim ID	PL01-c4r	PL01-c5r	PL01-c6r	PL01-d1r	PL01-d2r	PL01-d3r	PL01-d4r	PL01-d5r	PL01-e1r	PL01-e2r
Major element (wt.%)[b]										
SiO_2	-	47.52	47.91	48.16	51.81	46.65	49.03	-	45.35	46.46
TiO_2	-	0.18	0.12	0.09	0.11	0.05	0.00	-	0.01	0.00
Al_2O_3	-	32.33	32.03	31.73	29.21	33.16	31.25	-	34.12	33.52
Cr_2O_3	-	-	-	-	-	-	-	-	-	-
FeO[c]	-	1.02	0.94	0.99	0.95	0.89	1.07	-	0.70	0.83
MnO	-	0.09	0.07	0.00	0.01	0.00	0.02	-	0.04	0.00
MgO	-	0.11	0.09	0.14	0.13	0.04	0.07	-	0.05	0.05
CaO	-	16.36	16.18	16.22	13.35	17.27	15.42	-	18.42	17.24
Na_2O	-	2.26	2.41	2.52	4.04	1.85	2.99	-	1.25	1.82
K_2O	-	0.13	0.18	0.14	0.38	0.08	0.15	-	0.05	0.09
NiO	-	-	-	-	-	-	-	-	-	-
V_2O_3	-	-	-	-	-	-	-	-	-	-
P_2O_5	-	0.00	0.07	0.00	0.00	0.00	0.00	-	0.00	0.00
Total[d]	-	100.02	98.89	97.84	98.74	97.04	98.05	-	96.85	101.36
Cations	-							-		
Si	-	6.58	6.63	6.66	7.11	6.48	6.77	-	6.30	6.45
Ti	-	0.02	0.01	0.01	0.01	0.00	0.00	-	0.00	0.00
Al	-	5.28	5.22	5.17	4.73	5.43	5.09	-	5.59	5.49
Cr	-	-	-	-	-	-	-	-	-	-
Fe2+	-	0.12	0.11	0.11	0.11	0.10	0.12	-	0.08	0.10
Mn	-	0.01	0.01	0.00	0.00	0.00	0.00	-	0.01	0.00
Mg	-	0.02	0.02	0.03	0.03	0.01	0.01	-	0.01	0.01
Ca	-	2.43	2.40	2.40	1.96	2.57	2.28	-	2.74	2.56
Na	-	0.61	0.65	0.68	1.08	0.50	0.80	-	0.34	0.49
K	-	0.02	0.03	0.03	0.07	0.02	0.03	-	0.01	0.02
Ni	-	-	-	-	-	-	-	-	-	-
V	-	-	-	-	-	-	-	-	-	-
P	-	0.00	0.01	0.00	0.00	0.00	0.00	-	0.00	0.00
Cation total	-	15.09	15.09	15.09	15.10	15.11	15.10	-	15.08	15.12
Mg# / An[e]	-	79.9	78.7	77.9	64.5	83.7	74.0	-	89.0	83.9
Lab[f]	-	1	1	1	1	1	1	-	1	1

Table A3. (continued)

Volcanic cone										
Sample										
Mineral[a]	PL	PL	PL	PL	PL	PL	PL	PL	PL	PL
Core ID	PL01-e3c	PL01-e4c	PL01-e5c	PL02-a1c	PL02-a2c	PL02-a3c	PL02-a4c	PL02-a5c	PL02-b1c	PL02-b2c
Major element (wt.%) [b]										
SiO_2	53.70	49.68	48.15	52.95	49.29	45.08	52.15	52.20	48.59	51.95
TiO_2	0.04	0.00	0.08	0.11	0.15	0.04	0.01	0.00	0.00	0.11
Al_2O_3	28.19	31.08	32.03	28.78	31.46	34.50	29.34	29.25	31.94	29.53
Cr_2O_3	-	-	-	-	-	-	-	-	-	-
FeO[c]	0.81	0.96	0.87	0.81	0.56	0.51	0.75	0.91	0.78	0.86
MnO	0.00	0.02	0.06	0.21	0.00	0.03	0.00	0.00	0.00	0.06
MgO	0.15	0.05	0.05	0.07	0.07	0.07	0.06	0.12	0.15	0.11
CaO	11.80	14.85	16.03	12.21	15.12	18.59	12.93	12.85	15.83	12.80
Na_2O	4.66	3.10	2.61	4.39	3.19	1.14	4.24	4.22	2.54	4.09
K_2O	0.63	0.26	0.10	0.46	0.16	0.04	0.51	0.45	0.17	0.49
NiO	-	-	-	-	-	-	-	-	-	-
V_2O_3	-	-	-	-	-	-	-	-	-	-
P_2O_5	0.02	0.00	0.00	0.00	0.00	0.00	0.00	0.00	0.00	0.00
Total[d]	97.48	98.13	98.37	99.48	99.37	98.98	99.04	99.14	98.38	99.80
Cations										
Si	7.33	6.84	6.66	7.24	6.78	6.26	7.16	7.16	6.70	7.12
Ti	0.00	0.00	0.01	0.01	0.02	0.00	0.00	0.00	0.00	0.01
Al	4.54	5.05	5.22	4.64	5.10	5.65	4.75	4.73	5.19	4.77
Cr	-	-	-	-	-	-	-	-	-	-
Fe2+	0.09	0.11	0.10	0.09	0.06	0.06	0.09	0.10	0.09	0.10
Mn	0.00	0.00	0.01	0.02	0.00	0.00	0.00	0.00	0.00	0.01
Mg	0.03	0.01	0.01	0.01	0.01	0.01	0.01	0.03	0.03	0.02
Ca	1.73	2.19	2.38	1.79	2.23	2.77	1.90	1.89	2.34	1.88
Na	1.23	0.83	0.70	1.16	0.85	0.31	1.13	1.12	0.68	1.08
K	0.11	0.05	0.02	0.08	0.03	0.01	0.09	0.08	0.03	0.09
Ni	-	-	-	-	-	-	-	-	-	-
V	-	-	-	-	-	-	-	-	-	-
P	0.00	0.00	0.00	0.00	0.00	0.00	0.00	0.00	0.00	0.00
Cation total	15.06	15.08	15.11	15.04	15.08	15.07	15.13	15.11	15.06	15.08
Mg# / An[e]	58.4	72.5	77.3	60.7	72.4	89.9	62.7	62.8	77.5	63.5
Lab[f]	1	1	1	1	1	1	1	1	1	1
Mineral[a]	PL	PL	PL	PL	PL	PL	PL	PL	PL	PL
Rim ID	PL01-e3r	PL01-e4r	PL01-e5r	PL02-a1r	PL02-a2r	PL02-a3r	PL02-a4r	PL02-a5r	PL02-b1r	PL02-b2r
Major element (wt.%)[b]										
SiO_2	48.41	46.39	-	51.95	46.53	48.96	51.00	49.09	50.15	48.77
TiO_2	0.02	0.14	-	0.00	0.00	0.00	0.00	0.00	0.00	0.00
Al_2O_3	31.66	33.08	-	29.42	33.27	31.53	29.86	31.77	30.65	31.55
Cr_2O_3	-	-	-	-	-	-	-	-	-	-
FeO[c]	0.91	0.91	-	0.96	0.82	1.03	1.20	0.97	1.05	1.03
MnO	0.08	0.16	-	0.00	0.03	0.10	0.05	0.05	0.00	0.00
MgO	0.10	0.08	-	0.09	0.01	0.09	0.15	0.15	0.13	0.11
CaO	15.91	17.32	-	13.11	17.53	15.29	13.56	15.02	14.53	15.59
Na_2O	2.70	1.80	-	4.09	1.74	2.77	3.86	2.81	3.30	2.73
K_2O	0.20	0.12	-	0.37	0.07	0.22	0.32	0.14	0.20	0.22
NiO	-	-	-	-	-	-	-	-	-	-
V_2O_3	-	-	-	-	-	-	-	-	-	-
P_2O_5	0.00	0.00	-	0.00	0.00	0.00	0.00	0.00	0.00	0.00
Total[d]	96.58	96.27	-	98.99	97.77	98.66	98.48	102.83	99.51	97.42
Cations			-							
Si	6.70	6.44	-	7.12	6.45	6.76	7.00	6.76	6.90	6.73
Ti	0.00	0.01	-	0.00	0.00	0.00	0.00	0.00	0.00	0.00
Al	5.16	5.42	-	4.75	5.43	5.13	4.83	5.15	4.97	5.13
Cr	-	-	-	-	-	-	-	-	-	-
Fe2+	0.11	0.11	-	0.11	0.10	0.12	0.14	0.11	0.12	0.12
Mn	0.01	0.02	-	0.00	0.00	0.01	0.01	0.01	0.00	0.00
Mg	0.02	0.02	-	0.02	0.00	0.02	0.03	0.03	0.03	0.02
Ca	2.36	2.58	-	1.93	2.60	2.26	1.99	2.22	2.14	2.31
Na	0.72	0.48	-	1.09	0.47	0.74	1.03	0.75	0.88	0.73
K	0.03	0.02	-	0.07	0.01	0.04	0.06	0.02	0.04	0.04
Ni	-	-	-	-	-	-	-	-	-	-
V	-	-	-	-	-	-	-	-	-	-
P	0.00	0.00	-	0.00	0.00	0.00	0.00	0.00	0.00	0.00
Cation total	15.11	15.10	-	15.09	15.06	15.08	15.09	15.05	15.08	15.08
Mg# / An[e]	76.6	84.3	-	63.9	84.7	75.3	65.9	74.7	70.9	76.0
Lab[f]	1	1	-	1	1	1	1	1	1	1

Table A3. (continued)

Volcanic cone	OJSL									
Sample										
Mineral[a]	PL	PL	PL	PL	PL	PL	PL	PL	PL	PL
Core ID	PL02-b3c	PL02-b4c	PL02-c2c	PL02-c3c	PL01-a1c	PL01-a2c	PL01-a3c	PL01-a5c	PL01-b1c	PL01-b2c
Major element (wt.%) [b]										
SiO_2	52.26	47.28	48.76	47.05	43.91	52.17	51.89	46.48	52.83	47.46
TiO_2	0.00	0.00	0.08	0.07	0.07	0.09	0.04	0.03	0.00	0.04
Al_2O_3	29.24	32.86	31.38	33.12	35.06	29.57	29.54	33.30	28.71	32.81
Cr_2O_3	-	-	-	-	-	-	-	-	-	-
FeO[c]	0.74	0.95	1.00	0.72	0.79	0.63	0.81	0.91	0.85	0.80
MnO	0.00	0.02	0.00	0.00	0.00	0.00	0.00	0.00	0.03	0.00
MgO	0.13	0.04	0.13	0.05	0.03	0.00	0.05	0.12	0.14	0.03
CaO	13.05	16.65	15.67	16.86	19.31	12.99	13.10	17.18	12.56	16.70
Na_2O	4.23	2.09	2.76	2.03	0.81	4.09	4.09	1.89	4.37	2.07
K_2O	0.35	0.11	0.21	0.10	0.02	0.46	0.45	0.09	0.51	0.09
NiO	-	-	-	-	-	-	-	-	-	-
V_2O_3	-	-	-	-	-	-	-	-	-	-
P_2O_5	0.00	0.00	0.00	0.00	0.00	0.00	0.03	0.00	0.00	0.00
Total[d]	99.29	99.36	98.97	99.49	97.55	97.56	98.07	98.30	98.85	97.90
Cations										
Si	7.16	6.54	6.74	6.51	6.13	7.14	7.11	6.46	7.24	6.57
Ti	0.00	0.00	0.01	0.01	0.01	0.01	0.00	0.00	0.00	0.00
Al	4.72	5.36	5.12	5.40	5.77	4.77	4.77	5.45	4.63	5.35
Cr	-	-	-	-	-	-	-	-	-	-
Fe2+	0.08	0.11	0.12	0.08	0.09	0.07	0.09	0.11	0.10	0.09
Mn	0.00	0.00	0.00	0.00	0.00	0.00	0.00	0.00	0.00	0.00
Mg	0.03	0.01	0.03	0.01	0.01	0.00	0.01	0.02	0.03	0.01
Ca	1.92	2.47	2.32	2.50	2.89	1.90	1.92	2.56	1.84	2.48
Na	1.12	0.56	0.74	0.55	0.22	1.08	1.09	0.51	1.16	0.56
K	0.06	0.02	0.04	0.02	0.00	0.08	0.08	0.02	0.09	0.02
Ni	-	-	-	-	-	-	-	-	-	-
V	-	-	-	-	-	-	-	-	-	-
P	0.00	0.00	0.00	0.00	0.00	0.00	0.00	0.00	0.00	0.00
Cation total	15.09	15.07	15.12	15.08	15.12	15.05	15.07	15.13	15.09	15.08
Mg# / An[e]	63.2	81.5	75.8	82.0	92.9	63.8	63.8	83.4	61.3	81.6
Lab[f]	1	1	1	1	1	1	1	1	1	1
Mineral[a]	PL	PL	PL	PL	PL	PL	PL	PL	PL	PL
Rim ID	PL02-b3r	PL02-b4r	PL02-c2r	PL02-c3r	PL01-a1r	PL01-a2r	PL01-a3r	PL01-a5r	PL01-b1r	PL01-b2r
Major element (wt.%)[b]										
SiO_2	47.31	47.51	46.26	48.58	51.92	-	47.57	-	47.09	45.37
TiO_2	0.00	0.00	0.00	0.00	0.05	-	0.09	-	0.08	0.05
Al_2O_3	32.69	32.64	33.09	31.48	29.08	-	31.99	-	32.93	34.13
Cr_2O_3	-	-	-	-	-	-	-	-	-	-
FeO[c]	1.02	0.91	1.24	1.02	1.04	-	1.10	-	0.90	0.66
MnO	0.00	0.02	0.00	0.00	0.00	-	0.01	-	0.03	0.00
MgO	0.07	0.07	0.10	0.06	0.18	-	0.17	-	0.07	0.07
CaO	16.39	16.53	17.38	15.92	13.37	-	16.46	-	16.66	18.47
Na_2O	2.38	2.20	1.79	2.76	4.06	-	2.42	-	2.11	1.22
K_2O	0.14	0.12	0.13	0.18	0.30	-	0.18	-	0.08	0.03
NiO	-	-	-	-	-	-	-	-	-	-
V_2O_3	-	-	-	-	-	-	-	-	-	-
P_2O_5	0.00	0.00	0.00	0.00	0.00	-	0.00	-	0.05	0.00
Total[d]	99.16	97.85	98.65	97.02	96.09	-	98.94	-	101.48	98.28
Cations						-		-		
Si	6.56	6.57	6.42	6.72	7.14	-	6.60	-	6.52	6.31
Ti	0.00	0.00	0.00	0.00	0.01	-	0.01	-	0.01	0.00
Al	5.34	5.32	5.41	5.13	4.71	-	5.23	-	5.37	5.59
Cr	-	-	-	-	-	-	-	-	-	-
Fe2+	0.12	0.11	0.14	0.12	0.12	-	0.13	-	0.10	0.08
Mn	0.00	0.00	0.00	0.00	0.00	-	0.00	-	0.00	0.00
Mg	0.01	0.02	0.02	0.01	0.04	-	0.04	-	0.01	0.01
Ca	2.43	2.45	2.59	2.36	1.97	-	2.45	-	2.47	2.75
Na	0.64	0.59	0.48	0.74	1.08	-	0.65	-	0.57	0.33
K	0.03	0.02	0.02	0.03	0.05	-	0.03	-	0.01	0.00
Ni	-	-	-	-	-	-	-	-	-	-
V	-	-	-	-	-	-	-	-	-	-
P	0.00	0.00	0.00	0.00	0.00	-	0.00	-	0.01	0.00
Cation total	15.13	15.08	15.08	15.11	15.12	-	15.14	-	15.07	15.07
Mg# / An[e]	79.2	80.6	84.4	76.1	64.6	-	79.0	-	81.3	89.3
Lab[f]	1	1	1	1	1	-	1	-	1	1

Table A3. (continued)

Volcanic cone										
Sample										
Mineral[a]	PL	PL	PL	PL	PL	PL	PL	PL	PL	PL
Core ID	PL01-b4c	PL02-a1c	PL02-a2c	PL02-a3c	PL02-a4c	PL02-a5c	PL02-a6c	PL02-b1c	PL02-b2c	PL02-b3c
Major element (wt.%) [b]										
SiO_2	52.51	51.56	54.20	46.32	52.65	47.92	48.54	47.48	47.54	51.95
TiO_2	0.02	0.15	0.03	0.09	0.04	0.16	0.01	0.09	0.01	0.00
Al_2O_3	28.95	29.46	28.03	33.40	28.88	32.33	31.96	32.52	32.54	29.34
Cr_2O_3	-	-	-	-	-	-	-	-	-	-
FeO[c]	0.80	0.74	0.87	0.81	0.76	0.83	0.82	0.78	0.79	0.96
MnO	0.03	0.06	0.00	0.02	0.09	0.07	0.00	0.00	0.00	0.01
MgO	0.12	0.10	0.04	0.05	0.13	0.08	0.08	0.02	0.09	0.10
CaO	12.65	13.65	11.40	17.51	12.51	16.02	15.84	16.78	16.59	13.08
Na_2O	4.31	3.90	4.82	1.69	4.42	2.42	2.58	2.18	2.25	4.18
K_2O	0.52	0.37	0.60	0.10	0.47	0.16	0.10	0.14	0.18	0.36
NiO	-	-	-	-	-	-	-	-	-	-
V_2O_3	-	-	-	-	-	-	-	-	-	-
P_2O_5	0.08	0.00	0.02	0.00	0.05	0.00	0.07	0.00	0.00	0.00
Total[d]	98.15	99.11	98.16	98.49	98.67	98.21	98.44	98.42	98.47	98.74
Cations										
Si	7.19	7.08	7.39	6.43	7.20	6.63	6.69	6.58	6.59	7.12
Ti	0.00	0.02	0.00	0.01	0.00	0.02	0.00	0.01	0.00	0.00
Al	4.67	4.77	4.50	5.46	4.66	5.27	5.19	5.31	5.31	4.74
Cr	-	-	-	-	-	-	-	-	-	-
Fe2+	0.09	0.08	0.10	0.09	0.09	0.10	0.09	0.09	0.09	0.11
Mn	0.00	0.01	0.00	0.00	0.01	0.01	0.00	0.00	0.00	0.00
Mg	0.03	0.02	0.01	0.01	0.03	0.02	0.02	0.00	0.02	0.02
Ca	1.86	2.01	1.67	2.60	1.83	2.37	2.34	2.49	2.46	1.92
Na	1.14	1.04	1.28	0.45	1.17	0.65	0.69	0.59	0.60	1.11
K	0.09	0.07	0.10	0.02	0.08	0.03	0.02	0.02	0.03	0.06
Ni	-	-	-	-	-	-	-	-	-	-
V	-	-	-	-	-	-	-	-	-	-
P	0.01	0.00	0.00	0.00	0.01	0.00	0.01	0.00	0.00	0.00
Cation total	15.08	15.10	15.05	15.07	15.08	15.10	15.05	15.09	15.10	15.08
Mg# / An[e]	62.0	65.9	56.6	85.2	61.0	78.5	77.2	80.8	80.4	63.4
Lab[f]	1	1	1	1	1	1	1	1	1	1
Mineral[a]	PL	PL	PL	PL	PL	PL	PL	PL	PL	PL
Rim ID	PL01-b4r	PL02-a1r	PL02-a2r	PL02-a3r	PL02-a4r	PL02-a5r	PL02-a6r	PL02-b1r	PL02-b2r	PL02-b3r
Major element (wt.%)[b]										
SiO_2	-	49.26	50.10	47.71	46.92	50.44	48.27	47.14	46.65	49.89
TiO_2	-	0.02	0.17	0.00	0.03	0.08	0.07	0.02	0.00	0.12
Al_2O_3	-	31.21	30.53	32.46	32.89	30.48	31.96	32.67	33.23	30.76
Cr_2O_3	-	-	-	-	-	-	-	-	-	-
FeO[c]	-	0.97	1.11	0.89	0.96	1.01	1.00	0.98	0.86	0.96
MnO	-	0.00	0.00	0.00	0.00	0.00	0.00	0.00	0.00	0.00
MgO	-	0.11	0.17	0.07	0.11	0.04	0.11	0.11	0.06	0.10
CaO	-	15.46	14.23	16.27	16.98	14.08	15.86	16.97	17.32	14.71
Na_2O	-	2.83	3.49	2.43	2.06	3.54	2.58	1.98	1.79	3.27
K_2O	-	0.12	0.20	0.17	0.04	0.32	0.14	0.13	0.08	0.18
NiO	-	-	-	-	-	-	-	-	-	-
V_2O_3	-	-	-	-	-	-	-	-	-	-
P_2O_5	-	0.00	0.00	0.00	0.00	0.00	0.00	0.00	0.00	0.00
Total[d]	-	96.43	98.59	100.88	97.51	98.63	97.17	98.32	96.65	98.37
Cations	-									
Si	-	6.79	6.89	6.60	6.51	6.94	6.66	6.54	6.46	6.87
Ti	-	0.00	0.02	0.00	0.00	0.01	0.01	0.00	0.00	0.01
Al	-	5.07	4.95	5.30	5.38	4.94	5.20	5.34	5.42	4.99
Cr	-	-	-	-	-	-	-	-	-	-
Fe2+	-	0.11	0.13	0.10	0.11	0.12	0.12	0.11	0.10	0.11
Mn	-	0.00	0.00	0.00	0.00	0.00	0.00	0.00	0.00	0.00
Mg	-	0.02	0.04	0.01	0.02	0.01	0.02	0.02	0.01	0.02
Ca	-	2.28	2.10	2.41	2.52	2.08	2.34	2.52	2.57	2.17
Na	-	0.76	0.93	0.65	0.55	0.94	0.69	0.53	0.48	0.87
K	-	0.02	0.04	0.03	0.01	0.06	0.02	0.02	0.02	0.03
Ni	-	-	-	-	-	-	-	-	-	-
V	-	-	-	-	-	-	-	-	-	-
P	-	0.00	0.01	0.00	0.00	0.00	0.01	0.00	0.01	0.00
Cation total	-	15.05	15.11	15.10	15.10	15.10	15.07	15.08	15.07	15.07
Mg# / An[e]	-	75.0	69.3	78.8	82.1	68.9	77.2	82.6	84.3	71.4
Lab[f]	-	1	1	1	1	1	1	1	1	1

Table A3. (continued)

Volcanic cone										Kishimadake
Sample										KSS
Mineral[a]	PL	PL	PL	PL	PL	PL	PL	PL	PL	PL
Core ID	PL02-b4c	PL02-b5c	PL02-b6c	PL02-c1c	PL02-c2c	PL02-c4c	PL02-c5c	PL02-c6c	PL02-d2c	PL-a1c
Major element (wt.%) [b]										
SiO_2	52.06	52.17	49.99	51.97	48.22	49.82	52.07	52.43	52.38	53.32
TiO_2	0.03	0.03	0.05	0.00	0.00	0.17	0.05	0.09	0.00	0.02
Al_2O_3	29.45	29.17	30.77	29.63	31.98	30.98	29.39	29.05	29.20	28.47
Cr_2O_3	-	-	-	-	-	-	-	-	-	-
FeO[c]	0.93	0.92	0.94	0.76	0.94	0.79	0.88	0.97	0.78	0.81
MnO	0.00	0.06	0.05	0.06	0.04	0.03	0.00	0.00	0.02	0.06
MgO	0.11	0.08	0.04	0.10	0.09	0.06	0.11	0.05	0.11	0.09
CaO	12.78	12.81	14.43	13.00	15.90	14.60	12.85	12.61	12.88	12.13
Na_2O	4.17	4.35	3.43	4.01	2.60	3.28	4.18	4.33	4.17	4.53
K_2O	0.47	0.41	0.27	0.39	0.23	0.27	0.47	0.46	0.46	0.57
NiO	-	-	-	-	-	-	-	-	-	-
V_2O_3	-	-	-	-	-	-	-	-	-	-
P_2O_5	0.00	0.01	0.03	0.08	0.00	0.00	0.00	0.00	0.00	0.00
Total[d]	98.23	98.16	98.39	98.35	98.82	97.77	97.89	97.21	97.98	98.30
Cations										
Si	7.13	7.15	6.88	7.11	6.67	6.86	7.14	7.18	7.18	7.29
Ti	0.00	0.00	0.01	0.00	0.00	0.02	0.01	0.01	0.00	0.00
Al	4.76	4.71	4.99	4.78	5.21	5.03	4.75	4.69	4.72	4.59
Cr	-	-	-	-	-	-	-	-	-	-
Fe2+	0.11	0.10	0.11	0.09	0.11	0.09	0.10	0.11	0.09	0.09
Mn	0.00	0.01	0.01	0.01	0.00	0.00	0.00	0.00	0.00	0.01
Mg	0.02	0.02	0.01	0.02	0.02	0.01	0.02	0.01	0.02	0.02
Ca	1.88	1.88	2.13	1.91	2.36	2.15	1.89	1.85	1.89	1.78
Na	1.11	1.16	0.91	1.06	0.70	0.88	1.11	1.15	1.11	1.20
K	0.08	0.07	0.05	0.07	0.04	0.05	0.08	0.08	0.08	0.10
Ni	-	-	-	-	-	-	-	-	-	-
V	-	-	-	-	-	-	-	-	-	-
P	0.00	0.00	0.00	0.01	0.00	0.00	0.00	0.00	0.00	0.00
Cation total	15.09	15.10	15.10	15.06	15.11	15.09	15.10	15.08	15.09	15.08
Mg# / An[e]	62.9	61.8	70.1	64.3	77.1	71.0	63.0	61.7	63.0	59.7
Lab[f]	1	1	1	1	1	1	1	1	1	1
Mineral[a]	PL	PL	PL	PL	PL	PL	PL	PL	PL	PL
Rim ID	PL02-b4r	PL02-b5r	PL02-b6r	PL02-c1r	PL02-c2r	PL02-c4r	PL02-c5r	PL02-c6r	PL02-d2r	PL-a1r
Major element (wt.%)[b]										
SiO_2	46.34	-	51.23	48.38	47.10	48.57	47.15	48.73	48.18	47.95
TiO_2	0.12	-	0.03	0.09	0.08	0.12	0.00	0.13	0.03	0.00
Al_2O_3	33.30	-	29.55	32.12	32.74	31.58	32.90	31.65	31.94	32.18
Cr_2O_3	-	-	-	-	-	-	-	-	-	-
FeO[c]	0.89	-	1.23	1.08	0.97	1.20	0.94	1.04	0.83	0.99
MnO	0.00	-	0.00	0.00	0.00	0.00	0.00	0.00	0.00	0.03
MgO	0.10	-	0.15	0.07	0.02	0.14	0.06	0.10	0.06	0.12
CaO	17.30	-	13.38	15.63	16.83	15.48	16.65	15.39	16.18	16.21
Na_2O	1.81	-	4.13	2.49	2.15	2.68	2.17	2.76	2.62	2.35
K_2O	0.12	-	0.30	0.15	0.11	0.22	0.13	0.19	0.15	0.17
NiO	-	-	-	-	-	-	-	-	-	-
V_2O_3	-	-	-	-	-	-	-	-	-	-
P_2O_5	0.00	-	0.00	0.00	0.00	0.00	0.00	0.00	0.00	0.00
Total[d]	96.58	-	99.49	101.30	98.75	98.44	98.32	97.96	96.89	99.20
Cations		-								
Si	6.44	-	7.04	6.68	6.54	6.71	6.52	6.73	6.66	6.64
Ti	0.01	-	0.00	0.01	0.01	0.01	0.00	0.01	0.00	0.00
Al	5.45	-	4.79	5.23	5.36	5.14	5.36	5.15	5.21	5.25
Cr	-	-	-	-	-	-	-	-	-	-
Fe2+	0.10	-	0.14	0.12	0.11	0.14	0.11	0.12	0.10	0.11
Mn	0.00	-	0.00	0.00	0.00	0.00	0.00	0.00	0.00	0.00
Mg	0.02	-	0.03	0.01	0.00	0.03	0.01	0.02	0.01	0.02
Ca	2.57	-	1.97	2.31	2.50	2.29	2.47	2.28	2.40	2.40
Na	0.49	-	1.10	0.67	0.58	0.72	0.58	0.74	0.70	0.63
K	0.02	-	0.05	0.03	0.02	0.04	0.02	0.03	0.03	0.03
Ni	-	-	-	-	-	-	-	-	-	-
V	-	-	-	-	-	-	-	-	-	-
P	0.00	-	0.00	0.00	0.00	0.00	0.00	0.00	0.00	0.00
Cation total	15.10	-	15.12	15.06	15.12	15.08	15.07	15.08	15.11	15.08
Mg# / An[e]	84.0	-	64.2	77.5	81.2	76.1	81.0	75.5	77.4	79.2
Lab[f]	1	-	1	1	1	1	1	1	1	1

Table A3. (continued)

Volcanic cone										
Sample										
Mineral[a]	PL	PL	PL	PL	PL	PL	PL	PL	PL	PL
Core ID	PL-a2c	PL-a3c	PL-a4c	PL-a5c	PL-a6c	PL-b1c	PL-b2c	PL-b3c	PL-b4c	PL-b5c
Major element (wt.%) [b]										
SiO_2	52.81	53.26	52.28	46.20	51.42	48.68	53.90	44.29	53.10	53.08
TiO_2	0.00	0.06	0.05	0.04	0.01	0.06	0.15	0.05	0.09	0.07
Al_2O_3	28.84	28.97	29.19	33.36	29.80	31.85	27.91	34.95	28.64	28.55
Cr_2O_3	-	-	-	-	-	-	-	-	-	-
FeO[c]	0.71	0.49	0.74	0.86	0.78	0.66	0.84	0.54	0.83	0.81
MnO	0.00	0.00	0.00	0.00	0.06	0.00	0.00	0.12	0.00	0.00
MgO	0.10	0.07	0.07	0.04	0.10	0.03	0.04	0.00	0.06	0.09
CaO	12.65	12.12	12.89	17.60	13.56	15.93	11.51	19.11	12.17	12.23
Na_2O	4.29	4.49	4.26	1.81	3.81	2.67	4.90	0.86	4.48	4.52
K_2O	0.58	0.51	0.47	0.09	0.46	0.12	0.67	0.08	0.63	0.65
NiO	-	-	-	-	-	-	-	-	-	-
V_2O_3	-	-	-	-	-	-	-	-	-	-
P_2O_5	0.02	0.04	0.05	0.00	0.00	0.00	0.06	0.00	0.00	0.00
Total[d]	97.73	98.28	98.79	98.71	98.27	97.55	98.34	98.87	98.77	98.37
Cations										
Si	7.23	7.26	7.16	6.42	7.06	6.71	7.36	6.17	7.26	7.26
Ti	0.00	0.01	0.01	0.00	0.00	0.01	0.02	0.01	0.01	0.01
Al	4.65	4.65	4.71	5.46	4.82	5.18	4.49	5.74	4.62	4.60
Cr	-	-	-	-	-	-	-	-	-	-
Fe2+	0.08	0.06	0.08	0.10	0.09	0.08	0.10	0.06	0.10	0.09
Mn	0.00	0.00	0.00	0.00	0.01	0.00	0.00	0.01	0.00	0.00
Mg	0.02	0.01	0.01	0.01	0.02	0.01	0.01	0.00	0.01	0.02
Ca	1.85	1.77	1.89	2.62	2.00	2.35	1.68	2.85	1.78	1.79
Na	1.14	1.19	1.13	0.49	1.01	0.71	1.30	0.23	1.19	1.20
K	0.10	0.09	0.08	0.02	0.08	0.02	0.12	0.01	0.11	0.11
Ni	-	-	-	-	-	-	-	-	-	-
V	-	-	-	-	-	-	-	-	-	-
P	0.00	0.00	0.01	0.00	0.00	0.00	0.01	0.00	0.00	0.00
Cation total	15.07	15.04	15.08	15.12	15.09	15.07	15.09	15.08	15.08	15.08
Mg# / An[e]	61.9	59.8	62.6	84.2	66.4	76.8	56.4	92.5	59.9	59.9
Lab[f]	1	1	1	1	1	1	1	1	1	1
Mineral[a]	PL	PL	PL	PL	PL	PL	PL	PL	PL	PL
Rim ID	PL-a2r	PL-a3r	PL-a4r	PL-a5r	PL-a6r	PL-b1r	PL-b2r	PL-b3r	PL-b4r	PL-b5r
Major element (wt.%)[b]										
SiO_2	52.65	47.85	47.58	46.11	47.21	48.08	52.73	44.80	47.03	48.51
TiO_2	0.03	0.00	0.00	0.06	0.04	0.03	0.05	0.00	0.02	0.15
Al_2O_3	28.77	32.36	32.23	33.28	32.39	32.06	28.64	34.72	32.69	31.61
Cr_2O_3	-	-	-	-	-	-	-	-	-	-
FeO[c]	0.94	1.00	0.99	1.08	1.14	0.96	1.12	0.65	0.89	1.14
MnO	0.02	0.16	0.00	0.00	0.04	0.00	0.00	0.05	0.00	0.00
MgO	0.05	0.08	0.13	0.09	0.15	0.11	0.12	0.00	0.10	0.05
CaO	12.56	15.95	16.58	17.56	16.78	15.96	12.38	18.67	16.86	15.61
Na_2O	4.38	2.46	2.31	1.65	2.11	2.61	4.43	1.00	2.23	2.75
K_2O	0.59	0.13	0.18	0.15	0.14	0.16	0.53	0.10	0.18	0.18
NiO	-	-	-	-	-	-	-	-	-	-
V_2O_3	-	-	-	-	-	-	-	-	-	-
P_2O_5	0.00	0.01	0.00	0.02	0.00	0.03	0.00	0.00	0.00	0.00
Total[d]	97.51	99.17	98.91	97.64	98.53	100.12	99.98	99.77	99.07	99.71
Cations										
Si	7.22	6.62	6.59	6.41	6.56	6.65	7.23	6.25	6.53	6.72
Ti	0.00	0.00	0.00	0.01	0.00	0.00	0.01	0.00	0.00	0.02
Al	4.65	5.27	5.27	5.45	5.30	5.22	4.63	5.71	5.35	5.16
Cr	-	-	-	-	-	-	-	-	-	-
Fe2+	0.11	0.11	0.11	0.12	0.13	0.11	0.13	0.08	0.10	0.13
Mn	0.00	0.02	0.00	0.00	0.01	0.00	0.00	0.01	0.00	0.00
Mg	0.01	0.02	0.03	0.02	0.03	0.02	0.02	0.00	0.02	0.01
Ca	1.85	2.36	2.46	2.61	2.50	2.36	1.82	2.79	2.51	2.31
Na	1.17	0.66	0.62	0.44	0.57	0.70	1.18	0.27	0.60	0.74
K	0.10	0.02	0.03	0.03	0.03	0.03	0.09	0.02	0.03	0.03
Ni	-	-	-	-	-	-	-	-	-	-
V	-	-	-	-	-	-	-	-	-	-
P	0.00	0.00	0.00	0.00	0.00	0.00	0.00	0.00	0.00	0.00
Cation total	15.11	15.08	15.11	15.09	15.13	15.09	15.11	15.13	15.14	15.12
Mg# / An[e]	61.3	78.1	79.9	85.6	81.4	77.1	60.7	91.2	80.7	75.7
Lab[f]	1	1	1	1	1	1	1	1	1	1

Table A3. (continued)

Volcanic cone										
Sample										
Mineral[a]	PL	PL	PL	PL	PL	PL	PL	PL	PL	PL
Core ID	PL-c1c	PL-c2c	PL-c3c	PL-c4c	PL-c5c	PL-c6c	PL-d1c	PL-d3c	PL-d4c	PL-d5c
Major element (wt.%) [b]										
SiO_2	48.74	52.13	53.58	52.17	45.30	51.73	52.23	51.96	52.86	52.81
TiO_2	0.00	0.08	0.08	0.06	0.03	0.13	0.03	0.16	0.00	0.01
Al_2O_3	31.58	29.43	28.53	29.08	34.10	29.35	29.04	29.24	28.90	29.01
Cr_2O_3	-	-	-	-	-	-	-	-	-	-
FeO[c]	1.01	0.77	0.66	0.88	0.66	0.92	0.92	0.81	0.80	0.75
MnO	0.04	0.03	0.05	0.07	0.00	0.11	0.04	0.06	0.00	0.00
MgO	0.06	0.07	0.04	0.13	0.04	0.09	0.12	0.08	0.08	0.01
CaO	15.46	13.01	11.67	12.93	18.40	13.24	12.91	12.99	12.30	12.38
Na_2O	2.88	4.03	4.84	4.35	1.35	4.05	4.23	4.15	4.45	4.53
K_2O	0.23	0.46	0.55	0.33	0.09	0.35	0.48	0.54	0.60	0.50
NiO	-	-	-	-	-	-	-	-	-	-
V_2O_3	-	-	-	-	-	-	-	-	-	-
P_2O_5	0.00	0.00	0.00	0.00	0.03	0.01	0.00	0.00	0.02	0.00
Total[d]	99.33	98.87	98.61	98.84	98.68	98.76	100.19	99.24	98.96	99.55
Cations										
Si	6.73	7.15	7.31	7.16	6.30	7.10	7.17	7.13	7.23	7.24
Ti	0.00	0.01	0.01	0.01	0.00	0.01	0.00	0.02	0.00	0.00
Al	5.14	4.76	4.59	4.70	5.59	4.75	4.70	4.73	4.66	4.69
Cr	-	-	-	-	-	-	-	-	-	-
Fe2+	0.12	0.09	0.07	0.10	0.08	0.11	0.11	0.09	0.09	0.09
Mn	0.00	0.00	0.01	0.01	0.00	0.01	0.00	0.01	0.00	0.00
Mg	0.01	0.01	0.01	0.03	0.01	0.02	0.02	0.02	0.02	0.00
Ca	2.29	1.91	1.71	1.90	2.74	1.95	1.90	1.91	1.80	1.82
Na	0.77	1.07	1.28	1.16	0.36	1.08	1.13	1.10	1.18	1.20
K	0.04	0.08	0.09	0.06	0.02	0.06	0.08	0.10	0.10	0.09
Ni	-	-	-	-	-	-	-	-	-	-
V	-	-	-	-	-	-	-	-	-	-
P	0.00	0.00	0.00	0.00	0.00	0.00	0.00	0.00	0.00	0.00
Cation total	15.10	15.08	15.08	15.13	15.10	15.09	15.11	15.11	15.08	15.13
Mg# / An[e]	74.8	64.1	57.2	62.1	88.4	64.4	62.7	63.5	60.4	60.3
Lab[f]	1	1	1	1	1	1	1	1	1	1
Mineral[a]	PL	PL	PL	PL	PL	PL	PL	PL	PL	PL
Rim ID	PL-c1r	PL-c2r2	PL-c3r	PL-c4r	PL-c5r	PL-c6r	PL-d1r	PL-d3r	PL-d4r	PL-d5r
Major element (wt.%)[b]										
SiO_2	50.45	47.17	47.83	48.74	48.30	50.39	51.78	47.01	47.38	48.79
TiO_2	0.04	0.00	0.00	0.00	0.04	0.07	0.15	0.00	0.08	0.00
Al_2O_3	30.45	32.51	32.25	31.51	31.88	30.48	29.33	32.74	32.34	31.50
Cr_2O_3	-	-	-	-	-	-	-	-	-	-
FeO[c]	0.83	1.04	0.98	0.73	0.85	0.99	1.02	0.98	0.92	1.03
MnO	0.11	0.05	0.00	0.00	0.03	0.00	0.11	0.00	0.00	0.00
MgO	0.12	0.06	0.05	0.10	0.09	0.06	0.08	0.12	0.14	0.15
CaO	14.25	16.93	16.24	15.78	16.00	14.21	13.07	16.90	16.68	15.47
Na_2O	3.47	2.07	2.48	2.89	2.59	3.43	4.05	2.07	2.21	2.82
K_2O	0.27	0.16	0.16	0.22	0.21	0.38	0.41	0.18	0.24	0.23
NiO	-	-	-	-	-	-	-	-	-	-
V_2O_3	-	-	-	-	-	-	-	-	-	-
P_2O_5	0.00	0.00	0.00	0.03	0.00	0.00	0.00	0.00	0.00	0.01
Total[d]	98.74	97.84	98.74	98.49	98.61	100.38	100.29	98.96	97.36	100.66
Cations										
Si	6.94	6.55	6.62	6.73	6.67	6.94	7.11	6.53	6.58	6.74
Ti	0.00	0.00	0.00	0.00	0.00	0.01	0.02	0.00	0.01	0.00
Al	4.94	5.32	5.26	5.13	5.19	4.94	4.75	5.36	5.29	5.13
Cr	-	-	-	-	-	-	-	-	-	-
Fe2+	0.10	0.12	0.11	0.08	0.10	0.11	0.12	0.11	0.11	0.12
Mn	0.01	0.01	0.00	0.00	0.00	0.00	0.01	0.00	0.00	0.00
Mg	0.03	0.01	0.01	0.02	0.02	0.01	0.02	0.02	0.03	0.03
Ca	2.10	2.52	2.41	2.33	2.37	2.10	1.92	2.51	2.48	2.29
Na	0.93	0.56	0.67	0.78	0.69	0.91	1.08	0.56	0.59	0.76
K	0.05	0.03	0.03	0.04	0.04	0.07	0.07	0.03	0.04	0.04
Ni	-	-	-	-	-	-	-	-	-	-
V	-	-	-	-	-	-	-	-	-	-
P	0.00	0.00	0.00	0.00	0.00	0.00	0.00	0.00	0.00	0.00
Cation total	15.10	15.12	15.11	15.11	15.08	15.09	15.10	15.12	15.13	15.11
Mg# / An[e]	69.3	81.8	78.2	74.9	77.5	69.8	64.0	81.8	80.8	75.1
Lab[f]	1	1	1	1	1	1	1	1	1	1

Table A3. (continued)

Volcanic cone						Nakadake				
Sample						NKD14				
Mineral[a]	PL	PL	PL	PL	PL	CPX	CPX	CPX	CPX	CPX
Core ID	PL-e3c	PL-e4c	PL-e5c	PL-e6c	L03-b2c(PL)	a1c	a2c	a3c	a5c	b1c
Major element (wt.%) [b]										
SiO_2	53.46	45.81	52.07	52.68	51.84	50.87	51.53	51.21	50.91	51.07
TiO_2	0.11	0.00	0.02	0.00	0.13	0.59	0.60	0.66	0.76	0.59
Al_2O_3	28.15	33.87	29.28	28.99	29.61	2.30	2.00	2.42	2.75	2.50
Cr_2O_3	-	-	-	-	-	0.01	0.00	0.00	0.01	0.02
FeO[c]	0.89	0.73	0.71	0.85	0.86	11.84	10.82	11.59	10.99	11.45
MnO	0.00	0.00	0.00	0.06	0.04	0.37	0.38	0.36	0.37	0.32
MgO	0.12	0.01	0.11	0.06	0.07	15.10	15.60	15.73	14.96	15.32
CaO	12.00	17.83	13.25	12.42	12.94	18.53	18.75	17.64	18.87	18.37
Na_2O	4.59	1.67	4.07	4.46	3.94	0.30	0.26	0.26	0.23	0.26
K_2O	0.58	0.07	0.48	0.47	0.57	0.00	0.01	0.01	0.01	0.01
NiO	-	-	-	-	-	0.01	0.02	0.00	0.04	0.02
V_2O_3	-	-	-	-	-	0.09	0.03	0.11	0.10	0.06
P_2O_5	0.10	0.01	0.00	0.00	0.00	-	-	-	-	-
Total[d]	99.67	99.12	99.36	98.78	98.78	99.65	99.88	100.19	100.03	100.14
Cations										
Si	7.30	6.36	7.14	7.22	7.12	7.65	7.70	7.66	7.63	7.64
Ti	0.01	0.00	0.00	0.00	0.01	0.07	0.07	0.07	0.09	0.07
Al	4.53	5.54	4.73	4.68	4.79	0.41	0.35	0.43	0.49	0.45
Cr	-	-	-	-	-	0.00	0.00	0.00	0.00	0.00
Fe2+	0.10	0.08	0.08	0.10	0.10	1.49	1.35	1.45	1.38	1.53
Mn	0.00	0.00	0.00	0.01	0.00	0.05	0.05	0.05	0.05	0.05
Mg	0.02	0.00	0.02	0.01	0.01	3.38	3.48	3.51	3.34	3.47
Ca	1.76	2.65	1.95	1.82	1.90	2.98	3.00	2.83	3.03	2.83
Na	1.21	0.45	1.08	1.19	1.05	0.09	0.08	0.07	0.07	0.06
K	0.10	0.01	0.08	0.08	0.10	0.00	0.00	0.00	0.00	0.00
Ni	-	-	-	-	-	0.00	0.00	0.00	0.00	0.00
V	-	-	-	-	-	0.01	0.00	0.01	0.01	0.00
P	0.01	0.00	0.00	0.00	0.00	-	-	-	-	-
Cation total	15.04	15.09	15.08	15.11	15.08	16.12	16.09	16.08	16.07	16.10
Mg# / An[e]	59.3	85.5	64.4	60.5	64.4	69.4	72.0	70.8	70.8	70.4
Lab[f]	1	1	1	1	1	2	2	2	2	2
Mineral[a]	PL	PL	PL	PL	PL	CPX	CPX	CPX	CPX	CPX
Rim ID	PL-e3r	PL-e4r	PL-e5r	PL-e6r	L03-b2r(PL)	a1r	a2r	a3r	a5r	b1r
Major element (wt.%)[b]										
SiO_2	47.88	46.57	52.20	47.86	48.80	50.86	51.42	51.44	50.97	51.51
TiO_2	0.01	0.00	0.00	0.02	0.00	0.66	0.55	0.58	0.69	0.59
Al_2O_3	32.18	33.19	29.29	32.29	31.72	2.66	2.17	2.10	2.85	2.20
Cr_2O_3	-	-	-	-	-	0.06	0.00	0.01	0.00	0.00
FeO[c]	1.04	0.79	1.02	1.02	0.83	11.01	11.29	11.18	12.07	11.45
MnO	0.03	0.00	0.02	0.05	0.09	0.34	0.40	0.37	0.42	0.37
MgO	0.05	0.03	0.12	0.11	0.08	15.24	15.53	15.70	15.16	15.37
CaO	16.11	17.58	12.78	16.16	15.63	18.93	18.33	18.32	17.55	18.17
Na_2O	2.53	1.74	4.16	2.37	2.65	0.21	0.23	0.25	0.26	0.24
K_2O	0.17	0.10	0.39	0.12	0.19	0.00	0.01	0.00	0.00	0.01
NiO	-	-	-	-	-	0.00	0.01	0.00	0.00	0.00
V_2O_3	-	-	-	-	-	0.03	0.07	0.03	0.03	0.09
P_2O_5	0.00	0.00	0.00	0.00	0.00	-	-	-	-	-
Total[d]	100.54	97.77	99.65	99.67	100.24	99.34	100.32	99.92	99.34	99.90
Cations										
Si	6.63	6.47	7.16	6.62	6.74	7.62	7.69	7.69	7.64	7.71
Ti	0.00	0.00	0.00	0.00	0.00	0.07	0.06	0.07	0.08	0.07
Al	5.25	5.43	4.73	5.27	5.16	0.47	0.38	0.37	0.50	0.39
Cr	-	-	-	-	-	0.01	0.00	0.00	0.00	0.00
Fe2+	0.12	0.09	0.12	0.12	0.10	1.38	1.41	1.40	1.51	1.43
Mn	0.00	0.00	0.00	0.01	0.01	0.04	0.05	0.05	0.05	0.05
Mg	0.01	0.01	0.02	0.02	0.02	3.40	3.46	3.50	3.39	3.43
Ca	2.39	2.62	1.88	2.40	2.31	3.04	2.94	2.94	2.82	2.91
Na	0.68	0.47	1.11	0.63	0.71	0.06	0.07	0.07	0.08	0.07
K	0.03	0.02	0.07	0.02	0.03	0.00	0.00	0.00	0.00	0.00
Ni	-	-	-	-	-	0.00	0.00	0.00	0.00	0.00
V	-	-	-	-	-	0.00	0.01	0.00	0.00	0.01
P	0.00	0.00	0.00	0.00	0.00	-	-	-	-	-
Cation total	15.11	15.11	15.09	15.09	15.08	16.10	16.08	16.09	16.07	16.06
Mg# / An[e]	77.9	84.8	62.9	79.2	76.5	71.2	71.0	71.4	69.1	70.5
Lab[f]	1	1	1	1	1	2	2	2	2	2

Table A3. (continued)

Volcanic cone										
Sample										
Mineral[a]	CPX	CPX	CPX	CPX	CPX	CPX	CPX	CPX	CPX	CPX
Core ID	b2c	b3c	b4c	b5c	c1c	c2c	c3c	c4c	c5c	d1c
Major element (wt.%) [b]										
SiO_2	51.33	51.07	51.17	51.03	51.15	50.78	51.45	50.80	51.01	51.24
TiO_2	0.62	0.61	0.62	0.53	0.58	0.67	0.58	0.63	0.39	0.62
Al_2O_3	2.43	2.33	2.51	2.36	2.39	2.77	2.35	2.55	4.17	2.24
Cr_2O_3	0.00	0.01	0.01	0.02	0.01	0.00	0.02	0.00	0.06	0.01
FeO[c]	11.83	11.12	11.69	11.51	11.61	11.68	11.10	12.10	6.98	11.86
MnO	0.36	0.39	0.38	0.39	0.37	0.42	0.32	0.44	0.20	0.42
MgO	15.33	15.63	15.30	15.68	15.36	15.37	15.35	15.22	15.04	15.17
CaO	17.78	18.56	18.00	18.20	18.16	17.98	18.52	17.97	21.83	18.06
Na_2O	0.24	0.26	0.27	0.27	0.26	0.22	0.25	0.28	0.24	0.25
K_2O	0.00	0.01	0.00	0.00	0.00	0.01	0.00	0.00	0.00	0.00
NiO	0.01	0.00	0.00	0.00	0.00	0.00	0.01	0.00	0.01	0.00
V_2O_3	0.07	0.00	0.05	0.00	0.12	0.08	0.04	0.01	0.07	0.12
P_2O_5	-	-	-	-	-	-	-	-	-	-
Total[d]	100.12	99.44	100.06	99.81	100.04	100.00	99.78	99.95	100.31	99.71
Cations										
Si	7.65	7.68	7.65	7.67	7.65	7.66	7.61	7.69	7.63	7.55
Ti	0.07	0.07	0.07	0.07	0.06	0.07	0.08	0.07	0.07	0.04
Al	0.44	0.43	0.41	0.44	0.42	0.42	0.49	0.41	0.45	0.73
Cr	0.00	0.00	0.00	0.00	0.00	0.00	0.00	0.00	0.00	0.01
Fe2+	1.44	1.48	1.39	1.46	1.44	1.46	1.46	1.39	1.52	0.86
Mn	0.04	0.05	0.05	0.05	0.05	0.05	0.05	0.04	0.06	0.03
Mg	3.42	3.42	3.49	3.42	3.50	3.43	3.43	3.42	3.41	3.32
Ca	2.95	2.85	2.98	2.89	2.92	2.92	2.89	2.97	2.89	3.46
Na	0.08	0.07	0.07	0.08	0.08	0.08	0.06	0.07	0.08	0.07
K	0.00	0.00	0.00	0.00	0.00	0.00	0.00	0.00	0.00	0.00
Ni	0.00	0.00	0.00	0.00	0.00	0.00	0.00	0.00	0.00	0.00
V	0.01	0.01	0.00	0.01	0.00	0.01	0.01	0.01	0.00	0.01
P	-	-	-	-	-	-	-	-	-	-
Cation total	16.10	16.06	16.12	16.08	16.12	16.09	16.09	16.07	16.11	16.07
Mg# / An[e]	69.8	71.5	70.0	70.8	70.2	70.1	71.1	69.1	79.3	69.5
Lab[f]	2	2	2	2	2	2	2	2	2	2
Mineral[a]	CPX	CPX	CPX	CPX	CPX	CPX	CPX	CPX	CPX	CPX
Rim ID	b2r	b3r	b4r	b5r	c1r	c2r	c3r	c4r	c5r	d1r
Major element (wt.%)[b]										
SiO_2	51.73	51.37	51.18	51.43	51.17	50.75	51.34	51.95	51.20	51.56
TiO_2	0.48	0.61	0.60	0.54	0.65	0.62	0.65	0.50	0.63	0.56
Al_2O_3	1.75	2.30	2.50	2.25	2.31	2.51	2.75	1.93	2.55	2.24
Cr_2O_3	0.03	0.01	0.00	0.02	0.01	0.03	0.01	0.02	0.00	0.01
FeO[c]	11.22	11.39	11.98	11.38	11.37	11.14	10.87	11.44	11.91	11.38
MnO	0.40	0.34	0.39	0.38	0.38	0.41	0.32	0.45	0.36	0.38
MgO	16.22	15.27	15.50	15.48	15.43	15.53	14.83	15.76	14.89	15.44
CaO	17.85	18.33	17.42	18.15	18.42	18.61	18.93	17.64	18.20	18.14
Na_2O	0.22	0.25	0.27	0.30	0.22	0.27	0.24	0.20	0.24	0.25
K_2O	0.00	0.00	0.02	0.02	0.00	0.02	0.01	0.00	0.00	0.00
NiO	0.02	0.00	0.04	0.00	0.00	0.02	0.00	0.00	0.01	0.02
V_2O_3	0.09	0.12	0.10	0.05	0.04	0.08	0.05	0.11	0.01	0.03
P_2O_5	-	-	-	-	-	-	-	-	-	-
Total[d]	99.29	100.27	100.58	100.27	99.90	100.17	100.01	100.54	100.72	100.22
Cations										
Si	7.73	7.69	7.67	7.70	7.66	7.61	7.67	7.76	7.68	7.71
Ti	0.05	0.07	0.07	0.06	0.07	0.07	0.07	0.06	0.07	0.06
Al	0.31	0.41	0.44	0.40	0.41	0.44	0.48	0.34	0.45	0.39
Cr	0.00	0.00	0.00	0.00	0.00	0.00	0.00	0.00	0.00	0.00
Fe2+	1.40	1.43	1.50	1.42	1.42	1.40	1.36	1.43	1.49	1.42
Mn	0.05	0.04	0.05	0.05	0.05	0.05	0.04	0.06	0.05	0.05
Mg	3.61	3.41	3.46	3.45	3.44	3.47	3.30	3.51	3.33	3.44
Ca	2.86	2.94	2.80	2.91	2.96	2.99	3.03	2.82	2.92	2.91
Na	0.06	0.07	0.08	0.09	0.06	0.08	0.07	0.06	0.07	0.07
K	0.00	0.00	0.00	0.00	0.00	0.00	0.00	0.00	0.00	0.00
Ni	0.00	0.00	0.00	0.00	0.00	0.00	0.00	0.00	0.00	0.00
V	0.01	0.01	0.01	0.01	0.01	0.01	0.01	0.01	0.00	0.00
P	-	-	-	-	-	-	-	-	-	-
Cation total	16.09	16.07	16.08	16.09	16.09	16.13	16.04	16.04	16.06	16.06
Mg# / An[e]	72.0	70.5	69.8	70.8	70.7	71.3	70.9	71.1	69.0	70.8
Lab[f]	2	2	2	2	2	2	2	2	2	2

Table A3. (continued)

Volcanic cone	Kamikomezuka									
Sample	KKO									
Mineral[a]	CPX	CPX	CPX	CPX	CPX	CPX	CPX	CPX	CPX	CPX
Core ID	d2c	d3c	d4c	d5c	e1c	a1c	a6c	b2c	b5c	c6c
Major element (wt.%) [b]										
SiO_2	50.82	51.27	51.77	51.04	50.82	51.50	51.19	51.20	51.35	51.58
TiO_2	0.64	0.52	0.47	0.61	0.74	0.55	0.68	0.50	0.65	0.58
Al_2O_3	2.59	2.28	1.79	2.66	2.93	2.10	2.66	2.49	2.29	2.04
Cr_2O_3	0.00	0.00	0.01	0.03	0.05	0.00	0.02	0.00	0.00	0.01
FeO[c]	11.76	11.27	11.52	11.13	11.23	11.67	11.51	10.08	11.69	12.47
MnO	0.38	0.35	0.39	0.36	0.37	0.40	0.37	0.30	0.36	0.42
MgO	15.13	15.36	15.58	15.18	14.65	15.14	15.15	15.61	14.83	14.08
CaO	18.41	18.65	18.16	18.68	18.90	18.30	18.08	19.39	18.50	18.49
Na_2O	0.28	0.26	0.24	0.26	0.24	0.28	0.24	0.28	0.26	0.27
K_2O	0.00	0.00	0.00	0.02	0.00	0.00	0.00	0.01	0.01	0.00
NiO	0.00	0.00	0.02	0.00	0.00	0.05	0.00	0.03	0.01	0.01
V_2O_3	0.00	0.03	0.04	0.02	0.05	0.02	0.10	0.10	0.05	0.05
P_2O_5	-	-	-	-	-	-	-	-	-	-
Total[d]	99.59	100.42	100.55	100.24	99.46	99.39	99.53	99.24	99.67	100.30
Cations										
Si	7.69	7.63	7.68	7.75	7.64	7.62	7.72	7.66	7.65	7.70
Ti	0.07	0.07	0.06	0.05	0.07	0.08	0.06	0.08	0.06	0.07
Al	0.40	0.46	0.40	0.32	0.47	0.52	0.37	0.47	0.44	0.41
Cr	0.00	0.00	0.00	0.00	0.00	0.01	0.00	0.00	0.00	0.00
Fe2+	1.49	1.48	1.41	1.44	1.39	1.41	1.46	1.44	1.26	1.47
Mn	0.05	0.05	0.04	0.05	0.05	0.05	0.05	0.05	0.04	0.05
Mg	3.39	3.39	3.43	3.48	3.39	3.27	3.38	3.38	3.47	3.31
Ca	2.90	2.96	2.99	2.91	3.00	3.04	2.94	2.90	3.10	2.97
Na	0.07	0.08	0.08	0.07	0.08	0.07	0.08	0.07	0.08	0.08
K	0.00	0.00	0.00	0.00	0.00	0.00	0.00	0.00	0.00	0.00
Ni	0.00	0.00	0.00	0.00	0.00	0.00	0.01	0.00	0.00	0.00
V	0.01	0.00	0.00	0.00	0.00	0.01	0.00	0.01	0.01	0.01
P	-	-	-	-	-	-	-	-	-	-
Cation total	16.08	16.11	16.10	16.07	16.09	16.07	16.07	16.06	16.11	16.06
Mg# / An[e]	69.6	70.9	70.7	70.9	69.9	69.8	70.1	73.4	69.3	66.8
Lab[f]	2	2	2	2	2	2	2	2	2	2
Mineral[a]	CPX	CPX	CPX	CPX	CPX	CPX	CPX	CPX	CPX	CPX
Rim ID	d2r	d3r	d4r	d5r	e1r	a1r	a6r	b2r	b5r	c6r
Major element (wt.%)[b]										
SiO_2	51.96	51.67	51.39	51.64	51.90	49.57	52.04	51.69	49.94	51.07
TiO_2	0.62	0.56	0.54	0.51	0.46	0.86	0.44	0.54	0.74	0.59
Al_2O_3	2.31	2.32	2.20	2.16	2.06	5.08	2.03	2.20	4.00	3.44
Cr_2O_3	0.00	0.04	0.03	0.02	0.03	0.08	0.03	0.03	0.01	0.09
FeO[c]	11.01	10.91	11.18	10.93	11.40	9.24	10.38	10.05	10.98	9.03
MnO	0.37	0.37	0.37	0.34	0.40	0.20	0.41	0.33	0.29	0.28
MgO	15.33	15.32	15.11	15.68	15.60	13.66	15.95	15.80	14.04	14.93
CaO	18.02	18.45	18.86	18.39	17.86	21.00	18.51	19.04	19.60	20.29
Na_2O	0.29	0.26	0.23	0.31	0.23	0.28	0.17	0.18	0.26	0.23
K_2O	0.07	0.01	0.01	0.01	0.01	0.00	0.01	0.03	0.00	0.01
NiO	0.00	0.04	0.02	0.00	0.00	0.02	0.00	0.00	0.00	0.00
V_2O_3	0.02	0.06	0.07	0.00	0.06	0.00	0.05	0.11	0.13	0.05
P_2O_5	-	-	-	-	-	-	-	-	-	-
Total[d]	100.10	100.70	100.67	101.23	99.28	100.60	99.03	100.61	100.52	100.18
Cations										
Si	7.75	7.72	7.70	7.71	7.75	7.41	7.75	7.70	7.50	7.60
Ti	0.07	0.06	0.06	0.06	0.05	0.10	0.05	0.06	0.08	0.07
Al	0.41	0.41	0.39	0.38	0.36	0.90	0.36	0.39	0.71	0.60
Cr	0.00	0.00	0.00	0.00	0.00	0.01	0.00	0.00	0.00	0.01
Fe2+	1.37	1.36	1.40	1.36	1.42	1.15	1.29	1.25	1.38	1.12
Mn	0.05	0.05	0.05	0.04	0.05	0.03	0.05	0.04	0.04	0.04
Mg	3.41	3.41	3.37	3.49	3.47	3.04	3.54	3.51	3.14	3.31
Ca	2.88	2.95	3.03	2.94	2.86	3.36	2.95	3.04	3.15	3.23
Na	0.08	0.08	0.07	0.09	0.07	0.08	0.05	0.05	0.08	0.07
K	0.01	0.00	0.00	0.00	0.00	0.00	0.00	0.01	0.00	0.00
Ni	0.00	0.00	0.00	0.00	0.00	0.00	0.00	0.00	0.00	0.00
V	0.00	0.01	0.01	0.00	0.01	0.00	0.01	0.01	0.02	0.01
P	-	-	-	-	-	-	-	-	-	-
Cation total	16.03	16.05	16.08	16.08	16.05	16.08	16.05	16.07	16.09	16.06
Mg# / An[e]	71.3	71.4	70.7	71.9	70.9	72.5	73.3	73.7	69.5	74.7
Lab[f]	2	2	2	2	2	2	2	2	2	2

Table A3. (continued)

Volcanic cone			Ojodake							
Sample			OJSU							
Mineral[a]	CPX	CPX	CPX	CPX	CPX	CPX	CPX	CPX	CPX	CPX
Core ID	d2c	e3c	a2c	a3c	a5c	a6c	b1c	b2c	b4c	c1c
Major element (wt.%) [b]										
SiO_2	51.37	51.20	51.25	51.98	51.00	51.60	50.85	51.14	51.70	51.49
TiO_2	0.59	0.63	0.61	0.56	0.66	0.57	0.60	0.62	0.71	0.55
Al_2O_3	2.70	2.49	2.25	2.32	2.41	2.14	2.62	2.13	2.05	2.40
Cr_2O_3	0.01	0.02	0.03	0.02	0.01	0.01	0.04	0.00	0.00	0.00
FeO[c]	11.33	11.96	12.36	10.85	12.36	11.85	12.47	11.94	11.83	11.50
MnO	0.36	0.38	0.37	0.32	0.40	0.35	0.43	0.42	0.34	0.37
MgO	14.96	15.53	14.94	15.80	14.91	15.05	14.88	15.27	15.44	15.53
CaO	18.34	17.31	17.77	17.74	17.83	18.04	17.63	18.02	17.56	17.73
Na_2O	0.27	0.32	0.29	0.29	0.31	0.28	0.32	0.29	0.25	0.29
K_2O	0.00	0.01	0.00	0.00	0.00	0.00	0.01	0.00	0.00	0.01
NiO	0.00	0.01	0.02	0.00	0.00	0.00	0.03	0.00	0.03	0.00
V_2O_3	0.08	0.15	0.11	0.13	0.12	0.11	0.13	0.17	0.09	0.13
P_2O_5	-	-	-	-	-	-	-	-	-	-
Total[d]	99.81	98.61	99.03	99.04	99.16	98.05	98.43	98.16	98.63	98.82
Cations										
Si	7.76	7.68	7.67	7.70	7.74	7.66	7.73	7.65	7.68	7.73
Ti	0.07	0.07	0.07	0.07	0.06	0.07	0.06	0.07	0.07	0.08
Al	0.36	0.48	0.44	0.40	0.41	0.43	0.38	0.46	0.38	0.36
Cr	0.00	0.00	0.00	0.00	0.00	0.00	0.00	0.00	0.00	0.00
Fe2+	1.57	1.42	1.50	1.55	1.35	1.55	1.49	1.57	1.50	1.48
Mn	0.05	0.05	0.05	0.05	0.04	0.05	0.04	0.06	0.05	0.04
Mg	3.16	3.34	3.47	3.34	3.50	3.34	3.36	3.33	3.42	3.44
Ca	2.98	2.94	2.78	2.86	2.83	2.87	2.90	2.84	2.90	2.81
Na	0.08	0.08	0.09	0.09	0.08	0.09	0.08	0.09	0.08	0.07
K	0.00	0.00	0.00	0.00	0.00	0.00	0.00	0.00	0.00	0.00
Ni	0.00	0.00	0.00	0.00	0.00	0.00	0.00	0.00	0.00	0.00
V	0.01	0.01	0.02	0.01	0.02	0.01	0.01	0.02	0.02	0.01
P	-	-	-	-	-	-	-	-	-	-
Cation total	16.03	16.05	16.08	16.07	16.03	16.09	16.05	16.09	16.10	16.04
Mg# / An[e]	70.2	69.8	68.3	72.2	68.3	69.3	68.0	69.5	69.9	70.6
Lab[f]	2	2	2	2	2	2	2	2	2	2
Mineral[a]	CPX	CPX	CPX	CPX	CPX	CPX	CPX	CPX	CPX	CPX
Rim ID	d2r	e3r	a2r	a3r	a5r	a6r	b1r	b2r	b4r	c1r
Major element (wt.%)[b]										
SiO_2	52.03	50.61	-	51.58	51.63	50.66	52.14	50.89	51.43	52.33
TiO_2	0.46	0.60	-	0.63	0.56	0.59	0.49	0.55	0.55	0.44
Al_2O_3	2.73	3.70	-	2.63	2.87	3.61	2.16	3.53	3.39	1.97
Cr_2O_3	0.08	0.10	-	0.02	0.01	0.04	0.00	0.06	0.04	0.03
FeO[c]	7.89	8.47	-	10.28	9.77	8.76	9.56	8.44	8.93	9.69
MnO	0.21	0.21	-	0.37	0.30	0.26	0.37	0.24	0.26	0.37
MgO	15.35	15.05	-	15.57	15.47	15.85	16.03	15.53	15.41	16.00
CaO	21.02	21.01	-	18.55	18.95	19.84	18.92	20.29	19.56	18.83
Na_2O	0.18	0.22	-	0.29	0.34	0.28	0.22	0.30	0.27	0.21
K_2O	0.00	0.01	-	0.00	0.00	0.01	0.01	0.01	0.01	0.01
NiO	0.00	0.00	-	0.00	0.00	0.00	0.00	0.05	0.00	0.00
V_2O_3	0.05	0.02	-	0.07	0.10	0.09	0.10	0.10	0.14	0.10
P_2O_5	-	-	-	-	-	-	-	-	-	-
Total[d]	100.78	100.46	-	98.63	99.08	100.34	99.62	99.64	100.85	99.40
Cations			-							
Si	7.70	7.53	-	7.68	7.68	7.53	7.74	7.56	7.63	7.77
Ti	0.05	0.07	-	0.07	0.06	0.07	0.05	0.06	0.06	0.05
Al	0.48	0.65	-	0.46	0.50	0.63	0.38	0.62	0.59	0.34
Cr	0.01	0.01	-	0.00	0.00	0.01	0.00	0.01	0.01	0.00
Fe2+	0.98	1.05	-	1.28	1.22	1.09	1.19	1.05	1.11	1.20
Mn	0.03	0.03	-	0.05	0.04	0.03	0.05	0.03	0.03	0.05
Mg	3.39	3.34	-	3.46	3.43	3.51	3.55	3.44	3.41	3.54
Ca	3.33	3.35	-	2.96	3.02	3.16	3.01	3.23	3.11	3.00
Na	0.05	0.06	-	0.08	0.10	0.08	0.06	0.09	0.08	0.06
K	0.00	0.00	-	0.00	0.00	0.00	0.00	0.00	0.00	0.00
Ni	0.00	0.00	-	0.00	0.00	0.00	0.00	0.01	0.00	0.00
V	0.01	0.00	-	0.01	0.01	0.01	0.01	0.01	0.02	0.01
P	-	-	-	-	-	-	-	-	-	-
Cation total	16.03	16.10	-	16.05	16.05	16.12	16.04	16.10	16.04	16.03
Mg# / An[e]	77.6	76.0	-	73.0	73.8	76.3	74.9	76.6	75.5	74.6
Lab[f]	2	2	-	2	2	2	2	2	2	2

Table A3. (continued)

Volcanic cone										
Sample										
Mineral[a]	CPX	CPX	CPX	CPX	CPX	CPX	CPX	CPX	CPX	CPX
Core ID	c3c	c4c	c5c	d1c	d4c	e1c	e2c	e3c	e5c	e6c
Major element (wt.%) [b]										
SiO_2	52.16	51.20	51.30	51.45	52.18	51.49	51.34	51.69	51.36	51.24
TiO_2	0.52	0.66	0.56	0.60	0.57	0.55	0.67	0.56	0.66	0.63
Al_2O_3	2.09	2.54	2.68	2.13	2.34	2.27	2.59	2.39	2.37	2.36
Cr_2O_3	0.00	0.00	0.00	0.01	0.00	0.00	0.00	0.02	0.01	0.02
FeO[c]	11.18	12.16	10.71	11.39	10.51	11.41	10.93	11.06	11.84	12.48
MnO	0.37	0.40	0.36	0.42	0.35	0.35	0.36	0.31	0.36	0.44
MgO	15.10	15.17	15.14	15.41	15.66	14.83	15.31	15.77	14.99	14.86
CaO	18.22	17.40	18.80	18.21	18.01	18.68	18.37	17.81	17.92	17.59
Na_2O	0.25	0.33	0.26	0.24	0.26	0.30	0.25	0.25	0.29	0.27
K_2O	0.00	0.00	0.00	0.00	0.01	0.00	0.00	0.00	0.00	0.01
NiO	0.00	0.00	0.01	0.00	0.00	0.00	0.03	0.02	0.00	0.01
V_2O_3	0.11	0.13	0.19	0.14	0.12	0.12	0.13	0.11	0.19	0.10
P_2O_5	-	-	-	-	-	-	-	-	-	-
Total[d]	98.87	99.10	98.42	99.26	99.37	98.24	98.21	98.87	98.99	99.87
Cations										
Si	7.70	7.78	7.67	7.66	7.70	7.76	7.71	7.67	7.71	7.70
Ti	0.06	0.06	0.07	0.06	0.07	0.06	0.06	0.08	0.06	0.07
Al	0.42	0.37	0.45	0.47	0.38	0.41	0.40	0.46	0.42	0.42
Cr	0.00	0.00	0.00	0.00	0.00	0.00	0.00	0.00	0.00	0.00
Fe2+	1.44	1.39	1.52	1.34	1.43	1.31	1.43	1.37	1.38	1.48
Mn	0.05	0.05	0.05	0.05	0.05	0.04	0.04	0.05	0.04	0.05
Mg	3.46	3.36	3.39	3.37	3.44	3.47	3.31	3.41	3.51	3.35
Ca	2.84	2.91	2.79	3.01	2.92	2.87	3.00	2.94	2.84	2.88
Na	0.09	0.07	0.09	0.08	0.07	0.07	0.09	0.07	0.07	0.08
K	0.00	0.00	0.00	0.00	0.00	0.00	0.00	0.00	0.00	0.00
Ni	0.00	0.00	0.00	0.00	0.00	0.00	0.00	0.00	0.00	0.00
V	0.02	0.01	0.02	0.02	0.02	0.01	0.01	0.02	0.01	0.02
P	-	-	-	-	-	-	-	-	-	-
Cation total	16.07	16.01	16.07	16.06	16.07	16.01	16.06	16.06	16.05	16.05
Mg# / An[e]	70.7	69.0	71.6	70.7	72.6	69.8	71.4	71.8	69.3	68.0
Lab[f]	2	2	2	2	2	2	2	2	2	2
Mineral[a]	CPX	CPX	CPX	CPX	CPX	CPX	CPX	CPX	CPX	CPX
Rim ID	c3r	c4r	c5r	d1r	d4r	e1r	e2r	e3r	e5r	e6r
Major element (wt.%)[b]										
SiO_2	51.70	51.57	51.21	51.07	51.17	51.78	51.72	51.22	51.65	50.98
TiO_2	0.57	0.53	0.50	0.76	0.54	0.52	0.50	0.62	0.51	0.55
Al_2O_3	2.73	2.97	2.84	3.06	3.10	2.89	2.34	3.38	2.24	3.28
Cr_2O_3	0.01	0.01	0.05	0.00	0.02	0.07	0.02	0.05	0.01	0.05
FeO[c]	9.97	8.38	8.21	10.42	8.58	8.02	9.13	8.40	9.66	8.23
MnO	0.31	0.29	0.23	0.34	0.20	0.19	0.34	0.25	0.32	0.23
MgO	15.37	15.87	15.53	14.86	15.63	15.71	15.91	15.56	16.09	15.61
CaO	18.97	19.95	21.03	19.06	20.39	20.45	19.70	20.17	19.11	20.62
Na_2O	0.27	0.28	0.24	0.26	0.22	0.24	0.24	0.27	0.26	0.29
K_2O	0.00	0.02	0.00	0.00	0.02	0.00	0.01	0.00	0.01	0.01
NiO	0.00	0.00	0.03	0.03	0.00	0.00	0.00	0.00	0.00	0.04
V_2O_3	0.10	0.12	0.13	0.15	0.12	0.12	0.11	0.09	0.13	0.11
P_2O_5	-	-	-	-	-	-	-	-	-	-
Total[d]	98.26	100.07	98.19	99.02	98.59	99.78	98.36	100.20	99.90	100.17
Cations										
Si	7.69	7.64	7.61	7.63	7.60	7.67	7.69	7.60	7.69	7.57
Ti	0.06	0.06	0.06	0.09	0.06	0.06	0.06	0.07	0.06	0.06
Al	0.48	0.52	0.50	0.54	0.54	0.50	0.41	0.59	0.39	0.57
Cr	0.00	0.00	0.01	0.00	0.00	0.01	0.00	0.01	0.00	0.01
Fe2+	1.24	1.04	1.02	1.30	1.07	0.99	1.13	1.04	1.20	1.02
Mn	0.04	0.04	0.03	0.04	0.03	0.02	0.04	0.03	0.04	0.03
Mg	3.41	3.51	3.44	3.31	3.46	3.47	3.52	3.44	3.57	3.46
Ca	3.02	3.17	3.35	3.05	3.25	3.24	3.14	3.21	3.05	3.28
Na	0.08	0.08	0.07	0.08	0.06	0.07	0.07	0.08	0.08	0.08
K	0.00	0.00	0.00	0.00	0.00	0.00	0.00	0.00	0.00	0.00
Ni	0.00	0.00	0.00	0.00	0.00	0.00	0.00	0.00	0.00	0.00
V	0.01	0.01	0.02	0.02	0.01	0.01	0.01	0.01	0.02	0.01
P	-	-	-	-	-	-	-	-	-	-
Cation total	16.04	16.07	16.11	16.05	16.09	16.05	16.08	16.07	16.09	16.11
Mg# / An[e]	73.3	77.2	77.1	71.8	76.4	77.7	75.6	76.8	74.8	77.2
Lab[f]	2	2	2	2	2	2	2	2	2	2

Table A3. (continued)

Volcanic cone										
Sample	OJSL									
Mineral[a]	CPX	CPX	CPX	CPX	CPX	CPX	CPX	CPX	CPX	CPX
Core ID	a1c	a2c	a3c	a5c	a6c	b1c	b2c	b3c	b4c	b6c
Major element (wt.%) [b]										
SiO_2	50.84	51.08	-	51.06	51.49	50.62	51.53	51.20	51.01	50.98
TiO_2	0.64	0.56	-	0.57	0.56	0.69	0.59	0.60	0.71	0.62
Al_2O_3	2.28	2.30	-	2.63	2.23	2.57	2.20	2.57	2.51	2.74
Cr_2O_3	0.00	0.01	-	0.01	0.00	0.02	0.01	0.04	0.00	0.00
FeO[c]	12.08	12.39	-	11.61	11.43	10.97	11.05	10.77	12.55	11.81
MnO	0.47	0.43	-	0.32	0.35	0.32	0.41	0.34	0.44	0.36
MgO	15.22	15.33	-	15.00	15.56	15.41	15.65	15.38	15.10	15.09
CaO	18.02	17.48	-	18.39	18.01	18.95	18.17	18.66	17.28	17.93
Na_2O	0.29	0.29	-	0.30	0.25	0.30	0.28	0.30	0.27	0.31
K_2O	0.00	0.01	-	0.00	0.00	0.01	0.01	0.01	0.01	0.01
NiO	0.00	0.01	-	0.00	0.00	0.00	0.00	0.01	0.00	0.04
V_2O_3	0.15	0.11	-	0.12	0.12	0.15	0.10	0.12	0.13	0.12
P_2O_5	-	-	-	-	-	-	-	-	-	-
Total[d]	99.43	100.29	-	98.66	100.42	99.24	99.50	99.03	100.04	98.54
Cations			-							
Si	7.69	7.64	-	7.77	7.65	7.70	7.59	7.70	7.65	7.66
Ti	0.07	0.07	-	0.07	0.06	0.06	0.08	0.07	0.07	0.08
Al	0.42	0.40	-	0.41	0.46	0.39	0.45	0.39	0.45	0.44
Cr	0.00	0.00	-	0.00	0.00	0.00	0.00	0.00	0.00	0.00
Fe2+	1.57	1.52	-	1.68	1.46	1.43	1.38	1.38	1.35	1.58
Mn	0.06	0.06	-	0.06	0.04	0.04	0.04	0.05	0.04	0.06
Mg	3.33	3.41	-	3.18	3.35	3.47	3.44	3.49	3.43	3.38
Ca	2.83	2.90	-	2.73	2.95	2.89	3.04	2.91	2.99	2.78
Na	0.08	0.09	-	0.09	0.09	0.07	0.09	0.08	0.09	0.08
K	0.00	0.00	-	0.00	0.00	0.00	0.00	0.00	0.00	0.00
Ni	0.00	0.00	-	0.00	0.00	0.00	0.00	0.00	0.00	0.00
V	0.01	0.02	-	0.02	0.01	0.01	0.02	0.01	0.01	0.02
P	-	-	-	-	-	-	-	-	-	-
Cation total	16.06	16.12	-	16.00	16.09	16.07	16.14	16.08	16.09	16.07
Mg# / An[e]	69.2	68.8	-	69.7	70.8	71.5	71.6	71.8	68.2	69.5
Lab[f]	2	2	-	2	2	2	2	2	2	2
Mineral[a]	CPX	CPX	CPX	CPX	CPX	CPX	CPX	CPX	CPX	CPX
Rim ID	a1r	a2r	a3r	a5r	a6r	b1r	b2r	b3r	b4r	b6r
Major element (wt.%)[b]										
SiO_2	51.38	50.64	51.81	51.54	50.72	50.93	51.63	51.15	51.27	51.63
TiO_2	0.50	0.55	0.54	0.52	0.65	0.53	0.54	0.51	0.51	0.49
Al_2O_3	2.94	3.61	2.45	3.21	3.50	2.91	2.47	3.15	3.27	2.85
Cr_2O_3	0.02	0.03	0.02	0.05	0.05	0.02	0.01	0.09	0.04	0.01
FeO[c]	8.79	9.11	10.73	8.22	8.08	8.76	11.61	8.31	7.76	9.36
MnO	0.27	0.29	0.41	0.25	0.23	0.24	0.33	0.25	0.17	0.31
MgO	15.69	16.27	15.99	15.68	15.55	15.96	15.79	15.62	15.46	15.88
CaO	20.02	19.11	17.61	20.14	20.86	20.25	17.24	20.52	21.14	19.07
Na_2O	0.26	0.22	0.27	0.24	0.24	0.28	0.27	0.27	0.25	0.27
K_2O	0.01	0.00	0.00	0.00	0.00	0.00	0.00	0.00	0.00	0.02
NiO	0.00	0.04	0.03	0.00	0.04	0.00	0.00	0.01	0.00	0.00
V_2O_3	0.11	0.12	0.13	0.13	0.08	0.13	0.12	0.12	0.13	0.12
P_2O_5	-	-	-	-	-	-	-	-	-	-
Total[d]	99.83	100.26	99.84	99.08	99.34	98.78	99.53	98.56	101.71	99.12
Cations										
Si	7.63	7.52	7.71	7.63	7.58	7.70	7.60	7.60	7.54	7.67
Ti	0.06	0.06	0.06	0.06	0.06	0.06	0.06	0.06	0.07	0.05
Al	0.51	0.63	0.43	0.56	0.51	0.43	0.55	0.57	0.61	0.50
Cr	0.00	0.00	0.00	0.01	0.00	0.00	0.01	0.01	0.01	0.00
Fe2+	1.09	1.13	1.34	1.02	1.09	1.45	1.03	0.96	1.00	1.16
Mn	0.03	0.04	0.05	0.03	0.03	0.04	0.03	0.02	0.03	0.04
Mg	3.47	3.60	3.55	3.46	3.54	3.51	3.46	3.42	3.44	3.51
Ca	3.19	3.04	2.81	3.20	3.23	2.76	3.27	3.36	3.32	3.03
Na	0.08	0.06	0.08	0.07	0.08	0.08	0.08	0.07	0.07	0.08
K	0.00	0.00	0.00	0.00	0.00	0.00	0.00	0.00	0.00	0.00
Ni	0.00	0.01	0.00	0.00	0.00	0.00	0.00	0.00	0.00	0.00
V	0.01	0.01	0.01	0.02	0.02	0.01	0.01	0.02	0.01	0.01
P	-	-	-	-	-	-	-	-	-	-
Cation total	16.09	16.12	16.04	16.05	16.14	16.05	16.10	16.08	16.11	16.06
Mg# / An[e]	76.1	76.1	72.6	77.3	77.4	76.5	70.8	77.0	78.0	75.2
Lab[f]	2	2	2	2	2	2	2	2	2	2

Table A3. (continued)

Volcanic cone										
Sample										
Mineral[a]	CPX	CPX	CPX	CPX	CPX	CPX	CPX	CPX	CPX	CPX
Core ID	c1c	c2c	c4c	c5c	c6c	d1c	d2c	d5c	d6c	e1c
Major element (wt.%) [b]										
SiO_2	51.94	51.39	52.00	51.35	50.87	51.54	51.24	50.82	51.72	51.71
TiO_2	0.51	0.62	0.50	0.65	0.59	0.60	0.57	0.61	0.53	0.55
Al_2O_3	2.09	2.30	1.89	2.42	3.07	2.11	2.39	2.60	2.20	2.39
Cr_2O_3	0.00	0.00	0.00	0.00	0.04	0.03	0.00	0.00	0.00	0.00
FeO[c]	11.24	10.99	9.72	11.64	11.22	11.77	10.95	11.53	10.90	10.28
MnO	0.38	0.34	0.49	0.39	0.34	0.43	0.40	0.38	0.33	0.34
MgO	15.90	15.57	15.12	15.10	15.15	15.02	15.89	15.58	15.87	14.90
CaO	17.52	18.41	19.77	17.97	18.29	18.12	18.18	18.05	18.09	19.39
Na_2O	0.27	0.22	0.35	0.29	0.27	0.28	0.26	0.28	0.23	0.30
K_2O	0.00	0.01	0.01	0.00	0.02	0.00	0.00	0.00	0.00	0.00
NiO	0.00	0.00	0.04	0.03	0.01	0.00	0.01	0.00	0.00	0.01
V_2O_3	0.15	0.14	0.10	0.15	0.14	0.09	0.11	0.15	0.13	0.13
P_2O_5	-	-	-	-	-	-	-	-	-	-
Total[d]	98.49	100.23	98.67	99.48	98.63	98.97	99.27	100.00	100.00	99.39
Cations										
Si	7.64	7.74	7.68	7.76	7.69	7.61	7.72	7.66	7.62	7.71
Ti	0.07	0.06	0.07	0.06	0.07	0.07	0.07	0.06	0.07	0.06
Al	0.48	0.37	0.41	0.33	0.43	0.54	0.37	0.42	0.46	0.39
Cr	0.00	0.00	0.00	0.00	0.00	0.00	0.00	0.00	0.00	0.00
Fe2+	1.48	1.40	1.37	1.21	1.46	1.40	1.47	1.37	1.45	1.36
Mn	0.05	0.05	0.04	0.06	0.05	0.04	0.05	0.05	0.05	0.04
Mg	3.37	3.53	3.47	3.36	3.37	3.38	3.36	3.54	3.48	3.53
Ca	2.88	2.80	2.95	3.16	2.88	2.93	2.91	2.91	2.90	2.89
Na	0.09	0.08	0.06	0.10	0.08	0.08	0.08	0.07	0.08	0.07
K	0.00	0.00	0.00	0.00	0.00	0.00	0.00	0.00	0.00	0.00
Ni	0.00	0.00	0.00	0.00	0.00	0.00	0.00	0.00	0.00	0.00
V	0.02	0.02	0.02	0.01	0.02	0.02	0.01	0.01	0.02	0.02
P	-	-	-	-	-	-	-	-	-	-
Cation total	16.08	16.05	16.07	16.07	16.06	16.08	16.06	16.10	16.12	16.06
Mg# / An[e]	71.6	71.6	73.5	69.8	70.6	69.5	72.1	70.7	72.2	72.1
Lab[f]	2	2	2	2	2	2	2	2	2	2
Mineral[a]	CPX	CPX	CPX	CPX	CPX	CPX	CPX	CPX	CPX	CPX
Rim ID	c1r	c2r	c4r	c5r	c6r	d1r	d2r	d5r	d6r	e1r
Major element (wt.%)[b]										
SiO_2	50.97	51.43	50.42	50.13	51.61	50.70	50.91	52.37	-	51.05
TiO_2	0.55	0.52	0.63	0.57	0.52	0.63	0.57	0.47	-	0.54
Al_2O_3	3.07	2.95	3.82	4.45	2.10	3.52	3.29	1.70	-	3.40
Cr_2O_3	0.02	0.02	0.07	0.04	0.02	0.00	0.06	0.02	-	0.06
FeO[c]	9.26	8.27	8.60	7.87	9.97	8.40	8.42	9.94	-	8.31
MnO	0.30	0.23	0.26	0.20	0.36	0.24	0.21	0.39	-	0.22
MgO	15.87	15.69	15.09	14.81	16.25	15.33	15.54	16.20	-	15.36
CaO	19.57	20.51	20.75	21.53	18.76	20.78	20.65	18.58	-	20.72
Na_2O	0.27	0.27	0.27	0.29	0.23	0.31	0.24	0.24	-	0.22
K_2O	0.01	0.00	0.00	0.00	0.00	0.00	0.00	0.00	-	0.00
NiO	0.00	0.00	0.00	0.00	0.07	0.00	0.00	0.00	-	0.02
V_2O_3	0.12	0.12	0.09	0.13	0.11	0.10	0.09	0.08	-	0.10
P_2O_5	-	-	-	-	-	-	-	-	-	-
Total[d]	100.26	99.99	98.84	99.80	98.41	99.29	98.09	100.15	-	99.51
Cations									-	
Si	7.59	7.63	7.51	7.46	7.69	7.54	7.57	7.78	-	7.58
Ti	0.06	0.06	0.07	0.06	0.06	0.07	0.06	0.05	-	0.06
Al	0.54	0.52	0.67	0.78	0.37	0.62	0.58	0.30	-	0.60
Cr	0.00	0.00	0.01	0.00	0.00	0.00	0.01	0.00	-	0.01
Fe2+	1.15	1.03	1.07	0.98	1.24	1.05	1.05	1.24	-	1.03
Mn	0.04	0.03	0.03	0.03	0.05	0.03	0.03	0.05	-	0.03
Mg	3.52	3.47	3.35	3.28	3.61	3.40	3.44	3.59	-	3.40
Ca	3.12	3.26	3.31	3.43	2.99	3.31	3.29	2.96	-	3.30
Na	0.08	0.08	0.08	0.08	0.07	0.09	0.07	0.07	-	0.06
K	0.00	0.00	0.00	0.00	0.00	0.00	0.00	0.00	-	0.00
Ni	0.00	0.00	0.00	0.00	0.01	0.00	0.00	0.00	-	0.00
V	0.01	0.01	0.01	0.02	0.01	0.01	0.01	0.01	-	0.01
P	-	-	-	-	-	-	-	-	-	-
Cation total	16.12	16.08	16.11	16.12	16.09	16.12	16.11	16.05	-	16.08
Mg# / An[e]	75.3	77.2	75.8	77.0	74.4	76.5	76.7	74.4	-	76.7
Lab[f]	2	2	2	2	2	2	2	2	-	2

Table A3. (continued)

Volcanic cone							Kishimadake			
Sample							KSS			
Mineral[a]	CPX	CPX	CPX	CPX	CPX	CPX	CPX	CPX	CPX	CPX
Core ID	e2c	e3c	e5c	e6c	f1c	f2c	a1c	a2c	a3c	a5c
Major element (wt.%) [b]										
SiO_2	51.35	51.23	51.31	51.32	51.35	51.62	50.99	51.31	49.94	52.42
TiO_2	0.64	0.57	0.63	0.55	0.67	0.67	0.62	0.67	0.72	0.32
Al_2O_3	2.35	2.57	2.16	2.32	2.30	2.55	3.31	2.24	2.42	1.35
Cr_2O_3	0.02	0.00	0.01	0.00	0.02	0.04	0.00	0.02	0.01	0.01
FeO[c]	12.56	11.25	12.01	11.48	11.68	12.47	8.63	12.75	12.20	20.29
MnO	0.45	0.32	0.36	0.39	0.39	0.42	0.21	0.43	0.35	0.64
MgO	15.00	15.70	15.24	15.70	15.30	14.92	14.89	14.52	15.30	22.84
CaO	17.23	17.93	17.87	17.83	17.87	16.93	20.99	17.73	18.70	2.03
Na_2O	0.34	0.29	0.30	0.28	0.26	0.33	0.26	0.26	0.29	0.06
K_2O	0.00	0.00	0.00	0.00	0.00	0.00	0.01	0.00	0.01	0.00
NiO	0.00	0.01	0.00	0.01	0.02	0.00	0.00	0.00	0.00	0.01
V_2O_3	0.07	0.14	0.11	0.12	0.12	0.06	0.08	0.06	0.05	0.02
P_2O_5	-	-	-	-	-	-	-	-	-	-
Total[d]	99.08	99.28	98.73	100.20	99.67	98.85	99.87	100.33	98.88	101.14
Cations										
Si	7.72	7.70	7.66	7.70	7.68	7.69	7.73	7.59	7.71	7.54
Ti	0.06	0.07	0.06	0.07	0.06	0.08	0.08	0.07	0.08	0.08
Al	0.42	0.42	0.45	0.38	0.41	0.41	0.45	0.58	0.40	0.43
Cr	0.00	0.00	0.00	0.00	0.00	0.00	0.01	0.00	0.00	0.00
Fe2+	1.28	1.58	1.41	1.51	1.44	1.46	1.56	1.08	1.60	1.54
Mn	0.04	0.06	0.04	0.05	0.05	0.05	0.05	0.03	0.05	0.04
Mg	3.32	3.35	3.50	3.41	3.50	3.42	3.33	3.31	3.26	3.44
Ca	3.10	2.77	2.87	2.87	2.86	2.87	2.72	3.35	2.86	3.03
Na	0.09	0.10	0.08	0.09	0.08	0.08	0.09	0.08	0.08	0.09
K	0.00	0.00	0.00	0.00	0.00	0.00	0.00	0.00	0.00	0.00
Ni	0.00	0.00	0.00	0.00	0.00	0.00	0.00	0.00	0.00	0.00
V	0.02	0.01	0.02	0.01	0.02	0.01	0.01	0.01	0.01	0.01
P	-	-	-	-	-	-	-	-	-	-
Cation total	16.05	16.06	16.09	16.08	16.09	16.06	16.02	16.08	16.04	16.20
Mg# / An[e]	68.0	71.3	69.3	70.9	70.0	68.1	75.5	67.0	69.1	66.7
Lab[f]	2	2	2	2	2	2	2	2	2	2
Mineral[a]	CPX	CPX	CPX	CPX	CPX	CPX	CPX	CPX	CPX	CPX
Rim ID	e2r	e3r	e5r	e6r	f1r	f2r	a1r	a2r	a3r	a5r
Major element (wt.%)[b]										
SiO_2	51.31	51.26	51.49	51.55	51.04	51.84	51.06	51.32	51.76	52.08
TiO_2	0.58	0.58	0.55	0.51	0.55	0.52	0.54	0.53	0.55	0.58
Al_2O_3	2.45	3.29	3.19	2.93	3.35	3.22	3.06	2.87	2.51	2.01
Cr_2O_3	0.00	0.03	0.04	0.00	0.03	0.03	0.07	0.03	0.03	0.00
FeO[c]	11.01	8.39	8.27	8.31	8.38	7.98	8.30	8.24	10.00	11.14
MnO	0.37	0.22	0.21	0.25	0.25	0.22	0.23	0.23	0.36	0.43
MgO	15.96	15.39	15.69	15.85	16.07	15.58	15.33	15.40	15.86	14.60
CaO	17.89	20.45	20.12	20.23	19.94	20.29	21.14	21.04	18.58	18.83
Na_2O	0.26	0.29	0.29	0.23	0.24	0.25	0.22	0.27	0.27	0.24
K_2O	0.02	0.00	0.01	0.00	0.00	0.00	0.00	0.00	0.01	0.02
NiO	0.05	0.00	0.01	0.00	0.00	0.00	0.01	0.00	0.00	0.03
V_2O_3	0.11	0.08	0.14	0.12	0.15	0.08	0.04	0.05	0.07	0.04
P_2O_5	-	-	-	-	-	-	-	-	-	-
Total[d]	98.91	99.86	100.22	100.95	99.61	100.60	99.09	100.44	99.55	99.08
Cations										
Si	7.66	7.61	7.63	7.64	7.57	7.66	7.60	7.63	7.70	7.79
Ti	0.06	0.06	0.06	0.06	0.06	0.06	0.06	0.06	0.06	0.06
Al	0.43	0.58	0.56	0.51	0.59	0.56	0.54	0.50	0.44	0.35
Cr	0.00	0.00	0.00	0.00	0.00	0.00	0.01	0.00	0.00	0.00
Fe2+	1.38	1.04	1.02	1.03	1.04	0.99	1.03	1.02	1.24	1.39
Mn	0.05	0.03	0.03	0.03	0.03	0.03	0.03	0.03	0.05	0.06
Mg	3.55	3.41	3.47	3.50	3.55	3.43	3.40	3.41	3.52	3.25
Ca	2.86	3.25	3.19	3.21	3.17	3.21	3.37	3.35	2.96	3.02
Na	0.07	0.08	0.08	0.07	0.07	0.07	0.06	0.08	0.08	0.07
K	0.00	0.00	0.00	0.00	0.00	0.00	0.00	0.00	0.00	0.00
Ni	0.01	0.00	0.00	0.00	0.00	0.00	0.00	0.00	0.00	0.00
V	0.01	0.01	0.02	0.01	0.02	0.01	0.00	0.01	0.01	0.01
P	-	-	-	-	-	-	-	-	-	-
Cation total	16.09	16.07	16.06	16.07	16.10	16.03	16.10	16.10	16.06	16.01
Mg# / An[e]	72.1	76.6	77.2	77.3	77.4	77.7	76.7	76.9	73.9	70.0
Lab[f]	2	2	2	2	2	2	2	2	2	2

Table A3. (continued)

Volcanic cone										
Sample										
Mineral[a]	CPX	CPX	CPX	CPX	CPX	CPX	CPX	CPX	CPX	CPX
Core ID	b3c	b4c	b5c	c1c	c2c	c3c	c4c	c5c	d1c	d3c
Major element (wt.%) [b]										
SiO_2	51.52	50.84	50.50	51.47	51.28	51.60	51.57	51.18	51.01	51.50
TiO_2	0.57	0.63	0.59	0.64	0.60	0.58	0.58	0.56	0.73	0.62
Al_2O_3	2.14	2.65	2.45	1.85	2.13	2.02	2.38	2.45	2.50	2.30
Cr_2O_3	0.00	0.00	0.03	0.00	0.01	0.02	0.00	0.03	0.02	0.01
FeO[c]	12.18	12.37	11.88	12.04	11.10	11.87	9.98	11.71	11.65	11.39
MnO	0.43	0.39	0.38	0.42	0.46	0.34	0.40	0.37	0.39	0.40
MgO	14.63	15.14	15.17	14.99	14.88	14.46	15.28	15.24	15.22	14.47
CaO	18.16	17.61	18.71	18.26	19.22	18.74	19.50	18.14	18.10	18.93
Na_2O	0.31	0.25	0.26	0.28	0.27	0.29	0.27	0.25	0.28	0.27
K_2O	0.00	0.02	0.00	0.00	0.00	0.02	0.00	0.00	0.00	0.01
NiO	0.00	0.02	0.00	0.01	0.01	0.00	0.00	0.00	0.01	0.00
V_2O_3	0.06	0.08	0.03	0.06	0.04	0.07	0.06	0.07	0.09	0.09
P_2O_5	-	-	-	-	-	-	-	-	-	-
Total[d]	99.32	99.54	98.90	99.78	99.46	99.34	98.89	99.61	100.78	100.04
Cations										
Si	7.73	7.64	7.60	7.73	7.69	7.75	7.69	7.67	7.65	7.72
Ti	0.06	0.07	0.07	0.07	0.07	0.07	0.06	0.06	0.08	0.07
Al	0.38	0.47	0.44	0.33	0.38	0.36	0.42	0.43	0.44	0.41
Cr	0.00	0.00	0.00	0.00	0.00	0.00	0.00	0.00	0.00	0.00
Fe2+	1.53	1.55	1.50	1.51	1.39	1.49	1.24	1.47	1.46	1.43
Mn	0.05	0.05	0.05	0.05	0.06	0.04	0.05	0.05	0.05	0.05
Mg	3.27	3.39	3.40	3.36	3.33	3.24	3.40	3.40	3.40	3.23
Ca	2.92	2.83	3.02	2.94	3.09	3.01	3.12	2.91	2.91	3.04
Na	0.09	0.07	0.08	0.08	0.08	0.09	0.08	0.07	0.08	0.08
K	0.00	0.00	0.00	0.00	0.00	0.00	0.00	0.00	0.00	0.00
Ni	0.00	0.00	0.00	0.00	0.00	0.00	0.00	0.00	0.00	0.00
V	0.01	0.01	0.00	0.01	0.01	0.01	0.01	0.01	0.01	0.01
P	-	-	-	-	-	-	-	-	-	-
Cation total	16.05	16.09	16.15	16.07	16.09	16.05	16.07	16.08	16.09	16.04
Mg# / An[e]	68.2	68.6	69.5	68.9	70.5	68.5	73.2	69.9	70.0	69.4
Lab[f]	2	2	2	2	2	2	2	2	2	2
Mineral[a]	CPX	CPX	CPX	CPX	CPX	CPX	CPX	CPX	CPX	CPX
Rim ID	b3r	b4r	b5r	c1r	c2r	c3r	c4r	c5r	d1r	d3r
Major element (wt.%)[b]										
SiO_2	51.22	51.51	51.06	50.90	49.87	50.45	51.57	51.09	50.88	50.64
TiO_2	0.58	0.43	0.56	0.55	0.63	0.82	0.50	0.56	0.53	0.65
Al_2O_3	3.04	2.32	3.02	3.17	3.82	3.34	3.02	2.98	2.92	3.08
Cr_2O_3	0.02	0.01	0.05	0.02	0.01	0.00	0.10	0.07	0.05	0.01
FeO[c]	7.77	8.23	7.90	8.38	8.31	8.44	8.75	8.07	8.22	9.38
MnO	0.26	0.26	0.25	0.25	0.21	0.22	0.23	0.21	0.25	0.24
MgO	15.40	16.22	15.34	15.34	15.18	15.02	15.84	15.38	15.52	15.25
CaO	21.48	20.73	21.56	21.09	21.61	21.41	19.67	21.32	21.36	20.38
Na_2O	0.21	0.19	0.24	0.23	0.24	0.24	0.25	0.24	0.20	0.28
K_2O	0.01	0.01	0.00	0.01	0.03	0.01	0.02	0.00	0.00	0.00
NiO	0.00	0.01	0.00	0.03	0.01	0.02	0.00	0.03	0.00	0.01
V_2O_3	0.02	0.06	0.02	0.03	0.06	0.04	0.05	0.04	0.06	0.07
P_2O_5	-	-	-	-	-	-	-	-	-	-
Total[d]	98.73	100.02	100.28	99.28	99.47	99.98	99.91	100.77	100.39	100.30
Cations										
Si	7.61	7.65	7.59	7.58	7.45	7.52	7.65	7.60	7.58	7.56
Ti	0.06	0.05	0.06	0.06	0.07	0.09	0.06	0.06	0.06	0.07
Al	0.53	0.41	0.53	0.56	0.67	0.59	0.53	0.52	0.51	0.54
Cr	0.00	0.00	0.01	0.00	0.00	0.00	0.01	0.01	0.01	0.00
Fe2+	0.97	1.02	0.98	1.04	1.04	1.05	1.08	1.00	1.02	1.17
Mn	0.03	0.03	0.03	0.03	0.03	0.03	0.03	0.03	0.03	0.03
Mg	3.41	3.59	3.40	3.40	3.38	3.34	3.50	3.41	3.45	3.40
Ca	3.42	3.30	3.43	3.36	3.46	3.42	3.13	3.40	3.41	3.26
Na	0.06	0.05	0.07	0.07	0.07	0.07	0.07	0.07	0.06	0.08
K	0.00	0.00	0.00	0.00	0.01	0.00	0.00	0.00	0.00	0.00
Ni	0.00	0.00	0.00	0.00	0.00	0.00	0.00	0.00	0.00	0.00
V	0.00	0.01	0.00	0.00	0.01	0.00	0.01	0.00	0.01	0.01
P	-	-	-	-	-	-	-	-	-	-
Cation total	16.09	16.12	16.11	16.12	16.18	16.12	16.06	16.11	16.13	16.13
Mg# / An[e]	77.9	77.8	77.6	76.5	76.5	76.0	76.4	77.3	77.1	74.4
Lab[f]	2	2	2	2	2	2	2	2	2	2

Table A3. (continued)

Volcanic cone			Nakadake			Kamikomezuka				
Sample			NKD14			KKO				
Mineral[a]	CPX	CPX	OPX		OPX	OPX		OPX		OPX
Core ID	d4c	d5c	4-R1		4-R5	1-C1		1-C2		1-C3
Major element (wt.%) [b]										
SiO_2	50.71	51.03	53.31		53.22	52.64		52.91		52.91
TiO_2	0.62	0.64	0.32		0.26	0.34		0.34		0.33
Al_2O_3	2.04	2.57	1.26		1.26	1.49		1.54		1.53
Cr_2O_3	0.00	0.00	0.02		0.00	0.00		0.00		0.00
FeO[c]	13.32	11.79	17.80		17.88	19.50		19.21		19.49
MnO	0.52	0.43	0.53		0.52	0.52		0.54		0.47
MgO	14.85	14.95	23.26		24.39	23.31		23.15		23.08
CaO	17.63	18.26	3.42		2.22	2.14		2.16		2.11
Na_2O	0.28	0.26	0.06		0.14	0.06		0.05		0.05
K_2O	0.01	0.00	0.01		0.00	0.00		0.01		0.02
NiO	0.00	0.00	0.00		0.01	0.00		0.03		0.00
V_2O_3	0.02	0.07	0.01		0.09	0.00		0.05		0.00
P_2O_5	-	-	-		-	-		-		-
Total[d]	99.25	100.43	99.13		100.24	99.91		100.23		100.08
Cations										
Si	7.66	7.66	7.84		7.81	7.79		7.81		7.82
Ti	0.07	0.07	0.04		0.03	0.04		0.04		0.04
Al	0.36	0.45	0.22		0.22	0.26		0.27		0.27
Cr	0.00	0.00	0.00		0.00	0.00		0.00		0.00
Fe2+	1.68	1.48	2.19		2.20	2.41		2.37		2.41
Mn	0.07	0.05	0.07		0.07	0.07		0.07		0.06
Mg	3.34	3.34	5.10		5.34	5.14		5.10		5.08
Ca	2.85	2.94	0.54		0.35	0.34		0.34		0.33
Na	0.08	0.08	0.02		0.04	0.02		0.01		0.01
K	0.00	0.00	0.00		0.00	0.00		0.00		0.00
Ni	0.00	0.00	0.00		0.00	0.00		0.00		0.00
V	0.00	0.01	0.00		0.01	0.00		0.01		0.00
P	-	-	-		-	-		-		-
Cation total	16.13	16.08	16.02		16.06	16.05		16.02		16.02
Mg# / An[e]	66.5	69.3	70.0		70.9	68.1		68.2		67.9
Lab[f]	2	2	2		2	2		2		2
Mineral[a]	CPX	CPX	CPX[g]	OL[g]	CPX[g]	CPX[g]	OL[g]	CPX[g]	OL[g]	CPX[g]
Rim ID	d4r	d5r	4-R2	4-R1-2	4-R6	1-R1	1-R1-2	1-R2	1-R2-2	1-R3
Major element (wt.%)[b]										
SiO_2	51.35	52.01	51.29	36.77	50.83	53.48	37.95	51.88	38.34	53.34
TiO_2	0.59	0.57	0.56	0.01	0.78	0.27	0.03	0.50	0.00	0.25
Al_2O_3	3.00	2.03	2.31	0.01	2.63	1.05	0.03	3.04	0.03	1.23
Cr_2O_3	0.04	0.00	0.02	0.00	0.04	0.02	0.01	0.05	0.00	0.02
FeO[c]	9.58	13.64	11.16	29.59	11.03	9.64	23.11	8.47	22.24	8.99
MnO	0.33	0.46	0.36	0.61	0.30	0.29	0.41	0.29	0.37	0.36
MgO	15.19	15.09	15.59	32.66	15.55	17.65	38.12	14.93	38.66	17.08
CaO	19.57	15.94	18.39	0.24	18.55	17.38	0.20	20.49	0.24	18.41
Na_2O	0.24	0.23	0.25	0.02	0.29	0.18	0.00	0.30	0.01	0.25
K_2O	0.01	0.02	0.01	0.00	0.00	0.00	0.01	0.05	0.00	0.00
NiO	0.01	0.00	0.03	0.04	0.00	0.01	0.07	0.00	0.03	0.02
V_2O_3	0.09	0.02	0.03	0.04	0.02	0.04	0.08	0.00	0.09	0.05
P_2O_5	-	-	-	-	-	-	-	-	-	-
Total[d]	99.22	98.75	99.67	100.92	101.00	98.55	100.77	99.85	101.78	101.85
Cations										
Si	7.65	7.80	7.67	5.97	7.61	7.89	5.96	7.69	5.99	7.87
Ti	0.07	0.06	0.06	0.00	0.09	0.03	0.00	0.06	0.00	0.03
Al	0.53	0.36	0.41	0.00	0.46	0.18	0.00	0.53	0.01	0.21
Cr	0.01	0.00	0.00	0.00	0.00	0.00	0.00	0.01	0.00	0.00
Fe2+	1.19	1.71	1.40	4.02	1.38	1.19	3.03	1.05	2.91	1.11
Mn	0.04	0.06	0.05	0.08	0.04	0.04	0.05	0.04	0.05	0.04
Mg	3.37	3.37	3.48	7.90	3.47	3.88	8.92	3.30	9.00	3.76
Ca	3.12	2.56	2.95	0.04	2.97	2.75	0.03	3.26	0.04	2.91
Na	0.07	0.07	0.07	0.01	0.08	0.05	0.00	0.09	0.00	0.07
K	0.00	0.00	0.00	0.00	0.00	0.00	0.00	0.01	0.00	0.00
Ni	0.00	0.00	0.00	0.01	0.00	0.00	0.01	0.00	0.00	0.00
V	0.01	0.00	0.00	0.01	0.00	0.00	0.01	0.00	0.01	0.01
P	-	-	-	-	-	-	-	-	-	-
Cation total	16.05	15.99	16.09	18.03	16.11	16.01	18.03	16.03	18.01	16.02
Mg# / An[e]	73.9	66.4	71.4	66.3	71.5	76.5	74.6	75.9	75.6	77.2
Lab[f]	2	2	2	2	2	2	2	2	2	2

Table A3. (continued)

Volcanic cone									Ojodake	
Sample									OJSU	
Mineral[a]		OPX		OPX		OPX	OPX		OPX	OPX
Core ID		1-C4		1-C5		1-C6	1-C7		1-C8	1-C5
Major element (wt.%) [b]										
SiO_2		53.04		52.97		52.67	52.69		52.97	52.52
TiO_2		0.36		0.35		0.33	0.37		0.36	0.32
Al_2O_3		1.47		1.41		1.35	1.39		1.34	1.42
Cr_2O_3		0.02		0.00		0.00	0.00		0.00	0.00
FeO[c]		19.62		18.86		19.72	19.94		19.90	19.70
MnO		0.52		0.51		0.54	0.57		0.57	0.55
MgO		22.72		23.70		23.20	22.82		22.75	23.23
CaO		2.13		2.17		2.04	2.09		2.07	2.10
Na_2O		0.03		0.02		0.05	0.04		0.03	0.06
K_2O		0.01		0.01		0.00	0.00		0.01	0.00
NiO		0.00		0.00		0.00	0.00		0.00	0.00
V_2O_3		0.07		0.00		0.10	0.10		0.01	0.10
P_2O_5		-		-		-	-		-	-
Total[d]		100.79		100.12		99.07	100.44		100.28	100.53
Cations										
Si		7.84		7.81		7.80	7.81		7.84	7.78
Ti		0.04		0.04		0.04	0.04		0.04	0.04
Al		0.26		0.25		0.24	0.24		0.23	0.25
Cr		0.00		0.00		0.00	0.00		0.00	0.00
Fe2+		2.43		2.33		2.44	2.47		2.46	2.44
Mn		0.07		0.06		0.07	0.07		0.07	0.07
Mg		5.01		5.21		5.12	5.04		5.02	5.13
Ca		0.34		0.34		0.32	0.33		0.33	0.33
Na		0.01		0.00		0.01	0.01		0.01	0.02
K		0.00		0.00		0.00	0.00		0.00	0.00
Ni		0.00		0.00		0.00	0.00		0.00	0.00
V		0.01		0.00		0.01	0.01		0.00	0.01
P		-		-		-	-		-	-
Cation total		15.99		16.04		16.05	16.03		16.01	16.06
Mg# / An[e]		67.4		69.1		67.7	67.1		67.1	67.8
Lab[f]		2		2		2	2		2	2
Mineral[a]	OL[g]	CPX[g]	OL[g]	CPX[g]	OL[g]	CPX[g]	CPX[g]	OL[g]	CPX[g]	CPX[g]
Rim ID	1-R3-2	1-R4	1-R4-2	1-R5	1-R5-2	1-R6	1-R7	1-R7-2	1-R8	1-R5
Major element (wt.%)[b]										
SiO_2	38.43	53.78	38.74	51.03	-	52.47	51.33	38.23	51.66	51.57
TiO_2	0.00	0.26	0.02	0.57	-	0.33	0.49	0.05	0.45	0.47
Al_2O_3	0.03	1.15	0.03	3.54	-	1.82	3.01	0.01	2.68	2.82
Cr_2O_3	0.00	0.01	0.03	0.00	-	0.02	0.08	0.02	0.05	0.03
FeO[c]	21.95	10.27	22.14	8.48	-	9.29	8.14	22.34	8.52	9.52
MnO	0.41	0.36	0.37	0.26	-	0.33	0.20	0.39	0.26	0.30
MgO	38.90	18.14	38.43	15.82	-	17.28	15.45	38.72	16.08	16.37
CaO	0.23	15.74	0.20	19.97	-	18.20	20.94	0.20	20.04	18.59
Na_2O	0.03	0.21	0.02	0.26	-	0.20	0.28	0.00	0.21	0.25
K_2O	0.00	0.01	0.01	0.01	-	0.00	0.02	0.00	0.00	0.01
NiO	0.03	0.00	0.02	0.00	-	0.00	0.00	0.00	0.00	0.00
V_2O_3	0.00	0.07	0.00	0.07	-	0.06	0.05	0.04	0.05	0.06
P_2O_5	-	-	-	-	-	-	-	-	-	-
Total[d]	101.80	100.65	101.46	101.23	-	99.09	99.67	100.53	99.36	100.80
Cations					-					
Si	5.99	7.91	6.04	7.57	-	7.76	7.62	5.97	7.66	7.65
Ti	0.00	0.03	0.00	0.06	-	0.04	0.06	0.01	0.05	0.05
Al	0.00	0.20	0.01	0.62	-	0.32	0.53	0.00	0.47	0.49
Cr	0.00	0.00	0.00	0.00	-	0.00	0.01	0.00	0.01	0.00
Fe2+	2.86	1.26	2.89	1.05	-	1.15	1.01	2.92	1.06	1.18
Mn	0.05	0.04	0.05	0.03	-	0.04	0.02	0.05	0.03	0.04
Mg	9.04	3.98	8.93	3.50	-	3.81	3.42	9.02	3.55	3.62
Ca	0.04	2.48	0.03	3.17	-	2.88	3.33	0.03	3.18	2.96
Na	0.01	0.06	0.01	0.07	-	0.06	0.08	0.00	0.06	0.07
K	0.00	0.00	0.00	0.00	-	0.00	0.00	0.00	0.00	0.00
Ni	0.00	0.00	0.00	0.00	-	0.00	0.00	0.00	0.00	0.00
V	0.00	0.01	0.00	0.01	-	0.01	0.01	0.01	0.01	0.01
P	-	-	-	-	-	-	-	-	-	-
Cation total	18.01	15.98	17.96	16.09	-	16.07	16.09	18.02	16.08	16.08
Mg# / An[e]	76.0	75.9	75.6	76.9	-	76.8	77.2	75.5	77.1	75.4
Lab[f]	2	2	2	2	-	2	2	2	2	2

Table A3. (continued)

Volcanic cone										
Sample										
Mineral[a]	OPX	OPX		OPX		OPX		OPX		OPX
Core ID	1-C6	1-C7		1-C8		1-C9		1-C10		1-C11
Major element (wt.%) [b]										
SiO_2	52.28	53.42		52.72		52.82		53.37		53.02
TiO_2	0.32	0.27		0.28		0.44		0.27		0.28
Al_2O_3	1.35	1.32		1.47		1.31		1.25		1.28
Cr_2O_3	0.00	0.00		0.00		0.00		0.00		0.04
FeO[c]	19.63	18.37		19.61		19.06		18.34		18.29
MnO	0.57	0.54		0.57		0.48		0.52		0.55
MgO	23.60	23.97		23.10		23.73		24.03		24.44
CaO	2.12	2.04		2.18		2.11		2.06		2.05
Na_2O	0.06	0.04		0.05		0.05		0.01		0.00
K_2O	0.00	0.00		0.00		0.00		0.00		0.01
NiO	0.01	0.00		0.00		0.00		0.09		0.00
V_2O_3	0.04	0.04		0.04		0.00		0.05		0.03
P_2O_5	-	-		-		-		-		-
Total[d]	100.96	99.23		99.72		100.35		99.75		100.45
Cations										
Si	7.75	7.85		7.80		7.79		7.84		7.80
Ti	0.04	0.03		0.03		0.05		0.03		0.03
Al	0.24	0.23		0.26		0.23		0.22		0.22
Cr	0.00	0.00		0.00		0.00		0.00		0.00
Fe2+	2.43	2.26		2.43		2.35		2.25		2.25
Mn	0.07	0.07		0.07		0.06		0.07		0.07
Mg	5.21	5.25		5.10		5.22		5.26		5.36
Ca	0.34	0.32		0.34		0.33		0.32		0.32
Na	0.02	0.01		0.01		0.01		0.00		0.00
K	0.00	0.00		0.00		0.00		0.00		0.00
Ni	0.00	0.00		0.00		0.00		0.01		0.00
V	0.01	0.00		0.00		0.00		0.01		0.00
P	-	-		-		-		-		-
Cation total	16.10	16.01		16.04		16.05		16.02		16.06
Mg# / An[e]	68.2	69.9		67.7		68.9		70.0		70.4
Lab[f]	2	2		2		2		2		2
Mineral[a]	CPX[g]	CPX[g]	OL[g]	CPX[g]	OL[g]	CPX[g]	OL[g]	CPX[g]	OL[g]	CPX[g]
Rim ID	1-R6	1-R7	1-R7-2	1-R8	1-R8-2	1-R9	1-R9-2	1-R10	1-R10-2	1-R11
Major element (wt.%)[b]										
SiO_2	52.40	52.16	37.69	52.71	37.86	51.54	38.24	51.27	37.86	52.52
TiO_2	0.42	0.39	0.02	0.31	0.00	0.54	0.00	0.49	0.00	0.27
Al_2O_3	1.96	1.80	0.01	1.45	0.01	2.75	0.03	3.28	0.00	1.44
Cr_2O_3	0.00	0.01	0.00	0.00	0.00	0.00	0.00	0.05	0.00	0.01
FeO[c]	9.03	9.09	23.76	9.19	24.15	8.48	23.38	8.78	23.35	9.20
MnO	0.32	0.32	0.48	0.31	0.45	0.26	0.38	0.24	0.44	0.28
MgO	16.58	16.40	37.73	16.79	37.30	15.78	37.75	15.23	38.10	17.05
CaO	18.95	19.52	0.22	18.89	0.21	20.29	0.17	20.39	0.24	18.94
Na_2O	0.28	0.25	0.00	0.29	0.01	0.25	0.00	0.26	0.00	0.25
K_2O	0.02	0.00	0.00	0.01	0.00	0.02	0.01	0.00	0.00	0.00
NiO	0.02	0.02	0.08	0.00	0.01	0.00	0.04	0.01	0.01	0.00
V_2O_3	0.00	0.04	0.02	0.06	0.00	0.10	0.00	0.00	0.00	0.04
P_2O_5	-	-	-	-	-	-	-	-	-	-
Total[d]	101.55	99.12	100.24	99.69	100.18	100.01	101.52	99.23	98.78	100.11
Cations										
Si	7.76	7.74	5.94	7.81	5.97	7.65	6.00	7.62	5.95	7.78
Ti	0.05	0.04	0.00	0.03	0.00	0.06	0.00	0.06	0.00	0.03
Al	0.34	0.31	0.00	0.25	0.00	0.48	0.01	0.57	0.00	0.25
Cr	0.00	0.00	0.00	0.00	0.00	0.00	0.00	0.01	0.00	0.00
Fe2+	1.12	1.13	3.13	1.14	3.19	1.05	3.07	1.09	3.07	1.14
Mn	0.04	0.04	0.06	0.04	0.06	0.03	0.05	0.03	0.06	0.04
Mg	3.66	3.63	8.87	3.71	8.77	3.49	8.83	3.37	8.93	3.77
Ca	3.01	3.11	0.04	3.00	0.04	3.23	0.03	3.25	0.04	3.01
Na	0.08	0.07	0.00	0.08	0.00	0.07	0.00	0.07	0.00	0.07
K	0.00	0.00	0.00	0.00	0.00	0.00	0.00	0.00	0.00	0.00
Ni	0.00	0.00	0.01	0.00	0.00	0.00	0.00	0.00	0.00	0.00
V	0.00	0.00	0.00	0.01	0.00	0.01	0.00	0.00	0.00	0.00
P	-	-	-	-	-	-	-	-	-	-
Cation total	16.06	16.09	18.06	16.07	18.03	16.08	18.00	16.07	18.05	16.09
Mg# / An[e]	76.6	76.3	73.9	76.5	73.4	76.8	74.2	75.6	74.4	76.8
Lab[f]	2	2	2	2	2	2	2	2	2	2

Table A3. (continued)

Volcanic cone										
Sample				OJSL						
Mineral[a]		OPX		OPX		OPX		OPX		OPX
Core ID		1-C12		1-C1		1-C2		1-C4		1-C5
Major element (wt.%) [b]										
SiO_2		53.17		52.94		53.09		52.86		53.22
TiO_2		0.37		0.30		0.31		0.32		0.31
Al_2O_3		1.28		1.33		1.14		1.50		1.52
Cr_2O_3		0.00		0.03		0.01		0.00		0.00
FeO[c]		19.22		20.41		20.12		19.72		20.10
MnO		0.53		0.64		0.62		0.52		0.58
MgO		23.33		22.19		22.54		22.87		22.02
CaO		2.05		2.08		2.06		2.11		2.13
Na_2O		0.04		0.07		0.05		0.05		0.05
K_2O		0.00		0.00		0.00		0.01		0.00
NiO		0.00		0.00		0.06		0.00		0.01
V_2O_3		0.00		0.00		0.00		0.03		0.06
P_2O_5		-		-		-		-		-
Total[d]		100.44		101.38		100.39		101.65		99.93
Cations										
Si		7.84		7.86		7.87		7.82		7.88
Ti		0.04		0.03		0.04		0.04		0.03
Al		0.22		0.23		0.20		0.26		0.27
Cr		0.00		0.00		0.00		0.00		0.00
Fe2+		2.37		2.53		2.49		2.44		2.49
Mn		0.07		0.08		0.08		0.07		0.07
Mg		5.13		4.91		4.98		5.04		4.86
Ca		0.32		0.33		0.33		0.33		0.34
Na		0.01		0.02		0.01		0.01		0.01
K		0.00		0.00		0.00		0.00		0.00
Ni		0.00		0.00		0.01		0.00		0.00
V		0.00		0.00		0.00		0.00		0.01
P		-		-		-		-		-
Cation total		16.01		16.00		16.00		16.02		15.96
Mg# / An[e]		68.4		66.0		66.6		67.4		66.1
Lab[f]		2		2		2		2		2
Mineral[a]	OL[g]	CPX[g]	OL[g]	CPX[g]	OL[g]	CPX[g]	OL[g]	CPX[g]	OL[g]	CPX[g]
Rim ID	1-R11-2	1-R12	1-R12-2	1-R1	1-R1-2	1-R2	1-R2-2	1-R4	1-R4-2	1-R5
Major element (wt.%)[b]										
SiO_2	38.03	51.39	38.17	51.71	-	52.25	-	51.41	-	-
TiO_2	0.00	0.48	0.05	0.48	-	0.48	-	0.61	-	-
Al_2O_3	0.00	3.04	0.03	2.60	-	1.98	-	3.10	-	-
Cr_2O_3	0.00	0.00	0.00	0.01	-	0.00	-	0.01	-	-
FeO[c]	23.73	8.39	23.28	8.58	-	9.29	-	8.98	-	-
MnO	0.41	0.18	0.43	0.27	-	0.27	-	0.28	-	-
MgO	37.58	15.87	37.76	16.06	-	15.68	-	14.95	-	-
CaO	0.24	20.33	0.24	20.01	-	19.67	-	20.37	-	-
Na_2O	0.01	0.26	0.00	0.28	-	0.28	-	0.22	-	-
K_2O	0.01	0.00	0.02	0.00	-	0.01	-	0.00	-	-
NiO	0.00	0.02	0.00	0.00	-	0.03	-	0.01	-	-
V_2O_3	0.00	0.05	0.01	0.00	-	0.07	-	0.04	-	-
P_2O_5	-	-	-	-	-	-	-	-	-	-
Total[d]	101.86	99.56	100.11	101.20	-	98.58	-	101.43	-	-
Cations					-		-		-	-
Si	5.98	7.62	5.99	7.67	-	7.76	-	7.65	-	-
Ti	0.00	0.05	0.01	0.05	-	0.05	-	0.07	-	-
Al	0.00	0.53	0.00	0.45	-	0.35	-	0.54	-	-
Cr	0.00	0.00	0.00	0.00	-	0.00	-	0.00	-	-
Fe2+	3.12	1.04	3.06	1.06	-	1.15	-	1.12	-	-
Mn	0.05	0.02	0.06	0.03	-	0.03	-	0.04	-	-
Mg	8.81	3.51	8.84	3.55	-	3.47	-	3.31	-	-
Ca	0.04	3.23	0.04	3.18	-	3.13	-	3.25	-	-
Na	0.00	0.07	0.00	0.08	-	0.08	-	0.06	-	-
K	0.00	0.00	0.00	0.00	-	0.00	-	0.00	-	-
Ni	0.00	0.00	0.00	0.00	-	0.00	-	0.00	-	-
V	0.00	0.01	0.00	0.00	-	0.01	-	0.00	-	-
P	-	-	-	-	-	-	-	-	-	-
Cation total	18.02	16.09	18.00	16.09	-	16.05	-	16.04	-	-
Mg# / An[e]	73.8	77.1	74.3	76.9	-	75.1	-	74.8	-	-
Lab[f]	2	2	2	2	-	2	-	2	-	-

Table A3. (continued)

Volcanic cone										
Sample										
Mineral[a]		OPX		OPX		OPX		OPX	OPX	
Core ID		1-C7		1-C8		1-C9		1-C10	1-C11	
Major element (wt.%) [b]										
SiO_2		52.72		-		52.84		52.50	53.30	
TiO_2		0.34		-		0.29		0.34	0.28	
Al_2O_3		1.30		-		1.31		1.28	1.12	
Cr_2O_3		0.03		-		0.01		0.01	0.01	
FeO[c]		21.01		-		20.41		20.74	18.61	
MnO		0.59		-		0.55		0.58	0.51	
MgO		21.87		-		22.58		22.27	23.99	
CaO		2.10		-		1.96		2.08	2.09	
Na_2O		0.03		-		0.03		0.05	0.06	
K_2O		0.00		-		0.01		0.00	0.01	
NiO		0.00		-		0.00		0.07	0.00	
V_2O_3		0.00		-		0.00		0.08	0.01	
P_2O_5		-		-		-		-	-	
Total[d]		99.26		-		101.76		99.92	101.62	
Cations				-						
Si		7.85		-		7.84		7.81	7.84	
Ti		0.04		-		0.03		0.04	0.03	
Al		0.23		-		0.23		0.22	0.20	
Cr		0.00		-		0.00		0.00	0.00	
Fe2+		2.62		-		2.53		2.58	2.29	
Mn		0.07		-		0.07		0.07	0.06	
Mg		4.85		-		4.99		4.94	5.26	
Ca		0.34		-		0.31		0.33	0.33	
Na		0.01		-		0.01		0.02	0.02	
K		0.00		-		0.00		0.00	0.00	
Ni		0.00		-		0.00		0.01	0.00	
V		0.00		-		0.00		0.01	0.00	
P		-		-		-		-	-	
Cation total		16.00		-		16.02		16.04	16.04	
Mg# / An[e]		65.0		-		66.4		65.7	69.7	
Lab[f]		2		-		2		2	2	
Mineral[a]	OL[g]	CPX[g]	OL[g]	CPX[g]	OL[g]	CPX[g]	OL[g]	CPX[g]	CPX[g]	OL[g]
Rim ID	1-R5-2	1-R7	1-R7-2	1-R8	1-R8-2	1-R9	1-R9-2	1-R10	1-R11	1-R11-2
Major element (wt.%)[b]										
SiO_2	-	50.98	38.64	-	-	53.02	37.77	51.06	52.82	-
TiO_2	-	0.51	0.01	-	-	0.37	0.04	0.57	0.40	-
Al_2O_3	-	3.44	0.04	-	-	1.56	0.29	3.43	1.56	-
Cr_2O_3	-	0.05	0.00	-	-	0.00	0.00	0.02	0.00	-
FeO[c]	-	8.92	23.76	-	-	9.81	24.74	10.32	9.71	-
MnO	-	0.24	0.43	-	-	0.35	0.45	0.34	0.35	-
MgO	-	15.19	36.85	-	-	16.91	36.39	16.91	16.97	-
CaO	-	20.28	0.25	-	-	17.62	0.23	17.07	17.82	-
Na_2O	-	0.25	0.00	-	-	0.25	0.00	0.24	0.27	-
K_2O	-	0.01	0.00	-	-	0.00	0.00	0.00	0.00	-
NiO	-	0.04	0.02	-	-	0.00	0.07	0.02	0.05	-
V_2O_3	-	0.09	0.00	-	-	0.10	0.02	0.02	0.05	-
P_2O_5	-	-	-	-	-	-	-	-	-	-
Total[d]	-	99.73	98.70	-	-	101.59	101.42	99.71	101.88	-
Cations	-			-	-					-
Si	-	7.59	6.07	-	-	7.84	5.97	7.58	7.82	-
Ti	-	0.06	0.00	-	-	0.04	0.01	0.06	0.04	-
Al	-	0.60	0.01	-	-	0.27	0.05	0.60	0.27	-
Cr	-	0.01	0.00	-	-	0.00	0.00	0.00	0.00	-
Fe2+	-	1.11	3.12	-	-	1.21	3.27	1.28	1.20	-
Mn	-	0.03	0.06	-	-	0.04	0.06	0.04	0.04	-
Mg	-	3.37	8.63	-	-	3.73	8.58	3.74	3.74	-
Ca	-	3.23	0.04	-	-	2.79	0.04	2.71	2.83	-
Na	-	0.07	0.00	-	-	0.07	0.00	0.07	0.08	-
K	-	0.00	0.00	-	-	0.00	0.00	0.00	0.00	-
Ni	-	0.01	0.00	-	-	0.00	0.01	0.00	0.01	-
V	-	0.01	0.00	-	-	0.01	0.00	0.00	0.01	-
P	-	-	-	-	-	-	-	-	-	-
Cation total	-	16.08	17.93	-	-	16.01	17.99	16.09	16.04	-
Mg# / An[e]	-	75.2	73.4	-	-	75.5	72.4	74.5	75.7	-
Lab[f]	-	2	2	-	-	2	2	2	2	-

Table A3. (continued)

Volcanic cone	Kishimadake									
Sample	KSS									
Mineral[a]	OPX	OPX	OPX	OPX	OPX	OPX		OPX		OPX
Core ID	1-C13	1-C14	1-C15	3-C4	3-C5	3-C6		3-C7		3-C8
Major element (wt.%) [b]										
SiO_2	53.08	52.83	53.15	52.93	53.08	52.76		52.83		52.76
TiO_2	0.38	0.34	0.38	0.34	0.38	0.31		0.27		0.33
Al_2O_3	1.22	1.23	1.22	1.04	1.28	1.36		1.56		1.45
Cr_2O_3	0.01	0.00	0.00	0.00	0.01	0.01		0.00		0.00
FeO[c]	18.78	19.94	19.85	20.53	19.41	19.82		19.20		19.24
MnO	0.54	0.50	0.50	0.66	0.57	0.50		0.47		0.46
MgO	23.88	23.06	22.79	22.41	23.14	23.01		23.43		23.54
CaO	2.07	1.99	2.00	2.05	2.06	2.19		2.12		2.15
Na_2O	0.03	0.04	0.04	0.02	0.03	0.04		0.03		0.05
K_2O	0.00	0.00	0.01	0.00	0.00	0.00		0.00		0.00
NiO	0.00	0.02	0.00	0.00	0.02	0.00		0.02		0.00
V_2O_3	0.00	0.04	0.05	0.01	0.02	0.00		0.06		0.01
P_2O_5	-	-	-	-	-	-		-		-
Total[d]	100.52	101.48	101.39	99.56	100.99	100.22		99.37		98.54
Cations										
Si	7.82	7.82	7.86	7.86	7.84	7.81		7.80		7.79
Ti	0.04	0.04	0.04	0.04	0.04	0.03		0.03		0.04
Al	0.21	0.21	0.21	0.18	0.22	0.24		0.27		0.25
Cr	0.00	0.00	0.00	0.00	0.00	0.00		0.00		0.00
Fe2+	2.31	2.47	2.46	2.55	2.40	2.45		2.37		2.38
Mn	0.07	0.06	0.06	0.08	0.07	0.06		0.06		0.06
Mg	5.24	5.09	5.02	4.96	5.10	5.08		5.16		5.18
Ca	0.33	0.32	0.32	0.33	0.33	0.35		0.33		0.34
Na	0.01	0.01	0.01	0.01	0.01	0.01		0.01		0.02
K	0.00	0.00	0.00	0.00	0.00	0.00		0.00		0.00
Ni	0.00	0.00	0.00	0.00	0.00	0.00		0.00		0.00
V	0.00	0.01	0.01	0.00	0.00	0.00		0.01		0.00
P	-	-	-	-	-	-		-		-
Cation total	16.04	16.03	15.99	16.01	16.01	16.04		16.04		16.05
Mg# / An[e]	69.4	67.3	67.2	66.0	68.0	67.4		68.5		68.6
Lab[f]	2	2	2	2	2	2		2		2
Mineral[a]	CPX[g]	CPX[g]	CPX[g]	CPX[g]	CPX[g]	CPX[g]	OL[g]	CPX[g]	OL[g]	CPX[g]
Rim ID	1-R13	1-R14	1-R15	3-R4	3-R5	3-R6	3-R6-2	3-R7	3-R7-2	3-R8
Major element (wt.%)[b]										
SiO_2	51.17	-	-	51.89	51.06	52.63	38.19	52.35	37.57	51.87
TiO_2	0.47	-	-	0.50	0.54	0.37	0.00	0.42	0.00	0.50
Al_2O_3	3.26	-	-	2.33	3.47	1.56	0.03	2.19	0.02	2.34
Cr_2O_3	0.02	-	-	0.00	0.13	0.00	0.03	0.00	0.01	0.02
FeO[c]	9.39	-	-	9.55	8.12	10.15	23.47	9.15	24.83	9.50
MnO	0.22	-	-	0.34	0.25	0.37	0.39	0.24	0.48	0.27
MgO	15.93	-	-	16.45	15.77	17.01	37.59	15.94	36.85	16.84
CaO	19.12	-	-	18.60	20.39	17.58	0.22	19.39	0.17	18.39
Na_2O	0.31	-	-	0.23	0.22	0.26	0.02	0.26	0.00	0.21
K_2O	0.01	-	-	0.01	0.01	0.00	0.01	0.01	0.01	0.00
NiO	0.03	-	-	0.01	0.00	0.00	0.05	0.01	0.01	0.00
V_2O_3	0.07	-	-	0.10	0.04	0.06	0.00	0.05	0.03	0.05
P_2O_5	-	-	-	-	-	-	-	-	-	-
Total[d]	100.49	-	-	100.08	100.26	99.60	99.99	99.56	98.67	100.42
Cations		-	-							
Si	7.60	-	-	7.70	7.57	7.80	6.00	7.76	5.95	7.69
Ti	0.05	-	-	0.06	0.06	0.04	0.00	0.05	0.00	0.06
Al	0.57	-	-	0.41	0.61	0.27	0.01	0.38	0.00	0.41
Cr	0.00	-	-	0.00	0.02	0.00	0.00	0.00	0.00	0.00
Fe2+	1.17	-	-	1.18	1.01	1.26	3.08	1.13	3.29	1.18
Mn	0.03	-	-	0.04	0.03	0.05	0.05	0.03	0.06	0.03
Mg	3.53	-	-	3.64	3.49	3.76	8.80	3.52	8.70	3.72
Ca	3.04	-	-	2.96	3.24	2.79	0.04	3.08	0.03	2.92
Na	0.09	-	-	0.07	0.06	0.07	0.01	0.07	0.00	0.06
K	0.00	-	-	0.00	0.00	0.00	0.00	0.00	0.00	0.00
Ni	0.00	-	-	0.00	0.00	0.00	0.01	0.00	0.00	0.00
V	0.01	-	-	0.01	0.00	0.01	0.00	0.01	0.00	0.01
P	-	-	-	-	-	-	-	-	-	-
Cation total	16.10	-	-	16.07	16.09	16.05	18.00	16.04	18.05	16.08
Mg# / An[e]	75.1	-	-	75.4	77.6	74.9	74.1	75.6	72.6	76.0
Lab[f]	2	2	2	2	2	2	2	2	2	2

Table A3. (continued)

Volcanic cone									
Sample									
Mineral[a]		OPX	OPX		OPX	OPX	OPX		OPX	OPX
Core ID		3-C9	3-C10		3-C11	3-C13	3-C14		3-R15-2	3-C17
Major element (wt.%) [b]										
SiO_2		52.40	52.76		53.50	52.87	52.89		52.29	52.30
TiO_2		0.32	0.35		0.29	0.33	0.34		0.35	0.34
Al_2O_3		1.27	1.12		1.37	1.44	1.23		1.04	1.06
Cr_2O_3		0.01	0.00		0.00	0.00	0.02		0.00	0.02
FeO[c]		22.35	20.42		18.32	18.43	19.14		23.09	22.61
MnO		0.61	0.59		0.51	0.53	0.50		0.68	0.66
MgO		20.88	22.77		23.78	24.22	23.72		20.61	21.12
CaO		2.09	1.97		2.10	2.11	2.07		1.84	1.84
Na_2O		0.04	0.02		0.03	0.02	0.03		0.04	0.04
K_2O		0.00	0.00		0.00	0.00	0.00		0.00	0.00
NiO		0.01	0.00		0.00	0.03	0.01		0.03	0.01
V_2O_3		0.03	0.00		0.08	0.01	0.04		0.03	0.00
P_2O_5		-	-		-	-	-		-	-
Total[d]		99.11	98.78		100.18	99.91	100.10		100.81	100.42
Cations										
Si		7.85	7.83		7.86	7.78	7.81		7.86	7.85
Ti		0.04	0.04		0.03	0.04	0.04		0.04	0.04
Al		0.22	0.20		0.24	0.25	0.21		0.18	0.19
Cr		0.00	0.00		0.00	0.00	0.00		0.00	0.00
Fe2+		2.80	2.54		2.25	2.27	2.36		2.90	2.84
Mn		0.08	0.07		0.06	0.07	0.06		0.09	0.08
Mg		4.66	5.04		5.21	5.31	5.22		4.62	4.72
Ca		0.34	0.31		0.33	0.33	0.33		0.30	0.30
Na		0.01	0.01		0.01	0.01	0.01		0.01	0.01
K		0.00	0.00		0.00	0.00	0.00		0.00	0.00
Ni		0.00	0.00		0.00	0.00	0.00		0.00	0.00
V		0.00	0.00		0.01	0.00	0.00		0.00	0.00
P		-	-		-	-	-		-	-
Cation total		16.00	16.03		15.99	16.06	16.05		16.01	16.03
Mg# / An[e]		62.5	66.5		69.8	70.1	68.8		61.4	62.5
Lab[f]		2	2		2	2	2		2	2
Mineral[a]	OL[g]	CPX[g]	CPX[g]	OL[g]	CPX[g]	CPX[g]	CPX[g]	OL[g]	CPX[g]	CPX[g]
Rim ID	3-R8-2	3-R9	3-R10	3-R10-2	3-R11	3-R13	3-R14	3-R14-2	3-C15	3-R17
Major element (wt.%)[b]										
SiO_2	38.16	-	51.88	38.12	53.47	52.75	52.33	37.91	51.76	51.37
TiO_2	0.02	-	0.47	0.00	0.27	0.40	0.41	0.00	0.62	0.52
Al_2O_3	0.01	-	2.58	0.02	1.08	1.52	1.71	0.04	1.95	2.90
Cr_2O_3	0.00	-	0.00	0.00	0.00	0.00	0.00	0.00	0.00	0.03
FeO[c]	23.60	-	9.33	24.70	9.65	9.07	9.08	24.07	12.81	8.39
MnO	0.45	-	0.28	0.43	0.36	0.31	0.26	0.50	0.52	0.24
MgO	37.60	-	15.60	36.51	17.09	16.86	16.42	37.22	13.72	15.49
CaO	0.16	-	19.53	0.20	17.84	18.86	19.41	0.23	18.27	20.77
Na_2O	0.00	-	0.25	0.00	0.18	0.22	0.27	0.00	0.28	0.27
K_2O	0.01	-	0.00	0.00	0.00	0.00	0.00	0.00	0.00	0.00
NiO	0.00	-	0.00	0.00	0.00	0.00	0.00	0.02	0.00	0.00
V_2O_3	0.00	-	0.08	0.01	0.08	0.00	0.10	0.03	0.06	0.02
P_2O_5	-	-	-	-	-	-	-	-	-	-
Total[d]	100.75	-	100.86	100.42	100.67	100.57	100.57	101.79	99.97	101.24
Cations		-								
Si	6.00	-	7.71	6.02	7.90	7.81	7.76	5.98	7.79	7.63
Ti	0.00	-	0.05	0.00	0.03	0.04	0.05	0.00	0.07	0.06
Al	0.00	-	0.45	0.00	0.19	0.26	0.30	0.01	0.35	0.51
Cr	0.00	-	0.00	0.00	0.00	0.00	0.00	0.00	0.00	0.00
Fe2+	3.10	-	1.16	3.26	1.19	1.12	1.13	3.17	1.61	1.04
Mn	0.06	-	0.04	0.06	0.05	0.04	0.03	0.07	0.07	0.03
Mg	8.81	-	3.45	8.60	3.76	3.72	3.63	8.75	3.08	3.43
Ca	0.03	-	3.11	0.03	2.82	2.99	3.09	0.04	2.95	3.31
Na	0.00	-	0.07	0.00	0.05	0.06	0.08	0.00	0.08	0.08
K	0.00	-	0.00	0.00	0.00	0.00	0.00	0.00	0.00	0.00
Ni	0.00	-	0.00	0.00	0.00	0.00	0.00	0.00	0.00	0.00
V	0.00	-	0.01	0.00	0.01	0.00	0.01	0.00	0.01	0.00
P	-	-	-	-	-	-	-	-	-	-
Cation total	18.00	-	16.05	17.98	16.00	16.05	16.07	18.02	16.00	16.09
Mg# / An[e]	74.0	-	74.9	72.5	75.9	76.8	76.3	73.4	65.6	76.7
Lab[f]	2	-	2	2	2	2	2	2	2	2

Table A3. (continued)

Volcanic cone						
Sample						
Mineral[a]		OPX	OPX		OPX	
Core ID		3-C18	3-C19		3-C21	
Major element (wt.%) [b]						
SiO_2		53.15	53.30		52.75	
TiO_2		0.32	0.33		0.35	
Al_2O_3		1.33	1.32		1.61	
Cr_2O_3		0.00	0.01		0.00	
FeO[c]		18.95	19.16		19.04	
MnO		0.56	0.48		0.51	
MgO		23.43	23.21		23.32	
CaO		2.18	2.12		2.22	
Na_2O		0.05	0.04		0.03	
K_2O		0.01	0.00		0.00	
NiO		0.00	0.03		0.07	
V_2O_3		0.03	0.00		0.09	
P_2O_5		-	-		-	
Total[d]		100.68	101.13		100.96	
Cations						
Si		7.84	7.86		7.79	
Ti		0.04	0.04		0.04	
Al		0.23	0.23		0.28	
Cr		0.00	0.00		0.00	
Fe2+		2.34	2.36		2.35	
Mn		0.07	0.06		0.06	
Mg		5.15	5.10		5.13	
Ca		0.34	0.34		0.35	
Na		0.01	0.01		0.01	
K		0.00	0.00		0.00	
Ni		0.00	0.00		0.01	
V		0.00	0.00		0.01	
P		-	-		-	
Cation total		16.02	16.00		16.03	
Mg# / An[e]		68.8	68.3		68.6	
Lab[f]		2	2		2	
Mineral[a]	OL[g]	CPX[g]	CPX[g]	OL[g]	CPX[g]	OL[g]
Rim ID	3-R17-2	3-R18	3-R19	3-R19-2	3-R21	3-R21-2
Major element (wt.%)[b]						
SiO_2	-	51.22	52.74	38.18	52.77	38.45
TiO_2	-	0.65	0.43	0.01	0.29	0.00
Al_2O_3	-	2.94	1.64	0.03	1.38	0.01
Cr_2O_3	-	0.01	0.00	0.01	0.01	0.00
FeO[c]	-	8.89	9.15	23.88	9.46	23.35
MnO	-	0.22	0.35	0.44	0.28	0.41
MgO	-	15.57	16.51	37.15	16.82	37.48
CaO	-	20.14	18.83	0.25	18.71	0.22
Na_2O	-	0.29	0.22	0.01	0.22	0.03
K_2O	-	0.00	0.00	0.00	0.01	0.00
NiO	-	0.00	0.00	0.01	0.03	0.04
V_2O_3	-	0.06	0.11	0.02	0.02	0.00
P_2O_5	-	-	-	-	-	-
Total[d]	-	100.76	100.50	101.53	100.14	100.19
Cations	-					
Si	-	7.62	7.81	6.01	7.82	6.03
Ti	-	0.07	0.05	0.00	0.03	0.00
Al	-	0.52	0.29	0.01	0.24	0.00
Cr	-	0.00	0.00	0.00	0.00	0.00
Fe2+	-	1.11	1.13	3.14	1.17	3.06
Mn	-	0.03	0.04	0.06	0.04	0.05
Mg	-	3.45	3.64	8.72	3.72	8.77
Ca	-	3.21	2.99	0.04	2.97	0.04
Na	-	0.08	0.06	0.00	0.06	0.01
K	-	0.00	0.00	0.00	0.00	0.00
Ni	-	0.00	0.00	0.00	0.00	0.01
V	-	0.01	0.01	0.00	0.00	0.00
P	-	-	-	-	-	-
Cation total	-	16.09	16.03	17.99	16.06	17.97
Mg# / An[e]	-	75.7	76.3	73.5	76.0	74.1
Lab[f]	-	2	2	2	2	2

(Footnote for **Table A3**)

[a] OL: olivine, PL: plagioclase, CPX: clinopyroxene, OPX: orthopyroxene.

[b] All oxides were normalized to 100 wt.%.

[c] Total iron as FeO.

[d] Analyzed total by EPMA.

[e] Mg# = Mg/(Fe+Mg), An = Ca/(Ca+Na), in mole%.

[f] 1: Kumamoto University, 2: University of Tokyo.

[g] Composition of both olivine and clinopyroxene are shown as reaction rim of orthopyroxene.

* Analyzed by old EDS (INCA system; Oxford Instruments).

A4. Supplementary discussion

Magma mixing model

We quantitatively tested the mixing hypothesis, because the modern post-caldera magamas of Aso show abundant textural evidence. A two-component mixing model calculation of two distinct magmas was tested on the major element variation of melt inclusions. In this mixing calculation, first, the mixing equation was rearranged to $C^i_{obs} - C^i_B = x\left(C^i_A - C^i_B\right)$ and the x (mixing proportion) was determined with the linear regression of $C^i_{obs} - C^i_B$ and $C^i_A - C^i_B$. Here, the parameters are, each major element *i*, and subscripts obs, A, and B refer to the observed mixture, components A (silicic), and B (mafic), respectively; *x* is the weight proportion of component A in the mixture (Fourcade and Allegre 1981; Schiano *et al.* 2010). Second, x is determined for each melt inclusions using the model mafic and silicic end-member compositions. An example of such fit shows that the slope, that is x, can be determined with reasonable confidence (Fig. A4-1). With the determination of x for every melt inclusion, the quality of the mixing model fit was examined by comparing the modelled oxide abundance C^i_{model} and the observed oxide abundance C^i_{obs}. Fig. A4-2 shows that the sum of the absolute values of relative residual for each melt inclusion plotted against x, mixing proportion. One can conclude that the mixing model was applied to the melt inclusion dataset with reasonable success, because there is no systematic bias of the model deviation with respect to the mixing proportion, and the total deviation is about 0.5 except for two samples. This means nearly all samples plot within 0.5% deviation from any oxide, and the deviation with respect to each oxide is about 8.5 % relative on average. The anomalous point is due to its low TiO_2 concentration, 3 times lower than others, contributing significantly to normalized residual.

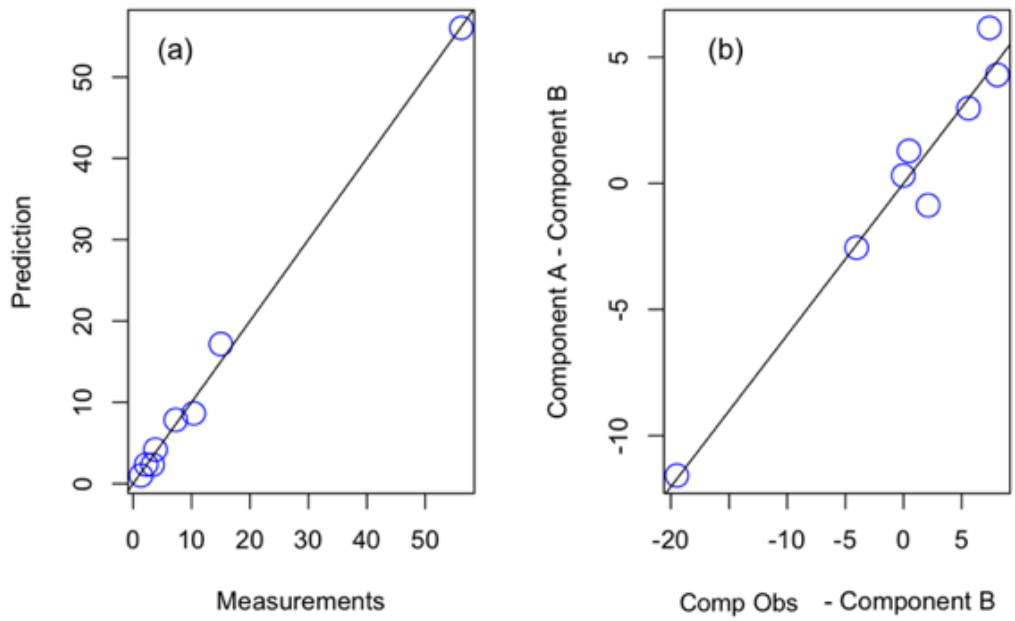

Figure **A4-1.** An example result of mixing inversion fit. (a) A comparison between the measured values and modelled (predicted) values. Units are in wt. %, and the line is one-to one slope. (b) A result of the linear regression.

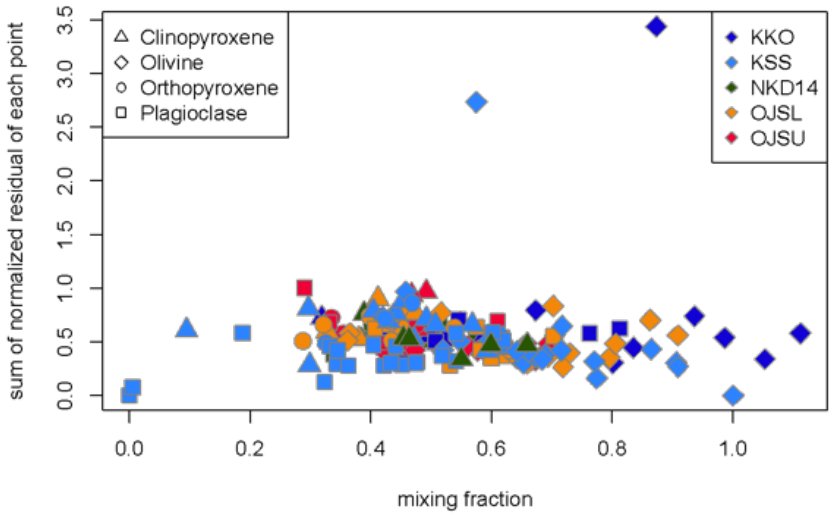

Figure **A4-2.** The sum of normalized residual of each point. Lack of systematic trend against calculated mixing fraction indicates that the model is unbiased. The normalized residual is the absolute value of difference between observation and model divided by the number of oxides.

For a successful model, we chose a pair of end-members compositions from the melt inclusions: the most primitive basaltic melt (Melt ID: KSS-2-m1 hosted in an olivine) and the most SiO_2-rich dacitic melt (Melt ID: KSS-d2-m1 hosted in a plagioclase) as a mafic and silicic end-member, respectively. The model was verified by the melt inclusions hosted in all minerals. It should be noted that we did not find any systematic deviation from the mixing trend with respect to mineral hosts (Fig. A4-2). In any case, all melt inclusions (even those hosted in other crystals), whole rocks, groundmass glasses plot along the linear trend of olivine-hosted melt inclusions (Fig. A4-3). The conclusion from this model is most likely applicable to the magmas of post-caldera activity of Aso.

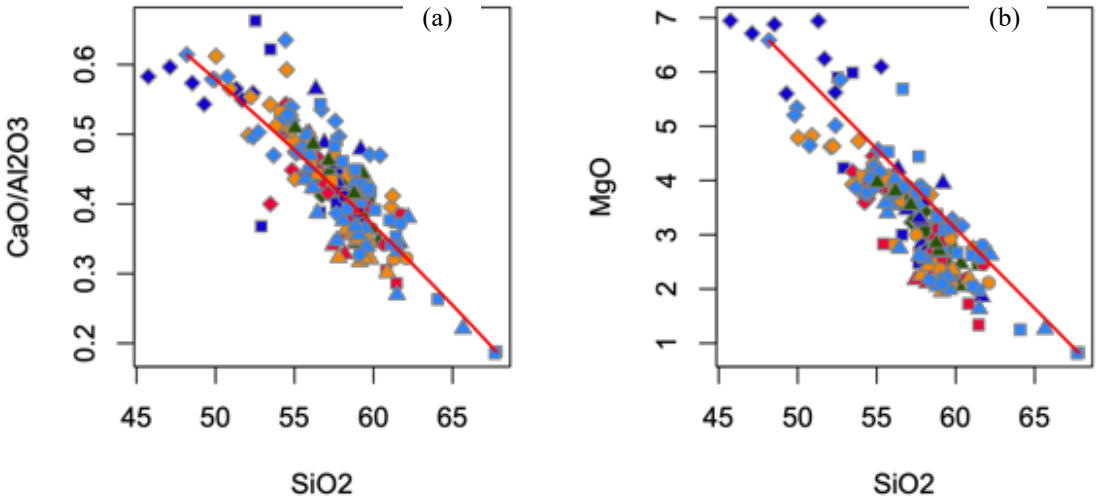

Figure **A4-3.** Major element oxide concentrations of melt inclusions. The red line is the trajectory of the mixing trend originating from the mafic end-member to the silicic end-member. Colors symbols are the same as Fig. A4-2.

Fig. A4-4 and A4-5 shows the series of panels comparing the melt inclusion compositions and the model mixing trajectory (red line). All the compositions are presented with ratios of concentration with K_2O as the denominator. This is to suppress any potential bias introduced by the post-entrapment crystallization correction. The ratios of incompatible

elements to olivine remain the same value throughout the potential crystallization in the inclusion. As one can confirm that there is good agreement between the melt inclusions and the mixing model. The calculated mixing proportion can be applied for a set of volatile elements (H_2O, S, and Cl, A4-4). F were omitted from the assessment since F concentration of felsic endmember was not measured. H_2O concentration of mafic endmember was taken from the plagioclase-olivine-liquid hygrometer-estimated value (4.68 wt.%) rather than from the measured melt inclusion because of possible diffusive H-loss (e.g. Portnyagin *et al.* 2008). It is notable that KSS melt inclusions appear to follow the model well, whereas NKD melt inclusions deviate to lower values. This can be interpreted as the extensive degassing of NKD samples. Some outliers with high values (Cl/K_2O) are potentially recording localized or episodic mobility of halogens during volcanic degassing.

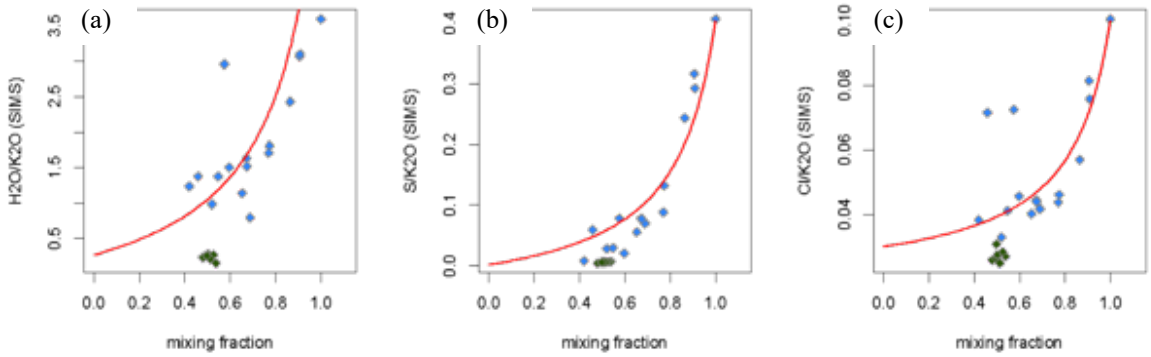

Figure **A4-4.** K_2O normalized volatile element concentration (SIMS data only) is plotted against the mixing fraction. The red line is the trajectory of the mixing trend originating from the mafic end-member to the silicic end-member at the bottom left of each plot Only KSS and NKD samples were analyzed for the volatile elements.

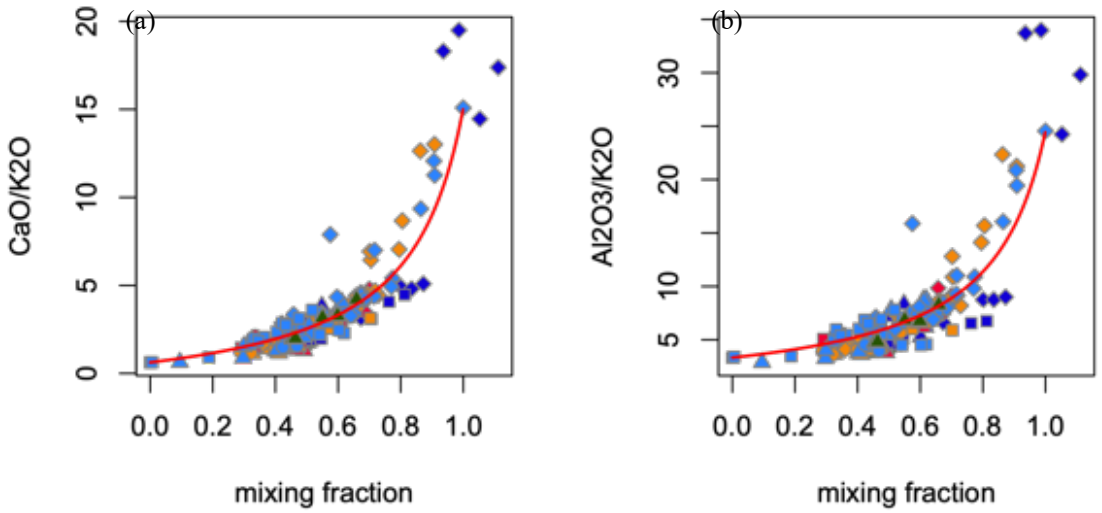

Figure **A4-5.** K_2O normalized major element concentration is plotted against the mixing fraction. The red line is the trajectory of the mixing trend originating from the mafic end-member (at mixing fraction equal to one) to the silicic end-member. Globally, no group of samples significantly and systematically deviates from the model, showing that the mixing model is applicable to all sets of the data.

Calculation of the total mass of emitted gas and exsolved volatile from erupted magma

Petrological information (e.g. measured contents, and hygrometer) recorded in melt inclusions gives estimates of the expected mass of volcanic gas for the eruption of the Nakadake 2014 - 2015 event. The total emitted mass of SO_2 gas during the 2014 - 2015 eruption was calculated from the average SO_2 emission rate of 2000 - 3100 ton/day for the observation from November 18, 2014 to January 9, 2015 (JMA 2016). The emitted gas masses of other volatile species such as H_2O, CO_2, and HCl are calculated from the measured gas composition using Multi-GAS and alkali filter pack techniques (Shinohara 2013; Shinohara *et al.* 2018) in combination with calculated total emitted mass of SO_2 gas.

The amount of volcanic gases derived from dissolved volatiles in pre-eruptive magmas is calculated based on the following equation after Shinohara (2008):

$$M_i^{gas} = M^{magma}(C_i^{initial} - C_i^{residual})F^{melt}$$

where M_i^{gas} and M^{magma} are masses of the volcanic gases and magmas, $C_i^{initial}$ and $C_i^{residual}$ are concentrations of volatile species *i* dissolved in a pre-eruptive melt (calculated from max volatiles/K_2O ratio of melt inclusions) and in a post-eruptive melt (groundmass glass), and F^{melt} is a silicate melt mass fraction of a magma calculated by K_2O contents in bulk rock and groundmass glasses assuming perfectly incompatible to phenocryst minerals. In this study, to assess the excess degassing of Nakadake 2014-2015 event at first, we compared the expected mass of volcanic gas estimated from erupted material, thus NKD14, with emitted gas masses (actual observation). Highest volatiles/K_2O ratio of NKD14 were used in this calculation for pre-eruptive concentration in NKD14 magma with assumption of no pre-eruptive gas phase in the magma chamber (Table 3.5). As it is described in main text, the mass of gas emission calculated this manner is lower than the integrated gas emission during the eruption.

Comparison of degassing models

In order to choose the degassing model that suits our sample, we tested two degassing models, D-compress (Burgisser *et al.* 2015) and SolEx (Witham *et al.* 2012), and compared the results with the observed compositional trend (Fig. A4-6). The degassing paths modelled by D-compress (red lines) show moderate decrease of S with a decrease of H_2O, whereas the paths of SolEx (black lines) show dramatic depression of sulfur with the initial decrease of H_2O, and fits globally with the observed trend (Fig. A4-6a). The SolEx results indicate negligible degassing of Cl, which is also consistent with our observation (Fig. A4-6b). However, some previous studies reported the inconsistency between SolEx paths and observed melt compositions (e.g. Werner *et al.* 2020). Furthermore, unlike D-compress, which accounts for chemical potential of gas species, SolEx treats the behavior of S with variable partition coefficient with pressure while not accounting for other parameters, such as oxygen fugacity

change with decompression. Lastly, because the compositional trend of volatile elements in the melt inclusions is a result of degassing, mixing, and probably crystal fractionation, the disparity of melt composition from the degassing path is likely due to such processes. On top of this, diffusive H-loss of melt inclusion can reduce H_2O while keeping S concentration. Similarly, many Cl points are shifted to a higher value compared to the SolEx path, which can be explained by mixing and crystal fractionation as Cl is incompatible in minerals. Here, our point is that the trend of the volatile element depletion is better explained by SolEx than D-compress, while it is far from a perfect fit.

An ideal case, would be to use the method for predicting gas evolution using pressure-dependent bulk partitioning coefficients derived from the observed trend (Werner *et al.* 2020; Johnson *et al.* 2010; Sisson and Layne 1993; Spilliaert *et al.* 2006). However, this method requires a well-documented sample set representing the degassing and crystallization, but without mixing. In our case, the variation of major and some volatile elements is clearly controlled by mixing, while H_2O and CO_2 are degassed. It was not possible to separate these processes, and derive degassing controlled S partition coefficient, like in those studies. Thus, we did not pursue this approach, and accepted to use SolEx for the degassing modelling of our sample.

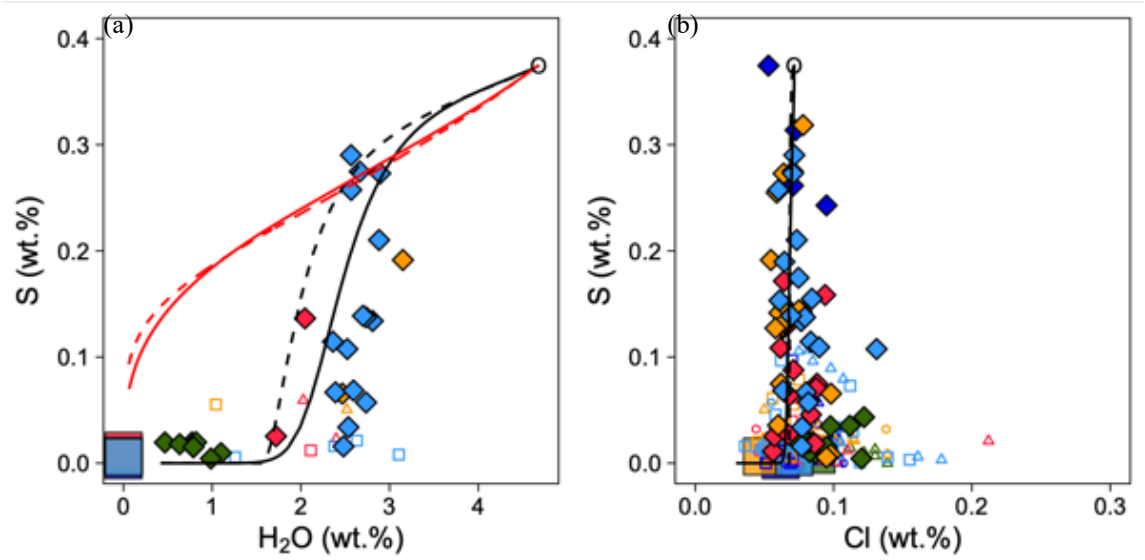

Figure **A4-6.** Comparison of degassing models. Red and black lines correspond to the modelled degassing paths of D-compress (Butgisser et al. 2015) and SolEx (Witham et al. 2012), respectively. Solid and dashed line indicates the closed-system and the open-system degassing, respectively. Initial volatile concentration used for the degassing model is plotted as an open circle, with H_2O = 4.68 wt. %, S = 3750 ppm, Cl = 716 ppm (Our mafic endmember composition before degassing). The paths shown in figures are the case of 650 ppm initial CO_2 in mafic endmember melt (KSS-OL-2-m1) with FMQ+1.4 and 1090 ˚C. Changing the initial CO_2 concentration did not change the paths significantly. Measured volatile concentrations of individual melt inclusion and average values of groundmass glasses are plotted as the same symbols as in Figure 3.3. H_2O concentrations of groundmass glasses are assumed to be 0.01wt.%.

Comparison of H_2O-CO_2 solubility models

Depth of magma degassing in this paper is closely tied to the model of H_2O-CO_2 solubility in magma. Therefore, we compared four widely available programs and compared against recent experimental calibration of pure H_2O and CO_2 solubilities accounting for magma compositions (Fig. A4-7). We have calculated isobar contours for 50, 100, 200, and 400 MPa, at 1090 ˚C (except for the model Iacono was at 1100 ˚C), and for the composition of KSS-Ol-2-m1. The four models were, SolEx (Witham *et al.* 2012), VolatileCalc (Newman and

Lowenstern 2002), MagmaSat (Ghiorso and Gualda 2015), and “Iacono model” (Iacono-Marziano *et al.* 2012). On the horizontal and vertical axes, the solubility values are calculated by Shishkina *et al.* (2014). From the figure, one can conclude that there is an excellent agreement with the solubility of pure water for all models up to 100 MPa. Similarly, all studies, except VolatileCalc agree well with the solubility of pure CO_2. As VolatileCalc uses only SiO_2 content to account for compositional effect of solubility, to some extent, the disparity is understandable and shows the limits of VolatileCalc. “Iacono model” deviates significantly, above 200 MPa here. It should be noted that their web-based calculator is the only one that reports the uncertainty of the model, and the uncertainty for the solubility at high pressure conditions is larger. While intermediate curvature is different, MagmaSat (a companion calculator of RhyoliteMELTS) and SolEx appear to give consistently close results. As stated in the text, in this paper, we used SolEx for the pressure calculation, and for low pressure, low CO_2, felsic composition, we used a value from MagmaSat.

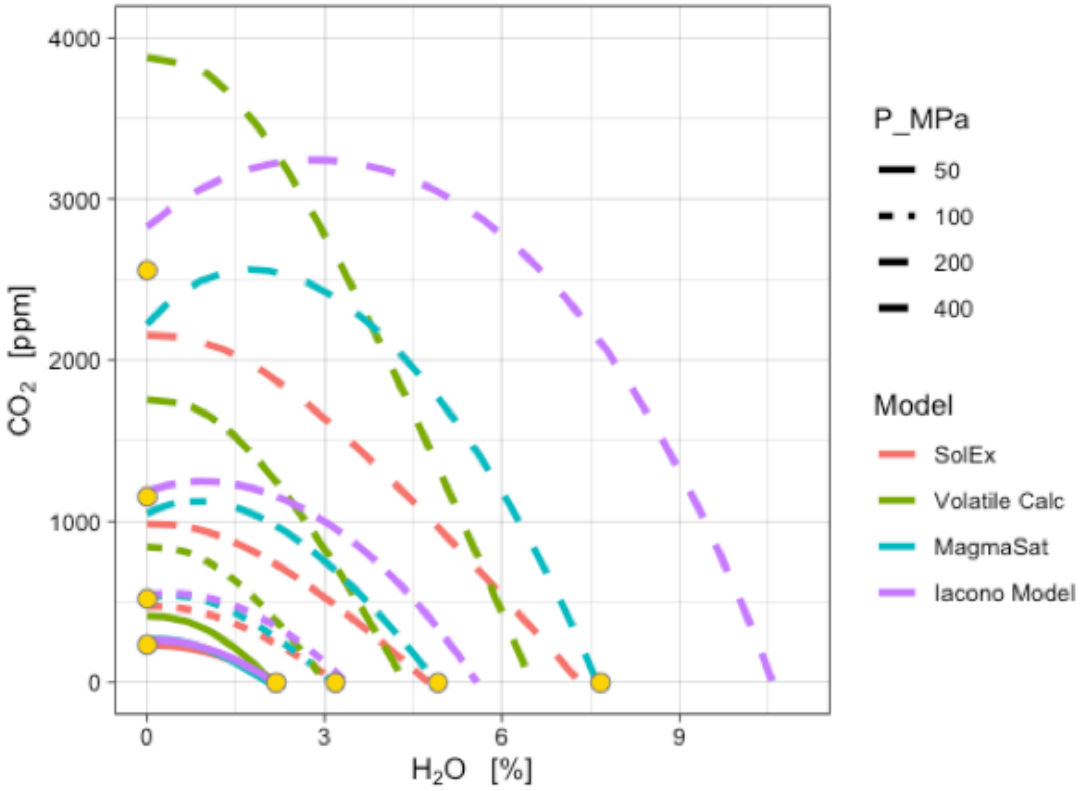

Figure **A4-7.** Comparison of H_2O-CO_2 solubility model. Isobars of 50, 100, 200, and 400 are shown. Colors indicate the different model: SolEx (Witham *et al.*, 2012), VolatileCalc (Newman and Lowenstern, 2002), MagmaSat (Ghiorso and Gaulda, 2015), and "Iacono model" (Iacono-Marziano *et al.*, 2015). Yellow circles are results of Shishkina *et al.* (2014) model.

Microscopic photo of typical melt inclusions

The photos shown below are typical olivine-hosted melt inclusions (Fig. A4-8). Melt inclusions are clear and often contain angular opaque mineral (Fig. A4-8a). Size of melt inclusions varies from 10 to over 100 μm scale (Fig. A4-8b). Shrinkage bubbles were commonly observed and often present several in one inclusion (Fig. A4-8c). Cylindrical melt pockets, called embayment (e.g. Liu *et al.* 2007), were commonly observed in some olivine among all tephra samples (Fig. A4-8c).

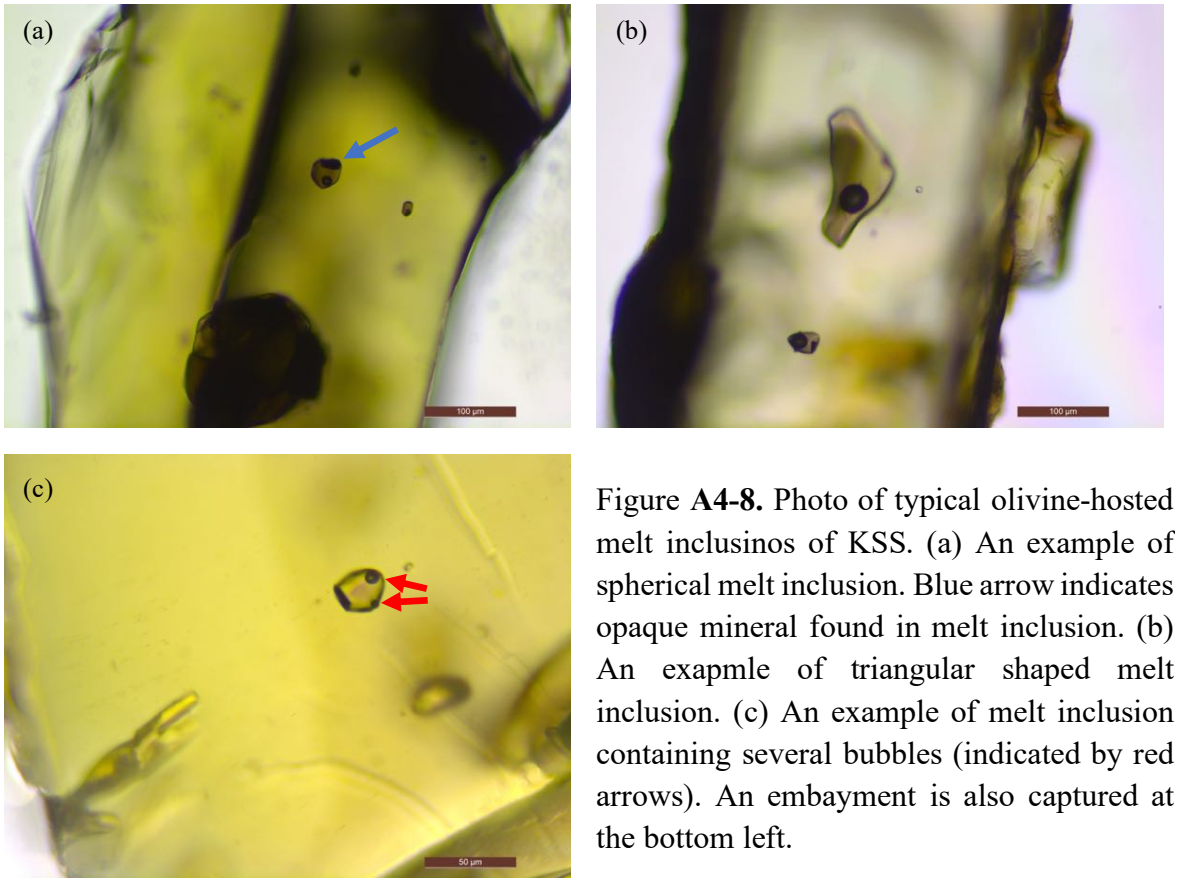

Figure **A4-8.** Photo of typical olivine-hosted melt inclusinos of KSS. (a) An example of spherical melt inclusion. Blue arrow indicates opaque mineral found in melt inclusion. (b) An exapmle of triangular shaped melt inclusion. (c) An example of melt inclusion containing several bubbles (indicated by red arrows). An embayment is also captured at the bottom left.

Supplementary references

Burgisser, A., Alletti, M. & Scaillet, B. (2015). Simulating the behavior of volatiles belonging to the C-O-H-S system in silicate melts under magmatic conditions with the software D-Compress. *Computers and Geosciences* **79**, 1–14.

Fourcade, S. & Allegre, C. J. (1981). Trace element behavior in granite genesis: a case study The calc-alkaline plutonic association from the Querigut Complex (Pyrénées, France). *Contributions to Mineralogy and Petrology* **76**, 177–195.

Ghiorso, M. S. & Gualda, G. A. R. (2015). An H_2O–CO_2 mixed fluid saturation model compatible with rhyolite-MELTS. *Contributions to Mineralogy and Petrology* **169**, 1–30.

Iacono-Marziano, G., Morizet, Y., Le Trong, E. & Gaillard, F. (2012). New experimental data and semi-empirical parameterization of H_2O-CO_2 solubility in mafic melts. *Geochimica et Cosmochimica Acta* **97**, 1–23.

Japan Meteorological Agency (2016). Volcanic activity of Asosan volcano —October 2014–February 2015—. *Report of Coordinating Comittee for Prediction of Volcanic Eruption*

120, 166-186 (in Japanese).

Johnson, E. R., Wallace, P. J., Cashman, K. V. & Granados, H. D. (2010). Degassing of volatiles (H_2O, CO_2, S, Cl) during ascent, crystallization, and eruption at mafic monogenetic volcanoes in central Mexico. *Journal of Volcanology and Geothermal Research* **197**, 225–238.

Liu, Y., Anderson, A. T. & Wilson, C. J. N. (2007). Melt pockets in phenocrysts and decompression rates of silicic magmas before fragmentation. *Journal of Geophysical Research: Solid Earth* **112**, B06204.

Newman, S. & Lowenstern, J. B. (2002). VolatileCalc: a silicate melt–H_2O–CO_2 solution model written in Visual Basic for excel. *Computers and Geosciences* **28**, 597–604.

Portnyagin, M., Almeev, R., Matveev, S. & Holtz, F. (2008). Experimental evidence for rapid water exchange between melt inclusions in olivine and host magma. *Earth and Planetary Science Letters* **272**, 541–552.

Schiano, P., Monzier, M., Eissen, J.-P., Martin, H. & Koga, K. T. (2010). Simple mixing as the major control of the evolution of volcanic suites in the Ecuadorian Andes. *Contributions to Mineralogy and Petrology* **160**, 297–312.

Shinohara, H. (2008). Excess degassing from volcanoes and its role on eruptive and intrusive activity. *Reviews of Geophysics* **46**, RG4005.

Shinohara, H. (2013). Volatile flux from subduction zone volcanoes: insights from a detailed evaluation of the fluxes from volcanoes in Japan. *Journal of Volcanology and Geothermal Research* **268**, 46–63.

Shinohara, H., Yokoo, A. & Kazahaya, R. (2018). Variation of volcanic gas composition during the eruptive period in 2014–2015 at Nakadake crater, Aso volcano, Japan. *Earth, Planets and Space* **70**, 151.

Shishkina, T. A., Botcharnikov, R. E., Holtz, F., Almeev, R. R., Jazwa, A. M. & Jakubiak, A. A. (2014). Compositional and pressure effects on the solubility of H_2O and CO_2 in mafic melts. *Chemical Geology* **388**, 112–129.

Sisson, T. W. & Layne, G. D. (1993). H_2O in basalt and basaltic andesite glass inclusions from four subduction-related volcanoes. *Earth and Planetary Science Letters* **117**, 619–635.

Spilliaert, N., Métrich, N. & Allard, P. (2006). S-Cl-F degassing pattern of water-rich alkali basalt: modelling and relationship with eruption styles on Mount Etna volcano. *Earth and Planetary Science Letters* **248**, 772–786.

Werner, C., Rasmussen, D. J., Plank, T., Kelly, P. J., Kern, C., Lopez, T., Gliss, J., Power, J. A., Roman, D. C., Izbekov, P. & Lyons, J. (2020). Linking subsurface to surface using

gas emission and melt inclusion data at Mount Cleveland volcano, Alaska. *Geochemistry, Geophysics, Geosystems* **125**, e2019GC008882.

Witham, F., Blundy, J., Kohn, S. C., Lesne, P., Dixon, J., Churakov, S. V. & Botcharnikov, R. (2012). SolEx: a model for mixed COHSCl-volatile solubilities and exsolved gas compositions in basalt. *Computers and Geosciences* **45**, 87–97.

Appendix B
Supplementary materials for Chapter 4

Table B1. Physical descriptions of olivine-hosted melt inclusions

Sample ID	Melt ID	MI shape	MI length (μm)	MI width (μm)	Vapor bubble length (μm)	Vapor bubble width (μm)	Vapor bubble[a] (vol.%)	Oxide length (μm)	Oxide width (μm)	Homogenized T_{heat} (°C)[b]	Texture/Color
ON2S	AMa-I	Angular	37.962	35.719	20.501	20.501	17.25	-	-	1321	Glassy, tan-colored, faceted
	AP-IV	Ellipsoidal	32.211	16.773	8.190	8.190	4.15	-	-	1335	Glassy, tan-colored
	BEc-II	Ellipsoidal	27.158	15.479	7.049	7.049	3.91	-	-	1331	Glassy, colorless
	BEc-III	Ellipsoidal	29.271	21.179	7.665	7.665	2.88	-	-	1331	Glassy, colorless
	BFa-I	Ellipsoidal	34.375	20.159	7.689	7.689	2.41	-	-	1353	Glassy, colorless
	CSa-III	Wormy	38.532	22.306	11.132	11.132	5.32	5.760	5.760	1331	Glassy, tan-colored
	DF-IV	Ellipsoidal	25.565	18.524	6.744	6.744	2.94	-	-	1304	Glassy, colorless
	DL-I	Ellipsoidal	55.726	39.498	21.869	21.869	9.98	-	-	1331	Glassy, tan-colored
	DS-III	Ellipsoidal	15.989	11.162	-	-	None	-	-	1338	Glassy, light brown
	DZ-I	Tubular	154.101	21.146	41.919	19.971	9.07	-	-	1337	Glassy, colorless
	EDa-I	Ellipsoidal	57.872	34.400	23.900	23.900	14.86	-	-	1347	Glassy, tan-colored
	U-I	Tubular	161.443	17.097	17.761	11.894	1.27	7.124	4.887	-	Glassy, light brown
	Z-I	Spherical	37.824	34.166	12.803	12.803	4.51	-	-	1364	Glassy, tan-colored, "raisin" aspect
YF1L	AFa-III	Ellipsoidal	28.306	20.065	10.875	10.875	9.36	-	-	1341	Glassy, tan-colored
	AFb-I	Ellipsoidal	35.064	30.324	14.932	14.932	9.58	-	-	1341	Glassy, colorless, smooth-walled
	AH-I	Rectangular	55.988	38.554	19.062	19.062	6.98	16.358	11.981	1268	Glassy, light brown, crystals remained
	AZ-I	Ellipsoidal	39.370	30.434	18.054	18.054	14.37	9.558	9.558	1319	Glassy, colorless, "raisin" aspect
	AZ-III	Spherical	25.099	24.626	9.550	9.550	5.67	-	-	1319	Glassy, light brown, crystals remained
	BD-I	Ellipsoidal	39.929	29.837	13.584	13.584	6.03	-	-	1332	Glassy, light brown, crystals remained
	BK-II	Ellipsoidal	50.280	39.590	17.886	17.886	6.40	-	-	1385	Glassy, dark brown, crystals remained
	BLa-II	Angular	56.097	26.555	12.555	12.555	3.21	-	-	1350	Glassy, light brown
	BLa-III	Tubular	68.039	17.291	11.439	11.439	2.98	-	-	1350	Glassy, light brown
	BM-I	Ellipsoidal	56.149	30.283	17.366	17.366	7.13	-	-	1321	Glassy, dark brown, crystals remained
	BO-I	Spherical	39.965	39.397	14.128	14.128	4.51	-	-	1336	Glassy, light brown
	BQ-I	Crescent	136.526	69.176	28.844	28.844	2.47	-	-	1357	Glassy, light brown, "raisin" aspect, crystals remained
					36.989	36.989	5.21	-	-		
	BQ-II	Ellipsoidal	56.375	50.069	25.130	25.130	10.56	-	-	1357	Glassy, light brown, "raisin" aspect, crystals remained
	BQ-III	Ellipsoidal	36.085	27.207	10.603	10.603	3.84	-	-	1357	Glassy, light brown, "raisin" aspect
	BSb-III	Spherical	29.339	28.174	8.041	8.041	2.19	-	-	1353	Glassy, light brown, "raisin" aspect
					8.245	8.245	2.36	-	-		
	BSc-II	Spherical	40.641	37.621	15.182	15.182	5.85	-	-	1353	Glassy, light brown, crystals remained
	F-I	Ellipsoidal	100.642	77.219	23.708	23.708	1.93	-	-	1358	Glassy, dark brown, crystals remained
	F-II	Ellipsoidal	106.276	60.293	30.988	30.988	5.58	-	-	1358	Glassy, dark brown, crystals remained
KJ5S	AD-V	Ellipsoidal	51.988	38.089	14.476	14.476	3.40	-	-	-	Glassy, light brown, "raisin" aspect
	AE-I	Ellipsoidal	93.332	66.895	23.818	23.818	2.70	-	-	-	Glassy, brown, "raisin" aspect, immiscible liquid
	AE-II	Ellipsoidal	162.492	144.253	39.052	39.052	1.66	-	-	-	Glassy, dark brown, immiscible liquid
	AF-I	Spherical	92.011	90.795	29.896	29.896	3.53	19.114	19.114	-	Glassy, dark brown, immiscible liquid
	AGa-I	Ellipsoidal	84.638	78.773	16.029	16.029	0.76	-	-	-	Glassy, dark brown
					14.432	14.432	0.55	-	-		
	AGb-IV	Ellipsoidal	144.351	104.373	35.184	35.184	2.44	45.598	44.636	-	Glassy, dark brown
					8.573	8.573	0.04	-	-		
	AGb-V	Ellipsoidal	72.299	61.967	22.227	22.227	3.65	-	-	-	Glassy, dark brown
	AI-I	Ellipsoidal	54.945	48.257	18.975	18.975	4.99	-	-	-	Glassy, dark brown
					12.657	12.657	1.48	-	-		
	AK-I	Ellipsoidal	50.666	41.479	12.687	12.687	2.11	-	-	-	Glassy, brown
					9.243	9.243	0.82	-	-		
	AK-II	Ellipsoidal	22.754	18.719	5.980	5.980	2.42	-	-	-	Glassy, brown
	B-I	Ellipsoidal	146.361	110.979	37.780	37.780	2.58	-	-	-	Glassy, dark brown
	K-I	Ellipsoidal	118.300	99.911	36.439	36.439	4.66	68.600	58.084	-	Glassy, dark brown
	L-I	Ellipsoidal	46.783	34.797	12.267	12.267	2.78	-	-	-	Glassy, brown
	S-III	Ellipsoidal	50.582	42.099	14.817	12.664	2.61	-	-	-	Glassy, brown
	U-I	Ellipsoidal	61.908	53.699	13.371	13.371	1.24	-	-	-	Glassy, brown
	V-I	Ellipsoidal	93.011	60.132	8.337	8.337	0.14	-	-	-	Glassy, light brown, necking-down
					7.266	7.266	0.09	-	-		
					11.056	11.056	0.32	-	-		
					10.040	10.040	0.24	-	-		
	Y-I	Ellipsoidal	194.695	155.561	54.524	54.524	3.06	-	-	-	Glassy, brown, "raisin" aspect
	Y-II	Ellipsoidal	107.645	79.621	27.997	27.997	2.73	-	-	-	Glassy, brown, "raisin" aspect
KSS	AA-I	Ellipsoidal	76.01	62.21	24.24	24.24	4.36	-	-	-	Glassy, light brown
	AA-II	Ellipsoidal	125.65	102.85	43.25	24.11	2.38	-	-	-	Glassy, light brown, "raisin" aspect
	AA-III	Ellipsoidal	99.42	74.16	28.39	28.39	3.58	-	-	-	Glassy, light brown
	AB-I	Tubular with neck	165.42	43.41	31.38	31.38	4.17	32.410	12.300	-	Glassy, light brown
	D-I	Spherical	49.652	49.333	15.020	15.020	2.80	-	-	-	Glassy, light brown
	D-II	Irregular	39.001	30.337	9.384	9.384	2.01	-	-	-	Glassy, light brown
	E-I	Ellipsoidal	58.144	45.094	-	-	None	16.275	16.275	-	Glassy, light brown
								15.935	15.935		

Table B1. (continued)

Sample ID	Melt ID	MI shape	MI length (μm)	MI width (μm)	Vapor bubble length (μm)	Vapor bubble width (μm)	Vapor bubble[a] (vol.%)	Oxide length (μm)	Oxide width (μm)	Homogenized T_{heat} (°C)[b]	Texture/Color
	E-II	Ellipsoidal	77.154	51.867	5.061	5.061	0.05	17.809	16.045	-	Glassy, light brown
								19.913	12.071		
								16.906	10.688		
	G-I	Ellipsoidal	38.763	35.114	12.801	12.801	4.17	-	-	-	Glassy, light brown
	G-II	Angular	60.801	44.861	13.412	13.412	1.67	-	-	-	Glassy, light brown, necking-down
	G-III	Spherical	27.738	26.010	-	-	None	-	-	-	Glassy, light brown
	H-I	Ellipsoidal	63.120	57.742	13.633	13.633	1.29	29.056	29.056	-	Glassy, light brown, faceted
	K-II	Tubular	97.283	41.236	16.575	16.575	1.64	-	-	-	Glassy, light brown
	L-I	Ellipsoidal	499.597	152.834	69.554	69.554	1.35	-	-	-	Glassy, light brown
	S-I	Tear-drop	69.003	33.369	16.141	16.141	3.57	-	-	-	Glassy, light brown
	W-I	Ellipsoidal	61.614	48.358	9.275	9.275	0.49	-	-	-	Glassy, light brown
KROHTH	A-I	Ellipsoidal	49.160	39.913	10.639	10.639	1.38	-	-	-	Glassy, light brown
	A-II	Ellipsoidal	37.082	32.102	5.901	5.901	0.50	-	-	-	Glassy, light brown
	C-I	Spherical	55.906	55.313	8.586	8.586	0.37	-	-	-	Glassy, light brown
					6.319	6.319	0.15	-	-		
					7.540	7.540	0.25	-	-		
					6.717	6.717	0.18	-	-		
	E-I	Spherical	67.540	64.506	2.259	2.259	0.00	-	-	-	Glassy, light brown
					2.527	2.527	0.01	-	-		
					1.384	1.384	0.00	-	-		
					1.037	1.037	0.00	-	-		
					1.977	1.977	0.00	-	-		
	E-II	Spherical	49.209	46.862	-	-	Unrecognized	-	-	-	Glassy, light brown
	E-III	Irregular	122.737	115.323	28.882	28.882	1.43	-	-	-	Glassy, light brown, necking-down
					25.894	25.894	1.03	-	-		
	F-I	Ellipsoidal	67.593	56.155	11.860	11.860	0.71	-	-	-	Glassy, light brown
	G-I	Ellipsoidal	43.702	35.508	-	-	None	-	-	-	Glassy, light brown
	H-I	Ellipsoidal	68.056	74.100	3.240	3.240	0.01	-	-	-	Glassy, light brown
	I-I	Ellipsoidal	72.526	61.558	-	-	None	-	-	-	Glassy, light brown
	K-I	Ellipsoidal	52.112	41.286	5.243	5.243	0.14	-	-	-	Glassy, light brown
	L-II	Ellipsoidal	46.050	38.665	-	-	None	-	-	-	Glassy, light brown
KRSM11	A-I	Ellipsoidal	90.797	65.263	16.146	16.146	0.91	-	-	-	Glassy, light brown, "raisin" aspect
					12.403	12.403	0.41	-	-		
	A-II	Ellipsoidal	54.235	44.238	12.610	12.610	1.70	-	-	-	Glassy, light brown, "raisin" aspect
	A-III	Ellipsoidal	48.010	42.008	11.060	11.060	1.49	5.830	5.830	-	Glassy, light brown, "raisin" aspect
	B-I	Tear-drop	206.610	81.451	20.887	20.887	0.38	-	-	-	Glassy, light brown
					13.056	13.056	0.09	-	-		
					21.517	17.742	0.31	-	-		
	C-I	Ellipsoidal	69.483	55.614	12.572	12.572	0.82	-	-	-	Glassy, light brown
	D-I	Ellipsoidal	97.514	48.248	18.164	18.164	1.75	-	-	-	Glassy, light brown, "raisin" aspect
	D-II	Ellipsoidal	38.676	29.349	5.841	5.841	0.52	-	-	-	Glassy, light brown, "raisin" aspect, possibly miss counted other bubble
	E-I	Ellipsoidal	83.022	65.809	14.279	14.279	0.72	-	-	-	Glassy, light brown
	E-II	Ellipsoidal	172.439	105.404	29.179	29.179	0.98	-	-	-	Glassy, light brown
	G-I	Ellipsoidal	130.013	76.350	43.134	43.134	7.84	-	-	-	Glassy, light brown
	H-I	Ellipsoidal	146.263	48.150	14.231	14.231	0.42	-	-	-	Glassy, light brown, faceted
					15.974	15.974	0.60	-	-		
	K-III	Irregular	104.270	34.755	14.662	14.662	1.25	-	-	-	Glassy, light brown
	K-V	Tubular	116.269	46.229	14.791	14.791	0.74	-	-	-	Glassy, light brown, "raisin" aspect
	L-I	Ellipsoidal	65.650	48.477	9.580	9.580	0.49	11.733	11.733	-	Glassy, light brown, "raisin" aspect
					10.183	10.183	0.59	-	-		
	L-II	Ellipsoidal	49.918	32.594	20.767	20.767	13.34	-	-	-	Glassy, light brown, "raisin" aspect
	L-III	Irregular	58.217	38.858	12.652	12.652	1.84	-	-	-	Glassy, light brown, "raisin" aspect, necking-down
	L-IV	Ellipsoidal	64.855	44.695	-	-	None	-	-	-	Glassy, light brown, "raisin" aspect
SM1S	AA-I	Angular	38.520	35.219	-	-	Not found	-	-	-	Glassy, dark brown
	AE-I	Ellipsoidal	71.314	59.329	21.392	21.392	3.54	-	-	-	Glassy, dark brown
	AJ-I	Ellipsoidal	55.039	37.517	23.436	23.436	13.47	-	-	-	Glassy, dark brown
	AL-II	Ellipsoidal	97.951	66.590	37.766	37.766	10.04	-	-	-	Glassy, dark brown
	AM-II	Ellipsoidal	28.802	24.062	6.251	6.251	1.33	-	-	-	
	AR-VI	Ellipsoidal	35.294	30.476	-	-	Not found	-	-	-	Glassy, dark brown
	BA-I	Spherical	37.069	34.821	-	-	Not found	-	-	-	Glassy, dark brown
	BA-IV	Ellipsoidal	19.856	14.832	-	-	Not found	-	-	-	Glassy, dark brown
	BC-I	Ellipsoidal	57.036	39.493	18.387	18.387	5.72	-	-	-	Glassy, dark brown
	S-II	Ellipsoidal	70.367	53.159	-	-	Unknown	-	-	-	Glassy, dark brown, multiple tiny bubbles on the MI wall.
	S-III	Ellipsoidal	90.403	59.575	-	-	Unknown	-	-	-	Glassy, dark brown, multiple tiny bubbles on the MI wall, immiscible liquid
	T-II	Ellipsoidal	38.586	32.589	13.478	13.478	5.47	-	-	-	Glassy, dark brown

Table B1. (continued)

Sample ID	Melt ID	MI shape	MI length (μm)	MI width (μm)	Vapor bubble length (μm)	Vapor bubble width (μm)	Vapor bubble[a] (vol.%)	Oxide length (μm)	Oxide width (μm)	Homogenized T_{heat} (°C)[b]	Texture/Color
	Y-I	Ellipsoidal	87.466	70.307	-	-	Unrecognized	53.381	53.381	-	Glassy, dark brown
	Y-IV	Ellipsoidal	32.662	29.313	9.201	9.201	2.63	-	-	-	Glassy, dark brown
	Z-I	Ellipsoidal	100.864	75.216	21.220	21.220	1.43	-	-	-	Glassy, dark brown
	Z-III	Ellipsoidal	132.843	87.796	-	-	Unrecognized	-	-	-	Crystallized, dark brown
KM1S12a	A-I	Ellipsoidal	54.158	42.327	13.601	13.601	2.28	-	-	-	Glassy, dark brown
	AE-I	Ellipsoidal	83.127	70.698	26.352	21.812	3.06	-	-	-	Glassy, dark brown
	AE-II	Ellipsoidal	37.572	32.253	2.937	2.937	0.06	-	-	-	Glassy, dark brown, multiple tiny bubbles on the MI wall.
	AE-III	Ellipsoidal	49.748	39.984	12.177	12.177	2.05	15.308	6.440	-	Glassy, dark brown
	AE-IV	Ellipsoidal	26.728	22.594	1.462	1.462	0.02	-	-	-	Glassy, dark brown
	AF-I	Spherical	40.772	39.034	17.827	14.254	6.42	-	-	-	Glassy, light brown
	AH-II	Ellipsoidal	88.353	67.488	23.732	23.732	2.88	-	-	-	Glassy, dark brown
	AJ-I	Ellipsoidal	66.211	47.173	8.832	8.832	0.39	-	-	-	Glassy, light brown
					7.760	7.760	0.26	-	-		
	AK-III	Ellipsoidal	95.102	38.979	27.928	27.928	8.77	-	-	-	Glassy, dark brown
	J-I	Ellipsoidal	111.728	96.503	25.283	25.283	1.44	14.038	14.038	-	Glassy, dark brown, faceted
					19.312	19.312	0.64	-	-		
	J-II	Ellipsoidal	57.226	40.589	12.599	12.599	1.76	-	-	-	Glassy, dark brown
	K-II	Ellipsoidal	46.151	41.301	14.339	14.339	3.54	-	-	-	Glassy, dark brown
	O-I	Ellipsoidal	53.795	38.048	9.861	9.861	1.02	-	-	-	Glassy, dark brown
					10.917	10.917	1.38	-	-		
	Q-I	Ellipsoidal	58.596	39.593	11.219	11.219	1.25	14.931	7.226	-	Glassy, dark brown, faceted
	U-VI	spherical	46.738	44.886	13.437	13.437	2.55	9.270	9.270	-	Glassy, dark brown
								5.269	5.269		
	Z-I	Ellipsoidal	42.833	32.746	7.447	7.447	0.80	11.029	3.314	-	Glassy, light brown
					6.539	6.539	0.54	13.861	5.861		
					7.989	7.989	0.98	-	-		
	Z-II	Ellipsoidal	31.085	27.652	8.417	8.417	2.36	-	-	-	Glassy, light brown
FKONON	A-I	Wormy	-	-	9.926	9.926	-	-	-	-	Glassy, tan-colored, faceted
					7.336	7.336		-	-		
					7.165	7.165		-	-		
	B-I	Ellipsoidal	286.808	65.902	13.654	13.654	0.08	-	-	-	Glassy, colorless
					10.032	10.032	0.03	-	-		
					9.190	9.190	0.02	-	-		
					8.375	8.375	0.02	-	-		
					10.420	10.420	0.03	-	-		
					12.870	12.870	0.06	-	-		
					10.876	10.876	0.04	-	-		
					9.970	9.970	0.03	-	-		
					11.456	11.456	0.05	-	-		
					12.176	12.176	0.05	-	-		
	D-I	Wormy	-	-	12.536	12.536	-	-	-	-	Glassy, tan-colored, "raisin" aspect
					9.295	9.295		-	-		
					10.741	10.741		-	-		
	D-II	Wormy	57.537	29.809	12.110	12.110	2.37	-	-	-	Glassy, tan-colored
	F-I	Tubular	90.034	18.149	6.990	6.990	0.39	-	-	-	Glassy, tan-colored
					11.629	11.629	1.78	-	-		
	I-I	Ellipsoidal	39.280	25.510	9.578	9.578	2.71	-	-	-	Glassy, tan-colored, faceted
	K-I	Crescent	82.929	31.741	10.935	10.935	0.87	-	-	-	Glassy, tan-colored, faceted
					6.583	6.583	0.19	-	-		
					8.311	8.311	0.38	-	-		
	K-II	Crescent	81.516	32.758	12.364	12.364	1.24	-	-	-	Glassy, tan-colored, faceted
	M-I	Tear-drop	31.070	14.840	6.709	6.709	2.85	-	-	-	Glassy, tan-colored
	N-I	Spherical	51.111	48.405	12.752	12.752	1.68	-	-	-	Glassy, tan-colored, faceted
	N-II	Ellipsoidal	26.837	20.262	6.219	6.219	1.88	-	-	-	Glassy, tan-colored, faceted
	O-I	Ellipsoidal	76.112	51.132	15.758	15.758	1.58	-	-	-	Glassy, tan-colored, "raisin" aspect
	O-II	Irregular	-	-	-	-	-	-	-	-	Glassy, tan-colored
	P-II	Triangular	47.046	31.843	10.567	10.567	2.00	-	-	-	Glassy, tan-colored

[a] Vapor bubble volume assuming ellipsoidal or spherical shape for melt inclusion and vapor bubble. Length of third axis c was calculated as the arithmetic mean of the two visible axes (c = (a + b)/2). The volume of solid mineral inclusion was excluded from the melt inclusion volume. Influence of subtraction was 0 - 0.30 vol.%, except one large oxide (68.6 μm) affecting 0.91 vol% change.

[b] Max temperature of heating experiment.

Table B2. Melt inclusion compositions corrected for post-entrapment crystallization and bubble

Sample ID	Melt ID	SiO_2 (wt. %)	TiO_2	Al_2O_3	FeO^{Total}	MnO	MgO	CaO	Na_2O	K_2O	P_2O_5	H_2O (wt. %)	CO_2^{Melt} (ppm)	S (ppm)	Cl (ppm)	F (ppm)	P_2O_5 (SIMS) (wt. %)	CO_2^{Total} (ppm)	1 s.e.[a] (rel. %)	T_{trap}[b] (°C)	PEC%[c]	Li (ppm)	Sc	V	Cu	Rb	Sr	Y
ON2S	AMa-I	44.52	2.51	15.14	13.44	0.21	10.74	7.86	2.06	1.02	0.67	–	–	–	–	–	–	–	–	1264	0	–	–	–	–	–	–	–
	AP-IV	43.54	2.33	14.56	15.68	0.12	9.34	8.75	3.12	1.04	0.62	–	–	1778	665	942	–	–	–	1233	5.8	–	20.0	233.7	45.6	26.44	755.9	15.9
	BEc-III	42.94	2.51	15.39	14.63	0.12	8.38	9.96	3.15	1.01	0.85	–	–	1652	673	1000	–	–	–	1211	2.5	–	27.1	223.2	28.2	24.70	841.8	18.9
	CSa-III	43.23	2.07	12.86	18.18	0.25	11.20	7.17	2.46	0.78	0.62	0.30	11	2403	541	882	0.61	263	48	1276	14.7	14.59	18.3	118.6	93.8	20.33	625.5	11.9
	DF-IV	44.46	2.04	16.23	13.70	0.17	8.21	9.49	3.25	0.95	0.89	–	–	2158	612	773	–	–	–	1208	5.9	–	–	–	–	–	–	–
	DL-I	43.53	2.59	16.66	13.57	0.16	11.16	6.23	1.79	1.16	0.80	–	–	1462	238	1029	–	–	–	1283	0	20.21	22.5	224.8	70.9	47.61	477.7	35.4
	DS-III	45.37	1.85	11.87	18.12	0.24	12.14	7.67	1.04	0.66	0.66	–	–	–	–	–	–	–	–	1286	8.8	–	–	–	–	–	–	–
	DZ-I	43.76	2.81	16.27	15.29	0.20	10.47	7.55	1.24	0.81	0.41	–	–	582	89	778	–	–	–	1260	0.4	71.22	30.6	265.7	–	44.14	435.3	18.7
	EDa-I	48.07	1.65	15.41	16.56	0.25	14.55	0.71	0.84	0.63	0.13	–	–	–	–	–	–	–	–	1359	0	–	–	–	–	–	–	–
	U-I	58.58	1.83	14.58	8.38	0.11	6.04	5.58	2.35	2.79	0.89	0.25	1	142	1194	1166	0.86	5	40	1166	11.5	–	–	–	–	–	–	–
	Z-I	42.68	2.61	16.15	13.25	0.28	9.05	10.43	3.29	0.97	0.80	0.42	117	2078	783	1160	0.80	2195	47	1220	0	6.90	19.8	229.3	24.5	20.63	818.6	15.1
YF1L	AFa-III	40.34	1.25	18.98	15.18	0.23	8.44	11.65	2.70	0.60	0.09	0.01	2	2624	772	614	0.20	2	49	1221	1.3	–	54.4	378.0	80.6	8.14	836.1	16.3
	AFb-I	42.30	1.27	17.87	14.85	0.26	11.49	10.17	2.07	0.47	0.11	0.03	2	757	401	552	0.15	2	49	1281	0	2.31	48.7	344.2	178.5	6.31	408.1	13.7
	AH-I	44.08	1.18	17.52	10.94	0.22	10.06	11.40	2.96	0.43	0.07	0.55	58	2894	1407	521	0.17	2635	49	1229	0	–	63.2	380.6	17.3	4.93	610.9	14.4
	AZ-I	42.09	1.18	18.13	14.17	0.21	10.46	11.90	2.13	0.41	0.09	–	–	–	–	–	–	–	–	1249	0	–	53.0	683.1	74.7	6.69	440.6	17.4
	AZ-III	41.54	1.13	18.08	14.03	0.20	10.20	11.94	2.67	0.53	0.27	0.07	59	2714	1250	514	0.20	1732	48	1249	0	–	66.3	424.7	34.1	9.08	925.5	17.7
	BD-I	42.19	1.18	17.99	13.12	0.13	11.07	11.65	2.87	0.39	0.03	0.22	129	2934	1272	446	0.15	4028	48	1260	0	–	66.1	374.3	45.5	4.42	587.0	14.9
	BK-II	40.95	1.06	17.53	15.09	0.07	11.08	10.34	2.70	0.52	0.16	0.17	91	3743	1255	511	0.19	2816	48	1270	0	–	40.1	309.4	45.7	5.80	633.9	13.5
	BLa-II	40.85	1.12	16.93	16.50	0.26	9.99	10.75	2.63	0.51	0.24	0.06	30	3364	1228	603	0.20	472	47	1251	0	–	53.2	380.0	54.4	7.58	822.3	14.7
	BLa-III	40.65	1.11	16.45	18.10	0.24	9.90	10.71	2.54	0.53	0.21	0.05	2	3793	1180	630	0.19	27	46	1249	1.9	–	52.3	371.5	70.9	7.42	774.6	14.5
	BM-I	42.05	1.12	17.55	12.63	0.12	11.72	11.16	2.96	0.39	0.13	0.39	185	3263	1437	488	0.18	6450	49	1268	0	–	63.1	414.4	51.4	4.32	576.7	14.1
	BO-I	40.81	1.12	17.43	14.67	0.14	10.49	10.89	2.69	0.51	0.19	0.13	49	3432	1206	602	0.21	1123	48	1259	0	–	60.3	400.0	42.2	7.64	747.8	13.9
	BQ-I	42.67	0.98	16.12	14.45	0.15	13.80	8.89	2.37	0.52	0.16	0.20	2	227	667	509	0.19	57	48	1321	0	–	33.2	315.7	61.2	5.98	432.1	12.4
	BQ-II	41.04	1.05	16.01	15.81	0.22	13.18	9.57	2.20	0.51	0.12	–	–	–	–	–	–	–	–	1311	0	–	47.4	407.7	88.7	7.95	550.9	14.8
	BQ-III	40.58	1.17	16.79	16.74	0.14	10.12	10.52	2.59	0.55	0.26	0.02	44	3487	1212	594	0.20	773	47	1257	0	–	53.1	344.9	37.4	8.16	819.6	15.8
	BSb-III	41.08	1.18	19.20	13.82	0.26	9.03	11.30	2.72	0.61	0.16	–	–	–	–	–	–	–	–	1228	0	–	–	–	–	–	–	–
	BSc-II	40.72	0.86	16.97	14.79	0.12	12.14	10.47	2.76	0.53	0.32	0.08	56	3328	1180	588	0.20	1393	48	1293	0	–	40.8	314.5	26.0	6.29	707.9	13.3
	F-I	42.05	1.09	16.93	14.05	0.17	13.29	9.67	2.57	0.57	0.07	0.20	113	3079	1242	459	0.18	1005	44	1310	0	–	34.3	370.9	49.2	7.06	598.3	14.0
	F-II	41.68	1.07	18.03	15.01	0.06	11.30	10.42	2.94	0.58	0.20	0.27	190	3573	1242	511	0.20	4781	48	1267	0	–	46.1	396.6	46.8	8.41	770.3	15.0
KJ5S	AD-V	51.94	0.93	16.49	10.58	0.22	4.25	7.26	2.87	0.96	0.18	4.39	223	2752	1006	500	0.29	711	34	1014	2	9.35	23.3	237.9	7.1	18.57	544.9	16.9
	AE-I	52.88	0.93	16.67	8.81	0.29	3.92	7.16	2.96	1.08	0.26	4.62	203	2547	1053	516	0.31	566	32	1004	0	10.33	23.0	223.1	16.9	22.34	561.2	17.3
	AE-II	51.77	1.05	16.86	9.33	0.24	4.61	7.33	2.91	1.02	0.30	4.64	307	2807	1000	485	0.29	587	24	1019	0	12.12	23.8	245.3	24.9	19.97	568.9	16.8
	AF-I	51.87	1.04	17.28	8.82	0.12	3.98	7.53	3.17	1.08	0.18	4.57	340	2810	1032	504	0.31	1061	34	1006	0	11.36	24.1	252.1	22.7	19.25	589.6	17.3
	AGa-I	52.29	0.95	17.26	8.99	0.11	4.57	7.06	3.11	1.08	0.23	4.57	339	2799	1036	504	0.31	597	22	1020	0	10.59	22.5	234.7	26.5	19.97	562.3	16.8
	AGb-IV	53.05	1.01	16.91	8.79	0.16	4.42	6.73	3.22	1.29	0.35	4.51	293	2433	1053	520	0.32	743	30	1018	0	11.35	21.4	240.4	21.3	25.58	556.2	17.3

Table B2. (continued)

Sample ID	Melt ID	SiO_2 (wt. %)	TiO_2	Al_2O_3	FeO^{Total}	MnO	MgO	CaO	Na_2O	K_2O	P_2O_5	H_2O (wt. %)	CO_2^{Melt} (ppm)	S (ppm)	Cl (ppm)	F (ppm)	P_2O_5 (SIMS) (wt. %)	CO_2^{Total} (ppm)	1 s.e.[a] (rel. %)	T_{trap}[b] (°C)	PEC%[c]	Li (ppm)	Sc	V	Cu	Rb	Sr	Y
	AGb-V	53.04	0.99	17.29	8.68	0.23	3.79	7.41	2.90	1.19	0.39	4.49	348	2899	1104	523	0.31	1210	36	1001	0.5	10.90	23.2	233.5	16.1	22.13	578.3	17.7
	AI-I	51.84	0.96	17.30	9.39	0.20	3.87	7.58	2.74	1.03	0.24	4.49	259	3156	1072	506	0.29	259	40	1003	0.8	8.08	23.4	252.9	20.2	20.16	566.4	17.3
	AK-I	52.32	0.92	17.52	9.61	0.19	3.97	7.87	2.89	0.92	0.24	4.66	377	3063	1096	538	0.30	1025	32	1002	0	6.57	23.9	240.3	11.4	18.96	613.5	18.2
	AK-II	52.24	1.06	18.53	8.12	0.25	3.59	7.80	2.84	1.07	0.30	–	–	2598	1032	517	–	–	–	1000	6.5	–	25.2	291.5	39.0	22.98	693.7	20.2
	B-I	52.09	0.78	16.97	9.42	0.25	4.08	7.45	2.89	1.07	0.34	4.71	272	2876	1087	514	0.30	698	31	1004	0.8	11.48	24.2	249.5	22.1	20.45	567.7	17.4
	K-I	52.38	1.06	17.46	9.04	0.22	4.20	7.55	2.97	0.98	0.21	4.72	276	2831	1031	492	0.30	1013	36	1007	0	11.32	23.3	241.5	17.7	19.22	586.5	16.7
	L-I	52.23	0.97	17.33	9.07	0.20	3.89	7.46	2.98	1.05	0.28	4.64	416	2943	1104	525	0.31	1090	31	1001	1.2	9.55	23.1	248.9	9.1	19.31	578.5	17.6
	S-III	52.42	0.96	17.46	9.34	0.25	4.09	7.45	2.86	1.02	0.30	4.56	313	2999	1081	508	0.30	829	31	1007	1.6	10.89	23.4	247.5	11.2	19.51	580.2	16.8
	U-I	53.87	1.02	16.94	8.77	0.25	3.85	7.28	3.11	1.05	0.26	4.52	371	2473	1103	515	0.31	678	23	1002	0.4	8.59	19.3	186.1	6.7	20.66	491.2	15.2
	V-I	54.26	0.91	16.93	8.59	0.21	3.62	7.13	3.04	1.16	0.15	4.35	116	2210	1080	487	0.30	195	20	1000	1.7	9.97	22.8	219.7	7.8	27.98	539.8	18.7
	Y-I	51.19	0.96	16.95	9.60	0.23	4.88	7.26	3.01	0.99	0.24	4.43	171	2601	973	475	0.30	496	33	1029	0	11.11	23.8	232.3	24.3	20.71	572.2	17.2
	Y-II	51.43	0.86	16.74	10.05	0.20	4.71	7.20	2.99	1.01	0.28	4.65	225	2657	1020	500	0.30	565	30	1021	0	11.19	22.5	230.7	22.0	20.84	570.1	16.8
KSS	AA-I	48.52	1.24	18.23	10.15	0.27	4.67	10.47	2.67	1.02	0.26	2.86	91	2786	707	388	0.24	1679	47	1048	1.4	7.37	33.6	483.8	203.0	25.95	624.6	16.6
	AA-II	53.72	1.03	15.20	10.79	0.20	4.83	7.28	2.84	1.96	0.35	2.17	60	1179	747	612	0.35	1071	47	1076	5.8	16.43	28.7	332.6	196.3	55.26	482.3	21.8
	AA-III	48.81	1.04	18.77	9.50	0.07	4.28	10.67	2.70	1.02	0.29	2.88	74	2691	749	388	0.24	1282	47	1038	0.5	4.78	32.1	414.5	156.3	26.90	653.7	16.0
	AB-I	49.10	0.97	19.70	8.59	0.17	4.39	11.29	2.89	1.07	0.14	2.48	192	2824	740	358	0.23	5472	48	1048	0.5	8.75	29.9	342.0	172.6	22.93	716.7	15.6
	D-I	49.04	1.00	17.24	12.17	0.30	4.70	8.93	2.69	1.06	0.30	2.91	121	2729	748	579	0.24	1029	44	1053	2.4	14.98	31.5	499.5	158.2	29.04	622.9	16.5
	E-I	60.73	0.94	13.99	9.90	0.20	2.90	6.08	2.93	2.41	0.52	–	–	883	742	789	–	–	–	1021	0.4	–	–	–	–	–	–	–
	E-II	58.98	0.96	14.18	10.18	0.17	3.03	5.98	3.15	2.43	0.36	2.58	230	994	885	913	0.50	275	8	1027	1.1	–	–	–	–	–	–	–
	G-I	53.35	1.00	15.53	10.53	0.18	3.79	8.25	2.83	1.54	0.33	2.66	108	694	531	583	0.36	2011	47	1038	1	19.33	38.0	410.6	268.1	43.57	555.8	24.7
	G-II	54.74	1.15	15.93	10.00	0.17	3.87	7.11	3.02	2.18	0.33	2.58	45	1247	830	639	0.35	408	44	1045	2	17.34	27.0	313.1	162.5	62.92	479.3	22.8
	G-III	52.43	1.38	15.43	10.58	0.07	3.71	8.54	2.81	1.44	0.49	–	–	–	–	–	–	–	–	1037	1.6	–	33.8	487.4	182.6	48.76	606.3	31.9
	H-I	57.48	0.62	13.94	11.38	0.20	3.40	6.38	3.16	1.61	0.23	2.42	369	1111	1067	868	0.35	2317	42	1039	2.5	23.71	30.0	260.3	197.2	38.01	867.2	33.2
	K-II	47.72	0.95	19.53	9.33	0.09	4.74	10.73	2.63	0.90	0.29	3.02	242	2952	736	364	0.23	1404	41	1045	1.5	7.98	27.7	364.0	137.4	20.40	664.0	14.2
	L-I	47.84	0.92	19.13	9.26	0.09	4.93	10.56	2.68	0.92	0.11	3.10	201	2792	719	354	0.23	960	40	1048	1.7	6.92	28.3	363.9	161.4	22.41	664.9	14.6
	W-I	54.64	1.26	15.31	10.63	0.22	3.87	6.60	3.15	2.02	0.48	2.20	43	968	825	632	0.36	182	38	1057	2.3	19.35	28.7	329.6	191.7	56.89	473.7	24.0
KROHTH	A-I	55.39	1.09	16.06	9.54	0.20	4.13	7.37	2.88	0.95	0.28	3.19	57	790	758	325	0.17	226	37	1033	5.9	–	–	–	–	–	–	–
	A-II	55.51	1.00	16.38	10.05	0.14	4.28	7.63	2.88	0.90	0.08	3.32	85	841	757	341	0.18	162	24	1032	6	–	–	–	–	–	–	–
	E-I	54.79	1.07	16.09	9.57	0.13	3.92	7.70	2.82	0.95	0.19	3.53	86	802	782	339	0.17	88	1	1020	1.7	15.43	35.9	396.3	116.9	26.24	301.1	20.1
	E-II	54.94	1.10	16.15	9.28	0.09	4.00	7.53	2.86	0.94	0.22	3.46	78	637	773	333	0.18	78	–	1024	2.3	14.90	34.2	365.3	107.9	25.44	291.0	19.4
	E-III	54.80	0.79	16.16	9.46	0.23	4.04	7.58	2.95	1.03	0.15	2.84	62	816	747	324	0.16	636	45	1039	1.9	–	–	–	–	–	–	–
	F-I	54.32	0.97	16.33	9.81	0.21	4.23	7.54	2.96	1.00	0.05	3.51	60	859	767	336	0.17	121	25	1028	0.6	15.48	34.2	370.4	118.0	26.97	301.2	19.5
	G-I	54.98	0.95	16.13	9.85	0.16	4.22	7.52	2.82	0.99	0.19	3.43	106	800	754	338	0.17	106	–	1029	2.8	15.52	34.4	358.1	108.6	24.95	289.4	19.2
	H-I	54.78	0.99	16.16	9.19	0.25	3.81	7.50	3.15	0.93	0.15	3.40	53	700	767	329	0.17	54	1	1022	1.8	15.70	34.6	375.0	117.4	27.00	300.0	19.9
	I-I	55.34	0.98	15.98	9.16	0.31	3.94	7.48	2.75	1.02	0.21	3.46	76	818	757	338	0.17	76	–	1022	1.4	16.37	35.2	373.2	123.3	30.45	304.2	20.4
	K-I	56.56	1.10	15.75	8.72	0.11	3.77	7.04	3.12	1.00	0.18	3.26	4	272	761	312	0.20	5	11	1025	0	14.24	31.6	294.4	101.4	27.49	282.2	19.3
	L-II	54.62	1.01	15.92	9.57	0.14	4.12	7.88	2.98	0.90	0.19	3.43	48	769	744	340	0.18	48	–	1026	1.7	15.94	35.3	385.3	113.5	28.83	311.0	20.1

Table B2. (continued)

Sample ID	Melt ID	SiO_2 (wt. %)	TiO_2	Al_2O_3	FeO^{Total}	MnO	MgO	CaO	Na_2O	K_2O	P_2O_5	H_2O (wt. %)	CO_2^{Melt} (ppm)	S (ppm)	Cl (ppm)	F (ppm)	P_2O_5 (SIMS) (wt. %)	CO_2^{Total} (ppm)	1 s.e.[a] (rel. %)	T_{trap}[b] (°C)	PEC%[c]	Li (ppm)	Sc	V	Cu	Rb	Sr	Y
KRSM11	A-I	53.96	0.71	17.05	8.07	0.15	3.80	7.29	2.81	1.15	0.14	4.56	262	1826	767	391	0.16	524	25	1000	0	14.95	27.6	288.8	82.7	35.40	300.6	17.6
	A-II	53.56	0.86	17.10	8.64	0.27	3.90	7.34	2.68	1.12	0.21	4.49	256	1805	771	401	0.15	576	28	1003	1.1	9.00	28.0	300.8	77.7	39.01	304.1	18.0
	A-III	53.61	0.77	17.13	7.95	0.17	3.56	7.86	2.83	1.04	0.23	4.43	280	1863	760	387	0.16	631	28	995	0.7	12.15	29.4	264.7	77.6	35.28	310.8	17.9
	B-I	53.61	0.86	16.87	8.15	0.09	3.75	7.42	2.61	1.11	0.13	4.51	304	1855	750	372	0.15	474	18	999	1.4	14.93	29.6	298.6	94.2	33.96	301.5	17.5
	C-I	54.44	0.78	17.31	7.79	0.27	3.42	7.53	2.72	1.26	0.15	4.39	240	1793	780	407	0.16	416	21	993	1.3	14.35	27.7	262.7	81.9	35.50	305.0	18.1
	D-I	52.24	0.89	18.10	8.58	0.23	3.68	8.65	2.71	0.86	0.15	4.50	202	1940	708	333	0.14	446	27	994	1.2	13.34	32.9	320.0	59.6	27.31	328.2	17.3
	D-II	54.47	0.74	17.53	8.55	0.12	3.93	7.87	2.61	1.10	0.12	4.16	231	1820	773	401	0.15	333	15	1007	3.3	–	26.1	291.0	36.3	36.89	333.8	19.0
	E-I	53.27	0.90	16.97	8.41	0.13	3.80	7.72	2.71	1.02	0.11	4.56	318	1864	755	376	0.15	478	17	998	1.6	14.92	30.0	303.1	65.7	32.97	309.4	17.8
	E-II	52.47	0.87	17.30	8.37	0.20	3.76	8.34	2.65	0.85	0.18	4.59	325	1957	715	336	0.14	555	21	995	2.2	12.89	32.3	313.6	49.7	26.72	319.5	17.1
	G-I	53.72	0.81	17.16	8.19	0.10	3.81	7.64	2.71	1.02	0.15	4.44	369	1938	743	364	0.15	369	43	1001	2.1	14.95	30.6	303.8	97.5	33.51	306.7	17.7
	H-I	53.36	0.82	17.35	8.22	0.31	3.80	7.79	2.73	1.10	0.09	4.28	207	1841	739	363	0.15	372	22	1003	1.3	–	–	–	–	–	–	–
	K-V	52.64	0.83	17.65	8.81	0.26	4.20	8.11	2.36	0.93	0.16	4.29	250	1870	705	334	0.14	387	18	1011	3.6	–	31.8	326.7	85.8	33.50	361.7	20.3
	L-I	53.39	0.71	16.93	8.55	0.20	3.88	7.70	2.64	1.04	0.12	4.41	199	1844	740	374	0.15	376	24	1003	1	13.82	29.5	282.8	51.8	32.23	311.1	17.5
	L-II	51.14	0.70	15.98	8.25	0.19	3.71	7.18	2.67	0.96	0.16	–	–	–	–	–	–	–	–	1002	0.9	–	–	–	–	–	–	–
	L-III	53.36	0.82	16.98	8.14	0.13	3.68	7.95	2.60	0.99	0.05	4.47	220	1842	739	370	0.15	502	28	996	0.1	10.20	30.6	303.9	50.4	33.04	321.6	18.2
	L-IV	52.89	0.79	16.89	9.02	0.12	4.09	7.51	2.64	1.13	0.12	4.51	277	1816	766	399	0.15	277	–	1007	2.5	14.35	28.9	290.1	43.3	33.03	297.2	17.6
SM1S	AA-I	45.82	1.08	18.35	12.37	0.20	5.88	13.26	2.02	0.35	0.10	0.97	418	2694	704	245	0.13	418	–	1120	5.4	–	47.3	442.5	35.2	4.59	269.3	17.7
	AE-I	49.25	1.19	19.05	10.50	0.25	5.59	10.10	3.31	0.66	0.26	0.82	95	2043	726	232	0.25	3177	48	1129	3.9	–	31.5	275.2	172.0	30.48	176.6	18.7
	AJ-I	45.66	1.18	18.61	13.08	0.09	6.61	11.01	2.83	0.18	0.13	0.56	695	3057	565	132	0.14	695	49	1159	8.9	–	–	–	–	–	–	–
	AL-II	45.83	0.86	19.39	12.02	0.23	6.02	11.79	2.24	0.94	0.11	1.22	339	2523	497	273	0.13	339	49	1122	0	1.98	41.9	406.2	41.8	17.07	345.3	16.8
	AM-II	46.75	1.25	18.00	14.62	0.28	5.82	11.43	2.98	0.19	0.19	–	–	2674	332	55	–	–	–	1136	6.5	–	40.9	502.5	42.4	5.17	356.1	22.4
	AR-VI	45.00	1.04	18.46	14.27	0.30	7.30	11.30	1.74	0.54	0.19	–	–	2047	442	63	–	–	–	1168	4.9	–	41.3	443.5	40.4	7.66	295.3	18.9
	BA-I	45.87	1.31	18.98	13.02	0.19	6.42	12.25	2.36	0.41	0.13	0.42	255	2762	530	321	0.14	255	–	1155	4.6	2.07	44.5	457.2	40.3	8.38	332.9	17.4
	BC-I	45.41	1.19	20.64	11.56	0.10	6.61	12.36	2.18	0.37	0.09	0.23	294	1847	513	260	0.14	294	49	1167	4.9	–	40.1	438.0	42.6	9.24	355.0	17.9
	S-II	46.68	1.19	18.17	14.98	0.11	6.19	8.97	3.55	0.18	0.14	1.28	126	3439	639	333	0.17	126	–	1132	5.9	1.38	52.3	470.0	64.6	3.43	222.5	20.0
	S-III	46.18	1.01	17.83	14.22	0.25	5.94	11.09	2.36	1.16	0.24	–	–	–	–	–	–	–	–	1140	3.5	–	–	–	–	–	–	–
	T-II	44.59	1.20	20.32	12.33	0.19	6.30	12.94	2.29	0.40	0.11	0.25	259	2571	527	287	0.13	259	49	1158	4.3	–	50.3	473.0	50.2	8.79	360.5	18.7
	Y-I	47.14	1.06	19.87	11.18	0.21	6.15	12.17	2.12	0.66	0.01	–	–	3530	415	–	–	–	–	1138	2	–	–	–	–	–	–	–
	Y-IV	46.37	1.06	20.50	11.43	0.21	6.17	12.71	2.24	0.40	0.12	0.37	527	2598	472	249	0.13	7583	47	1150	2.3	–	–	–	–	–	–	–
	Z-I	47.11	1.19	18.27	10.53	0.20	6.38	12.37	2.07	0.76	0.13	–	–	–	–	–	–	–	–	1143	0	3.52	41.7	405.9	61.4	26.81	251.8	18.1
KM1S12a	A-I	51.75	1.16	17.63	9.16	0.16	3.54	8.14	2.72	0.63	0.36	5.39	187	2215	1023	611	0.23	380	25	979	2.5	–	–	–	–	–	–	–
	AE-I	50.47	1.00	17.25	10.26	0.18	4.13	8.70	2.38	0.43	0.18	4.81	485	2724	833	521	0.20	1127	29	1000	2	7.61	30.2	265.4	26.6	8.63	257.8	21.8
	AE-II	50.66	1.14	17.89	10.08	0.21	3.97	8.39	2.28	0.60	0.15	–	–	–	–	–	–	–	–	996	4.8	–	–	–	–	–	–	–
	AE-III	50.33	0.93	18.29	9.39	0.15	3.62	9.23	2.55	0.43	0.11	5.10	338	2657	889	611	0.22	680	25	982	1.1	3.29	32.5	214.6	14.6	9.18	270.1	23.9
	AF-I	50.68	1.11	17.91	8.93	0.23	3.72	8.83	2.49	0.65	0.55	5.28	115	1691	870	504	0.55	115	38	983	4.6	4.40	29.1	210.0	4.5	18.81	236.6	24.5
	AH-II	52.15	1.04	17.77	8.55	0.07	3.53	8.41	2.87	0.67	0.19	4.51	214	1392	973	558	0.26	680	34	992	5.6	6.33	32.1	251.4	5.9	15.58	249.4	25.5
	AJ-I	51.70	1.20	16.78	9.68	0.34	3.95	7.95	2.21	0.65	0.31	5.93	143	2135	988	621	0.24	181	11	981	2.1	7.30	34.3	269.5	13.5	14.26	281.9	25.8

Table B2. (continued)

Sample ID	Melt ID	SiO_2 (wt. %)	TiO_2	Al_2O_3	FeO^{Total}	MnO	MgO	CaO	Na_2O	K_2O	P_2O_5	H_2O (wt. %)	CO_2^{Melt} (ppm)	S (ppm)	Cl (ppm)	F (ppm)	P_2O_5 (SIMS) (wt. %)	CO_2^{Total} (ppm)	1 s.e.[a] (rel. %)	T_{trap}[b] (°C)	PEC%[c]	Li (ppm)	Sc	V	Cu	Rb	Sr	Y
	J-I	49.93	1.11	17.70	9.38	0.27	4.72	8.50	2.53	0.50	0.11	6.06	556	2326	938	557	0.24	881	18	996	0	5.60	34.2	263.9	5.8	10.44	274.6	23.0
	J-II	49.77	1.18	17.68	9.72	0.15	4.12	8.60	2.53	0.47	0.15	5.17	–	2205	784	516	0.24	–	–	996	0	5.12	34.0	265.3	4.5	9.11	281.3	23.7
	K-II	51.82	1.02	17.67	9.49	0.15	3.61	8.48	2.74	0.67	0.39	4.96	76	1856	985	595	0.25	238	34	986	5.2	7.67	33.4	298.8	9.8	14.55	274.7	26.8
	O-I	53.88	0.99	16.93	9.20	0.19	3.63	7.20	3.30	0.75	0.17	–	–	1168	827	391	–	–	–	990	5.3	–	–	–	–	–	–	–
	Q-I	51.07	0.72	17.81	9.20	0.08	3.48	9.45	2.48	0.50	0.11	4.35	139	2663	890	615	0.22	287	26	990	3.6	7.29	43.2	256.0	26.4	10.00	286.3	27.0
	U-VI	51.52	1.13	18.11	8.20	0.16	3.24	8.63	2.81	0.59	0.30	4.48	86	2336	986	597	0.23	237	32	986	4.1	1.80	33.2	271.8	10.0	13.49	275.6	25.5
	Z-I	53.43	1.06	17.85	8.30	0.23	3.19	8.35	3.04	0.74	0.25	4.27	81	1914	1009	611	0.26	242	33	988	4.1	5.10	33.7	262.1	9.9	16.09	289.1	28.9
	Z-II	54.83	0.86	18.06	7.87	0.16	3.19	7.28	2.79	0.86	0.31	–	–	1426	967	303	–	–	–	980	5.7	–	–	–	–	–	–	–
FKONON	A-I	48.36	1.94	18.59	8.64	0.17	5.61	10.56	2.92	0.95	0.28	2.01	2502	1278	581	495	0.34	2502	–	1091	1.8	–	27.2	251.9	21.8	29.71	511.8	21.4
	B-I	49.34	1.76	18.56	8.98	0.14	5.67	10.07	3.26	1.01	0.31	1.99	1101	1200	603	519	0.37	2341	26	1093	3.1	–	29.1	327.1	10.8	32.43	529.2	20.4
	D-I	48.57	1.65	18.39	9.26	0.14	5.67	10.14	3.11	1.03	0.41	1.82	1851	1334	607	520	0.38	1851	–	1099	2	–	26.7	261.0	24.3	31.56	534.5	23.2
	D-II	48.59	1.67	16.95	11.40	0.14	6.77	7.86	3.80	1.44	0.33	1.54	1971	1032	852	578	0.42	9569	40	1139	7.4	4.47	19.4	158.2	35.7	37.07	522.5	22.6
	F-I	48.86	1.93	19.09	9.11	0.21	4.53	10.87	3.16	1.04	0.23	1.89	2183	1189	626	543	0.39	9812	39	1070	0.7	–	27.4	255.1	15.3	27.58	514.0	22.8
	I-I	48.81	1.74	19.12	9.40	0.19	5.05	10.62	3.19	1.00	0.20	1.67	2338	1396	572	482	0.34	12148	40	1089	0	–	27.2	250.1	34.2	26.19	489.0	19.6
	K-I	48.01	1.81	18.97	8.97	0.23	5.61	10.40	2.99	1.03	0.44	1.77	2253	1269	566	491	0.36	7353	35	1099	0.8	–	29.5	258.1	29.5	28.60	529.7	21.5
	K-II	48.84	1.77	18.65	9.03	0.07	5.70	10.34	3.04	1.00	0.40	1.76	2219	1245	562	495	0.36	6628	33	1100	1.1	–	27.8	265.1	19.5	29.94	556.9	23.0
	N-I	48.74	1.82	19.10	9.08	0.11	5.03	10.23	3.23	1.13	0.45	1.89	2713	1199	635	518	0.47	8840	35	1083	0.2	–	28.0	238.8	21.1	31.24	494.8	20.5
	N-II	48.27	1.99	19.25	8.94	0.20	4.89	9.74	3.35	1.24	0.34	–	–	–	–	–	–	–	–	1091	2.6	–	46.7	275.3	38.9	40.10	562.5	25.5
	O-I	47.95	1.82	19.35	8.57	0.23	5.17	10.63	3.29	1.12	0.32	1.62	2495	1126	593	534	0.41	8245	35	1095	0	–	29.4	268.8	12.5	32.48	550.5	22.1
	O-II	48.29	1.87	18.63	9.05	0.16	5.47	10.39	2.98	1.02	0.25	–	–	–	–	–	–	–	–	1099	0.7	–	26.9	254.2	37.1	28.45	503.1	19.8
	P-II	48.97	1.82	18.88	9.25	0.13	5.36	10.36	3.27	0.97	0.39	1.67	2324	1250	592	511	0.39	9507	38	1096	0.7	–	29.9	247.4	21.0	29.98	495.8	21.2

Table B2. (continued)

Sample ID	Melt ID	Zr	Nb	Ba	La	Ce	Pr	Nd	Sm	Eu	Gd	Dy	Er	Yb	Lu	Hf	Ta	Pb	Th	U
ON2S	AMa-I	–	–	–	–	–	–	–	–	–	–	–	–	–	–	–	–	–	–	–
	AP-IV	183.0	28.71	322.1	34.56	81.52	9.80	40.05	7.26	2.14	5.28	4.20	1.79	1.26	0.19	4.66	1.45	6.51	3.82	0.72
	BEc-III	192.7	29.69	329.0	36.58	84.90	11.01	42.28	8.21	2.56	5.51	3.99	1.87	1.45	0.15	4.78	1.46	6.01	3.56	0.61
	CSa-III	143.3	23.66	256.6	25.37	60.23	7.63	30.97	5.56	1.61	4.33	3.00	1.31	0.84	0.15	3.24	1.16	3.37	2.51	0.47
	DF-IV	–	–	–	–	–	–	–	–	–	–	–	–	–	–	–	–	–	–	–
	DL-I	156.1	26.16	7690.1	109.94	109.31	17.38	65.24	10.07	2.95	8.66	5.22	2.57	1.66	0.24	4.11	1.25	5.41	3.08	0.65
	DS-III	–	–	–	–	–	–	–	–	–	–	–	–	–	–	–	–	–	–	–
	DZ-I	200.3	32.47	1308.5	35.37	52.68	8.07	30.95	5.95	1.60	4.16	3.18	1.52	1.03	0.21	5.40	1.58	6.11	4.04	0.55
	EDa-I	–	–	–	–	–	–	–	–	–	–	–	–	–	–	–	–	–	–	–
	U-I	–	–	–	–	–	–	–	–	–	–	–	–	–	–	–	–	–	–	–
	Z-I	153.5	26.84	283.6	33.83	80.73	10.31	39.29	7.64	2.28	5.77	3.41	1.75	1.26	0.12	3.96	1.36	4.79	3.26	0.66
YF1L	AFa-III	50.6	2.67	210.8	9.52	22.67	3.37	15.26	4.17	1.19	3.28	3.25	1.78	1.44	0.23	1.33	–	3.38	1.54	0.52
	AFb-I	42.0	2.19	133.4	6.68	18.74	2.72	12.62	3.51	1.13	3.18	2.75	1.33	1.47	0.20	1.31	0.10	3.73	1.30	0.40
	AH-I	43.0	2.46	136.2	6.34	15.76	2.30	10.93	3.01	1.05	2.82	2.94	1.62	1.49	0.26	1.40	0.12	2.32	0.72	0.23
	AZ-I	52.3	2.23	135.0	7.61	21.80	3.23	15.45	4.30	1.25	4.26	3.53	1.75	1.79	0.21	1.44	0.15	4.20	1.46	0.61
	AZ-III	52.5	2.66	237.4	9.89	24.40	3.22	15.54	3.58	1.36	4.16	3.05	2.28	1.57	0.25	1.77	0.20	2.33	1.46	0.44
	BD-I	43.7	2.38	125.5	6.28	15.59	2.26	11.14	2.85	0.85	2.63	2.98	1.89	1.35	0.18	1.34	0.10	1.75	0.71	0.24
	BK-II	40.1	2.12	150.8	6.84	16.54	2.39	11.36	2.91	1.05	2.85	2.67	1.53	1.35	0.18	1.27	0.09	2.22	1.05	0.31
	BLa-II	46.6	2.66	202.0	8.80	21.04	2.84	12.57	3.34	1.14	3.44	2.97	1.53	1.34	0.25	1.30	0.16	3.06	1.31	0.39
	BLa-III	47.1	2.36	195.4	8.43	20.23	2.69	14.38	3.53	1.25	3.27	2.62	1.47	1.30	0.16	1.55	–	2.97	1.39	0.42
	BM-I	41.8	2.31	127.3	5.90	15.08	2.22	10.58	2.87	1.17	2.70	2.73	1.63	1.62	0.18	1.32	0.09	1.91	0.68	0.19
	BO-I	42.5	2.26	199.2	7.87	18.68	2.95	11.44	2.14	1.31	2.58	3.22	1.59	1.17	0.09	1.76	0.06	2.67	1.68	0.39
	BQ-I	41.2	2.20	137.3	5.65	15.49	2.43	11.64	3.12	1.07	2.53	2.42	1.53	1.55	0.18	1.14	0.11	3.18	1.18	0.35
	BQ-II	45.5	2.41	138.3	7.10	19.08	2.67	12.57	3.36	1.08	3.74	2.74	1.94	1.29	0.25	1.56	0.19	3.07	1.38	0.46
	BQ-III	50.5	2.44	220.6	9.51	19.58	3.40	13.07	3.60	1.18	2.42	2.32	1.80	1.85	0.22	1.04	–	3.05	1.41	0.38
	BSb-III	–	–	–	–	–	–	–	–	–	–	–	–	–	–	–	–	–	–	–
	BSc-II	40.6	2.10	181.5	7.88	18.88	2.69	12.08	2.90	1.03	2.99	2.51	1.40	1.45	0.18	1.23	0.09	2.36	1.33	0.35
	F-I	42.5	2.35	191.5	7.17	19.02	2.62	12.92	3.79	1.03	3.05	2.68	1.58	1.20	0.14	1.40	–	4.69	1.41	0.48
	F-II	47.0	2.27	204.5	8.57	20.01	2.65	13.00	3.46	1.13	2.89	2.82	1.73	1.66	0.24	1.57	–	3.51	1.56	0.56
KJ5S	AD-V	76.1	5.58	301.5	13.06	29.29	3.71	16.03	3.79	1.19	3.58	3.12	1.93	1.80	0.27	2.05	0.29	7.20	1.68	0.39
	AE-I	82.6	6.27	331.8	13.89	30.93	3.96	17.12	4.15	1.22	3.28	3.29	1.75	1.92	0.28	2.44	0.34	7.65	2.02	0.50
	AE-II	77.2	5.59	313.6	12.65	28.62	3.65	15.85	3.72	1.16	3.28	3.15	1.81	1.71	0.27	2.13	0.31	6.75	1.68	0.39
	AF-I	81.5	5.89	315.6	12.82	28.94	3.72	16.27	3.89	1.19	3.32	3.22	1.89	1.79	0.25	2.19	0.31	6.94	1.71	0.39
	AGa-I	78.8	5.80	318.4	13.03	29.35	3.63	16.08	3.64	1.17	3.40	3.08	1.85	1.78	0.25	2.11	0.30	7.21	1.67	0.41
	AGb-IV	87.5	6.48	356.0	13.89	31.27	3.94	17.08	3.94	1.21	3.54	3.21	1.87	1.81	0.27	2.33	0.33	7.29	2.06	0.46

Table B2. (continued)

Sample ID	Melt ID	Zr	Nb	Ba	La	Ce	Pr	Nd	Sm	Eu	Gd	Dy	Er	Yb	Lu	Hf	Ta	Pb	Th	U
	AGb-V	81.6	6.13	336.6	13.88	31.09	3.97	17.01	3.93	1.21	3.50	3.17	1.94	1.81	0.25	2.28	0.31	7.56	1.71	0.37
	AI-I	78.7	5.79	315.4	13.27	29.48	3.78	16.31	3.87	1.24	3.66	3.45	2.10	1.96	0.27	2.28	0.29	7.84	1.69	0.40
	AK-I	79.7	6.11	320.6	13.51	31.03	3.98	17.05	4.01	1.25	3.72	3.36	1.90	1.84	0.29	2.30	0.31	7.41	1.65	0.39
	AK-II	106.9	5.51	359.0	14.60	30.65	4.31	15.82	3.96	0.90	4.50	3.70	2.86	1.34	0.34	1.88	0.51	8.02	1.85	0.52
	B-I	80.1	5.85	313.4	13.32	30.13	3.79	16.46	3.92	1.24	3.48	3.17	1.95	1.97	0.30	2.21	0.30	6.93	1.78	0.42
	K-I	78.0	5.66	314.9	12.58	28.11	3.58	15.86	3.44	1.14	3.56	3.00	1.79	1.80	0.27	2.12	0.29	6.93	1.61	0.38
	L-I	80.0	5.83	315.4	13.76	30.24	3.77	16.78	3.69	1.24	3.69	3.42	1.86	1.80	0.27	2.10	0.29	7.29	1.79	0.40
	S-III	79.7	5.83	314.0	12.95	29.70	3.81	16.20	3.90	1.20	3.55	3.35	1.93	1.75	0.27	2.15	0.31	6.83	1.70	0.41
	U-I	75.6	5.54	294.0	12.63	28.17	3.50	15.44	3.55	1.10	3.17	2.96	1.64	1.68	0.23	1.99	0.30	6.96	1.82	0.44
	V-I	90.6	6.81	384.1	15.41	34.54	4.07	18.17	4.18	1.34	3.96	3.33	2.10	1.65	0.28	2.15	0.39	7.64	2.38	0.56
	Y-I	80.8	5.86	325.0	13.33	29.52	3.85	16.48	3.74	1.20	3.52	3.22	1.76	1.85	0.27	2.20	0.33	6.79	1.78	0.45
	Y-II	80.6	5.82	323.6	13.26	29.76	3.79	16.51	3.83	1.21	3.40	3.14	1.89	1.87	0.28	2.19	0.30	7.04	1.87	0.43
KSS	AA-I	60.4	3.01	239.0	9.94	23.09	3.09	13.86	3.53	1.06	3.33	3.14	1.77	1.74	0.27	1.81	0.19	6.59	2.19	0.65
	AA-II	114.9	6.34	361.5	16.90	38.63	4.98	21.14	5.00	1.36	4.44	4.24	2.46	2.29	0.34	3.01	0.40	10.89	5.11	1.42
	AA-III	58.7	2.95	250.7	10.30	23.70	3.11	13.78	3.15	1.08	3.41	3.18	1.89	1.73	0.22	1.70	0.20	6.73	2.16	0.63
	AB-I	54.7	2.58	242.9	9.70	22.21	2.92	13.35	3.21	1.10	3.06	2.97	1.73	1.55	0.24	1.57	0.17	6.20	1.98	0.61
	D-I	59.2	2.91	254.6	9.95	22.96	3.04	13.95	3.52	1.11	3.11	3.09	1.75	1.73	0.26	1.77	0.20	7.09	2.13	0.62
	E-I	–	–	–	–	–	–	–	–	–	–	–	–	–	–	–	–	–	–	–
	E-II	–	–	–	–	–	–	–	–	–	–	–	–	–	–	–	–	–	–	–
	G-I	88.1	4.45	305.5	12.20	28.74	3.73	16.89	4.46	1.22	4.26	4.60	2.91	2.95	0.40	2.42	0.31	9.62	3.39	1.07
	G-II	124.9	7.64	391.6	18.44	42.72	5.12	23.17	5.18	1.33	4.64	4.36	2.42	2.36	0.37	3.33	0.50	11.97	5.76	1.72
	G-III	131.7	6.41	381.4	18.64	44.23	5.81	24.75	7.43	1.81	5.34	6.30	3.43	3.32	0.46	3.65	0.36	12.00	5.75	1.60
	H-I	99.6	4.25	357.2	14.78	37.11	5.23	26.23	7.62	1.82	6.91	6.17	3.59	3.48	0.50	2.61	0.29	7.56	3.39	1.05
	K-II	48.3	2.40	223.0	8.76	20.36	2.71	12.24	3.08	0.97	2.86	2.60	1.46	1.47	0.20	1.29	0.15	5.93	1.74	0.53
	L-I	50.6	2.47	226.5	9.13	20.95	2.81	12.23	2.83	1.00	2.80	2.75	1.64	1.45	0.21	1.51	0.17	5.99	1.94	0.55
	W-I	121.1	6.95	377.1	17.51	40.04	5.02	22.36	5.20	1.35	4.77	4.37	2.65	2.65	0.42	3.26	0.48	10.81	5.25	1.58
KROHTH	A-I	–	–	–	–	–	–	–	–	–	–	–	–	–	–	–	–	–	–	–
	A-II	–	–	–	–	–	–	–	–	–	–	–	–	–	–	–	–	–	–	–
	E-I	63.3	2.97	191.9	9.04	20.81	2.60	12.10	3.21	1.01	3.35	3.62	2.30	2.39	0.35	1.84	0.21	8.07	2.07	0.58
	E-II	63.8	2.99	185.5	8.82	20.25	2.54	11.99	3.14	0.96	3.23	3.59	2.19	2.27	0.32	1.84	0.21	7.71	2.07	0.57
	E-III	–	–	–	–	–	–	–	–	–	–	–	–	–	–	–	–	–	–	–
	F-I	64.8	3.00	197.0	9.14	20.54	2.61	11.97	3.12	0.94	3.13	3.52	2.18	2.35	0.34	1.87	0.21	8.02	2.34	0.64
	G-I	65.6	3.06	190.7	9.12	21.11	2.58	12.11	3.35	0.97	3.30	3.50	2.34	2.18	0.31	1.97	0.20	7.70	2.28	0.65
	H-I	63.8	3.00	191.1	8.95	20.60	2.60	11.75	3.20	0.99	3.32	3.60	2.28	2.29	0.34	1.79	0.20	8.14	2.07	0.57
	I-I	67.5	3.13	205.4	9.37	21.53	2.70	12.24	3.19	1.01	3.26	3.56	2.37	2.33	0.32	1.92	0.22	8.34	2.30	0.63
	K-I	67.1	3.07	201.3	9.43	21.52	2.77	12.35	3.50	1.02	3.18	3.44	2.18	2.11	0.31	1.99	0.22	7.88	2.20	0.59
	L-II	66.7	3.14	202.9	9.36	21.64	2.67	12.24	3.20	1.01	3.27	3.70	2.26	2.35	0.36	1.90	0.21	8.76	2.24	0.63

Table B2. (continued)

Sample ID	Melt ID	Zr	Nb	Ba	La	Ce	Pr	Nd	Sm	Eu	Gd	Dy	Er	Yb	Lu	Hf	Ta	Pb	Th	U
KRSM11	A-I	72.1	2.92	207.4	9.09	20.76	2.54	11.35	2.96	0.84	2.93	3.19	1.91	2.00	0.32	2.07	0.21	9.08	3.11	0.83
	A-II	76.2	2.99	217.6	9.68	21.53	2.74	11.76	2.86	0.82	3.13	3.15	1.96	1.77	0.32	2.28	0.18	9.62	3.29	0.84
	A-III	72.9	2.89	202.6	9.36	21.03	2.62	11.63	3.03	0.83	3.20	3.52	2.11	2.05	0.35	2.17	0.19	10.28	3.05	0.80
	B-I	68.2	2.80	195.3	8.81	19.92	2.46	10.95	2.92	0.86	2.85	3.18	1.93	2.01	0.30	1.97	0.20	8.97	2.83	0.76
	C-I	74.8	2.99	217.0	9.57	22.06	2.79	12.37	3.22	0.90	2.90	3.19	2.16	2.10	0.29	2.11	0.23	10.61	3.33	0.85
	D-I	59.2	2.39	173.6	7.89	18.16	2.28	10.39	2.83	0.85	2.73	3.19	1.94	2.04	0.30	1.68	0.18	8.47	2.32	0.61
	D-II	76.5	3.04	214.8	9.87	21.63	2.95	12.32	3.19	0.83	2.87	3.13	2.30	2.21	0.28	2.00	0.16	10.10	3.42	0.81
	E-I	70.6	2.84	194.3	8.94	20.39	2.47	11.30	2.80	0.87	2.90	3.17	1.98	1.99	0.30	2.03	0.19	9.08	2.91	0.79
	E-II	59.4	2.36	170.2	7.81	18.19	2.26	10.57	2.78	0.86	2.61	3.06	1.90	2.08	0.31	1.63	0.17	8.13	2.33	0.64
	G-I	68.7	2.74	195.2	8.86	20.24	2.48	11.08	2.89	0.86	2.89	3.21	1.97	2.08	0.29	1.90	0.20	9.22	2.86	0.78
	H-I	–	–	–	–	–	–	–	–	–	–	–	–	–	–	–	–	–	–	–
	K-V	71.5	3.00	215.3	10.03	21.96	2.58	12.35	3.03	0.92	3.07	3.34	2.41	1.88	0.32	1.89	–	9.63	2.66	0.84
	L-I	67.1	2.74	199.4	8.87	20.74	2.55	11.39	3.07	0.85	3.08	3.29	1.97	2.12	0.30	1.88	0.19	9.21	2.80	0.79
	L-II	–	–	–	–	–	–	–	–	–	–	–	–	–	–	–	–	–	–	–
	L-III	69.3	2.88	200.1	8.90	20.20	2.52	11.59	2.71	0.89	2.59	3.27	2.07	2.15	0.30	2.07	0.18	8.79	2.94	0.74
	L-IV	70.4	2.85	200.6	9.43	21.51	2.61	11.85	3.02	0.82	3.14	3.30	2.20	1.84	0.29	1.80	0.21	9.49	3.09	0.74
SM1S	AA-I	35.6	3.30	120.1	5.06	12.39	1.83	9.17	2.66	1.02	3.02	3.33	2.17	2.02	0.27	1.19	0.17	2.62	0.72	0.19
	AE-I	66.9	6.73	120.7	9.65	23.42	2.83	12.90	3.92	1.30	3.11	3.83	2.11	1.74	0.25	2.10	0.33	9.99	1.63	0.42
	AJ-I	–	–	–	–	–	–	–	–	–	–	–	–	–	–	–	–	–	–	–
	AL-II	32.3	3.04	89.2	4.57	11.30	1.58	8.07	2.57	0.86	2.63	3.25	1.81	1.71	0.26	0.97	0.18	2.09	0.69	0.20
	AM-II	49.6	4.41	99.8	7.07	17.06	2.25	10.77	3.29	1.31	4.09	4.53	2.26	1.98	0.33	1.36	0.22	3.35	1.13	0.25
	AR-VI	34.9	3.22	90.9	5.28	12.32	1.80	8.61	2.79	1.11	3.38	3.68	2.27	2.08	0.34	1.00	0.13	2.57	0.70	0.20
	BA-I	35.8	3.41	97.1	5.27	12.89	1.86	8.91	2.70	0.90	3.21	3.20	2.02	1.98	0.28	1.19	0.17	2.32	0.77	0.21
	BC-I	32.9	3.36	96.3	4.79	12.08	1.76	8.35	2.43	0.99	2.90	3.19	2.23	2.11	0.33	1.10	0.15	3.39	0.68	0.20
	S-II	41.0	3.66	68.0	5.68	14.35	1.80	10.63	3.68	1.10	2.95	3.69	2.34	1.87	0.30	1.26	0.17	3.25	0.83	0.18
	S-III	–	–	–	–	–	–	–	–	–	–	–	–	–	–	–	–	–	–	–
	T-II	36.4	3.27	97.0	5.01	12.56	1.79	8.78	2.49	1.01	2.89	3.17	2.22	2.06	0.33	1.18	0.19	2.52	0.78	0.20
	Y-I	–	–	–	–	–	–	–	–	–	–	–	–	–	–	–	–	–	–	–
	Y-IV	–	–	–	–	–	–	–	–	–	–	–	–	–	–	–	–	–	–	–
	Z-I	35.7	3.10	92.5	4.85	11.76	1.74	8.63	2.59	0.95	3.02	3.46	2.08	1.88	0.30	1.15	0.17	3.86	0.71	0.18
KM1S12a	A-I	–	–	–	–	–	–	–	–	–	–	–	–	–	–	–	–	–	–	–
	AE-I	57.6	2.75	81.0	6.13	16.07	2.34	11.40	3.26	1.02	3.58	3.95	2.39	2.45	0.36	1.70	0.13	3.75	0.72	0.20
	AE-II	–	–	–	–	–	–	–	–	–	–	–	–	–	–	–	–	–	–	–
	AE-III	61.4	2.96	86.4	6.77	18.21	2.60	12.35	3.54	1.08	3.64	4.21	2.60	2.46	0.34	1.77	0.10	3.74	0.82	0.23
	AF-I	79.5	3.94	115.7	8.87	22.72	3.09	14.97	3.91	1.27	4.24	4.59	2.84	2.70	0.38	2.39	0.19	5.53	1.65	0.36
	AH-II	90.9	4.41	112.8	9.72	26.14	3.59	17.04	4.54	1.41	4.44	4.74	3.04	2.66	0.41	2.44	0.21	5.68	1.16	0.26
	AJ-I	77.6	3.79	118.5	8.90	22.96	3.22	15.62	4.27	1.30	4.48	4.68	3.03	2.74	0.44	2.15	0.15	4.59	1.22	0.29

Table B2. (continued)

Sample ID	Melt ID	Zr	Nb	Ba	La	Ce	Pr	Nd	Sm	Eu	Gd	Dy	Er	Yb	Lu	Hf	Ta	Pb	Th	U
	J-I	67.5	3.24	93.5	7.01	18.57	2.62	12.70	3.48	1.05	3.63	4.17	2.58	2.59	0.37	1.93	0.15	3.99	0.89	0.23
	J-II	69.1	3.36	92.8	7.33	19.38	2.72	13.06	3.65	1.19	3.98	4.50	2.59	2.66	0.41	2.00	0.17	3.81	0.84	0.20
	K-II	81.5	3.91	118.2	8.96	23.32	3.23	15.53	4.47	1.38	4.60	4.87	3.17	3.00	0.40	2.28	0.17	4.65	1.28	0.35
	O-I	–	–	–	–	–	–	–	–	–	–	–	–	–	–	–	–	–	–	–
	Q-I	70.2	3.36	98.3	7.48	19.49	2.81	13.54	3.53	1.19	4.33	4.54	3.04	3.14	0.50	2.05	0.16	3.96	0.82	0.18
	U-VI	77.1	3.66	114.0	8.44	22.00	3.04	14.40	3.94	1.31	4.53	4.80	2.75	2.79	0.43	2.22	0.16	4.88	1.15	0.31
	Z-I	93.5	4.36	136.0	10.06	26.66	3.70	17.42	4.42	1.31	4.80	5.45	3.20	3.25	0.51	2.75	0.19	5.54	1.44	0.39
	Z-II	–	–	–	–	–	–	–	–	–	–	–	–	–	–	–	–	–	–	–
FKONON	A-I	94.6	25.97	337.4	17.09	34.46	4.05	17.24	4.00	1.40	3.96	4.19	2.31	2.18	0.32	2.35	1.29	1.67	2.50	0.49
	B-I	100.7	25.33	386.2	20.71	43.26	4.32	19.31	5.83	1.61	4.58	4.32	2.82	2.27	0.31	2.15	1.41	2.20	2.21	0.44
	D-I	114.1	27.54	372.7	19.27	37.95	4.89	19.12	4.33	1.72	4.81	4.95	2.32	1.82	0.27	3.06	1.36	2.18	2.71	0.64
	D-II	109.9	32.73	487.6	26.62	50.79	5.58	22.66	5.26	1.62	4.24	4.21	2.55	2.34	0.35	2.39	1.47	3.26	3.12	0.64
	F-I	106.1	26.03	351.2	18.24	38.16	4.43	19.09	4.55	1.67	4.98	4.84	2.47	2.54	0.30	2.81	1.51	2.35	2.30	0.57
	I-I	87.7	23.00	310.5	15.52	31.27	3.66	15.78	3.41	1.46	3.78	3.81	2.04	1.93	0.29	2.42	1.14	1.93	2.22	0.44
	K-I	104.3	22.90	327.2	15.73	30.78	3.49	16.21	4.26	1.48	3.21	4.35	2.75	2.35	0.35	1.96	1.48	2.76	2.37	0.37
	K-II	106.1	25.41	343.4	17.87	33.69	3.95	16.18	4.12	1.64	4.52	3.64	2.74	1.78	0.30	2.43	1.36	2.51	2.19	0.46
	N-I	96.2	27.38	363.9	18.42	35.71	4.24	17.21	4.00	1.51	3.98	4.15	2.33	1.98	0.29	2.41	1.44	2.10	2.57	0.55
	N-II	127.9	34.50	471.4	22.05	42.94	4.78	18.91	4.42	0.95	–	5.98	1.55	3.54	0.25	2.18	1.38	3.79	3.53	0.60
	O-I	104.9	27.78	365.1	18.65	36.98	4.51	18.55	4.55	1.56	4.68	4.33	2.48	2.13	0.31	2.66	1.46	1.93	2.57	0.52
	O-II	90.5	24.60	329.1	16.62	32.78	4.08	16.66	4.12	1.50	3.93	3.97	2.26	1.92	0.29	2.59	1.22	1.80	2.35	0.48
	P-II	102.3	26.26	343.3	18.16	35.88	4.18	17.58	4.31	1.56	4.18	3.94	2.41	2.03	0.30	2.37	1.29	1.98	2.43	0.53

[a] Relative uncertainty (1σ) on total CO_2 in percent assigned 50% error to each MI volume estimation based on the numerical simulation of Tucker et al. (2019) regarding arithmetic mean asumption for the third axis.

[b] Temperature calculated based on corrected melt composition after Sugawara (2000) and Médard and Grove (2008). Average H_2O concentrations of each samples were assumed for not analyzed melt inclusion. Pressures were set at 1 kbar as pressure effects over several kbars are negligible.

[c] Degree of post-entrapment crystallization in wt.% based on adding calculation.

Table B3. Uncorrected major element and sulfur speciation analyses of melt inclusions

Sample ID	Melt ID	SiO_2 (wt. %)	*1 s.d.*	TiO_2	*1 s.d.*	Al_2O_3	*1 s.d.*	FeO^{Total}	*1 s.d.*	MnO	*1 s.d.*	MgO	*1 s.d.*	CaO	*1 s.d.*	Na_2O	*1 s.d.*	K_2O	*1 s.d.*	P_2O_5	*1 s.d.*	Total	S^{6+}/S^{Total}	*1 s.e.*
ON2S	AMa-I	44.52	*1.16*	2.51	*0.28*	15.14	*0.21*	13.44	*0.60*	0.21	*0.16*	10.74	*0.51*	7.86	*0.34*	2.06	*0.12*	1.02	*0.05*	0.67	*0.15*	98.18	-	-
	AP-IV	43.80	*1.14*	2.46	*0.27*	15.43	*0.21*	15.50	*0.65*	0.13	*0.16*	7.39	*0.41*	9.27	*0.37*	3.30	*0.15*	1.10	*0.05*	0.66	*0.15*	99.05	-	-
	BEc-III	43.03	*1.13*	2.57	*0.29*	15.78	*0.21*	14.53	*0.63*	0.13	*0.17*	7.52	*0.42*	10.21	*0.39*	3.23	*0.14*	1.03	*0.05*	0.87	*0.16*	98.90	-	-
	BFa-I	43.12	*1.13*	2.62	*0.29*	15.90	*0.21*	14.61	*0.63*	0.21	*0.17*	7.21	*0.41*	10.16	*0.39*	3.27	*0.15*	1.00	*0.05*	0.81	*0.16*	98.90	-	-
	CSa-III	43.92	*1.14*	2.39	*0.28*	14.90	*0.20*	17.78	*0.70*	0.28	*0.19*	6.56	*0.39*	8.30	*0.35*	2.85	*0.14*	0.91	*0.04*	0.72	*0.15*	98.62	0.07	*0.02*
	DF-IV	44.78	*1.16*	2.16	*0.26*	17.21	*0.23*	13.37	*0.60*	0.18	*0.17*	6.17	*0.37*	10.06	*0.39*	3.44	*0.15*	1.01	*0.05*	0.95	*0.18*	99.34	0.06	*0.04*
	DL-I	43.53	*1.14*	2.59	*0.28*	16.66	*0.22*	13.57	*0.61*	0.16	*0.16*	11.16	*0.52*	6.23	*0.30*	1.79	*0.11*	1.16	*0.05*	0.80	*0.16*	97.65	-	-
	DS-III	45.94	*1.18*	2.02	*0.25*	12.96	*0.18*	18.05	*0.70*	0.26	*0.19*	9.40	*0.47*	8.37	*0.35*	1.14	*0.09*	0.72	*0.04*	0.72	*0.15*	99.58	-	-
	DZ-I	43.77	*1.14*	2.82	*0.29*	16.33	*0.22*	15.28	*0.65*	0.20	*0.17*	10.33	*0.50*	7.58	*0.34*	1.24	*0.09*	0.82	*0.04*	0.42	*0.13*	98.81	-	-
	EDa-I	48.07	*1.23*	1.65	*0.23*	15.41	*0.21*	16.56	*0.67*	0.25	*0.17*	14.55	*0.61*	0.71	*0.11*	0.84	*0.08*	0.63	*0.04*	0.13	*0.08*	98.78	-	-
	U-I	61.04	*1.43*	2.05	*0.26*	16.35	*0.21*	6.64	*0.43*	0.13	*0.15*	2.04	*0.20*	6.26	*0.31*	2.64	*0.13*	3.12	*0.08*	0.99	*0.18*	101.26	-	-
	Z-I	42.68	*1.12*	2.61	*0.28*	16.15	*0.22*	13.25	*0.60*	0.28	*0.17*	9.05	*0.46*	10.43	*0.40*	3.29	*0.15*	0.97	*0.05*	0.80	*0.16*	99.51	0.13	*0.14*
YF1L	AFa-III	40.36	*1.08*	1.26	*0.21*	19.22	*0.25*	15.14	*0.64*	0.24	*0.16*	7.99	*0.43*	11.80	*0.42*	2.74	*0.13*	0.61	*0.04*	0.09	*0.09*	99.46	-	-
	AFb-I	42.30	*1.12*	1.27	*0.20*	17.87	*0.23*	14.85	*0.63*	0.26	*0.16*	11.49	*0.53*	10.17	*0.39*	2.07	*0.12*	0.47	*0.03*	0.11	*0.09*	100.87	0.43	*0.23*
	AH-I	44.08	*1.15*	1.18	*0.21*	17.52	*0.23*	10.94	*0.54*	0.22	*0.16*	10.06	*0.49*	11.40	*0.42*	2.96	*0.14*	0.43	*0.03*	0.07	*0.08*	98.86	-	-
	AZ-I	42.09	*1.11*	1.18	*0.20*	18.13	*0.24*	14.17	*0.62*	0.21	*0.17*	10.46	*0.50*	11.90	*0.42*	2.13	*0.12*	0.41	*0.03*	0.09	*0.09*	100.76	-	-
	AZ-III	41.54	*1.10*	1.13	*0.21*	18.08	*0.24*	14.03	*0.61*	0.20	*0.17*	10.20	*0.49*	11.94	*0.42*	2.67	*0.13*	0.53	*0.04*	0.27	*0.11*	100.59	-	-
	BD-I	42.19	*1.11*	1.18	*0.20*	17.99	*0.23*	13.12	*0.60*	0.13	*0.17*	11.07	*0.52*	11.65	*0.42*	2.87	*0.14*	0.39	*0.03*	0.03	*0.10*	100.62	-	-
	BK-II	40.95	*1.09*	1.06	*0.20*	17.53	*0.23*	15.09	*0.64*	0.07	*0.17*	11.08	*0.52*	10.34	*0.40*	2.70	*0.13*	0.52	*0.04*	0.16	*0.10*	99.51	0.10	*0.04*
	BLa-II	40.85	*1.09*	1.12	*0.20*	16.93	*0.22*	16.50	*0.67*	0.26	*0.18*	9.99	*0.49*	10.75	*0.40*	2.63	*0.13*	0.51	*0.04*	0.24	*0.10*	99.79	-	-
	BLa-III	40.68	*1.09*	1.13	*0.20*	16.76	*0.22*	18.10	*0.70*	0.25	*0.18*	9.27	*0.47*	10.91	*0.40*	2.59	*0.13*	0.54	*0.04*	0.21	*0.10*	100.44	-0.01	*0.01*
	BM-I	42.05	*1.11*	1.12	*0.21*	17.55	*0.23*	12.63	*0.58*	0.12	*0.17*	11.72	*0.54*	11.16	*0.41*	2.96	*0.14*	0.39	*0.03*	0.13	*0.09*	99.83	-0.02	*0.03*
	BO-I	40.81	*1.09*	1.12	*0.20*	17.43	*0.23*	14.67	*0.63*	0.14	*0.18*	10.49	*0.50*	10.89	*0.41*	2.69	*0.13*	0.51	*0.04*	0.19	*0.09*	98.94	-	-
	BQ-I	42.67	*1.13*	0.98	*0.19*	16.12	*0.22*	14.45	*0.63*	0.15	*0.18*	13.80	*0.59*	8.89	*0.37*	2.37	*0.12*	0.52	*0.04*	0.16	*0.10*	100.10	-	-
	BQ-II	41.04	*1.10*	1.05	*0.20*	16.01	*0.22*	15.81	*0.65*	0.22	*0.17*	13.18	*0.58*	9.57	*0.38*	2.20	*0.12*	0.51	*0.03*	0.12	*0.10*	99.71	-	-
	BQ-III	40.58	*1.09*	1.17	*0.20*	16.79	*0.22*	16.74	*0.68*	0.14	*0.18*	10.12	*0.50*	10.52	*0.40*	2.59	*0.13*	0.55	*0.04*	0.26	*0.10*	99.46	-	-
	BSb-III	41.08	*1.09*	1.18	*0.21*	19.20	*0.25*	13.82	*0.61*	0.26	*0.17*	9.03	*0.46*	11.30	*0.41*	2.72	*0.13*	0.61	*0.04*	0.16	*0.10*	99.34	-	-
	BSc-II	40.72	*1.09*	0.86	*0.19*	16.97	*0.23*	14.79	*0.64*	0.12	*0.16*	12.14	*0.55*	10.47	*0.40*	2.76	*0.13*	0.53	*0.04*	0.32	*0.11*	99.66	0.02	*0.04*

Table B3. (continued)

Sample ID	Melt ID	SiO_2 (wt. %)	*1 s.d.*	TiO_2	*1 s.d.*	Al_2O_3	*1 s.d.*	FeO^{Total}	*1 s.d.*	MnO	*1 s.d.*	MgO	*1 s.d.*	CaO	*1 s.d.*	Na_2O	*1 s.d.*	K_2O	*1 s.d.*	P_2O_5	*1 s.d.*	Total	S^{6+}/S^{Total}	*1 s.e.*
	F-I	42.05	*1.11*	1.09	*0.20*	16.93	*0.22*	14.05	*0.62*	0.17	*0.17*	13.29	*0.58*	9.67	*0.38*	2.57	*0.13*	0.57	*0.04*	0.07	*0.10*	100.45	-	-
	F-II	41.68	*1.11*	1.07	*0.20*	18.03	*0.24*	15.01	*0.64*	0.06	*0.15*	11.30	*0.53*	10.42	*0.39*	2.94	*0.14*	0.58	*0.04*	0.20	*0.10*	101.28	-	-
KJ5S	AD-V	52.23	*1.29*	0.95	*0.19*	16.82	*0.22*	10.27	*0.53*	0.22	*0.17*	3.61	*0.27*	7.41	*0.33*	2.93	*0.14*	0.98	*0.05*	0.18	*0.09*	95.58	-	-
	AE-I	52.88	*1.29*	0.93	*0.19*	16.67	*0.22*	8.81	*0.49*	0.29	*0.17*	3.92	*0.28*	7.16	*0.33*	2.96	*0.13*	1.08	*0.05*	0.26	*0.10*	94.96	-	-
	AE-II	51.77	*1.28*	1.05	*0.19*	16.86	*0.22*	9.33	*0.50*	0.24	*0.17*	4.61	*0.31*	7.33	*0.33*	2.91	*0.13*	1.02	*0.05*	0.30	*0.10*	95.41	-	-
	AF-I	51.87	*1.28*	1.04	*0.19*	17.28	*0.22*	8.82	*0.49*	0.12	*0.15*	3.98	*0.29*	7.53	*0.34*	3.17	*0.14*	1.08	*0.05*	0.18	*0.11*	95.07	-	-
	AGa-I	52.29	*1.29*	0.95	*0.19*	17.26	*0.22*	8.99	*0.50*	0.11	*0.16*	4.57	*0.31*	7.06	*0.33*	3.11	*0.14*	1.08	*0.05*	0.23	*0.10*	95.65	-	-
	AGb-IV	53.05	*1.30*	1.01	*0.20*	16.91	*0.22*	8.79	*0.49*	0.16	*0.16*	4.42	*0.30*	6.73	*0.32*	3.22	*0.14*	1.29	*0.05*	0.35	*0.11*	95.94	-	-
	AGb-V	53.12	*1.30*	0.99	*0.19*	17.37	*0.23*	8.60	*0.48*	0.23	*0.17*	3.62	*0.27*	7.45	*0.34*	2.92	*0.13*	1.20	*0.05*	0.39	*0.12*	95.89	-	-
	AI-I	51.95	*1.28*	0.97	*0.19*	17.44	*0.23*	9.26	*0.50*	0.20	*0.16*	3.61	*0.27*	7.64	*0.34*	2.76	*0.13*	1.04	*0.05*	0.24	*0.11*	95.11	0.63	*0.04*
	AK-I	52.32	*1.29*	0.92	*0.19*	17.52	*0.23*	9.61	*0.51*	0.19	*0.16*	3.97	*0.29*	7.87	*0.34*	2.89	*0.13*	0.92	*0.04*	0.24	*0.11*	96.46	-	-
	AK-II	53.24	*1.30*	1.13	*0.20*	19.77	*0.25*	6.71	*0.43*	0.27	*0.17*	1.57	*0.18*	8.32	*0.36*	3.03	*0.13*	1.15	*0.05*	0.32	*0.10*	95.52	-	-
	B-I	52.20	*1.29*	0.79	*0.18*	17.11	*0.22*	9.30	*0.50*	0.25	*0.17*	3.82	*0.28*	7.51	*0.34*	2.91	*0.13*	1.08	*0.05*	0.34	*0.12*	95.31	-	-
	K-I	52.38	*1.29*	1.06	*0.19*	17.46	*0.23*	9.04	*0.50*	0.22	*0.17*	4.20	*0.29*	7.55	*0.34*	2.97	*0.14*	0.98	*0.05*	0.21	*0.10*	96.06	-	-
	L-I	52.41	*1.29*	0.98	*0.19*	17.54	*0.23*	8.88	*0.49*	0.20	*0.18*	3.50	*0.27*	7.55	*0.34*	3.02	*0.14*	1.06	*0.05*	0.29	*0.10*	95.41	0.65	*0.04*
	S-III	52.65	*1.29*	0.98	*0.19*	17.74	*0.23*	9.09	*0.50*	0.26	*0.18*	3.56	*0.27*	7.57	*0.34*	2.91	*0.13*	1.04	*0.05*	0.31	*0.12*	96.10	-	-
	U-I	53.93	*1.32*	1.03	*0.19*	17.01	*0.22*	8.70	*0.49*	0.26	*0.17*	3.72	*0.28*	7.31	*0.33*	3.13	*0.14*	1.05	*0.05*	0.26	*0.09*	96.40	0.61	*0.04*
	V-I	54.54	*1.34*	0.92	*0.19*	17.22	*0.23*	8.30	*0.49*	0.21	*0.18*	3.05	*0.26*	7.25	*0.34*	3.09	*0.14*	1.18	*0.05*	0.16	*0.11*	95.92	0.77	*0.05*
	Y-I	51.19	*1.27*	0.96	*0.19*	16.95	*0.22*	9.60	*0.51*	0.23	*0.18*	4.88	*0.32*	7.26	*0.33*	3.01	*0.14*	0.99	*0.05*	0.24	*0.10*	95.32	-	-
	Y-II	51.43	*1.27*	0.86	*0.19*	16.74	*0.22*	10.05	*0.52*	0.20	*0.16*	4.71	*0.31*	7.20	*0.33*	2.99	*0.14*	1.01	*0.05*	0.28	*0.11*	95.47	0.65	*0.10*
KSS	AA-I	48.66	*1.22*	1.25	*0.21*	18.48	*0.24*	9.98	*0.52*	0.27	*0.17*	4.18	*0.30*	10.62	*0.40*	2.71	*0.13*	1.04	*0.05*	0.26	*0.11*	97.45	0.56	*0.06*
	AA-II	54.67	*1.33*	1.09	*0.20*	16.11	*0.21*	9.87	*0.52*	0.21	*0.18*	2.97	*0.25*	7.72	*0.34*	3.01	*0.14*	2.08	*0.07*	0.37	*0.12*	98.10	0.74	*0.23*
	AA-III	48.86	*1.23*	1.05	*0.19*	18.86	*0.24*	9.44	*0.51*	0.07	*0.16*	4.10	*0.29*	10.72	*0.40*	2.71	*0.13*	1.02	*0.05*	0.29	*0.10*	97.14	-	-
	AB-I	49.15	*1.23*	0.98	*0.20*	19.79	*0.25*	8.54	*0.48*	0.17	*0.18*	4.20	*0.30*	11.35	*0.42*	2.90	*0.13*	1.08	*0.05*	0.14	*0.10*	98.30	-	-
	D-I	49.31	*1.24*	1.02	*0.20*	17.66	*0.23*	11.85	*0.57*	0.31	*0.19*	3.92	*0.29*	9.14	*0.37*	2.75	*0.13*	1.09	*0.05*	0.31	*0.11*	97.36	0.63	*0.10*
	E-I	60.83	*1.43*	0.94	*0.19*	14.05	*0.19*	9.81	*0.52*	0.20	*0.16*	2.78	*0.24*	6.10	*0.30*	2.94	*0.13*	2.42	*0.07*	0.53	*0.14*	100.61	-	-
	E-II	59.22	*1.40*	0.97	*0.19*	14.34	*0.20*	9.94	*0.52*	0.17	*0.18*	2.71	*0.24*	6.05	*0.30*	3.19	*0.14*	2.45	*0.07*	0.37	*0.13*	99.41	0.44	*0.23*
	G-I	53.50	*1.31*	1.01	*0.19*	15.69	*0.21*	10.37	*0.53*	0.18	*0.16*	3.47	*0.27*	8.34	*0.36*	2.86	*0.13*	1.55	*0.06*	0.33	*0.10*	97.29	0.97	*0.22*
	G-II	55.08	*1.33*	1.18	*0.21*	16.25	*0.21*	9.66	*0.51*	0.17	*0.17*	3.23	*0.26*	7.25	*0.33*	3.08	*0.14*	2.22	*0.07*	0.34	*0.12*	98.47	-	-
	G-III	52.67	*1.29*	1.41	*0.22*	15.68	*0.21*	10.31	*0.53*	0.07	*0.16*	3.20	*0.26*	8.68	*0.36*	2.86	*0.13*	1.46	*0.06*	0.50	*0.12*	96.84	-	-

Table B3. (continued)

Sample ID	Melt ID	SiO_2 (wt. %)	*1 s.d.*	TiO_2	*1 s.d.*	Al_2O_3	*1 s.d.*	FeO^{Total}	*1 s.d.*	MnO	*1 s.d.*	MgO	*1 s.d.*	CaO	*1 s.d.*	Na_2O	*1 s.d.*	K_2O	*1 s.d.*	P_2O_5	*1 s.d.*	Total	S^{6+}/S^{Total}	*1 s.e.*
	H-I	58.01	*1.38*	0.64	*0.17*	14.30	*0.19*	10.85	*0.54*	0.20	*0.17*	2.70	*0.24*	6.55	*0.31*	3.24	*0.14*	1.65	*0.06*	0.24	*0.10*	98.38	-	-
	K-II	47.86	*1.21*	0.97	*0.19*	19.82	*0.25*	9.16	*0.50*	0.10	*0.16*	4.19	*0.29*	10.90	*0.41*	2.67	*0.13*	0.91	*0.04*	0.29	*0.10*	96.86	0.66	*0.07*
	L-I	47.99	*1.21*	0.94	*0.19*	19.45	*0.25*	9.08	*0.50*	0.09	*0.15*	4.31	*0.30*	10.74	*0.40*	2.73	*0.13*	0.94	*0.05*	0.11	*0.09*	96.39	0.62	*0.02*
	W-I	55.04	*1.33*	1.28	*0.21*	15.66	*0.21*	10.22	*0.53*	0.23	*0.17*	3.16	*0.26*	6.75	*0.32*	3.23	*0.14*	2.07	*0.07*	0.49	*0.13*	98.13	-	-
KROHTH	A-I	56.48	*1.36*	1.16	*0.20*	17.03	*0.22*	8.39	*0.48*	0.22	*0.16*	2.30	*0.22*	7.82	*0.34*	3.06	*0.14*	1.00	*0.05*	0.29	*0.10*	97.76	0.51	*0.23*
	A-II	56.63	*1.36*	1.06	*0.20*	17.40	*0.23*	8.92	*0.49*	0.15	*0.17*	2.42	*0.22*	8.10	*0.35*	3.06	*0.14*	0.96	*0.05*	0.08	*0.10*	98.77	-	-
	E-I	55.08	*1.12*	1.09	*0.13*	16.37	*0.18*	9.30	*0.34*	0.14	*0.11*	3.36	*0.19*	7.83	*0.24*	2.87	*0.09*	0.96	*0.03*	0.19	*0.06*	97.19	0.94	*0.25*
	E-II	55.34	*1.34*	1.13	*0.20*	16.53	*0.22*	8.89	*0.50*	0.09	*0.16*	3.25	*0.26*	7.70	*0.34*	2.93	*0.14*	0.96	*0.05*	0.23	*0.09*	97.04	-	-
	E-III	55.12	*1.34*	0.81	*0.19*	16.47	*0.22*	9.15	*0.50*	0.23	*0.18*	3.42	*0.26*	7.72	*0.34*	3.01	*0.14*	1.05	*0.05*	0.15	*0.10*	97.14	-	-
	F-I	54.42	*1.33*	0.98	*0.19*	16.43	*0.22*	9.72	*0.51*	0.21	*0.17*	4.03	*0.29*	7.58	*0.34*	2.97	*0.14*	1.01	*0.05*	0.05	*0.11*	97.40	0.52	*0.29*
	G-I	55.47	*1.34*	0.98	*0.20*	16.59	*0.22*	9.39	*0.51*	0.16	*0.16*	3.31	*0.26*	7.74	*0.34*	2.90	*0.14*	1.02	*0.05*	0.20	*0.11*	97.74	-	-
	H-I	55.09	*1.34*	1.01	*0.20*	16.46	*0.22*	8.89	*0.49*	0.25	*0.18*	3.22	*0.26*	7.63	*0.34*	3.21	*0.14*	0.94	*0.05*	0.15	*0.10*	96.84	0.83	*0.25*
	I-I	55.58	*1.36*	1.00	*0.19*	16.21	*0.22*	8.94	*0.50*	0.31	*0.18*	3.48	*0.27*	7.59	*0.35*	2.79	*0.14*	1.03	*0.05*	0.21	*0.10*	97.14	-	-
	K-I	56.56	*1.36*	1.10	*0.20*	15.75	*0.21*	8.72	*0.49*	0.11	*0.16*	3.77	*0.28*	7.04	*0.33*	3.12	*0.14*	1.00	*0.05*	0.18	*0.10*	97.35	-	-
	L-II	54.91	*1.35*	1.03	*0.20*	16.20	*0.22*	9.30	*0.51*	0.14	*0.16*	3.56	*0.28*	8.01	*0.35*	3.03	*0.14*	0.92	*0.05*	0.19	*0.10*	97.29	0.58	*0.25*
KRSM11	A-I	53.96	*1.33*	0.71	*0.18*	17.05	*0.22*	8.07	*0.48*	0.15	*0.17*	3.80	*0.28*	7.29	*0.34*	2.81	*0.13*	1.15	*0.05*	0.14	*0.09*	95.13	0.93	*0.06*
	A-II	53.73	*1.33*	0.86	*0.18*	17.29	*0.23*	8.47	*0.49*	0.28	*0.17*	3.53	*0.27*	7.42	*0.34*	2.71	*0.13*	1.13	*0.05*	0.21	*0.10*	95.64	-	-
	A-III	53.72	*1.33*	0.78	*0.18*	17.25	*0.23*	7.83	*0.47*	0.17	*0.16*	3.32	*0.27*	7.92	*0.35*	2.85	*0.13*	1.05	*0.05*	0.23	*0.11*	95.11	-	-
	B-I	53.83	*1.33*	0.87	*0.19*	17.11	*0.23*	7.93	*0.48*	0.09	*0.17*	3.27	*0.26*	7.52	*0.35*	2.65	*0.13*	1.13	*0.05*	0.13	*0.09*	94.52	-	-
	C-I	54.65	*1.35*	0.79	*0.19*	17.53	*0.23*	7.57	*0.46*	0.28	*0.17*	2.98	*0.25*	7.63	*0.35*	2.75	*0.13*	1.28	*0.05*	0.16	*0.09*	95.61	0.88	*0.12*
	D-I	52.41	*1.31*	0.90	*0.19*	18.32	*0.24*	8.39	*0.49*	0.23	*0.17*	3.27	*0.27*	8.75	*0.37*	2.75	*0.13*	0.87	*0.05*	0.16	*0.09*	96.05	0.55	*0.10*
	D-II	55.02	*1.35*	0.77	*0.18*	18.12	*0.23*	7.99	*0.48*	0.12	*0.16*	2.83	*0.24*	8.14	*0.36*	2.70	*0.13*	1.13	*0.05*	0.12	*0.08*	96.93	-	-
	E-I	53.52	*1.33*	0.91	*0.19*	17.25	*0.23*	8.16	*0.48*	0.13	*0.18*	3.26	*0.26*	7.84	*0.35*	2.75	*0.13*	1.04	*0.05*	0.11	*0.10*	94.96	-	-
	E-II	52.79	*1.29*	0.89	*0.19*	17.69	*0.23*	8.00	*0.47*	0.21	*0.18*	3.02	*0.25*	8.53	*0.36*	2.71	*0.13*	0.87	*0.04*	0.18	*0.09*	94.88	0.84	*0.02*
	G-I	54.05	*1.32*	0.82	*0.17*	17.52	*0.23*	7.84	*0.46*	0.10	*0.14*	3.10	*0.25*	7.80	*0.34*	2.77	*0.13*	1.04	*0.05*	0.15	*0.08*	95.19	0.68	*0.19*
	H-I	53.56	*1.31*	0.83	*0.19*	17.57	*0.23*	8.02	*0.47*	0.31	*0.18*	3.35	*0.26*	7.89	*0.35*	2.76	*0.13*	1.12	*0.05*	0.09	*0.10*	95.50	-	-
	K-V	53.17	*1.32*	0.86	*0.19*	18.29	*0.24*	8.22	*0.48*	0.27	*0.17*	2.99	*0.25*	8.40	*0.36*	2.44	*0.13*	0.96	*0.05*	0.17	*0.08*	95.78	-	-
	L-I	53.55	*1.31*	0.72	*0.17*	17.10	*0.22*	8.40	*0.48*	0.21	*0.17*	3.54	*0.27*	7.78	*0.34*	2.66	*0.13*	1.05	*0.05*	0.13	*0.10*	95.14	-	-
	L-II	51.26	*1.27*	0.71	*0.18*	16.13	*0.21*	8.11	*0.47*	0.19	*0.17*	3.40	*0.26*	7.24	*0.33*	2.70	*0.13*	0.97	*0.05*	0.16	*0.10*	90.86	-	-
	L-III	53.37	*1.31*	0.82	*0.18*	17.00	*0.22*	8.12	*0.47*	0.13	*0.16*	3.65	*0.27*	7.95	*0.35*	2.60	*0.13*	0.99	*0.05*	0.05	*0.11*	94.67	-	-

Table B3. (continued)

Sample ID	Melt ID	SiO_2 (wt. %)	*1 s.d.*	TiO_2	*1 s.d.*	Al_2O_3	*1 s.d.*	FeO^{Total}	*1 s.d.*	MnO	*1 s.d.*	MgO	*1 s.d.*	CaO	*1 s.d.*	Na_2O	*1 s.d.*	K_2O	*1 s.d.*	P_2O_5	*1 s.d.*	Total	S^{6+}/S^{Total}	*1 s.e.*
	L-IV	53.27	*1.30*	0.81	*0.19*	17.31	*0.22*	8.62	*0.49*	0.13	*0.18*	3.25	*0.26*	7.70	*0.34*	2.71	*0.13*	1.16	*0.05*	0.13	*0.09*	95.09	-	-
SM1S	AA-I	46.23	*1.18*	1.14	*0.20*	19.36	*0.25*	11.82	*0.56*	0.21	*0.18*	4.03	*0.29*	14.00	*0.46*	2.14	*0.12*	0.37	*0.03*	0.11	*0.09*	99.40	0.93	*0.07*
	AE-I	49.67	*1.24*	1.24	*0.21*	19.80	*0.25*	10.09	*0.52*	0.26	*0.18*	4.20	*0.30*	10.50	*0.40*	3.44	*0.15*	0.68	*0.04*	0.27	*0.11*	100.15	0.31	*0.07*
	AJ-I	46.34	*1.19*	1.29	*0.22*	20.35	*0.26*	12.13	*0.57*	0.09	*0.17*	3.65	*0.28*	12.03	*0.43*	3.10	*0.14*	0.19	*0.03*	0.15	*0.11*	99.32	0.51	*0.03*
	AL-II	45.83	*1.18*	0.86	*0.19*	19.39	*0.25*	12.02	*0.57*	0.23	*0.18*	6.02	*0.36*	11.79	*0.42*	2.24	*0.12*	0.94	*0.05*	0.11	*0.10*	99.42	-	-
	AM-II	47.36	*1.20*	1.33	*0.21*	19.20	*0.24*	13.83	*0.61*	0.29	*0.18*	3.80	*0.29*	12.20	*0.43*	3.18	*0.14*	0.21	*0.03*	0.20	*0.11*	101.61	-	-
	AR-VI	45.32	*1.17*	1.09	*0.20*	19.39	*0.25*	13.91	*0.62*	0.31	*0.19*	5.67	*0.35*	11.86	*0.42*	1.83	*0.11*	0.56	*0.04*	0.20	*0.10*	100.14	-	-
	BA-I	46.21	*1.18*	1.38	*0.21*	19.87	*0.25*	12.60	*0.58*	0.20	*0.16*	4.86	*0.32*	12.82	*0.44*	2.47	*0.12*	0.43	*0.03*	0.13	*0.10*	100.98	-	-
	BC-I	45.74	*1.18*	1.25	*0.21*	21.68	*0.27*	11.10	*0.55*	0.10	*0.17*	4.91	*0.32*	12.98	*0.45*	2.29	*0.12*	0.39	*0.03*	0.09	*0.08*	100.54	0.03	*0.05*
	S-II	47.20	*1.22*	1.26	*0.21*	19.28	*0.25*	14.36	*0.64*	0.12	*0.18*	4.33	*0.31*	9.52	*0.39*	3.77	*0.16*	0.19	*0.03*	0.15	*0.09*	100.18	0.52	*0.09*
	S-III	46.46	*1.20*	1.04	*0.20*	18.47	*0.24*	13.87	*0.63*	0.26	*0.17*	4.81	*0.33*	11.48	*0.43*	2.45	*0.13*	1.20	*0.05*	0.25	*0.11*	100.28	-	-
	T-II	44.85	*1.18*	1.26	*0.21*	21.21	*0.27*	11.93	*0.58*	0.20	*0.18*	4.82	*0.33*	13.51	*0.46*	2.39	*0.13*	0.41	*0.03*	0.12	*0.08*	100.70	0.23	*0.12*
	Y-I	47.30	*1.20*	1.08	*0.20*	20.27	*0.25*	11.01	*0.54*	0.21	*0.17*	5.44	*0.34*	12.41	*0.43*	2.16	*0.12*	0.68	*0.04*	0.01	*0.09*	100.56	-	-
	Y-IV	46.54	*1.19*	1.08	*0.20*	20.97	*0.26*	11.23	*0.55*	0.22	*0.17*	5.36	*0.34*	13.01	*0.45*	2.29	*0.12*	0.41	*0.03*	0.12	*0.10*	101.24	-	-
	Z-I	47.11	*1.20*	1.19	*0.20*	18.27	*0.24*	10.53	*0.53*	0.20	*0.18*	6.38	*0.37*	12.37	*0.43*	2.07	*0.11*	0.76	*0.04*	0.13	*0.10*	99.01	-	-
KM1S12a	A-I	52.11	*1.28*	1.19	*0.20*	18.08	*0.23*	8.68	*0.49*	0.17	*0.17*	2.76	*0.24*	8.34	*0.36*	2.78	*0.13*	0.65	*0.04*	0.36	*0.11*	95.12	-	-
	AE-I	50.73	*1.26*	1.02	*0.19*	17.60	*0.23*	9.93	*0.52*	0.18	*0.15*	3.49	*0.27*	8.88	*0.37*	2.43	*0.12*	0.44	*0.03*	0.18	*0.10*	94.88	0.32	*0.12*
	AE-II	51.31	*1.27*	1.20	*0.21*	18.77	*0.24*	9.18	*0.50*	0.22	*0.16*	2.48	*0.23*	8.80	*0.36*	2.39	*0.12*	0.63	*0.04*	0.16	*0.09*	95.14	-	-
	AE-III	50.47	*1.26*	0.94	*0.19*	18.49	*0.24*	9.21	*0.50*	0.15	*0.18*	3.26	*0.26*	9.33	*0.38*	2.58	*0.13*	0.44	*0.03*	0.11	*0.09*	94.99	-	-
	AF-I	51.30	*1.27*	1.16	*0.20*	18.75	*0.24*	8.06	*0.47*	0.24	*0.19*	2.25	*0.21*	9.24	*0.37*	2.61	*0.13*	0.68	*0.04*	0.57	*0.14*	94.86	-	-
	AH-II	53.01	*1.30*	1.10	*0.20*	18.79	*0.24*	7.35	*0.45*	0.08	*0.16*	1.80	*0.20*	8.89	*0.37*	3.04	*0.14*	0.70	*0.04*	0.21	*0.11*	94.97	0.76	*0.10*
	AJ-I	52.00	*1.28*	1.22	*0.21*	17.13	*0.22*	9.30	*0.50*	0.35	*0.18*	3.29	*0.26*	8.12	*0.35*	2.25	*0.12*	0.67	*0.04*	0.32	*0.10*	94.65	0.32	*0.12*
	J-I	49.93	*1.25*	1.11	*0.20*	17.70	*0.23*	9.38	*0.50*	0.27	*0.17*	4.72	*0.31*	8.50	*0.36*	2.53	*0.12*	0.50	*0.04*	0.11	*0.10*	94.74	0.72	*0.03*
	J-II	49.77	*1.25*	1.18	*0.20*	17.68	*0.23*	9.72	*0.51*	0.15	*0.16*	4.12	*0.29*	8.60	*0.36*	2.53	*0.13*	0.47	*0.03*	0.15	*0.09*	94.36	0.78	*0.19*
	K-II	52.60	*1.29*	1.07	*0.20*	18.62	*0.24*	8.39	*0.48*	0.16	*0.17*	2.05	*0.20*	8.93	*0.37*	2.89	*0.13*	0.70	*0.04*	0.41	*0.12*	95.83	-	-
	O-I	54.79	*1.33*	1.05	*0.20*	17.85	*0.23*	8.08	*0.47*	0.20	*0.16*	2.02	*0.21*	7.60	*0.34*	3.48	*0.15*	0.79	*0.04*	0.18	*0.11*	96.03	-	-
	Q-I	51.58	*1.28*	0.75	*0.18*	18.46	*0.24*	8.49	*0.48*	0.09	*0.17*	2.36	*0.22*	9.80	*0.39*	2.57	*0.13*	0.52	*0.04*	0.11	*0.09*	94.73	-	-
	U-VI	52.12	*1.28*	1.18	*0.21*	18.87	*0.24*	7.32	*0.45*	0.17	*0.18*	1.97	*0.20*	8.99	*0.37*	2.93	*0.13*	0.61	*0.04*	0.32	*0.11*	94.47	-	-
	Z-I	54.11	*1.32*	1.10	*0.20*	18.59	*0.24*	7.42	*0.45*	0.24	*0.16*	1.92	*0.20*	8.70	*0.36*	3.16	*0.14*	0.77	*0.04*	0.26	*0.11*	96.26	0.85	-
	Z-II	55.88	*1.35*	0.91	*0.19*	19.12	*0.24*	6.53	*0.42*	0.17	*0.16*	1.48	*0.18*	7.71	*0.34*	2.96	*0.13*	0.91	*0.05*	0.33	*0.12*	96.00	-	-

Table B3. (continued)

Sample ID	Melt ID	SiO_2 (wt. %)	*1 s.d.*	TiO_2	*1 s.d.*	Al_2O_3	*1 s.d.*	FeO^{Total}	*1 s.d.*	MnO	*1 s.d.*	MgO	*1 s.d.*	CaO	*1 s.d.*	Na_2O	*1 s.d.*	K_2O	*1 s.d.*	P_2O_5	*1 s.d.*	Total	S^{6+}/S^{Total}	*1 s.e.*
FKONON	A-I	48.52	*1.22*	1.97	*0.25*	18.93	*0.24*	8.49	*0.48*	0.17	*0.17*	4.93	*0.32*	10.75	*0.40*	2.97	*0.13*	0.97	*0.05*	0.28	*0.11*	97.98	0.37	*0.13*
	B-I	49.66	*1.24*	1.82	*0.25*	19.15	*0.24*	8.70	*0.49*	0.15	*0.17*	4.49	*0.31*	10.38	*0.40*	3.36	*0.14*	1.04	*0.05*	0.32	*0.12*	99.07	-	-
	D-I	48.76	*1.23*	1.68	*0.24*	18.76	*0.24*	9.09	*0.50*	0.14	*0.17*	4.92	*0.32*	10.34	*0.40*	3.17	*0.14*	1.05	*0.05*	0.42	*0.12*	98.33	-	-
	D-II	49.32	*1.24*	1.80	*0.24*	18.25	*0.24*	10.76	*0.54*	0.15	*0.18*	4.12	*0.30*	8.47	*0.36*	4.09	*0.16*	1.55	*0.06*	0.35	*0.14*	98.86	0.39	*0.19*
	F-I	48.93	*1.23*	1.95	*0.25*	19.22	*0.24*	9.03	*0.50*	0.21	*0.19*	4.27	*0.30*	10.95	*0.41*	3.18	*0.14*	1.05	*0.05*	0.24	*0.11*	99.03	-	-
	I-I	48.81	*1.23*	1.74	*0.24*	19.12	*0.24*	9.40	*0.50*	0.19	*0.16*	5.05	*0.33*	10.62	*0.40*	3.19	*0.14*	1.00	*0.05*	0.20	*0.11*	99.33	0.50	*0.11*
	K-I	48.08	*1.22*	1.83	*0.25*	19.12	*0.24*	8.91	*0.49*	0.23	*0.17*	5.31	*0.34*	10.49	*0.40*	3.01	*0.14*	1.04	*0.05*	0.44	*0.13*	98.45	-	-
	K-II	48.94	*1.23*	1.79	*0.24*	18.85	*0.24*	8.94	*0.49*	0.07	*0.17*	5.28	*0.33*	10.45	*0.40*	3.07	*0.14*	1.01	*0.05*	0.41	*0.12*	98.82	0.38	*0.05*
	N-I	48.76	*1.23*	1.82	*0.24*	19.14	*0.24*	9.06	*0.50*	0.11	*0.16*	4.95	*0.32*	10.25	*0.40*	3.24	*0.14*	1.13	*0.05*	0.45	*0.13*	98.91	-	-
	N-II	48.51	*1.22*	2.04	*0.26*	19.75	*0.25*	8.66	*0.48*	0.20	*0.18*	3.93	*0.29*	10.00	*0.39*	3.44	*0.15*	1.27	*0.05*	0.35	*0.11*	98.16	-	-
	O-I	47.95	*1.21*	1.82	*0.25*	19.35	*0.25*	8.57	*0.48*	0.23	*0.17*	5.17	*0.33*	10.63	*0.40*	3.29	*0.14*	1.12	*0.05*	0.32	*0.13*	98.44	0.47	*0.04*
	O-II	48.35	*1.22*	1.88	*0.25*	18.76	*0.24*	8.99	*0.50*	0.16	*0.16*	5.21	*0.33*	10.46	*0.40*	3.00	*0.14*	1.03	*0.05*	0.25	*0.11*	98.10	-	-
	P-II	49.04	*1.23*	1.83	*0.24*	19.01	*0.24*	9.19	*0.50*	0.13	*0.15*	5.10	*0.33*	10.43	*0.40*	3.30	*0.14*	0.98	*0.05*	0.39	*0.12*	99.40	-	-

Table B4. Volatile and P_2O_5 concentrations uncorrected for post-entrapment modification and S isotope compositions of olivine-hosted melt inclusions

Volcano	Sample ID	Melt ID	H_2O wt%	*2 s.e.*	CO_2 ppm	*2 s.e.*	S ppm	*2 s.e.*	Cl ppm	*2 s.e.*	F ppm	*2 s.e.*	P_2O_5 wt%	*2 s.e.*	$\delta^{34}S_{V\text{-}CDT}$ ‰	*2 s.e.*	SIMS lab*
Oninomi	ON2S	AP-IV†	-	-	-	-	1884	*128*	705	*85*	999	*114*	-	-	1.60	*0.79*	1
		BEc-III†	-	-	-	-	1694	*33*	690	*55*	1026	*278*	-	-	1.65	*0.79*	1
		CSa-III	0.34	*0.0007*	13	*1*	2783	*31*	627	*3*	1021	*3*	0.70	*0.0026*	-0.32	*0.79*	1
		DF-IV†	-	-	-	-	2289	*119*	649	*64*	820	*187*	-	-	0.77	*0.97*	1
		DL-I†	-	-	-	-	1462	*86*	238	*73*	1029	*168*	-	-	1.56	*0.79*	1
		DZ-I†	-	-	-	-	584	*90*	90	*55*	781	*355*	-	-	3.63	*1.16*	1
		U-I	0.28	*0.0015*	1	*0*	159	*1*	1339	*5*	1308	*7*	0.96	*0.0052*	0.70	*1.88*	2
		Z-I	0.42	*0.0012*	117	*1*	2078	*15*	783	*2*	1160	*3*	0.80	*0.0042*	1.45	*0.79*	1
Yufu	YF1L	AFa-III	0.01	*0.0004*	2	*0*	2658	*17*	782	*3*	622	*2*	0.20	*0.0008*	6.60	*1.13*	1
		AFb-I	0.03	*0.0004*	2	*0*	757	*7*	401	*4*	552	*2*	0.15	*0.0015*	6.52	*1.13*	1
		AH-I	0.55	*0.0032*	58	*2*	2894	*44*	1407	*5*	521	*2*	0.17	*0.0020*	6.76	*1.13*	1
		AZ-III	0.07	*0.0008*	59	*1*	2714	*154*	1250	*8*	514	*5*	0.20	*0.0017*	6.10	*1.13*	1
		BD-I	0.22	*0.0014*	129	*2*	2934	*242*	1272	*5*	446	*3*	0.15	*0.0009*	5.18	*1.13*	1
		BK-II	0.17	*0.0025*	91	*1*	3743	*158*	1255	*12*	511	*4*	0.19	*0.0014*	5.09	*1.13*	1
		BLa-II	0.06	*0.0010*	30	*1*	3364	*56*	1228	*5*	603	*3*	0.20	*0.0015*	3.39	*1.13*	1
		BLa-III	0.05	*0.0003*	2	*0*	3866	*115*	1202	*7*	642	*2*	0.20	*0.0012*	4.91	*1.13*	1
		BM-I	0.39	*0.0020*	185	*2*	3263	*112*	1437	*7*	488	*2*	0.18	*0.0009*	5.72	*0.79*	1
		BO-I	0.13	*0.0010*	49	*0*	3432	*81*	1206	*3*	602	*2*	0.21	*0.0015*	5.26	*0.79*	1
		BQ-I	0.20	*0.0013*	2	*0*	227	*2*	667	*3*	509	*2*	0.19	*0.0016*	-	-	-
		BQ-III	0.02	*0.0003*	44	*1*	3487	*51*	1212	*4*	594	*3*	0.20	*0.0014*	4.73	*0.79*	1
		BSc-II	0.08	*0.0008*	56	*1*	3328	*65*	1180	*6*	588	*3*	0.20	*0.0015*	6.25	*0.79*	1
		F-I	0.20	*0.0043*	113	*2*	3079	*100*	1242	*29*	459	*9*	0.18	*0.0020*	4.60	*1.13*	1
		F-II	0.27	*0.0017*	190	*2*	3573	*158*	1242	*6*	511	*2*	0.20	*0.0007*	-	-	-
Kuju	KJ5S	AD-V	4.48	*0.0221*	227	*2*	2807	*13*	1026	*5*	510	*3*	0.30	*0.0016*	8.01	*0.47*	2
		AE-I	4.62	*0.0198*	203	*3*	2547	*15*	1053	*7*	516	*3*	0.31	*0.0038*	6.31	*1.02*	1
		AE-II	4.64	*0.0285*	307	*4*	2807	*19*	1000	*7*	485	*4*	0.29	*0.0032*	5.49	*1.02*	1

Table B4. (continued)

Volcano	Sample ID	Melt ID	H_2O wt%	*2 s.e.*	CO_2 ppm	*2 s.e.*	S ppm	*2 s.e.*	Cl ppm	*2 s.e.*	F ppm	*2 s.e.*	P_2O_5 wt%	*2 s.e.*	$\delta^{34}S_{V\text{-}CDT}$ ‰	*2 s.e.*	SIMS lab*
		AF-I	4.57	*0.0219*	340	*4*	2810	*14*	1032	*7*	504	*3*	0.31	*0.0024*	6.56	*1.02*	1
		AGa-I	4.57	*0.0229*	339	*2*	2799	*15*	1036	*5*	504	*4*	0.31	*0.0036*	7.66	*1.14*	1
		AGb-IV	4.51	*0.0323*	293	*2*	2433	*17*	1053	*8*	520	*4*	0.32	*0.0021*	7.63	*1.14*	1
		AGb-V	4.51	*0.0266*	350	*2*	2914	*13*	1109	*7*	525	*3*	0.31	*0.0030*	7.65	*1.14*	1
		AI-I	4.53	*0.0210*	261	*2*	3182	*16*	1081	*5*	510	*4*	0.30	*0.0024*	7.19	*1.14*	1
		AK-I	4.66	*0.0230*	377	*2*	3063	*13*	1096	*5*	538	*2*	0.30	*0.0021*	7.59	*1.14*	1
		AK-II†	-	-	-	-	2772	*73*	1101	*57*	552	*161*	-	-	7.44	*1.14*	1
		B-I	4.75	*0.0185*	274	*2*	2899	*13*	1096	*5*	518	*2*	0.30	*0.0018*	6.87	*0.50*	2
		K-I	4.72	*0.0147*	276	*2*	2831	*8*	1031	*5*	492	*2*	0.30	*0.0026*	6.90	*0.48*	2
		L-I	4.70	*0.0125*	421	*3*	2979	*10*	1117	*4*	531	*3*	0.31	*0.0017*	6.55	*0.53*	2
		S-III	4.63	*0.0242*	318	*2*	3047	*14*	1099	*5*	516	*2*	0.31	*0.0029*	4.90	*0.48*	2
		U-I	4.54	*0.0146*	373	*3*	2483	*5*	1108	*4*	517	*2*	0.31	*0.0024*	6.49	*0.48*	2
		V-I	4.42	*0.0208*	118	*1*	2248	*9*	1098	*3*	495	*3*	0.31	*0.0015*	7.46	*0.54*	2
		Y-I	4.43	*0.0277*	171	*3*	2601	*16*	973	*6*	475	*3*	0.30	*0.0032*	7.76	*0.45*	2
		Y-II	4.65	*0.0153*	225	*2*	2657	*10*	1020	*3*	500	*2*	0.30	*0.0020*	7.21	*0.58*	2
Aso	KSS	AA-I	2.90	*0.0119*	93	*1*	2825	*9*	717	*3*	393	*2*	0.24	*0.0023*	7.21	*0.62*	2
		AA-II	2.30	*0.0142*	64	*1*	1249	*6*	792	*4*	648	*3*	0.37	*0.0031*	7.48	*1.21*	1
		AA-III	2.89	*0.0136*	75	*1*	2704	*12*	753	*4*	390	*1*	0.24	*0.0020*	6.93	*0.54*	2
		AB-I	2.50	*0.0103*	193	*2*	2838	*13*	744	*3*	360	*2*	0.23	*0.0016*	6.47	*0.54*	2
		D-I	2.98	*0.0087*	124	*2*	2795	*5*	766	*4*	594	*2*	0.25	*0.0021*	7.65	*0.50*	2
		E-I†	-	-	-	-	887	*72*	745	*32*	792	*303*	-	-	4.40	*0.78*	2
		E-II	2.61	*0.0114*	233	*2*	1005	*7*	895	*3*	923	*4*	0.51	*0.0029*	5.71	*0.64*	2
		G-I	2.69	*0.0211*	109	*2*	701	*5*	536	*5*	589	*4*	0.36	*0.0038*	6.85	*0.82*	2
		G-II	2.63	*0.0220*	46	*1*	1272	*11*	846	*5*	652	*2*	0.35	*0.0027*	8.07	*0.68*	2
		H-I	2.48	*0.0093*	378	*2*	1139	*8*	1094	*6*	890	*3*	0.36	*0.0026*	7.81	*0.81*	2
		K-II	3.07	*0.0113*	246	*3*	2996	*14*	747	*4*	370	*2*	0.23	*0.0026*	6.34	*0.55*	2
		L-I	3.15	*0.0167*	205	*2*	2840	*13*	731	*5*	360	*2*	0.23	*0.0018*	7.26	*0.49*	2
		S-I	1.89	*0.0325*	142	*23*	3203	*42*	929	*12*	505	*6*	0.28	*0.0024*	-	-	-
		W-I	2.25	*0.0131*	44	*1*	990	*4*	845	*3*	646	*3*	0.37	*0.0019*	6.56	*0.81*	2

Table B4. (continued)

Volcano	Sample ID	Melt ID	H_2O wt%	*2 s.e.*	CO_2 ppm	*2 s.e.*	S ppm	*2 s.e.*	Cl ppm	*2 s.e.*	F ppm	*2 s.e.*	P_2O_5 wt%	*2 s.e.*	$\delta^{34}S_{V\text{-}CDT}$ ‰	*2 s.e.*	SIMS lab*
Kirishima	KROHTH	A-I	3.38	*0.0111*	61	*0*	838	*5*	804	*4*	345	*2*	0.18	*0.0020*	5.34	*0.80*	2
		A-II	3.52	*0.0183*	90	*1*	893	*2*	803	*4*	362	*2*	0.19	*0.0012*	8.07	*0.47*	2
		C-I	3.20	*0.0811*	83	*2*	845	*12*	740	*18*	320	*6*	0.18	*0.0018*	9.24	*2.88*	2
		E-I	3.60	*0.0090*	88	*1*	816	*3*	795	*4*	345	*1*	0.18	*0.0010*	8.09	*0.68*	2
		E-II	3.54	*0.0118*	80	*1*	652	*2*	791	*3*	341	*2*	0.18	*0.0013*	7.16	*0.55*	2
		E-III	2.90	*0.0088*	63	*1*	831	*3*	761	*2*	331	*1*	0.17	*0.0015*	8.38	*0.39*	2
		F-I	3.53	*0.0127*	60	*1*	864	*4*	772	*4*	338	*2*	0.17	*0.0019*	7.93	*0.70*	2
		G-I	3.52	*0.0303*	109	*1*	823	*4*	775	*5*	347	*3*	0.18	*0.0015*	7.33	*0.67*	2
		H-I	3.46	*0.0123*	54	*1*	713	*2*	781	*3*	335	*1*	0.18	*0.0012*	9.31	*0.99*	2
		I-I	3.51	*0.0146*	77	*2*	829	*3*	767	*3*	343	*2*	0.17	*0.0013*	7.85	*0.69*	2
		K-I	3.26	*0.0126*	4	*0*	272	*2*	761	*3*	312	*1*	0.20	*0.0012*	7.24	*0.97*	2
		L-II	3.49	*0.0215*	49	*1*	782	*4*	757	*5*	346	*2*	0.19	*0.0017*	8.33	*0.70*	2
	KRSM11	A-I	4.56	*0.0126*	262	*1*	1826	*7*	767	*3*	391	*2*	0.16	*0.0012*	8.83	*0.55*	2
		A-II	4.54	*0.0229*	259	*1*	1825	*10*	779	*5*	405	*3*	0.15	*0.0013*	8.34	*0.50*	2
		A-III	4.46	*0.0242*	282	*1*	1876	*7*	765	*4*	389	*2*	0.16	*0.0015*	8.53	*0.46*	2
		B-I	4.57	*0.0237*	308	*2*	1881	*7*	760	*4*	377	*2*	0.15	*0.0012*	8.39	*0.56*	2
		C-I	4.45	*0.0176*	243	*3*	1816	*5*	790	*3*	413	*1*	0.16	*0.0011*	8.48	*0.42*	2
		D-I	4.56	*0.0199*	204	*1*	1963	*9*	716	*3*	337	*2*	0.15	*0.0013*	8.33	*0.48*	2
		D-II	4.30	*0.0180*	238	*2*	1881	*6*	799	*4*	414	*2*	0.16	*0.0015*	8.20	*0.48*	2
		E-I	4.64	*0.0210*	323	*3*	1894	*9*	767	*6*	382	*2*	0.15	*0.0012*	8.33	*0.48*	2
		E-II	4.69	*0.0127*	332	*4*	2001	*7*	731	*3*	343	*1*	0.15	*0.0015*	9.43	*0.47*	2
		G-I	4.54	*0.0212*	377	*2*	1979	*9*	759	*5*	371	*2*	0.15	*0.0012*	7.92	*0.50*	2
		H-I	4.34	*0.0161*	209	*2*	1865	*7*	749	*4*	368	*2*	0.15	*0.0013*	8.64	*0.50*	2
		K-III	4.40	*0.0154*	130	*9*	1894	*8*	721	*4*	335	*1*	0.15	*0.0015*	8.15	*0.57*	2
		K-V	4.44	*0.0158*	259	*2*	1939	*10*	730	*3*	346	*2*	0.15	*0.0017*	9.11	*0.40*	2
		L-I	4.45	*0.0221*	201	*7*	1862	*8*	747	*4*	378	*2*	0.15	*0.0017*	8.43	*0.43*	2
		L-III	4.48	*0.0163*	220	*1*	1844	*7*	740	*4*	370	*2*	0.15	*0.0011*	-	-	-
		L-IV	4.63	*0.0220*	284	*2*	1862	*7*	785	*3*	409	*3*	0.16	*0.0015*	9.23	*0.42*	2
Sumiyoshiike	SM1S	AA-I	1.03	*0.0062*	441	*40*	2843	*62*	743	*6*	259	*2*	0.14	*0.0017*	6.42	*1.02*	1

Table B4. (continued)

Volcano	Sample ID	Melt ID	H_2O wt%	*2 s.e.*	CO_2 ppm	*2 s.e.*	S ppm	*2 s.e.*	Cl ppm	*2 s.e.*	F ppm	*2 s.e.*	P_2O_5 wt%	*2 s.e.*	$\delta^{34}S_{V\text{-}CDT}$ ‰	*2 s.e.*	SIMS lab*
		AE-I	0.85	*0.0070*	99	*2*	2124	*46*	755	*11*	241	*2*	0.26	*0.0022*	6.88	*0.79*	1
		AJ-I	0.61	*0.0059*	760	*28*	3342	*57*	617	*3*	145	*1*	0.15	*0.0009*	6.36	*0.79*	1
		AL-II	1.22	*0.0054*	339	*3*	2523	*33*	497	*3*	273	*2*	0.13	*0.0016*	6.30	*1.02*	1
		AM-II†	-	-	-	-	2853	*78*	354	*58*	58	*72*	-	-	1.54	*1.34*	1
		AR-VI†	-	-	-	-	2150	*53*	464	*30*	66	*81*	-	-	6.19	*1.02*	1
		BA-I	0.44	*0.0015*	267	*2*	2892	*7*	555	*3*	336	*1*	0.15	*0.0008*	5.58	*1.02*	1
		BC-I	0.24	*0.0017*	309	*3*	1940	*13*	539	*4*	273	*2*	0.14	*0.0014*	5.76	*1.02*	1
		S-II	1.36	*0.0128*	134	*13*	3648	*92*	677	*6*	353	*3*	0.18	*0.0016*	3.65	*0.55*	2
		T-II	0.26	*0.0018*	271	*1*	2684	*7*	550	*3*	300	*1*	0.14	*0.0015*	4.87	*0.48*	2
		Y-I†	-	-	-	-	3601	*36*	424	*28*	-	-	-	-	5.93	*1.02*	1
		Y-IV	0.37	*0.0020*	540	*16*	2658	*37*	483	*2*	255	*1*	0.13	*0.0014*	-	-	-
Kaimondake	KM1S12a	A-I	5.52	*0.0319*	192	*9*	2271	*32*	1049	*7*	627	*6*	0.24	*0.0019*	6.66	*1.21*	1
		AE-I	4.90	*0.0167*	495	*13*	2779	*22*	850	*5*	531	*5*	0.20	*0.0023*	6.32	*0.79*	1
		AE-III	5.16	*0.0264*	342	*6*	2686	*24*	898	*9*	617	*4*	0.22	*0.0020*	7.06	*0.79*	1
		AF-I	5.53	*0.0631*	120	*2*	1771	*12*	910	*8*	527	*2*	0.57	*0.0034*	6.85	*0.79*	1
		AH-II	4.77	*0.0200*	226	*5*	1473	*9*	1029	*7*	590	*4*	0.27	*0.0020*	7.75	*0.81*	1
		AJ-I	6.05	*0.0257*	146	*5*	2181	*15*	1009	*5*	635	*4*	0.25	*0.0014*	7.77	*0.79*	1
		J-I	6.06	*0.0248*	556	*2*	2326	*8*	938	*2*	557	*2*	0.24	*0.0019*	7.07	*0.57*	2
		J-II	5.17	*0.0391*	-	-	2205	*8*	784	*5*	516	*4*	0.24	*0.0023*	8.73	*0.53*	2
		K-II	5.22	*0.0478*	80	*1*	1955	*10*	1038	*5*	626	*4*	0.26	*0.0023*	8.23	*1.21*	1
		O-I†	-	-	-	-	1231	*87*	872	*60*	412	*237*	-	-	8.17	*0.62*	2
		Q-I	4.51	*0.0102*	144	*2*	2761	*9*	923	*3*	638	*2*	0.23	*0.0018*	8.20	*0.58*	2
		U-VI	4.67	*0.0174*	89	*1*	2434	*11*	1028	*4*	622	*2*	0.24	*0.0015*	6.86	*0.64*	2
		Z-I	4.44	*0.0165*	84	*1*	1994	*7*	1051	*5*	636	*2*	0.28	*0.0029*	7.79	*0.79*	1
		Z-II†	-	-	-	-	1509	*95*	1024	*61*	321	*250*	-	-	7.35	*0.79*	1
Fukue	FKONON	A-I	2.05	*0.0056*	2547	*6*	1301	*4*	591	*2*	504	*2*	0.35	*0.0025*	2.31	*0.49*	2
		B-I	2.05	*0.0116*	1135	*5*	1238	*7*	622	*4*	536	*3*	0.38	*0.0013*	2.11	*0.56*	2
		D-I	1.85	*0.0077*	1888	*5*	1361	*7*	619	*3*	531	*3*	0.39	*0.0018*	1.38	*0.57*	2
		D-II	1.66	*0.0144*	2122	*6*	1111	*5*	918	*5*	622	*4*	0.45	*0.0025*	1.68	*0.57*	2

Table B4. (continued)

Volcano	Sample ID	Melt ID	H_2O wt%	*2 s.e.*	CO_2 ppm	*2 s.e.*	S ppm	*2 s.e.*	Cl ppm	*2 s.e.*	F ppm	*2 s.e.*	P_2O_5 wt%	*2 s.e.*	$\delta^{34}S_{V\text{-}CDT}$ ‰	*2 s.e.*	SIMS lab*
		F-I	1.91	*0.0064*	2198	*5*	1198	*6*	631	*3*	547	*2*	0.39	*0.0033*	2.32	*0.62*	2
		G-II	1.60	*0.0076*	2332	*8*	1214	*6*	624	*3*	559	*2*	0.39	*0.0024*	-	-	-
		I-I	1.67	*0.0069*	2338	*6*	1396	*6*	572	*3*	482	*2*	0.34	*0.0022*	0.97	*0.65*	2
		K-I	1.78	*0.0079*	2271	*7*	1279	*4*	570	*2*	495	*2*	0.36	*0.0022*	1.79	*0.63*	2
		K-II	1.78	*0.0050*	2244	*6*	1258	*5*	568	*3*	501	*2*	0.36	*0.0022*	1.85	*0.46*	2
		M-I	0.37	*0.0020*	1255	*4*	1093	*4*	586	*2*	508	*3*	0.39	*0.0022*	0.31	*0.55*	2
		N-I	1.89	*0.0055*	2719	*8*	1201	*5*	636	*2*	519	*1*	0.47	*0.0019*	0.49	*0.51*	2
		O-I	1.62	*0.0081*	2495	*3*	1126	*2*	593	*2*	534	*2*	0.41	*0.0026*	2.45	*0.70*	2
		P-II	1.68	*0.0080*	2341	*5*	1258	*5*	597	*3*	514	*2*	0.39	*0.0026*	1.76	*0.46*	2

*SIMS lab for S-isotope measurement: 1. Kochi Institute for Core Sample Research, JAMSTEC, Japan, 2. CRPG-CNRS-Nancy, France.

†: S, Cl and F were measured by EPMA.

Table B5. Measured trace element concentrations (uncorrected) in olivine hosted melt inclusions

Sample ID	Melt ID	Li (ppm)	*1 s.e.*	Sc	*1 s.e.*	V	*1 s.e.*	Cu	*1 s.e.*	Rb	*1 s.e.*	Sr	*1 s.e.*	Y	*1 s.e.*	Zr	*1 s.e.*	Nb	*1 s.e.*	Ba	*1 s.e.*	La	*1 s.e.*	Ce	*1 s.e.*	Pr	*1 s.e.*
ON2S	AP-IV	–	–	21.2	*1.3*	248	*8*	48	*4*	28.0	*1.0*	801	*32*	16.8	*0.6*	193.9	*6.5*	30.4	*1.3*	341	*13*	36.6	*1.5*	86.4	*3.5*	10.4	*0.5*
	BEc-III	–	–	27.8	*1.2*	229	*8*	29	*2*	25.3	*0.9*	863	*34*	19.4	*0.7*	197.6	*6.6*	30.4	*1.4*	337	*13*	37.5	*1.5*	87.1	*3.6*	11.3	*0.5*
	CSa-III	16.9	*1.6*	21.2	*1.0*	137	*5*	109	*5*	23.6	*0.9*	724	*32*	13.7	*0.5*	165.9	*5.9*	27.4	*1.1*	297	*12*	29.4	*1.2*	69.8	*2.3*	8.8	*0.3*
	DL-I	20.2	*1.3*	22.5	*0.8*	225	*8*	71	*4*	47.6	*1.9*	478	*17*	35.4	*1.5*	156.1	*6.1*	26.2	*1.0*	7690	*257*	109.9	*3.9*	109.3	*3.8*	17.4	*0.6*
	DZ-I	71.5	*5.3*	30.8	*1.6*	267	*9*	–[a]	*49*	44.3	*1.6*	437	*18*	18.8	*0.7*	201.2	*6.8*	32.6	*1.5*	1314	*52*	35.5	*1.5*	52.9	*2.2*	8.1	*0.4*
	Z-I	6.9	*1.0*	19.8	*0.9*	229	*9*	24	*1*	20.6	*0.8*	819	*35*	15.1	*0.6*	153.5	*5.4*	26.8	*1.0*	284	*11*	33.8	*1.3*	80.7	*2.7*	10.3	*0.4*
YF1L	AFa-III	–	–	55.2	*2.0*	383	*13*	82	*4*	8.3	*0.3*	847	*31*	16.6	*0.6*	51.3	*1.9*	2.7	*0.1*	214	*8*	9.6	*0.4*	23.0	*0.9*	3.4	*0.2*
	AFb-I	2.3	*0.7*	48.7	*2.0*	344	*13*	179	*7*	6.3	*0.3*	408	*17*	13.7	*0.5*	42.0	*1.5*	2.2	*0.1*	133	*5*	6.7	*0.3*	18.7	*0.6*	2.7	*0.1*
	AH-I	–	–	63.2	*2.2*	381	*14*	17	*1*	4.9	*0.2*	611	*22*	14.4	*0.6*	43.0	*1.7*	2.5	*0.1*	136	*5*	6.3	*0.2*	15.8	*0.6*	2.3	*0.1*
	AZ-I	–	–	53.0	*2.0*	683	*23*	75	*4*	6.7	*0.3*	441	*17*	17.4	*0.6*	52.3	*2.1*	2.2	*0.1*	135	*5*	7.6	*0.3*	21.8	*0.9*	3.2	*0.2*
	AZ-III	–	–	66.3	*2.5*	425	*14*	34	*3*	9.1	*0.4*	925	*35*	17.7	*0.6*	52.5	*2.2*	2.7	*0.2*	237	*9*	9.9	*0.4*	24.4	*1.0*	3.2	*0.2*
	BD-I	–	–	66.1	*2.7*	374	*14*	46	*2*	4.4	*0.2*	587	*24*	14.9	*0.5*	43.7	*1.6*	2.4	*0.1*	125	*5*	6.3	*0.3*	15.6	*0.5*	2.3	*0.1*
	BK-II	–	–	40.1	*1.4*	309	*12*	46	*3*	5.8	*0.2*	634	*22*	13.5	*0.5*	40.1	*1.5*	2.1	*0.1*	151	*7*	6.8	*0.3*	16.5	*0.7*	2.4	*0.1*
	BLa-II	–	–	53.2	*2.0*	380	*13*	54	*3*	7.6	*0.3*	822	*31*	14.7	*0.5*	46.6	*1.9*	2.7	*0.1*	202	*8*	8.8	*0.4*	21.0	*0.8*	2.8	*0.1*
	BLa-III	–	–	53.3	*2.0*	379	*13*	72	*4*	7.6	*0.3*	789	*30*	14.8	*0.5*	48.0	*1.9*	2.4	*0.1*	199	*8*	8.6	*0.4*	20.6	*0.8*	2.7	*0.1*
	BM-I	–	–	63.1	*2.6*	414	*15*	51	*2*	4.3	*0.2*	577	*24*	14.1	*0.5*	41.8	*1.5*	2.3	*0.1*	127	*5*	5.9	*0.2*	15.1	*0.5*	2.2	*0.1*
	BO-I	–	–	60.3	*2.2*	400	*15*	42	*3*	7.6	*0.4*	748	*27*	13.9	*0.6*	42.5	*1.9*	2.3	*0.1*	199	*7*	7.9	*0.3*	18.7	*0.7*	3.0	*0.2*
	BQ-I	–	–	33.2	*1.3*	316	*11*	61	*3*	6.0	*0.3*	432	*15*	12.4	*0.4*	41.2	*1.6*	2.2	*0.1*	137	*5*	5.7	*0.2*	15.5	*0.6*	2.4	*0.1*
	BQ-II	–	–	47.4	*1.9*	408	*14*	89	*5*	8.0	*0.4*	551	*21*	14.8	*0.5*	45.5	*2.1*	2.4	*0.1*	138	*6*	7.1	*0.3*	19.1	*0.8*	2.7	*0.1*
	BQ-III	–	–	53.1	*2.4*	345	*12*	37	*5*	8.2	*0.5*	820	*32*	15.8	*0.6*	50.5	*2.6*	2.4	*0.2*	221	*9*	9.5	*0.5*	19.6	*0.9*	3.4	*0.2*
	BSc-II	–	–	40.8	*1.4*	315	*12*	26	*2*	6.3	*0.2*	708	*24*	13.3	*0.5*	40.6	*1.5*	2.1	*0.1*	181	*8*	7.9	*0.3*	18.9	*0.7*	2.7	*0.1*
	F-I	–	–	34.3	*1.3*	371	*12*	49	*3*	7.1	*0.3*	598	*21*	14.0	*0.5*	42.5	*1.6*	2.4	*0.1*	192	*7*	7.2	*0.3*	19.0	*0.7*	2.6	*0.1*
	F-II	–	–	46.1	*1.8*	397	*13*	47	*3*	8.4	*0.4*	770	*29*	15.0	*0.5*	47.0	*1.9*	2.3	*0.1*	205	*8*	8.6	*0.4*	20.0	*0.8*	2.7	*0.1*
KJ5S	AD-V	9.5	*0.6*	23.8	*0.8*	243	*9*	7	*0*	19.0	*0.7*	556	*20*	17.3	*0.7*	77.6	*2.9*	5.7	*0.2*	308	*10*	13.3	*0.5*	29.9	*1.0*	3.8	*0.1*
	AE-I	10.3	*0.6*	23.0	*0.8*	223	*9*	17	*1*	22.3	*0.8*	561	*20*	17.3	*0.6*	82.6	*3.3*	6.3	*0.3*	332	*16*	13.9	*0.6*	30.9	*1.3*	4.0	*0.2*
	AE-II	12.1	*0.7*	23.8	*0.9*	245	*10*	25	*2*	20.0	*0.7*	569	*20*	16.8	*0.6*	77.2	*3.1*	5.6	*0.2*	314	*15*	12.7	*0.5*	28.6	*1.2*	3.7	*0.2*
	AF-I	11.4	*0.7*	24.1	*0.9*	252	*10*	23	*2*	19.3	*0.7*	590	*21*	17.3	*0.6*	81.5	*3.3*	5.9	*0.2*	316	*16*	12.8	*0.6*	28.9	*1.2*	3.7	*0.2*
	AGa-I	10.6	*0.6*	22.5	*0.8*	235	*10*	26	*2*	20.0	*0.7*	562	*20*	16.8	*0.6*	78.8	*3.2*	5.8	*0.2*	318	*16*	13.0	*0.6*	29.4	*1.3*	3.6	*0.2*
	AGb-IV	11.4	*0.7*	21.4	*0.8*	240	*10*	21	*2*	25.6	*0.9*	556	*20*	17.3	*0.6*	87.5	*3.6*	6.5	*0.3*	356	*18*	13.9	*0.6*	31.3	*1.4*	3.9	*0.2*
	AGb-V	11.0	*0.7*	23.4	*0.9*	235	*10*	16	*1*	22.2	*0.8*	581	*21*	17.7	*0.7*	82.0	*3.4*	6.2	*0.3*	338	*17*	14.0	*0.6*	31.3	*1.4*	4.0	*0.2*
	AI-I	8.1	*0.7*	23.6	*0.9*	255	*10*	20	*1*	20.3	*0.9*	571	*22*	17.5	*0.8*	79.4	*3.3*	5.8	*0.2*	318	*11*	13.4	*0.5*	29.7	*1.1*	3.8	*0.1*
	AK-I	6.6	*0.7*	23.9	*0.9*	240	*9*	11	*1*	19.0	*0.8*	613	*24*	18.2	*0.8*	79.7	*3.3*	6.1	*0.2*	321	*11*	13.5	*0.5*	31.0	*1.1*	4.0	*0.2*
	AK-II	–	–	26.9	*1.8*	311	*11*	42	*5*	24.5	*1.1*	740	*31*	21.5	*0.9*	114.1	*4.5*	5.9	*0.4*	383	*17*	15.6	*0.8*	32.7	*1.5*	4.6	*0.3*
	B-I	11.6	*0.6*	24.4	*0.8*	252	*9*	22	*1*	20.6	*0.7*	572	*19*	17.6	*0.6*	80.7	*2.9*	5.9	*0.2*	316	*13*	13.4	*0.5*	30.4	*1.1*	3.8	*0.1*
	K-I	11.3	*0.7*	23.3	*0.8*	241	*9*	18	*1*	19.2	*0.7*	586	*20*	16.7	*0.6*	78.0	*2.8*	5.7	*0.2*	315	*13*	12.6	*0.5*	28.1	*1.1*	3.6	*0.1*
	L-I	9.7	*0.6*	23.3	*0.8*	252	*9*	9	*1*	19.5	*0.7*	586	*21*	17.8	*0.7*	81.0	*3.0*	5.9	*0.2*	319	*11*	13.9	*0.5*	30.6	*1.0*	3.8	*0.1*

Table B5. (continued)

Sample ID	Melt ID	Li (ppm)	*1 s.e.*	Sc	*1 s.e.*	V	*1 s.e.*	Cu	*1 s.e.*	Rb	*1 s.e.*	Sr	*1 s.e.*	Y	*1 s.e.*	Zr	*1 s.e.*	Nb	*1 s.e.*	Ba	*1 s.e.*	La	*1 s.e.*	Ce	*1 s.e.*	Pr	*1 s.e.*
	S-III	11.1	*0.6*	23.8	*0.8*	251	*9*	11	*1*	19.8	*0.7*	590	*21*	17.1	*0.7*	81.0	*3.0*	5.9	*0.2*	319	*11*	13.2	*0.5*	30.2	*1.0*	3.9	*0.1*
	U-I	8.6	*0.5*	19.4	*0.7*	187	*7*	7	*1*	20.7	*0.7*	493	*16*	15.3	*0.5*	75.9	*2.7*	5.6	*0.2*	295	*12*	12.7	*0.5*	28.3	*1.0*	3.5	*0.1*
	V-I	10.1	*0.9*	23.2	*0.8*	223	*8*	8	*1*	28.5	*1.1*	549	*19*	19.0	*0.8*	92.1	*3.4*	6.9	*0.3*	391	*13*	15.7	*0.6*	35.1	*1.2*	4.1	*0.2*
	Y-I	11.1	*0.6*	23.8	*0.8*	232	*8*	24	*1*	20.7	*0.7*	572	*19*	17.2	*0.6*	80.8	*2.9*	5.9	*0.2*	325	*13*	13.3	*0.5*	29.5	*1.1*	3.9	*0.1*
	Y-II	11.2	*0.6*	22.5	*0.8*	231	*8*	22	*1*	20.8	*0.7*	570	*19*	16.8	*0.6*	80.6	*2.9*	5.8	*0.2*	324	*13*	13.3	*0.5*	29.8	*1.1*	3.8	*0.1*
KSS	AA-I	7.5	*0.5*	34.1	*1.2*	491	*18*	206	*11*	26.3	*0.9*	633	*21*	16.8	*0.6*	61.2	*2.2*	3.1	*0.1*	242	*10*	10.1	*0.4*	23.4	*0.9*	3.1	*0.1*
	AA-II	17.4	*0.9*	30.4	*1.0*	352	*13*	208	*11*	58.6	*2.0*	511	*17*	23.1	*0.8*	121.7	*4.3*	6.7	*0.2*	383	*15*	17.9	*0.7*	40.9	*1.5*	5.3	*0.2*
	AA-III	4.8	*0.6*	32.3	*1.1*	417	*15*	157	*7*	27.0	*1.0*	657	*23*	16.1	*0.6*	59.0	*2.2*	3.0	*0.1*	252	*8*	10.4	*0.4*	23.8	*0.8*	3.1	*0.1*
	AB-I	8.8	*0.5*	30.1	*1.0*	344	*12*	174	*8*	23.0	*0.8*	720	*25*	15.7	*0.6*	55.0	*2.0*	2.6	*0.1*	244	*8*	9.8	*0.3*	22.3	*0.8*	2.9	*0.1*
	D-I	15.3	*0.9*	32.2	*1.1*	512	*19*	162	*9*	29.8	*1.0*	638	*21*	16.9	*0.6*	60.6	*2.2*	3.0	*0.1*	261	*10*	10.2	*0.4*	23.5	*0.9*	3.1	*0.1*
	G-I	19.5	*1.0*	38.4	*1.3*	415	*14*	271	*11*	44.0	*1.5*	561	*19*	24.9	*0.8*	89.0	*3.0*	4.5	*0.2*	309	*11*	12.3	*0.4*	29.0	*1.0*	3.8	*0.1*
	G-II	17.7	*0.9*	27.5	*0.9*	319	*11*	166	*7*	64.2	*2.2*	489	*16*	23.3	*0.8*	127.4	*4.3*	7.8	*0.3*	400	*14*	18.8	*0.6*	43.6	*1.5*	5.2	*0.2*
	G-III	–	–	34.3	*1.5*	495	*17*	186	*8*	49.6	*1.7*	616	*23*	32.4	*1.1*	133.9	*4.6*	6.5	*0.3*	388	*15*	18.9	*0.8*	44.9	*1.7*	5.9	*0.3*
	H-I	24.3	*1.2*	30.8	*1.0*	267	*9*	202	*8*	39.0	*1.4*	889	*30*	34.1	*1.2*	102.1	*3.4*	4.4	*0.2*	366	*13*	15.2	*0.5*	38.1	*1.3*	5.4	*0.2*
	K-II	8.1	*0.4*	28.1	*1.0*	370	*13*	139	*6*	20.7	*0.7*	674	*23*	14.4	*0.5*	49.0	*1.7*	2.4	*0.1*	226	*8*	8.9	*0.3*	20.7	*0.7*	2.7	*0.1*
	L-I	7.0	*0.5*	28.8	*1.0*	370	*13*	164	*7*	22.8	*0.8*	676	*23*	14.8	*0.6*	51.5	*1.9*	2.5	*0.1*	230	*8*	9.3	*0.3*	21.3	*0.7*	2.9	*0.1*
	W-I	19.8	*1.0*	29.4	*1.0*	337	*12*	196	*8*	58.2	*2.0*	485	*16*	24.6	*0.8*	124.0	*4.2*	7.1	*0.2*	386	*13*	17.9	*0.6*	41.0	*1.4*	5.1	*0.2*
KROHTH	E-I	15.7	*0.8*	36.5	*1.2*	403	*14*	119	*5*	26.7	*0.9*	306	*10*	20.5	*0.7*	64.4	*2.1*	3.0	*0.1*	195	*7*	9.2	*0.3*	21.2	*0.7*	2.6	*0.1*
	E-II	15.3	*0.8*	35.0	*1.2*	374	*13*	110	*4*	26.0	*0.9*	298	*10*	19.8	*0.7*	65.3	*2.1*	3.1	*0.1*	190	*6*	9.0	*0.3*	20.7	*0.7*	2.6	*0.1*
	F-I	15.6	*0.8*	34.4	*1.1*	373	*13*	119	*5*	27.1	*0.9*	303	*10*	19.6	*0.6*	65.2	*2.1*	3.0	*0.1*	198	*7*	9.2	*0.3*	20.7	*0.7*	2.6	*0.1*
	G-I	16.0	*0.8*	35.4	*1.2*	368	*13*	112	*4*	25.7	*0.9*	298	*10*	19.7	*0.7*	67.5	*2.2*	3.2	*0.1*	196	*7*	9.4	*0.3*	21.7	*0.7*	2.7	*0.1*
	H-I	16.0	*0.8*	35.2	*1.2*	382	*13*	120	*5*	27.5	*0.9*	305	*10*	20.3	*0.7*	65.0	*2.1*	3.1	*0.1*	195	*7*	9.1	*0.3*	21.0	*0.7*	2.6	*0.1*
	I-I	16.6	*0.8*	35.7	*1.2*	378	*13*	125	*5*	30.9	*1.0*	308	*10*	20.6	*0.7*	68.5	*2.3*	3.2	*0.1*	208	*7*	9.5	*0.3*	21.8	*0.7*	2.7	*0.1*
	K-I	14.2	*0.7*	31.6	*1.1*	294	*10*	101	*4*	27.5	*0.9*	282	*9*	19.3	*0.6*	67.1	*2.2*	3.1	*0.1*	201	*7*	9.4	*0.3*	21.5	*0.7*	2.8	*0.1*
	L-II	16.2	*0.8*	35.9	*1.2*	392	*13*	115	*4*	29.3	*1.0*	316	*10*	20.5	*0.7*	67.9	*2.2*	3.2	*0.1*	206	*7*	9.5	*0.3*	22.0	*0.7*	2.7	*0.1*
KRSM11	A-I	15.0	*0.7*	27.6	*0.9*	289	*10*	83	*3*	35.4	*1.2*	301	*10*	17.6	*0.6*	72.1	*2.4*	2.9	*0.1*	207	*7*	9.1	*0.3*	20.8	*0.7*	2.5	*0.1*
	A-II	9.1	*0.7*	28.3	*1.0*	304	*11*	79	*4*	39.4	*1.4*	308	*11*	18.2	*0.7*	77.1	*2.8*	3.0	*0.1*	220	*7*	9.8	*0.3*	21.8	*0.7*	2.8	*0.1*
	A-III	12.2	*0.8*	29.7	*1.0*	267	*9*	78	*4*	35.5	*1.3*	313	*11*	18.0	*0.7*	73.5	*2.7*	2.9	*0.1*	204	*7*	9.4	*0.3*	21.2	*0.7*	2.6	*0.1*
	B-I	15.1	*0.8*	30.0	*1.0*	303	*10*	96	*4*	34.4	*1.2*	306	*10*	17.7	*0.6*	69.2	*2.3*	2.8	*0.1*	198	*7*	8.9	*0.3*	20.2	*0.7*	2.5	*0.1*
	C-I	14.5	*0.8*	28.1	*0.9*	266	*9*	83	*3*	36.0	*1.2*	309	*10*	18.4	*0.6*	75.8	*2.5*	3.0	*0.1*	220	*8*	9.7	*0.3*	22.4	*0.8*	2.8	*0.1*
	D-I	13.5	*0.7*	33.3	*1.1*	324	*11*	60	*2*	27.6	*0.9*	332	*11*	17.5	*0.6*	59.9	*2.0*	2.4	*0.1*	176	*6*	8.0	*0.3*	18.4	*0.6*	2.3	*0.1*
	D-II	–	–	27.0	*1.1*	301	*10*	38	*2*	38.1	*1.3*	345	*12*	19.7	*0.7*	79.1	*2.7*	3.1	*0.1*	222	*8*	10.2	*0.4*	22.4	*0.8*	3.1	*0.1*
	E-I	15.2	*0.8*	30.5	*1.0*	308	*11*	67	*3*	33.5	*1.1*	314	*10*	18.1	*0.6*	71.7	*2.4*	2.9	*0.1*	197	*7*	9.1	*0.3*	20.7	*0.7*	2.5	*0.1*
	E-II	13.2	*0.7*	33.0	*1.1*	321	*11*	51	*2*	27.3	*0.9*	327	*11*	17.4	*0.6*	60.8	*2.0*	2.4	*0.1*	174	*6*	8.0	*0.3*	18.6	*0.6*	2.3	*0.1*
	G-I	15.3	*0.8*	31.2	*1.0*	310	*11*	100	*4*	34.2	*1.2*	313	*10*	18.1	*0.6*	70.2	*2.3*	2.8	*0.1*	199	*7*	9.1	*0.3*	20.7	*0.7*	2.5	*0.1*
	K-V	–	–	33.0	*1.4*	339	*11*	89	*4*	34.7	*1.2*	375	*13*	21.1	*0.7*	74.1	*2.7*	3.1	*0.2*	223	*8*	10.4	*0.4*	22.8	*0.8*	2.7	*0.1*
	L-I	14.0	*0.7*	29.8	*1.0*	286	*10*	52	*2*	32.6	*1.1*	314	*11*	17.7	*0.6*	67.7	*2.3*	2.8	*0.1*	201	*7*	9.0	*0.3*	21.0	*0.7*	2.6	*0.1*
	L-III	10.2	*0.8*	30.7	*1.2*	304	*13*	50	*4*	33.1	*1.3*	322	*12*	18.2	*0.7*	69.3	*2.9*	2.9	*0.1*	200	*10*	8.9	*0.4*	20.2	*0.9*	2.5	*0.1*

Table B5. (continued)

Sample ID	Melt ID	Li (ppm)	*1 s.e.*	Sc	*1 s.e.*	V	*1 s.e.*	Cu	*1 s.e.*	Rb	*1 s.e.*	Sr	*1 s.e.*	Y	*1 s.e.*	Zr	*1 s.e.*	Nb	*1 s.e.*	Ba	*1 s.e.*	La	*1 s.e.*	Ce	*1 s.e.*	Pr	*1 s.e.*
	L-IV	14.7	*0.8*	29.7	*1.0*	297	*10*	44	*2*	33.9	*1.2*	305	*10*	18.0	*0.6*	72.2	*2.4*	2.9	*0.1*	206	*7*	9.7	*0.3*	22.1	*0.8*	2.7	*0.1*
SM1S	AA-I	–	–	49.9	*1.8*	467	*19*	37	*3*	4.8	*0.2*	284	*10*	18.7	*0.7*	37.6	*1.5*	3.5	*0.1*	127	*6*	5.3	*0.2*	13.1	*0.6*	1.9	*0.1*
	AE-I	–	–	32.7	*1.2*	286	*11*	179	*10*	31.7	*1.3*	184	*7*	19.4	*0.9*	69.6	*2.8*	7.0	*0.3*	126	*4*	10.0	*0.4*	24.4	*0.9*	2.9	*0.1*
	AL-II	2.0	*0.6*	41.9	*1.5*	406	*15*	42	*2*	17.1	*0.7*	345	*13*	16.8	*0.8*	32.3	*1.3*	3.0	*0.1*	89	*3*	4.6	*0.2*	11.3	*0.4*	1.6	*0.1*
	AM-II	–	–	43.7	*1.7*	536	*18*	45	*3*	5.5	*0.3*	380	*16*	23.9	*0.8*	52.9	*2.0*	4.7	*0.2*	106	*4*	7.5	*0.3*	18.2	*0.8*	2.4	*0.1*
	AR-VI	–	–	43.3	*1.6*	466	*16*	42	*3*	8.0	*0.3*	310	*11*	19.9	*0.7*	36.7	*1.5*	3.4	*0.2*	95	*4*	5.6	*0.2*	12.9	*0.5*	1.9	*0.1*
	BA-I	2.2	*0.4*	46.6	*1.7*	479	*19*	42	*3*	8.8	*0.3*	349	*12*	18.3	*0.7*	37.5	*1.5*	3.6	*0.1*	102	*5*	5.5	*0.2*	13.5	*0.6*	1.9	*0.1*
	BC-I	–	–	42.2	*1.5*	460	*17*	45	*3*	9.7	*0.4*	373	*14*	18.8	*0.8*	34.6	*1.4*	3.5	*0.1*	101	*3*	5.0	*0.2*	12.7	*0.5*	1.9	*0.1*
	S-II	1.5	*0.7*	55.5	*2.0*	499	*18*	69	*4*	3.6	*0.2*	236	*8*	21.2	*0.8*	43.5	*1.7*	3.9	*0.2*	72	*3*	6.0	*0.3*	15.2	*0.6*	1.9	*0.1*
	T-II	–	–	52.5	*1.8*	494	*18*	52	*3*	9.2	*0.4*	376	*13*	19.5	*0.8*	38.0	*1.5*	3.4	*0.1*	101	*4*	5.2	*0.2*	13.1	*0.5*	1.9	*0.1*
	Z-I	3.5	*0.3*	41.7	*1.5*	406	*16*	61	*4*	26.8	*1.0*	252	*9*	18.1	*0.7*	35.7	*1.4*	3.1	*0.1*	92	*4*	4.9	*0.2*	11.8	*0.5*	1.7	*0.1*
KM1S12a	AE-I	7.8	*0.5*	30.8	*1.1*	271	*10*	27	*2*	8.8	*0.3*	263	*9*	22.3	*0.8*	58.8	*2.2*	2.8	*0.1*	83	*4*	6.3	*0.3*	16.4	*0.7*	2.4	*0.1*
	AE-III	3.3	*0.6*	32.8	*1.2*	217	*8*	15	*1*	9.3	*0.4*	273	*10*	24.1	*1.1*	62.0	*2.5*	3.0	*0.1*	87	*3*	6.8	*0.3*	18.4	*0.6*	2.6	*0.1*
	AF-I	4.6	*0.4*	30.5	*1.1*	220	*8*	5	*0*	19.7	*0.7*	248	*9*	25.6	*0.9*	83.3	*3.2*	4.1	*0.2*	121	*5*	9.3	*0.4*	23.8	*1.0*	3.2	*0.1*
	AH-II	6.7	*0.5*	34.0	*1.2*	266	*10*	6	*1*	16.5	*0.6*	264	*9*	27.0	*1.0*	96.2	*3.7*	4.7	*0.2*	119	*5*	10.3	*0.4*	27.6	*1.1*	3.8	*0.2*
	AJ-I	7.5	*0.5*	35.0	*1.3*	275	*11*	14	*1*	14.6	*0.5*	288	*10*	26.4	*0.9*	79.2	*3.1*	3.9	*0.2*	121	*6*	9.1	*0.4*	23.5	*1.0*	3.3	*0.1*
	J-I	5.6	*0.4*	34.2	*1.2*	264	*10*	6	*0*	10.4	*0.4*	275	*9*	23.0	*0.8*	67.5	*2.5*	3.2	*0.1*	94	*4*	7.0	*0.3*	18.6	*0.7*	2.6	*0.1*
	J-II	5.1	*0.4*	34.0	*1.2*	265	*10*	4	*0*	9.1	*0.4*	281	*10*	23.7	*1.0*	69.1	*2.6*	3.4	*0.1*	93	*3*	7.3	*0.3*	19.4	*0.7*	2.7	*0.1*
	K-II	8.1	*0.5*	35.2	*1.2*	315	*12*	10	*1*	15.3	*0.5*	289	*10*	28.2	*1.0*	85.8	*3.2*	4.1	*0.2*	125	*5*	9.4	*0.4*	24.6	*0.9*	3.4	*0.1*
	Q-I	7.6	*0.7*	44.8	*1.6*	265	*10*	27	*2*	10.4	*0.4*	297	*11*	28.0	*1.1*	72.8	*2.8*	3.5	*0.1*	102	*4*	7.8	*0.3*	20.2	*0.7*	2.9	*0.1*
	U-VI	1.9	*0.7*	34.6	*1.2*	283	*10*	10	*1*	14.1	*0.6*	287	*10*	26.6	*1.1*	80.3	*3.1*	3.8	*0.2*	119	*4*	8.8	*0.3*	22.9	*0.8*	3.2	*0.1*
	Z-I	5.3	*0.6*	35.1	*1.2*	273	*10*	10	*1*	16.8	*0.7*	301	*11*	30.1	*1.3*	97.4	*3.8*	4.5	*0.2*	142	*5*	10.5	*0.4*	27.8	*1.0*	3.9	*0.1*
FKONON	A-I	–	–	27.7	*1.1*	256	*9*	22	*1*	30.3	*1.0*	521	*20*	21.8	*0.7*	96.3	*3.3*	26.4	*0.9*	343	*12*	17.4	*0.6*	35.1	*1.1*	4.1	*0.1*
	B-I	–	–	30.0	*1.7*	337	*12*	11	*4*	33.5	*1.3*	546	*20*	21.0	*0.8*	103.9	*4.0*	26.1	*1.1*	398	*15*	21.4	*0.9*	44.6	*1.8*	4.5	*0.3*
	D-I	–	–	27.2	*1.3*	266	*9*	25	*3*	32.2	*1.1*	545	*19*	23.7	*0.8*	116.4	*4.0*	28.1	*1.1*	380	*13*	19.7	*0.7*	38.7	*1.4*	5.0	*0.2*
	D-II	4.8	*0.7*	20.9	*0.8*	170	*6*	38	*2*	39.9	*1.4*	563	*22*	24.4	*0.8*	118.3	*4.0*	35.2	*1.3*	525	*19*	28.7	*1.0*	54.7	*1.8*	6.0	*0.2*
	F-I	–	–	27.6	*1.2*	257	*9*	15	*2*	27.8	*1.0*	518	*18*	22.9	*0.8*	106.9	*3.7*	26.2	*1.0*	354	*13*	18.4	*0.7*	38.4	*1.4*	4.5	*0.2*
	I-I	–	–	27.2	*1.1*	250	*9*	34	*2*	26.2	*0.9*	489	*19*	19.6	*0.7*	87.7	*3.0*	23.0	*0.8*	310	*11*	15.5	*0.6*	31.3	*1.0*	3.7	*0.1*
	K-I	–	–	29.7	*1.5*	260	*9*	30	*3*	28.8	*1.1*	534	*19*	21.7	*0.8*	105.2	*3.9*	23.1	*1.0*	330	*13*	15.9	*0.7*	31.0	*1.2*	3.5	*0.2*
	K-II	–	–	28.1	*1.2*	268	*9*	20	*2*	30.3	*1.1*	563	*20*	23.3	*0.8*	107.3	*3.7*	25.7	*1.0*	347	*13*	18.1	*0.7*	34.1	*1.3*	4.0	*0.2*
	N-I	–	–	28.0	*1.0*	239	*8*	21	*1*	31.3	*1.1*	496	*17*	20.6	*0.8*	96.4	*3.5*	27.4	*1.0*	365	*12*	18.5	*0.6*	35.8	*1.2*	4.3	*0.2*
	N-II	–	–	47.9	*3.4*	283	*10*	40	*9*	41.2	*1.7*	577	*21*	26.2	*1.1*	131.3	*6.0*	35.4	*1.6*	484	*19*	22.6	*1.0*	44.1	*1.8*	4.9	*0.3*
	O-I	–	–	29.4	*1.0*	269	*9*	13	*1*	32.5	*1.2*	550	*19*	22.1	*0.8*	104.9	*3.8*	27.8	*1.0*	365	*12*	18.7	*0.6*	37.0	*1.2*	4.5	*0.2*
	O-II	–	–	27.1	*1.0*	256	*9*	37	*2*	28.7	*1.0*	507	*18*	20.0	*0.7*	91.2	*3.0*	24.8	*0.9*	331	*12*	16.7	*0.6*	33.0	*1.2*	4.1	*0.2*
	P-II	–	–	30.1	*1.2*	249	*9*	21	*1*	30.2	*1.1*	499	*20*	21.3	*0.7*	103.0	*3.5*	26.4	*1.0*	346	*13*	18.3	*0.7*	36.1	*1.2*	4.2	*0.2*

Table B5. (continued)

Sample ID	Melt ID	Nd	*1 s.e.*	Sm	*1 s.e.*	Eu	*1 s.e.*	Gd	*1 s.e.*	Dy	*1 s.e.*	Er	*1 s.e.*	Yb	*1 s.e.*	Lu	*1 s.e.*	Hf	*1 s.e.*	Ta	*1 s.e.*	Pb	*1 s.e.*	Th	*1 s.e.*	U	*1 s.e.*
ON2S	AP-IV	42.4	*1.9*	7.7	*0.5*	2.27	*0.14*	5.6	*0.5*	4.5	*0.3*	1.9	*0.2*	1.3	*0.2*	0.21	*0.04*	4.9	*0.3*	1.54	*0.10*	6.90	*0.35*	4.05	*0.18*	0.77	*0.05*
	BEc-III	43.4	*1.9*	8.4	*0.5*	2.62	*0.13*	5.7	*0.4*	4.1	*0.3*	1.9	*0.2*	1.5	*0.2*	0.15	*0.03*	4.9	*0.3*	1.50	*0.08*	6.16	*0.30*	3.65	*0.16*	0.63	*0.04*
	CSa-III	35.9	*1.9*	6.4	*0.5*	1.87	*0.13*	5.0	*0.4*	3.5	*0.3*	1.5	*0.2*	1.0	*0.2*	0.17	*0.03*	3.8	*0.3*	1.34	*0.09*	3.90	*0.26*	2.91	*0.15*	0.55	*0.05*
	DL-I	65.2	*2.3*	10.1	*0.4*	2.95	*0.13*	8.7	*0.4*	5.2	*0.3*	2.6	*0.2*	1.7	*0.1*	0.24	*0.02*	4.1	*0.2*	1.25	*0.06*	5.41	*0.25*	3.08	*0.12*	0.65	*0.04*
	DZ-I	31.1	*1.5*	6.0	*0.5*	1.61	*0.13*	4.2	*0.5*	3.2	*0.3*	1.5	*0.3*	1.0	*0.3*	0.21	*0.04*	5.4	*0.4*	1.59	*0.11*	6.13	*0.34*	4.06	*0.19*	0.55	*0.05*
	Z-I	39.3	*2.0*	7.6	*0.5*	2.28	*0.14*	5.8	*0.4*	3.4	*0.3*	1.8	*0.2*	1.3	*0.2*	0.12	*0.03*	4.0	*0.3*	1.36	*0.09*	4.79	*0.29*	3.26	*0.16*	0.66	*0.06*
YF1L	AFa-III	15.5	*0.7*	4.2	*0.3*	1.21	*0.08*	3.3	*0.3*	3.3	*0.2*	1.8	*0.2*	1.5	*0.2*	0.23	*0.03*	1.4	*0.1*	–	–	3.42	*0.19*	1.56	*0.08*	0.53	*0.04*
	AFb-I	12.6	*0.6*	3.5	*0.2*	1.13	*0.07*	3.2	*0.2*	2.8	*0.2*	1.3	*0.1*	1.5	*0.1*	0.20	*0.03*	1.3	*0.1*	0.10	*0.02*	3.73	*0.20*	1.30	*0.07*	0.40	*0.03*
	AH-I	10.9	*0.4*	3.0	*0.2*	1.05	*0.05*	2.8	*0.2*	2.9	*0.1*	1.6	*0.1*	1.5	*0.1*	0.26	*0.02*	1.4	*0.1*	0.12	*0.01*	2.32	*0.11*	0.72	*0.03*	0.23	*0.02*
	AZ-I	15.5	*0.8*	4.3	*0.3*	1.25	*0.10*	4.3	*0.4*	3.5	*0.3*	1.8	*0.2*	1.8	*0.2*	0.21	*0.03*	1.4	*0.2*	0.15	*0.04*	4.20	*0.23*	1.46	*0.08*	0.61	*0.05*
	AZ-III	15.5	*0.8*	3.6	*0.3*	1.36	*0.11*	4.2	*0.4*	3.1	*0.3*	2.3	*0.2*	1.6	*0.2*	0.25	*0.04*	1.8	*0.2*	0.20	*0.05*	2.33	*0.18*	1.46	*0.09*	0.44	*0.04*
	BD-I	11.1	*0.6*	2.9	*0.2*	0.85	*0.06*	2.6	*0.2*	3.0	*0.2*	1.9	*0.1*	1.4	*0.1*	0.18	*0.02*	1.3	*0.1*	0.10	*0.02*	1.75	*0.11*	0.71	*0.04*	0.24	*0.02*
	BK-II	11.4	*0.4*	2.9	*0.1*	1.05	*0.05*	2.9	*0.2*	2.7	*0.1*	1.5	*0.1*	1.3	*0.1*	0.18	*0.01*	1.3	*0.1*	0.09	*0.01*	2.22	*0.12*	1.05	*0.04*	0.31	*0.02*
	BLa-II	12.6	*0.7*	3.3	*0.3*	1.14	*0.09*	3.4	*0.3*	3.0	*0.2*	1.5	*0.2*	1.3	*0.2*	0.25	*0.03*	1.3	*0.1*	0.16	*0.04*	3.06	*0.19*	1.31	*0.07*	0.39	*0.03*
	BLa-III	14.7	*0.7*	3.6	*0.3*	1.27	*0.10*	3.3	*0.3*	2.7	*0.2*	1.5	*0.2*	1.3	*0.2*	0.16	*0.03*	1.6	*0.2*	–	–	3.03	*0.19*	1.41	*0.08*	0.43	*0.04*
	BM-I	10.6	*0.5*	2.9	*0.2*	1.17	*0.06*	2.7	*0.2*	2.7	*0.2*	1.6	*0.1*	1.6	*0.1*	0.18	*0.02*	1.3	*0.1*	0.09	*0.02*	1.91	*0.11*	0.68	*0.04*	0.19	*0.02*
	BO-I	11.4	*0.7*	2.1	*0.3*	1.31	*0.13*	2.6	*0.4*	3.2	*0.3*	1.6	*0.2*	1.2	*0.2*	0.09	*0.03*	1.8	*0.2*	0.06	*0.04*	2.67	*0.24*	1.68	*0.12*	0.39	*0.05*
	BQ-I	11.6	*0.5*	3.1	*0.2*	1.07	*0.07*	2.5	*0.2*	2.4	*0.2*	1.5	*0.1*	1.6	*0.2*	0.18	*0.02*	1.1	*0.1*	0.11	*0.03*	3.18	*0.17*	1.18	*0.06*	0.35	*0.03*
	BQ-II	12.6	*0.7*	3.4	*0.3*	1.08	*0.11*	3.7	*0.4*	2.7	*0.3*	1.9	*0.2*	1.3	*0.3*	0.25	*0.04*	1.6	*0.2*	0.19	*0.05*	3.07	*0.20*	1.38	*0.08*	0.46	*0.04*
	BQ-III	13.1	*0.9*	3.6	*0.5*	1.18	*0.16*	2.4	*0.6*	2.3	*0.4*	1.8	*0.3*	1.9	*0.4*	0.22	*0.06*	1.0	*0.3*	–	–	3.05	*0.29*	1.41	*0.12*	0.38	*0.06*
	BSc-II	12.1	*0.5*	2.9	*0.2*	1.03	*0.06*	3.0	*0.2*	2.5	*0.1*	1.4	*0.1*	1.5	*0.1*	0.18	*0.01*	1.2	*0.1*	0.09	*0.01*	2.36	*0.13*	1.33	*0.06*	0.35	*0.02*
	F-I	12.9	*0.6*	3.8	*0.3*	1.03	*0.07*	3.1	*0.3*	2.7	*0.2*	1.6	*0.1*	1.2	*0.2*	0.14	*0.02*	1.4	*0.1*	–	–	4.69	*0.23*	1.41	*0.07*	0.48	*0.03*
	F-II	13.0	*0.7*	3.5	*0.3*	1.13	*0.08*	2.9	*0.3*	2.8	*0.2*	1.7	*0.2*	1.7	*0.2*	0.24	*0.03*	1.6	*0.2*	–	–	3.51	*0.20*	1.56	*0.08*	0.56	*0.04*
KJ5S	AD-V	16.4	*0.6*	3.9	*0.2*	1.22	*0.05*	3.7	*0.2*	3.2	*0.1*	2.0	*0.1*	1.8	*0.1*	0.28	*0.01*	2.1	*0.1*	0.30	*0.01*	7.35	*0.29*	1.71	*0.06*	0.40	*0.02*
	AE-I	17.1	*0.6*	4.2	*0.2*	1.22	*0.07*	3.3	*0.2*	3.3	*0.2*	1.7	*0.1*	1.9	*0.1*	0.28	*0.02*	2.4	*0.1*	0.34	*0.02*	7.65	*0.40*	2.02	*0.08*	0.50	*0.03*
	AE-II	15.9	*0.6*	3.7	*0.2*	1.16	*0.06*	3.3	*0.2*	3.2	*0.1*	1.8	*0.1*	1.7	*0.1*	0.27	*0.01*	2.1	*0.1*	0.31	*0.02*	6.75	*0.36*	1.68	*0.07*	0.39	*0.02*
	AF-I	16.3	*0.6*	3.9	*0.2*	1.19	*0.06*	3.3	*0.2*	3.2	*0.2*	1.9	*0.1*	1.8	*0.1*	0.25	*0.01*	2.2	*0.1*	0.31	*0.02*	6.94	*0.37*	1.71	*0.07*	0.39	*0.02*
	AGa-I	16.1	*0.6*	3.6	*0.2*	1.17	*0.06*	3.4	*0.2*	3.1	*0.1*	1.9	*0.1*	1.8	*0.1*	0.25	*0.01*	2.1	*0.1*	0.30	*0.02*	7.21	*0.39*	1.67	*0.07*	0.41	*0.02*
	AGb-IV	17.1	*0.6*	3.9	*0.2*	1.21	*0.07*	3.5	*0.2*	3.2	*0.2*	1.9	*0.1*	1.8	*0.1*	0.27	*0.01*	2.3	*0.1*	0.33	*0.02*	7.29	*0.40*	2.06	*0.08*	0.46	*0.03*
	AGb-V	17.1	*0.6*	4.0	*0.2*	1.22	*0.07*	3.5	*0.2*	3.2	*0.2*	2.0	*0.1*	1.8	*0.1*	0.26	*0.02*	2.3	*0.1*	0.31	*0.02*	7.60	*0.43*	1.72	*0.07*	0.37	*0.02*
	AI-I	16.4	*0.6*	3.9	*0.2*	1.25	*0.06*	3.7	*0.2*	3.5	*0.2*	2.1	*0.1*	2.0	*0.1*	0.27	*0.02*	2.3	*0.1*	0.29	*0.02*	7.90	*0.34*	1.70	*0.07*	0.40	*0.02*
	AK-I	17.1	*0.6*	4.0	*0.2*	1.25	*0.06*	3.7	*0.2*	3.4	*0.2*	1.9	*0.1*	1.8	*0.1*	0.29	*0.02*	2.3	*0.1*	0.31	*0.02*	7.41	*0.32*	1.65	*0.07*	0.39	*0.02*
	AK-II	16.9	*1.3*	4.2	*0.6*	0.96	*0.18*	4.8	*0.7*	4.0	*0.5*	3.1	*0.5*	1.4	*0.4*	0.36	*0.08*	2.0	*0.4*	0.54	*0.10*	8.56	*0.63*	1.97	*0.17*	0.55	*0.09*
	B-I	16.6	*0.6*	4.0	*0.2*	1.25	*0.06*	3.5	*0.2*	3.2	*0.1*	2.0	*0.1*	2.0	*0.1*	0.30	*0.02*	2.2	*0.1*	0.31	*0.02*	6.99	*0.32*	1.80	*0.07*	0.42	*0.02*
	K-I	15.9	*0.6*	3.4	*0.2*	1.14	*0.05*	3.6	*0.2*	3.0	*0.1*	1.8	*0.1*	1.8	*0.1*	0.27	*0.02*	2.1	*0.1*	0.29	*0.02*	6.93	*0.32*	1.61	*0.06*	0.38	*0.02*
	L-I	17.0	*0.6*	3.7	*0.2*	1.26	*0.06*	3.7	*0.2*	3.5	*0.2*	1.9	*0.1*	1.8	*0.1*	0.28	*0.02*	2.1	*0.1*	0.30	*0.02*	7.38	*0.30*	1.81	*0.07*	0.41	*0.02*

Table B5. (continued)

Sample ID	Melt ID	Nd	*1 s.e.*	Sm	*1 s.e.*	Eu	*1 s.e.*	Gd	*1 s.e.*	Dy	*1 s.e.*	Er	*1 s.e.*	Yb	*1 s.e.*	Lu	*1 s.e.*	Hf	*1 s.e.*	Ta	*1 s.e.*	Pb	*1 s.e.*	Th	*1 s.e.*	U	*1 s.e.*
	S-III	16.5	*0.6*	4.0	*0.2*	1.22	*0.05*	3.6	*0.2*	3.4	*0.1*	2.0	*0.1*	1.8	*0.1*	0.28	*0.02*	2.2	*0.1*	0.31	*0.02*	6.94	*0.28*	1.73	*0.07*	0.42	*0.02*
	U-I	15.5	*0.5*	3.6	*0.2*	1.11	*0.05*	3.2	*0.2*	3.0	*0.1*	1.6	*0.1*	1.7	*0.1*	0.23	*0.02*	2.0	*0.1*	0.30	*0.02*	6.99	*0.32*	1.83	*0.07*	0.44	*0.02*
	V-I	18.5	*0.8*	4.3	*0.3*	1.36	*0.09*	4.0	*0.3*	3.4	*0.2*	2.1	*0.2*	1.7	*0.2*	0.28	*0.03*	2.2	*0.2*	0.39	*0.04*	7.77	*0.37*	2.42	*0.11*	0.57	*0.04*
	Y-I	16.5	*0.6*	3.7	*0.2*	1.20	*0.05*	3.5	*0.2*	3.2	*0.1*	1.8	*0.1*	1.8	*0.1*	0.27	*0.01*	2.2	*0.1*	0.33	*0.02*	6.79	*0.31*	1.78	*0.07*	0.45	*0.02*
	Y-II	16.5	*0.6*	3.8	*0.2*	1.21	*0.05*	3.4	*0.2*	3.1	*0.1*	1.9	*0.1*	1.9	*0.1*	0.28	*0.01*	2.2	*0.1*	0.30	*0.01*	7.04	*0.32*	1.87	*0.07*	0.43	*0.02*
KSS	AA-I	14.1	*0.5*	3.6	*0.2*	1.08	*0.05*	3.4	*0.2*	3.2	*0.1*	1.8	*0.1*	1.8	*0.1*	0.27	*0.02*	1.8	*0.1*	0.19	*0.01*	6.68	*0.30*	2.22	*0.08*	0.66	*0.03*
	AA-II	22.4	*0.8*	5.3	*0.2*	1.44	*0.07*	4.7	*0.2*	4.5	*0.2*	2.6	*0.1*	2.4	*0.1*	0.36	*0.02*	3.2	*0.1*	0.42	*0.02*	11.54	*0.52*	5.41	*0.20*	1.51	*0.07*
	AA-III	13.9	*0.5*	3.2	*0.2*	1.09	*0.05*	3.4	*0.2*	3.2	*0.2*	1.9	*0.1*	1.7	*0.1*	0.23	*0.02*	1.7	*0.1*	0.20	*0.02*	6.76	*0.28*	2.17	*0.08*	0.63	*0.03*
	AB-I	13.4	*0.5*	3.2	*0.1*	1.11	*0.04*	3.1	*0.1*	3.0	*0.1*	1.7	*0.1*	1.6	*0.1*	0.24	*0.01*	1.6	*0.1*	0.17	*0.01*	6.23	*0.25*	1.99	*0.07*	0.61	*0.02*
	D-I	14.3	*0.5*	3.6	*0.2*	1.14	*0.06*	3.2	*0.2*	3.2	*0.1*	1.8	*0.1*	1.8	*0.1*	0.26	*0.02*	1.8	*0.1*	0.20	*0.01*	7.26	*0.33*	2.18	*0.08*	0.64	*0.03*
	G-I	17.1	*0.7*	4.5	*0.2*	1.23	*0.06*	4.3	*0.2*	4.7	*0.2*	2.9	*0.1*	3.0	*0.2*	0.40	*0.03*	2.4	*0.1*	0.31	*0.02*	9.72	*0.40*	3.42	*0.14*	1.08	*0.05*
	G-II	23.6	*0.9*	5.3	*0.2*	1.36	*0.06*	4.7	*0.2*	4.5	*0.2*	2.5	*0.1*	2.4	*0.1*	0.38	*0.02*	3.4	*0.1*	0.51	*0.02*	12.21	*0.48*	5.88	*0.22*	1.76	*0.07*
	G-III	25.2	*1.2*	7.6	*0.6*	1.84	*0.14*	5.4	*0.5*	6.4	*0.4*	3.5	*0.3*	3.4	*0.3*	0.47	*0.06*	3.7	*0.3*	0.37	*0.07*	12.19	*0.60*	5.84	*0.26*	1.63	*0.11*
	H-I	26.9	*1.0*	7.8	*0.3*	1.86	*0.08*	7.1	*0.3*	6.3	*0.2*	3.7	*0.2*	3.6	*0.2*	0.51	*0.02*	2.7	*0.1*	0.30	*0.02*	7.75	*0.31*	3.48	*0.13*	1.08	*0.05*
	K-II	12.4	*0.5*	3.1	*0.1*	0.98	*0.04*	2.9	*0.1*	2.6	*0.1*	1.5	*0.1*	1.5	*0.1*	0.20	*0.01*	1.3	*0.1*	0.15	*0.01*	6.02	*0.24*	1.77	*0.07*	0.54	*0.03*
	L-I	12.4	*0.4*	2.9	*0.1*	1.02	*0.04*	2.9	*0.1*	2.8	*0.1*	1.7	*0.1*	1.5	*0.1*	0.22	*0.01*	1.5	*0.1*	0.17	*0.01*	6.09	*0.25*	1.97	*0.07*	0.56	*0.03*
	W-I	22.9	*0.8*	5.3	*0.2*	1.38	*0.05*	4.9	*0.2*	4.5	*0.2*	2.7	*0.1*	2.7	*0.1*	0.43	*0.02*	3.3	*0.1*	0.49	*0.02*	11.06	*0.43*	5.37	*0.20*	1.62	*0.06*
KROHTH	E-I	12.3	*0.4*	3.3	*0.1*	1.03	*0.04*	3.4	*0.1*	3.7	*0.1*	2.3	*0.1*	2.4	*0.1*	0.35	*0.01*	1.9	*0.1*	0.21	*0.01*	8.21	*0.31*	2.11	*0.08*	0.59	*0.02*
	E-II	12.3	*0.4*	3.2	*0.1*	0.98	*0.04*	3.3	*0.1*	3.7	*0.1*	2.2	*0.1*	2.3	*0.1*	0.32	*0.01*	1.9	*0.1*	0.21	*0.01*	7.89	*0.30*	2.12	*0.08*	0.58	*0.02*
	F-I	12.0	*0.4*	3.1	*0.1*	0.94	*0.04*	3.2	*0.1*	3.5	*0.1*	2.2	*0.1*	2.4	*0.1*	0.35	*0.02*	1.9	*0.1*	0.21	*0.01*	8.07	*0.31*	2.36	*0.09*	0.65	*0.03*
	G-I	12.5	*0.5*	3.4	*0.2*	1.00	*0.05*	3.4	*0.2*	3.6	*0.2*	2.4	*0.1*	2.2	*0.1*	0.32	*0.02*	2.0	*0.1*	0.21	*0.01*	7.92	*0.32*	2.35	*0.09*	0.67	*0.03*
	H-I	12.0	*0.4*	3.3	*0.1*	1.01	*0.04*	3.4	*0.1*	3.7	*0.1*	2.3	*0.1*	2.3	*0.1*	0.34	*0.02*	1.8	*0.1*	0.20	*0.01*	8.29	*0.32*	2.11	*0.08*	0.58	*0.02*
	I-I	12.4	*0.4*	3.2	*0.1*	1.03	*0.04*	3.3	*0.1*	3.6	*0.1*	2.4	*0.1*	2.4	*0.1*	0.33	*0.01*	1.9	*0.1*	0.22	*0.01*	8.46	*0.32*	2.34	*0.08*	0.64	*0.03*
	K-I	12.4	*0.5*	3.5	*0.2*	1.02	*0.05*	3.2	*0.2*	3.4	*0.1*	2.2	*0.1*	2.1	*0.1*	0.31	*0.02*	2.0	*0.1*	0.22	*0.01*	7.88	*0.31*	2.20	*0.08*	0.59	*0.03*
	L-II	12.5	*0.4*	3.3	*0.1*	1.03	*0.04*	3.3	*0.1*	3.8	*0.1*	2.3	*0.1*	2.4	*0.1*	0.37	*0.02*	1.9	*0.1*	0.21	*0.01*	8.91	*0.34*	2.28	*0.08*	0.64	*0.03*
KRSM11	A-I	11.4	*0.4*	3.0	*0.1*	0.84	*0.04*	2.9	*0.1*	3.2	*0.1*	1.9	*0.1*	2.0	*0.1*	0.32	*0.02*	2.1	*0.1*	0.21	*0.01*	9.08	*0.35*	3.11	*0.11*	0.83	*0.03*
	A-II	11.9	*0.4*	2.9	*0.2*	0.83	*0.04*	3.2	*0.2*	3.2	*0.1*	2.0	*0.1*	1.8	*0.1*	0.32	*0.02*	2.3	*0.1*	0.19	*0.02*	9.73	*0.39*	3.33	*0.12*	0.85	*0.04*
	A-III	11.7	*0.4*	3.1	*0.2*	0.83	*0.04*	3.2	*0.2*	3.5	*0.2*	2.1	*0.1*	2.1	*0.1*	0.35	*0.02*	2.2	*0.1*	0.19	*0.02*	10.35	*0.42*	3.07	*0.11*	0.81	*0.04*
	B-I	11.1	*0.4*	3.0	*0.1*	0.88	*0.03*	2.9	*0.1*	3.2	*0.1*	2.0	*0.1*	2.0	*0.1*	0.30	*0.01*	2.0	*0.1*	0.20	*0.01*	9.10	*0.35*	2.87	*0.10*	0.77	*0.03*
	C-I	12.5	*0.5*	3.3	*0.2*	0.91	*0.05*	2.9	*0.2*	3.2	*0.2*	2.2	*0.1*	2.1	*0.1*	0.29	*0.02*	2.1	*0.1*	0.23	*0.02*	10.75	*0.43*	3.37	*0.13*	0.86	*0.04*
	D-I	10.5	*0.4*	2.9	*0.1*	0.86	*0.04*	2.8	*0.1*	3.2	*0.1*	2.0	*0.1*	2.1	*0.1*	0.31	*0.01*	1.7	*0.1*	0.18	*0.01*	8.57	*0.33*	2.34	*0.09*	0.62	*0.03*
	D-II	12.7	*0.6*	3.3	*0.2*	0.85	*0.07*	3.0	*0.3*	3.2	*0.2*	2.4	*0.2*	2.3	*0.2*	0.29	*0.03*	2.1	*0.2*	0.17	*0.04*	10.44	*0.44*	3.53	*0.14*	0.83	*0.05*
	E-I	11.5	*0.4*	2.9	*0.1*	0.88	*0.03*	3.0	*0.1*	3.2	*0.1*	2.0	*0.1*	2.0	*0.1*	0.31	*0.01*	2.1	*0.1*	0.19	*0.01*	9.23	*0.35*	2.96	*0.11*	0.81	*0.03*
	E-II	10.8	*0.4*	2.8	*0.1*	0.88	*0.04*	2.7	*0.1*	3.1	*0.1*	1.9	*0.1*	2.1	*0.1*	0.32	*0.02*	1.7	*0.1*	0.17	*0.01*	8.31	*0.32*	2.38	*0.09*	0.65	*0.03*
	G-I	11.3	*0.4*	3.0	*0.1*	0.88	*0.03*	3.0	*0.1*	3.3	*0.1*	2.0	*0.1*	2.1	*0.1*	0.30	*0.01*	1.9	*0.1*	0.20	*0.01*	9.42	*0.36*	2.92	*0.11*	0.80	*0.03*
	K-V	12.8	*0.6*	3.1	*0.3*	0.96	*0.08*	3.2	*0.3*	3.5	*0.3*	2.5	*0.2*	2.0	*0.3*	0.33	*0.04*	2.0	*0.2*	–	–	9.98	*0.47*	2.76	*0.13*	0.87	*0.06*
	L-I	11.5	*0.4*	3.1	*0.1*	0.85	*0.04*	3.1	*0.1*	3.3	*0.1*	2.0	*0.1*	2.1	*0.1*	0.30	*0.02*	1.9	*0.1*	0.19	*0.01*	9.30	*0.37*	2.83	*0.11*	0.80	*0.04*
	L-III	11.6	*0.5*	2.7	*0.2*	0.89	*0.06*	2.6	*0.2*	3.3	*0.2*	2.1	*0.1*	2.2	*0.2*	0.30	*0.02*	2.1	*0.1*	0.18	*0.02*	8.80	*0.51*	2.94	*0.13*	0.74	*0.05*

Table B5. (continued)

Sample ID	Melt ID	Nd	*1 s.e.*	Sm	*1 s.e.*	Eu	*1 s.e.*	Gd	*1 s.e.*	Dy	*1 s.e.*	Er	*1 s.e.*	Yb	*1 s.e.*	Lu	*1 s.e.*	Hf	*1 s.e.*	Ta	*1 s.e.*	Pb	*1 s.e.*	Th	*1 s.e.*	U	*1 s.e.*
	L-IV	12.2	*0.5*	3.1	*0.2*	0.85	*0.05*	3.2	*0.2*	3.4	*0.2*	2.3	*0.1*	1.9	*0.1*	0.29	*0.02*	1.9	*0.1*	0.22	*0.02*	9.73	*0.41*	3.17	*0.13*	0.76	*0.04*
SM1S	AA-I	9.7	*0.4*	2.8	*0.2*	1.07	*0.06*	3.2	*0.2*	3.5	*0.2*	2.3	*0.1*	2.1	*0.1*	0.28	*0.02*	1.3	*0.1*	0.18	*0.01*	2.77	*0.16*	0.76	*0.04*	0.20	*0.02*
	AE-I	13.4	*0.6*	4.1	*0.2*	1.35	*0.07*	3.2	*0.2*	4.0	*0.2*	2.2	*0.1*	1.8	*0.1*	0.26	*0.02*	2.2	*0.1*	0.35	*0.03*	10.39	*0.46*	1.69	*0.08*	0.44	*0.03*
	AL-II	8.1	*0.3*	2.6	*0.1*	0.86	*0.05*	2.6	*0.2*	3.3	*0.2*	1.8	*0.1*	1.7	*0.1*	0.26	*0.02*	1.0	*0.1*	0.18	*0.02*	2.09	*0.10*	0.69	*0.03*	0.20	*0.01*
	AM-II	11.5	*0.6*	3.5	*0.3*	1.40	*0.10*	4.4	*0.4*	4.8	*0.3*	2.4	*0.2*	2.1	*0.3*	0.35	*0.04*	1.5	*0.2*	0.23	*0.04*	3.58	*0.21*	1.20	*0.07*	0.27	*0.03*
	AR-VI	9.0	*0.5*	2.9	*0.3*	1.17	*0.08*	3.6	*0.3*	3.9	*0.2*	2.4	*0.2*	2.2	*0.2*	0.36	*0.04*	1.1	*0.1*	0.14	*0.04*	2.70	*0.16*	0.74	*0.05*	0.21	*0.02*
	BA-I	9.3	*0.4*	2.8	*0.2*	0.94	*0.06*	3.4	*0.2*	3.4	*0.2*	2.1	*0.1*	2.1	*0.1*	0.29	*0.02*	1.2	*0.1*	0.18	*0.02*	2.43	*0.14*	0.80	*0.04*	0.22	*0.02*
	BC-I	8.8	*0.4*	2.6	*0.1*	1.04	*0.05*	3.1	*0.2*	3.4	*0.2*	2.3	*0.1*	2.2	*0.1*	0.35	*0.02*	1.2	*0.1*	0.16	*0.02*	3.56	*0.17*	0.72	*0.04*	0.21	*0.02*
	S-II	11.3	*0.6*	3.9	*0.3*	1.17	*0.10*	3.1	*0.3*	3.9	*0.3*	2.5	*0.2*	2.0	*0.2*	0.32	*0.04*	1.3	*0.1*	0.18	*0.03*	3.45	*0.25*	0.88	*0.07*	0.19	*0.03*
	T-II	9.2	*0.4*	2.6	*0.2*	1.06	*0.06*	3.0	*0.2*	3.3	*0.2*	2.3	*0.1*	2.2	*0.2*	0.35	*0.03*	1.2	*0.1*	0.19	*0.02*	2.63	*0.14*	0.81	*0.04*	0.21	*0.02*
	Z-I	8.6	*0.3*	2.6	*0.1*	0.95	*0.05*	3.0	*0.2*	3.5	*0.2*	2.1	*0.1*	1.9	*0.1*	0.30	*0.02*	1.2	*0.1*	0.17	*0.01*	3.86	*0.20*	0.71	*0.03*	0.18	*0.01*
KM1S12a	AE-I	11.6	*0.4*	3.3	*0.2*	1.04	*0.05*	3.7	*0.2*	4.0	*0.2*	2.4	*0.1*	2.5	*0.1*	0.37	*0.02*	1.7	*0.1*	0.13	*0.01*	3.83	*0.19*	0.73	*0.03*	0.20	*0.01*
	AE-III	12.5	*0.5*	3.6	*0.2*	1.09	*0.05*	3.7	*0.2*	4.3	*0.2*	2.6	*0.1*	2.5	*0.1*	0.34	*0.02*	1.8	*0.1*	0.10	*0.01*	3.78	*0.17*	0.83	*0.04*	0.23	*0.02*
	AF-I	15.7	*0.6*	4.1	*0.2*	1.33	*0.07*	4.4	*0.2*	4.8	*0.2*	3.0	*0.1*	2.8	*0.2*	0.40	*0.02*	2.5	*0.1*	0.20	*0.01*	5.79	*0.29*	1.72	*0.07*	0.38	*0.02*
	AH-II	18.0	*0.6*	4.8	*0.2*	1.49	*0.08*	4.7	*0.3*	5.0	*0.2*	3.2	*0.2*	2.8	*0.2*	0.43	*0.02*	2.6	*0.1*	0.22	*0.01*	6.01	*0.30*	1.23	*0.05*	0.28	*0.02*
	AJ-I	16.0	*0.6*	4.4	*0.2*	1.33	*0.07*	4.6	*0.3*	4.8	*0.2*	3.1	*0.2*	2.8	*0.2*	0.45	*0.03*	2.2	*0.1*	0.16	*0.01*	4.69	*0.25*	1.24	*0.05*	0.30	*0.02*
	J-I	12.7	*0.5*	3.5	*0.2*	1.05	*0.05*	3.6	*0.2*	4.2	*0.2*	2.6	*0.1*	2.6	*0.1*	0.37	*0.02*	1.9	*0.1*	0.15	*0.01*	3.99	*0.19*	0.89	*0.04*	0.23	*0.01*
	J-II	13.1	*0.5*	3.7	*0.2*	1.19	*0.05*	4.0	*0.2*	4.5	*0.2*	2.6	*0.1*	2.7	*0.1*	0.41	*0.02*	2.0	*0.1*	0.17	*0.01*	3.81	*0.16*	0.84	*0.03*	0.20	*0.01*
	K-II	16.4	*0.6*	4.7	*0.2*	1.46	*0.07*	4.9	*0.2*	5.1	*0.2*	3.3	*0.2*	3.2	*0.2*	0.42	*0.02*	2.4	*0.1*	0.18	*0.01*	4.90	*0.23*	1.34	*0.05*	0.37	*0.02*
	Q-I	14.0	*0.5*	3.7	*0.2*	1.23	*0.06*	4.5	*0.2*	4.7	*0.2*	3.2	*0.2*	3.3	*0.2*	0.52	*0.03*	2.1	*0.1*	0.17	*0.02*	4.10	*0.19*	0.85	*0.04*	0.19	*0.02*
	U-VI	15.0	*0.6*	4.1	*0.2*	1.36	*0.07*	4.7	*0.3*	5.0	*0.2*	2.9	*0.2*	2.9	*0.2*	0.45	*0.03*	2.3	*0.1*	0.17	*0.02*	5.08	*0.23*	1.20	*0.05*	0.32	*0.02*
	Z-I	18.2	*0.7*	4.6	*0.2*	1.36	*0.06*	5.0	*0.3*	5.7	*0.2*	3.3	*0.2*	3.4	*0.2*	0.53	*0.03*	2.9	*0.1*	0.20	*0.02*	5.77	*0.25*	1.50	*0.06*	0.40	*0.02*
FKONON	A-I	17.6	*0.7*	4.1	*0.2*	1.43	*0.06*	4.0	*0.2*	4.3	*0.2*	2.4	*0.1*	2.2	*0.1*	0.33	*0.02*	2.4	*0.1*	1.31	*0.06*	1.70	*0.09*	2.55	*0.10*	0.50	*0.03*
	B-I	19.9	*1.3*	6.0	*0.7*	1.66	*0.21*	4.7	*0.7*	4.5	*0.5*	2.9	*0.4*	2.3	*0.5*	0.32	*0.07*	2.2	*0.4*	1.45	*0.15*	2.27	*0.30*	2.28	*0.19*	0.46	*0.08*
	D-I	19.5	*0.9*	4.4	*0.4*	1.75	*0.11*	4.9	*0.4*	5.1	*0.3*	2.4	*0.2*	1.9	*0.2*	0.28	*0.04*	3.1	*0.2*	1.39	*0.08*	2.22	*0.15*	2.76	*0.13*	0.65	*0.05*
	D-II	24.4	*1.1*	5.7	*0.3*	1.75	*0.10*	4.6	*0.3*	4.5	*0.3*	2.8	*0.2*	2.5	*0.2*	0.38	*0.03*	2.6	*0.2*	1.58	*0.08*	3.51	*0.19*	3.36	*0.14*	0.69	*0.05*
	F-I	19.2	*0.9*	4.6	*0.4*	1.68	*0.11*	5.0	*0.4*	4.9	*0.3*	2.5	*0.2*	2.6	*0.3*	0.31	*0.04*	2.8	*0.2*	1.52	*0.09*	2.37	*0.16*	2.32	*0.12*	0.58	*0.05*
	I-I	15.8	*0.7*	3.4	*0.2*	1.46	*0.08*	3.8	*0.3*	3.8	*0.2*	2.0	*0.1*	1.9	*0.2*	0.29	*0.03*	2.4	*0.1*	1.14	*0.06*	1.93	*0.12*	2.22	*0.10*	0.44	*0.03*
	K-I	16.3	*1.0*	4.3	*0.5*	1.49	*0.16*	3.2	*0.5*	4.4	*0.5*	2.8	*0.3*	2.4	*0.4*	0.36	*0.06*	2.0	*0.3*	1.49	*0.13*	2.78	*0.28*	2.39	*0.17*	0.37	*0.06*
	K-II	16.4	*0.8*	4.2	*0.3*	1.66	*0.11*	4.6	*0.4*	3.7	*0.3*	2.8	*0.2*	1.8	*0.2*	0.30	*0.04*	2.5	*0.2*	1.38	*0.08*	2.54	*0.17*	2.21	*0.11*	0.47	*0.04*
	N-I	17.2	*0.6*	4.0	*0.2*	1.52	*0.07*	4.0	*0.2*	4.2	*0.2*	2.3	*0.1*	2.0	*0.1*	0.30	*0.02*	2.4	*0.1*	1.45	*0.06*	2.10	*0.11*	2.58	*0.10*	0.55	*0.03*
	N-II	19.4	*1.5*	4.5	*0.9*	0.98	*0.19*	–	–	6.1	*0.8*	1.6	*0.5*	3.6	*0.7*	0.26	*0.10*	2.2	*0.5*	1.42	*0.22*	3.89	*0.46*	3.62	*0.27*	0.62	*0.11*
	O-I	18.6	*0.7*	4.6	*0.2*	1.56	*0.07*	4.7	*0.2*	4.3	*0.2*	2.5	*0.1*	2.1	*0.1*	0.31	*0.02*	2.7	*0.1*	1.46	*0.06*	1.93	*0.10*	2.57	*0.10*	0.52	*0.03*
	O-II	16.8	*0.7*	4.2	*0.2*	1.51	*0.07*	4.0	*0.2*	4.0	*0.2*	2.3	*0.1*	1.9	*0.1*	0.29	*0.02*	2.6	*0.1*	1.23	*0.06*	1.81	*0.10*	2.37	*0.10*	0.48	*0.03*
	P-II	17.7	*0.8*	4.3	*0.2*	1.57	*0.08*	4.2	*0.2*	4.0	*0.2*	2.4	*0.1*	2.0	*0.1*	0.30	*0.02*	2.4	*0.1*	1.30	*0.06*	1.99	*0.11*	2.45	*0.10*	0.53	*0.03*

Table B6. Calculated CO_2 concentration in bubble and parameters used to calculation.

Sample ID	Melt ID	T_{glass}[a] (°C)	V_limit[b] (vol.%)	P_{int}[c] (kbar)	ρ_m[d] (gm/cc)	$\rho_{H2O-CO2}$[e] (gm/cc)	xCO_2 vapor[f] (wt.%)	CO_2 in bubble (ppm)
ON2S	AMa-I	597	-	-	-	-	-	-
	AP-IV	592	-	-	-	-	-	-
	BEc-III	595	-	-	-	-	-	-
	CSa-III	590	7.93	0.052	2.899	0.023	70.5	291
	DF-IV	596	-	-	-	-	-	-
	DL-I	593	-	-	-	-	-	-
	DS-III	594	-	-	-	-	-	-
	DZ-I	600	-	-	-	-	-	-
	EDa-I	576	-	-	-	-	-	-
	U-I	653	3.62	0.012	2.561	0.003	27.9	5
	Z-I	588	7.06	0.261	2.883	0.142	93.6	2078
YF1L	AFa-III	648	6.18	0.005	2.934	0.003	99.8	92
	AFb-I	638	7.05	0.004	2.937	0.002	97.8	70
	AH-I	569	7.05	0.222	2.845	0.118	88.9	2578
	AZ-I	605	-	-	-	-	-	-
	AZ-III	631	6.81	0.153	2.928	0.087	99.7	1673
	BD-I	603	7.29	0.347	2.916	0.191	98.5	3899
	BK-II	607	7.45	0.225	2.944	0.127	98.6	2724
	BLa-II	629	6.99	0.071	2.961	0.041	99.5	442
	BLa-III	630	7.04	0.005	2.980	0.003	94.0	25
	BM-I	581	7.73	0.492	2.909	0.264	97.0	6265
	BO-I	616	7.17	0.124	2.938	0.071	98.6	1074
	BQ-I	599	8.23	0.013	2.932	0.005	46.1	54
	BQ-II	598	-	-	-	-	-	-
	BQ-III	639	6.95	0.099	2.966	0.056	100.0	729
	BSb-III	606	-	-	-	-	-	-
	BSc-II	622	7.66	0.118	2.950	0.068	99.5	1337
	F-I	602	8.06	0.245	2.937	0.138	98.3	892
	F-II	593	7.58	0.456	2.938	0.246	98.2	4591
KJ5S	AD-V	438	5.48	7.470	2.723	0.990	4.0	498
	AE-I	432	5.24	7.607	2.702	0.996	3.7	364
	AE-II	437	5.59	7.756	2.723	0.999	4.6	280
	AF-I	435	5.32	7.569	2.709	0.997	5.5	721
	AGa-I	434	5.48	7.718	2.715	1.001	5.4	258
	AGb-IV	431	5.41	7.555	2.704	0.998	4.9	450
	AGb-V	436	5.10	7.422	2.697	0.994	6.4	866
	AI-I	440	5.22	7.506	2.712	0.991	4.6	1093
	AK-I	438	5.29	7.712	2.722	1.000	6.0	648
	AK-II	439	-	-	-	-	-	-
	B-I	431	5.38	7.883	2.715	1.005	4.5	430
	K-I	436	5.37	7.810	2.717	1.000	4.3	737
	L-I	433	5.27	7.984	2.713	1.011	6.6	683
	S-III	436	5.30	7.724	2.712	1.000	5.4	524
	U-I	434	5.12	7.474	2.697	0.997	6.7	308
	V-I	435	4.93	6.914	2.671	0.975	2.8	80
	Y-I	440	5.69	7.159	2.720	0.979	3.0	326
	Y-II	434	5.70	7.774	2.732	0.998	3.4	340
KSS	AA-I	487	5.44	2.028	2.682	0.697	14.2	1610

Table B6. (continued)

Sample ID	Melt ID	T_{glass}[a] (˚C)	V_limit[b] (vol.%)	P_{int}[c] (kbar)	ρ_m[d] (gm/cc)	$\rho_{H2O-CO2}$[e] (gm/cc)	xCO_2 vapor[f] (wt.%)	CO_2 in bubble (ppm)
	AA-II	487	5.11	0.761	2.602	0.412	28.5	1071
	AA-III	486	5.18	1.932	2.667	0.705	12.8	1214
	AB-I	497	5.03	1.724	2.672	0.654	52.0	5306
	D-I	477	5.60	2.611	2.699	0.766	11.7	929
	E-I	470	-	-	-	-	-	-
	E-II	468	4.26	1.619	2.574	0.677	32.8	45
	G-I	478	4.82	1.548	2.627	0.663	18.2	1922
	G-II	476	4.75	1.148	2.596	0.598	9.6	369
	G-III	483	-	-	-	-	-	-
	H-I	471	4.48	2.038	2.605	0.715	56.2	1997
	K-II	484	5.38	2.991	2.690	0.795	24.4	1179
	L-I	481	5.47	2.990	2.685	0.794	19.3	772
	W-I	485	4.74	0.678	2.601	0.386	19.7	143
KROHTH	A-I	465	4.83	3.171	2.596	0.813	4.1	178
	A-II	463	4.92	3.564	2.612	0.837	5.1	82
	E-I	459	4.84	4.138	2.637	0.866	3.7	2
	E-II	460	4.83	4.000	2.627	0.859	3.6	Rejected[g]
	E-III	472	4.71	1.857	2.600	0.710	8.7	585
	F-I	458	5.03	3.902	2.647	0.855	2.7	62
	G-I	460	4.95	3.880	2.632	0.855	5.1	Rejected[g]
	H-I	458	4.80	3.544	2.620	0.838	3.0	1
	I-I	460	4.78	3.686	2.622	0.844	3.7	Rejected[g]
	K-I	462	4.58	2.862	2.600	0.795	0.3	1
	L-II	460	4.96	3.578	2.630	0.838	2.5	Rejected[g]
KRSM11	A-I	434	4.93	7.367	2.680	0.992	5.3	262
	A-II	437	5.04	7.329	2.688	0.989	5.2	323
	A-III	438	4.85	6.954	2.669	0.981	6.5	354
	B-I	437	4.93	7.584	2.681	0.998	6.0	173
	C-I	438	4.70	6.820	2.658	0.976	5.9	178
	D-I	444	5.03	6.838	2.686	0.969	3.9	247
	D-II	446	4.85	6.260	2.653	0.955	5.7	105
	E-I	437	5.03	7.586	2.687	0.998	6.1	162
	E-II	439	5.06	7.477	2.687	0.994	6.5	236
	G-I	438	4.94	7.423	2.677	0.996	7.7	2243
	H-I	443	4.93	6.390	2.665	0.958	4.6	167
	K-V	447	5.10	6.793	2.678	0.969	5.3	142
	L-I	440	5.00	6.891	2.677	0.975	4.6	179
	L-II	432	-	-	-	-	-	-
	L-III	441	4.89	6.929	2.675	0.974	4.2	283
	L-IV	436	5.19	7.580	2.693	0.997	5.4	Rejected[g]
SM1S	AA-I	553	5.61	2.645	2.828	0.792	94.9	Rejected[g]
	AE-I	561	5.05	0.527	2.723	0.272	90.5	3204
	AJ-I	579	5.66	3.599	2.849	0.898	98.3	41740
	AL-II	535	5.75	1.793	2.809	0.662	90.9	21499
	AM-II	568	-	-	-	-	-	-
	AR-VI	564	-	-	-	-	-	-
	BA-I	594	5.49	1.352	2.838	0.551	98.4	Rejected[g]
	BC-I	621	5.16	1.658	2.833	0.609	99.5	12225

Table B6. (continued)

Sample ID	Melt ID	T_{glass}[a] (˚C)	V_limit[b] (vol.%)	P_{int}[c] (kbar)	ρ_m[d] (gm/cc)	$\rho_{H2O-CO2}$[e] (gm/cc)	xCO_2 vapor[f] (wt.%)	CO_2 in bubble (ppm)
	S-II	523	6.09	0.847	2.779	0.402	79.3	Rejected[g]
	S-III	564	-	-	-	-	-	-
	T-II	615	5.26	1.463	2.851	0.569	99.4	10859
	Y-I	571	-	-	-	-	-	-
	Y-IV	600	5.13	2.725	2.849	0.790	99.2	7220
	Z-I	570	-	-	-	-	-	-
KM1S12a	A-I	426	5.34	9.443	2.735	1.038	2.3	197
	AE-I	445	5.48	8.347	2.745	1.012	5.8	655
	AE-II	440	-	-	-	-	-	-
	AE-III	441	5.27	8.459	2.735	1.014	4.6	346
	AF-I	429	5.43	9.055	2.720	1.027	1.6	390
	AH-II	437	5.05	7.701	2.678	0.997	4.6	493
	AJ-I	423	5.63	10.106	2.753	1.051	1.6	39
	J-I	430	5.94	9.827	2.762	1.048	4.1	325
	J-II	441	5.48	-	-	-	-	-
	K-II	430	5.30	8.528	2.709	1.014	1.3	171
	O-I	419	-	-	-	-	-	-
	Q-I	449	5.00	6.631	2.682	0.960	3.4	154
	U-VI	442	4.93	7.332	2.677	0.980	1.7	158
	Z-I	443	4.77	6.459	2.653	0.956	2.0	168
	Z-II	423	-	-	-	-	-	-
FKONON	A-I	516	5.49	6.603	2.802	1.115	90.2	Rejected[g]
	B-I	512	5.49	4.326	2.744	0.972	87.4	1279
	D-I	516	5.51	5.633	2.788	1.067	91.0	Rejected[g]
	D-II	512	6.12	5.098	2.785	1.040	92.4	8182
	F-I	520	5.10	6.050	2.797	1.088	91.2	7683
	I-I	524	5.24	6.141	2.815	1.096	93.1	9810
	K-I	521	5.47	6.135	2.809	1.094	92.0	5141
	K-II	521	5.44	6.143	2.802	1.095	92.1	4457
	N-I	516	5.27	6.544	2.807	1.117	91.6	6139
	N-II	527	-	-	-	-	-	-
	O-I	526	5.28	6.098	2.810	1.093	93.5	5750
	O-II	526	-	-	-	-	-	-
	P-II	524	5.33	6.097	2.808	1.093	93.0	7233

[a] Glass transition temperature estimated using measured MI composition and the equation of Giordano et al. (2008).

[b] Upper limit of bubble volume. Expected bubble volume based on the empirical thermal expansion of host-olivine and silicate melt simulated for post-entrapment cooling down to the glass transition temperature (ΔT = Ttrap - Tglass) using the calculator of Moore et al. (2015). Bubbles larger than this upper limit were excluded from this bubble CO_2 estimation.

[c] Internal pressure of MI at glass transition temperature based on the measured melt H_2O and CO_2 concentrations.

[d] Volumetric melt density at glass transition temperature computed using RhyoliteMELTS ver. 1.2.0 (Ghiorso and Sack, 1995; Gualda et al., 2012; Ghiorso and Gualda, 2015).

[e] Volumetric density of mixed H_2O-CO_2 fluid at glass transition temperature based on the high-pressure equation of state (Duan and Zhang, 2006).

[f] Weight fraction of CO_2 in vapor fluid calculated based on the solubility model using RhyoliteMELTS.

[g] MIs were excluded from this calculation due to the large bubble volume greater than the upper limit.

Table B7. Host olivine compositions

Sample ID	Host ID	SiO_2 (wt. %)	TiO_2	Al_2O_3	Cr_2O_3	FeO	MnO	MgO	CaO	NiO	Total	Fo content
ON2S	AMa	40.2	0.00	0.04	0.07	16.3	0.17	43.5	0.16	0.23	100.6	82.7
	AP	39.5	0.01	0.02	0.00	17.0	0.20	42.9	0.15	0.18	99.9	81.8
	BEc	39.5	0.09	0.04	0.08	17.5	0.18	42.8	0.16	0.18	100.5	81.4
	CSa	39.8	0.01	0.02	0.06	17.1	0.22	42.9	0.14	0.10	100.3	81.7
	DF	40.3	0.05	0.03	0.00	17.2	0.24	43.0	0.16	0.10	101.1	81.7
	DL	39.5	0.03	0.04	0.04	16.2	0.25	43.5	0.14	0.24	99.9	82.7
	DS	40.1	0.02	0.04	0.00	17.0	0.18	43.0	0.15	0.19	100.6	81.9
	DZ	40.0	0.02	0.04	0.11	16.6	0.21	43.3	0.15	0.20	100.6	82.4
	EDa	39.9	0.05	0.04	0.00	16.8	0.18	43.4	0.14	0.21	100.7	82.1
	U	39.8	0.00	0.02	0.05	17.2	0.17	42.8	0.15	0.23	100.4	81.6
	Z	40.1	0.00	0.03	0.05	15.9	0.23	43.7	0.15	0.22	100.4	83.1
	BFa	-	-	-	-	-	-	-	-	-	-	-
YF1L	AFa	39.4	0.00	0.01	0.04	17.6	0.28	42.8	0.13	0.02	100.3	81.2
	AFb	39.9	0.01	0.02	0.04	17.4	0.23	42.8	0.12	0.03	100.5	81.4
	AH	39.8	0.02	0.02	0.02	17.5	0.18	42.7	0.13	0.05	100.4	81.3
	AZ	39.9	0.03	0.01	0.00	17.7	0.24	42.7	0.14	0.05	100.8	81.1
	BD	40.0	0.00	0.01	0.02	17.6	0.25	43.0	0.13	0.05	101.1	81.3
	BK	39.7	0.00	0.01	0.00	18.0	0.28	42.4	0.13	0.00	100.6	80.7
	BLa	39.7	0.04	0.03	0.00	17.9	0.28	42.4	0.13	0.05	100.5	80.8
	BM	39.8	0.03	0.00	0.02	17.3	0.25	43.0	0.11	0.06	100.5	81.6
	BO	39.7	0.07	0.01	0.02	18.1	0.25	42.1	0.14	0.06	100.5	80.6
	BQ	39.7	0.02	0.01	0.02	17.8	0.24	42.4	0.14	0.02	100.4	80.9
	BSb	39.5	0.04	0.02	0.00	17.7	0.25	42.5	0.14	0.01	100.2	81.0
	BSc	39.5	0.04	0.02	0.00	17.7	0.25	42.5	0.14	0.01	100.2	81.0
	F	39.7	0.02	0.02	0.00	17.7	0.25	42.7	0.14	0.10	100.6	81.1
KJ5S	AD	38.6	0.00	0.01	0.00	24.0	0.42	37.4	0.12	0.00	100.5	73.6
	AE	38.7	0.00	0.01	0.00	23.7	0.42	37.5	0.12	0.01	100.4	73.8
	AF	38.5	0.04	0.03	0.00	24.3	0.36	37.3	0.12	0.00	100.7	73.3
	AGa	38.6	0.05	0.02	0.04	23.9	0.47	37.5	0.13	0.05	100.8	73.6
	AGb	38.9	0.03	0.01	0.00	24.3	0.44	37.7	0.12	0.01	101.5	73.5
	AI	38.6	0.02	0.02	0.00	23.9	0.46	37.5	0.11	0.00	100.5	73.7
	AK	38.3	0.02	0.02	0.00	23.8	0.40	37.7	0.13	0.02	100.4	73.8
	B	38.8	0.06	0.02	0.01	24.3	0.44	37.4	0.12	0.04	101.2	73.3
	K	38.5	0.00	0.03	0.06	23.9	0.42	37.5	0.12	0.02	100.5	73.7
	L	38.2	0.00	0.02	0.00	24.3	0.41	37.2	0.12	0.02	100.3	73.2
	S	38.4	0.01	0.02	0.00	24.2	0.42	37.5	0.12	0.00	100.7	73.4
	U	38.5	0.00	0.01	0.00	23.9	0.45	37.4	0.13	0.03	100.5	73.6
	V	38.1	0.02	0.02	0.00	24.3	0.37	37.0	0.11	0.01	100.0	73.1
	Y	38.6	0.02	0.02	0.00	23.9	0.48	37.5	0.12	0.05	100.7	73.6
KSS	AA	39.3	0.00	0.03	0.03	21.2	0.37	39.7	0.17	0.08	100.9	76.9
	AB	39.6	0.00	0.02	0.00	19.0	0.29	41.5	0.16	0.09	100.7	79.5
	D	38.4	0.01	0.01	0.02	24.0	0.41	37.0	0.19	0.07	100.0	73.3
	E	37.1	0.01	0.02	0.05	30.2	0.60	31.7	0.24	0.09	100.0	65.2
	G	38.3	0.02	0.02	0.00	25.3	0.46	36.1	0.25	0.09	100.5	71.8
	H	37.2	0.00	0.02	0.00	30.4	0.51	32.3	0.24	0.00	100.7	65.5
	K	39.4	0.00	0.03	0.02	19.6	0.36	41.2	0.18	0.08	100.9	78.9
	L	39.7	0.00	0.03	0.00	18.9	0.29	41.5	0.18	0.06	100.7	79.7
	W	38.1	0.02	0.01	0.01	26.5	0.48	35.4	0.21	0.13	100.9	70.4
KROHTH	A	38.4	0.04	0.02	0.06	24.6	0.50	37.3	0.16	0.06	101.2	73.0
	E	38.7	0.00	0.02	0.04	24.3	0.35	37.2	0.16	0.02	100.8	73.2
	F	38.3	0.00	0.03	0.05	24.7	0.44	37.3	0.16	0.01	101.1	72.9

Table B7. (continued)

Sample ID	Host ID	SiO_2 (wt. %)	TiO_2	Al_2O_3	Cr_2O_3	FeO	MnO	MgO	CaO	NiO	Total	Fo content
	G	38.1	0.04	0.02	0.00	24.4	0.40	37.2	0.16	0.03	100.4	73.1
	H	38.4	0.02	0.03	0.03	24.4	0.44	37.0	0.17	0.01	100.5	73.0
	I	38.4	0.00	0.02	0.02	24.4	0.41	37.3	0.17	0.07	100.7	73.2
	K	38.4	0.00	0.02	0.02	24.6	0.39	37.0	0.17	0.01	100.6	72.9
	L	38.6	0.03	0.04	0.02	24.3	0.42	36.9	0.17	0.04	100.5	73.0
KRSM11	A	38.8	0.01	0.03	0.01	23.3	0.35	37.9	0.14	0.08	100.6	74.3
	B	38.8	0.06	0.01	0.02	23.3	0.37	38.4	0.13	0.05	101.0	74.6
	C	38.8	0.00	0.03	0.01	23.7	0.34	38.2	0.13	0.05	101.2	74.2
	D	38.9	0.01	0.03	0.00	23.1	0.34	38.0	0.12	0.06	100.5	74.6
	E	39.0	0.01	0.03	0.00	23.7	0.36	38.6	0.13	0.07	101.9	74.4
	G	39.3	0.01	0.02	0.00	23.2	0.36	38.4	0.13	0.09	101.5	74.6
	H	38.8	0.08	0.03	0.00	23.0	0.35	38.5	0.15	0.04	101.0	74.9
	K	39.1	0.02	0.02	0.00	22.5	0.36	38.4	0.13	0.05	100.7	75.2
	L	38.7	0.02	0.01	0.06	23.4	0.41	38.1	0.13	0.05	100.9	74.4
SM1S	AA	39.7	0.00	0.02	0.01	19.5	0.28	41.0	0.21	0.01	100.7	78.9
	AE	39.5	0.01	0.02	0.00	19.1	0.34	41.7	0.16	0.06	100.9	79.5
	AJ	39.2	0.00	0.02	0.00	19.6	0.28	41.4	0.19	0.07	100.7	79.0
	AL	39.5	0.00	0.04	0.03	19.8	0.31	40.8	0.19	0.06	100.7	78.6
	AM	38.7	0.04	0.03	0.00	23.2	0.36	37.9	0.20	0.00	100.4	74.5
	AR	39.8	0.00	0.04	0.00	19.9	0.31	41.1	0.17	0.00	101.4	78.6
	BA	39.4	0.01	0.02	0.00	20.1	0.35	40.8	0.19	0.05	100.9	78.4
	BC	39.6	0.00	0.04	0.01	18.8	0.32	41.8	0.19	0.04	100.8	79.9
	S	39.1	0.00	0.03	0.06	22.5	0.38	38.7	0.18	0.00	101.0	75.4
	T	39.5	0.01	0.02	0.00	19.6	0.27	41.4	0.20	0.05	101.1	79.0
	Y	39.6	0.04	0.03	0.00	18.9	0.27	41.9	0.20	0.07	101.1	79.8
	Z	40.0	0.03	0.03	0.01	17.8	0.24	42.7	0.21	0.05	101.2	81.1
KM1S12a	A	38.2	0.00	0.02	0.04	25.2	0.49	36.7	0.14	0.00	100.7	72.2
	AE	38.2	0.01	0.02	0.00	25.0	0.46	36.4	0.13	0.00	100.3	72.2
	AF	38.5	0.00	0.02	0.00	23.9	0.38	37.8	0.12	0.05	100.8	73.8
	AH	38.4	0.05	0.03	0.00	24.8	0.48	36.6	0.13	0.02	100.5	72.5
	AJ	38.3	0.00	0.00	0.06	25.2	0.49	36.3	0.15	0.01	100.5	72.0
	J	38.1	0.01	0.02	0.00	24.7	0.52	36.8	0.11	0.00	100.2	72.7
	K	38.2	0.00	0.03	0.04	25.3	0.47	36.5	0.12	0.07	100.6	72.0
	O	38.2	0.01	0.02	0.00	26.2	0.58	36.4	0.13	0.00	101.6	71.3
	Q	37.5	0.00	0.04	0.00	25.5	0.50	36.2	0.15	0.04	100.0	71.7
	U	38.0	0.01	0.01	0.01	24.9	0.52	36.7	0.13	0.00	100.4	72.4
	Z	38.6	0.01	0.02	0.00	25.8	0.53	36.1	0.13	0.02	101.2	71.4
FKONON	A	40.1	0.00	0.07	0.00	16.1	0.23	43.6	0.20	0.18	100.5	82.8
	B	39.8	0.00	0.05	0.00	16.4	0.18	43.4	0.21	0.14	100.2	82.6
	D	39.7	0.02	0.05	0.03	16.9	0.23	43.4	0.20	0.17	100.8	82.1
	F	39.3	0.00	0.05	0.01	19.7	0.22	41.1	0.19	0.11	100.6	78.8
	I	39.1	0.04	0.06	0.03	19.9	0.27	40.7	0.20	0.13	100.5	78.5
	K	40.0	0.00	0.05	0.00	16.4	0.23	43.2	0.20	0.19	100.2	82.4
	N	39.7	0.00	0.07	0.00	18.0	0.26	42.0	0.21	0.23	100.5	80.6
	O	39.8	0.02	0.07	0.01	17.0	0.22	43.0	0.19	0.14	100.6	81.8
	P	39.6	0.04	0.06	0.00	17.5	0.25	42.9	0.20	0.10	100.7	81.3
Replesentative 1 s.d.		0.6	0.08	0.01	0.05	0.6	0.10	0.4	0.02	0.10	-	1.3

Table B8. Model parameters and estimated slab melt/fluid composition

	Source material		Estimated slab component				Bulk partition coefficient
	Bulk SED[a]	AOC[b]	SED fluid/melt[c]		AOC fluid/melt[c]	AOC fluid[d]	$D_{(AOC/fluid)}$[e]
Pressure (GPa)			3	4.2	4.2	4	
Fluid or melt Fraction			16%	14%	10%	5%[d]	
Li (ppm)	49.5	24.4				23.24	1.053
Rb	140.9	7.43	22.9	23.0	17.0	109	0.019
Sr	165	168	397	446	2768	305	0.526
Y	36.8	29.3	2.2	3.3	1.5	0.28	111.1
Zr	150	95.1	66	93	52	3.90	25.64
Nb	14.31	3.20	9.37	10.48	6.71	0.60	5.556
Ba	540	16.9	3121	2677	395	145	0.070
La	34.7	3.66	27.8	28.1	21.9	3.87	0.943
Ce	74.9	11.5	69.1	70.2	73.5	6.47	1.818
Pr	8.50	1.98	591	621	5.61		
Nd	30.9	10.5	16.4	17.8	18.9	1.60	6.849
Sm	5.62	3.28	1.81	2.20	1.83	0.22	15.38
Eu	1.23	1.19	0.31	0.39	0.45	0.06	20.83
Gd	5.13	4.29	0.86	1.13	0.90	0.14	33.33
Dy	3.80	5.00	0.31	0.44	0.39	0.05	100
Er	1.75	3.02				0.02	200
Yb	1.60	2.94	0.056	0.085	0.081	0.01	250
Lu	0.25	0.444	0.009	0.013	0.013	0.00	200
Hf	4.29	2.13	2.39	3.10	1.77	0.11	20.0
Ta	1.008	0.214	0.716	1.033	0.237	0.01	21.28
Pb	33.4	0.829	101	94.0	14.89	8.29	0.053
Th	14.2	0.197	26.2	26.3	1.6	0.09	2.273
U	0.99	0.214	1.45	1.65	0.74	0.22	0.980

[a] Composition of bulk sediment at ODP site 808 (Nankai trough) from Plank (2014).

[b] Composition of altered oceanic crust at DSDP site 442B (in Shikoku Basin) from Shu et al. (2017).

[c] Estimated using Arc Basalt Simulator (ABS5, Kimura, 2017).

[d] Estimeted composition of 5% fluid in equilibirum with AOC.

[e] AOC/fluid partition coefficients at 800 ˚C (4 GPa) with residual rutile from Kessel et al. (2005).

B9. Supplementary discussion

Heating experiment

All crystallized MIs of YF1L and ON2S were homogenized using a Vernadsky-type microscope heating stage following the procedure described by Le Voyer et al. (2010). Olivine surfaces were roughly polished (without exposing the MI) to observe the MI inside before homogenization. During the experiments, the oxygen fugacity was kept to reduced condition less than 10^{-19} atm with He gas purified by Zr at 650 ˚C, to avoid sample oxidation and to ensure an efficient quench. We measured the temperature inside the furnace using a Pt-Pt_{90}-Rh_{10} thermocouple welded to the sample holder and calibrated using Au as temperature standard (melting temperature at 1064 ˚C). Temperature increase was set at ~90 ˚C/min until ~920 ˚C, then reduced to ~30 ˚C/min until the last crystal disappeared. Total duration of one heating experiment was less than 30 minutes. The temperature required to homogenize the MI varied from 1268 to 1385 ˚C in this study. Given a 50 μm radius MI and 250 – 500 μm radius olivine, the expected water loss is negligible at these temperatures, even with the smaller increasing rate of 5 ˚C/min (Chen et al., 2011), and because we spent much less than 10 min above 1200 ˚C.

After homogenization, some daughter minerals in MIs of YF1L survived, even at temperatures as high as ~1380 ˚C, while ON2S MIs were mostly homogenized. In addition, bubbles were commonly observed in MIs at high temperature, indicating the difference between the initial trapping pressure and internal pressure of MI, due to the inelastic behavior of the olivine (Schiano and Bourdon, 1999; Le Voyer et al., 2010). In fact, this YF1L sample is a mafic enclave enclosed in a few meters-sized large lava blocks of a pyroclastic flow deposit induced by a gravitational collapse of summit lava (Kobayashi, 1984; Ohta et al., 1990). The slow-cooling history that YF1L magma experienced could have led to a significant diffusive H^+ loss.

Correction of post-entrapment diffusive Fe-loss

We compared uncorrected major element composition of MI with those of whole rock composition (Fig. B9-1), as an examination of possible post-entrapment diffusive Fe-Mg exchange (also named "Fe-loss" e.g. Danyushevsky et al., 2000). All MIs have similar composition to the reported whole rock values, except ON2S and YF1L. The MI from these two samples have less evolved composition and higher FeO^{Total} concentration compared to the whole rock trend, indicating no significant Fe-loss. However, since MIs of both ON2S and YF1L were homogenized by heating experiments, we checked the correlation between olivine-melt equilibrium and evolution of FeO^{Total} and MgO concentrations. Some MIs of KSS show relatively higher FeO^{Total} concentration compared to their whole rock, however, these compositions are similar to that of the glassy groundmass (Kawaguchi et al., 2021). KSS MIs and groundmass also show a decrease in Al_2O_3 concentrations indicating plagioclase crystallization. This is consistent with the abundant plagioclase phenocryst mode reported in KSS-related basalt - basaltic andesite rocks of Aso volcano (e.g., Miyoshi et al., 2005).

Figure B9-2 shows the comparison between the calculated olivine-melt Fe-Mg distribution coefficients $K_D^{Fe\text{-}Mg}$ of MIs and the expected evolution by heating experiment. While overheating of the MI would generate a positive correlation between FeO (or MgO) and $K_D^{Fe\text{-}Mg}$, the measured FeO^{Total} concentration of the YF1L-MI correlates negatively with the calculated $K_D^{Fe\text{-}Mg}$. This negative correlation is attributed to the diffusive Fe-Mg exchange because of the re-equilibration of the melt with its host olivine (Danyushevsky et al., 2000; Rowe et al., 2011). However, the determination of the initial FeO concentration is theoretically impossible. Therefore, MIs having higher $K_D^{Fe\text{-}Mg}$ value than equilibrium $K_D^{Fe\text{-}Mg}$ (Toplis, 2005) were not corrected for neither Fe-Mg exchange nor PEC. Even if the PEC was not corrected, the ratios of incompatible elements for olivine remain primary values. In case of YF1L, only equilibrium MIs in terms of $K_D^{Fe\text{-}Mg}$, which also show high FeO^{Total} concentration,

were used for the discussion using major elements if necessary. As most MIs of other samples have no significant correlation with $K_D^{Fe\text{-}Mg}$, we used their measured compositions for PEC correction.

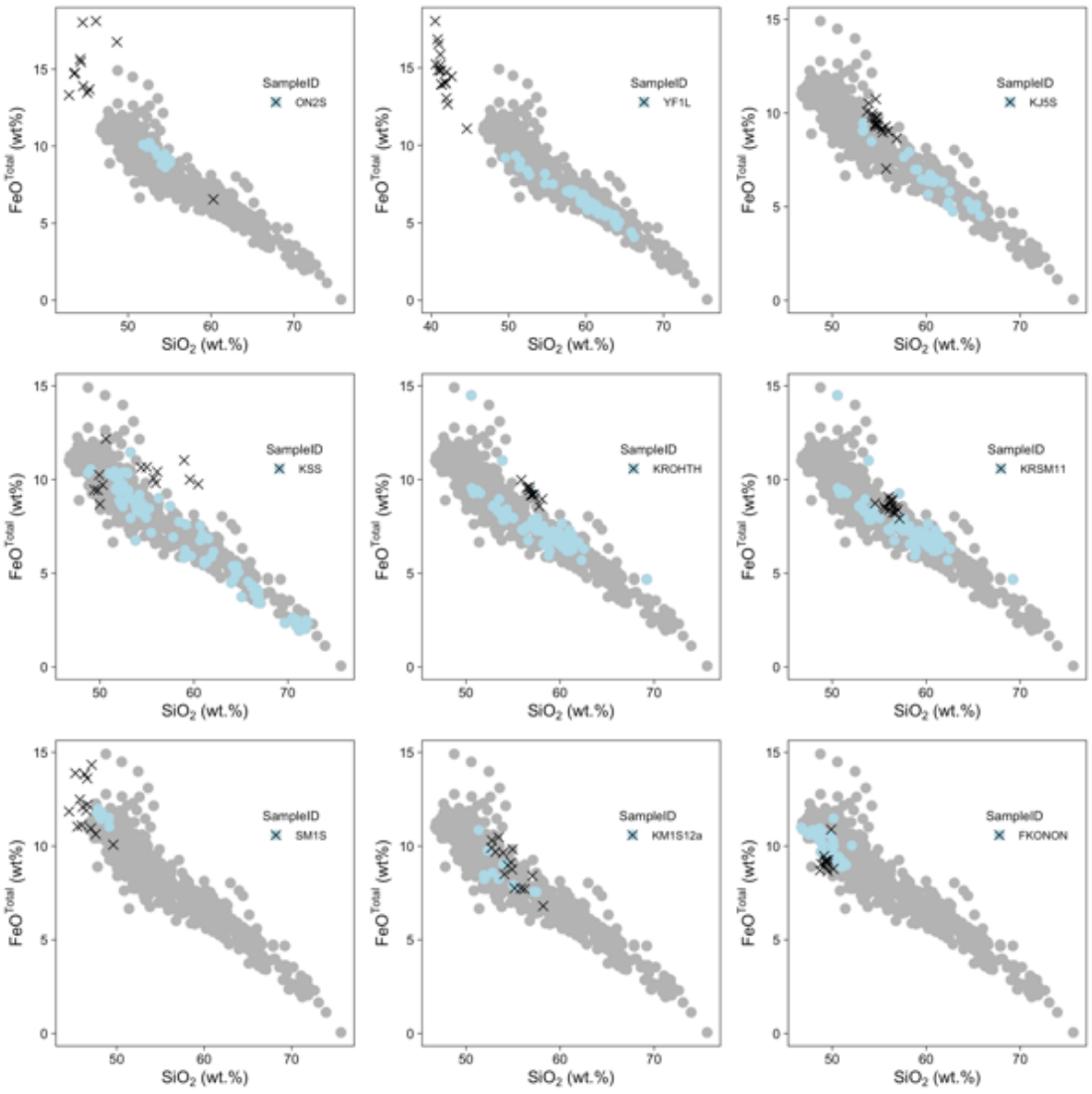

Figure **B9-1.** Variations in SiO_2 and FeO^{Total} concentrations of MI and reported whole rock data. All oxide concentrations are normalized to 100 wt. % on a volatile-free basis. Black cross and light blue solid circles represent MI (this study) and whole rock data (from literatures) of each volcanic group, respectively. Grey solid circle indicates reported whole rock data of volcanic products found in the entire studied area. Whole rock data: Sawamura and Matsui (1957), Shinno (1966), Nakamura (1971), Nakada (1986), Ohta and Aoki (1991), Ohta et al.

(1990, 1992), Imura and Kobayashi (2001), Kawanabe and Sakaguchi (2005), Sugimoto et al. (2006), Miyoshi et al. (2005, 2008a, 2008b, 2010, 2011), Kita et al. (2001, 2012), Hoang et al. (2013), Shibata et al. (2013, 2014), Tajima et al. (2013, 2014), Kawanabe et al. (2015), Yamasaki et al. (2016), Kuritani et al. (2017), Brown et al. (2020), Nche et al. (2021).

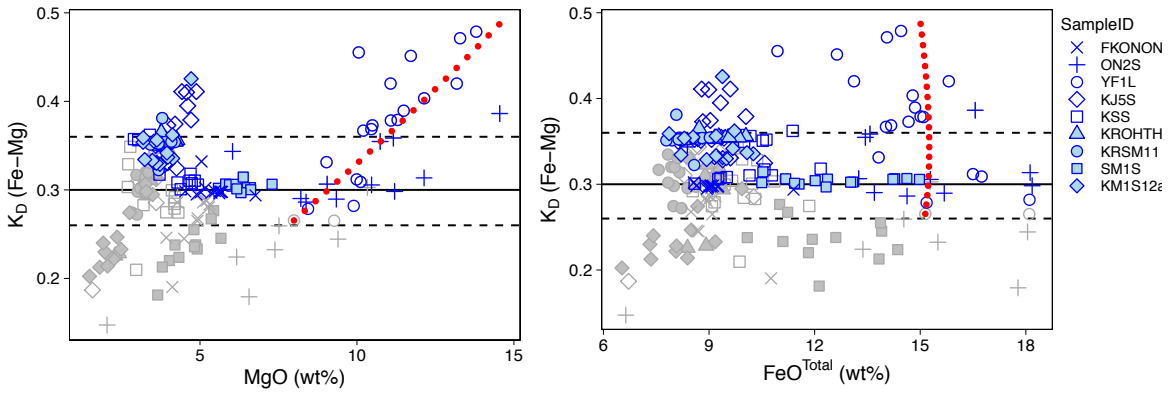

Figure **B9-2.** Calculated olivine-melt Fe-Mg distribution coefficients (K_D) as a function of FeO^{Total} and MgO concentrations in MI. Grey and blue symbols represent PEC-uncorrected and -corrected MI compositions, respectively. Black solid and dashed lines indicate the coefficient of K_D = 0.3 (Roeder and Emslie, 1970) and the range of calculated coefficients from 0.26 to 0.36 for MIs (Toplis, 2005), respectively. Red dotted line demonstrates the effect of overheating for a PEC-uncorrected MI (ID: YF1L-AFa-III). The negative correlation between FeO^{Total} and K_D is characteristic of diffusive Fe-Mg exchange because of host-melt re-equilibration (Danyushevsky et al., 2000; Rowe et al., 2011).

Identification of the primitive melt composition

Magmas erupted through a volcano rarely reflect on the composition corresponding to the condition of melting in the mantle. Olivine-hosted melt inclusions are considered to provide an access to the magmas which experienced minimum crustal modification, and crystallization because olivine is often the first crystal forming at the liquidus of basalts. In this study, we further examine the compositional variation of the melt inclusions with the method of Fourcade and Allegre (1981), and identified the potential mechanism responsible for variation and

identified the most primitive composition of the series. First, plots of Th/Nd vs. Th and Rb/Nd vs. Rb are examined to assess the role of crystal fractionation (Fig. B9-3). Compared to the illustration in the inset (Fig. B9-3a), compositional variation of melt inclusions does not reflect the crystal fractionation (except for Oninomi and evolved Aso magmas). These olivine-hosted melt inclusions therefore satisfy the necessary condition to be considered as the geological material potentially including primitive magma free of crustal modification. Further details of the assessment are explained below for each volcano.

Following the method, the following plots were presented below. Mixing processes produce a hyperbolic curve on C^I versus C^I/C^C plot (red line, plots of the first and third columns of Fig. B9-4) and a linear trend on the companion plot of $1/C^C$ versus C^I/C^C (red line, plots of the second and fourth columns, Fig. B9-4), here the superscript "I" indicates "incompatible element to solid", in which its partition coefficient solid/melt is smaller than the fraction of partial melt. The superscript "C" indicates "compatible element". C is the concentration. On the contrary, partial melting processes generate a straight line on C^I versus C^I/C^C plot (blue line, plots of the first and third columns of Fig. B9-4) and a hyperbolic curve on the companion plot (blue line, plots of the second and fourth columns, Fig. B9-4). Typically, C^I corresponds to the concentration in an incompatible element, such as Rb, Th, Nd and K_2O, and C^C corresponds to the concentration of a compatible element such as Sc, V, Sr and Eu. Then, we identify the most representative melt inclusions of the primary magma for each cone. In conclusion, Yufu, Aso, and Kaimondake record the mixing systematics, and Kuju and Kirishima-OH and -SM show the systematics of partial melting. Variation of Fukue is too small to make any reasonable assessment, and Oninomi is also inconclusive, perhaps somewhat an indication of crystal fractionation (Fig. B9-3). Lastly, Variation of Sumiyoshi-ike composition is complex and further discussion is required. As shown in Fig. B9-4, melt inclusions of Sumiyoshi-ike illustrate curves on both Rb versus Rb/V and the 1/Rb versus Rb/V (or Rb

versus Rb/Sr and 1/Rb versus Rb/Sr). Therefore, this systematic indicates that variations are due to neither the melting of a single source or the mixing of two end members.

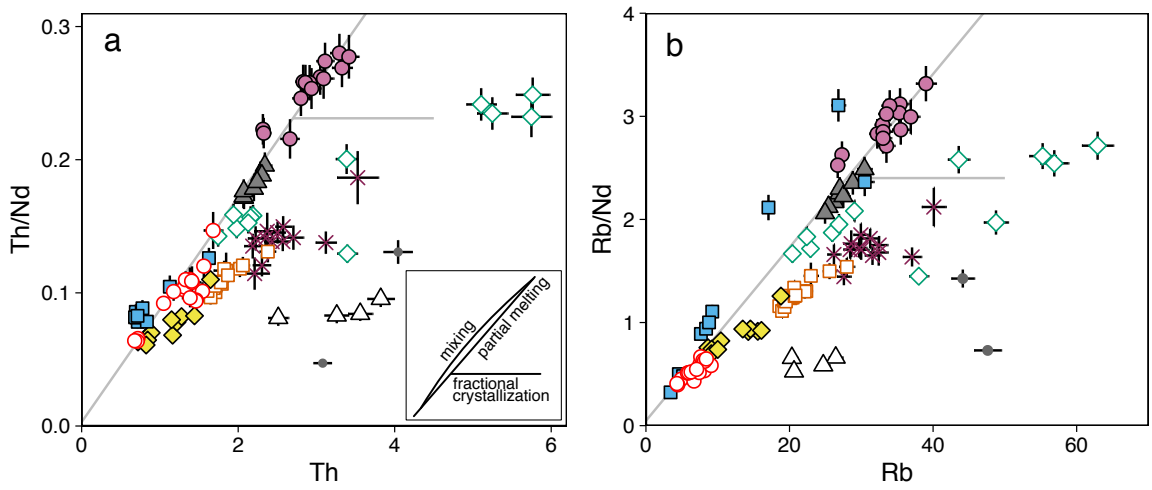

Figure **B9-3.** Variations in selected trace elements ratios and concentrations of melt inclusions. Symbols are the same as in Figure 4.2. Assimilated melt inclusions of Oninomi were plotted as grey dots (see main text for detailed explanations). Error bars are 1 sigma. Grey slope line shows a defined compositional variation array determined only for KROHTH and KRSM11.The significant variation of trace element ratios indicates magma mixing or partial melting has occurred. Theoretical correlation curves during fractional crystallization, partial melting and magma mixing (Schiano et al., 2010) were inserted in panel (a).

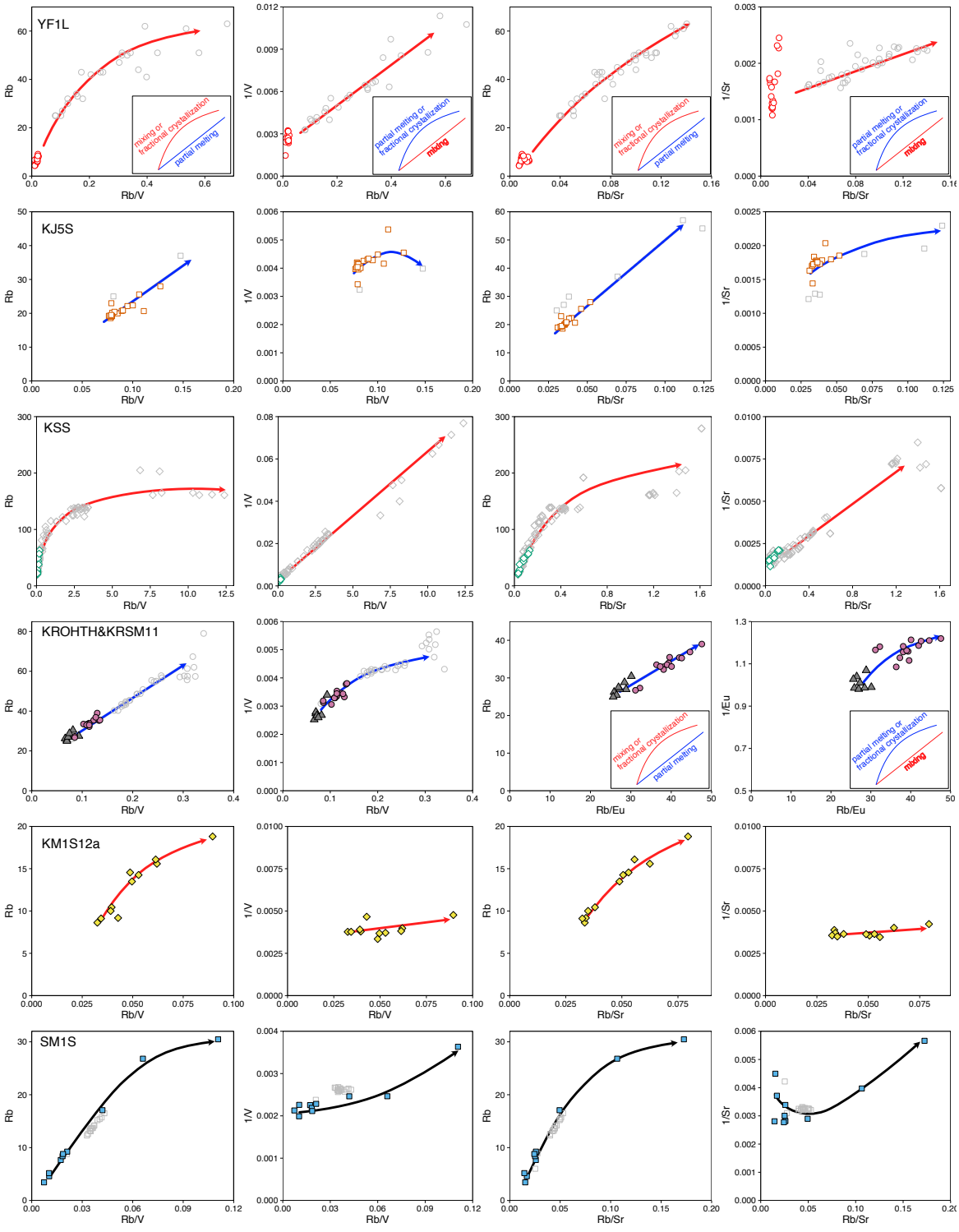

Figure **B9-4.** Variations in selected incompatible and compatible elements ratios of melt inclusions. Reported bulk rock data were shown as grey symbols. Symbols and data source are

the same as in Figure 4.2. In the insert are drawn the theoretical correlation curves during fractional crystallization, partial melting and magma mixing (Schiano et al., 2010) as reference. Red and blue arrows are trends corresponding to mixing and partial melting, respectively. Variations of Sumiyoshi-ike (SM1S) (shown as black arrow) are not possible to explain by neither two-component mixing nor partial melting of a single source.

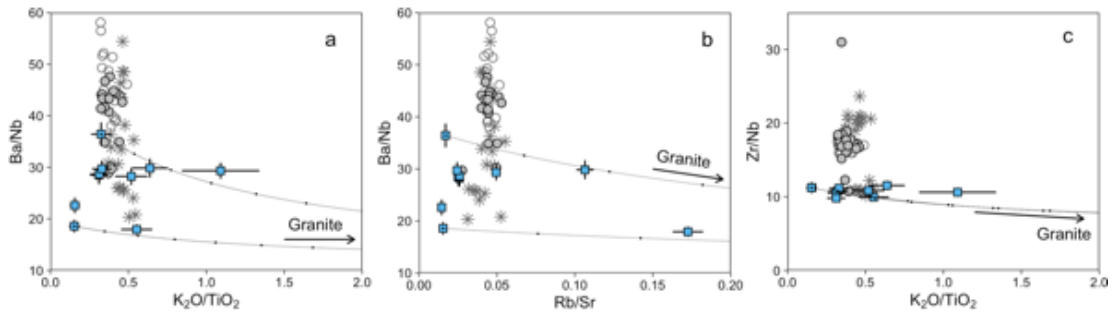

Figure **B9-5.** Variations in incompatible element concentrations of Sumiyoshi-ike (blue square). Reported bulk rock compositions of Sumiyoshi-ike (grey circle), Yonemaru (open circle) and Aojiki (asterisk) are also shown for comparison. Solid lines indicate bulk mixing lines between two representative melts (S-II and AA-1) and a regional granite (average of Takakumayama granite (N=7); Ishihara and Chappell, 2010). Error bar is 1σ. Tick marks on the mixing line is 5% step.

Trace element variation of Sumiyoshi-ike melt inclusions shows a complex process which is neither a simple melting, mixing nor crystal fractionation process (Fig. B9-4). Further examination of the melt inclusions in combination of whole rock basaltic data available for Sumiyoshi-ike and neighboring volcanoes (Yonemaru, 8.1 ka; Aojiki, ~100 ka; Moriwaki et al., 2002; Nagaoka et al., 2001; Nche et al., 2021) illustrate a multistage magmatic evolution. An obvious feature of the whole rock composition trend is a highly variable Ba/Nb for a limited variation of K_2O/TiO_2, Rb/Sr and Zr/Nb to some extent (Fig. B9-5abc). A previous model calculation shows that the magmas here may assimilate up to 7% of lower continental crust, to explain the trace element systematics (Nche et al., 2021). Similarly, reported bulk Pb-isotope composition of Sumiyoshi-ike ($^{208}Pb/^{204}Pb$ = 38.312 - 38.368, $^{207}Pb/^{204}Pb$ = 15.547 - 15.548, $^{206}Pb/^{204}Pb$ = 18.244 - 18.260; Shibata et al., 2013; Brown et al., 2020) represent an intermediate composition between mantle and crustal components (mixture of Shimanto

sedimentary rocks and Takakumayama granite; Brown et al., 2020). A mixing of mantle derived magma with granitic (or sedimentary) crust is an alternative mixing scenario. In either case, the variation of the highly incompatible element ratio is the best explained by a mixing process.

The melt inclusions from Sumiyoshi-ike distribute somewhat differently from the well-defined whole rock trend (Fig. B9-5). The melt inclusions record the variation of K_2O/TiO_2 and Rb/Sr greater than those of the whole rock while the Ba/Nb ratio of melt inclusions are lower than that of the whole rock. This illustrates that the melt inclusions records an additional process prior to the aforementioned mixing process, because olivine-hosted melt inclusions generally trap melts at earlier stages of magma evolution/crystal fractionation. The greater Ba/Nb variation in the whole rock can be interpreted as a consequence of crustal assimilation of Shimanto sedimentary rocks which compose the upper crust (Brown et al., 2020; Nche et al., 2021), and a magma evolution after the melt entrapment in olivine. The prior process is therefore expected to produce the variations of K_2O/TiO_2 and Rb/Sr, as well as limited variation in Ba/Nb. These variations are reproduced by a mixing between a magma, which has low-K_2O/TiO_2 and low-Rb/Sr corresponding to some melt inclusions, and Takakumayama granite, which has K_2O = 4.0 %, TiO_2 = 0.38 %; Rb = 173 ppm; Sr = 175 ppm (Ishihara and Chappell, 2010) suitable for high K_2O/TiO_2 and high-Rb/Sr end member found locally. This mixing scenario is in agreement with the Pb isotope mixing model for the whole rock (Shibata et al., 2013; Brown et al., 2020). Even when assimilation of a mafic lower crust is considered, this granite is a reasonable mixing end member, because a partial melt of a lower crust produces granitic composition (e.g., Qian and Hermann, 2013).

Putting these interpretations together, we think that the melt inclusions of Sumiyoshi-ike captured the early interactions of the primitive magma and the crust. Such interaction was not well-mixed and variable melt compositions are still found in the inclusions. The magma was then stored at depth and eventually well-mixed, erasing the variability of K_2O/TiO_2 and Rb/Sr. Based on this scenario, we attribute K_2O-rich melts of Sumiyoshi-ike inclusions as a signature

of crustal contamination. The melt with low K_2O (and K_2O/TiO_2) therefore most-likely represents the primitive magma before the crustal modification. We chose two primitive magmas for this study, because it was impossible to identify a unique low K_2O end member (Fig. B9-5). Both have low K_2O/TiO_2 and Rb/Sr but with two extreme values of Ba/Nb (for high Ba/Nb, AA-I, and for low Ba/Nb, S-II).

Sulfur isotope fractionation

Our approach is similar to those used in Marini et al. (1994, 1998) and Fiege et al. (2015). Because sulfur species of higher valance tend to be more enriched in the heavier isotope at the equilibrium ($\delta^{34}S_{SO_4} > \delta^{34}S_{SO_2} > \delta^{34}S_{S_2} > \delta^{34}S_{H_2S}$, Ohmoto and Goldhaber, 1997), the effect of sulfur degassing on $\delta^{34}S$ depends on sulfur species in gas phase and melt. In the case of the degassing of magmas, the equilibrium isotope fractionation factor between gas and silicate melt phases, $\alpha_{gas-melt}$, is theoretically explained as

$$
\begin{aligned}
&1000\, ln\, \alpha_{gas-melt} = \delta^{34}S_{gas} - \delta^{34}S_{melt} \\
&= \left[X\delta^{34}S_{SO_2} + (1-X)\delta^{34}S_{H_2S}\right] - \left[Y\delta^{34}S_{S^{2-}} + (1-Y)\delta^{34}S_{SO_4^{2-}}\right] \\
&= X1000\, ln\, \alpha_{SO_2-H_2S} + Y1000\, ln\, \alpha_{SO_4^{2-}-S^{2-}} + 1000\, ln\, \alpha_{H_2S-SO_4^{2-}}
\end{aligned}
$$

here X is the mole fraction of SO_2 in gaseous sulfur (SO_2 + H_2S) and Y is the mole fraction of sulfide sulfur in the total sulfur in the melt (Sakai et al., 1982; Marini et al., 2011). In this study, we assumed SO_4^{2-} contributes to SO_2 and S^{2-} contributes to H_2S, so that mole fraction X is expressed as X = 1 – Y. Fractionation factors of each reactions are determined by the experiments and previous studies (Miyoshi et al., 1984; Taylor, 1986):

$$1000\,ln\,\alpha_{SO_2-H_2S} = -0.42 \times \left(\frac{10^3}{T}\right)^3 + 4.367 \times \left(\frac{10^3}{T}\right)^2 - 0.105 \times \left(\frac{10^3}{T}\right) - 0.41$$

$$1000ln\,\alpha_{SO_4{}^{2-}-H_2S} = (6.5 \pm 0.3) \times \left(\frac{10^3}{T}\right)^2 \qquad (Eq.1)$$

$$1000ln\,\alpha_{SO_4{}^{2-}-S^{2-}} = 7.4 \times \left(\frac{10^3}{T}\right)^2 - 0.19 \qquad (Eq.2)\,.$$

As discussed by Fiege et al. (2015), the clear discrepancy between results of them and Miyoshi et al. (1984) at reduced condition indicates the temperature dependence determined by Miyoshi (1984) for $\alpha_{SO_4^{2-}-S^{2-}}$ (Eq. 2) is less likely applicable to the silicate system as the previous experiment conducted for molten salt. It is expected that the bonding energy of S^{2-} in a molten salt is probably different significantly from that in a Fe-bearing silicate melt. Since the relationship between atomic mass and bonding energy affects the equilibrium isotope fractionation (e.g., O'Neil, 1986), the differences are most likely related to the significant differences in melt composition and structure. On the contrary, Fiege et al. (2014) suggested that the temperature dependence determined by Miyoshi et al. (1984) for $\alpha_{SO_4^{2-}-H_2S}$ (Eq. 1) is probably applicable since the composition of the fluid and sulfate species in the salts are similar to those of silicate systems at relatively oxidized condition. Therefore, we adopted Eq. 1 for $\alpha_{SO_4^{2-}-H_2S}$ and experimentally updated temperature dependence for $\alpha_{H_2S-S^{2-}}$:

$$1000ln\,\alpha_{H_2S-S^{2-}} = 10.84 \times \left(\frac{10^3}{T}\right)^2 - 2.50 \qquad (Eq.3)$$

with one sigma of ~0.0010 (Fiege et al., 2015). Consequently, the α value for SO_4^{2-}-S^{2-} is theoretically constrained using Eq. 1 and Eq. 3 as

$$1000ln\ \alpha_{SO_4^{2-}-S^{2-}} = 1000ln\ \alpha_{SO_4^{2-}-H_2S} + 1000ln\ \alpha_{H_2S-S^{2-}}$$

Using these equations, $\alpha_{gas-melt}$ was calculated at a given fO_2 and temperature conditions. It is important to note that, at the magmatic temperature from ~1040 to 1200 ˚C, the effect of temperature variation on S-isotope fractionation between gas phase and melt is insignificant under relatively oxidized condition higher than ~FMQ+1, while are significant under relatively reduced condition of ~FMQ (Fiege et al., 2015).

The evolution of $\delta^{34}S$ values caused by isothermal open-system and closed-system degassing are expressed as

$$\delta^{34}S_{melt}^{final} = \delta^{34}S_{melt}^{initial} - (1-F) \times 1000ln\alpha_{gas-melt}$$

and

$$\delta^{34}S_{melt}^{final} = \delta^{34}S_{melt}^{initial} + 1000 \times (F^{\alpha_{gas-melt}-1} - 1)$$

respectively, where $F = C_S^{final}/C_S^{initial}$ is the fraction of sulfur remaining in the melt and $\alpha_{gas-melt}$ is the equilibrium isotope fractionation factor between gas phase and melt (Holloway and Blank, 1994; Marini et al., 1994). Calculated evolution of $\delta^{34}S$ of melt during open- and closed-system degassing are shown in Fig. B9-6 as a function of the remaining fraction of dissolved sulfur. This result shows the variations are maximum at open-system degassing and drastically increase during the last stage of degassing (after ~80% of initial S degassed).

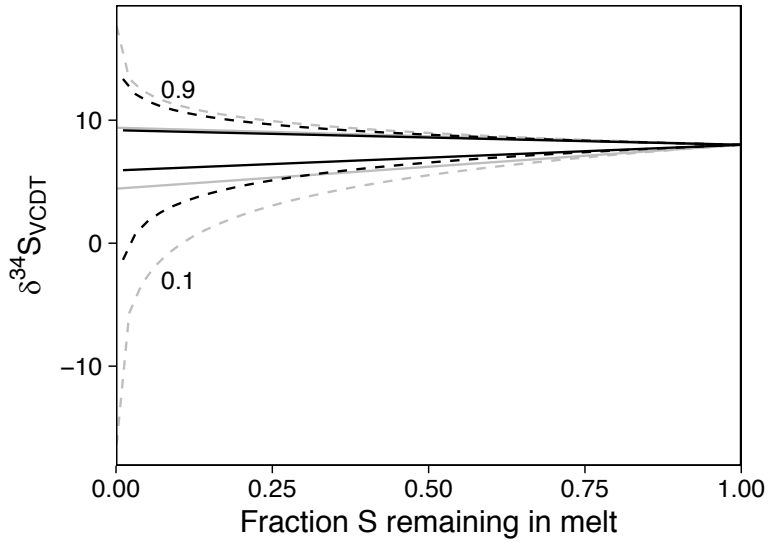

Figure **B9-6.** Evolution of melt $\delta^{34}S$ values caused by S degassing. Initial $\delta^{34}S$ value are set to 8 ‰. Evolution paths are primarily controlled by redox condition and S species in gas phase and melt rather than initial $\delta^{34}S$ value. Grey and blacklines represent temperature conditions at 900 ˚C and 1200 ˚C, respectively. Dashed and solid lines represent modeled evolution curves during open- and closed-system degassing, respectively. Numbers beside the dashed line indicate the fraction of dissolved sulfate in silicate melt.

Calculation of trace element composition in slab-component

Trace element composition of slab-components are estimated using Arc Basalt Simulator version 5 (ABS5, Kimura, 2017). In this ABS5 excel calculation sheet, mineral partition coefficients of trace elements are parameterized from experimental data as a function of temperature (Kimura et al., 2009), the bulk partition coefficients are used for element fractionations model during partial melting/dehydration, and calculated from mineral partition coefficients and composition-dependent mineral modes modelled by Perple_X thermodynamic program (Connolly and Kerrick, 1987; Connolly and Petrini, 2002). Pressure and temperature conditions of dehydration/melting are referenced to a geodynamic model of the convergent margin corner flow (Fig. B9-7a; Syracuse et al., 2010; van Keken et al., 2011).

We assumed slab-surface pressures of 3.0 and 4.2 GPa, for this study, based on the iso-depth contour beneath the volcanic front and the thermal model corresponding to the area (Fig. 4.1 and Fig. B9-7a). Trace element compositions of AOC and a sediment were assumed as those of Shikoku Basin basalt (Shu et al., 2017) and Nankai trench sediment, where Shikoku Basin is subducting (ODP site 808, Plank, 2014). The rest of the required inputs were as follows: slab solidus model, "W" wet solidus; slab P-T model (PvK2011), "44" Kyushu; for others see the Fig B9-8. Resulting trace element compositions of the slab components are reported in Table B8, and they are considered as possible flux coming out of the slab.

We also noted that ABS5 is inadequate in calculating slab-issued "fluid" significantly different from "melt" due to the design of the program. To cover the wider range of compositions derived from the slab, we calculated trace element concentrations of AOC-fluid using selected experimentally determined bulk partition coefficients of our choice (Kessel et al., 2005), and degree of partial dehydration was set at 5% (Fig. B9-7b).

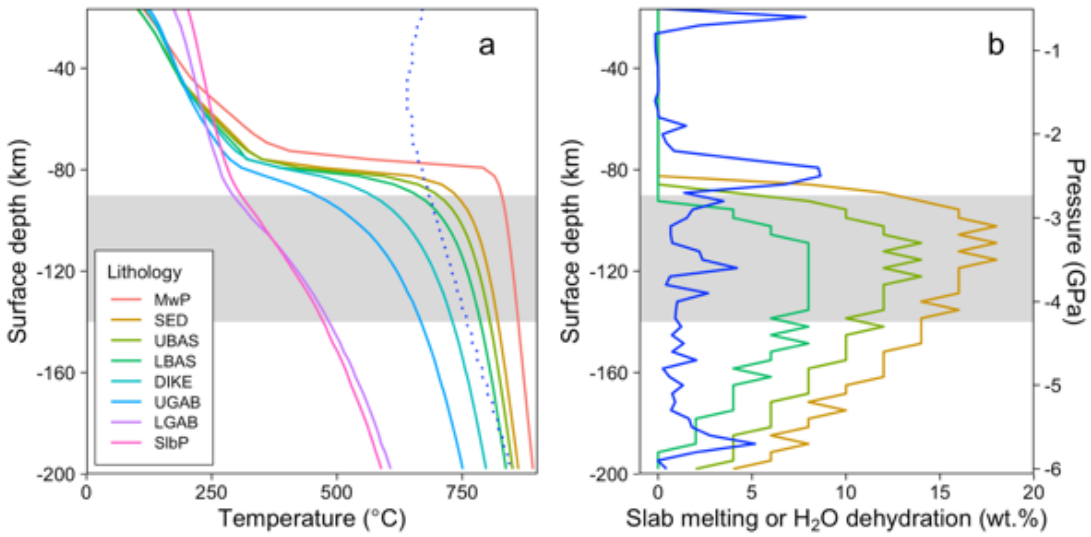

Figure **B9-7.** a) The pressure-temperature (P-T) paths along the subducted slab. Slab geotherm is from a geodynamic model for Kyushu (Syracuse et al., 2010; van Keken et al., 2011). Colored lines represent each slab layer surface defined in the ABS5 model. Dotted line is a wet solidus used in the ABS5 model for the both AOC and SED based on the experimental results (Hermann and Spandler, 2008; Schmidt et al., 2004; Skora and Blundy, 2010). b) Fraction of slab melt and total H_2O dehydrated. Blue line shows the weight fraction of total H_2O dehydrated from slab. Other colored lines show melt fraction in each slab layer. Degree of dehydration and melting of slab layers were calculated by ABS5. Phase proportions in slab layers are also simulated in ABS5 using Perple_X thermodynamic model version 7 (Connolly and Kerrick, 1987; Connolly and Petrini, 2002). Grey field indicates the depth of subducting slab surface beneath volcanic front ranging from 90 to 140 km depth (Fig. 4.1). MwP: mantle-wedge peridotite; SED: sediment; UBAS: upper basalt (altered oceanic crust); LBAS: lower basalt; DIKE: dike layer; UGAB: upper gabbro; LGAB: lower gabbro; SlbP: slab peridotite.

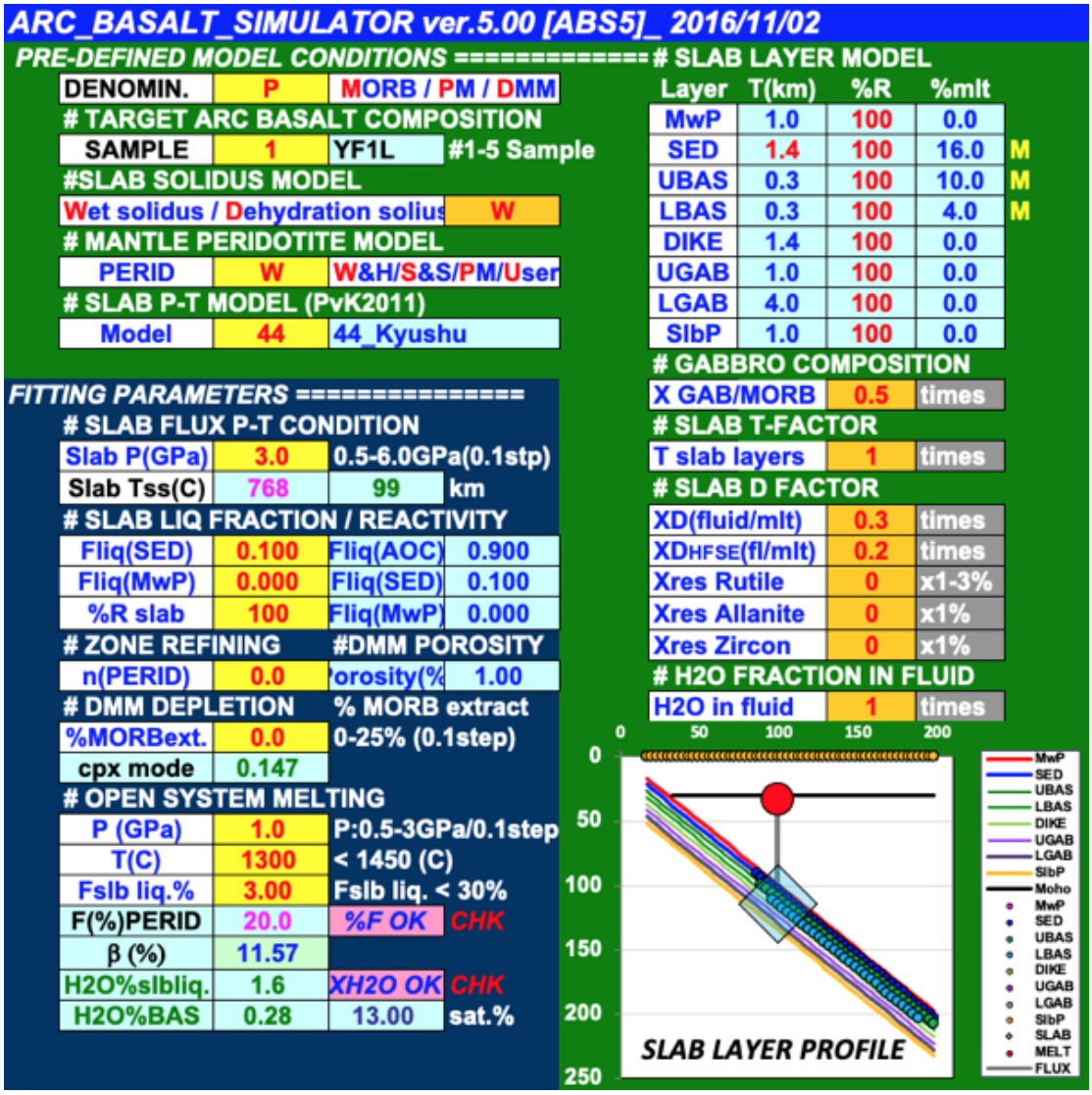

Figure **B9-8.** Screen capture of ABS5 control panel for input parameters (in this study). Note parameters in the "Fitting parameters" section are default (e.g., %R slab, SED/AOC ratio in fluid) except "Slab P(GPa)" since we did not not simulate any related internal slab-component mixing and flux melting in ABS5. We only calculated each slab-component. Residual rutile, allanite and zircon was set to zero. Details of ABS5 utilization are provided in Kimura (2017).

Supplementary references

Brown, J. R., Taylor, R. N. & Iguchi, M. (2020). Using high-resolution Pb isotopes to unravel the petrogenesis of Sakurajima volcano, Japan. *Bulletin of Volcanology* **82**, 36.

Chen, Y., Provost, A., Schiano, P. & Cluzel, N. (2011). The rate of water loss from olivine-hosted melt inclusions. *Contributions to Mineralogy and Petrology* **162**, 625–636.

Connolly, J. A. D. & Kerrick, D. M. (1987). An algorithm and computer program for calculating composition diagrams. *Calphad* **11**, 1–55.

Connolly, J. A. D. & Petrini, K. (2002). An automated strategy for calculation of phase diagram sections and retrieval of rock properties as a function of physical conditions. *Journal of Metamorphic Geology* **20**, 697–708.

Danyushevsky, L. V., Della-Pasqua, F. N. & Sokolov, S. (2000). Re-equilibration of melt inclusions trapped by magnesian olivine phenocrysts from subduction-related magmas: petrological implications. *Contributions to Mineralogy and Petrology* **138**, 68–83.

Fiege, A., Holtz, F., Shimizu, N., Mandeville, C. W., Behrens, H. & Knipping, J. L. (2014). Sulfur isotope fractionation between fluid and andesitic melt: an experimental study. *Geochimica et Cosmochimica Acta* **142**, 501–521.

Fiege, A., Holtz, F., Behrens, H., Mandeville, C. W., Shimizu, N., Crede, L. S. & Göttlicher, J. (2015). Experimental investigation of the S and S-isotope distribution between H2O–S ± Cl fluids and basaltic melts during decompression. *Chemical Geology* **393**–**394**, 36–54.

Fourcade, S. & Allegre, C. J. (1981). Trace element behavior in granite genesis: a case study The calc-alkaline plutonic association from the Querigut Complex (Pyrénées, France). *Contributions to Mineralogy and Petrology* **76**, 177–195.

Hacker, B. R. (2008). H_2O subduction beyond arcs. *Geochemistry Geophysics Geosystems* **9**, Q03001.

Hermann, J. & Spandler, C. J. (2008). Sediment melts at sub-arc depths: an experimental study. *Journal of Petrology* **49**, 717–740.

Holloway, J. R. & Blank, J. G. (1994). Application of experimental results to C-O-H species in natural melts. *Volatiles in Magmas*. Reviews in Mineralogy and geochemistry **30**, 187–230.

Huang, Z., Zhao, D., Hasegawa, A., Umino, N., Park, J.-H. & Kang, I.-B. (2013). Aseismic deep subduction of the Philippine Sea plate and slab window. *Journal of Asian Earth Sciences* **75**, 82–94.

Imura, R. & Kobayashi, T. (2001). *Geological map of Kirishima volcano, 1:50,000. Geological map of volcanoes 11*.

Ishihara, S. & Chappell, B. W. (2010). Chemical compositions of the Miocene granitoids of the Okueyama, Hoei mine and Takakumayama plutons, Outer Zone of SW Japan. *Bulletin of the Geological Survey of Japan* **61**, 17–38.

Kawaguchi, M., Hasenaka, T., Koga, K. T., Rose, E. F., Yasuda, A., Hokanishi, N., Mori, Y., Shimizu, K. & Ushikubo, T. (2021). Persistent gas emission originating from a deep basaltic magma reservoir of an active volcano : the case of Aso volcano, Japan. *Contributions to Mineralogy and Petrology* **176**, 6.

Kawanabe, Y., Hoshizumi, H., Itoh, J. & Yamasaki, S. (2015). *Geological map of Kuju volcano*. *Geological map of volcanoes 19*.

Kawanabe, Y. & Sakaguchi, K. (2005). *Geology of the Kaimon Dake district*. *Quadrangle Series, 1:50,000*. Geological Survey of Japan, AIST.

Kessel, R., Schmidt, M. W., Ulmer, P. & Pettke, T. (2005). Trace element signature of subduction-zone fluids, melts and supercritical liquids at 120-180 km depth. *Nature* **437**, 724–727.

Kimura, J.-I. (2017). Modeling chemical geodynamics of subduction zones using the Arc Basalt Simulator version 5. *Geosphere* **13**, 992–1025.

Kimura, J.-I., Hacker, B. R., van Keken, P. E., Kawabata, H., Yoshida, T. & Stern, R. J. (2009). Arc Basalt Simulator version 2, a simulation for slab dehydration and fluid-fluxed mantle melting for arc basalts: modeling scheme and application. *Geochemistry, Geophysics, Geosystems* **10**, Q09004.

Kita, I., Asakawa, Y., Yuri, T., Yasui, M., Shimoike, Y., Yamamoto, M., Hasegawa, H., Taguchi, S. & Sumino, H. (2012). Rifting of Kyushu, Japan, based on the fault-controlled concurrent eruption of oceanic island basalt-type and island arc-type lavas. *Bulletin of Volcanology* **74**, 1121–1139.

Kita, I., Yamamoto, M., Asakawa, Y., Nakagawa, M., Taguchi, S. & Hasegawa, H. (2001). Contemporaneous ascent of within-plate type and island-arc type magmas in the Beppu-Shimabara graben system, Kyushu island, Japan. *Journal of Volcanology and Geothermal Research* **111**, 99–109.

Kobayashi, T. (1984). Geology of Yufu-Tsurumi volcanoes and their latest eruptions. *The memoirs of the Geological Society of Japan* **24**, 93-108 (in Japanese with English abstract).

Kuritani, T., Sakuyama, T., Kamada, N., Yokoyama, T. & Nakagawa, M. (2017). Fluid-fluxed melting of mantle versus decompression melting of hydrous mantle plume as the cause of intraplate magmatism over a stagnant slab: implications from Fukue volcano group, SW Japan. *Lithos* **282**–**283**, 98–110.

Le Voyer, M., Rose-Koga, E. F., Shimizu, N., Grove, T. L. & Schiano, P. (2010). Two contrasting H_2O-rich components in primary melt inclusions from Mount Shasta. *Journal of Petrology* **51**, 1571–1595.

Marini, L., Chiappini, V., Cioni, R., Cortecci, G., Dinelli, E., Principe, C. & Ferrara, G. (1998). Effect of degassing on sulfur contents and $\delta^{34}S$ values in Somma-Vesuvius magmas. *Bulletin of Volcanology* **60**, 187–194.

Marini, L., Moretti, R. & Accornero, M. (2011). Sulfur isotopes in magmatic-hydrothermal systems, melts, and magmas. *Reviews in Mineralogy and Geochemistry* **73**, 423–492.

Marini, L., Paiotti, A., Principe, C., Ferrara, G. & Cioni, R. (1994). Isotopic ratio and concentration of sulfur in the undersaturated alkaline magmas of Vulture volcano (Italy). *Bulletin of Volcanology* **56**, 487–492.

Médard, E. & Grove, T. L. (2008). The effect of H_2O on the olivine liquidus of basaltic melts: experiments and thermodynamic models. *Contributions to Mineralogy and Petrology* **155**, 417–432.

Miyoshi, M., Fukuoka, T., Sano, T. & Hasenaka, T. (2008a). Subduction influence of Philippine Sea plate on the mantle beneath northern Kyushu, SW Japan: an examination of boron contents in basaltic rocks. *Journal of Volcanology and Geothermal Research* **171**, 73–87.

Miyoshi, M., Hasenaka, T. & Sano, T. (2005). Genetic relationship of the compositionally diverse magmas from Aso post-caldera volcanism. *Bulletin of the volcanological society of Japan* **50**, 269-283 (in Japanese with English abstract).

Miyoshi, M., Shibata, T., Yoshikawa, M., Sano, T., Shinmura, T. & Hasenaka, T. (2011). Genetic relationship between post-caldera and caldera-forming magmas from Aso volcano, SW Japan: constraints from Sr isotope and trace element compositions. *Journal of Mineralogical and Petrological Sciences* **106**, 114–119.

Miyoshi, M., Shimono, M., Hasenaka, T., Sano, T. & Fukuoka, T. (2008b). Determination of boron and other elements in volcanic rocks by prompt gamma-ray analysis: an application to magma genesis in Kyushu island, SW-Japan. *Journal of Radioanalytical and Nuclear Chemistry* **278**, 343–347.

Miyoshi, M., Shimono, M., Hasenaka, T., Sano, T., Mori, Y. & Fukuoka, T. (2010). Boron systematics of Hisatsu and Kirishima basaltic rocks from southern Kyushu, Japan. *Geochemical Journal* **44**, 359–369.

Miyoshi, T., Sakai, H. & Chiba, H. (1984). Experimental study of sulfur isotope fractionation factors between sulfate and sulfide in high temperature melts. *Geochemical Journal* **18**, 75–84.

Moriwaki, H., Matsushima, Y., Iwai, M., Arai, F. & Fujiwara, O. (2002). Holocene geomorphic evolution around the Aira caldera, south Japan. *The Quaternary Research* **41**, 253–268.

Moyen, J.-F. & Stevens, G. (2006). Experimental constraints on TTG petrogenesis: implications for Archean geodynamics. In: Benn, K., Mareschal, J.-C. & Condie, K. C. (eds) *Archean Geodynamics and Environments*, 149–175.

Nagaoka, S., Okuno, M. & Arai, F. (2001). Tephrostratigraphy and eruptive history of the Aira caldera volcano during 100-30 ka, Kyushu, Japan. *Journal of Geological Society of Japan* **107**, 432–450.

Nakada, S. (1986). Comparative study of chemistry of rocks from the Kirishima, and Daisen Volcanic Belts in Kyushu, southwest Japan. *Bulletin of the volcanological society of Japan* **31**, 95-110 (in Japanese with English abstract).

Nakamura, M. (1971). Petrology of Kaimon-dake volcano. *Journal of Geological Society of Japan* **77**, 359-364 (in Japanese with English abstract).

Nche, L. A., Hasegawa, T., Aka, F. T., Kobayashi, T., Németh, K., Asaah, A. N. E., Kaneda, Y., Nishihara, A., Bate-Tibang, E. E., Lebga, A. K., Tiabou, A. F., Ngwa, C. N. & Suh, C. E. (2021). Lithostratigraphy and geochemistry of Aojiki volcano and Sumiyoshiike and Yonemaru maars, Kamo Volcanic Field (Southern Kyushu), Japan. *Journal of Volcanology and Geothermal Research* **412**.

O'Neil, J. R. (1986). Theoretical and experimental aspects of isotopic fractionation. *Stable isotopes in high temperature geological processes*. Reviews in Mineralogy and geochemistry **16**, 1–40.

Ohmoto, H. & Goldhaber, M. B. (1997). Sulfur and carbon isotopes. *Geochemistry of Hydrothermal Ore Deposits*, 517–611.

Ohta, T. & Aoki, K. (1991). Origin of andesitic magma in Yufu-Tsurumi volcano group – a binary mixing model –. *Journal of Mineralogy, Petrology and Economic Geology* **86**, 1-15 (in Japanese with English abstract).

Ohta, T., Hasenaka, T., Ban, M. & Sasaki, M. (1992). Characteristic geology and petrology of non-arc type volcanism at Oninomi monogenetic volcano, Yufu-Tsurumi graben. *Bulletin of the volcanological society of Japan* **37**, 119-131 (in Japanese with English abstract).

Ohta, T., Hasenaka, T. & Fujimaki, H. (1990). Geology and petrography of Yufu-Tsurumi volcano group, Oita Prefecture. *Journal of Mineralogy, Petrology and Economic Geology* **85**, 113-129 (in Japanese with English abstract).

Plank, T. (2014). The chemical composition of subducting sediments. *Treatise on Geochemistry: Second Edition* **4**, 607–629.

Qian, Q. & Hermann, J. (2013). Partial melting of lower crust at 10-15 kbar: constraints on adakite and TTG formation. *Contributions to Mineralogy and Petrology* **165**, 1195–1224.

Roeder, P. L. & Emslie, R. F. (1970). Olivine-liquid equilibrium. *Contributions to Mineralogy and Petrology* **29**, 275–289.

Rowe, M. C., Peate, D. W. & Newbrough, A. (2011). Compositional and thermal evolution of olivine-hosted melt inclusions in small-volume basaltic eruptions: a "simple" example from Dotsero volcano, NW Colorado. *Contributions to Mineralogy and Petrology* **161**, 197–211.

Sakai, H., Casadevall, T. J. & Moore, J. G. (1982). Chemistry and isotope ratios of sulfur in basalts and volcanic gases at Kilauea volcano, Hawaii. *Geochimica et Cosmochimica Acta* **46**, 729–738.

Sawamura, K. & Matsui, K. (1957). *Explanatory text of the geological map of Japan, "Kirishimayama", Scale 1:50,000. Geological Survey of Japan*.

Schiano, P. & Bourdon, B. (1999). On the preservation of mantle information in ultramafic nodules: glass inclusions within minerals versus interstitial glasses. *Earth and Planetary Science Letters* **169**, 173–188.

Schiano, P., Monzier, M., Eissen, J.-P., Martin, H. & Koga, K. T. (2010). Simple mixing as the major control of the evolution of volcanic suites in the Ecuadorian Andes. *Contributions to Mineralogy*

and Petrology **160**, 297–312.

Schmidt, M. W., Vielzeuf, D. & Auzanneau, E. (2004). Melting and dissolution of subducting crust at high pressures: the key role of white mica. *Earth and Planetary Science Letters* **228**, 65–84.

Shibata, T., Suzuki, J., Yoshikawa, M., Kobayashi, T., Miki, D. & Takemura, K. (2013). Geochemical and Sr-Nd-Pb isotopic constraints on the origin and magmatic evolution of Quaternary lavas of Sakurajima volcano, southern Kyushu island, Japan. *Bulletin of the volcanological society of Japan* **58**, 43–58.

Shibata, T., Yoshikawa, M., Itoh, J., Ujike, O., Miyoshi, M. & Takemura, K. (2014). Along-arc geochemical variations in Quaternary magmas of northern Kyushu Island, Japan. *Geological Society Special Publication* **385**, 15–29.

Shinno, I. (1966). Petrology of the Kirishima volcano. *Journal of Mineralogy, Petrology and Economic Geology* **56**, 56-74 (in Japanese with English abstract).

Shu, Y., Nielsen, S. G., Zeng, Z., Shinjo, R., Blusztajn, J., Wang, X. & Chen, S. (2017). Tracing subducted sediment inputs to the Ryukyu arc-Okinawa Trough system: evidence from thallium isotopes. *Geochimica et Cosmochimica Acta*. Elsevier Ltd **217**, 462–491.

Skora, S. & Blundy, J. (2010). High-pressure hydrous phase relations of radiolarian clay and implications for the involvement of subducted sediment in arc magmatism. *Journal of Petrology* **51**, 2211–2243.

Sugimoto, T., Shibata, T., Yoshikawa, M. & Takemura, K. (2006). Sr-Nd-Pb isotopic and major and trace element compositions of the Yufu-Tsurumi volcanic rocks: implications for the magma genesis of the Yufu-Tsurumi volcanoes, northeast Kyushu, Japan. *Journal of Mineralogical and Petrological Sciences* **101**, 270–275.

Syracuse, E. M., van Keken, P. E. & Abers, G. A. (2010). The global range of subduction zone thermal models. *Physics of the Earth and Planetary Interiors* **183**, 73–90.

Tajima, Y., Hayashi, S., Yasuda, A. & Itoh, H. (2013). Tephrostratigraphy and eruptive history of Shinmoedake volcano of the Kirishima volcanoes, Kyushu, Japan. *The Quaternary Research* **52**, 151-171 (in Japanese with English abstract).

Tajima, Y., Matsuo, Y., Shoji, T. & Kobayashi, T. (2014). Eruptive history of Ebinokogen volcanic area of Kirishima volcanoes for the past 15,000 years in Kyushu, Japan. *Bulletin of the volcanological society of Japan* **59**, 55-75 (in Japanese with English abstract).

Taylor, B. E. (1986). Magmatic volatiles: isotopic variation of C, H, and S. *Stable Isotopes in High Temperature Geological Processes*. Reviews in Mineralogy and geochemistry **16**, 273–317.

Toplis, M. J. (2005). The thermodynamics of iron and magnesium partitioning between olivine and liquid: criteria for assessing and predicting equilibrium in natural and experimental systems. *Contributions to Mineralogy and Petrology* **149**, 22–39.

Van Keken, P. E., Hacker, B. R., Syracuse, E. M. & Abers, G. A. (2011). Subduction factory: 4. Depth-

dependent flux of H_2O from subducting slabs worldwide. *Journal of Geophysical Research: Solid Earth* **116**, B01401.

Yamasaki, S., Hoshizumi, H. & Matsumoto, A. (2016). Growth history of western to central part of Kuju volcanic group, Kyushu, Japan. *Bulletin of the Volcanological Society of Japan* **61**, 519-531 (in Japanese with English abstract).

Zellmer, G. F., Iizuka, Y., Miyoshi, M., Tamura, Y. & Tatsumi, Y. (2012). Lower crustal H_2O controls on the formation of adakitic melts. *Geology* **40**, 487–490.

B10. Microscopic photos of melt inclusions

<ON2S>
AMa-I (after heating)

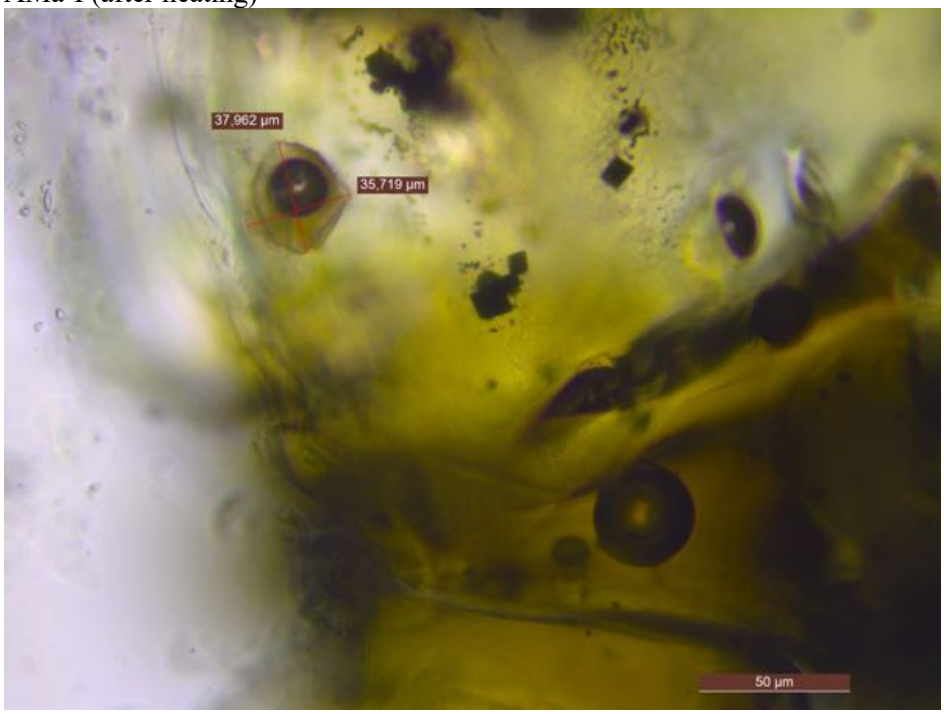

AP-IV (after heating)

BEc-II (after heating)

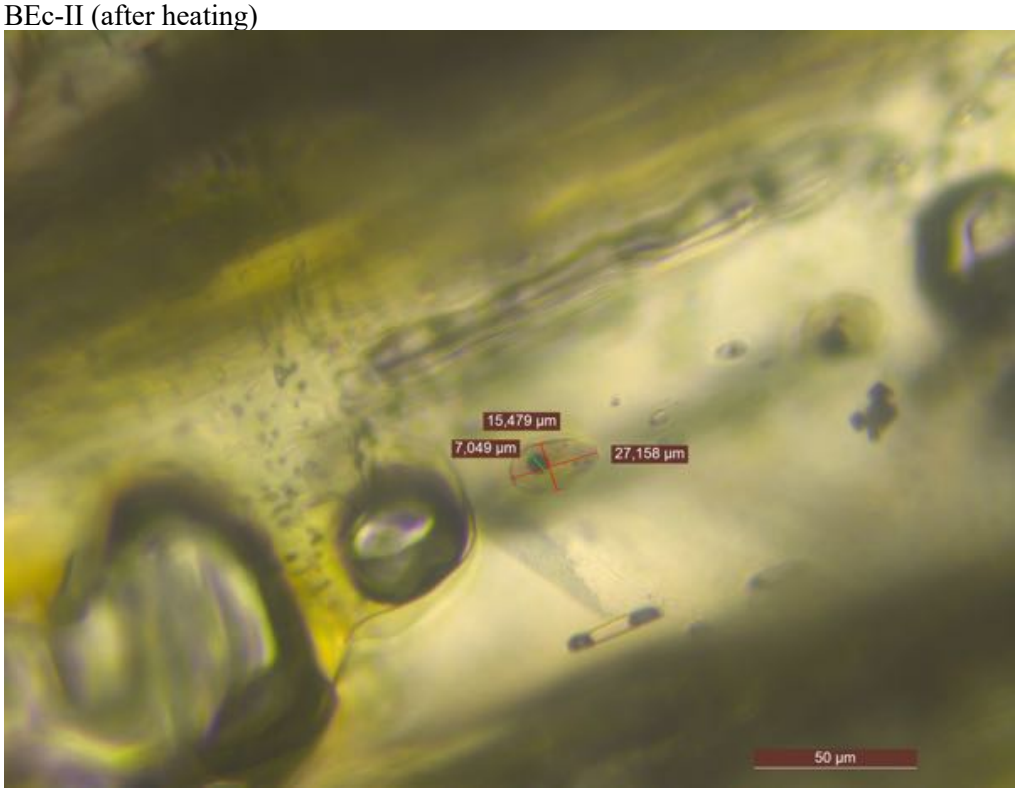

BEc-III (after heating)

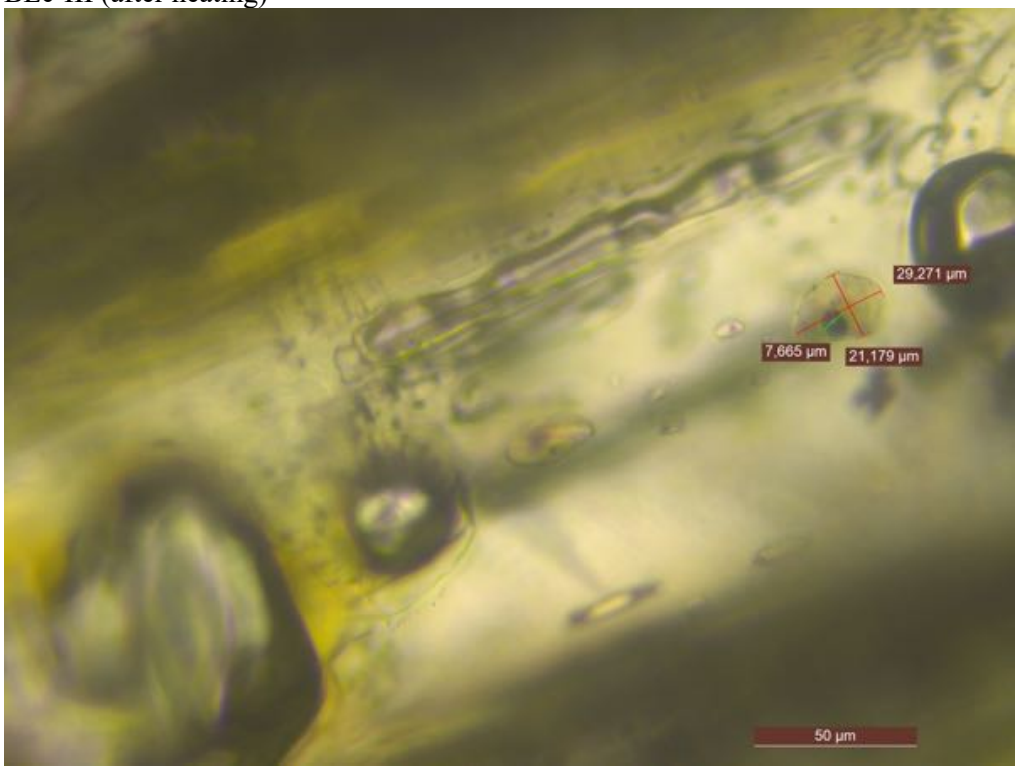

BFa-I (after heating)

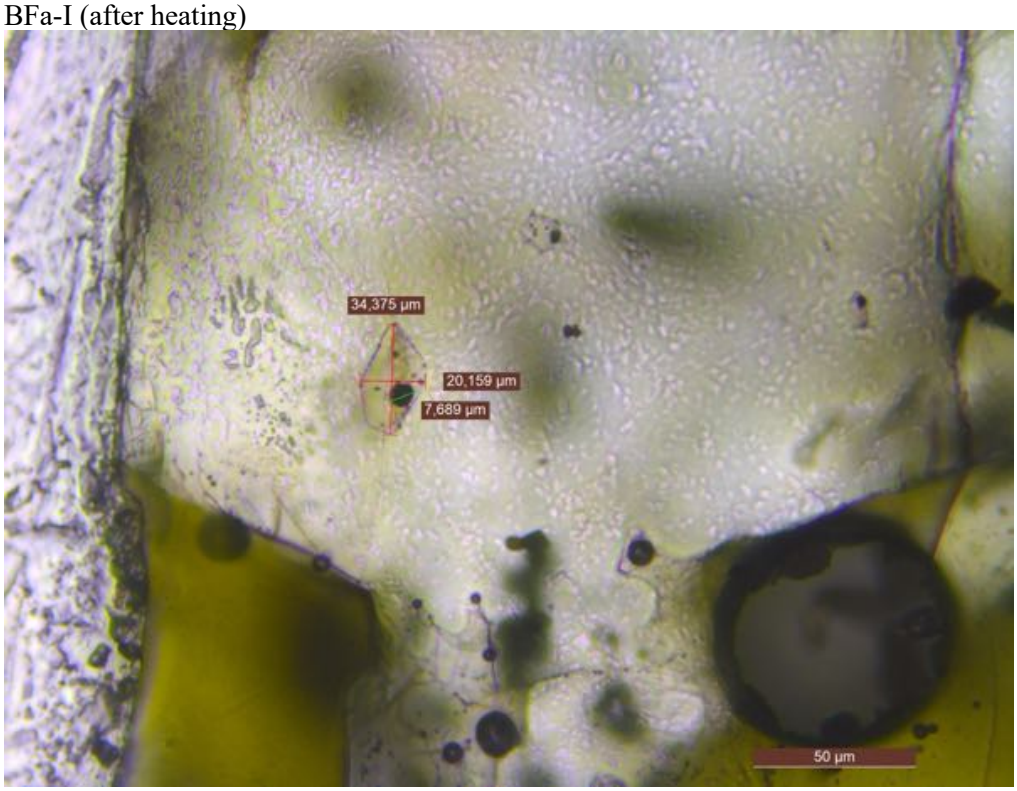

CSa-III (after heating)

DF-IV (after heating)

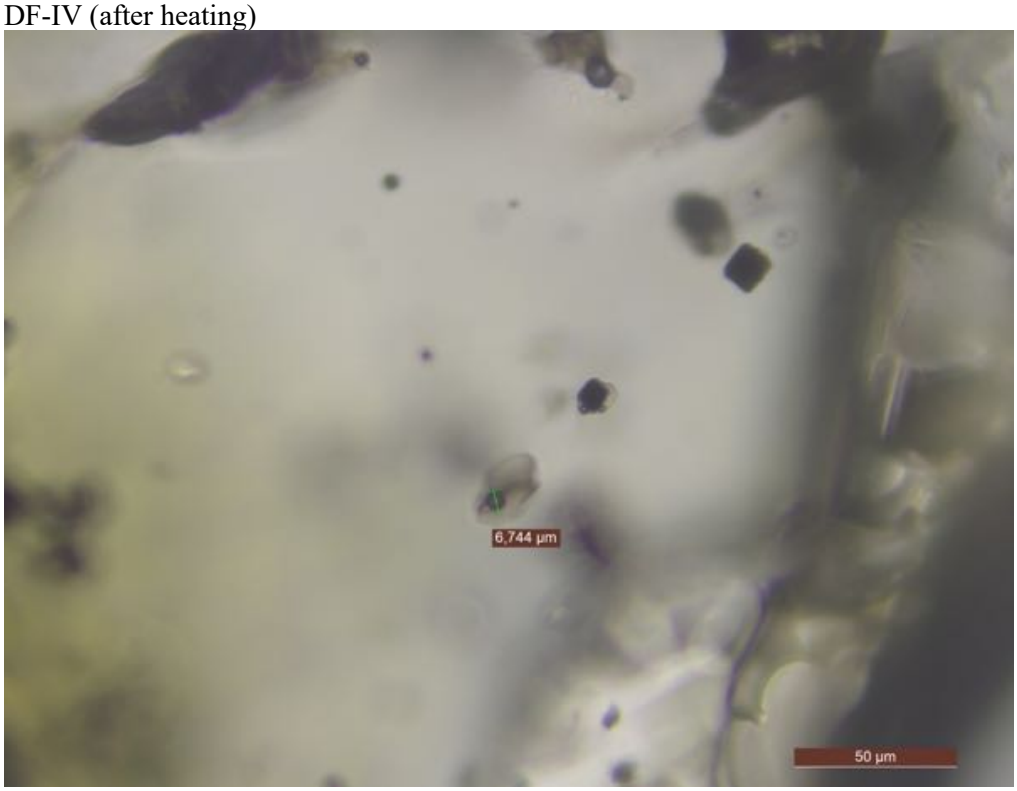

DL-I (after heating)

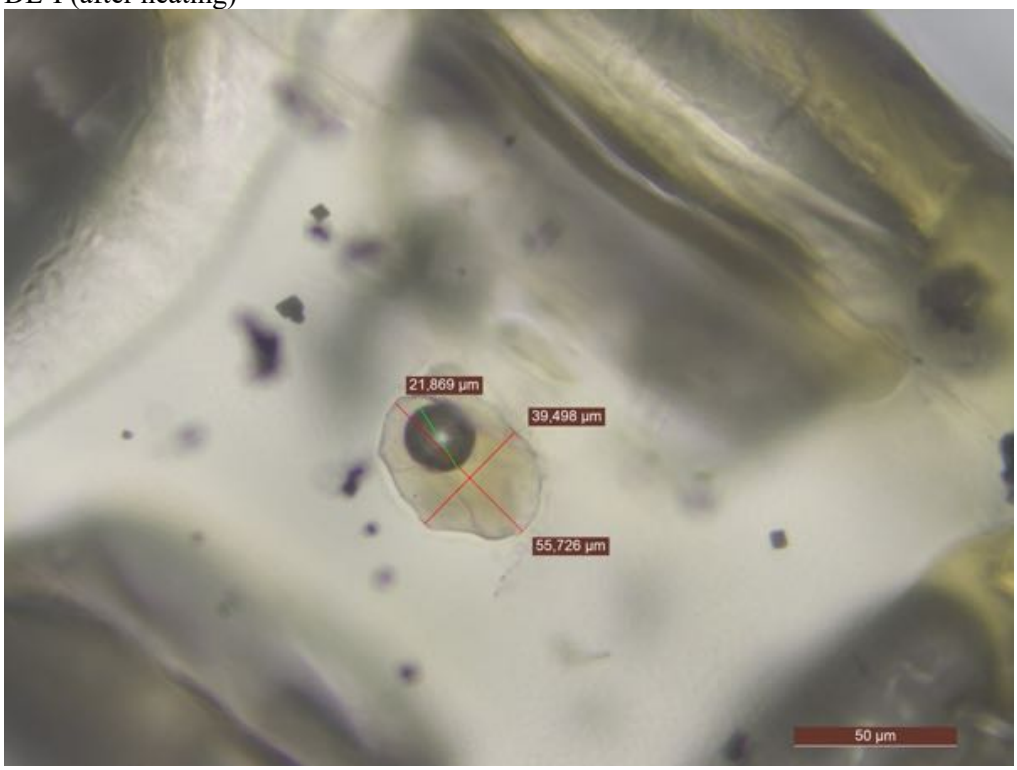

DS-III (after heating)

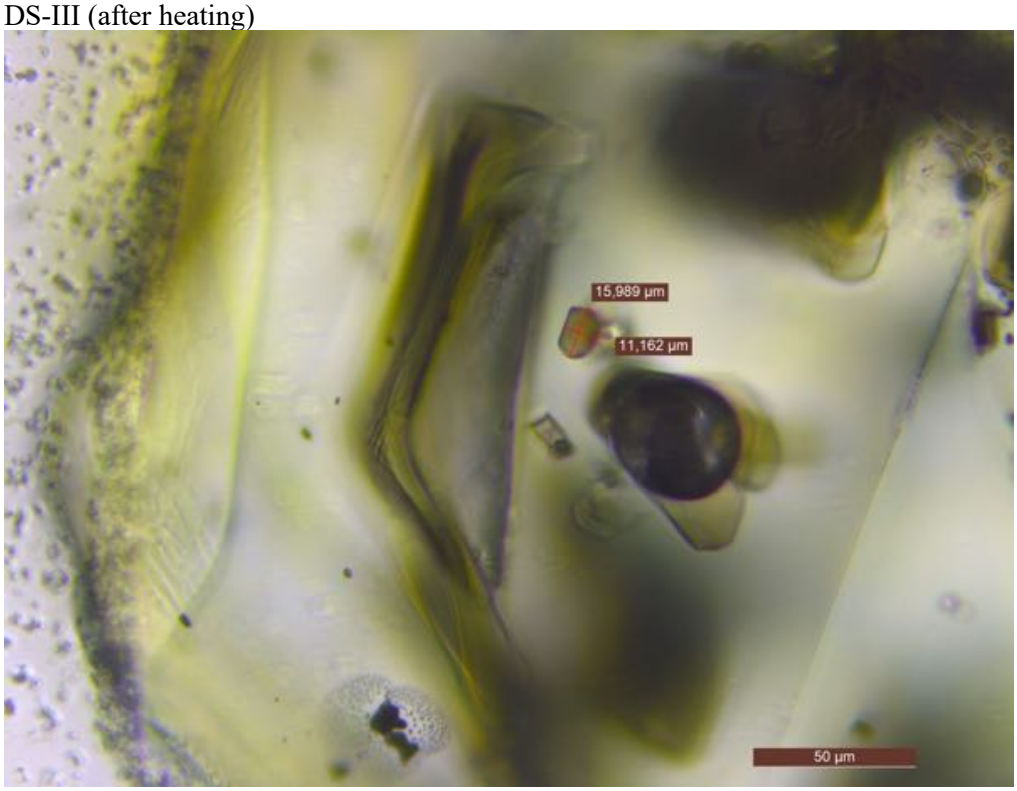

DZ-I (after heating)

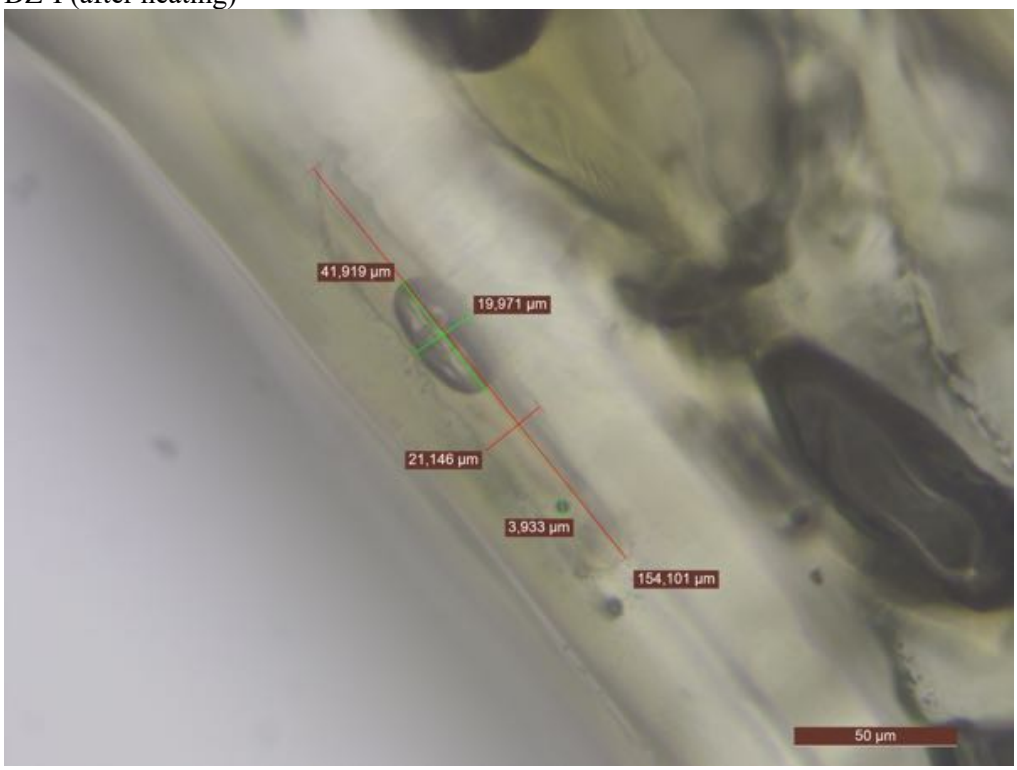

EDa-I (after heating)

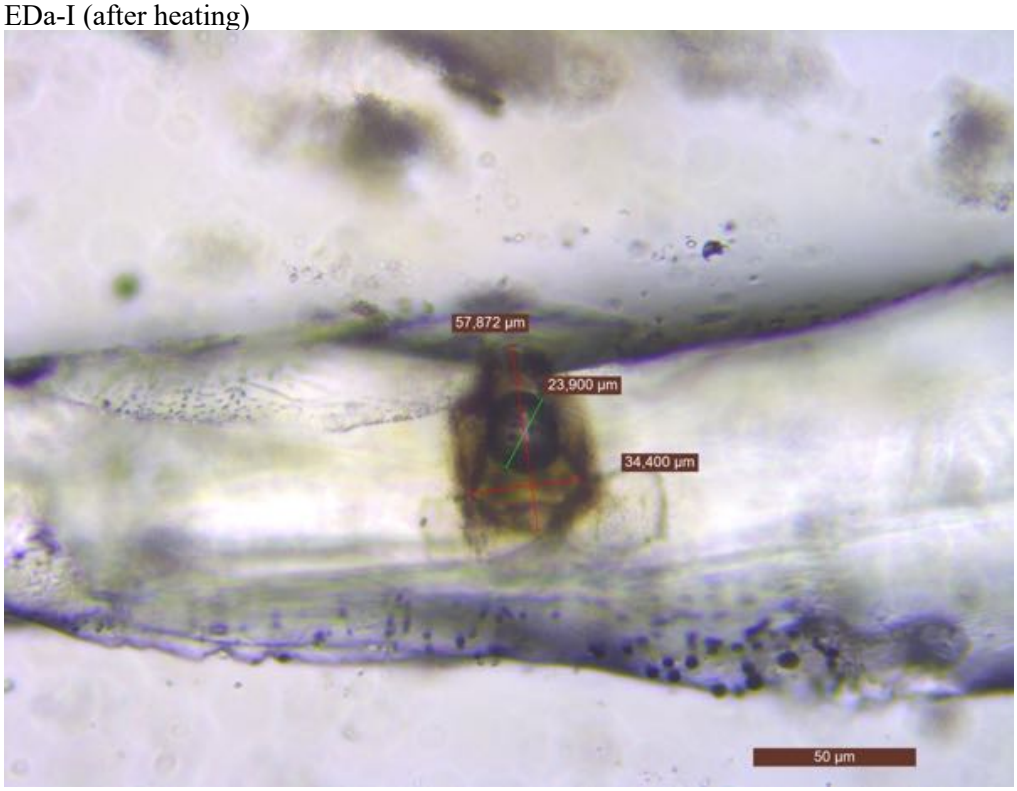

U-I (unheated)

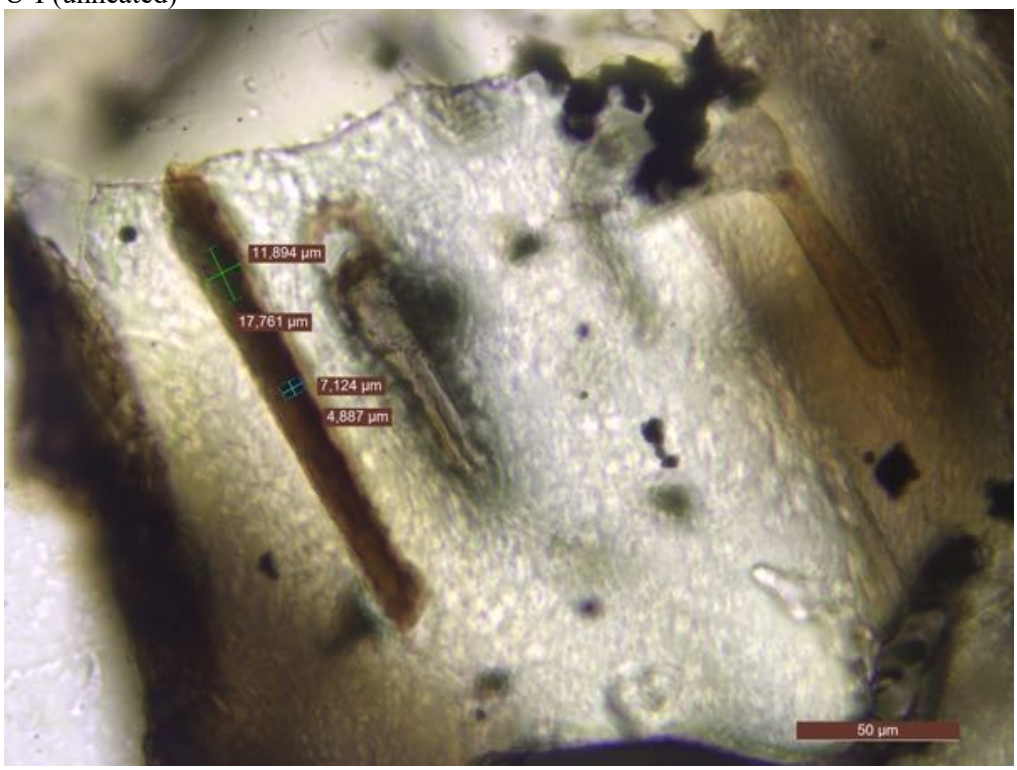

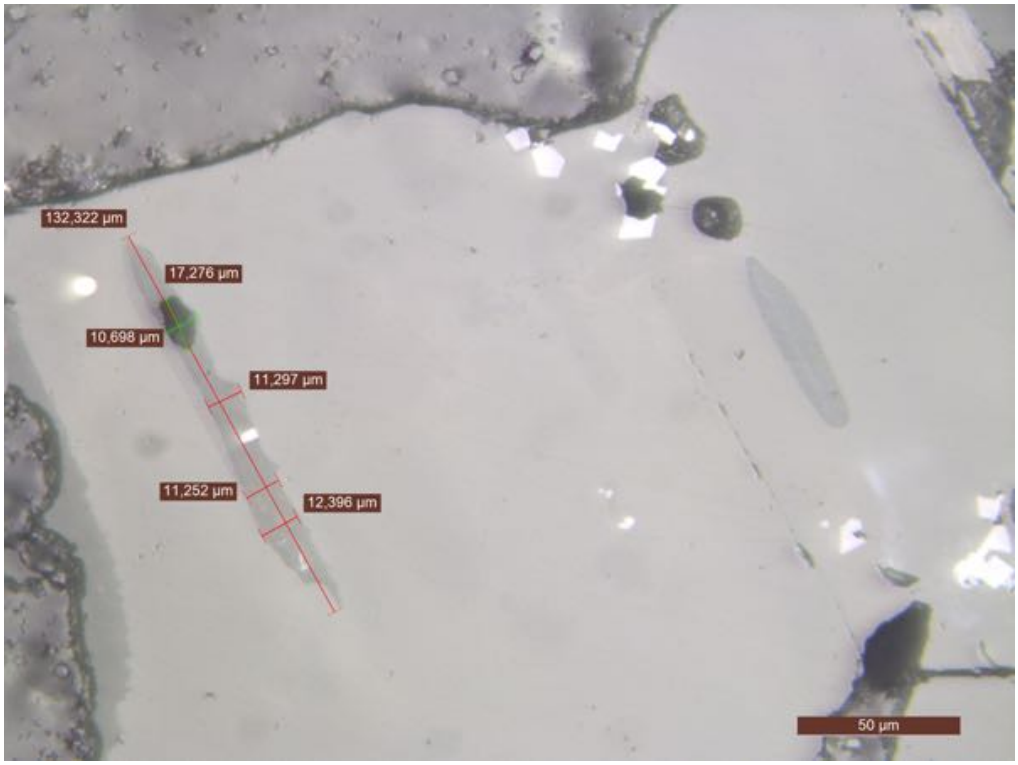

Z-I (after heating)

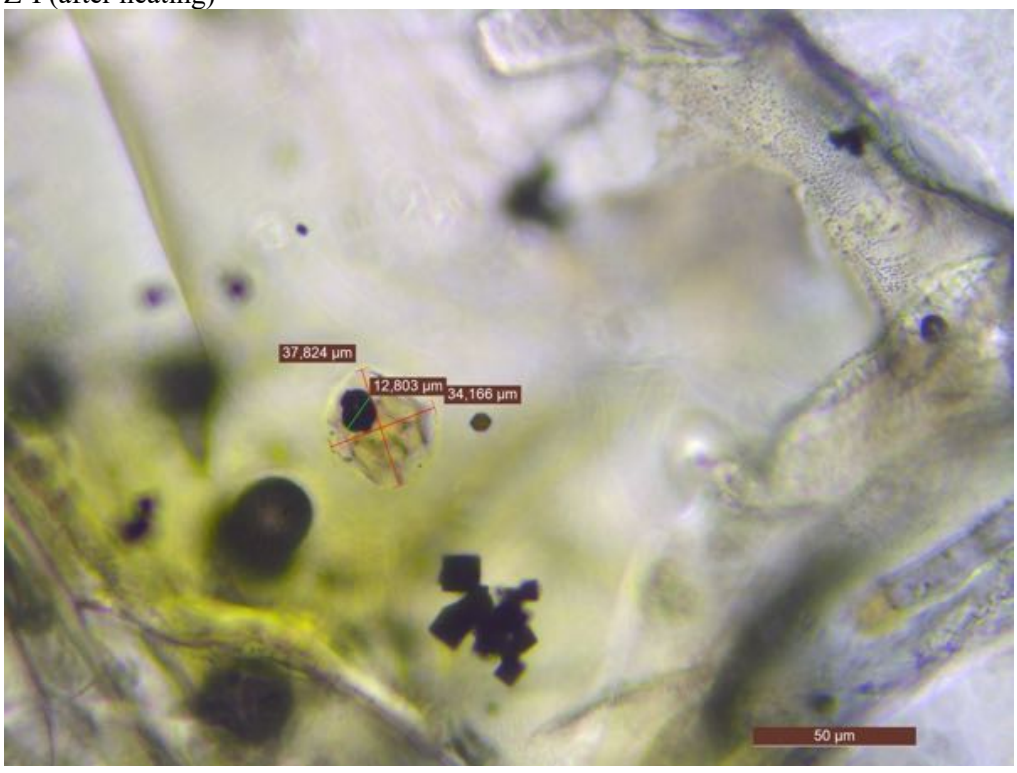

<YF1L>
AFa-III (after heating)

AFb-I (after heating)

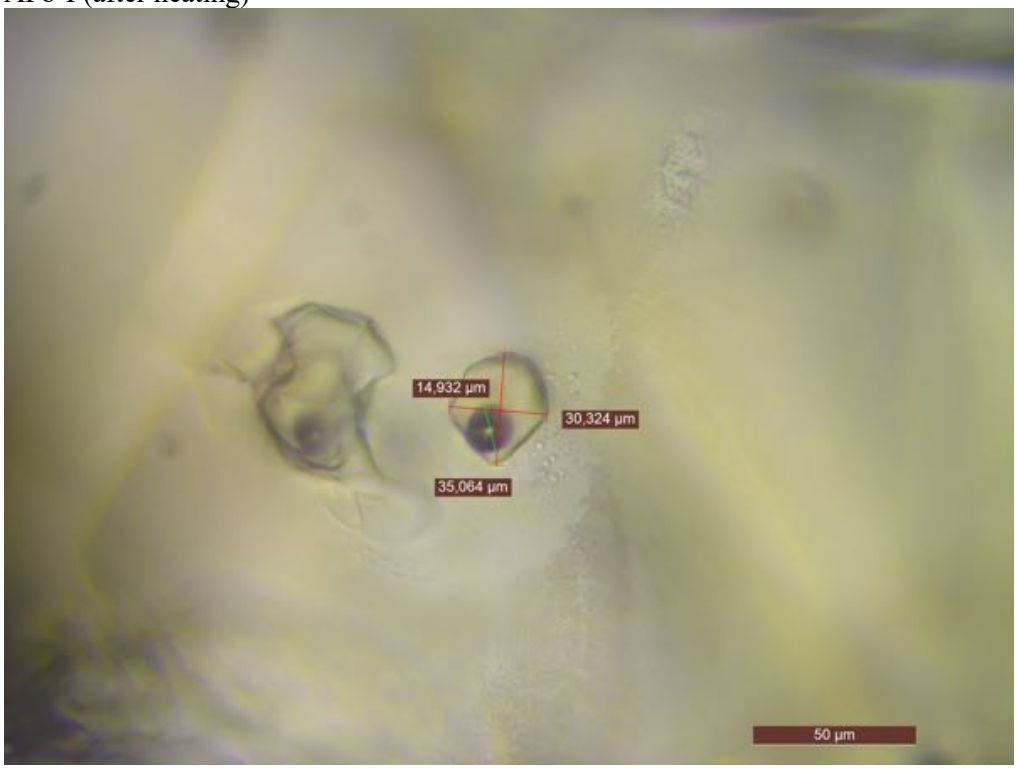

AFb-II (after heating)

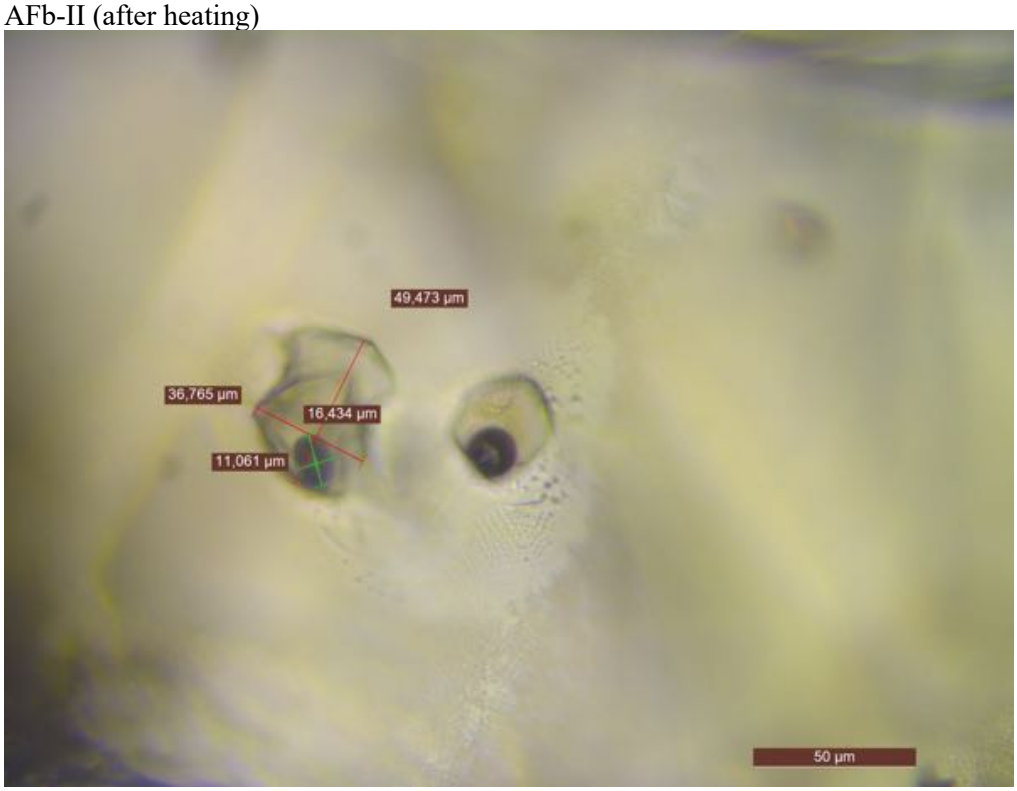

AH-I (after heating)

AZ-I (after heating)

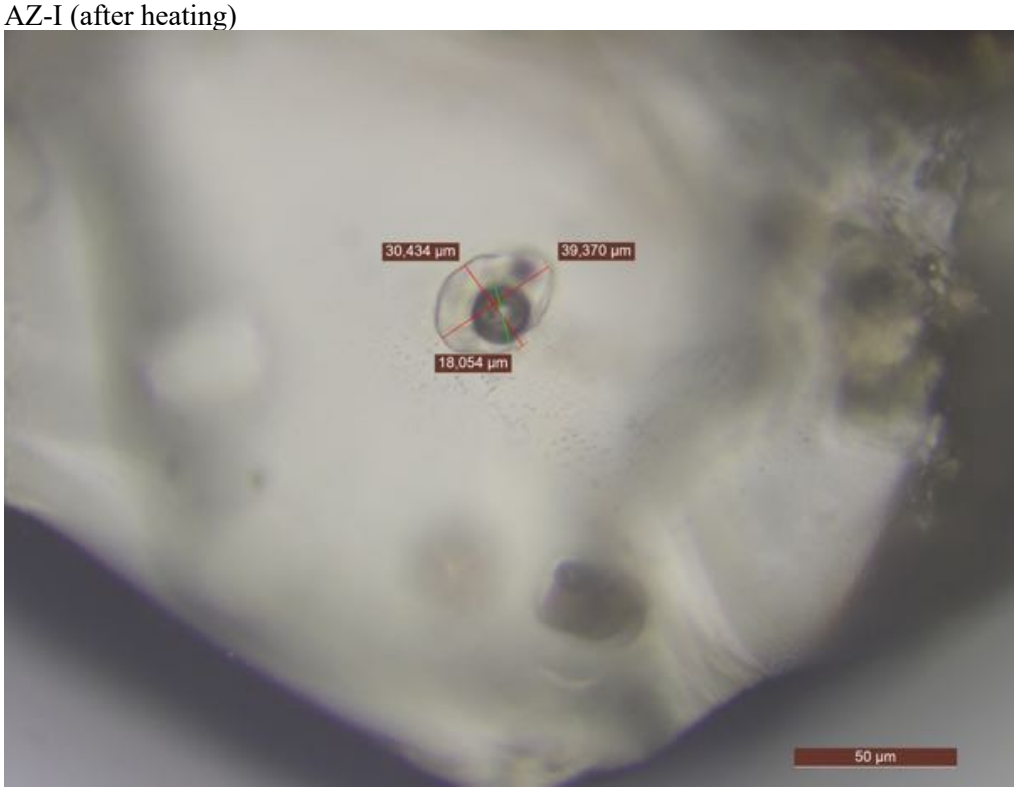

AZ-III (after heating)

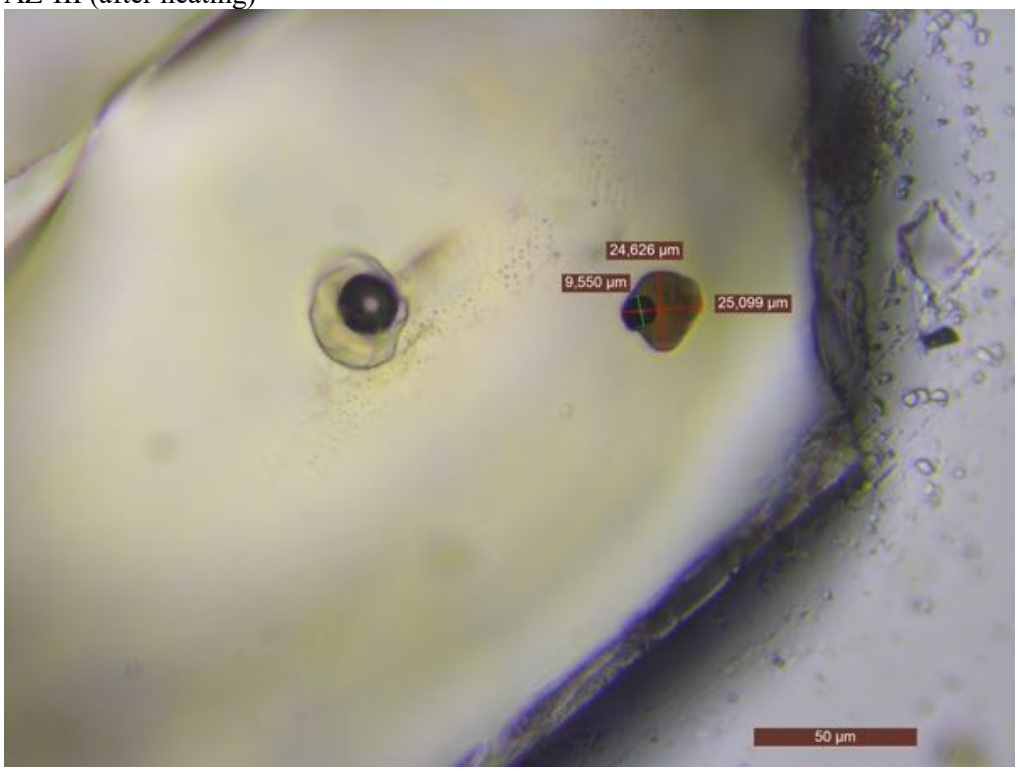

BD-I (after heating)

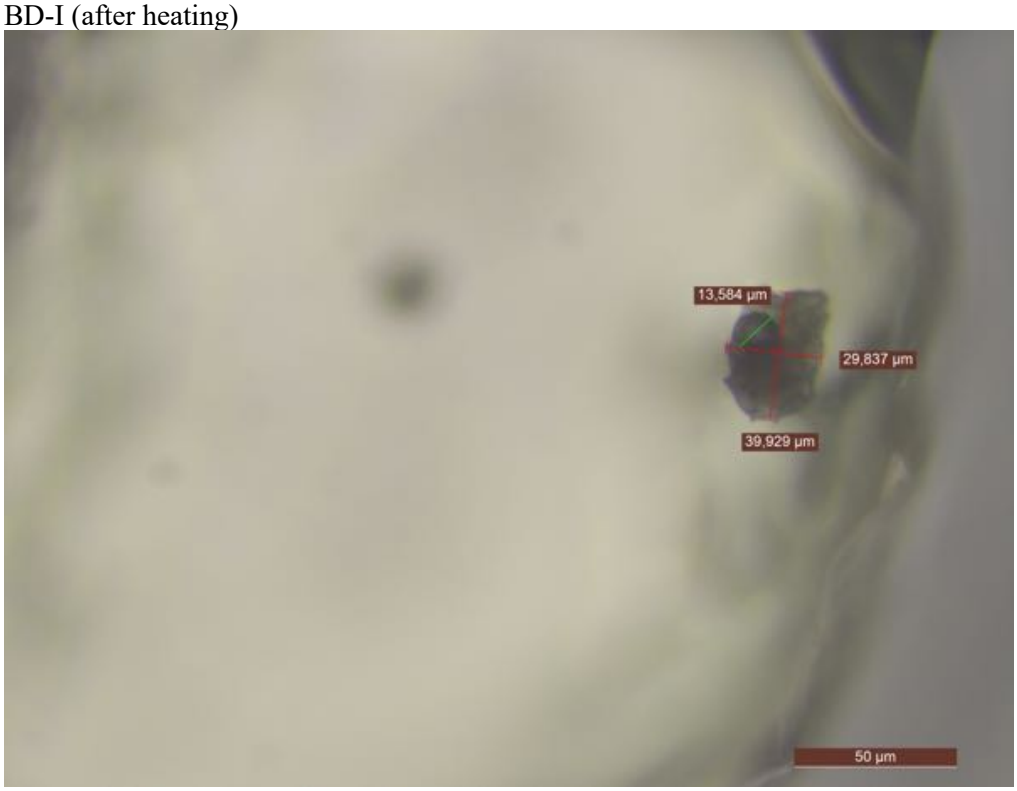

BK-II (after heating)

BLa-II (after heating)

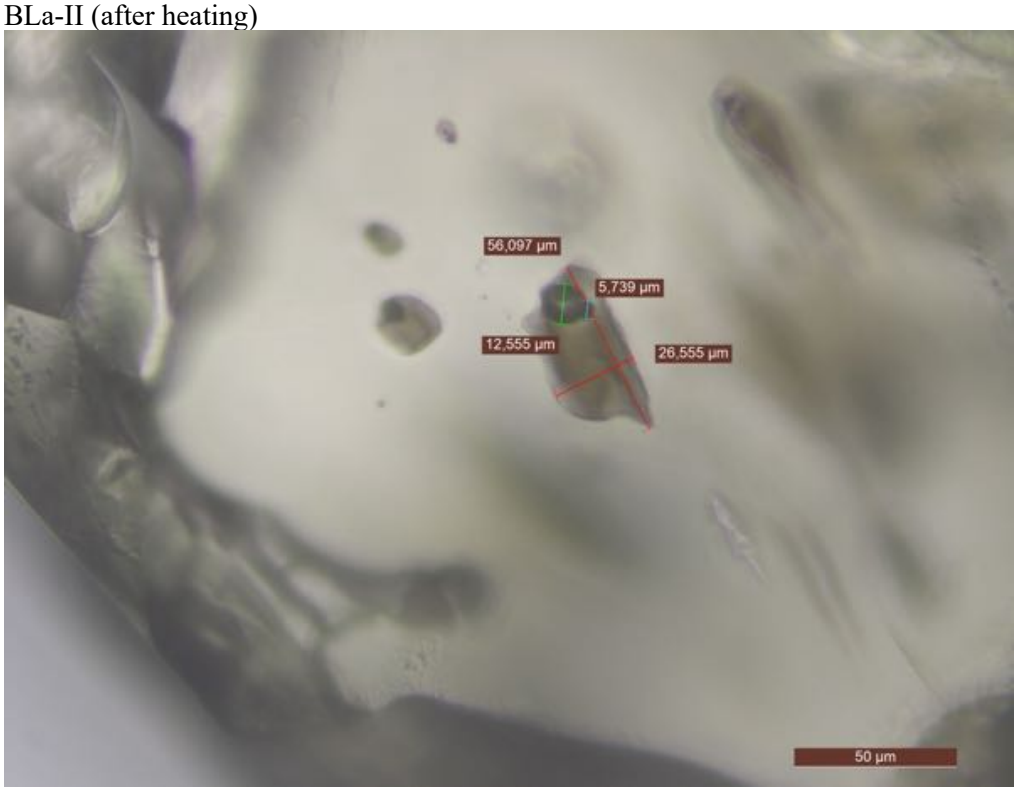

BLa-III (after heating)

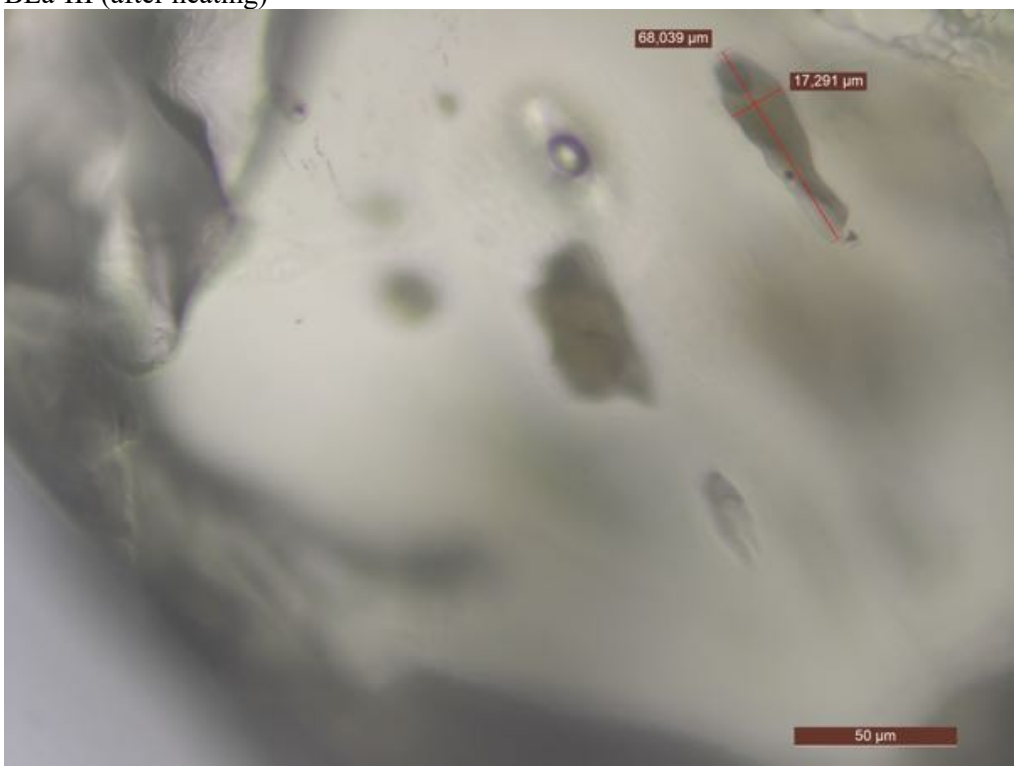

BM-I (after heating)

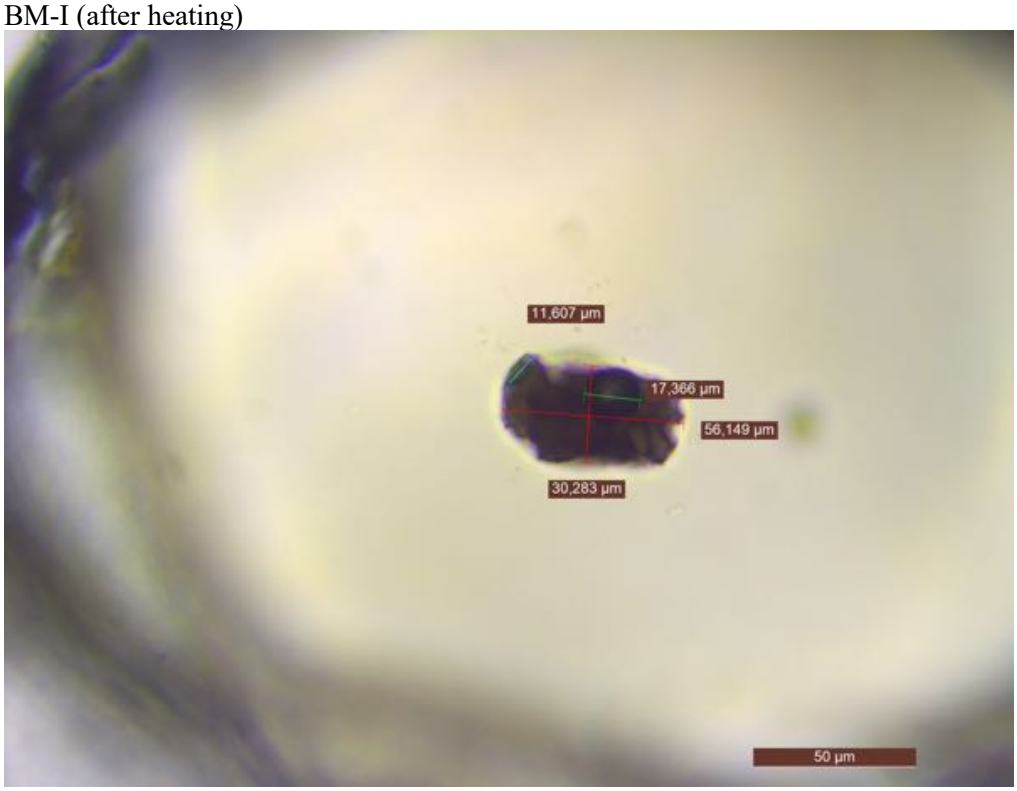

BO-I (after heating)

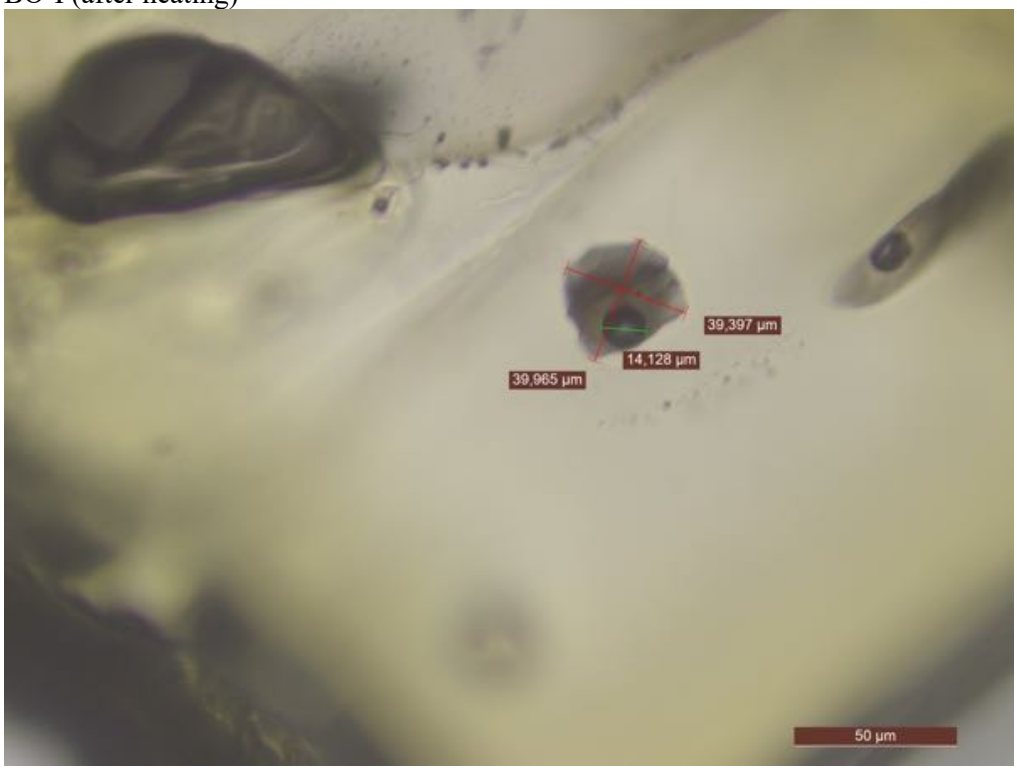

BQ-I (after heating)

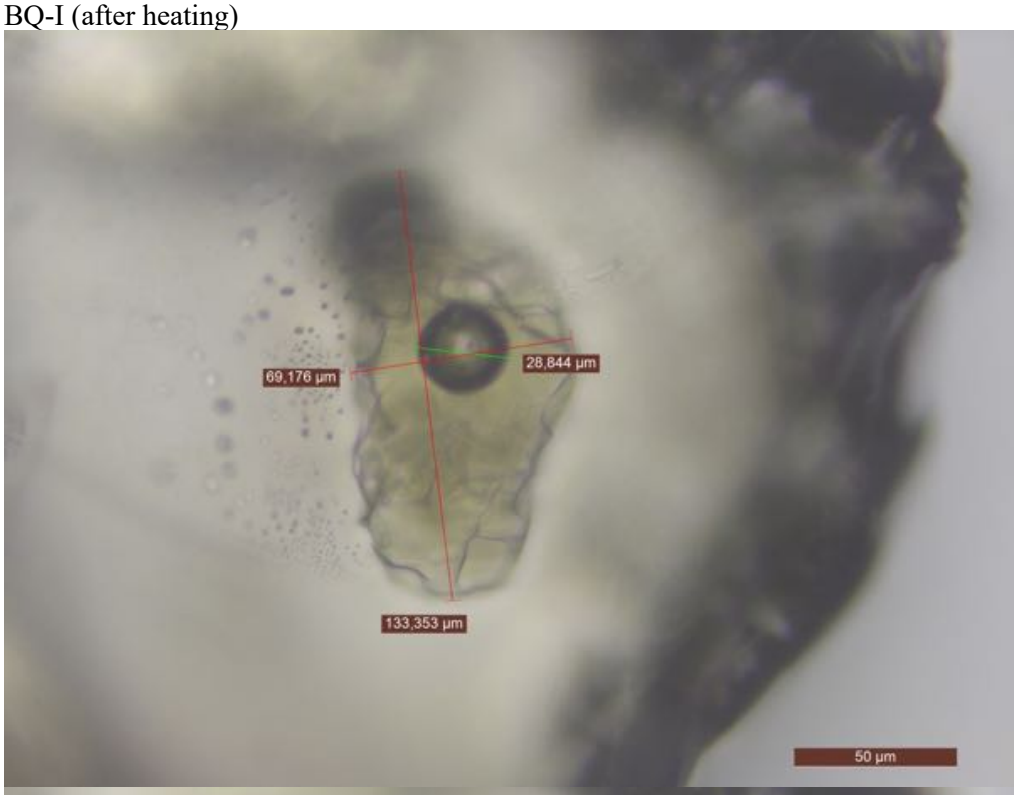

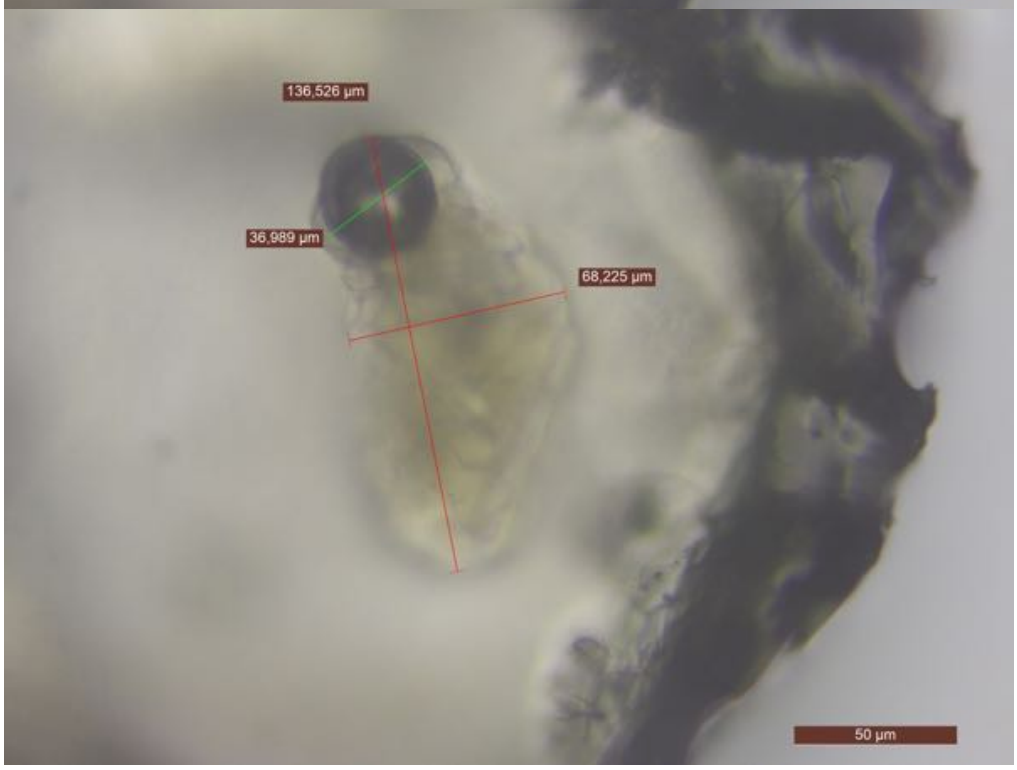

BQ-II (after heating)

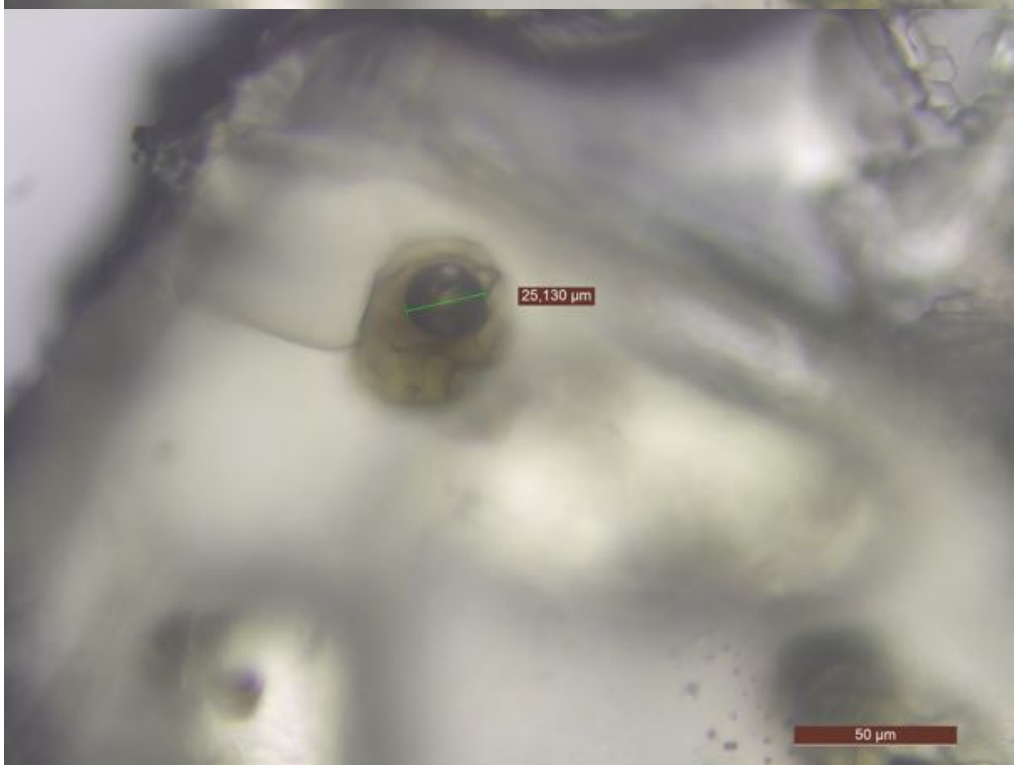

BQ-III (after heating)

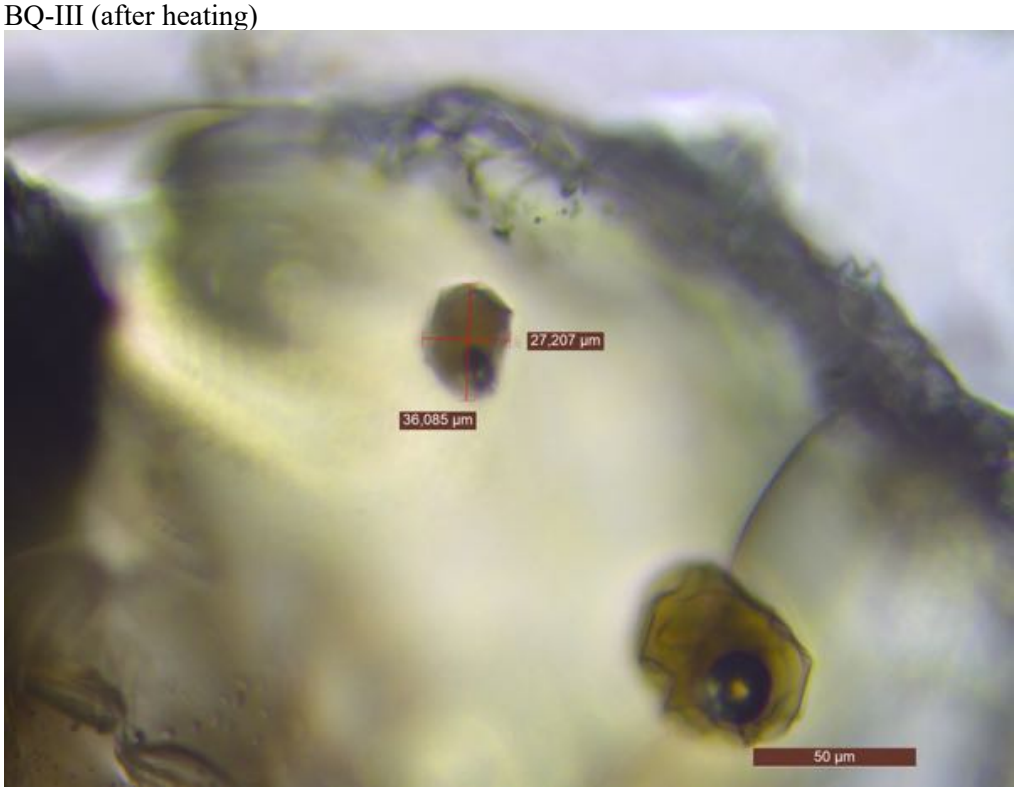

BSb-III (after heating)

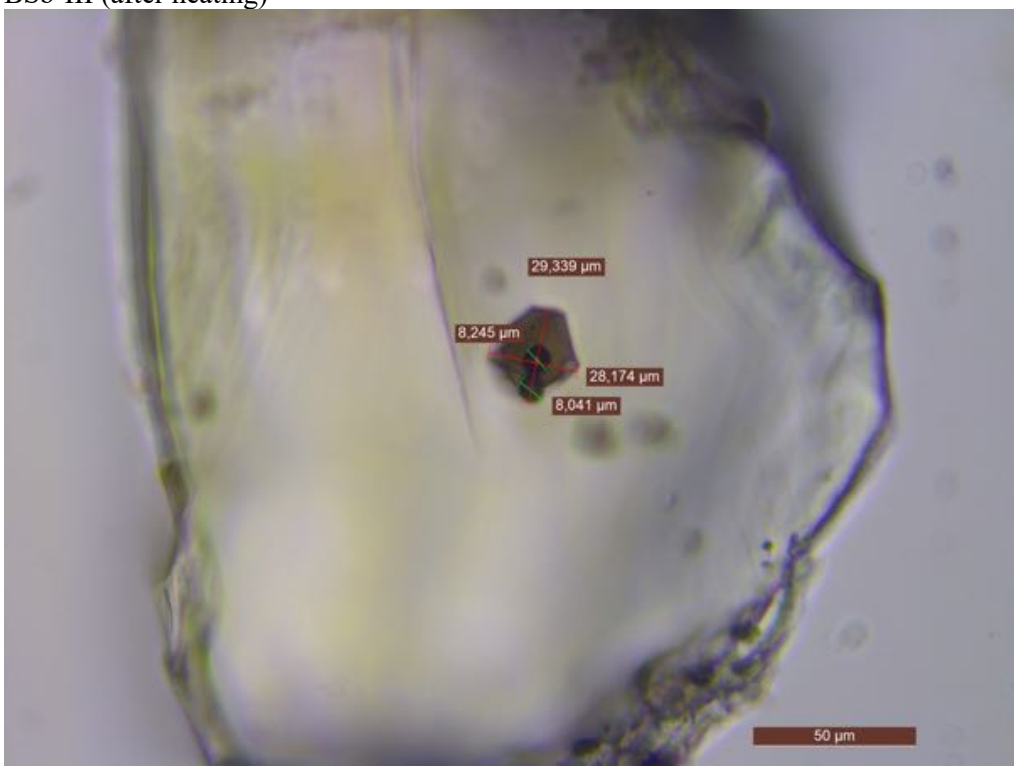

BSc-II (after heating)

F-I (after heating)

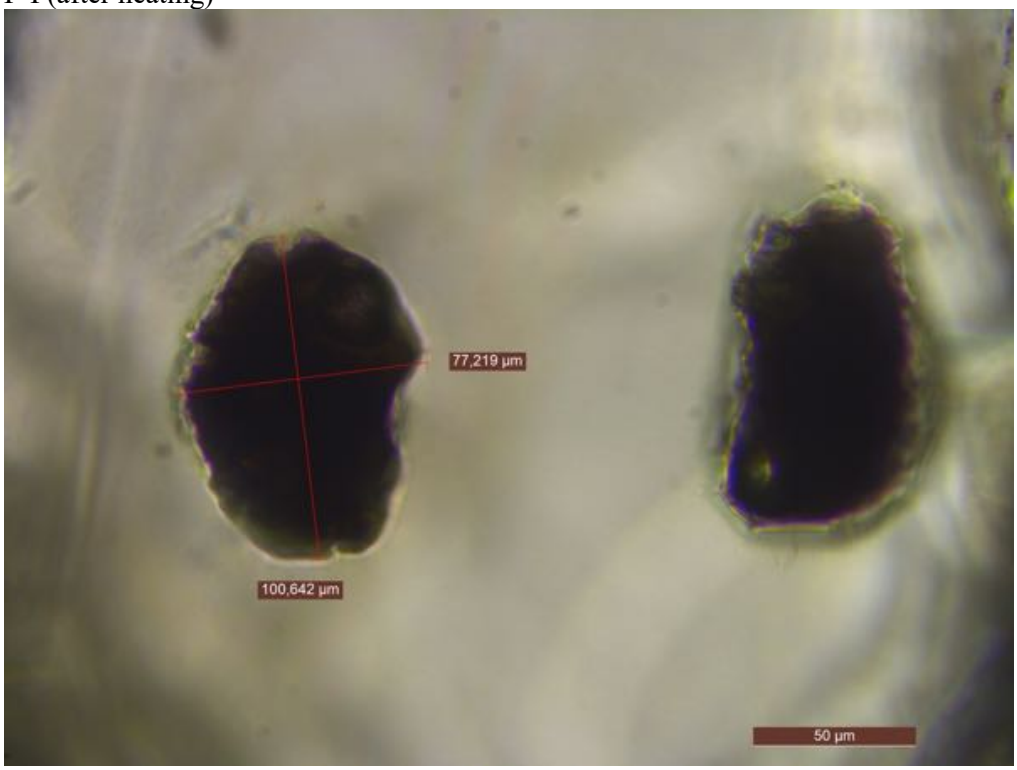

F-II (after heating)

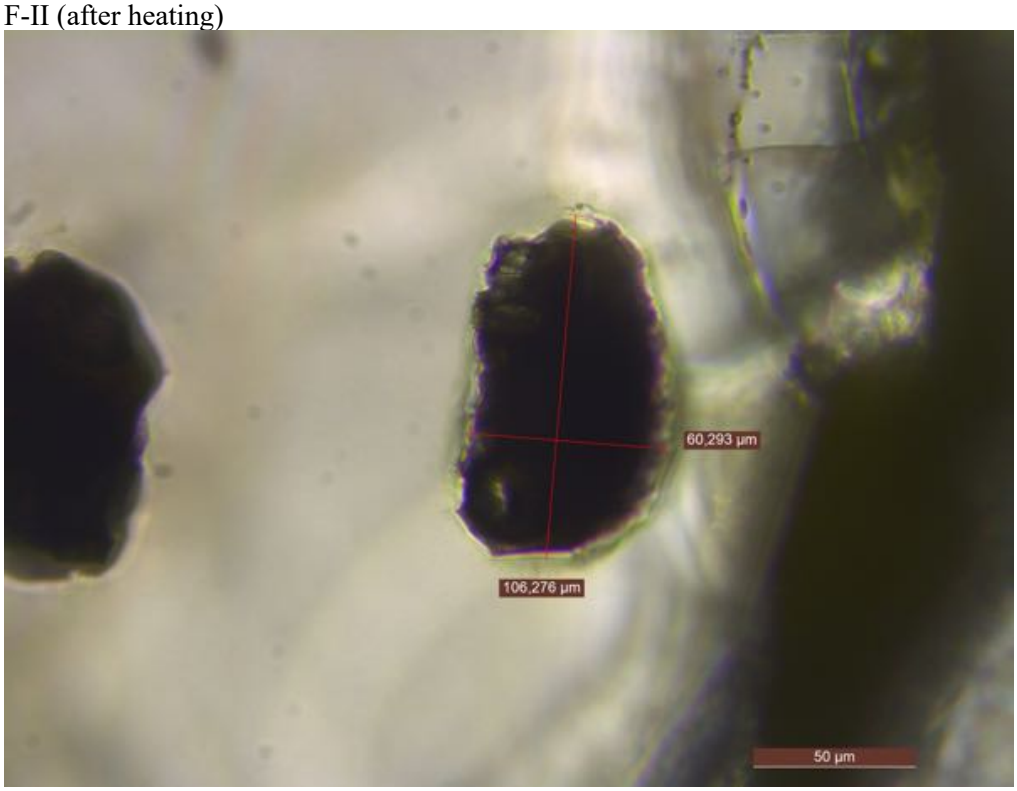

<KJ5S>
AD-V

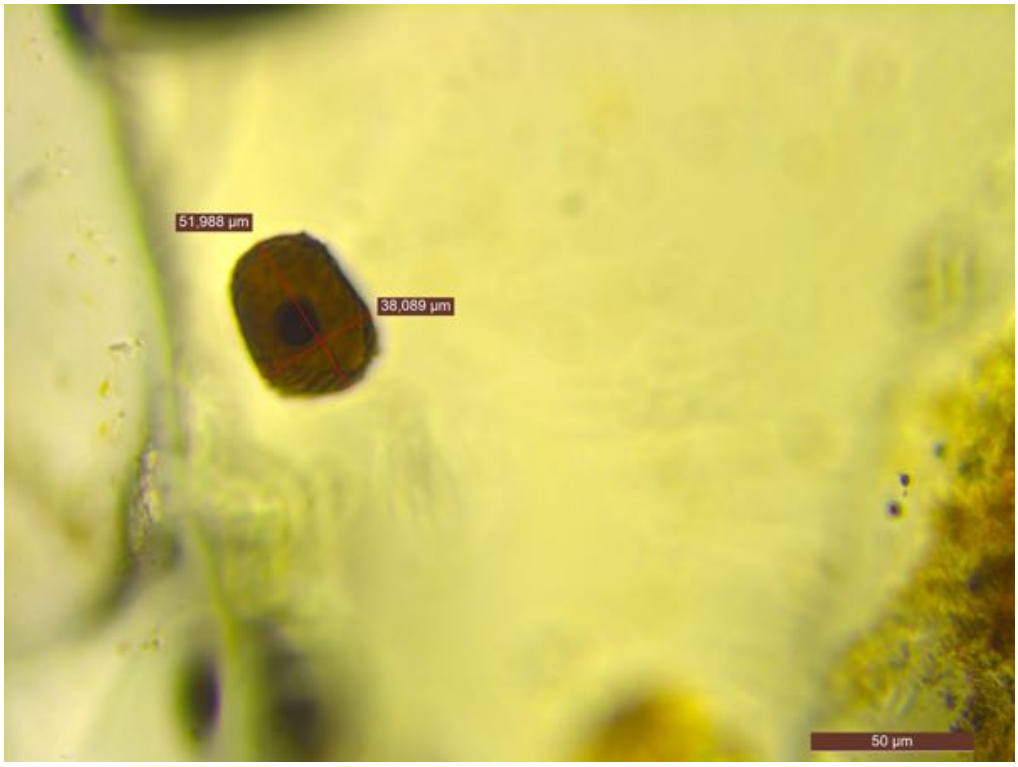

AE-I

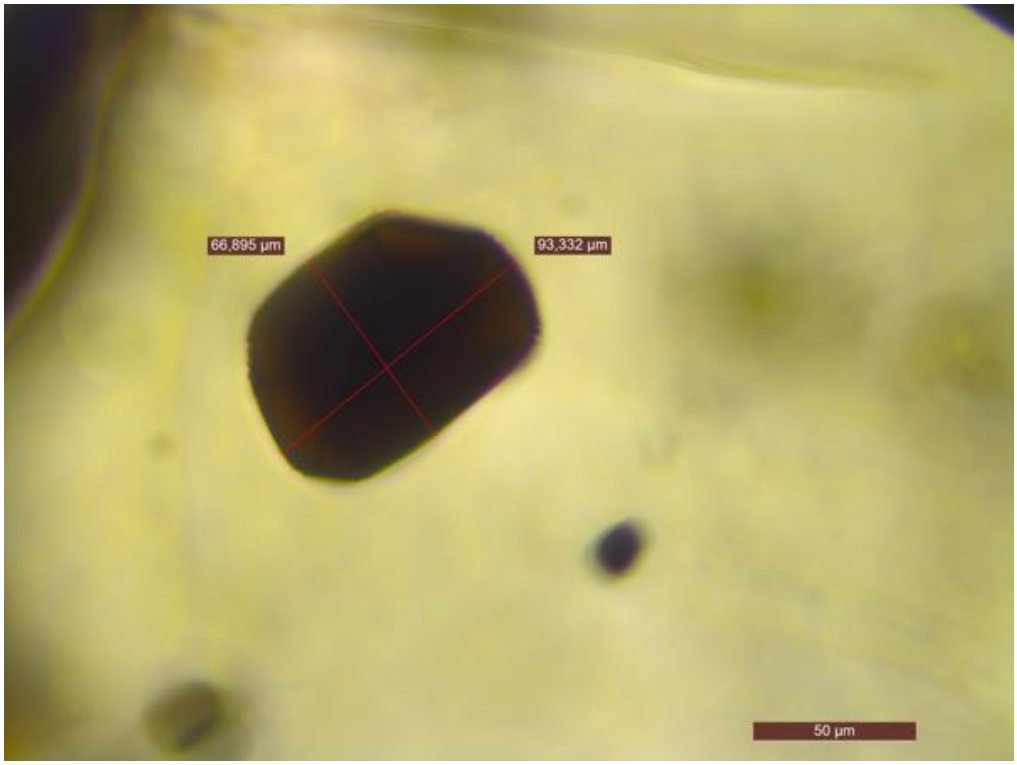

AE-II

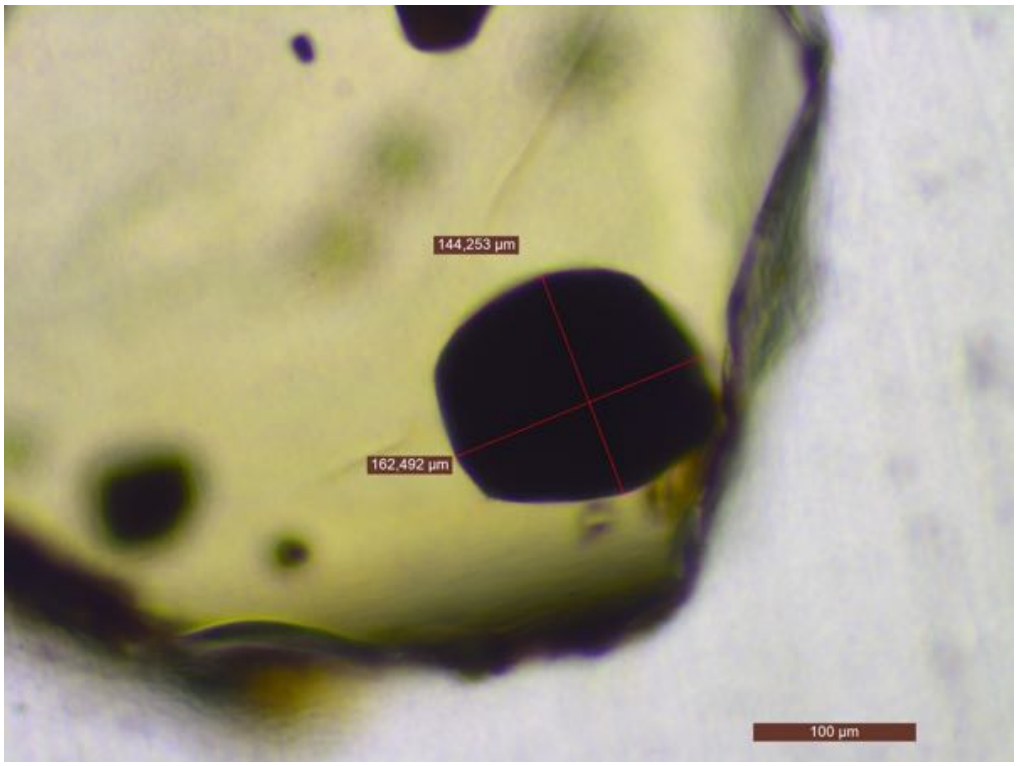

AF-I

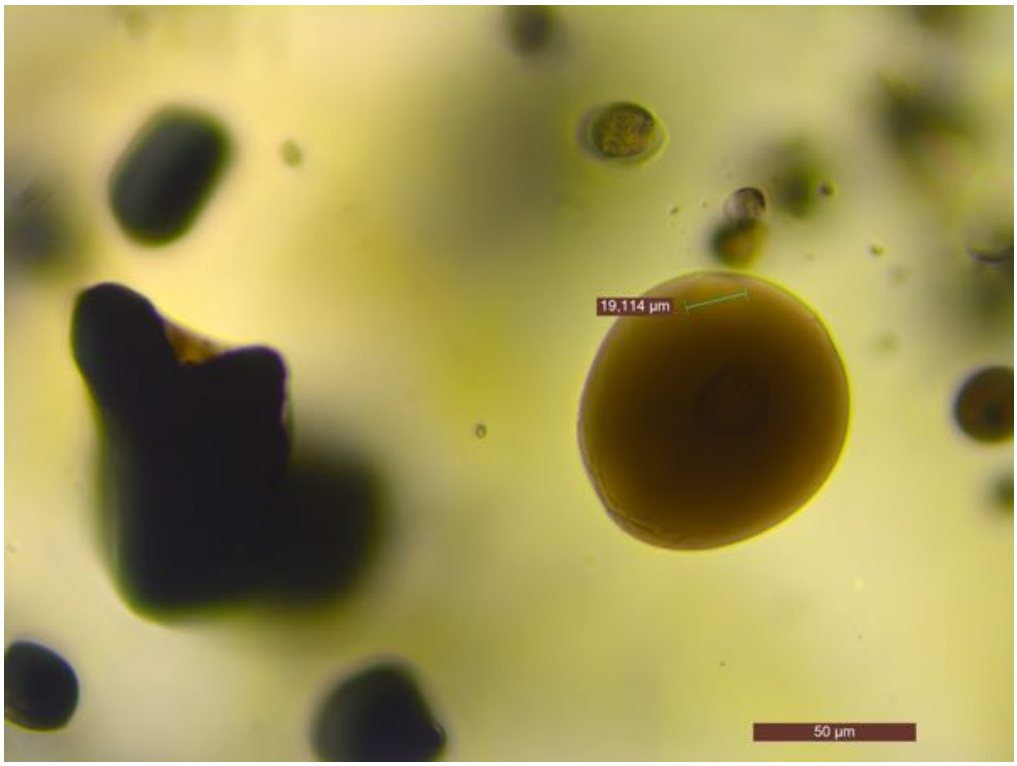

AGa-I

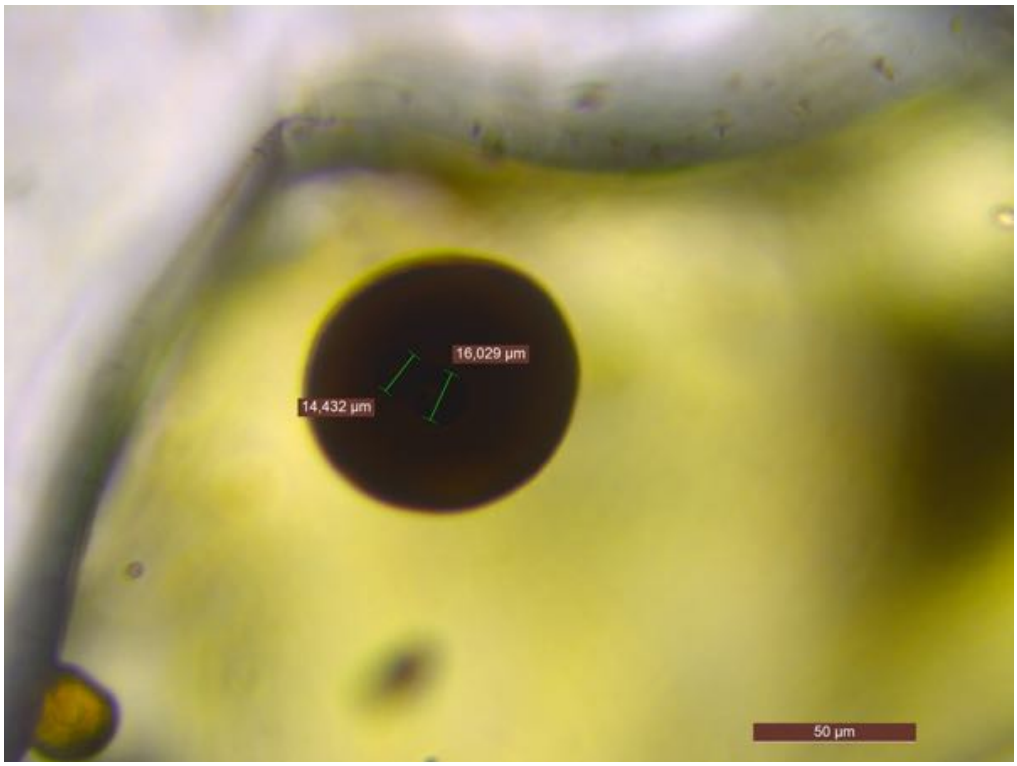

AGb-IV

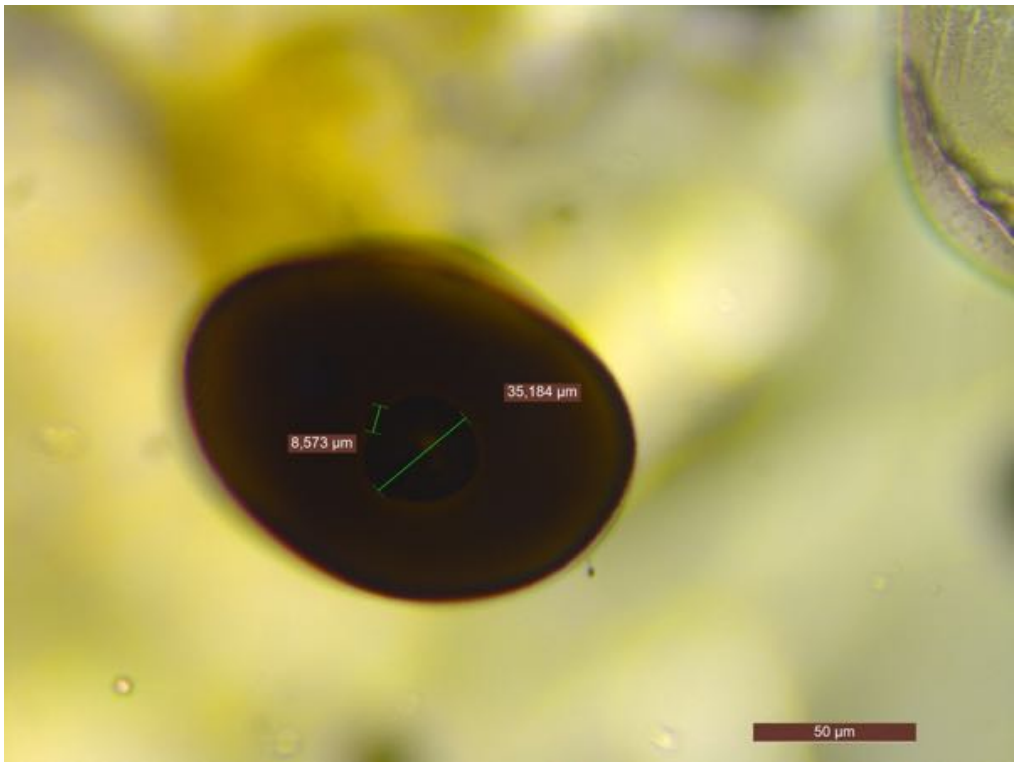

AGb-V

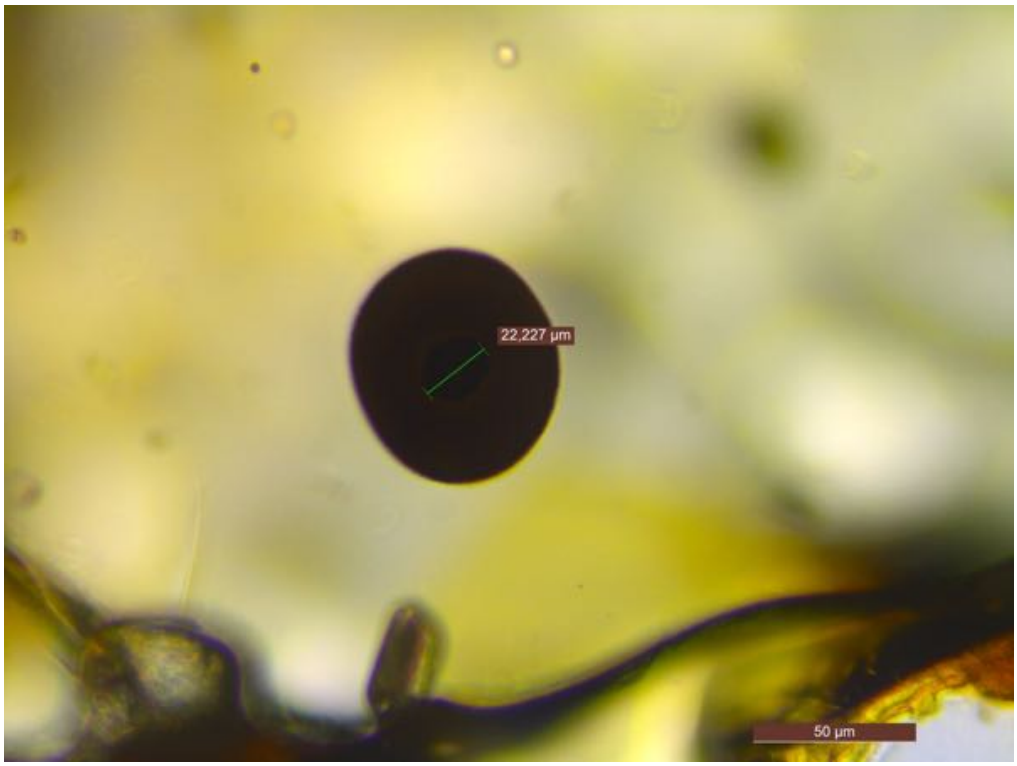

AI-I

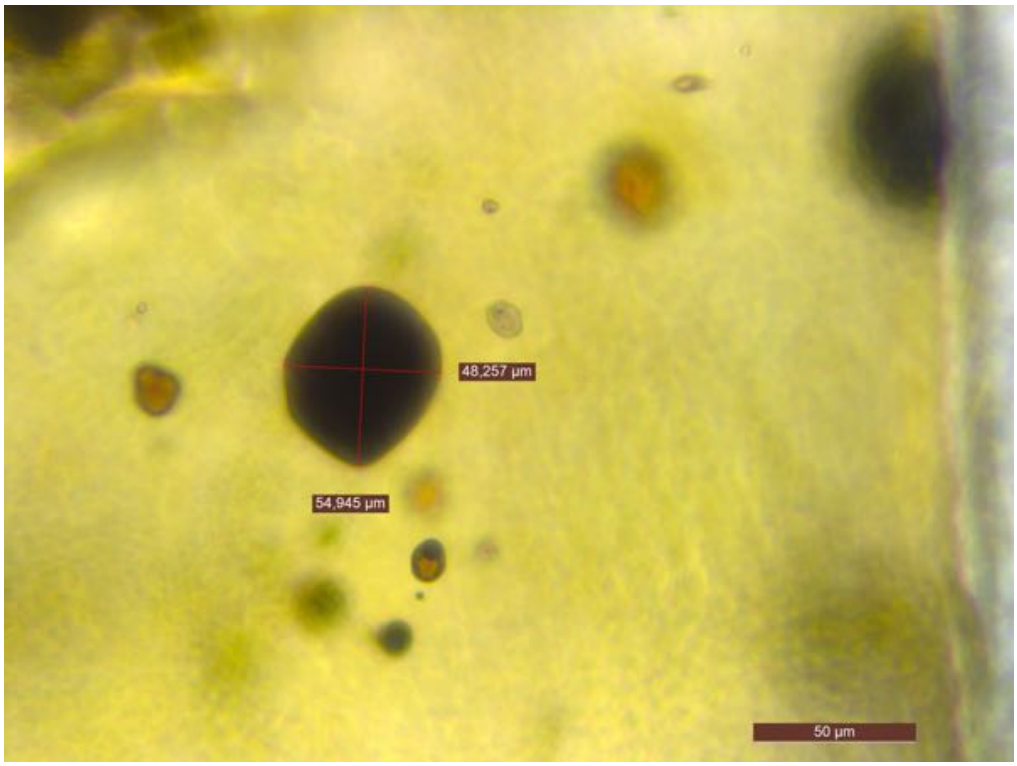

AK-I

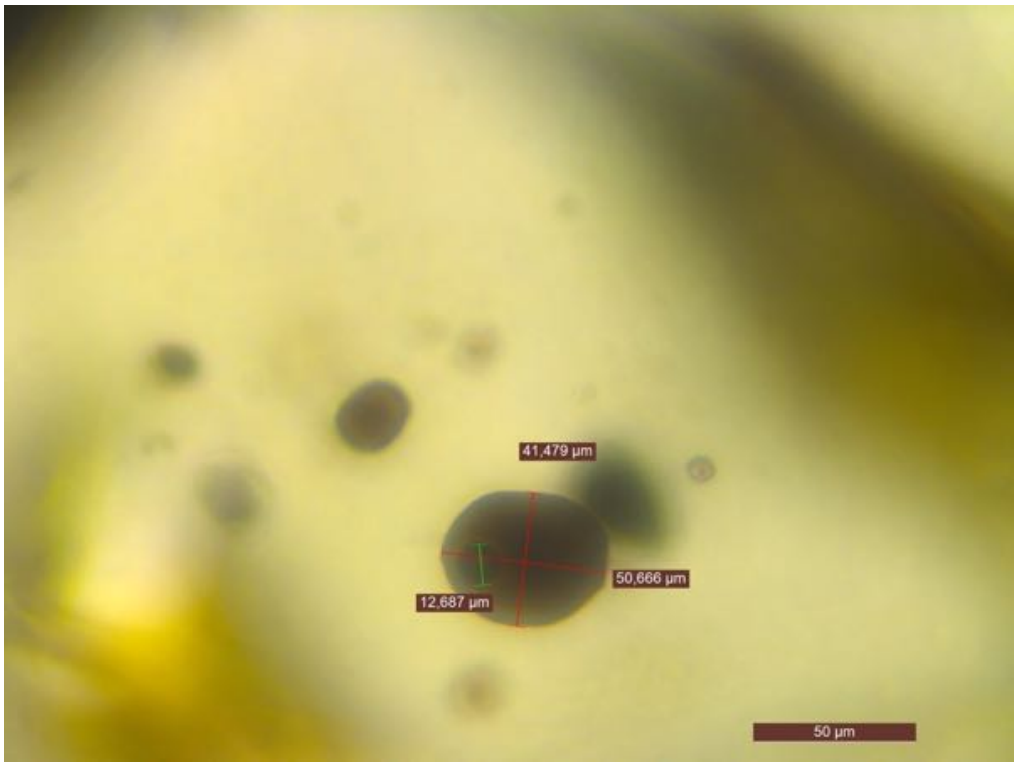

AK-II

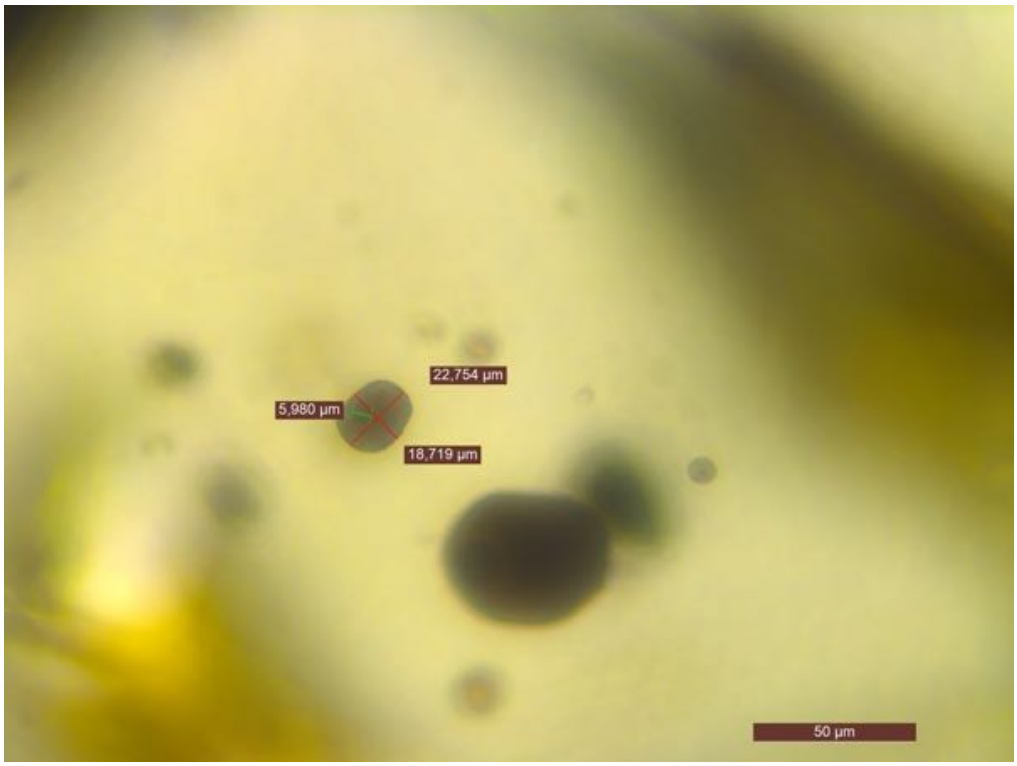

B-I

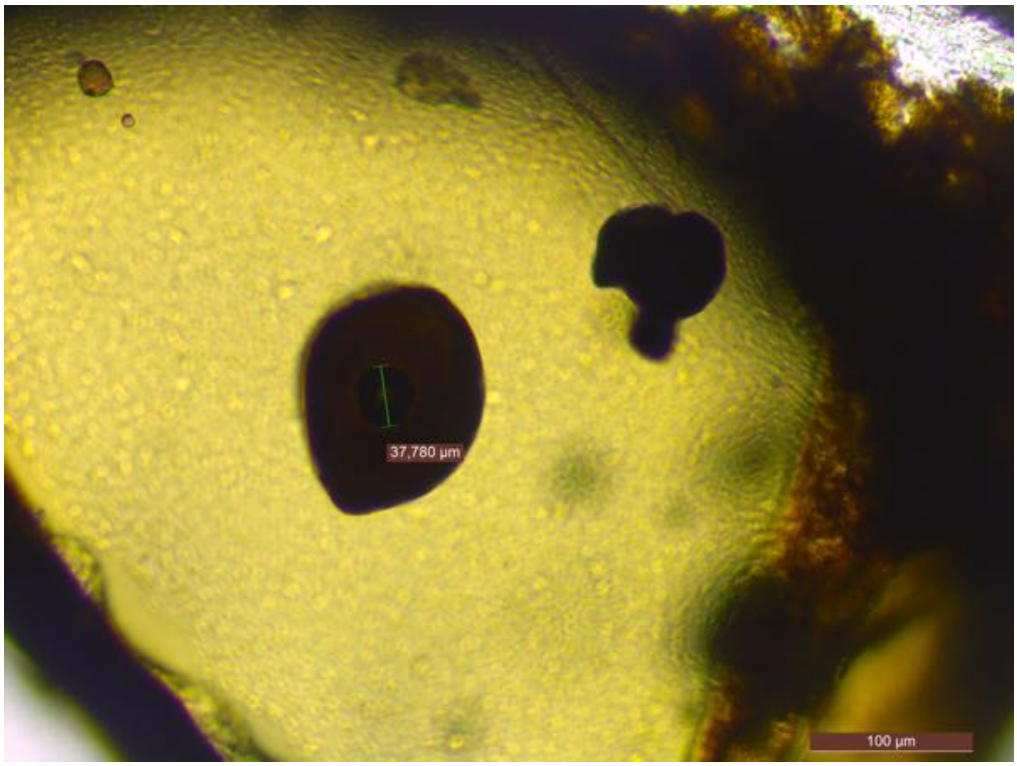

K-I

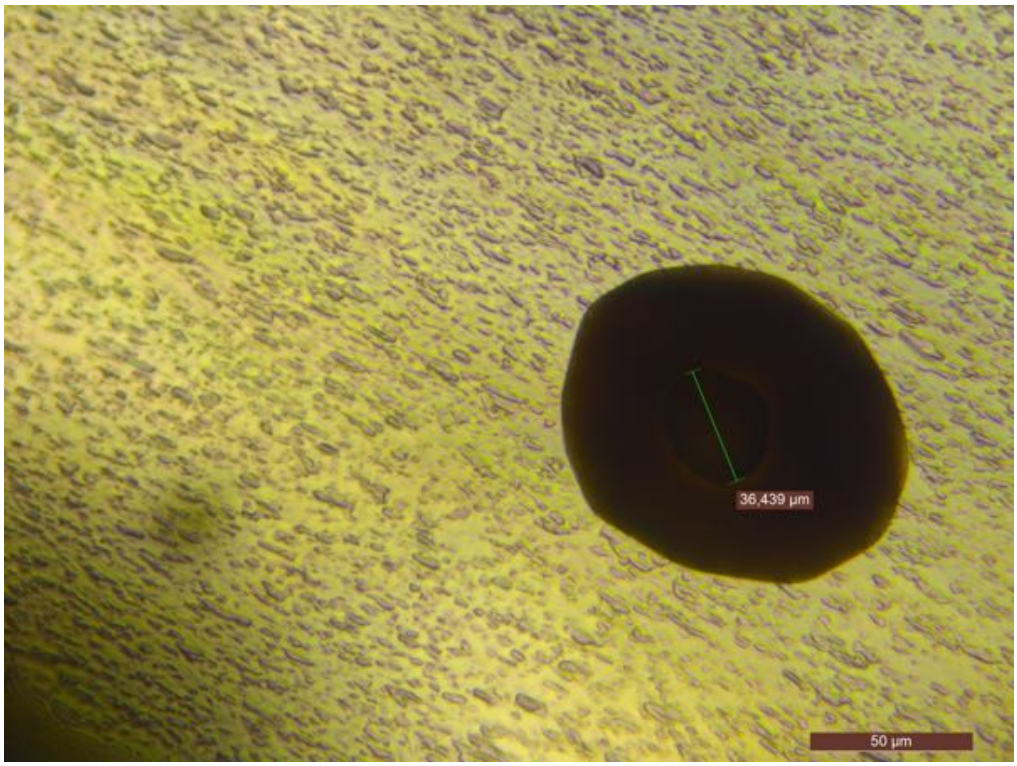

L-I

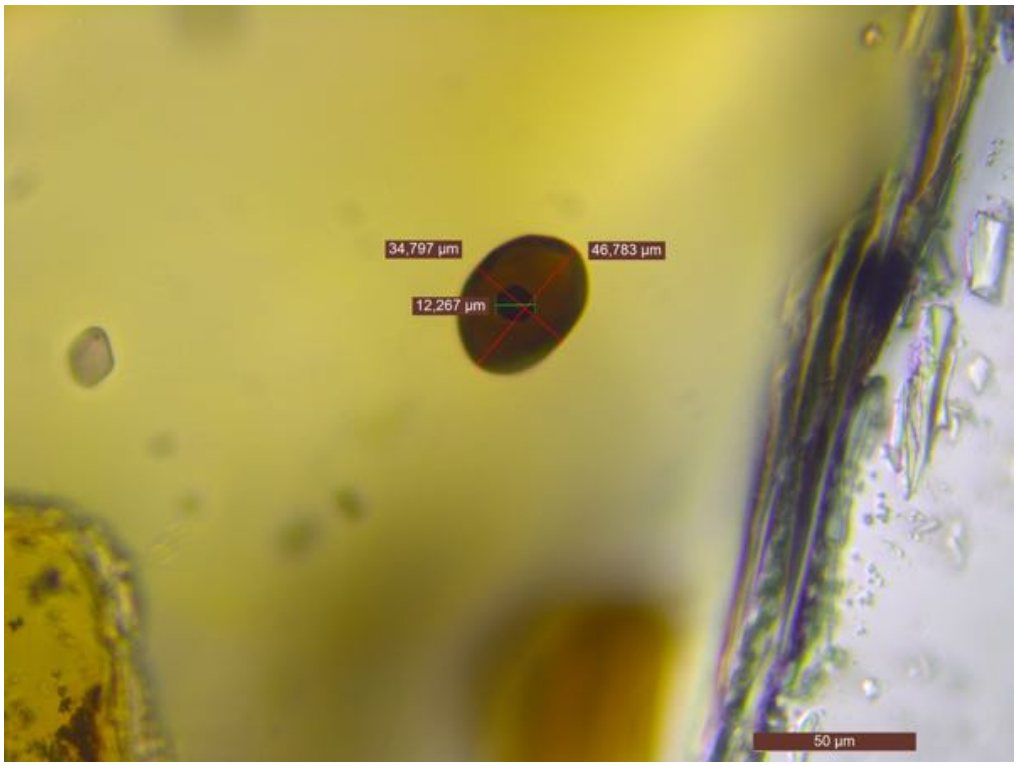
34,797 µm
46,783 µm
12,267 µm
50 µm

S-III

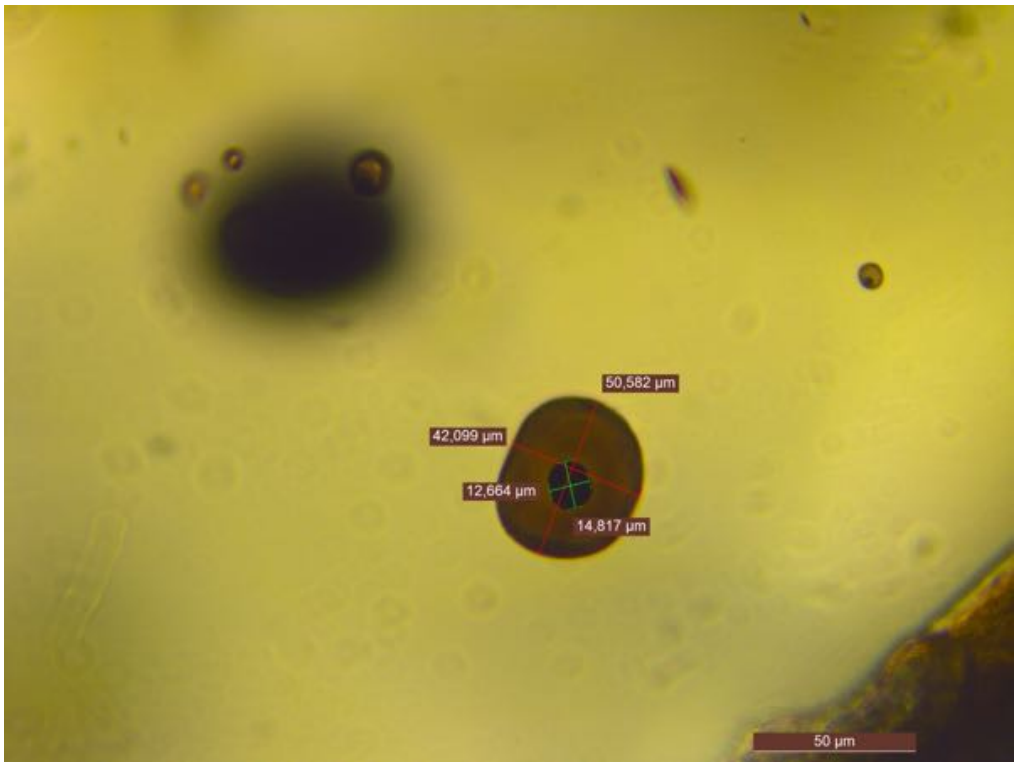
50,582 µm
42,099 µm
12,664 µm
14,817 µm
50 µm

U-I

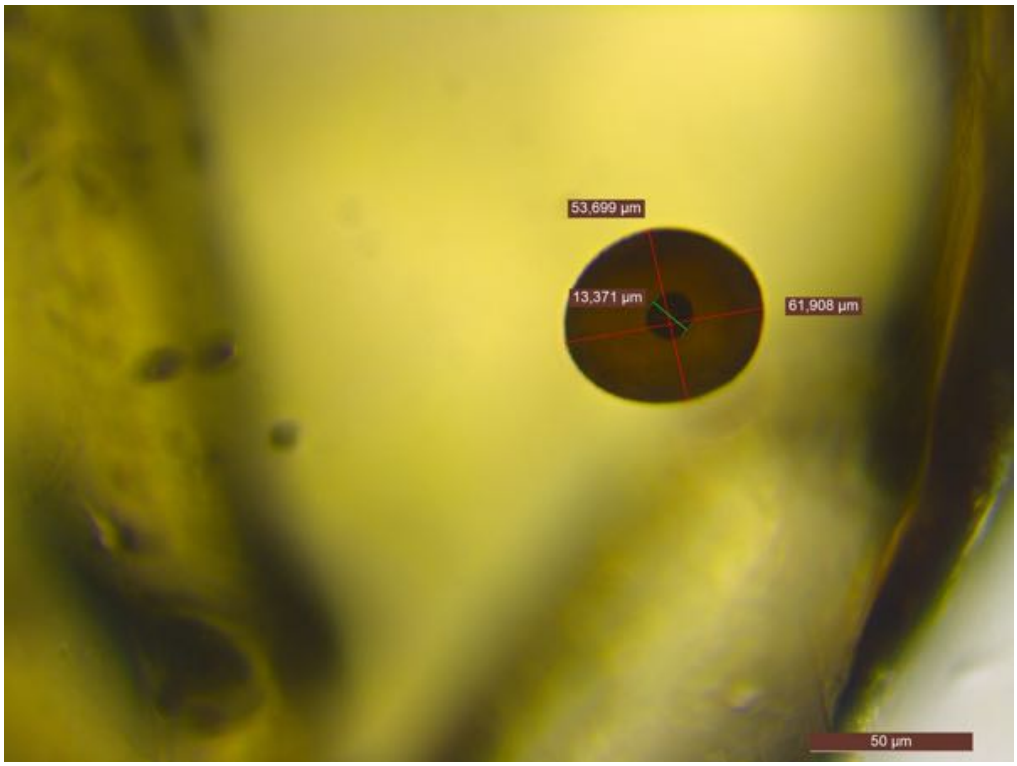

V-I

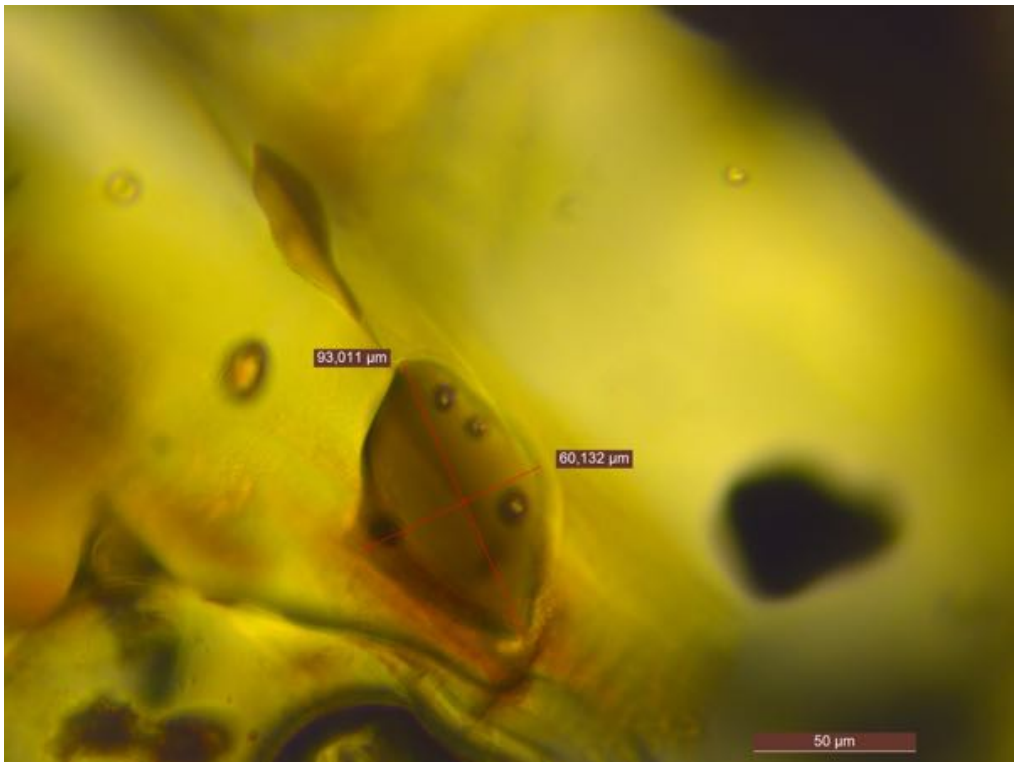

Y-I

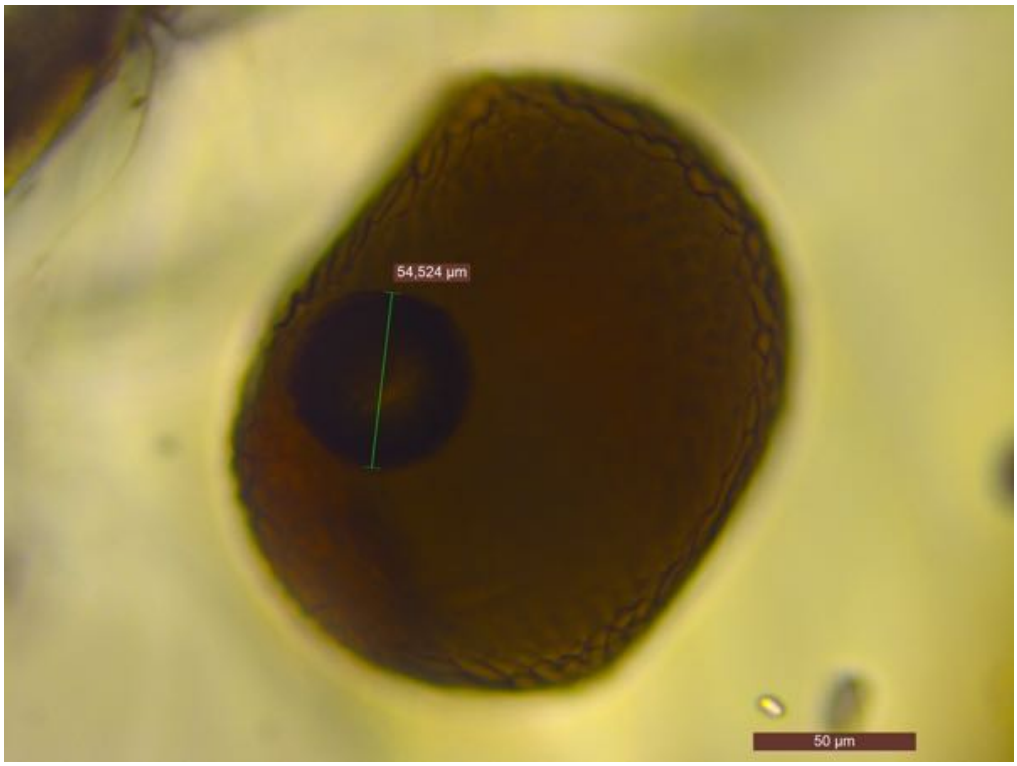

Y-II

<KSS>
AA-I

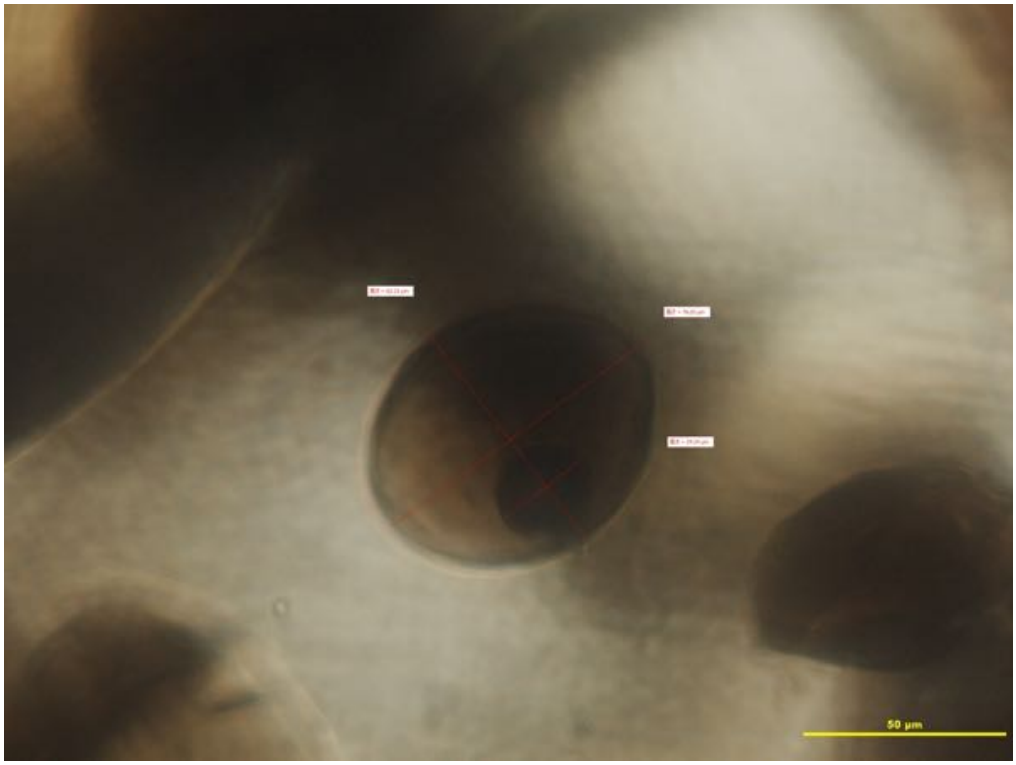

AA-II

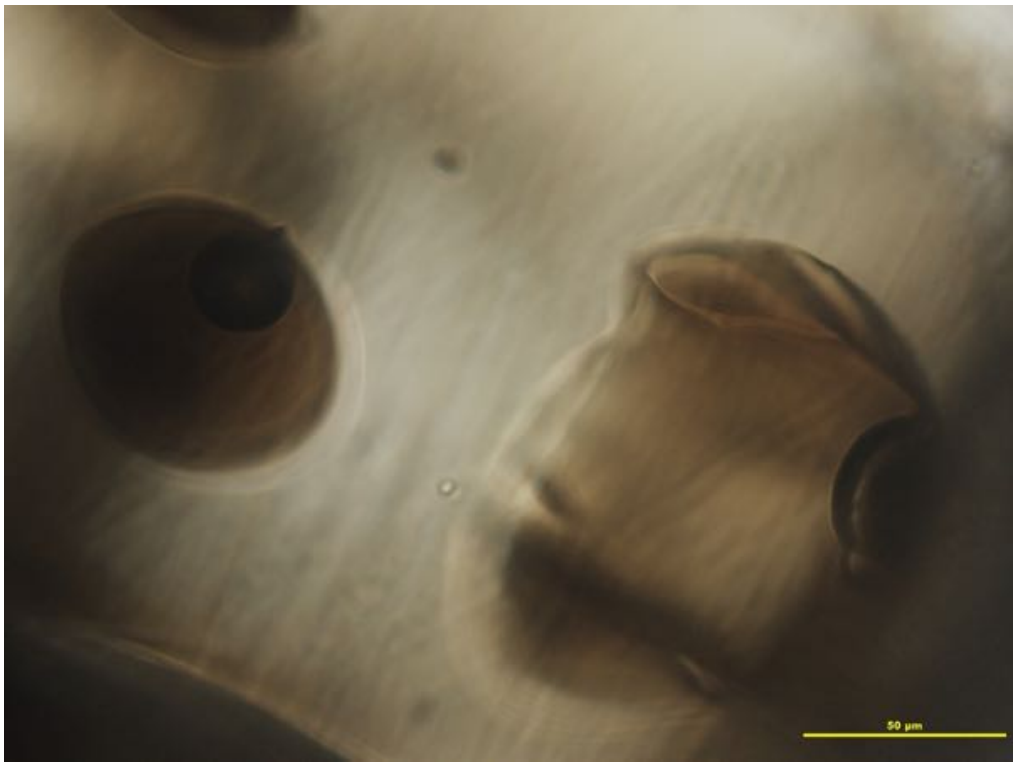

AA-III

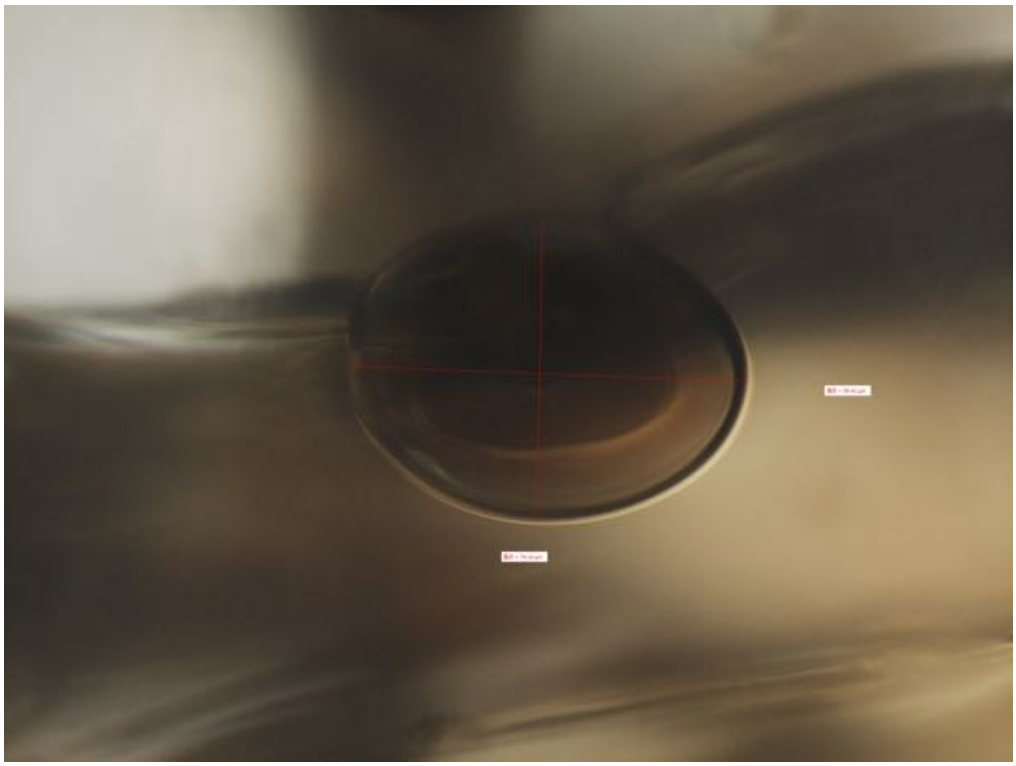

AB-I

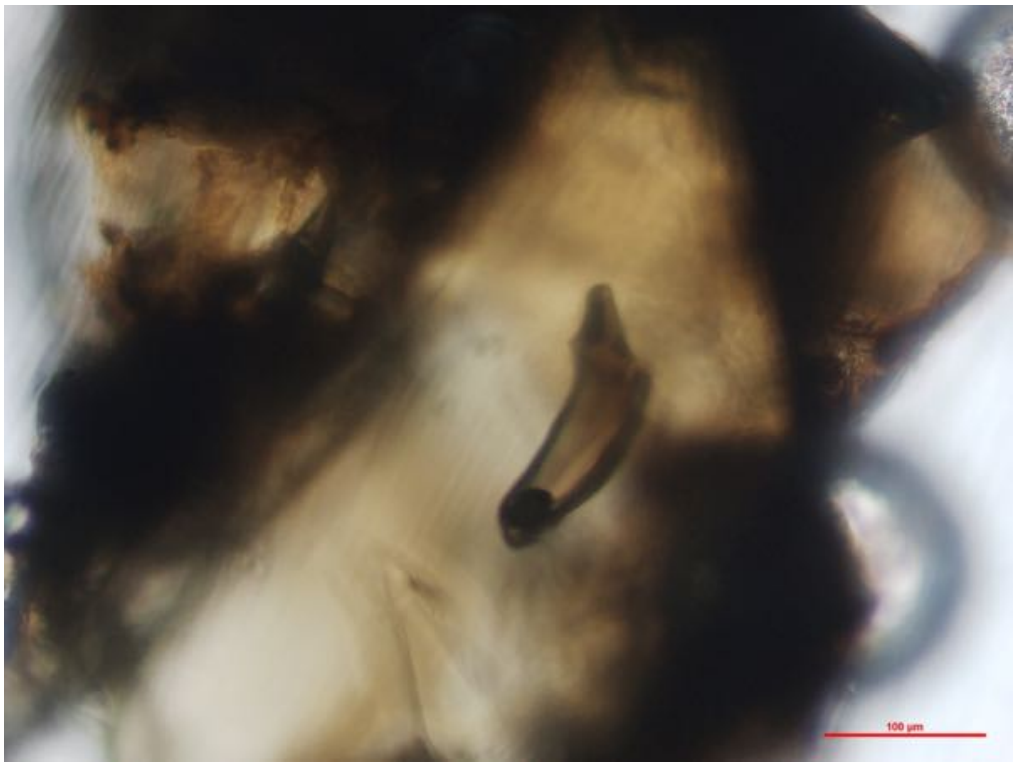

D-I

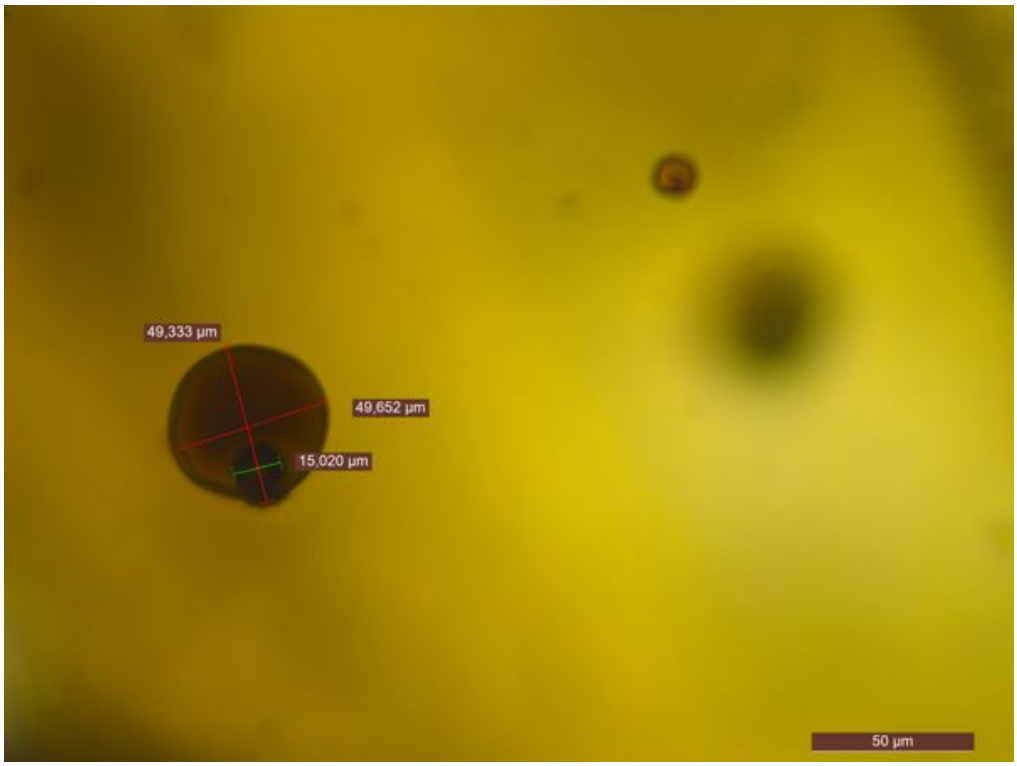

D-II

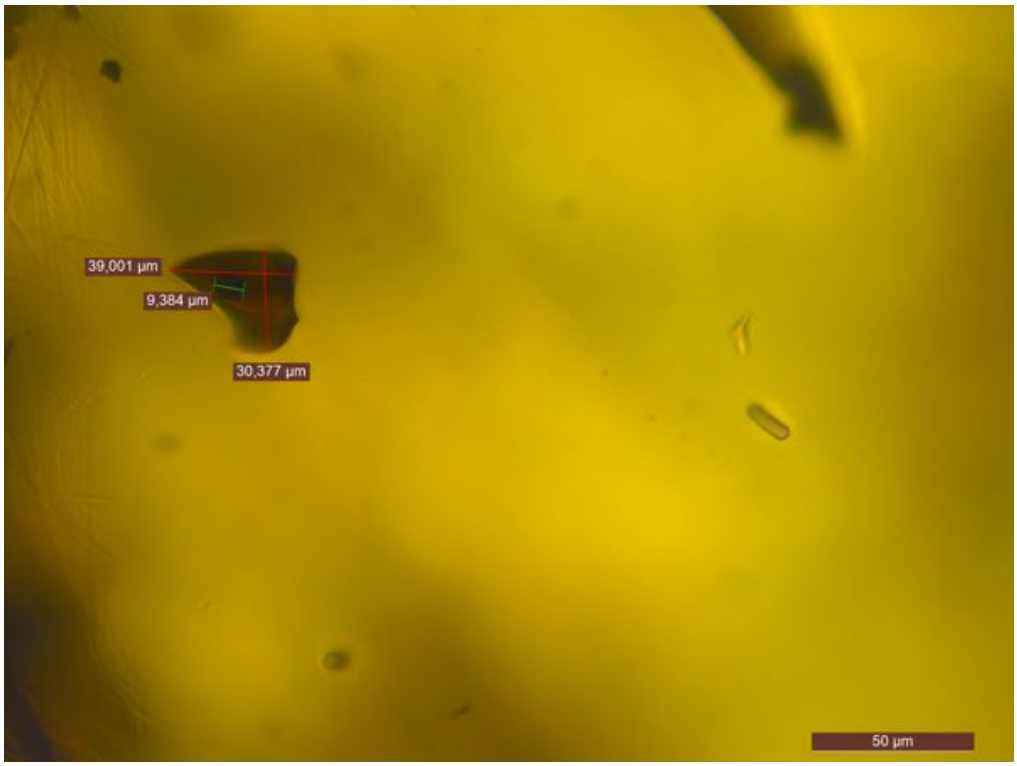

E-I

*Real scale is 50 µm. Length have to be divided by 4.

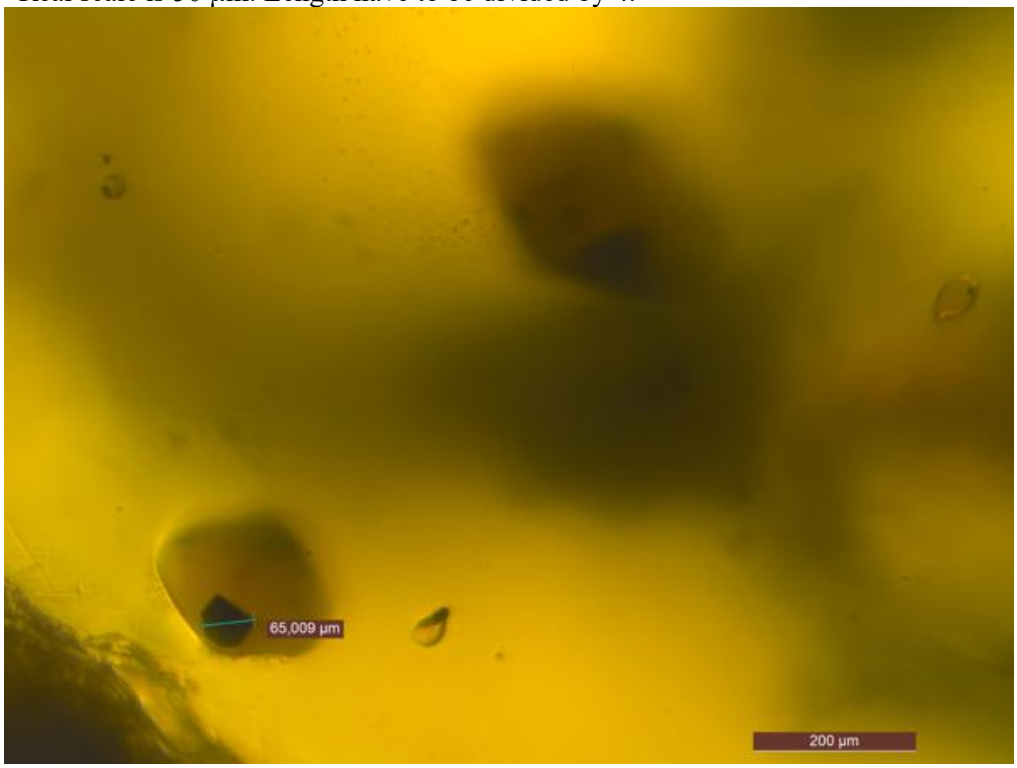

E-II

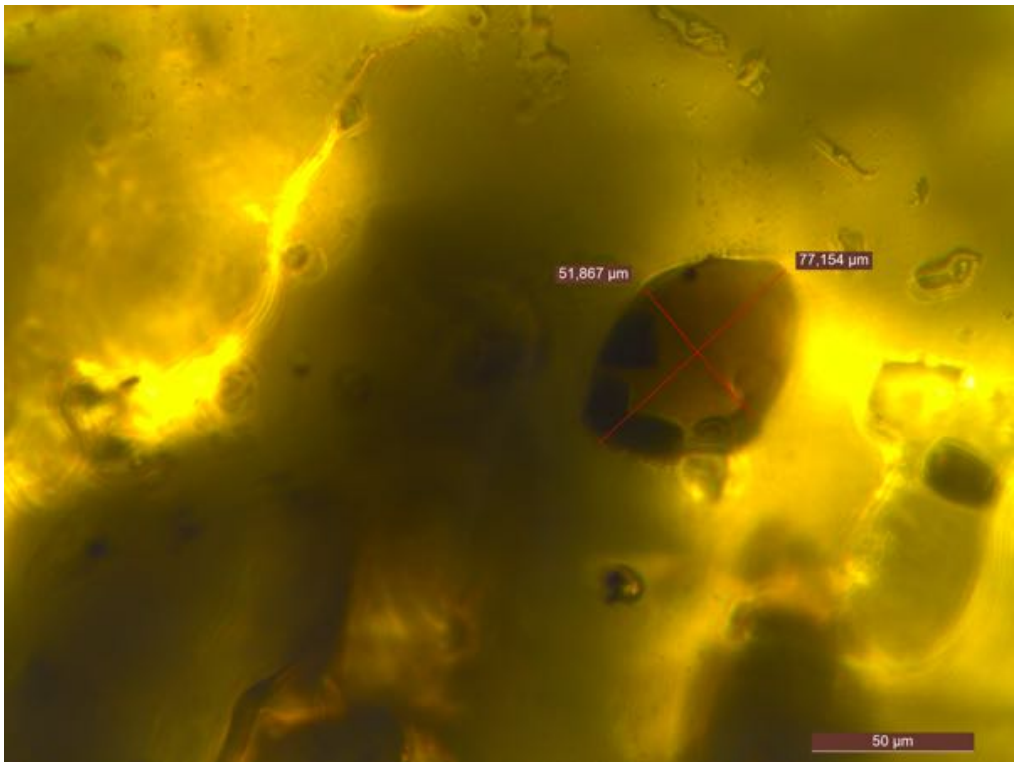

G-I

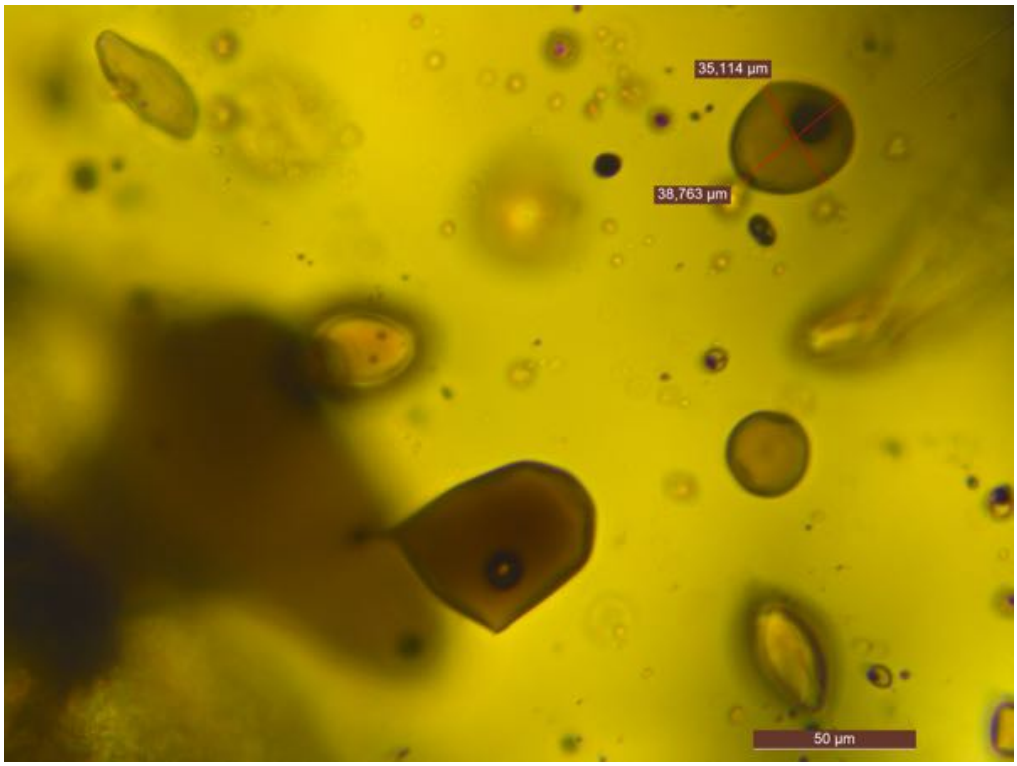

G-II

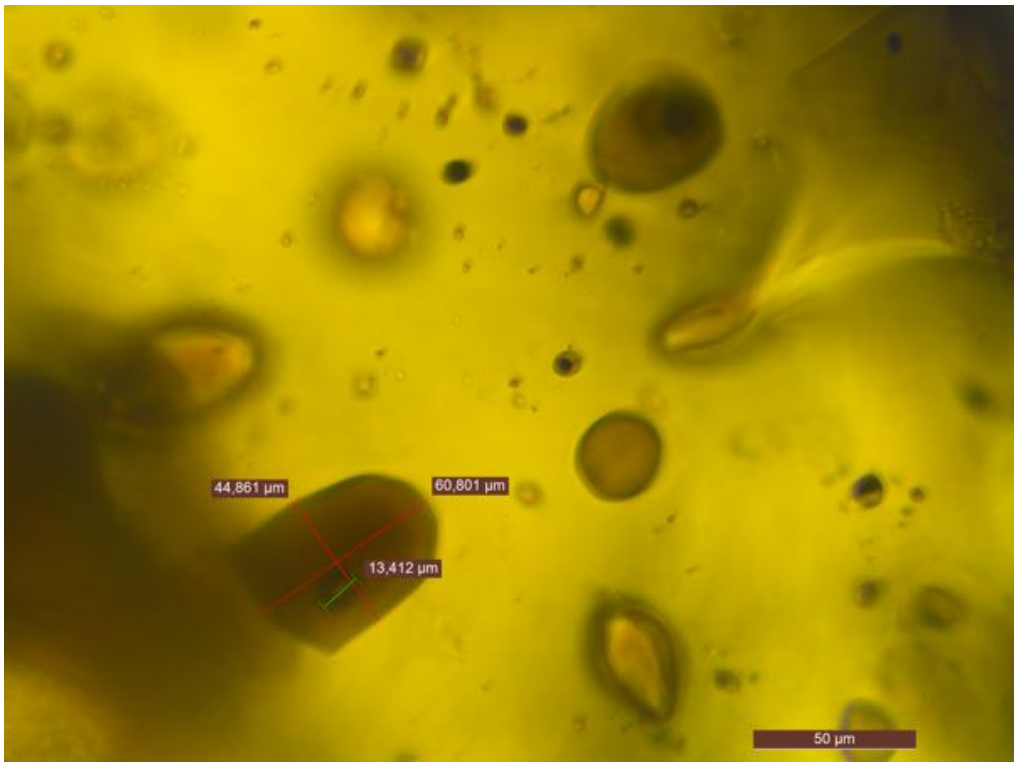

G-III

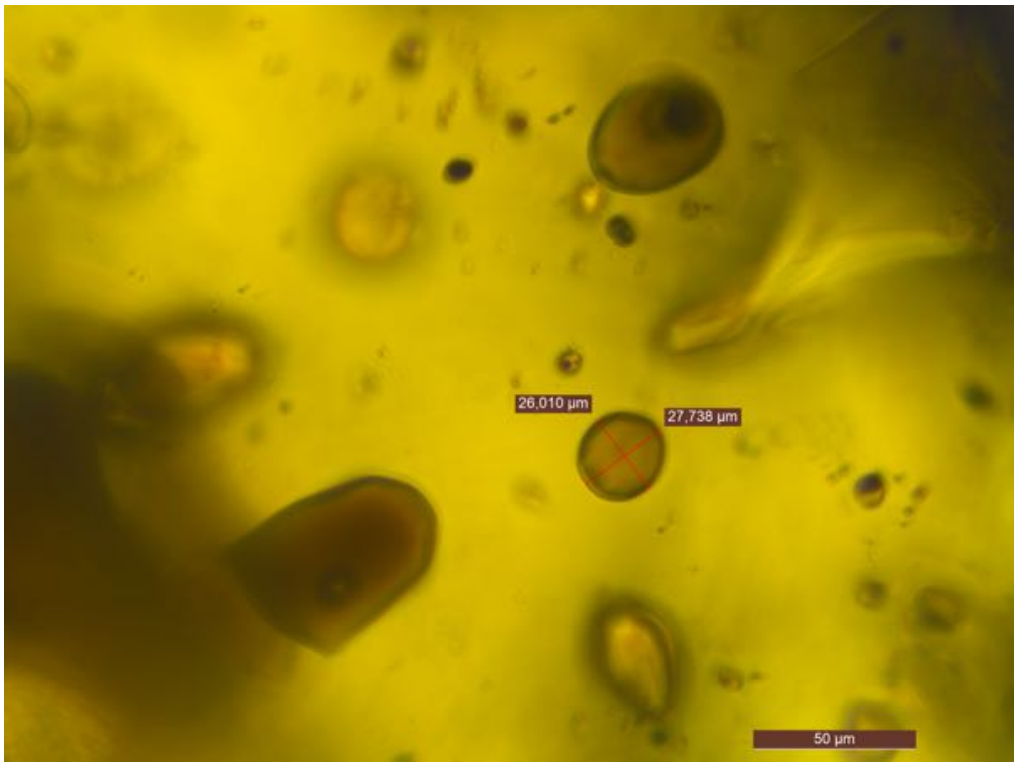

H-I

*Real scale is 50 µm. Length have to divided by 4.

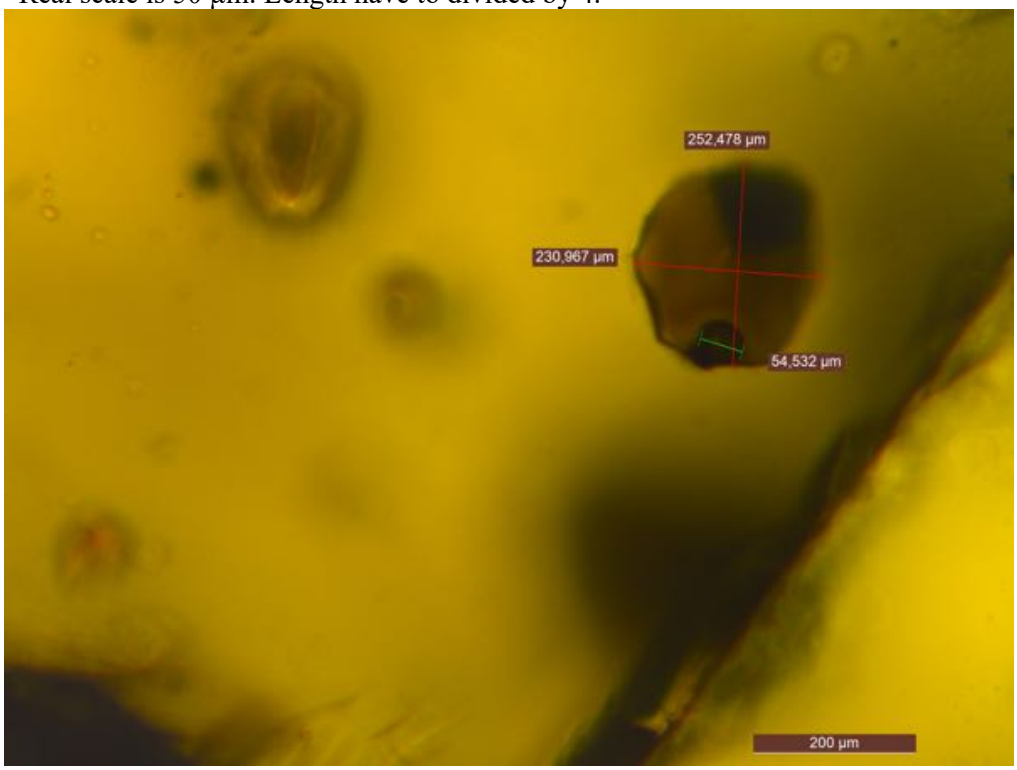

K-II

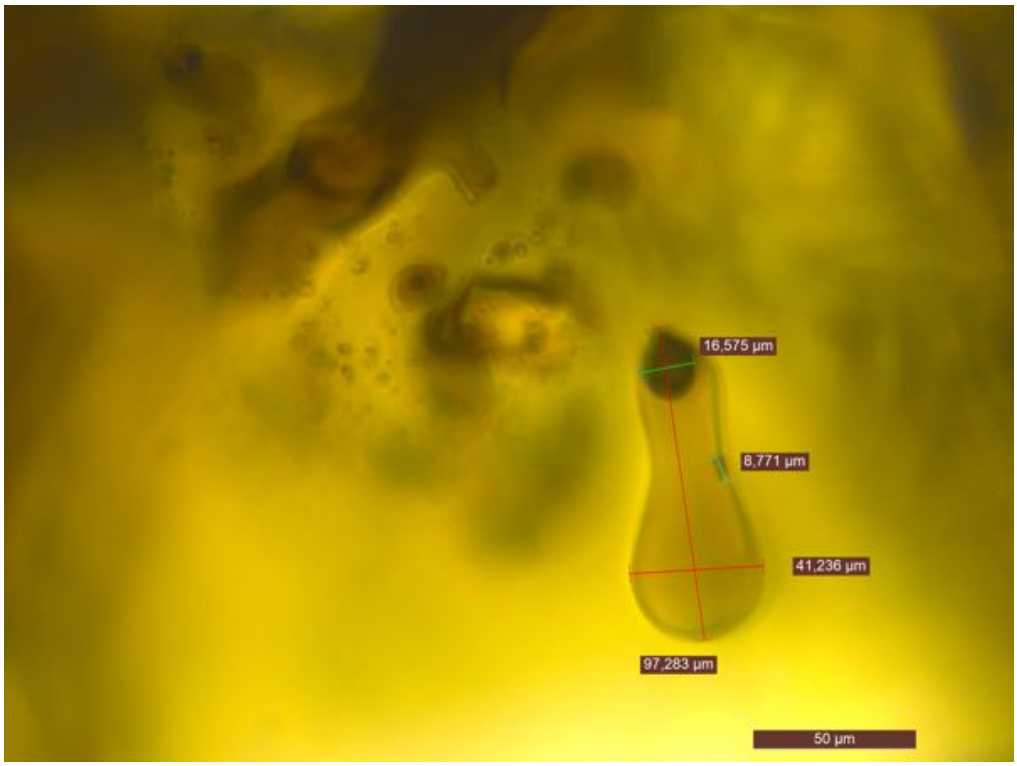

L-I

*Real scale of second photo is 50 µm. Length have to divided by 4.

S-I

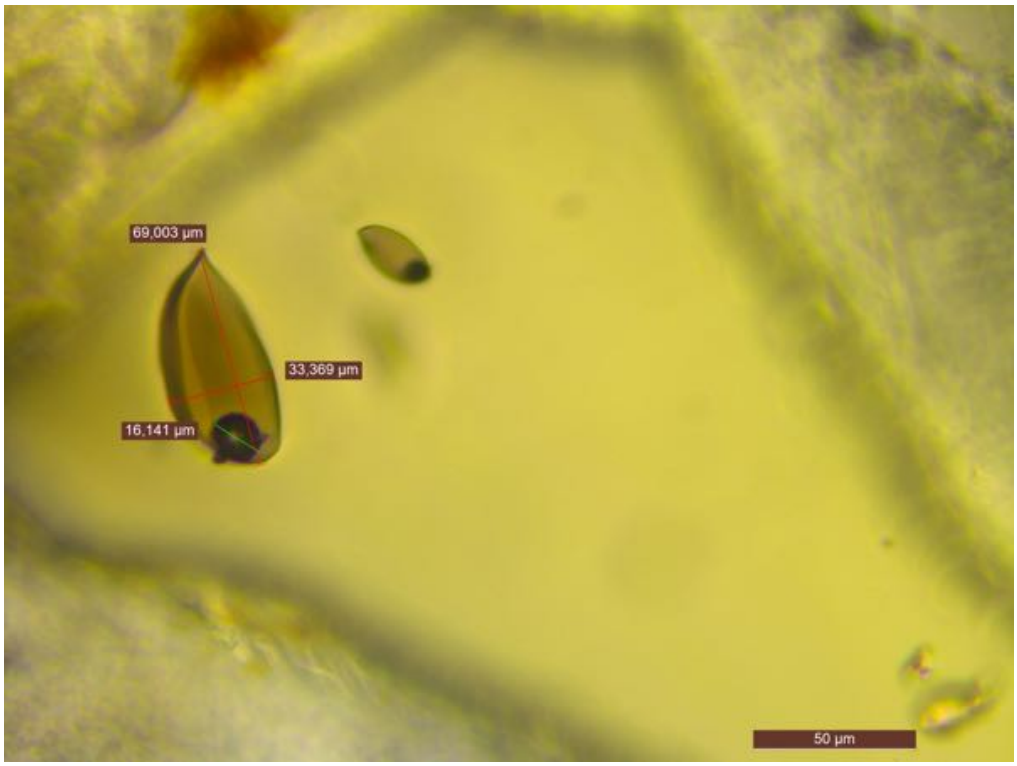

W-I

*Real scale of second photo is 50 µm. Length have to divided by 4.

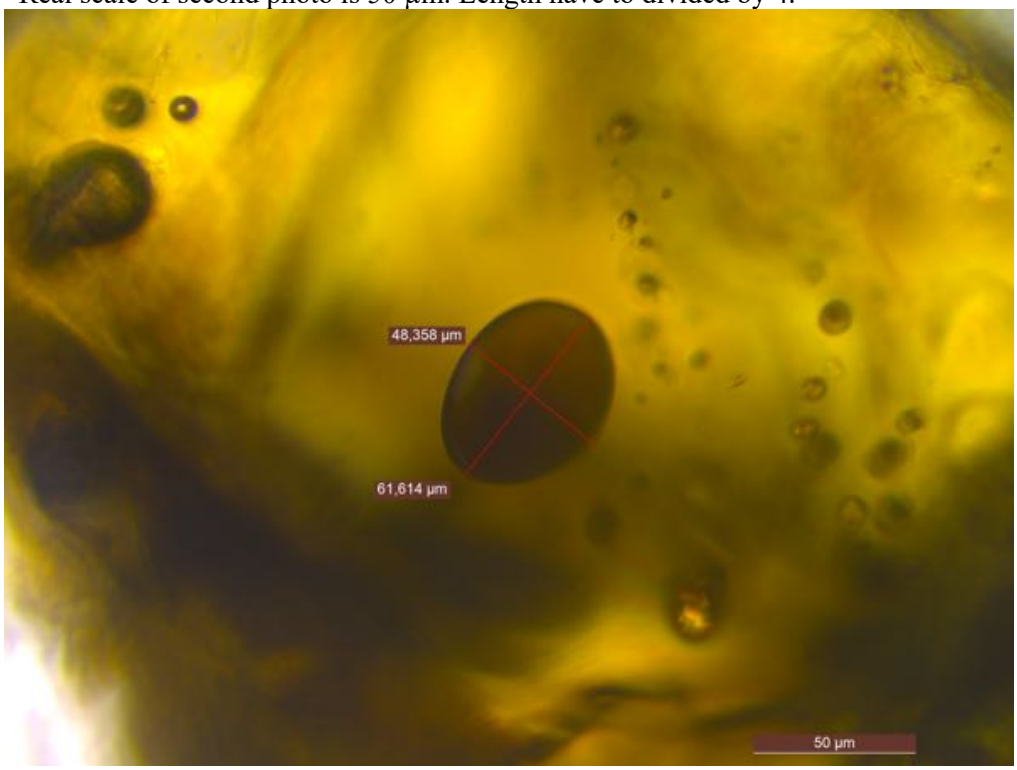

<KROHTH>
A-I

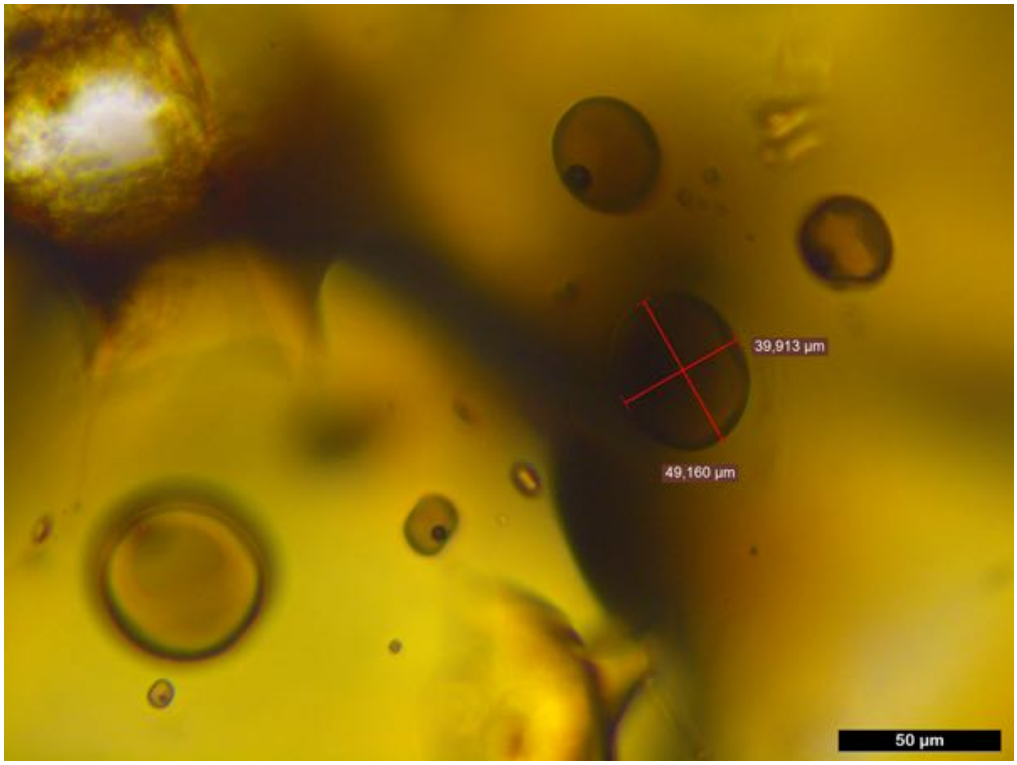

A-II

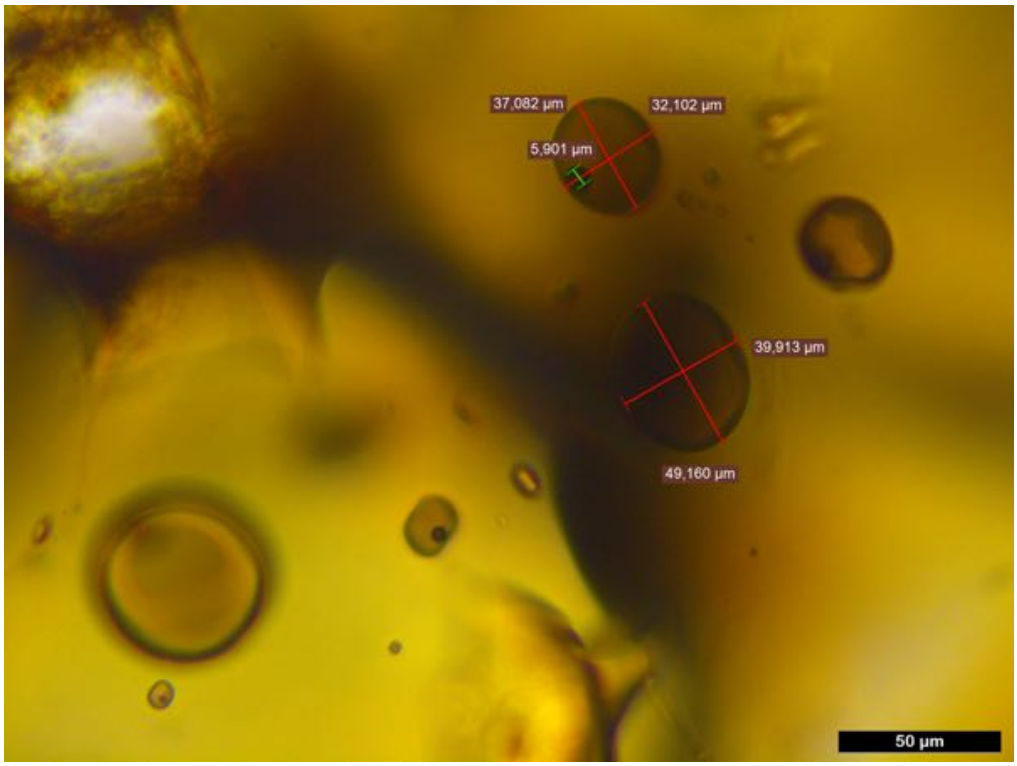

C-I

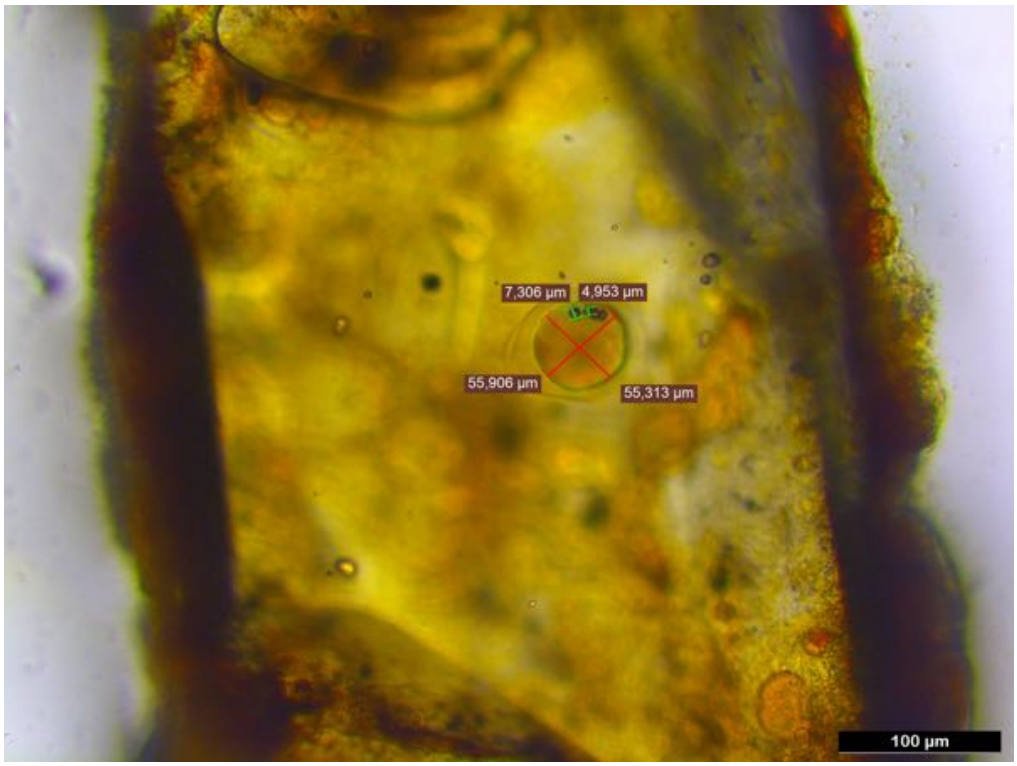
7,306 µm
4,953 µm
55,906 µm
55,313 µm
100 µm

E-I

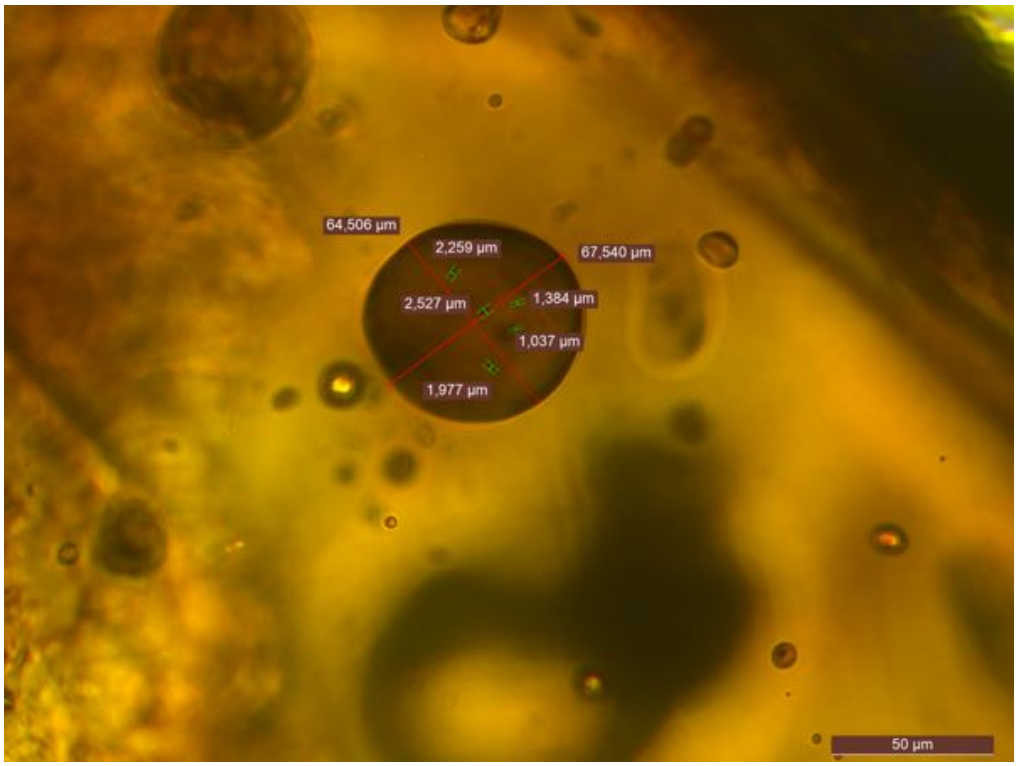
64,506 µm
2,259 µm
67,540 µm
2,527 µm
1,384 µm
1,037 µm
1,977 µm
50 µm

E-II

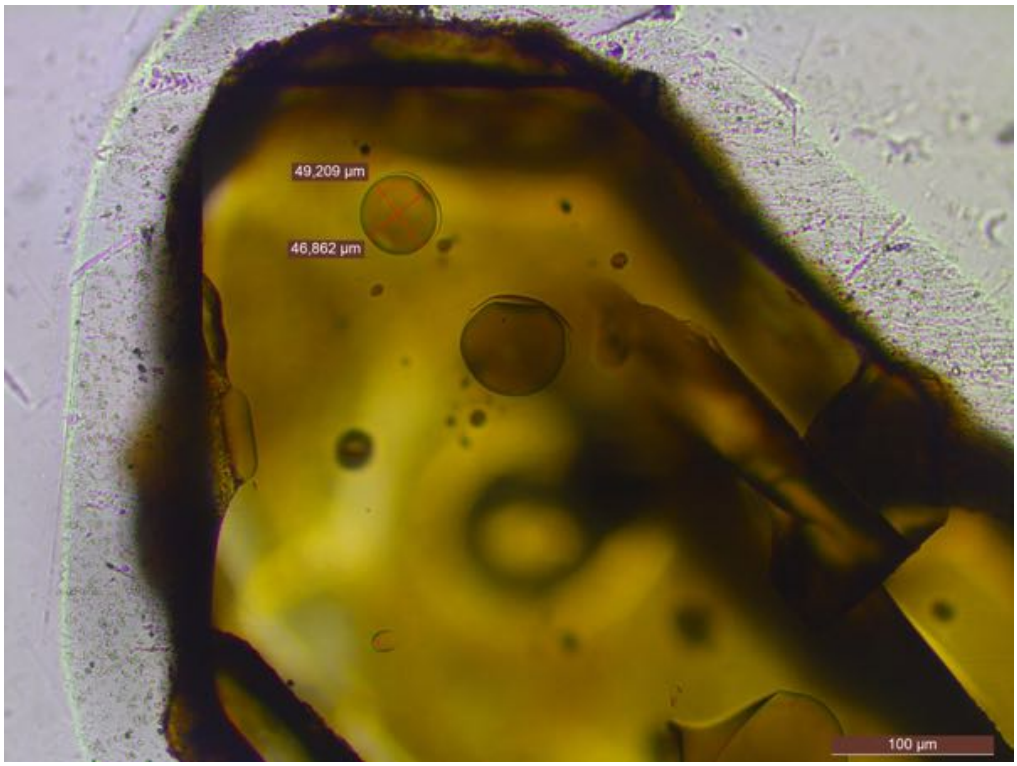
49,209 µm
46,862 µm
100 µm

E-III

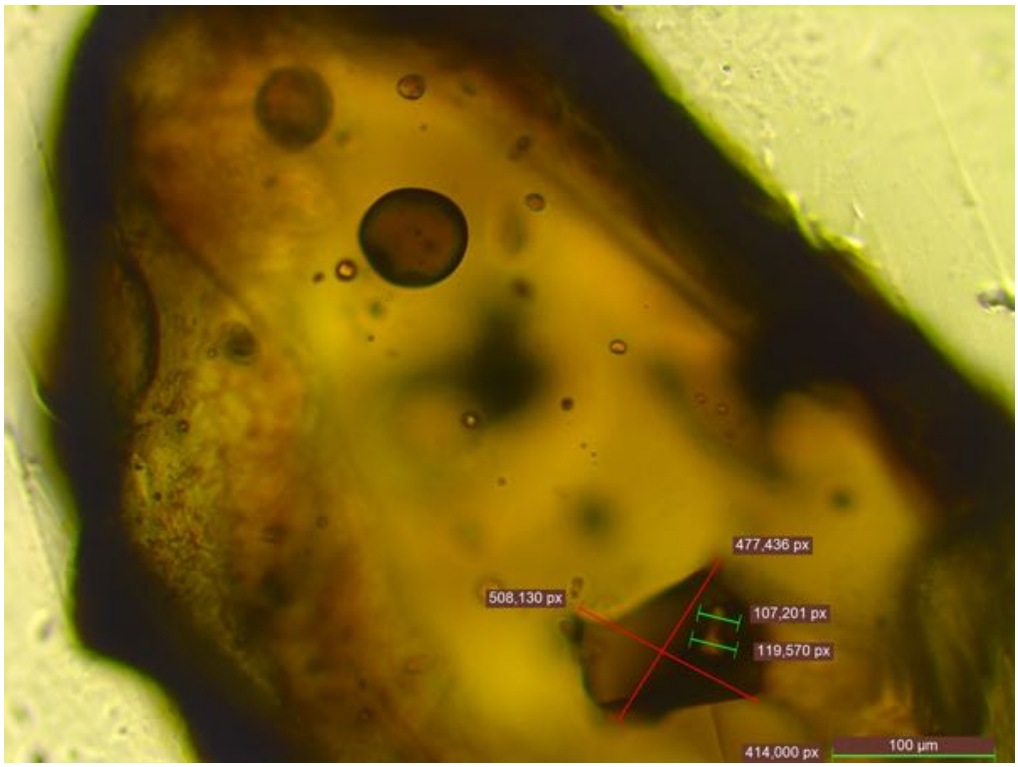
477,436 px
508,130 px
107,201 px
119,570 px
414,000 px
100 µm

F-I

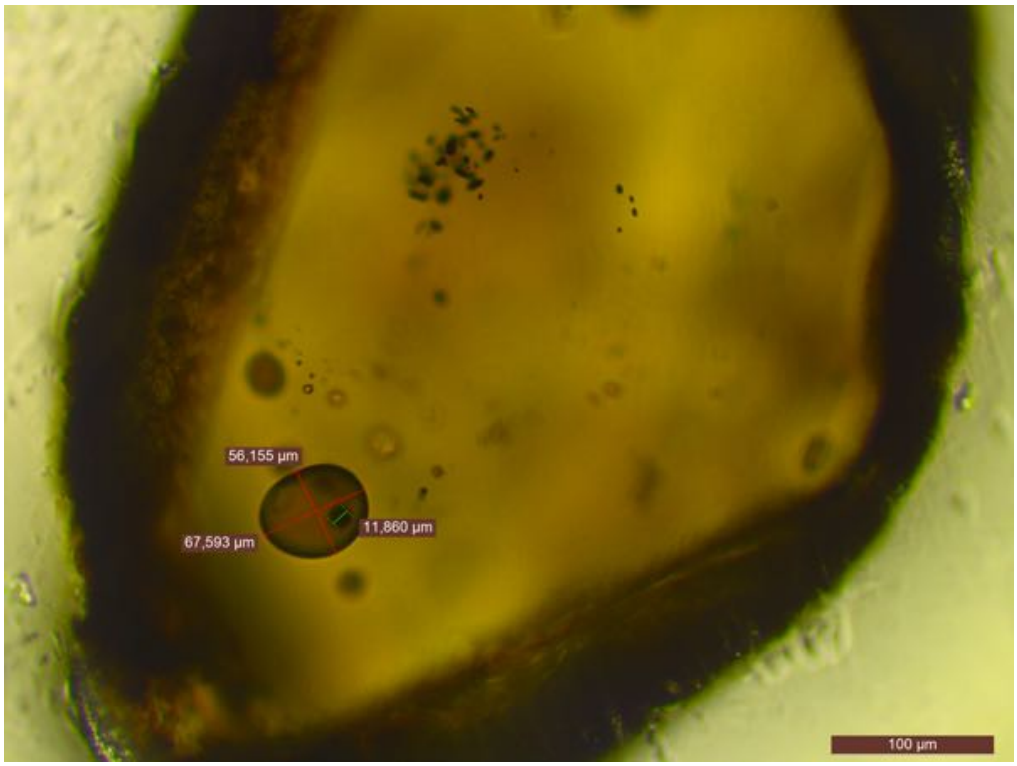

G-I

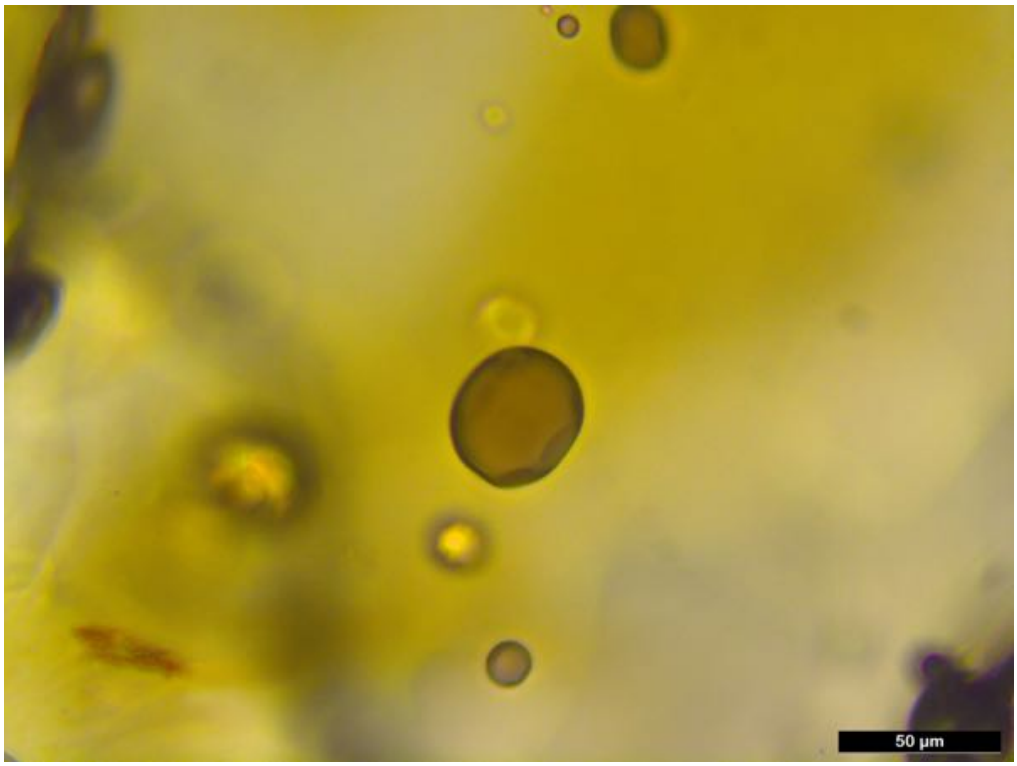

H-I

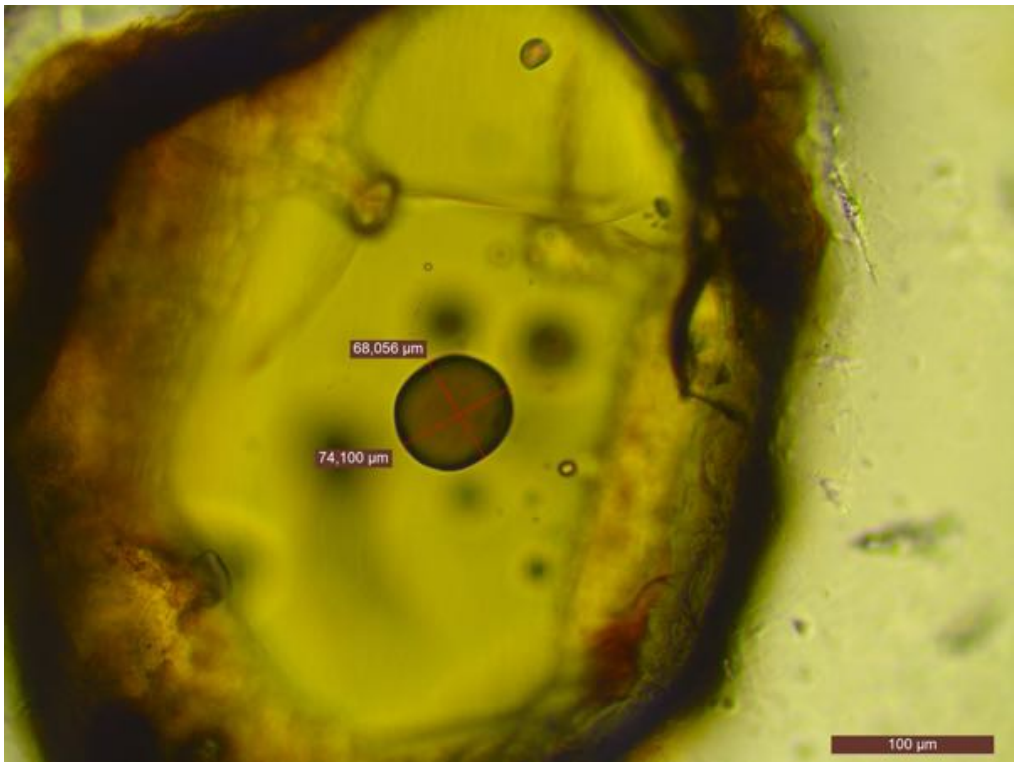

I-I

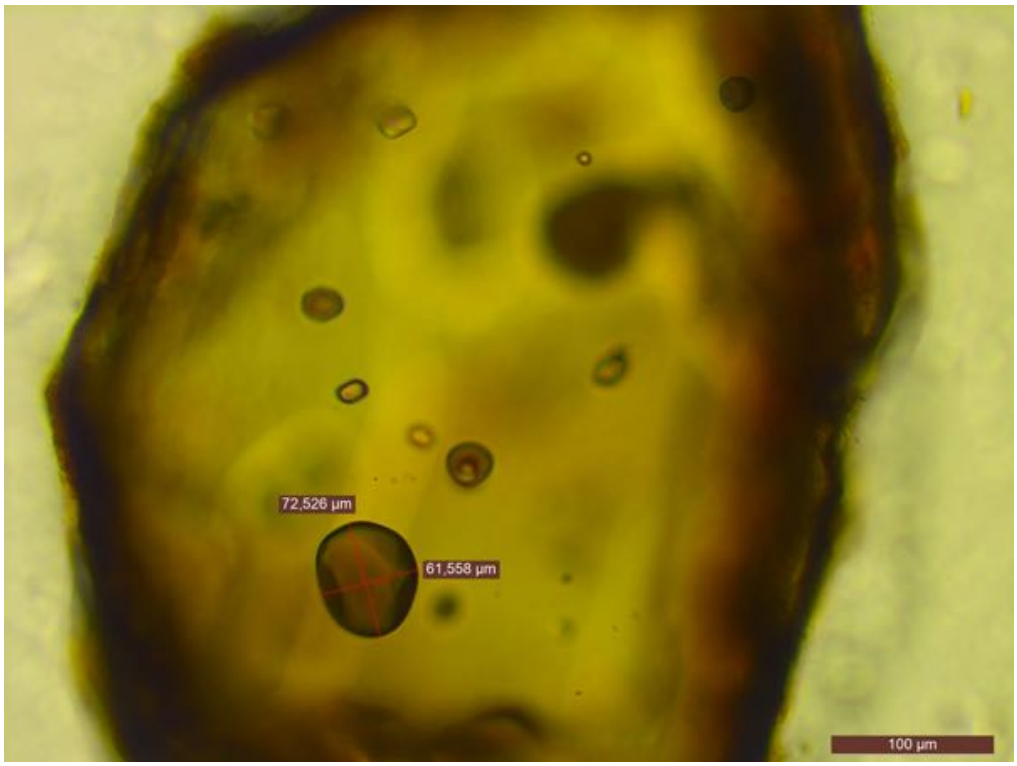

K-I

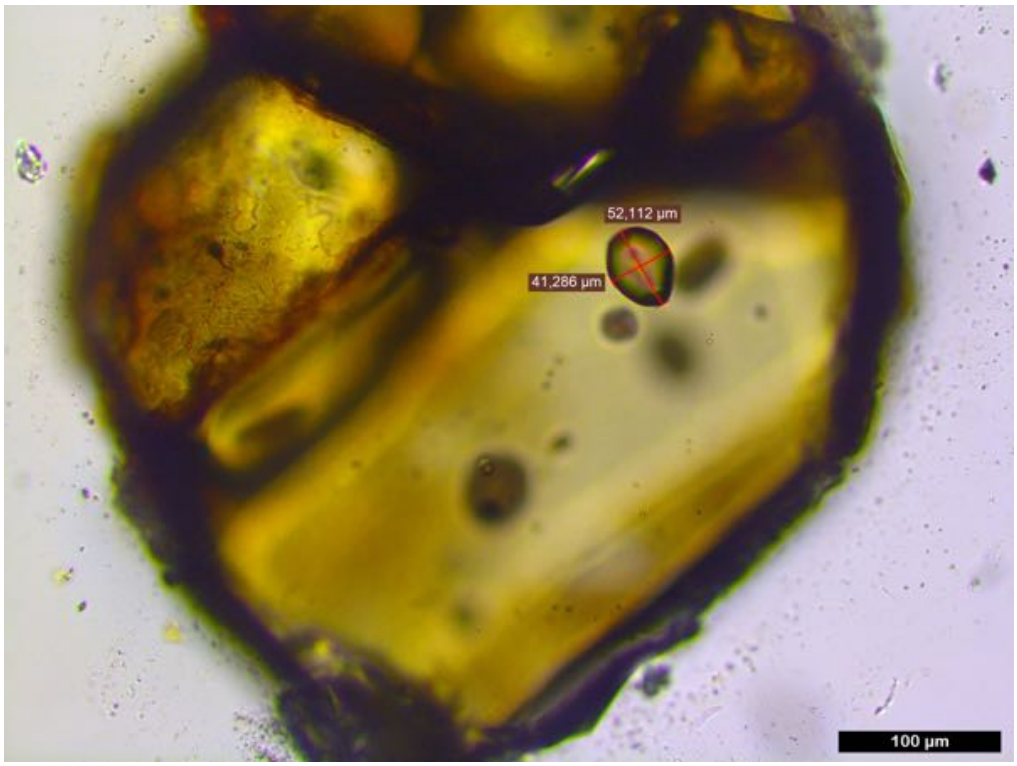

L-II

*First picture is same scale with second figure

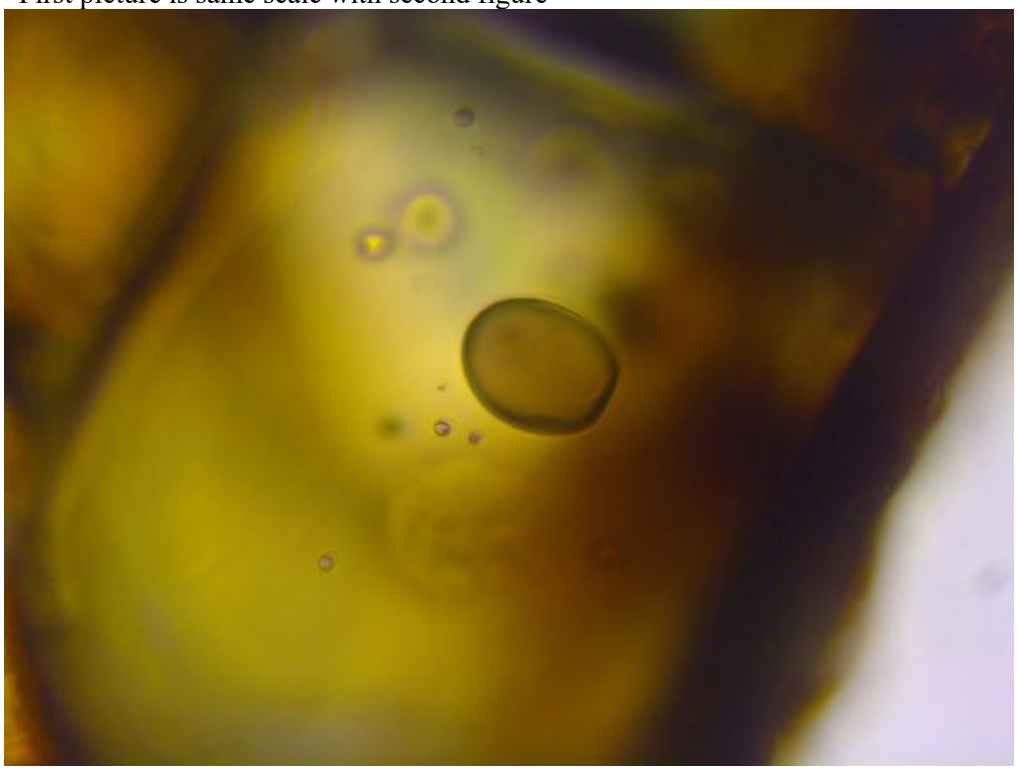

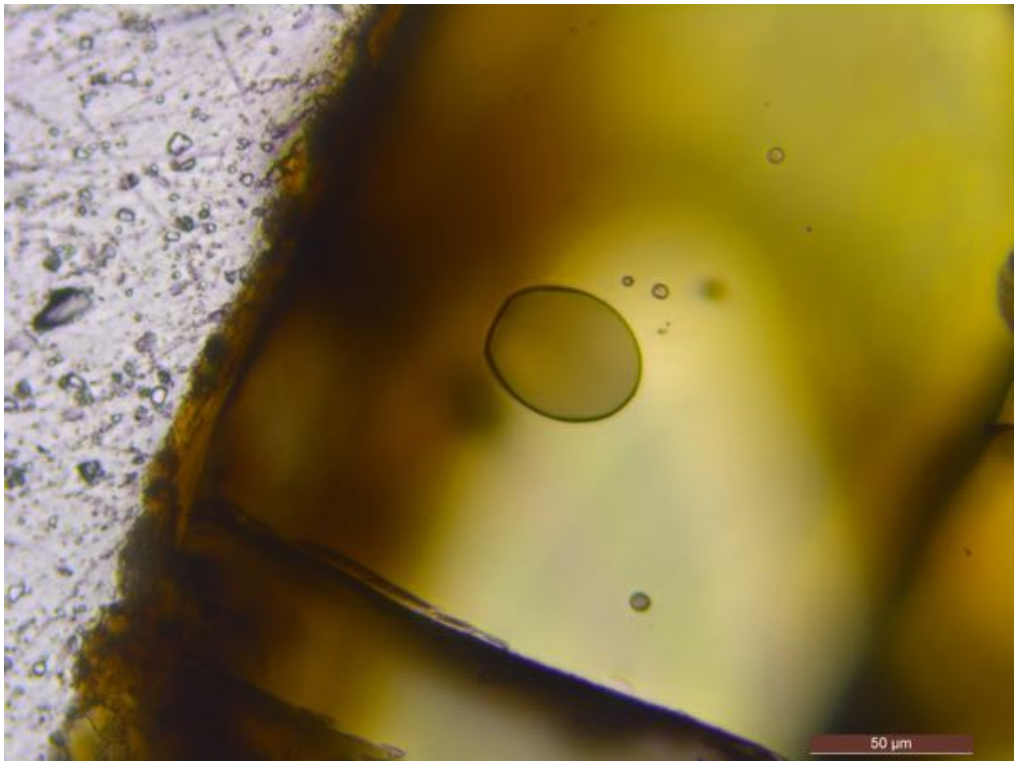
50 µm

<KRSM11>
A-I

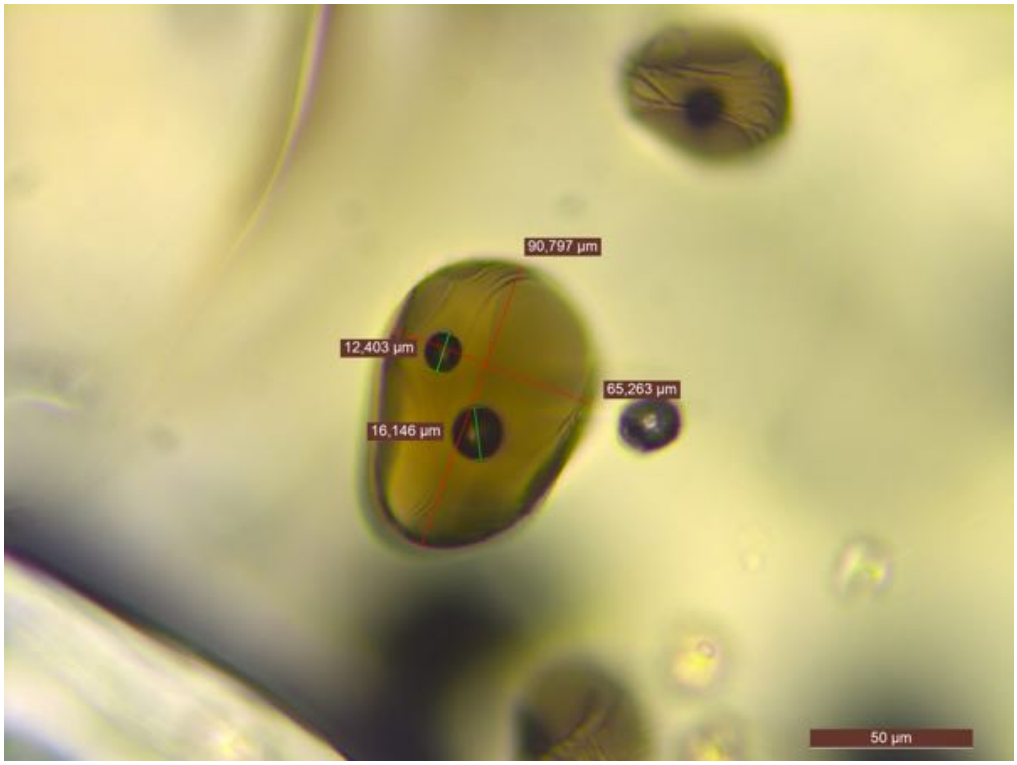

A-II

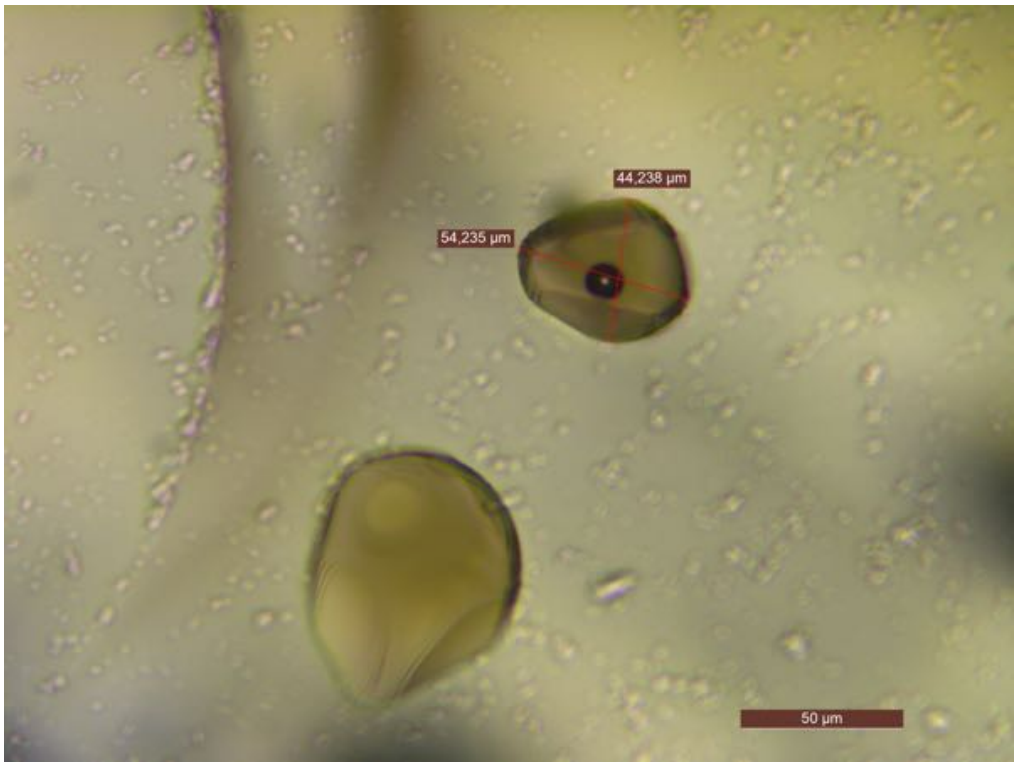

A-III


48,010 µm
42,008 µm
50 µm

B-I

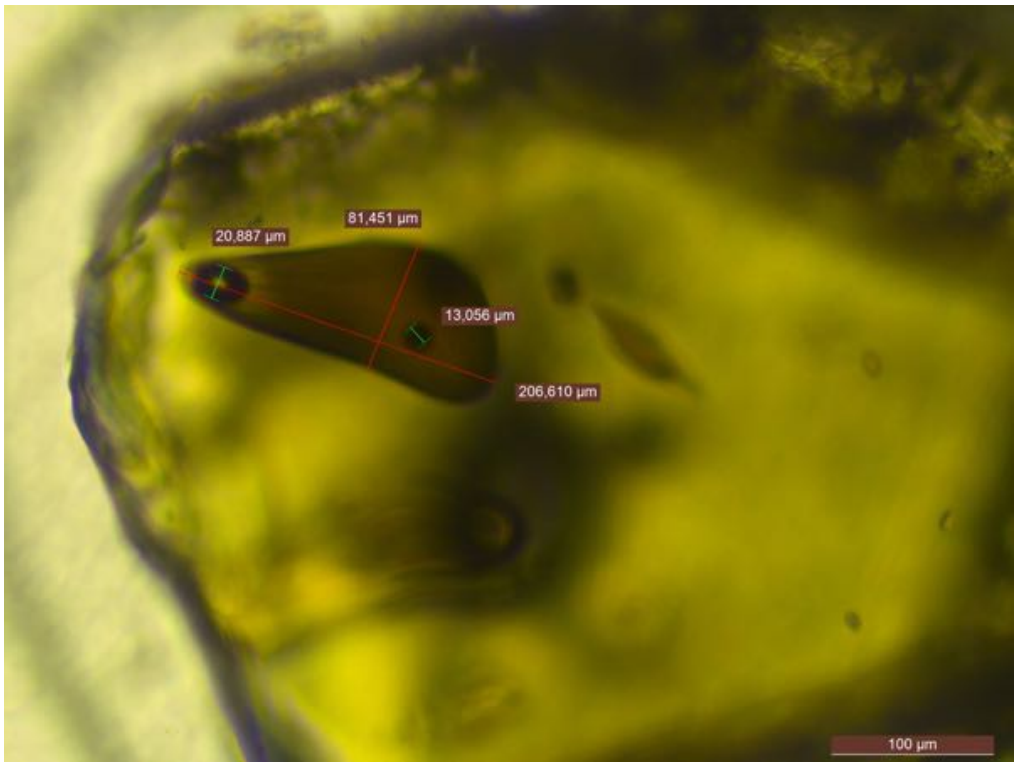
81,451 µm
20,887 µm
13,056 µm
206,610 µm
100 µm

C-I

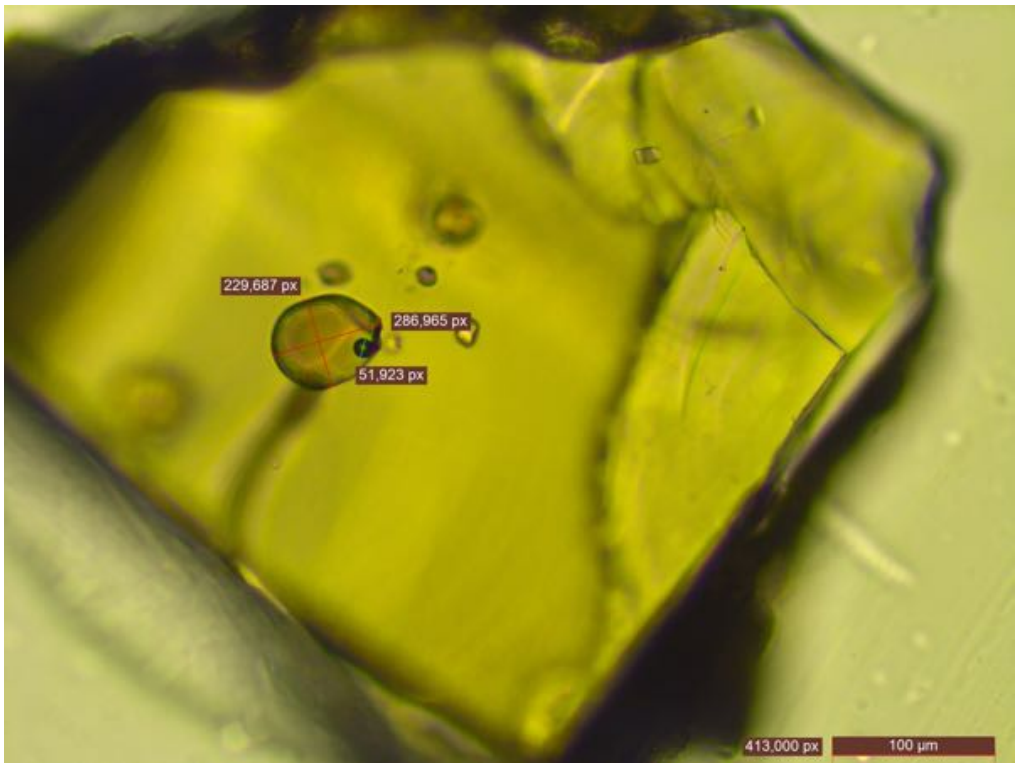
229,687 px
286,965 px
51,923 px
413,000 px
100 µm

D-I

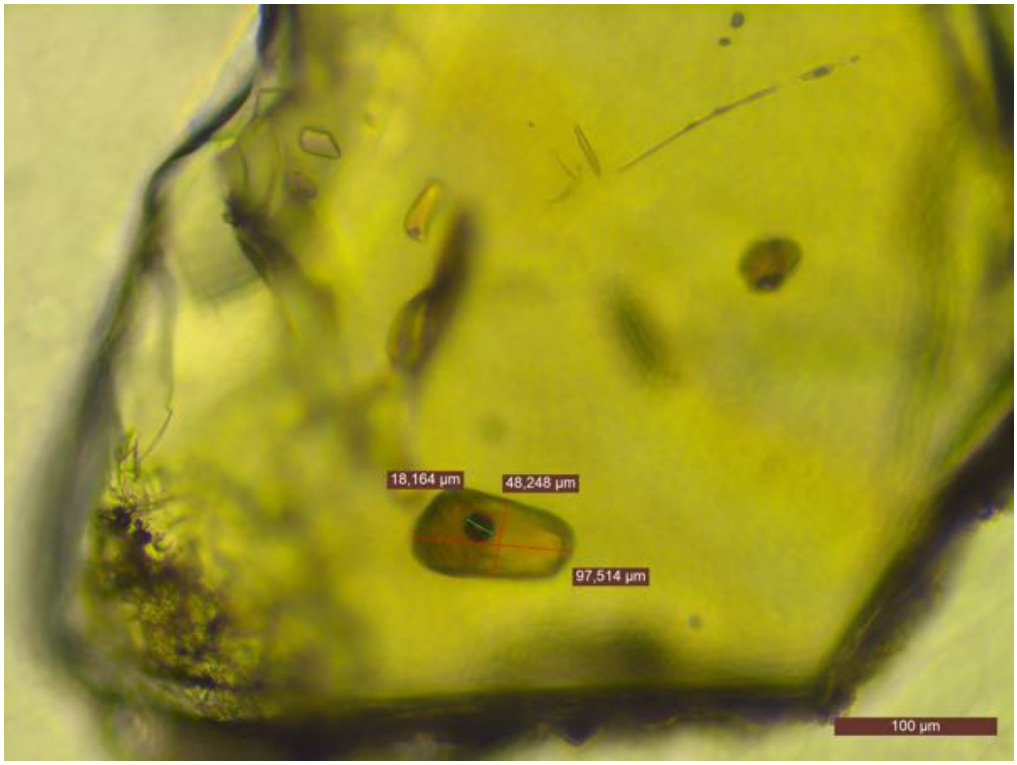
18,164 µm
48,248 µm
97,514 µm
100 µm

D-II

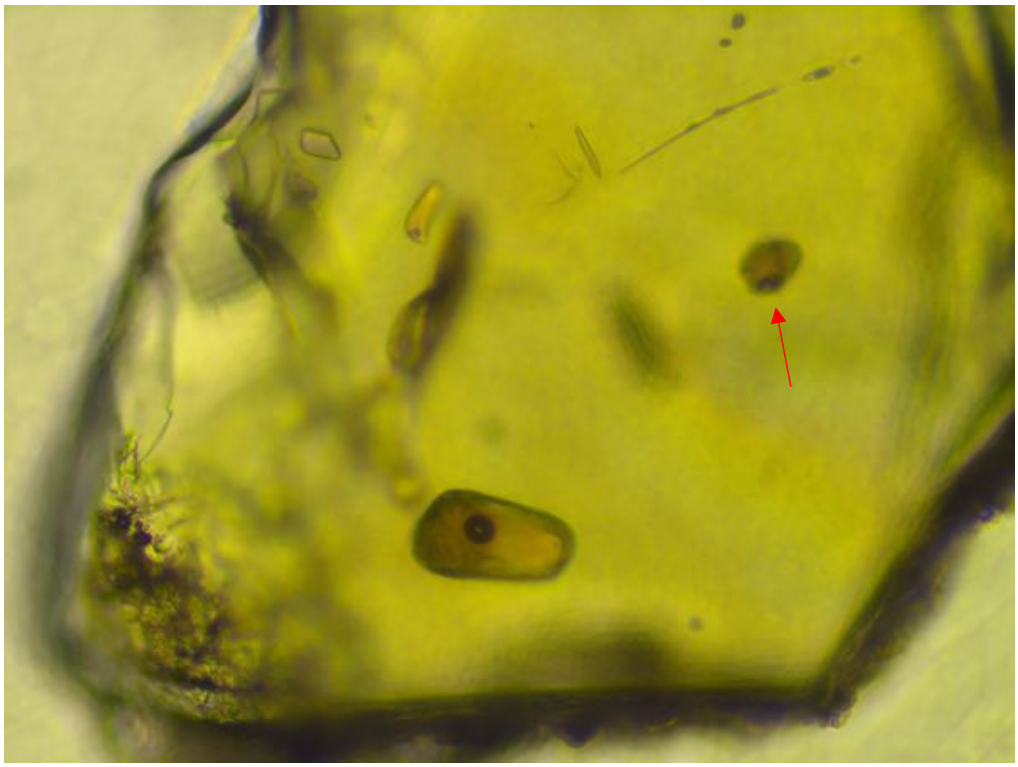

E-I

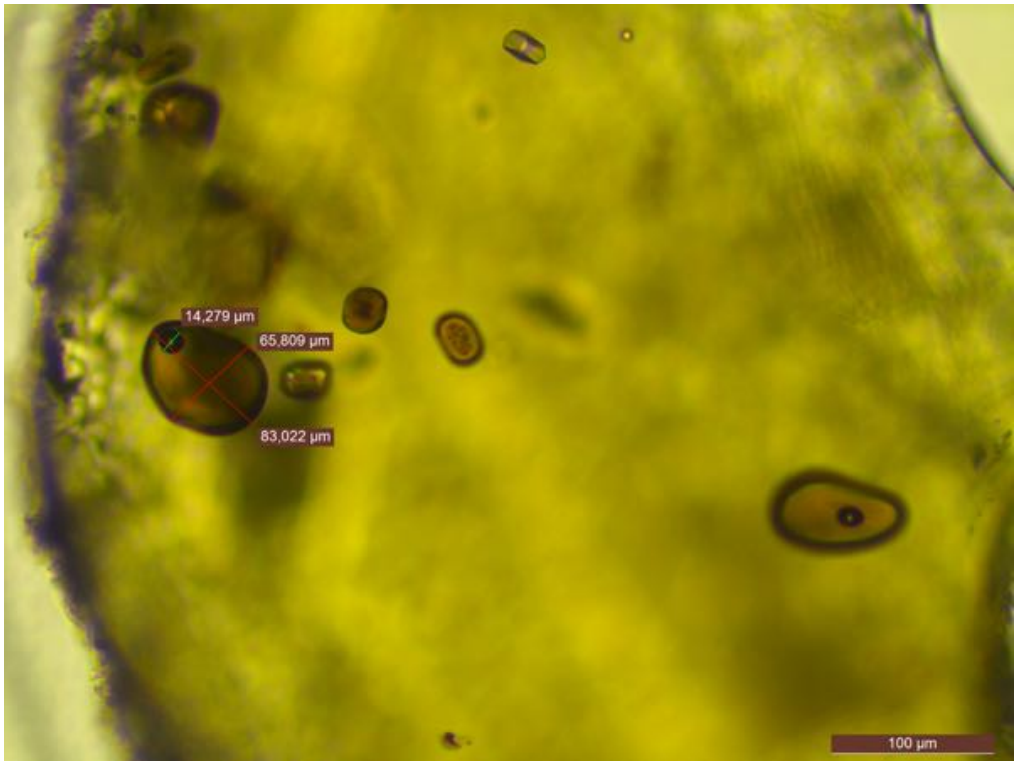

E-II

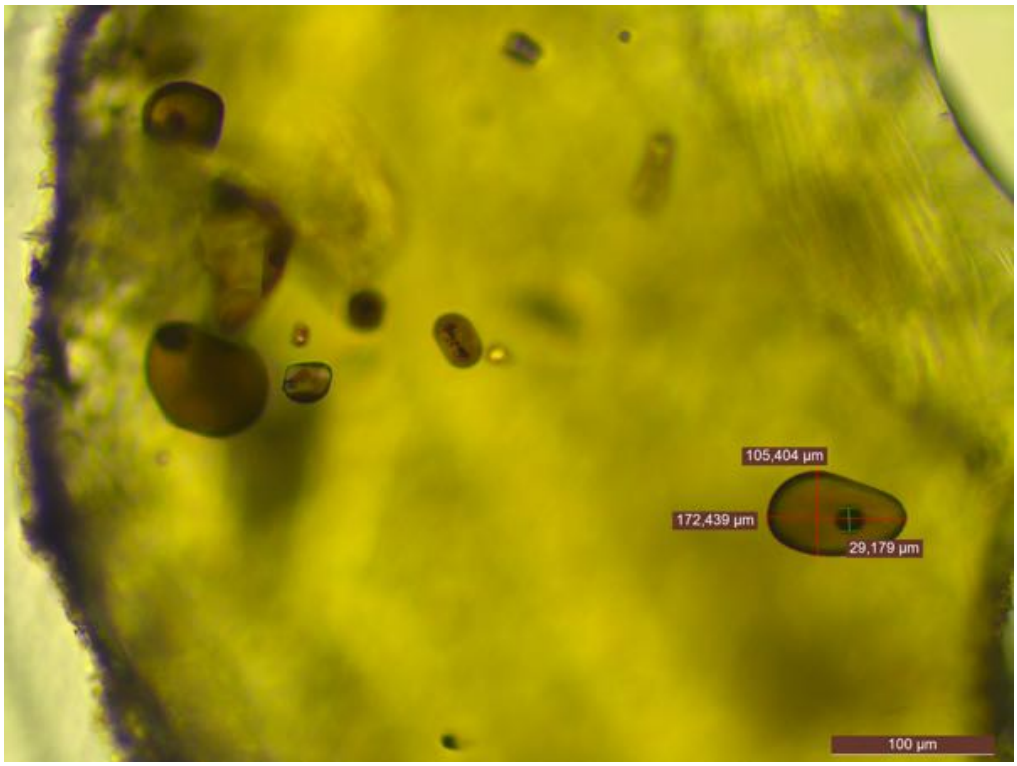
105,404 µm
172,439 µm
29,179 µm
100 µm

G-I


76,350 µm
43,134 µm
130,013 µm
100 µm

H-I

K-III

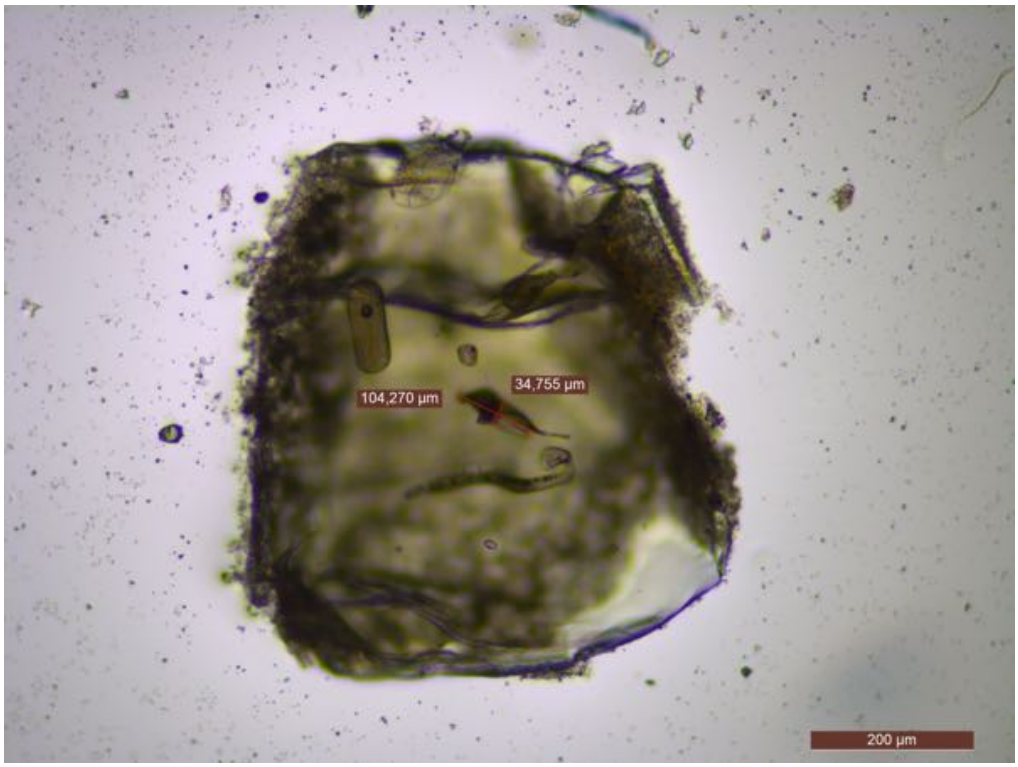

K-V


116,269 µm
46,229 µm
50 µm

L-I

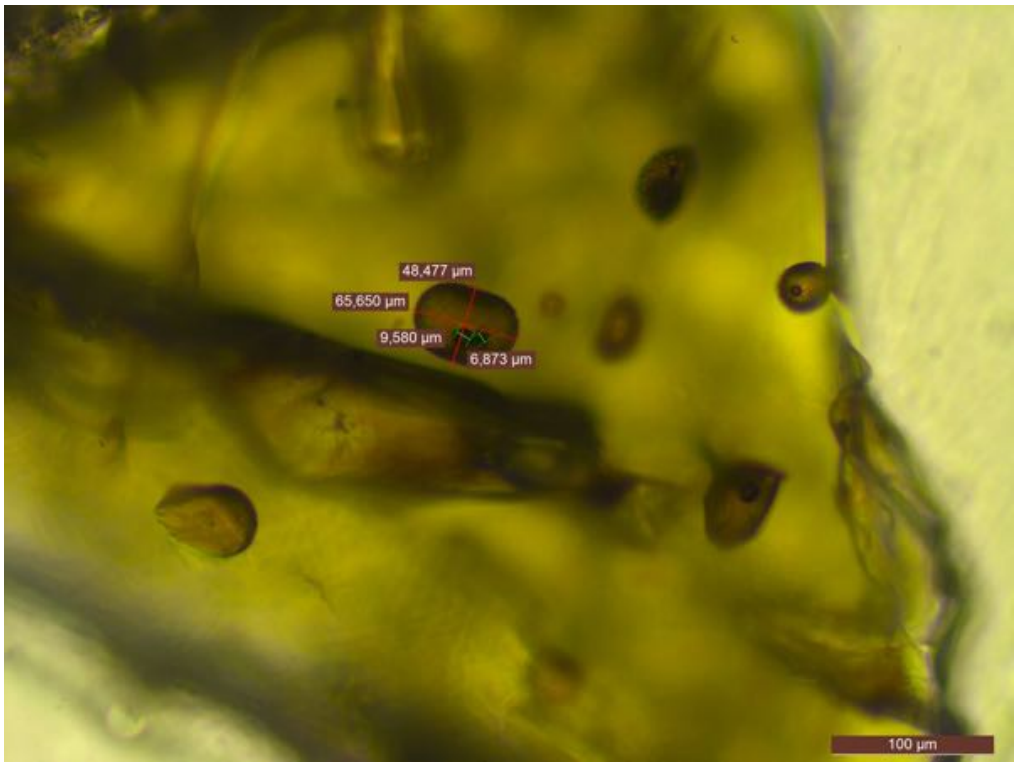
48,477 µm
65,650 µm
9,580 µm
6,873 µm
100 µm

L-II

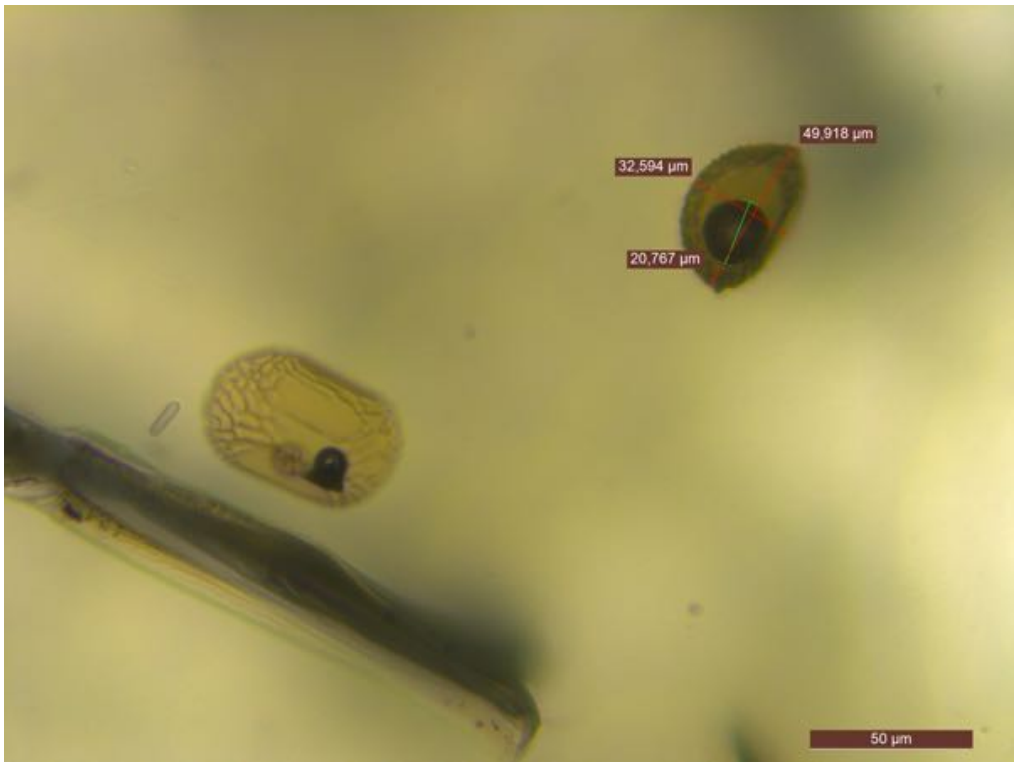
49,918 µm
32,594 µm
20,767 µm
50 µm

L-III

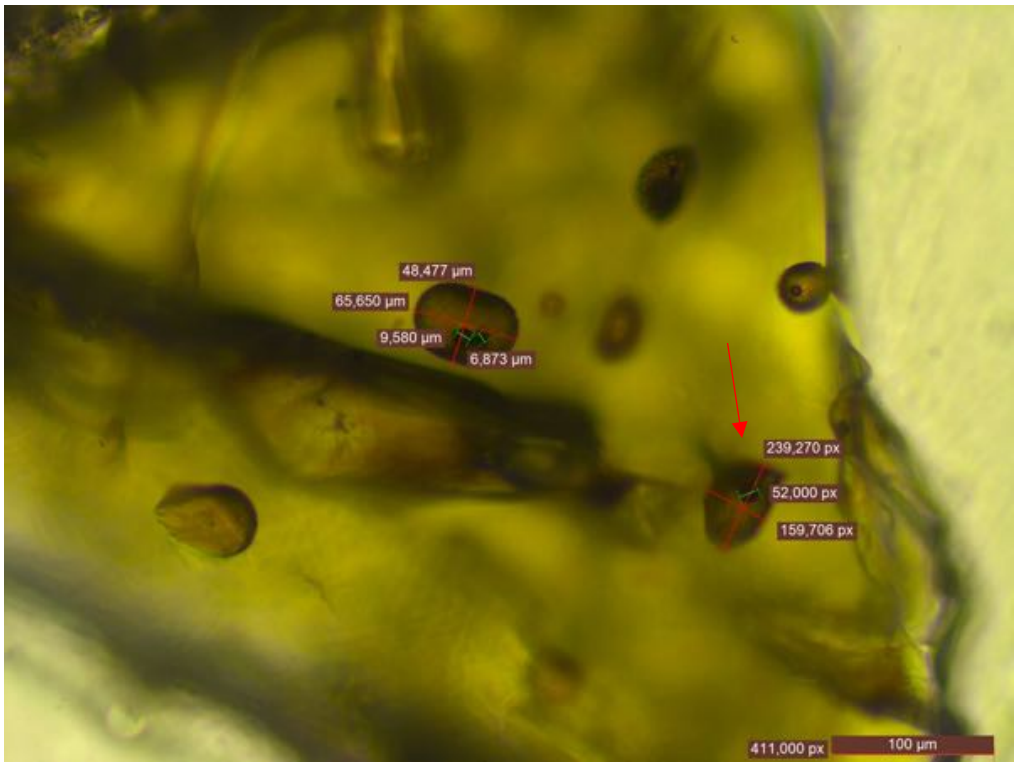
48,477 µm
65,650 µm
9,580 µm
6,873 µm
239,270 px
52,000 px
159,706 px
411,000 px
100 µm

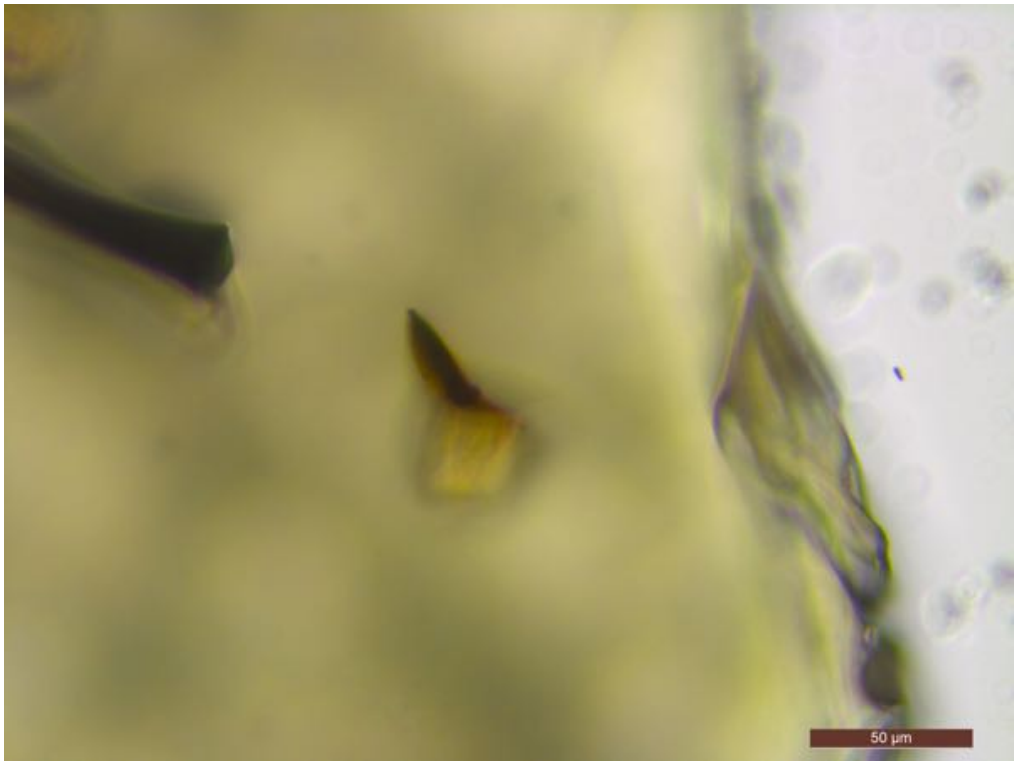
50 µm

L-IV

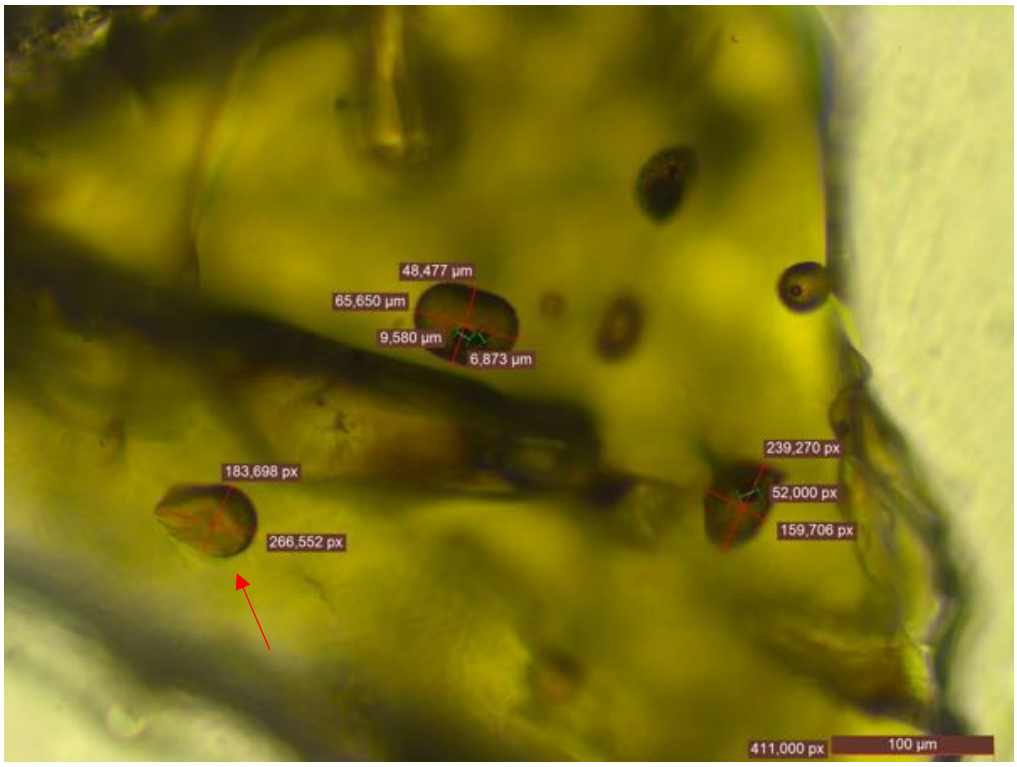
48,477 µm
65,650 µm
9,580 µm
6,873 µm
239,270 px
183,698 px
52,000 px
159,706 px
266,552 px
411,000 px
100 µm

<SM1S>
AA-I

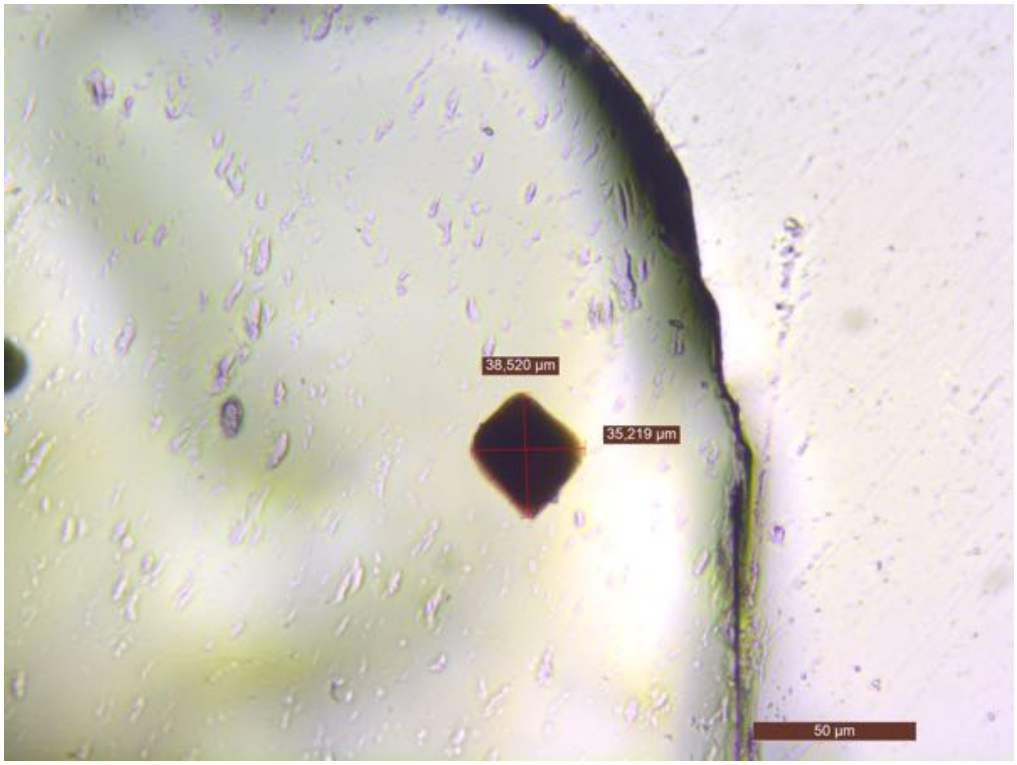

AE-I

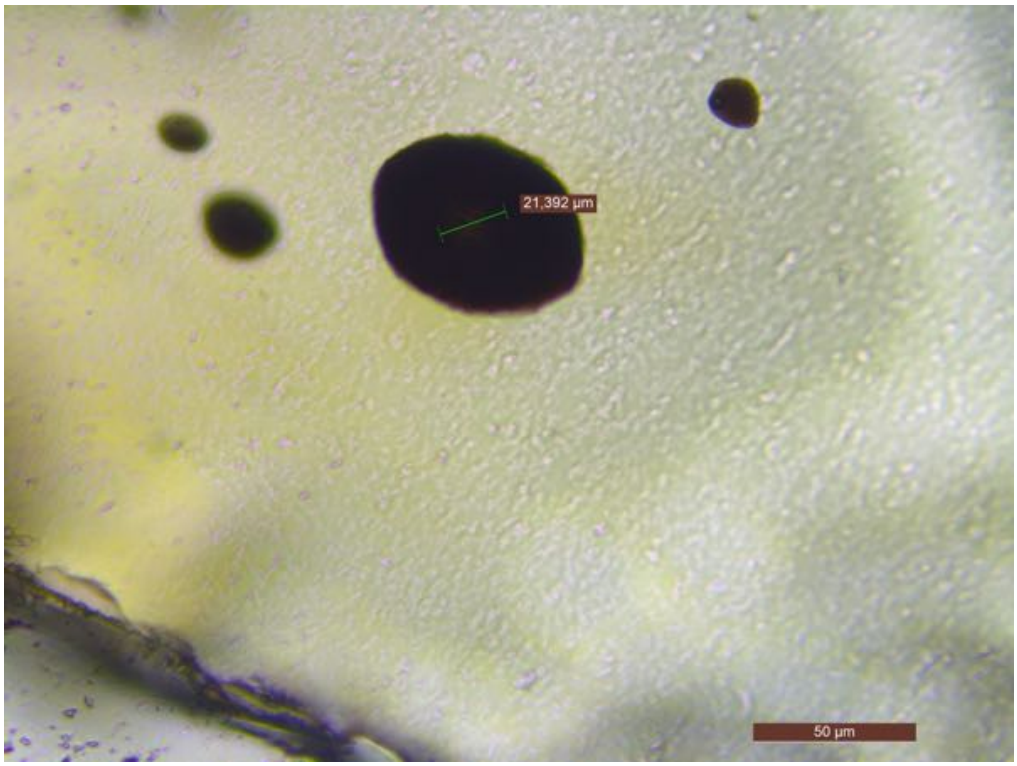

AJ-I

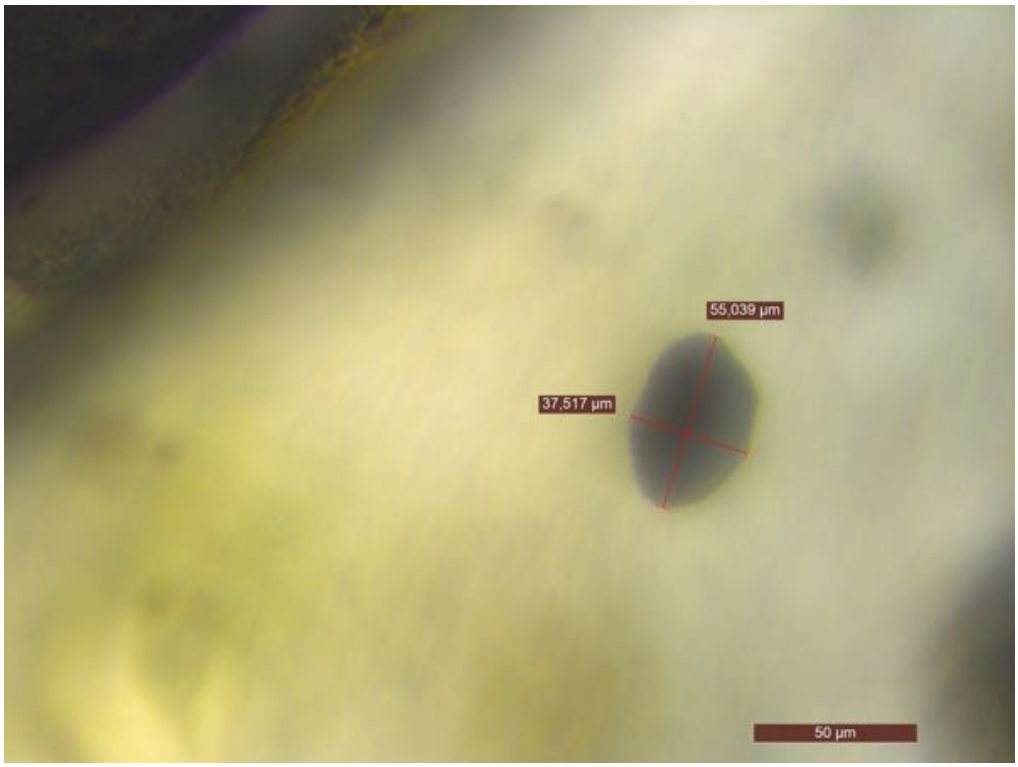

AL-II

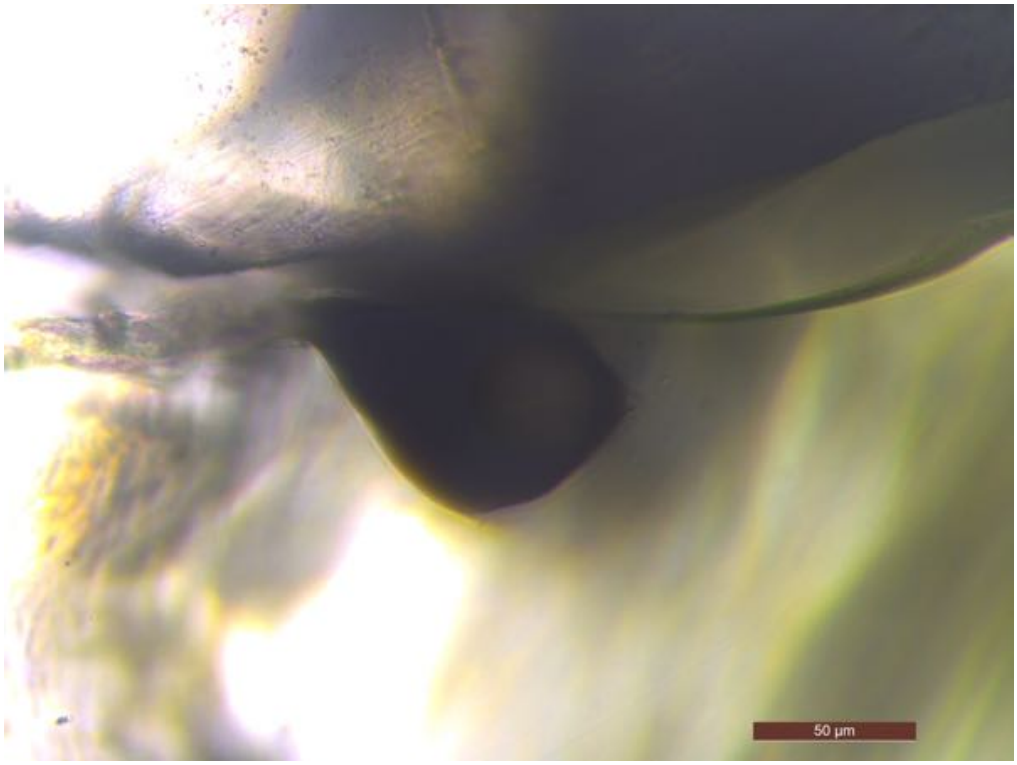

AM-II

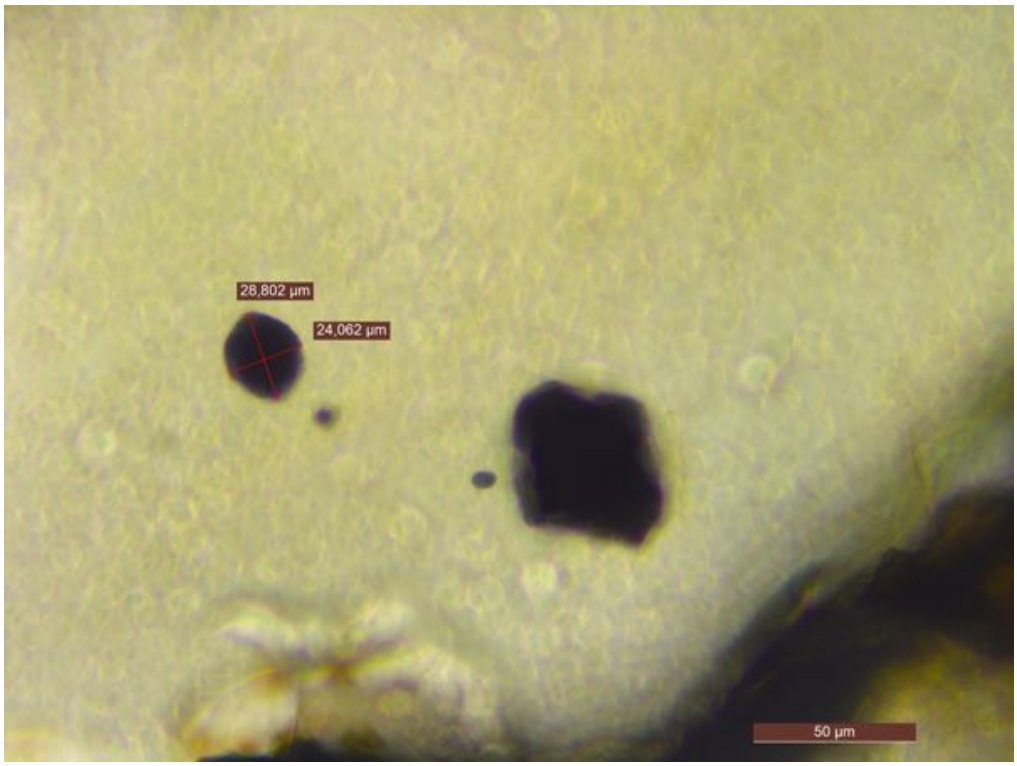

AR-VI

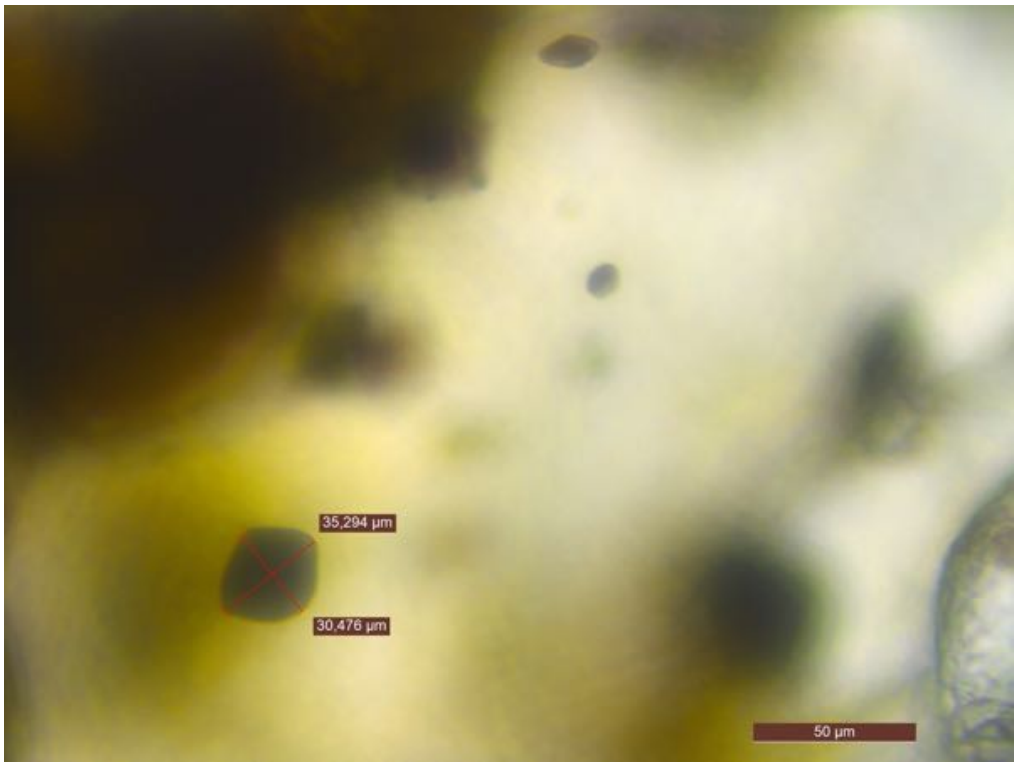

BA-I

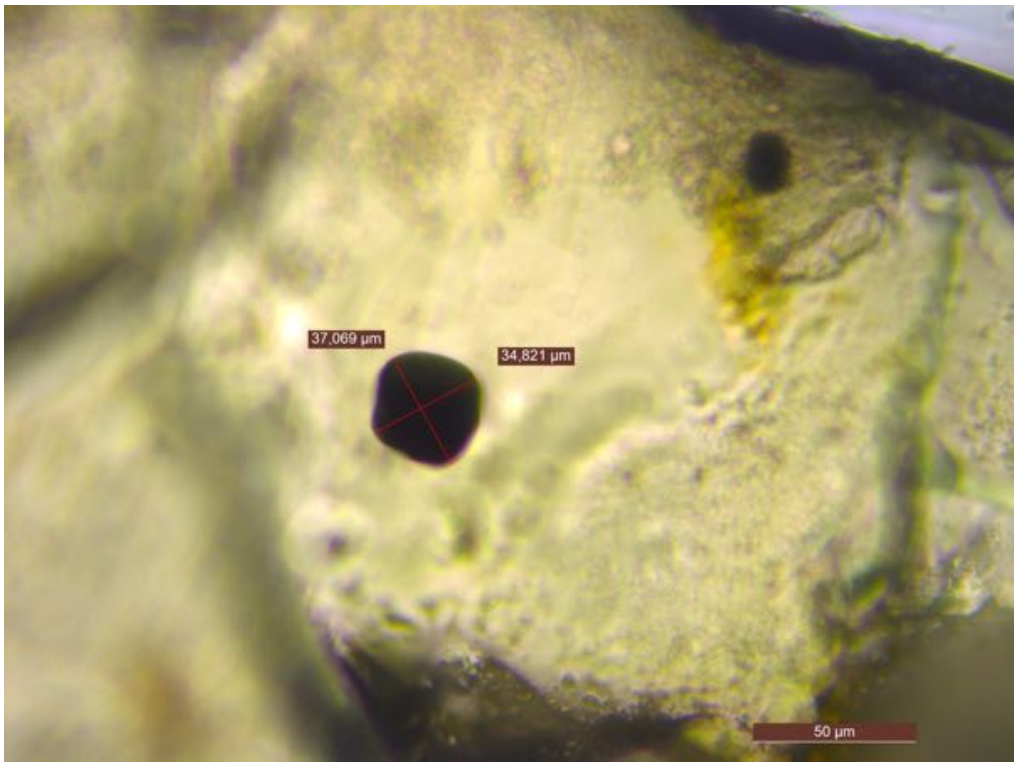

BA-IV

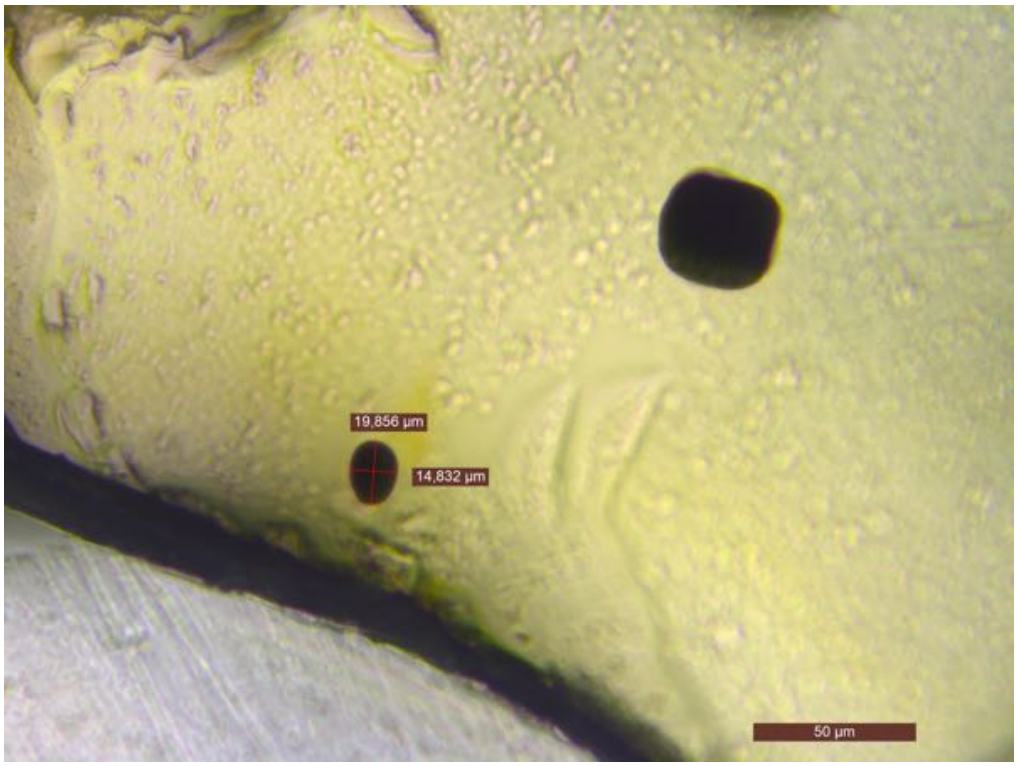

BC-I

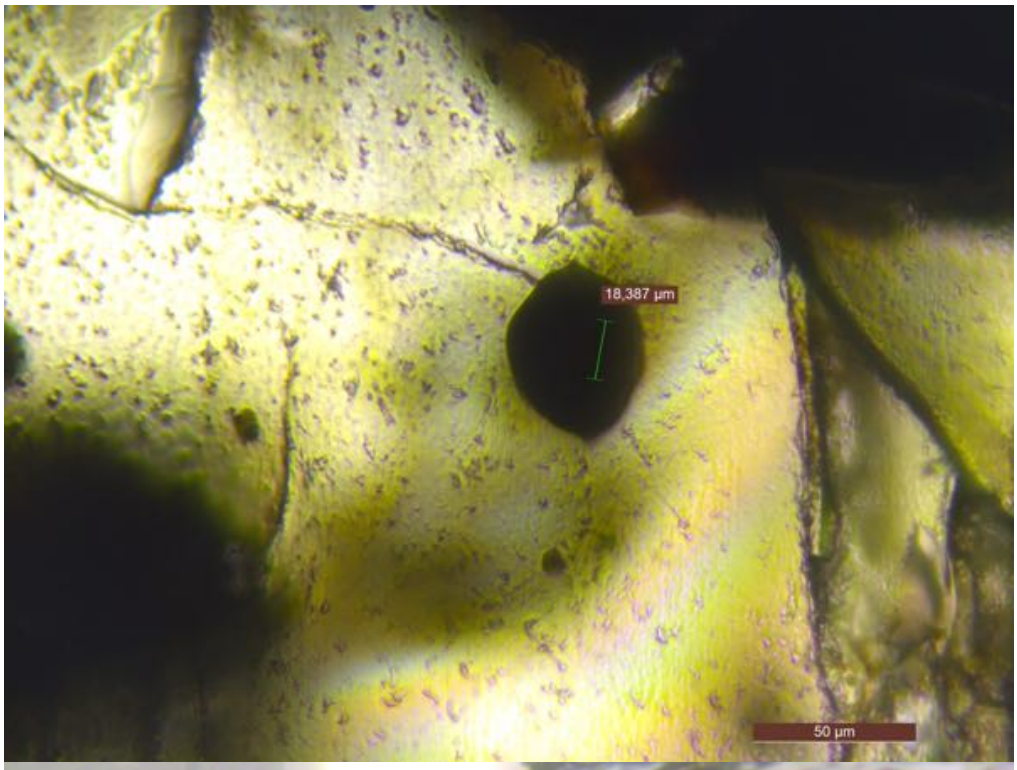

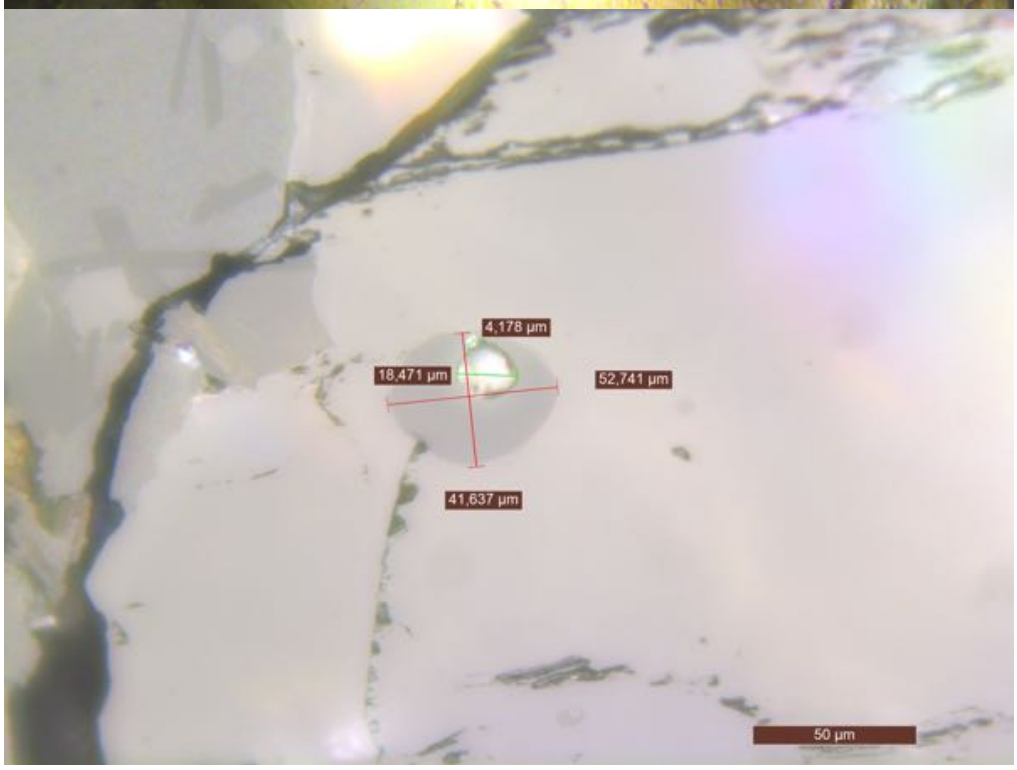

S-II

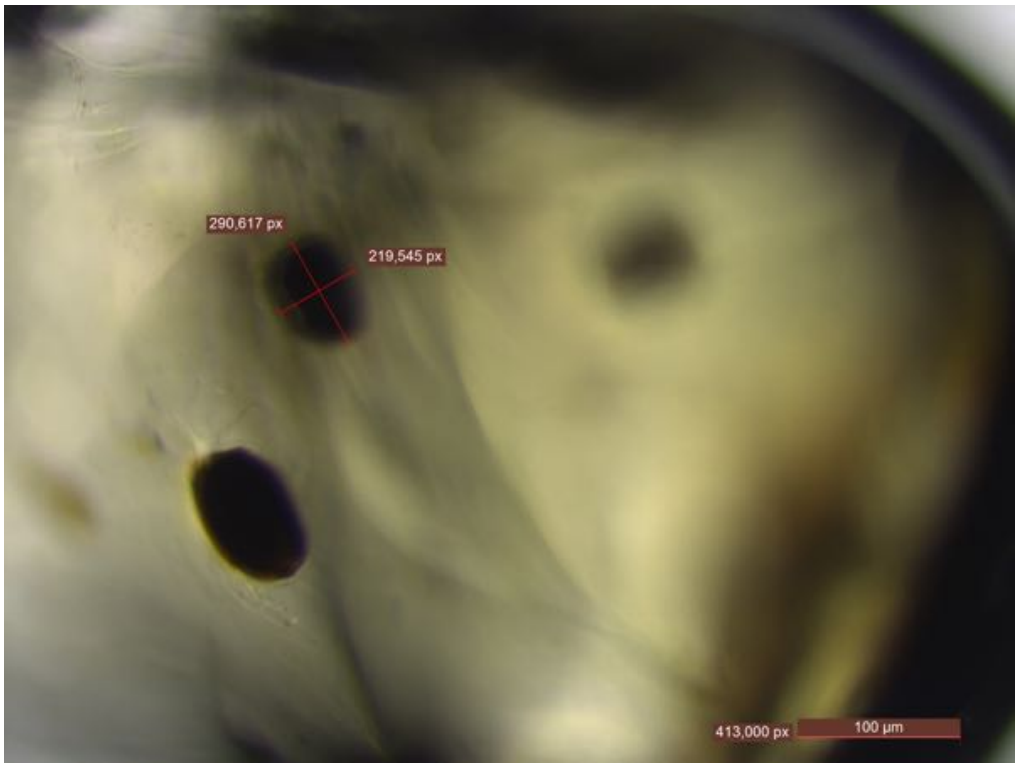
290,617 px
219,545 px
413,000 px
100 µm

S-III

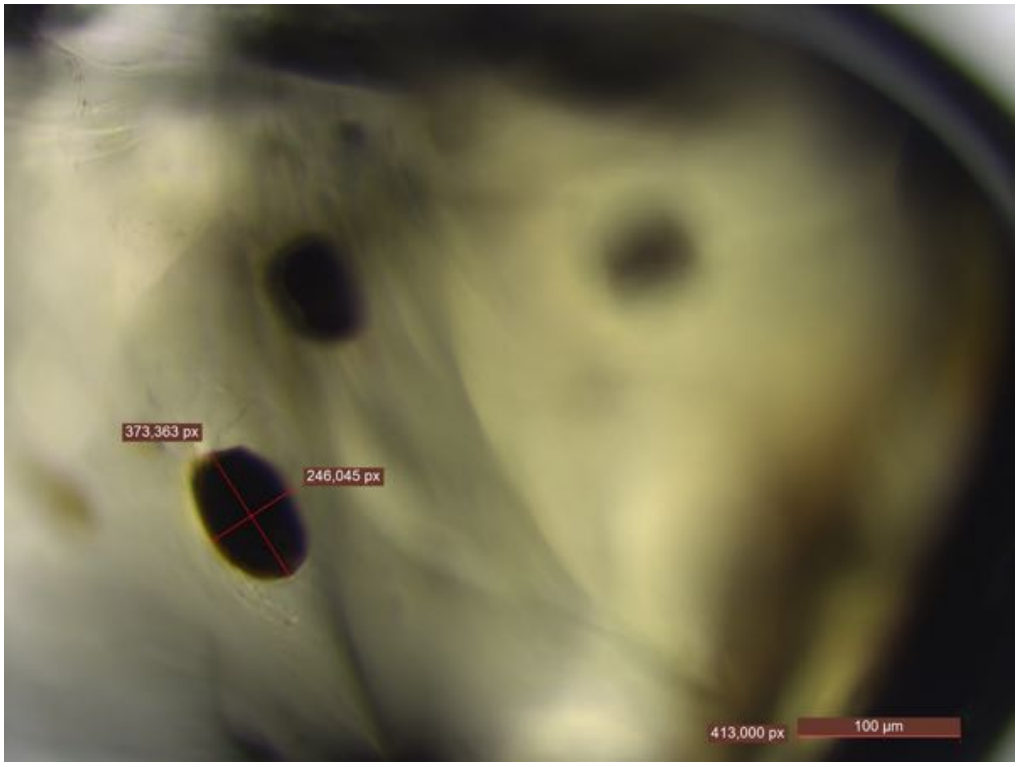
373,363 px
246,045 px
413,000 px
100 µm

T-II

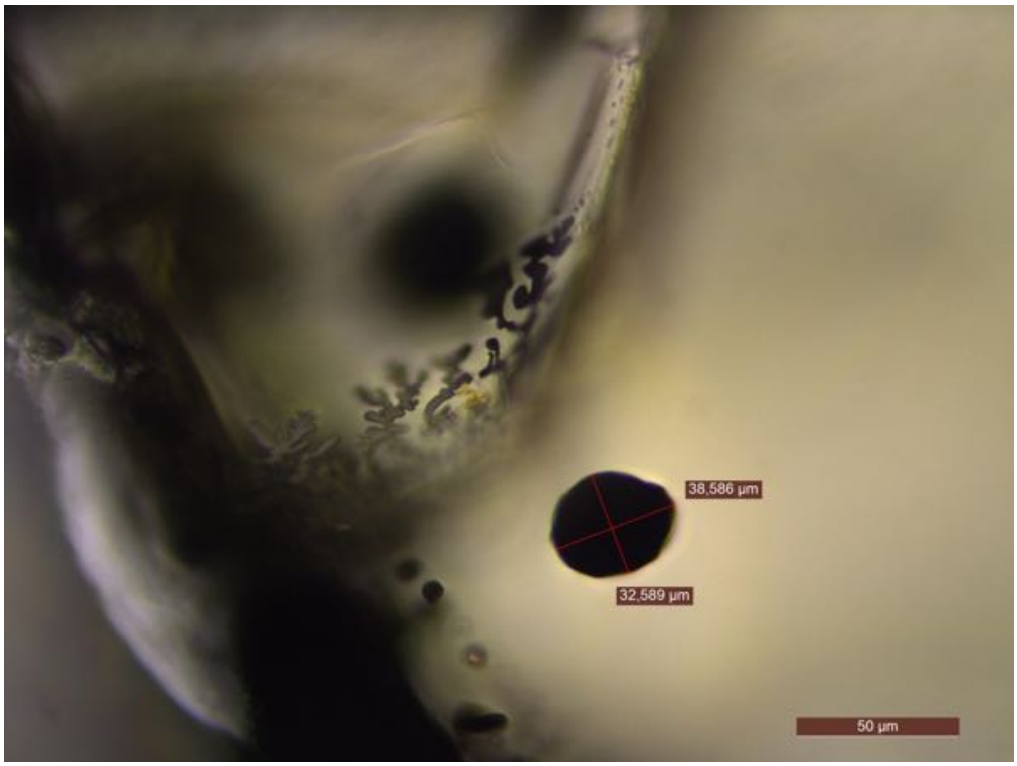

Y-I

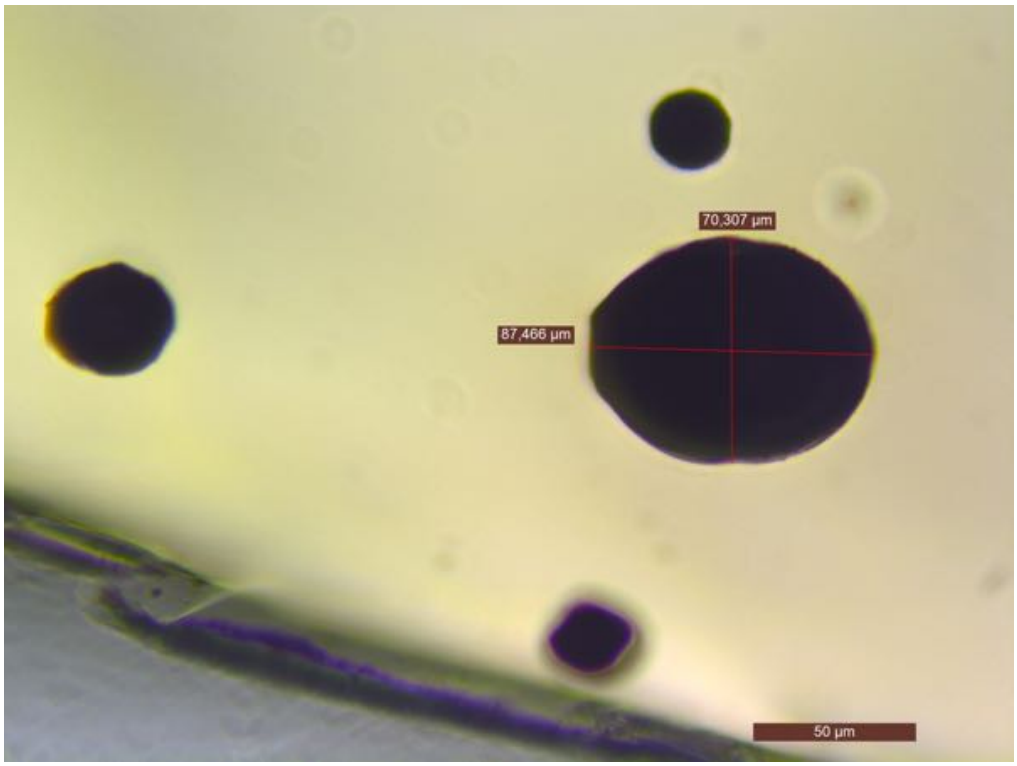

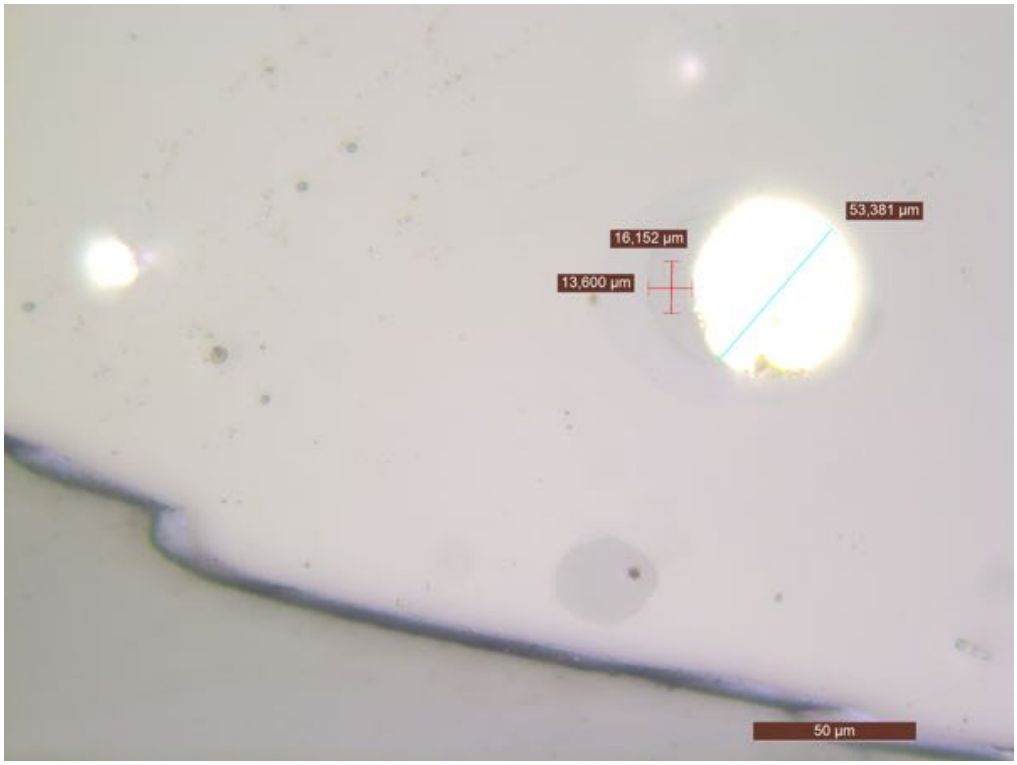

Y-IV

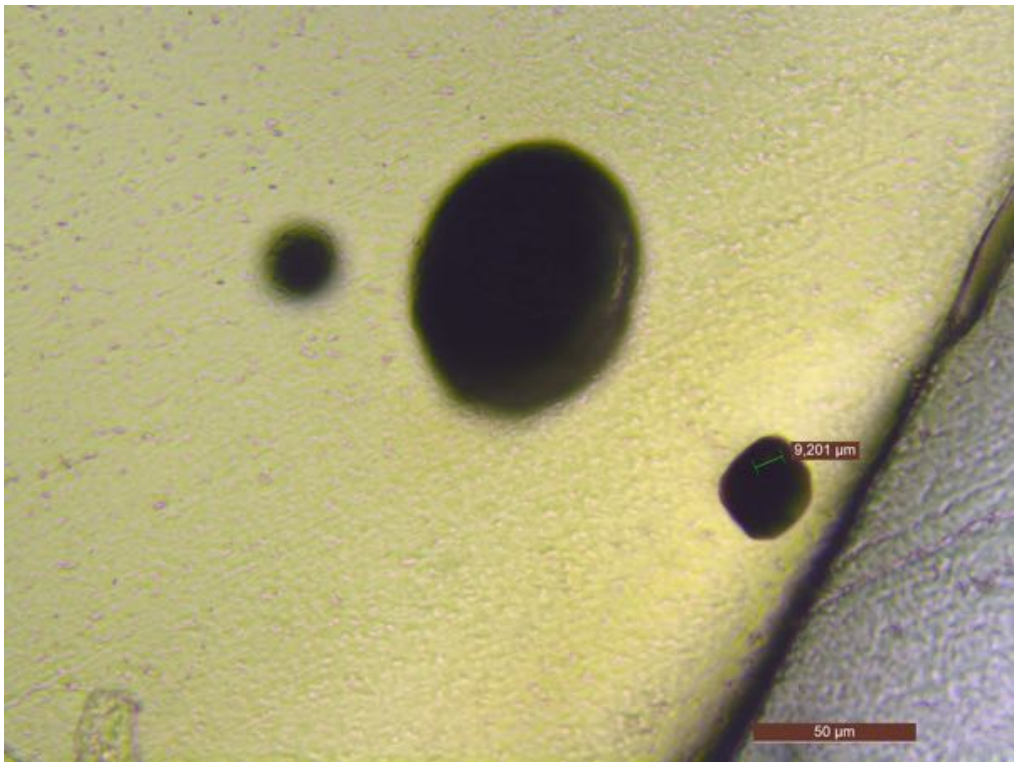

Z-I

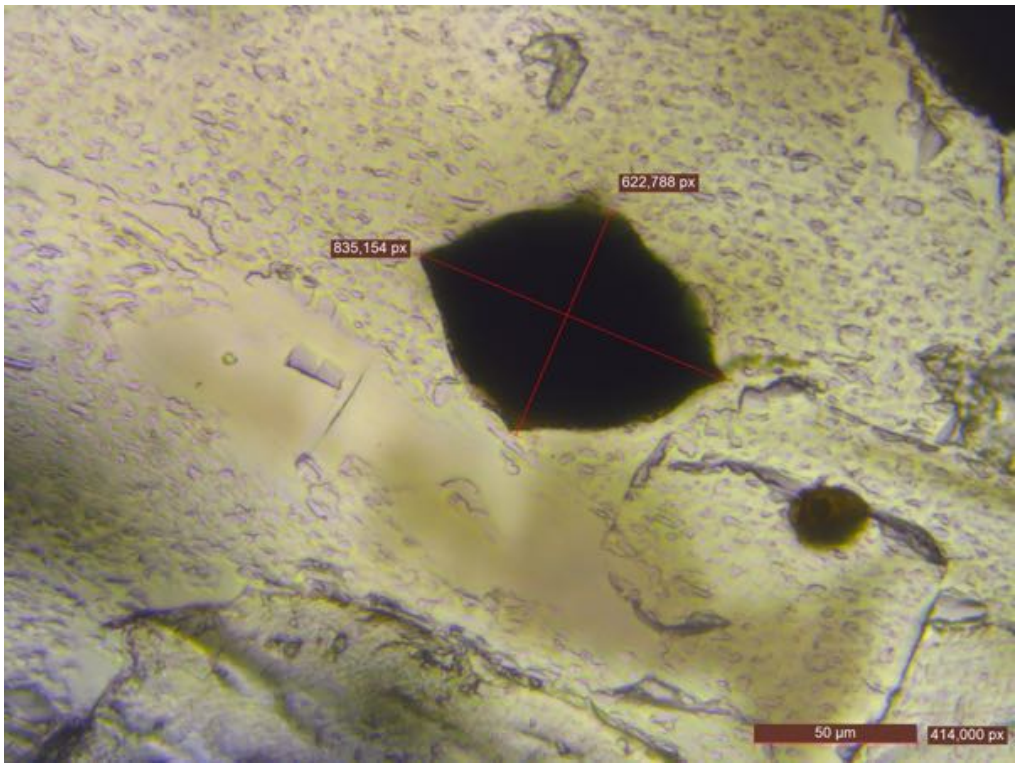

Z-III

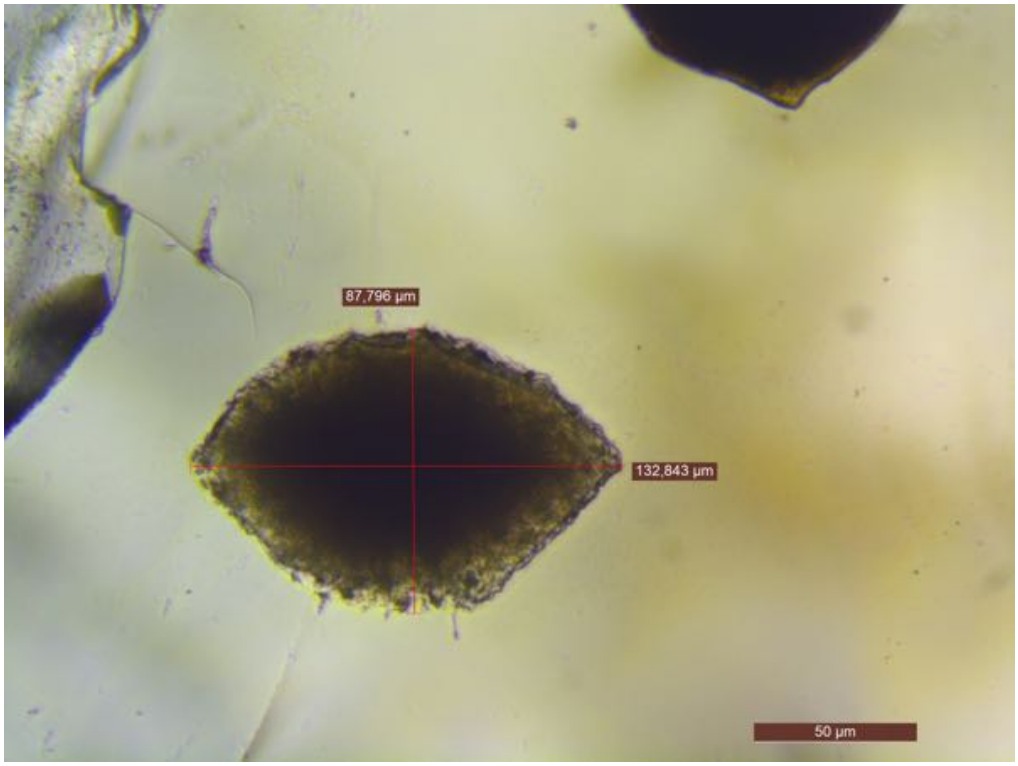

<KM1S12a>
A-I

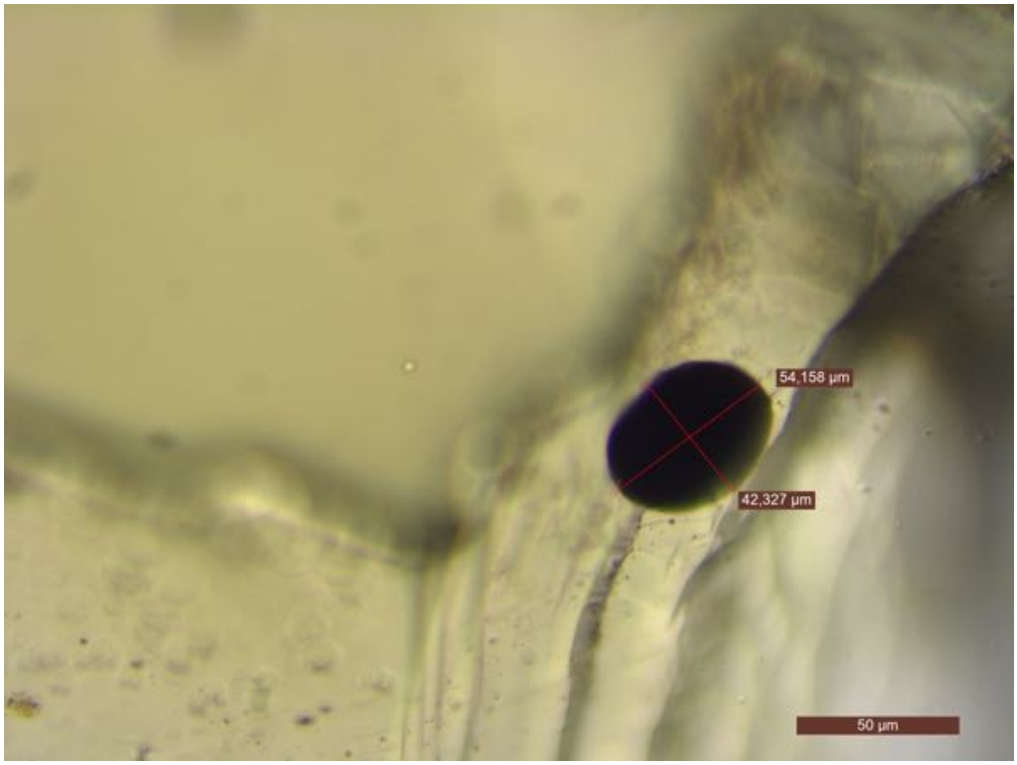

AE-I

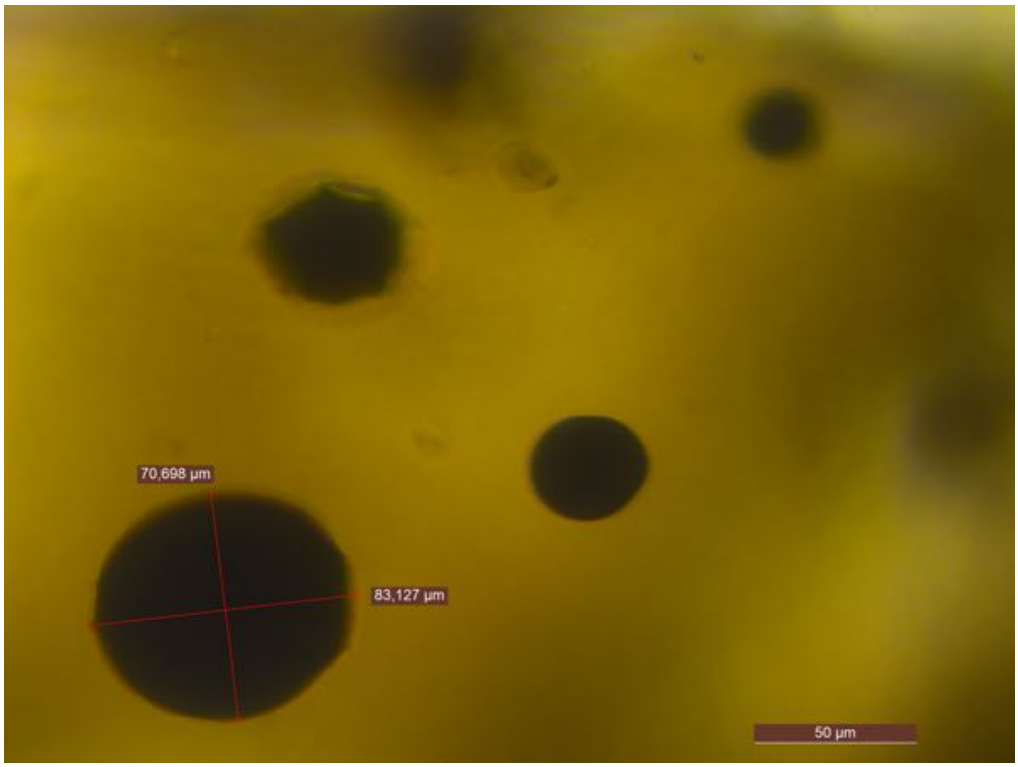

AE-II

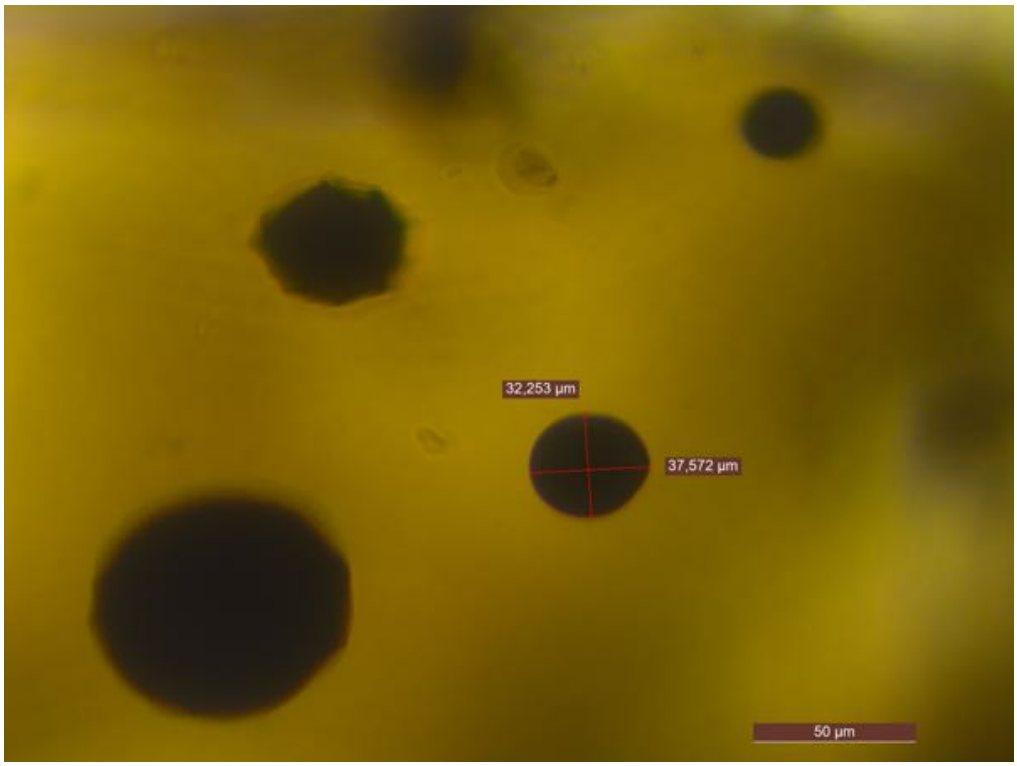

AE-III

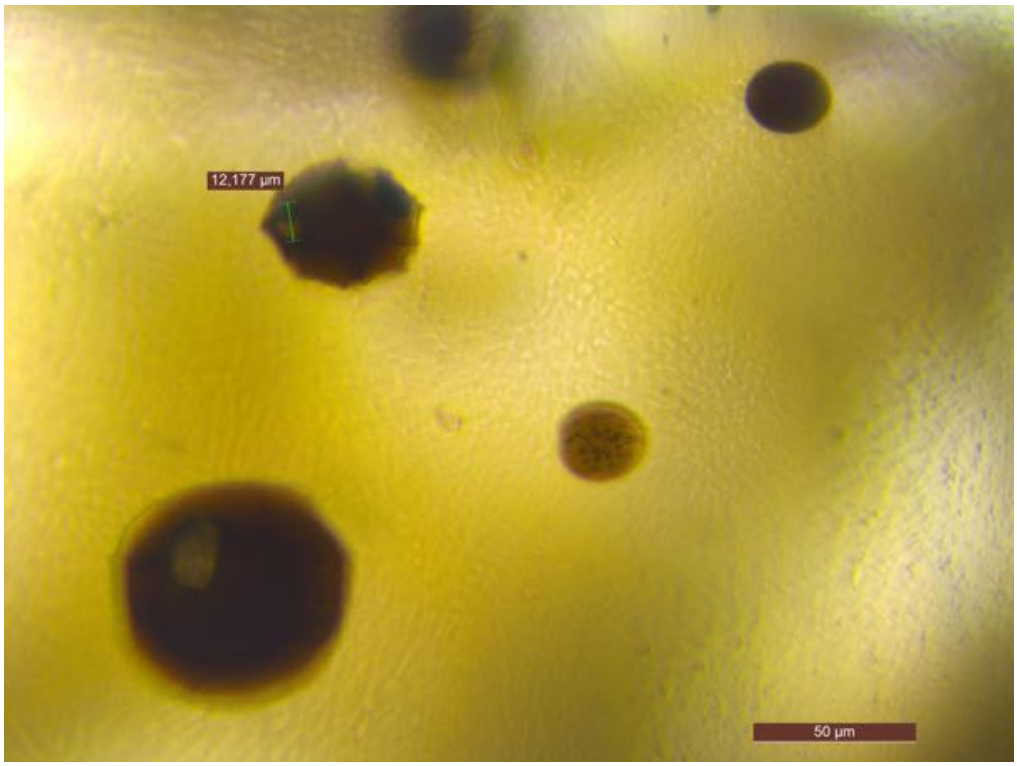

AE-IV

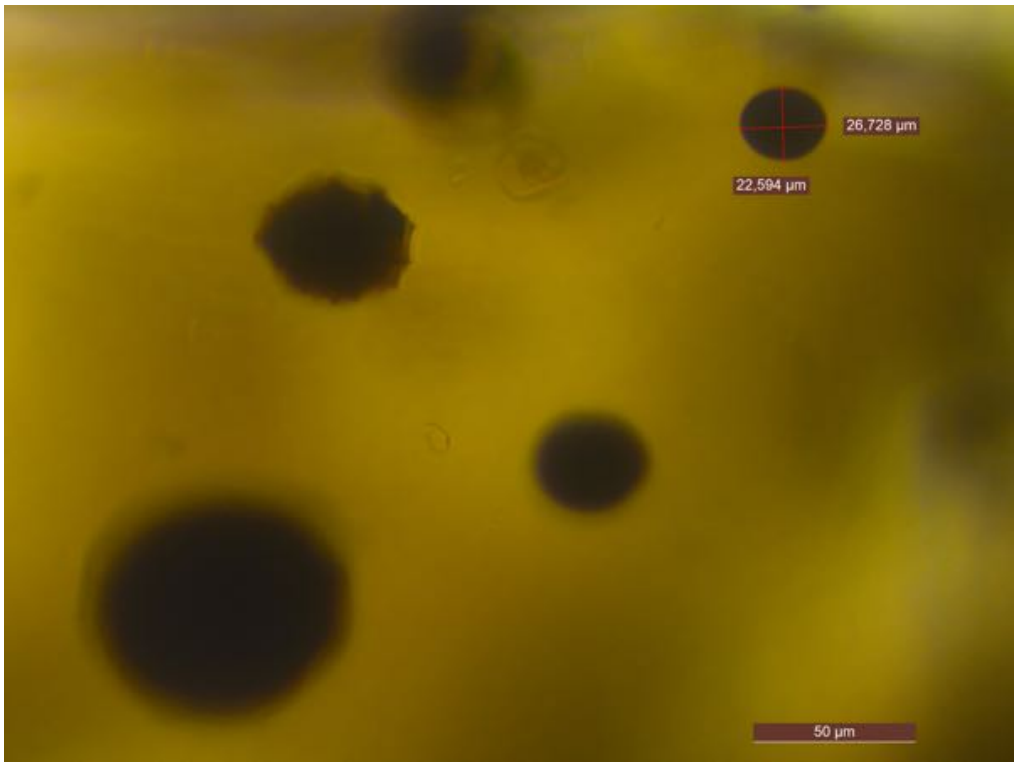

AF-I

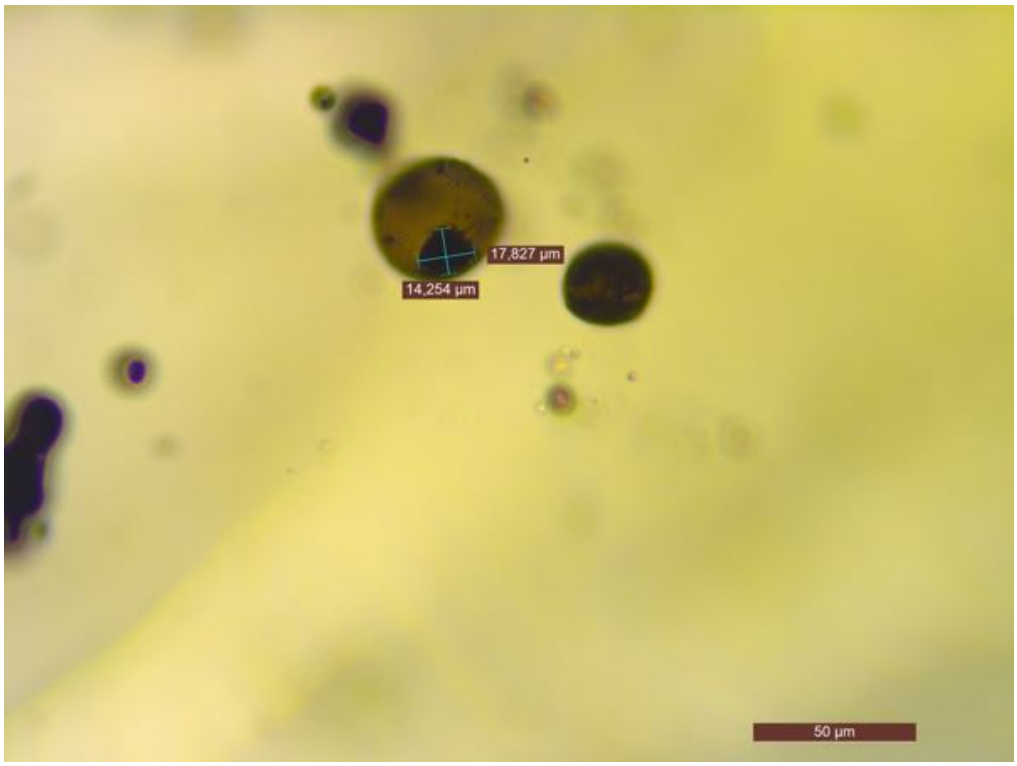

AH-II

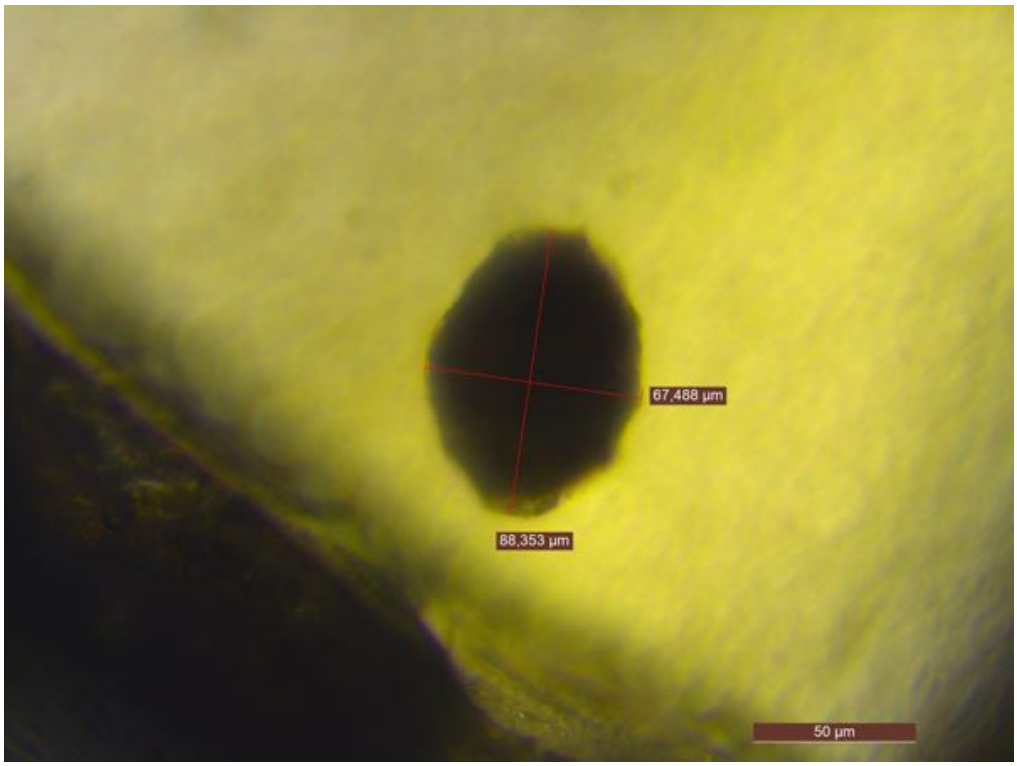

AJ-I

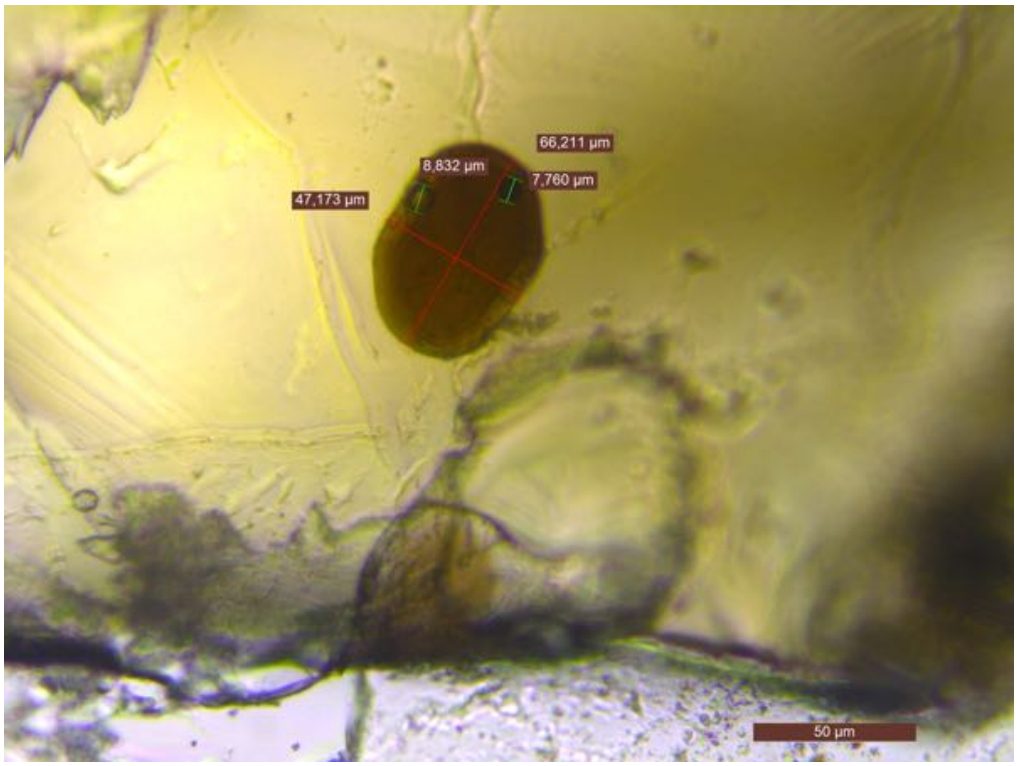

AK-III

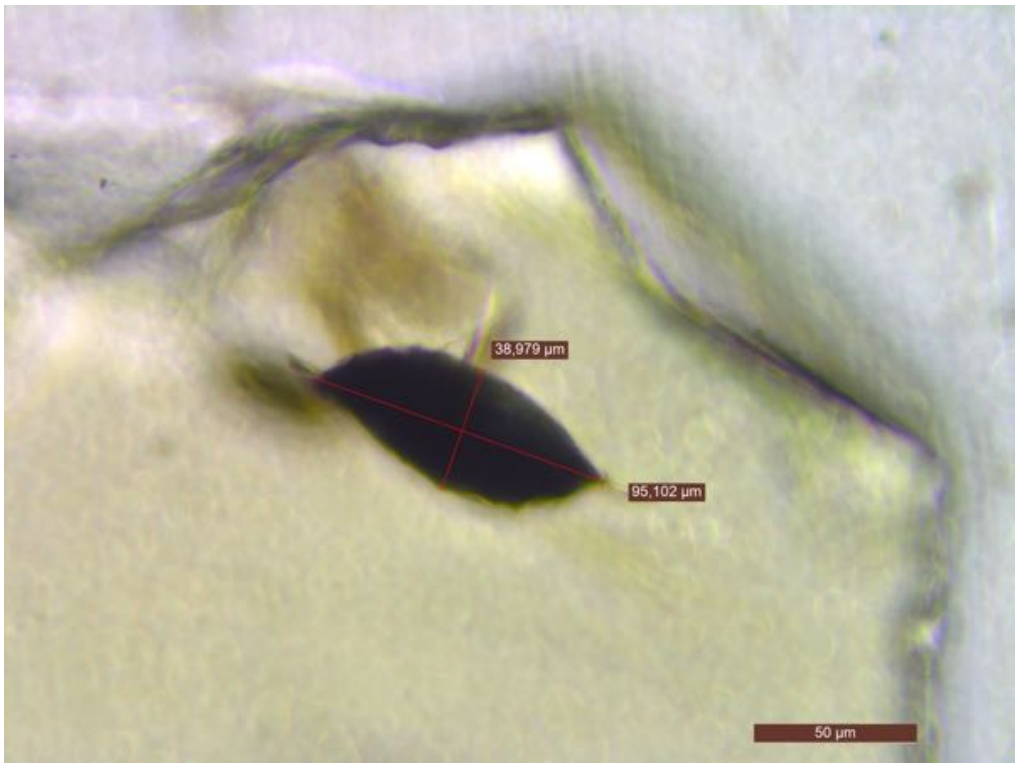

J-I

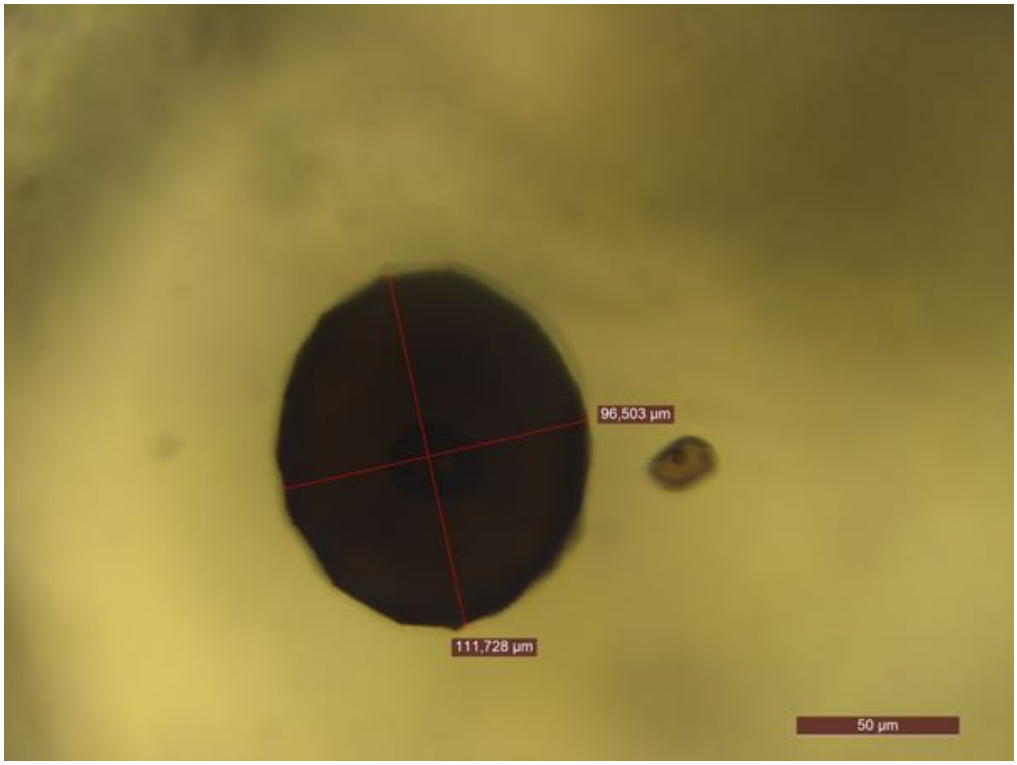

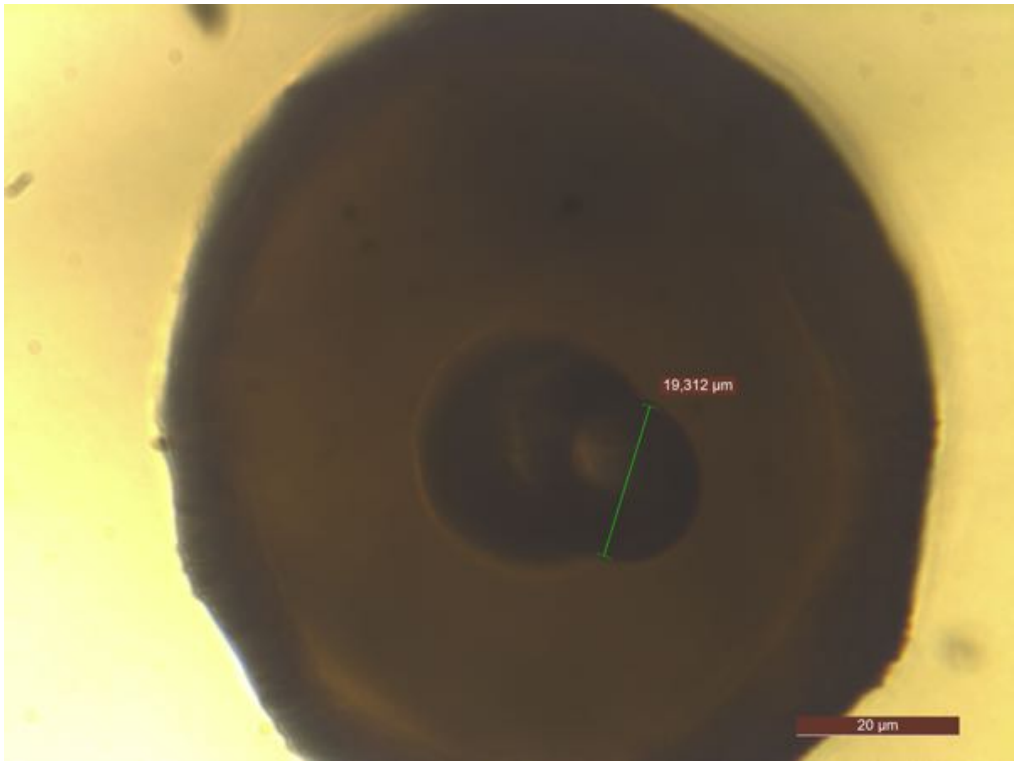

J-II

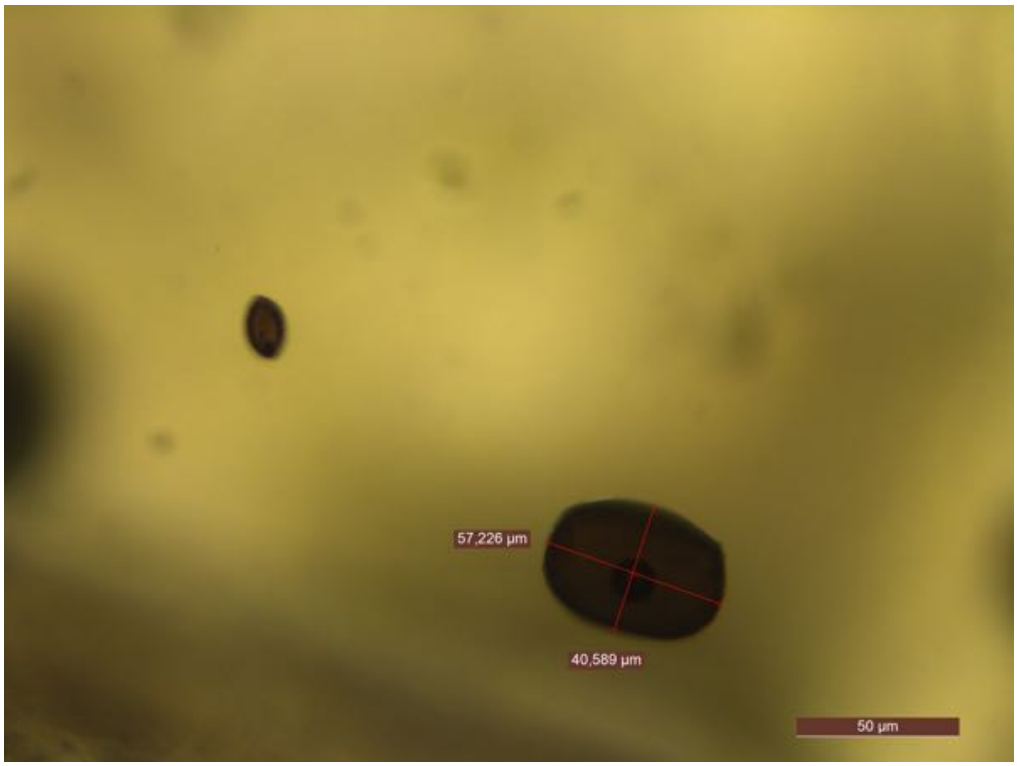

K-II

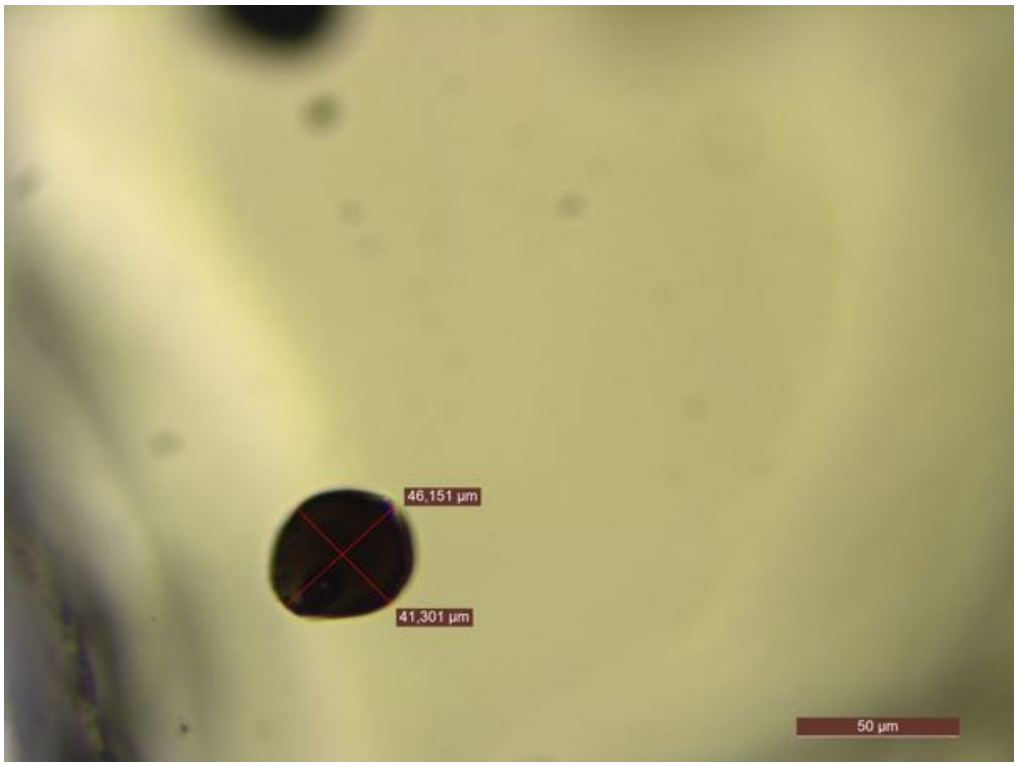

O-I

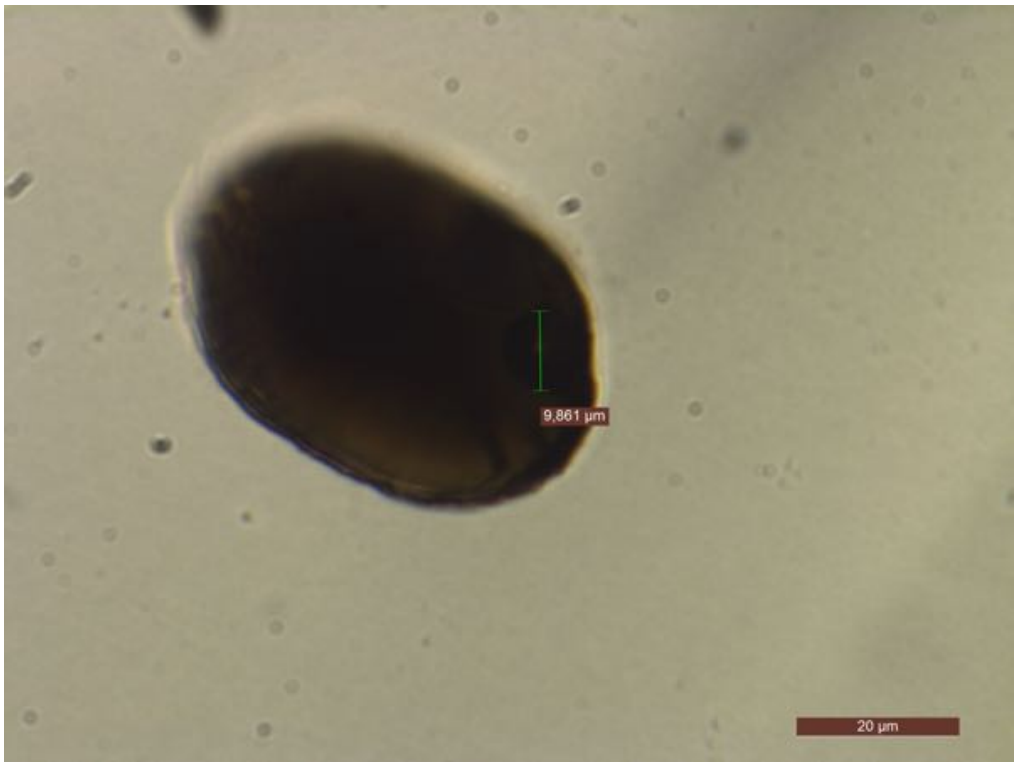

Q-I

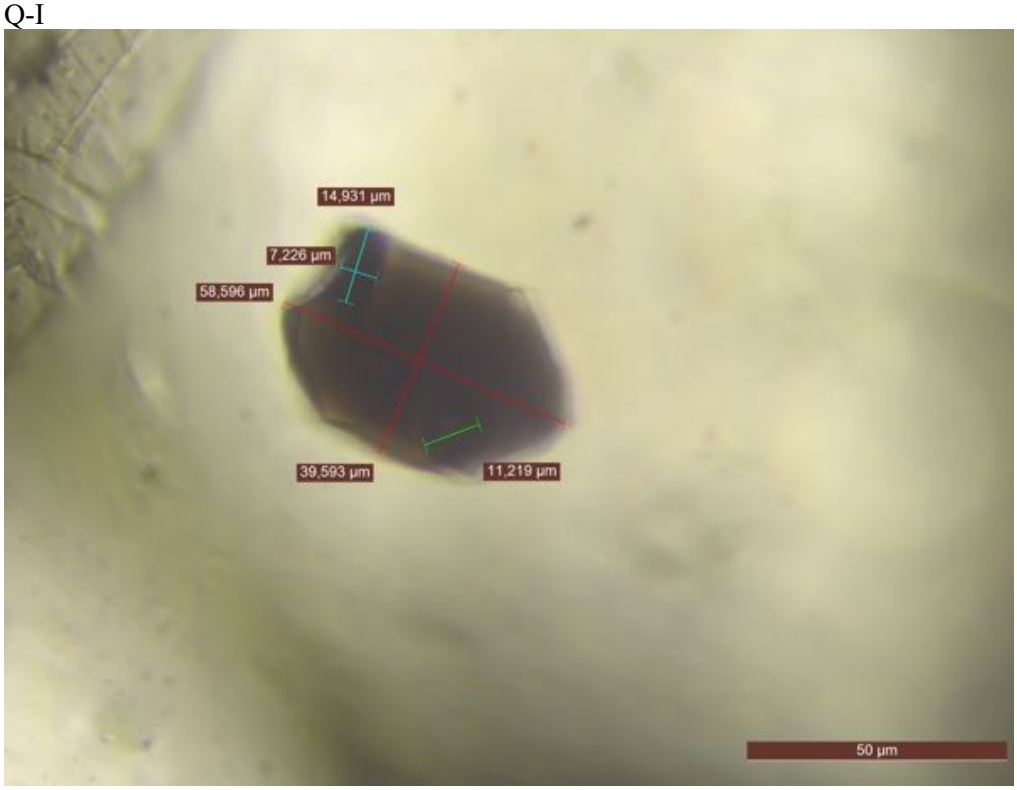
14,931 µm
7,226 µm
58,596 µm
39,593 µm
11,219 µm
50 µm

U-VI


46,738 µm
5,269 µm
44,886 µm
9,270 µm
13,437 µm
100 µm

Z-I

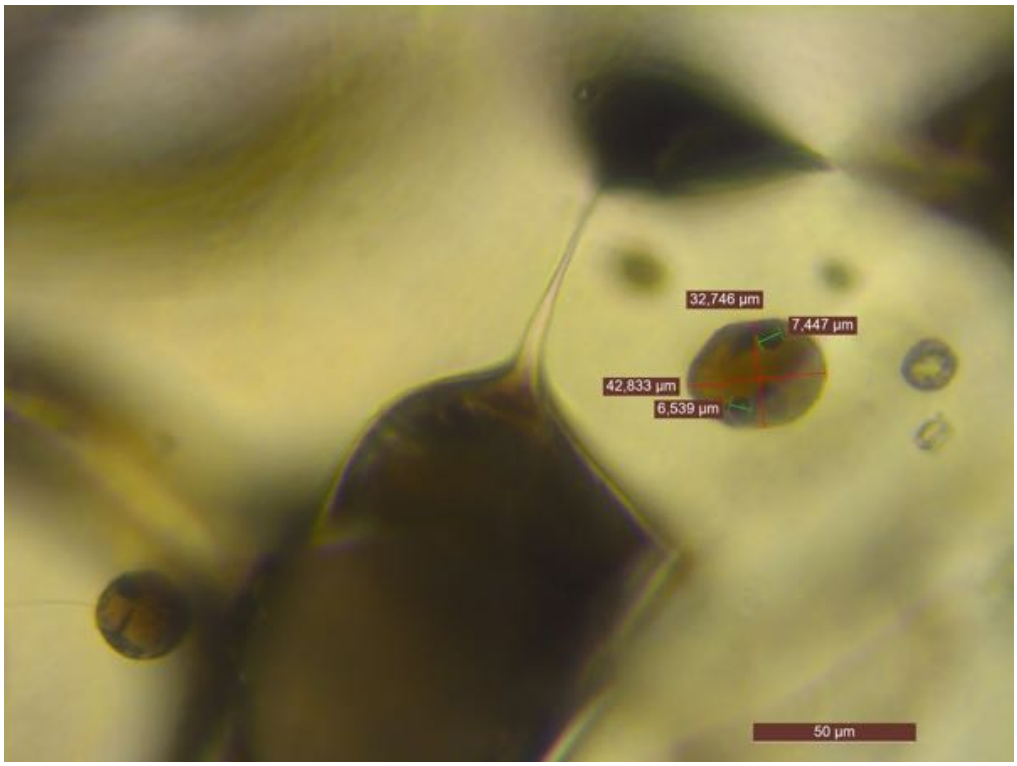
32,746 µm
7,447 µm
42,833 µm
6,539 µm
50 µm

Z-II

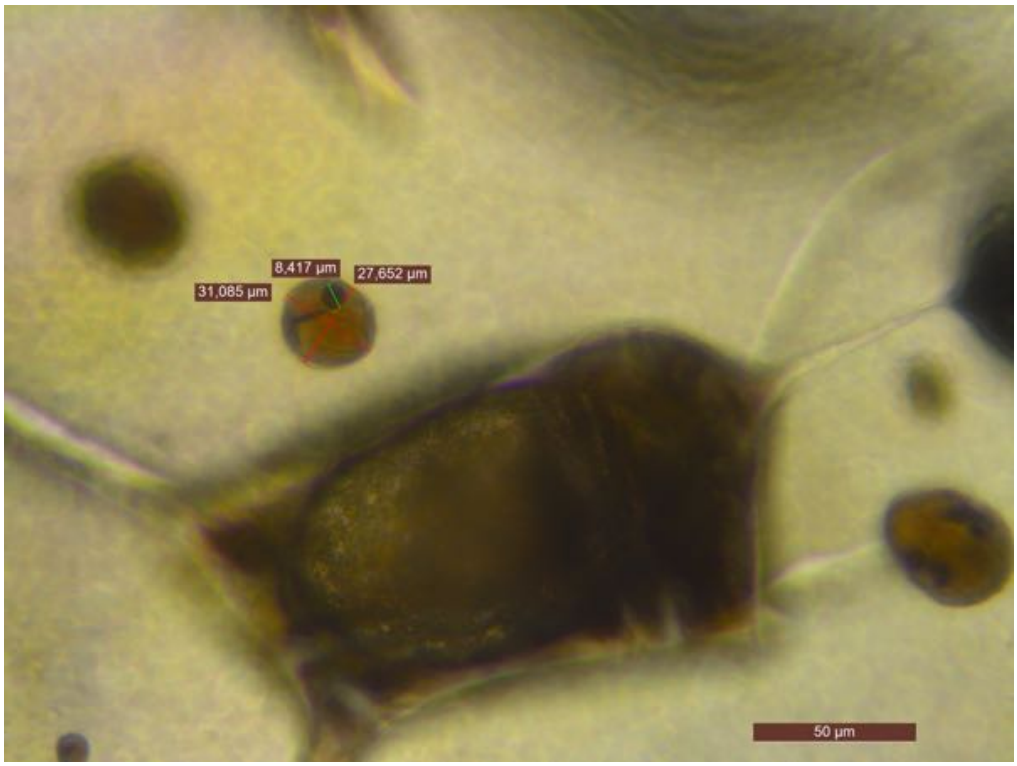
8,417 µm
27,652 µm
31,085 µm
50 µm

<FKONON>
A-I

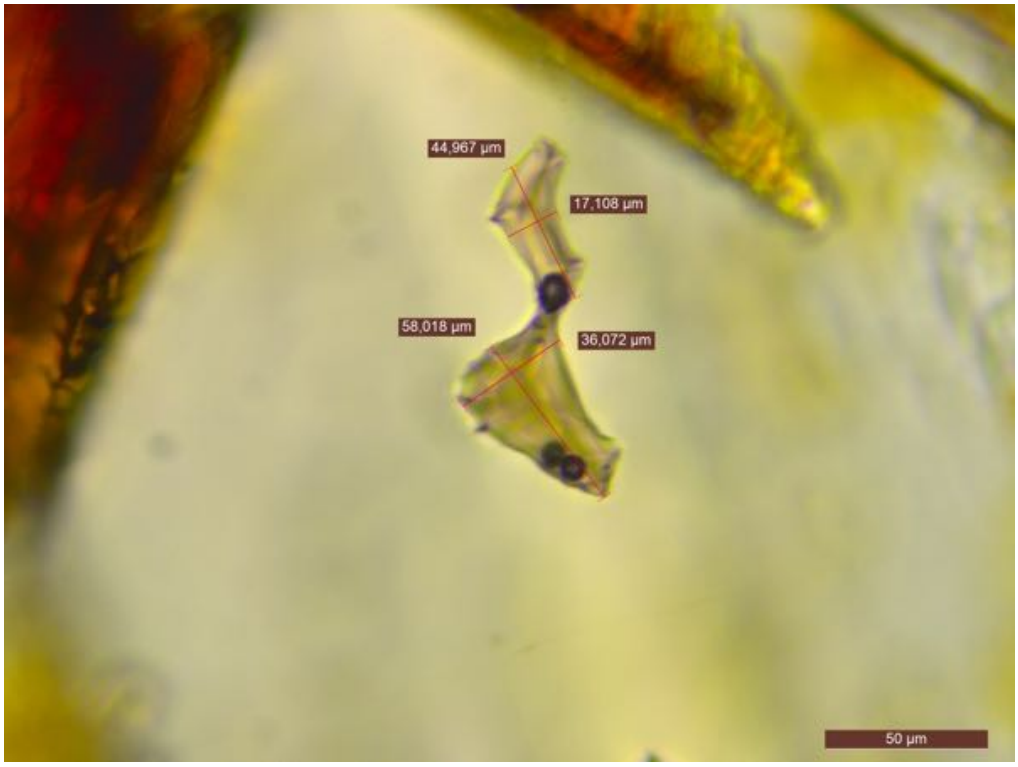
44,967 µm
17,108 µm
58,018 µm
36,072 µm
50 µm

B-I

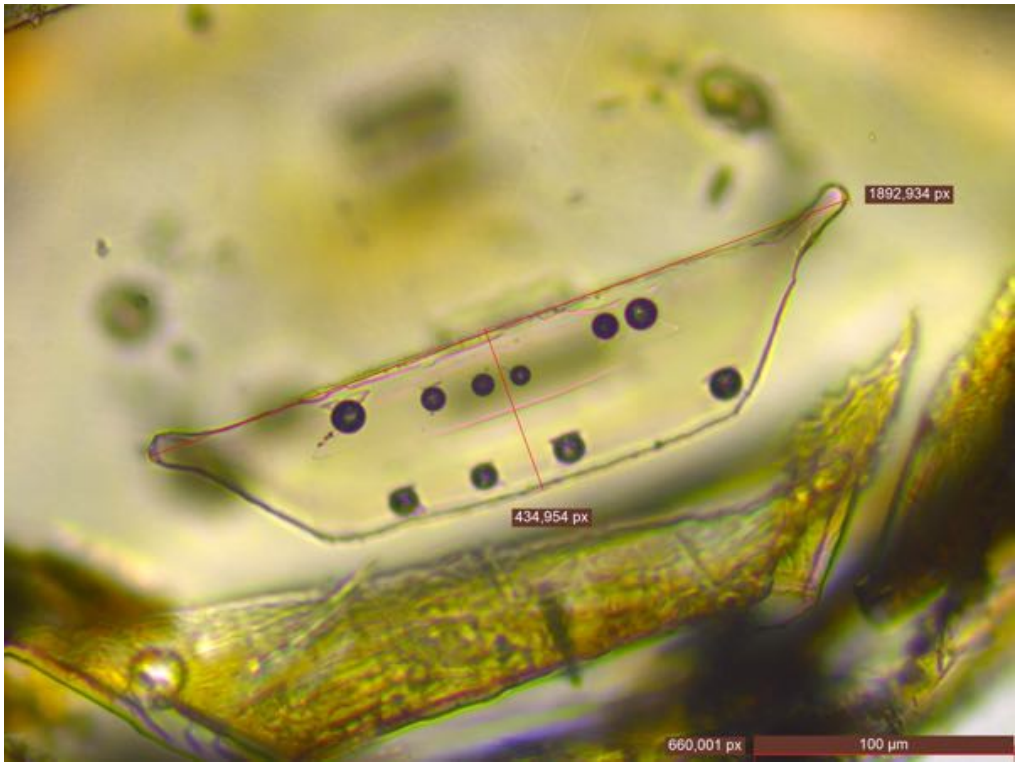
1892,934 px
434,954 px
660,001 px
100 µm

D-I

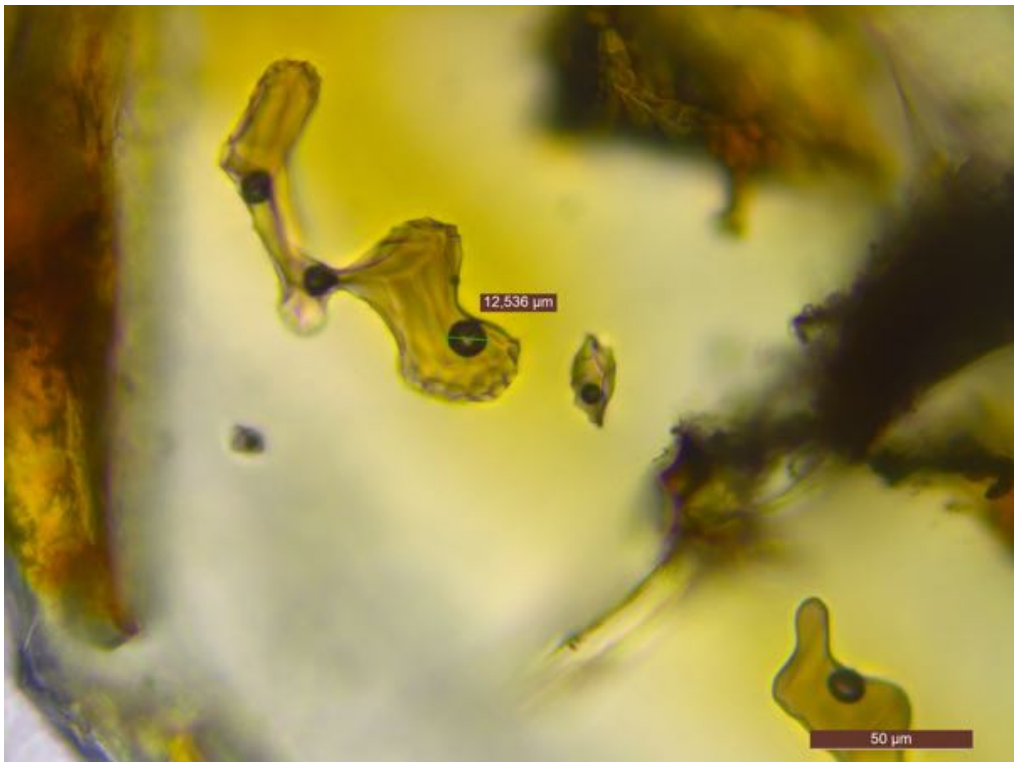

D-II

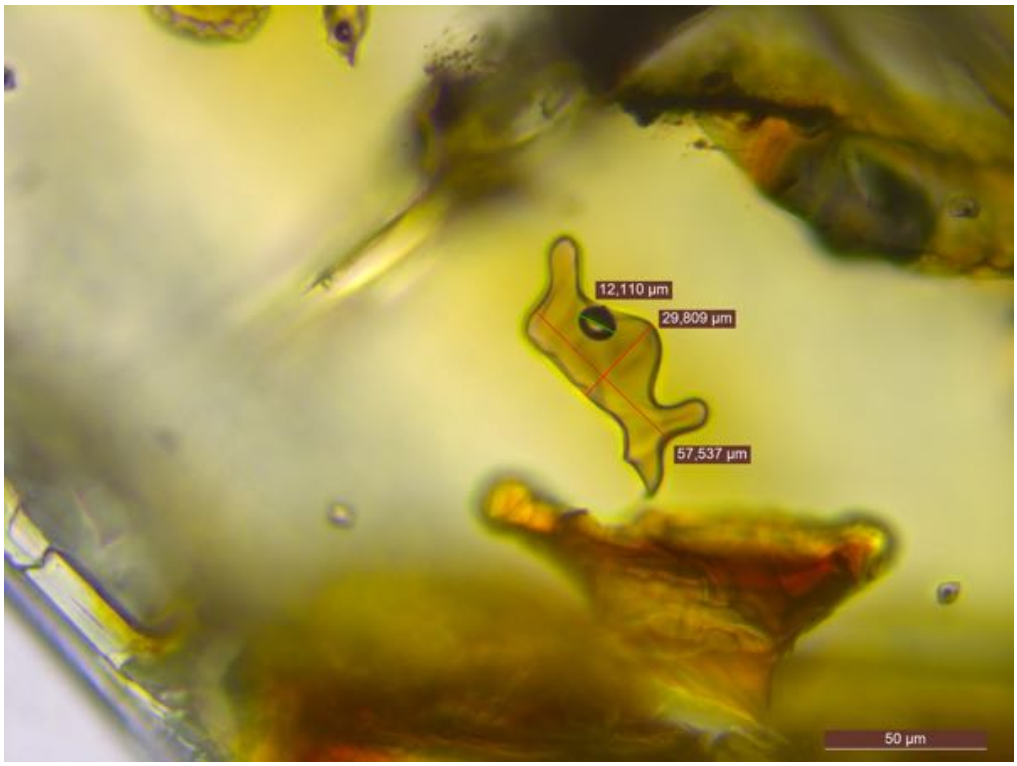

F-I

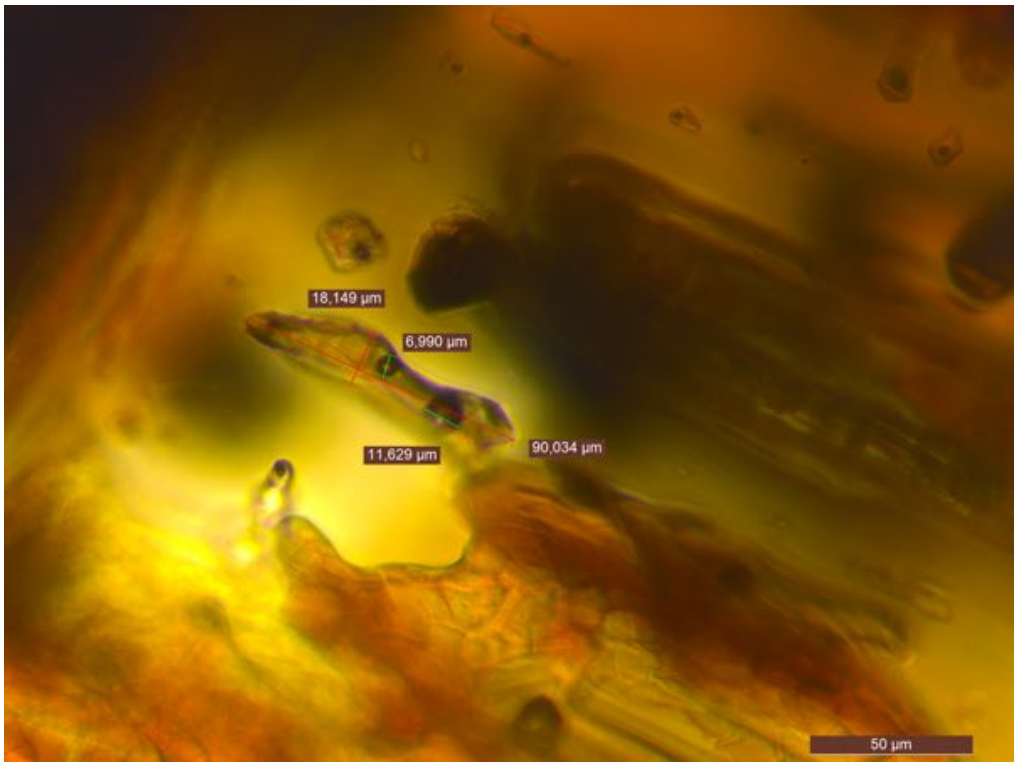
18,149 µm
6,990 µm
11,629 µm
90,034 µm
50 µm

I-I

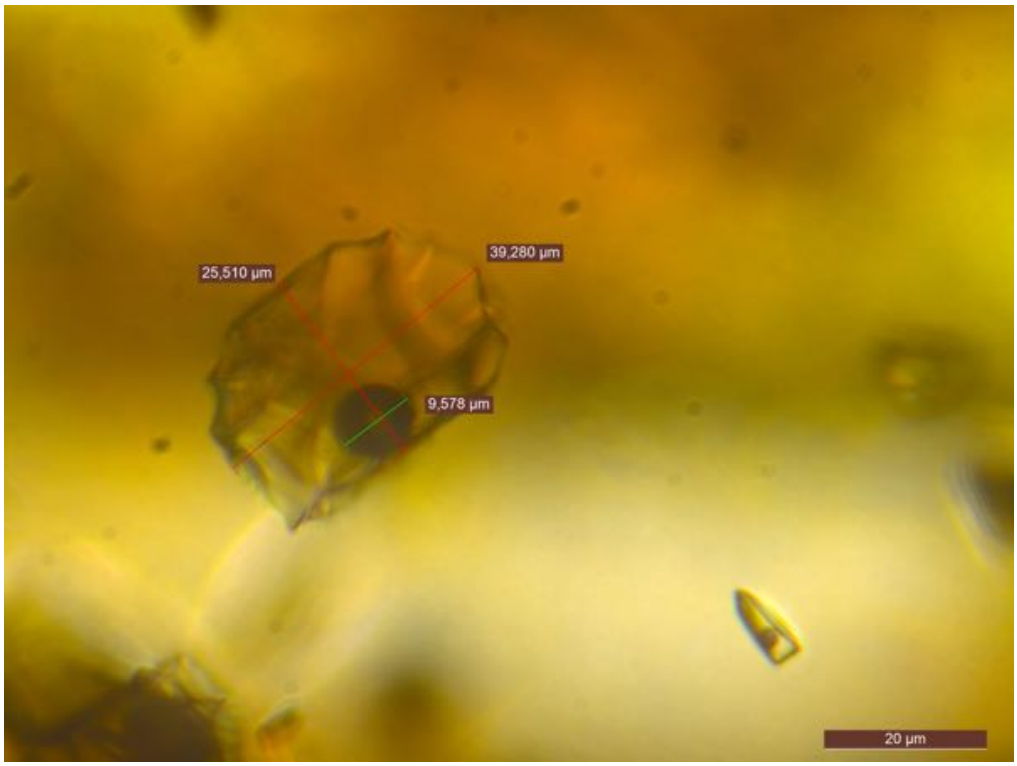
25,510 µm
39,280 µm
9,578 µm
20 µm

K-I

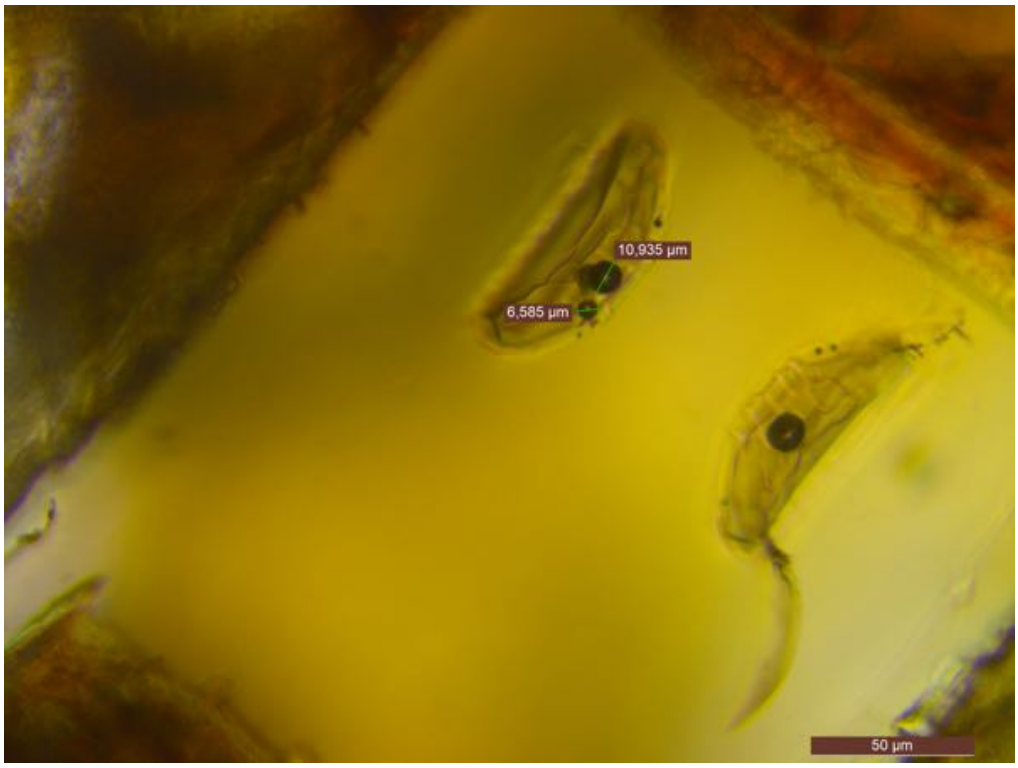

K-II

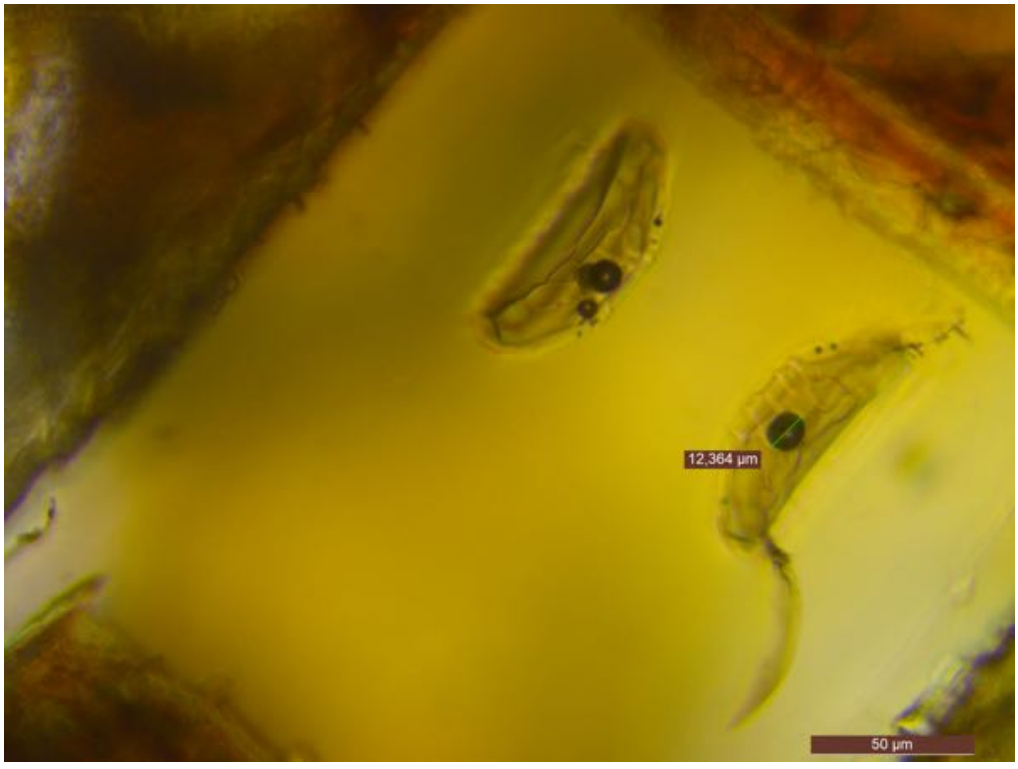

M-I


14,840 µm
31,070 µm
10,828 µm
6,709 µm
20 µm

N-I

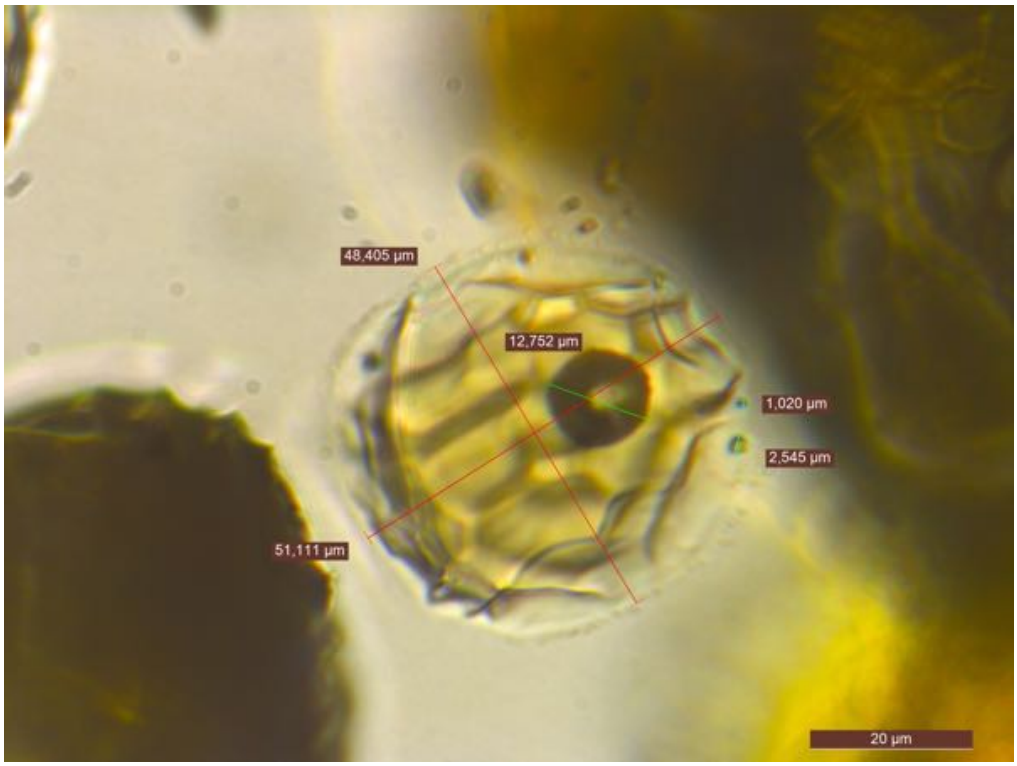
48,405 µm
12,752 µm
1,020 µm
2,545 µm
51,111 µm
20 µm

N-II

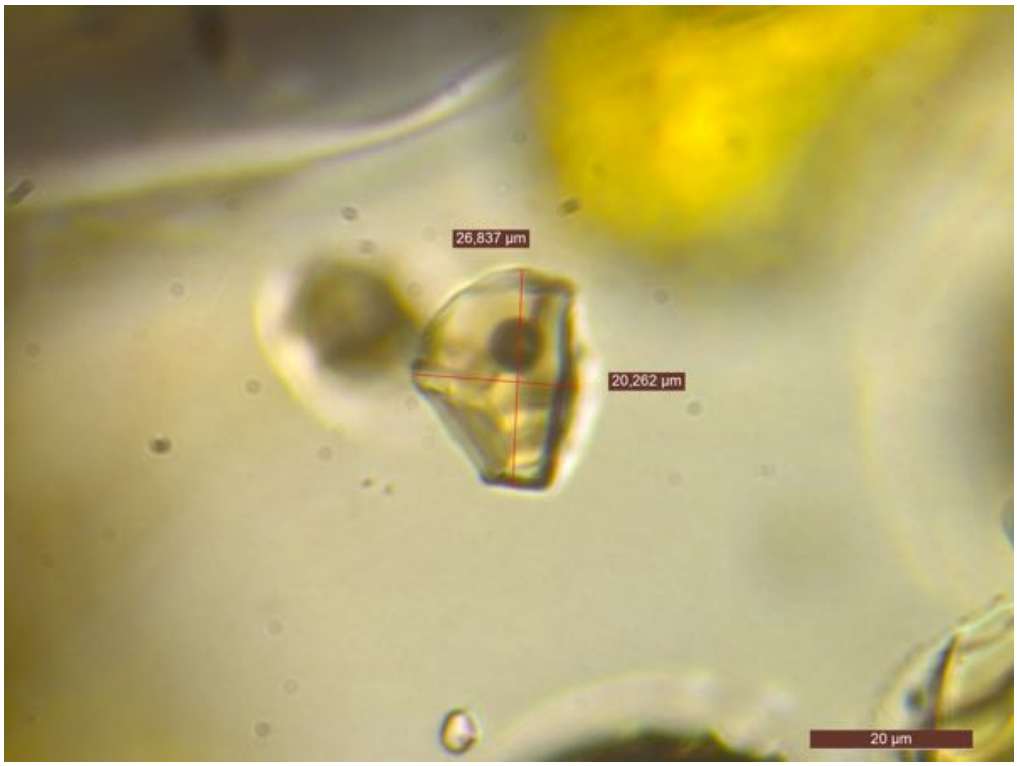

O-I

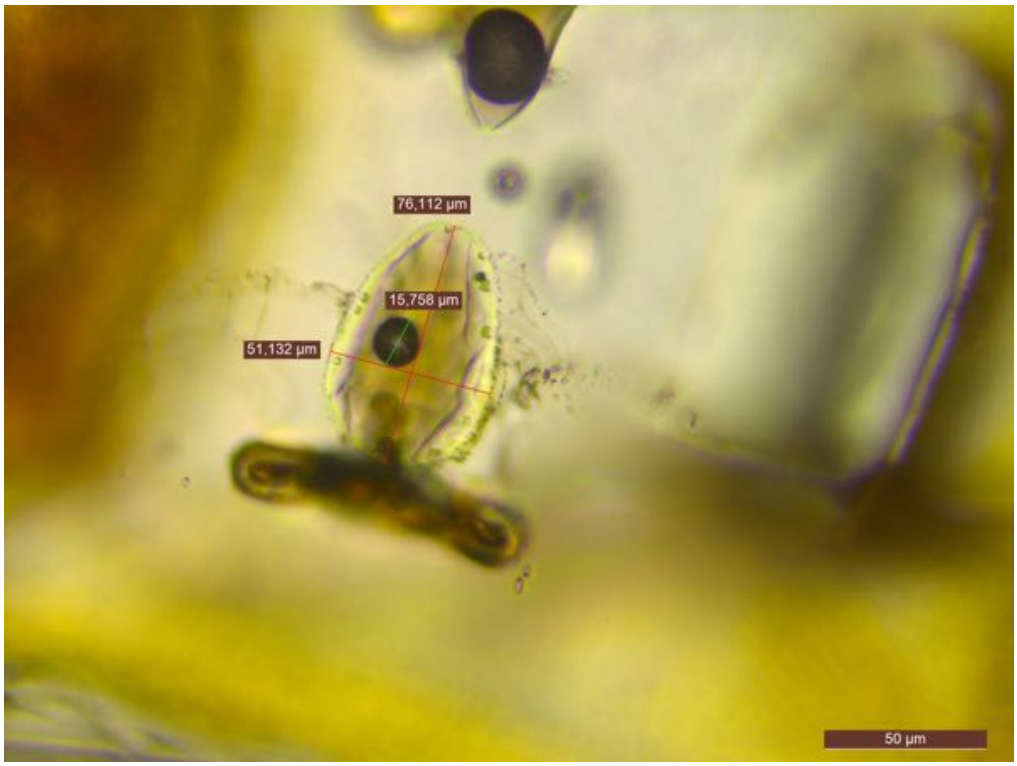

O-II

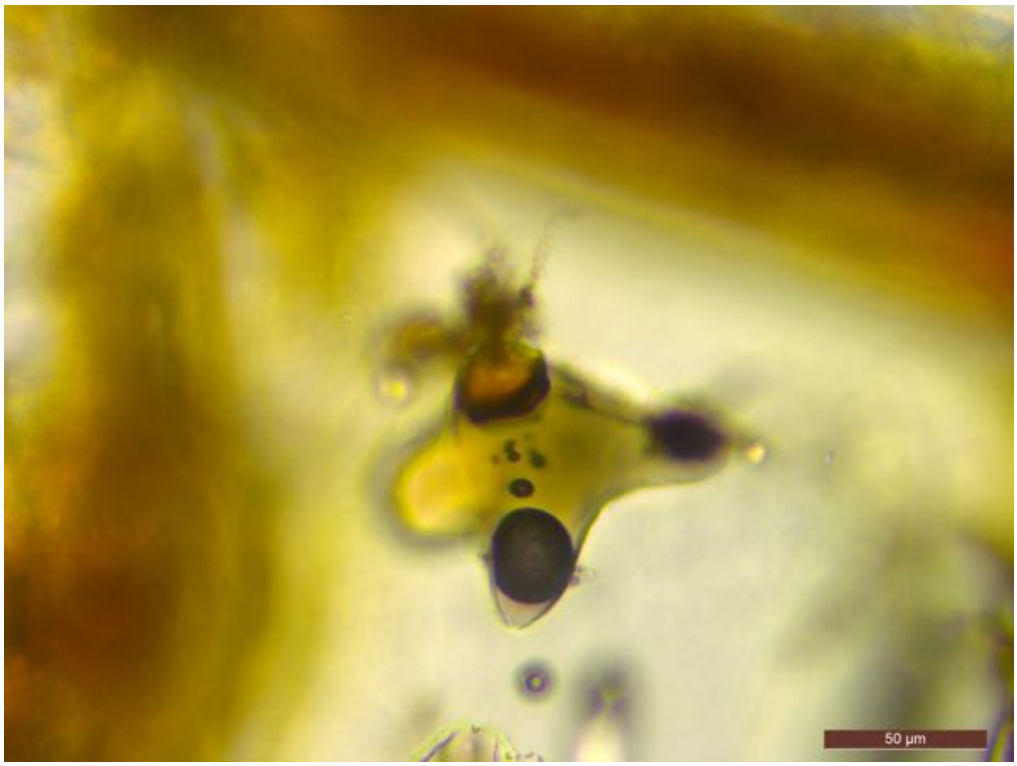

P-II